



Universiteit
Leiden
The Netherlands

CRB1 gene therapy coming of age: mechanistic insight and rAAV assays on mouse & human retinal organoid models

Buck, T.M.

Citation

Buck, T. M. (2022, September 28). *CRB1 gene therapy coming of age: mechanistic insight and rAAV assays on mouse & human retinal organoid models*. Retrieved from <https://hdl.handle.net/1887/3464695>

Version: Publisher's Version

License: [Licence agreement concerning inclusion of doctoral thesis in the Institutional Repository of the University of Leiden](#)

Downloaded from: <https://hdl.handle.net/1887/3464695>

Note: To cite this publication please use the final published version (if applicable).

***CRBI* gene therapy coming of age:
Mechanistic insight and rAAV assays on mouse & human
retinal organoid models**

Thilo Matthias Buck

ISBN: 978-94-6419-586-6.

Front cover art: With permission of Sirion-Biotech GmbH. © Drawing "Gene therapy AAV" by Sirion-Biotech GmbH, Gräfelfing 2022

Back cover art: Müller glial cell extracted from a human iPSC-derived control retinal organoid. Stained & imaged for glutamine synthetase (green), CD44 (red), vimentin (cyan), and DNA/DAPI (gray). © Drawing T.M. Buck, Leiden 2022

Printed by Gildeprint - www.gildeprint.nl

The printing of this thesis was financially supported by Stichting Blindenhulp, Den Haag.

Copyright © Thilo M. Buck, 2022.

All rights are reserved. No part of this publication may be reproduced, stored, or transmitted in any form or by any means without permission of the copyright owners.

***CRB1* gene therapy coming of age:
Mechanistic insight and rAAV assays on mouse & human retinal
organoid models**

Proefschrift

ter verkrijging van

de graad van doctor aan de Universiteit Leiden,
op gezag van rector magnificus prof. dr. ir. H. Bijl,
volgens besluit van het college voor promoties
te verdedigen op woensdag 28 september 2022

klokke 16.15 uur

door

Thilo M. Buck

geboren te Esslingen am Neckar, Germany

in 1988

Promotor: Prof. dr. G.P.M. Luyten

Co-Promotor: Dr. J. Wijnholds

Leden promotiecommissie:

Dr. A. Garanto Iglesias, Radboud UMC

Prof. dr. A.A.B. Bergen, Amsterdam UMC

Prof. dr. C.J.F. Boon, Amsterdam UMC and LUMC

Prof. dr. R.C. Hoeben

Prof. dr. M.J. Goumans

The research here described was conducted at the Department of Ophthalmology, at the Leiden University Medical Center (LUMC). The studies described in this thesis were financially supported by Foundation Fighting Blindness, The Netherlands Organisation for Health Research and Development: ZonMw, Curing Retinal Blindness Foundation, Stichting Retina Nederland Fonds, Landelijke St. Blinden en Slechtienden, Rotterdamse Stichting Blindenbelangen, St. Blindenhulp, St. Blinden-Penning, Algemene Nederlandse Vereniging ter Voorkoming van Blindheid (ANVVB), Gelderse Blinden Stichting and MaculaFonds.

CONTENTS

	Abbreviations	10
<hr/>		
CHAPTER 1	General introduction	
	1.1 Introduction: A short history on the apical polarity protein CRB1	14
	1.2 Recombinant Adeno-Associated Viral Vectors (rAAV)- Vector Elements in Ocular Gene Therapy Clinical Trials and Transgene Expression and Bioactivity Assays <i>Int. J. Mol. Sci., 2020, 21, 4197</i>	22
	1.3 Aims and outline of this thesis	61
<hr/>		
CHAPTER 2	AAV-CRB2 protects against vision loss in an inducible CRB1 retinitis pigmentosa mouse model <i>Molecular Therapy: Methods & Clinical Development, 2021, 20, 423-441</i>	90
<hr/>		
CHAPTER 3	AAV Serotype Testing on Cultured Human Donor Retinal Explants <i>Methods Mol Biol, 2018, 1715, 275-288</i>	136
<hr/>		
CHAPTER 4	Human iPSC-Derived Retinas Recapitulate the Fetal CRB1 CRB2 Complex Formation and Demonstrate that Photoreceptors and Müller Glia Are Targets of AAV5 <i>Stem Cell Reports, 2019, 12(5),906-919</i>	152
<hr/>		
CHAPTER 5	CRB1 is required for NOTCH1 interaction and RAB11A sorting vesicles in human retinal organoids <i>Submitted</i>	192
<hr/>		
CHAPTER 6	General Discussion	260
<hr/>		
CHAPTER 7	Summary	260
	Nederlandse Samenvatting	264
	Acknowledgements	269
	Curriculum Vitae	270
	List of Publications	271

to Claartje and Luna

ABBREVIATION

AAV	adeno-associated virus
AAV2-tYF	rAAV2-Y444F+Y500F+Y730F
Ad	adenovirus
AMD	age-related macular degeneration
AON	antisense oligonucleotides
BAA	biological activity assay
bGH	bovine growth hormone
CAG/CBA/ pCAGGS	CMV early enhancer element, promoter of the first exon and the first intron of chicken β -actin gene, splice acceptor of the rabbit β -globin intron
CB7	shortened CMV early enhancer element and a chicken β -actin promoter
CBh	CMV early enhancer element, a chicken β -actin promoter and a chimeric chicken β -Actin / minute virus of mice (MVM) viral protein (VP) intron
CB-SB	shortened CBA promoter containing a CMV early enhancer element
CMV	cytomegalovirus early enhancer element and promoter
EBV	Epstein Barr Virus
ERG	Electroretinogram (retinal function)
GCL	Ganglion cell layer
GMP	good manufacturing practice
hCAR	human cone arrestin
hCNGA3	Human (cone PRC) Cyclic Nucleotide Gated Channel Subunit Alpha 3
hCHM	Human CHM gene (encodes for the Rab escort protein 1 [REP1])
hGH	human growth hormone
hGRK1/hRK	human G protein-coupled rhodopsin kinase 1 promoter
hiPSC	human induced pluripotent stem cells
hRPE65p	human retinal pigment epithelium-specific 65 kDa protein (RPE65) promoter
hVMD2	human vitelliform macular dystrophy type 2 promoter (aka BEST1)
ILM	Inner Limiting Membrane
INL	Inner Nuclear Layer
IPL	Inner Plexiform Layer
IONs	inherited optic neuropathies
IRBP	interphotoreceptor retinoid-binding protein
IRDs	inherited retinal dystrophies
IRES	Internal ribosome entry site
ITR	palindromic inverted terminal repeats
ITR2	palindromic inverted terminal repeats AAV serotype 2
LCA	Leber congenital amaurosis

LV	lentivirus
mCAR	mouse cone arrestin
mRNA	Messenger RNA
miRNA	microRNA
MGC	Müller glial cell
MVM	minute virus of mice viral protein (VP intron)
NMT	novel medical therapy
OKT	Optokinetic headtracking response
OLM	Outer Limiting Membrane
ONL	Outer Nuclear Layer
OPL	Outer Plexiform Layer
pA	polyadenylation sequence
PBGD	Porphobilinogen deaminase
PRC	photoreceptor
PRE	post-transcriptional regulatory element
rAAV	recombinant adeno-associated virus
rBG	rabbit β -globin
rHSV	replication-defective recombinant herpes virus
RPE	Retinal Pigment Epithelium
SpA	synthetic polyadenylation signal
sBHK	suspension-adapted Baby Hamster Kidney fibroblasts
scAAV	self-complementary recombinant adeno-associated virus
Sf9	a clonal isolate of <i>Spodoptera frugiperda</i> (Fall Army worm) Sf21 cells
smCBA	truncated chimeric CMV/CBA promoter
ssAAV	single-stranded recombinant adeno-associated virus
SV40	late simian virus 40
TEA	transgene expression assay
TFBS	transcription factor binding sites
vg	viral genomes (<i>aka gc</i> , genome copies)
WPRE	Woodchuck hepatitis virus post-transcriptional regulatory element
wtAAV	Wild-type adeno-associated virus

Chapter 1

1.1 Introduction: A short history on the apical polarity protein CRB1

T.M. Buck

1.2 Recombinant Adeno-Associated Viral Vectors(rAAV)-Vector Elements in Ocular Gene Therapy Clinical Trials and Transgene Expression and Bioactivity Assays

T.M. Buck and J. Wijnholds

Int. J. Mol. Sci. 2020, 21, 4197

1.3 Aim and outline of this thesis

Inherited retinal dystrophies (IRDs) are disabling disorders of the visual system with so far, few to no treatment options available. More than 279 genes have been associated with IRDs including the Crumbs homolog-1 (*CRB1*) gene. *CRB1*-associated retinal dystrophies (RDs) have an autosomal recessive inheritance pattern requiring individuals to have two pathogenic variant alleles as either homozygous or compound heterozygote alleles. Clinical phenotypes range from retinitis pigmentosa (RP; 3-9% of all RP cases), Leber congenital amaurosis (LCA; 7-17% of all LCA cases), cone-rod dystrophies to sporadically foveal retinoschisis and macular dystrophy [1–6]. *CRB1*-associated RD patients in ophthalmic clinics may present with progressive visual loss, peripheral macular retinal thickening (but thinning over time), difficult to discern retinal layers, hyperopia, disruption of the normal blood-retinal barrier shown by cystoid fluid collections, reticular pseudo-drusenoid white spots or optic nerve disc drusen (i.e., acellular calcified deposits in ganglion cells), and preservation of para-arteria retinal pigment epithelium (RPE) [1,6,7]. Early phenotypes are found above the RPE at the outer limiting membrane (OLM) in the neuroretina where *CRB1* protein and other apical polarity regulators localize, pointing towards a primarily cell adhesion-related phenotype [8,9]. The OLM is established in the fetal neuroretina and hold in place by Müller glial cells (MGCs) and photoreceptors (PRs), establishing adherens junctions between PRs-PRs, MGCs-MGCs, and PRs-MGCs. Many RD-*CRB1*-like animal models, RP-*CRB1*-like patient-derived retinal organoids as well as the observation in RD-associated *CRB1* patients establishes a disease mechanism related to a loss of adhesion between the OLM participating cell types and a dysregulation of the apical-polarity signaling pathways [8–12].

In 1984 and further worked out in 1990, the *crb* gene was discovered in the apical membrane of epithelia cells in *Drosophila melanogaster* [13,14]. The first phenotype in *crb*-null embryos was described as “*many small holes in cuticle*” like a crumbling morphology giving it its name *crumbs*. Other *Crb* orthologues have since been found in insects and vertebrates alike. In vertebrates, the *CRB* gene has undergone several gene duplication events during evolution (ENSG00000134376 gene tree). Yet, the prototypic (human, mouse, rat) *CRB1/CRB2* as well as the *CRB* (fruit fly) protein is composed of a large extracellular domain containing many EGF-like domains and 3x LamG-like domains, a single-pass transmembrane domain, and a canonical short PDZ/ERLI intracellular domain [9,15,16]. The 37-aa intracellular C-terminal domain contains a FERM domain next to the transmembrane domain and a PDZ domain which form intracellular protein complexes interacting with the cell cytoskeleton. The human *CRB1* gene consists of 12 exons coding for 1406 amino acids (aa; 1405 aa in mice). In humans we also find the *CRB1* orthologues *CRB2*, *CRB3A*, and *CRB3B* with all being expressed in the retina. *CRB2* (1285 aa) is highly similar to *CRB1* but having less EGF-like domains and *CRB3* (~120 aa) lacks the extracellular domains. However, all apart from *CRB3B*, are able to form *CRB* or *PAR* apical polarity complexes by recruiting *PALS1* or *PAR6* [17–20]. Interestingly, *Crb2* and *Crb3* gene ablation in mice is lethal while *Crb1* is not [8,21,22].

What is more, mouse CRB2 protein (while *CRB3* expression is actively repressed) promotes cell ingressions in the epithelial-to-mesenchymal transition (EMT) during gastrulation – a key developmental stage needed to establish the ectoderm, mesoderm, and endoderm [23,24]. Also, human CRB2 protein is found earlier than CRB1 during retinal neurogenesis [9]. However, the function and cellular expression of CRB's (including CRB1) diverged between species evolution making inter-species comparisons complex. For example, a hallmark of human or mouse CRB1 function is to participate in the neuroretinal polarity complex but zebrafish CRB1 does not [25]. Further, several *CRB1*-like mouse models and human CRB1/CRB2 protein localization studies suggests that CRB1 and CRB2 have at least overlapping roles and being able to compensate the loss of the other in the neuroretina [12,15,26–32]. Interestingly, CRB1 has a more dominant role in humans compared to mice being expressed in both photoreceptors and Müller glial cells at the subapical region while in mice CRB1 is only found in early retinal progenitor cells and later in Müller glial cells (see Figure 1). Further complicating, a 1003-aa CRB1-B isoform (delineating it from the classical 1406 aa CRB1-A protein) was detected having a shorter extracellular domain and lacking the ERLI domain for binding to the polarity complex members. However its significance is still under dispute as the mouse *Crb1-B* knockout model had no evident retinal phenotype and the protein is by large expressed in the photoreceptor outer segments instead of at the subapical region where CRB1-A takes part in apico-polarity protein complexes CRUMBS and PAR [33] (**Figure 1**).

In 1999, the human *CRB1* gene was first associated as a retinal disease causing gene [35]. Over the years, more than 300 pathogenic *CRB1* variants have been found with the most frequently found on exon 2, 7 and 9 [6]. Common variants are p.(Glu222Lys), p.(Cys250Trp), p.(Cys948Tyr), and p.(Met1041Thr) (<https://databases.lovd.nl/shared/variants/CRB1>). The pathogenic variants are almost exclusively found in exons (94%) & splice regions (4%) and covering the whole *CRB1* exome. Interestingly, RD-associated *CRB1* variants display a low genotype-phenotype correlation, yet variants ablating CRB1 proteins have been more clearly associated with early retinal phenotypes [36].

With the advent of gene therapy showing safety and long-lasting expression by recombinant adeno-associated viral vectors (rAAVs) in many studies [37], several options were explored for developing candidate vectors for clinical trials. Different promoters (CAG, CMV, CMVmin, GFAP, RLBP1, CD44), different rAAV serotypes (rAAV2/2, rAAV2/5, rAAV2/6, rAAV2/6-derived ShH10^{Y445F}, rAAV2/9), and different *CRB1* isoforms were tested [28,38,39]. An early challenge was that the size of the *CRB1* transcript (4218 bp) coding for the large 1406-aa protein being close to the maximum packaging size of an rAAV (~4800 bp). And additional room is needed for a promoter and a polyadenylation sequence. It was approached in three directions: (a) expressing a short native *CRB1* (*sCRB1*) lacking

exon 3 and 4, (b) replacing *CRB1* with *CRB2* (3855 bp), (c) developing a short Müller & photoreceptor cell promoter. The s*CRB1* caused retinal degeneration when injected subretinal [39].

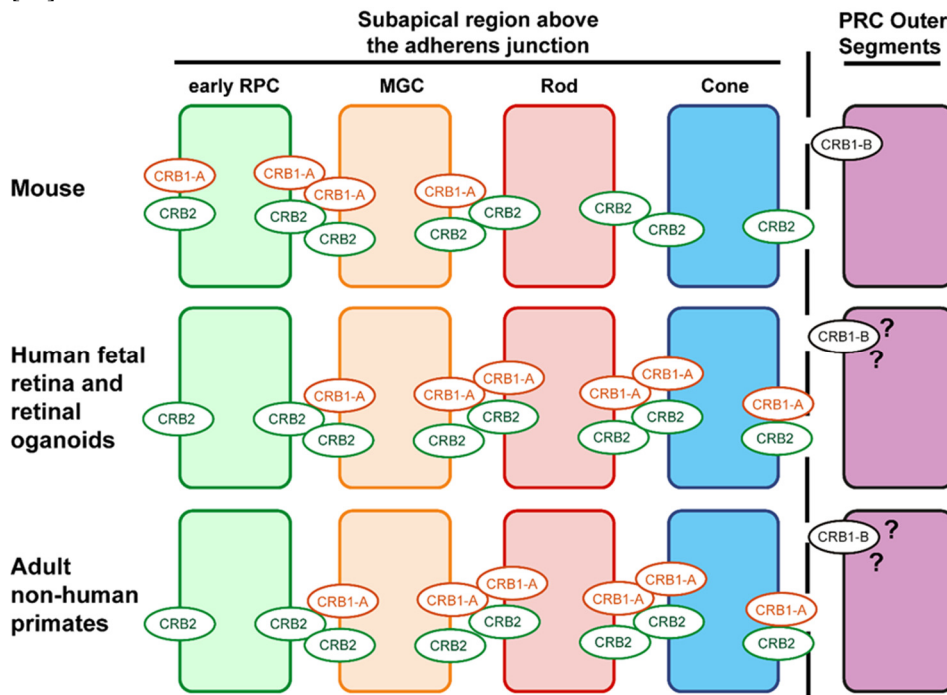


Figure 1. Cartoon representation of CRB1-A, CRB1-B and CRB2 protein location at the subapical region above the adherens junction (forming the outer limiting membrane) and in photoreceptor outer segments. The subcellular localization of CRB1-B in human photoreceptor outer segments is not known, therefore indicated in red with question mark. Figure adapted from [34]. MGC, Müller glial cells; PRC, photoreceptor; RPC, retinal progenitor cells.

Replacing *CRB1* with *CRB2* turned out to be a highly efficient vector showing repeatedly rescue or protection in *in vivo* mouse studies [12,28]. And the generation of a CMVmin promoter provided robust *CRB1* expression to Müller and photoreceptor cells also being able to protect the retinal morphological phenotype but not visual function [12,28]. Then, a different AAV serotypes were screened on potency in human retinal explants and human retinal organoids showing that rAAV5 and rAAV6-derived ShH10^{Y445F} can efficiently infect both cell types. Recently, also a natural occurring *Crb1* rat model became available which we had difficulties in showing efficient rAAV-mediated neuroretinal infection [40]. rAAV gene therapy studies in retinal organoids are also under way. It will be exciting to see what other research will define therapies for patients with *CRB1*-associated retinitis pigmentosa.

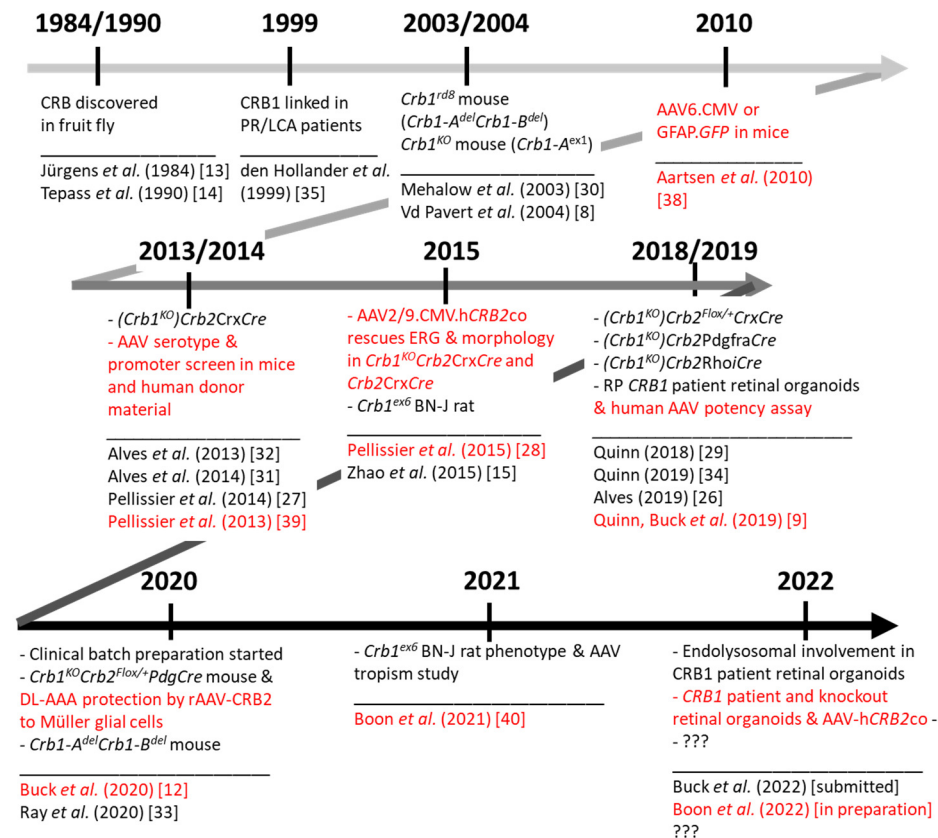


Figure 2. An incomplete short *CRB1* history. Focus: *CRB1*-like mouse models, *CRB1*-associated retinitis pigmentosa patient-derived retinal organoids and relevant rAAV gene therapy-related studies (in red).

REFERENCES

1. Nguyen, X.T.A.; Talib, M.; van Schooneveld, M.J.; Wijnholds, J.; van Genderen, M.M.; Schalijs-Delfos, N.E.; Klaver, C.C.W.; Talsma, H.E.; Fiocco, M.; Florijn, R.J.; et al. *CRB1*-Associated Retinal Dystrophies: A Prospective Natural History Study in Anticipation of Future Clinical Trials. *Am. J. Ophthalmol.* **2022**, *234*, 37–48.
2. Talib, M.; van Schooneveld, M.J.; van Genderen, M.M.; Wijnholds, J.; Florijn, R.J.; ten Brink, J.B.; Schalijs-Delfos, N.E.; Dagnelie, G.; Cremers, F.P.M.; Wolterbeek, R.; et al. Genotypic and Phenotypic Characteristics of *CRB1*-Associated Retinal Dystrophies: A Long-Term Follow-up Study. *Ophthalmology* **2017**, *124*, 884–895.
3. Vincent, A.; Ng, J.; Gerth-Kahlert, C.; Tavares, E.; Maynes, J.T.; Wright, T.; Tiwari, A.; Tumber, A.; Li, S.; Hanson, J.V.M.; et al. Biallelic Mutations in *CRB1* Underlie Autosomal Recessive Familial Foveal Retinoschisis. *Invest. Ophthalmol. Vis. Sci.* **2016**, *57*, 2637–2646.
4. Tsang, S.H.; Burke, T.; Oll, M.; Yzer, S.; Lee, W.; Xie, Y.A. (Angela); Allikmets, R. Whole Exome Sequencing Identifies *CRB1* Defect in an Unusual Maculopathy Phenotype. *Ophthalmology* **2014**, *121*, 1–10.
5. Khan, A.O.; Aldahmesh, M.A.; Abu-Safieh, L.; Alkuraya, F.S. Childhood cone-rod dystrophy with macular cystic degeneration from recessive *CRB1* mutation. *Ophthalmic Genet.* **2014**, *35*, 130–137.
6. Motta, F.L.; Salles, M.V.; Costa, K.A.; Filippelli-Silva, R.; Martin, R.P.; Sallum, J.M.F. The correlation between *CRB1* variants and the clinical severity of Brazilian patients with different inherited retinal dystrophy phenotypes. *Sci. Reports* **2017**, *7*, 1–9.
7. Ehrenberg, M.; Pierce, E.A.; Cox, G.F.; Fulton, A.B. *CRB1*: One gene, many phenotypes. *Semin. Ophthalmol.* **2013**, *28*, 397–405.

8. van de Pavert, S.A.; Kantardzhieva, A.; Malysheva, A.; Meuleman, J.; Versteeg, I.; Levelt, C.; Klooster, J.; Geiger, S.; Seeliger, M.W.; Rashbass, P.; et al. Crumbs homologue 1 is required for maintenance of photoreceptor cell polarization and adhesion during light exposure. *J. Cell Sci.* **2004**, *117*, 4169–4177.
9. Quinn, P.M.; Buck, T.M.; Mulder, A.A.; Ohonin, C.; Alves, C.H.; Vos, R.M.; Bialecka, M.; van Herwaarden, T.; van Dijk, E.H.C.C.; Talib, M.; et al. Human iPSC-Derived Retinas Recapitulate the Fetal CRB1 CRB2 Complex Formation and Demonstrate that Photoreceptors and Müller Glia Are Targets of AAV5. *Stem Cell Reports* **2019**, *12*, 906–919.
10. Boon, N.; Wijnholds, J.; Pellissier, L.P. Research Models and Gene Augmentation Therapy for CRB1 Retinal Dystrophies. *Front. Neurosci.* **2020**, *14*, 860.
11. Alves, C.H.; Pellissier, L.P.; Wijnholds, J. The CRB1 and adherens junction complex proteins in retinal development and maintenance. *Prog. Retin. Eye Res.* **2014**, *40*, 35–52.
12. Buck, T.M.; Vos, R.M.; Alves, C.H.; Wijnholds, J. AAV-CRB2 protects against vision loss in an inducible CRB1 retinitis pigmentosa mouse model. *Mol. Ther. - Methods Clin. Dev.* **2021**, *20*.
13. Jürgens, G.; Wieschaus, E.; Nüsslein-Volhard, C.; Kluding, H. Mutations affecting the pattern of the larval cuticle in *Drosophila melanogaster*: II. Zygotic loci on the third chromosome. *Wilehm Roux Arch Dev Biol* **1984**, *193*, 283–29.
14. Tepass, U.; Theres, C.; Knust, E. crumbs encodes an EGF-like protein expressed on apical membranes of *Drosophila* epithelial cells and required for organization of epithelia. *Cell* **1990**, *61*, 787–799.
15. Zhao, M.; Andrieu-Soler, C.; Kowalczyk, L.; Cortés, M.P.; Berdugo, M.; Dernigoghossian, M.; Halili, F.; Jeanny, J.C.; Goldenberg, B.; Savoldelli, M.; et al. A new CRB1 rat mutation links Müller glial cells to retinal telangiectasia. *J. Neurosci.* **2015**, *35*, 6093–6106.
16. Pellissier, L.P.; Alves, C.H.; Quinn, P.M.; Vos, R.M.; Tanimoto, N.; Lundvig, D.M.S.; Dudok, J.J.; Hooibrink, B.; Richard, F.; Beck, S.C.; et al. Targeted ablation of CRB1 and CRB2 in retinal progenitor cells mimics Leber congenital amaurosis. *PLoS Genet* **2013**, *9*, e1003976.
17. Quinn, P.M.; Pellissier, L.P.; Wijnholds, J. The CRB1 complex: Following the trail of Crumbs to a feasible gene therapy strategy. *Front. Neurosci.* **2017**, *11*, 175.
18. Roh, M.H.; Fan, S.; Liu, C.-J.; Margolis, B. The Crumbs3-Pals1 complex participates in the establishment of polarity in mammalian epithelial cells. *J. Cell Sci.* **2003**, *116*, 2895–2906.
19. Hurd, T.W.; Gao, L.; Roh, M.H.; Macara, I.G.; Margolis, B. Direct interaction of two polarity complexes implicated in epithelial tight junction assembly. *Nat. Cell Biol.* **2003**, *5*, 137–142.
20. Roh, M.H.; Makarova, O.; Liu, C.-J.; Shin, K.; Lee, S.; Laurinec, S.; Goyal, M.; Wiggins, R.; Margolis, B. The Maguk protein, Pals1, functions as an adapter, linking mammalian homologues of Crumbs and Discs Lost. *J. Cell Biol.* **2002**, *157*, 161–72.
21. Alves, C.H.; Sanz, A.S.; Park, B.; Pellissier, L.P.; Tanimoto, N.; Beck, S.C.; Huber, G.; Murtaza, M.; Richard, F.; Sridevi Gurubaran, I.; et al. Loss of CRB2 in the mouse retina mimics human retinitis pigmentosa due to mutations in the CRB1 gene. *Hum. Mol. Genet.* **2013**, *22*, 35–50.
22. Whiteman, E.L.; Fan, S.; Harder, J.L.; Walton, K.D.; Liu, C.-J.; Soofi, A.; Fogg, V.C.; Hershenson, M.B.; Dressler, G.R.; Deutsch, G.H.; et al. Crumbs3 Is Essential for Proper Epithelial Development and Viability. *Mol. Cell. Biol.* **2014**, *34*, 43.
23. Ramkumar, N.; Omelchenko, T.; Silva-Gagliardi, N.F.; McGlade, C.J.; Wijnholds, J.; Anderson, K. V. Crumbs2 promotes cell ingressation during the epithelial-to-mesenchymal transition at gastrulation. *Nat. Cell Biol.* **2016**, *18*, 1281–1291.
24. Whiteman, E.L.; Liu, C.J.; Fearon, E.R.; Margolis, B. The transcription factor snail represses Crumbs3 expression and disrupts apico-basal polarity complexes. *Oncogene* **2008**, *27*, 3875–3879.
25. Guo, C.; Deveau, C.; Zhang, C.; Nelson, R.; Wei, X. Zebrafish Crb1, Localizing Uniquely to the Cell Membranes around Cone Photoreceptor Axonemes, Alleviates Light Damage to Photoreceptors and Modulates Cones' Light Responsiveness. *J. Neurosci.* **2020**, *40*, 7065–7079.
26. Alves, C.H.; Boon, N.; Mulder, A.A.; Koster, A.J.; Jost, C.R.; Wijnholds, J. CRB2 Loss in Rod Photoreceptors Is Associated with Progressive Loss of Retinal Contrast Sensitivity. *Int. J. Mol. Sci.* **2019**, *20*, 4069.
27. Pellissier, L.P.; Lundvig, D.M.S.; Tanimoto, N.; Klooster, J.; Vos, R.M.; Richard, F.; Sothilingam, V.; Garcia Garrido, M.; Le Bivic, A.; Seeliger, M.W.; et al. CRB2 acts as a modifying factor of CRB1-related retinal dystrophies in mice. *Hum. Mol. Genet.* **2014**, *23*, 3759–3771.
28. Pellissier, L.P.; Quinn, P.M.; Henrique Alves, C.; Vos, R.M.; Klooster, J.; Flannery, J.G.; Alexander Heimel, J.; Wijnholds, J. Gene therapy into photoreceptors and Müller glial cells restores retinal structure and function in CRB1 retinitis pigmentosa mouse models. *Hum. Mol. Genet.* **2015**, *24*, 3104–3118.
29. Quinn, P.M.; Henrique Alves, C.; Klooster, J.; Wijnholds, J. CRB2 in immature photoreceptors determines the superior-inferior symmetry of the developing retina to maintain retinal structure and function. *Journals Gerontol. - Ser. A Biol. Sci. Med. Sci.* **2018**, *73*, 1010–1017.
30. Mehalow, A.K.; Kameya, S.; Smith, R.S.; Hawes, N.L.; Denegre, J.M.; Young, J. a.; Bechtold, L.; Haider, N.B.; Tepass, U.; Heckenlively, J.R.; et al. CRB1 is essential for external limiting membrane integrity and photoreceptor morphogenesis in the mammalian retina. *Hum. Mol. Genet.* **2003**, *12*, 2179–89.

31. Alves, C.H.; Pellissier, L.P.; Vos, R.M.; Garcia Garrido, M.; Sothilingam, V.; Seide, C.; Beck, S.C.; Klooster, J.; Furukawa, T.; Flannery, J.G.; et al. Targeted ablation of Crb2 in photoreceptor cells induces retinitis pigmentosa. *Hum. Mol. Genet.* **2014**, *23*, 3384–3401.
32. Alves, C.H.; Bossers, K.; Vos, R.M.; Essing, A.H.W.; Swagemakers, S.; van der Spek, P.J.; Verhaagen, J.; Wijnholds, J. Microarray and morphological analysis of early postnatal CRB2 mutant retinas on a pure C57BL/6J genetic background. *PLoS One* **2013**, *8*, e82532.
33. Ray, T.A.; Cochran, K.; Kozlowski, C.; Wang, J.; Alexander, G.; Cady, M.A.; Spencer, W.J.; Ruzycski, P.A.; Clark, B.S.; Laeremans, A.; et al. Comprehensive identification of mRNA isoforms reveals the diversity of neural cell-surface molecules with roles in retinal development and disease. *Nat. Commun.* **2020**, *11*, 1–20.
34. Quinn, P.M.; Mulder, A.A.; Henrique Alves, C.; Desrosiers, M.; de Vries, S.I.; Klooster, J.; Dalkara, D.; Koster, A.J.; Jost, C.R.; Wijnholds, J. Loss of CRB2 in Müller glial cells modifies a CRB1-associated retinitis pigmentosa phenotype into a Leber congenital amaurosis phenotype. *Hum. Mol. Genet.* **2019**, *28*, 105–123.
35. den Hollander, a I.; ten Brink, J.B.; de Kok, Y.J.; van Soest, S.; van den Born, L.I.; van Driel, M. a.; van de Pol, D.J.; Payne, a M.; Bhattacharya, S.S.; Kellner, U.; et al. Mutations in a human homologue of Drosophila crumbs cause retinitis pigmentosa (RP12). *Nat. Genet.* **1999**, *23*, 217–21.
36. den Hollander, a I.; Heckenlively, J.R.; van den Born, L.I.; de Kok, Y.J.; van der Velde-Visser, S.D.; Kellner, U.; Jurklies, B.; van Schooneveld, M.J.; Blankenagel, a; Rohrschneider, K.; et al. Leber congenital amaurosis and retinitis pigmentosa with Coats-like exudative vasculopathy are associated with mutations in the crumbs homologue 1 (CRB1) gene. *Am. J. Hum. Genet.* **2001**, *69*, 198–203.
37. Buck, T.M.; Wijnholds, J. Recombinant adeno-associated viral vectors (RAAV)-vector elements in ocular gene therapy clinical trials and transgene expression and bioactivity assays. *Int. J. Mol. Sci.* **2020**, *21*, 1–52.
38. Aartsen, W.M.; van Cleef, K.W.R.R.; Pellissier, L.P.; Hoek, R.M.; Vos, R.M.; Blits, B.; Ehlert, E.M.E.E.; Balaggan, K.S.; Ali, R.R.; Verhaagen, J.; et al. GFAP-driven GFP expression in activated mouse Müller glial cells aligning retinal blood vessels following intravitreal injection of AAV2/6 vectors. *PLoS One* **2010**, *5*, e12387.
39. Pellissier, L.P.; Hoek, R.M.; Vos, R.M.; Aartsen, W.M.; Klimczak, R.R.; Hoyng, S.A.; Flannery, J.G.; Wijnholds, J. Specific tools for targeting and expression in Müller glial cells. *Mol. Ther. — Methods Clin. Dev.* **2014**, *1*, 14009.
40. Boon, N.; Henrique Alves, C.; Mulder, A.A.; Andriessen, C.A.; Buck, T.M.; Quinn, P.M.J.; Vos, R.M.; Koster, A.J.; Jost, C.R.; Wijnholds, J. Defining phenotype, tropism, and retinal gene therapy using adeno-associated viral vectors (AAVs) in newborn brown norway rats with a spontaneous mutation in CRB1. *Int. J. Mol. Sci.* **2021**, *22*, 3563.

**1.2 Recombinant Adeno-Associated Viral Vectors(rAAV)-Vector
Elements in Ocular Gene Therapy Clinical Trials and Transgene
Expression and Bioactivity Assays**

T.M. Buck and J. Wijnholds

Int. J. Mol. Sci. 2020, 21, 4197

Abstract

Inherited retinal dystrophies and optic neuropathies cause chronic disabling loss of visual function. The development of recombinant adeno-associated viral vectors (rAAV) gene therapies in all disease fields have been promising, but the translation to the clinic has been slow. The safety and efficacy profiles of rAAV are linked to the dose of applied vectors. DNA changes in the rAAV gene cassette affect potency, the expression pattern (cell-specificity), and the production yield. Here, we present a library of rAAV vectors and elements that provide an intuitive workflow to design novel vectors. We first performed a meta-analysis on recombinant rAAV elements in clinical trials (2007-2019) for ocular gene therapies. We analyzed 32 unique rAAV gene cassettes used in 56 ocular clinical trials. The rAAV gene therapy vectors used six unique capsid variants, 16 different promoters, and six unique polyadenylation sequences. Further, we compiled a list of promoters, enhancers, and other sequences used in current rAAV gene cassettes in preclinical studies. Then, we give an update on pro-viral plasmid backbones used to produce the gene therapy vectors, inverted terminal repeats, production yield, and rAAV safety considerations. Finally, we assess rAAV transgene and bioactivity assays applied to cells or organoids *in vitro*, explants *ex vivo*, and clinical studies.

Introduction

Many reviews have been written on recombinant adeno-associated virus vector (rAAV) tropism in ocular tissue, rAAV host cell infection, and potential rAAV-treatable inherited retinal diseases [1–9]. Here, we review the ocular gene therapies developed over the past 20 years focused on the diversity of elements incorporated in rAAV vectors. Further, we discuss how the vectors were generated, tested, and further modified to increase the potency and safety of the gene expression vector. A library of validated elements allows researchers to streamline the modification of their vectors. Novel medical therapies, such as gene therapies, need to be carefully optimized to demonstrate efficacy and safety for human trials [10]. It is crucial to choose the most relevant biological model(s) (in vitro, in vivo, and ex vitro model) to test an optimized gene therapy vector in a transgene expression assay (TEA) and test the transgene activity in a biological activity assay (BAA). Novel developments in preclinical models, for example, human induced pluripotent stem cell (hiPSC) derived retinal organoid disease models, can result in FDA or EMA approval for phase I/II clinical trials. Such an approach, for example, reduced the need for further animal experimentations for the AAV2-hCHM (Sponsor: Spark Therapeutics) clinical trial preparation.

1.1. Why viral vector-based gene augmentation therapy for ocular diseases?

The environment of the eye offers a wide range of treatment possibilities because the blood-retinal barrier of the eye decreases viral vector diffusion to other organs and decreases systemic immune activation. The retina also consists of terminally differentiated cells reducing gene integration and chromosomal rearrangements. Also, many noninvasive techniques are available to monitor the treatment response. Treatments aim to slow the progression of the inherited retinopathies by reducing retinal cell death, augmenting retinal function, replacing cells, or creating an artificial retina (retinal prosthesis). Prevention of retinal cell death might be achieved by gene therapy, cell therapy, other drug treatment, dietary adjustment, and even by changes in lifestyle. There are few scientifically proven preventive or protective actions available to patients with inherited retinal diseases.. Some of the preventing measures might potentially decrease the quality of life, such as the continuous use of eye protection, photochromic lenses, or restriction to light exposure. Cigarette smoke or high Vitamine E intake can worsen ocular disease progression [11].

The ocular gene therapy strategy targets the basis of inherited retinopathies: The gene. The variant (disease-causing) gene can be silenced, replaced, or repaired by expressing a gene cassette in the target cell. The primary gene cassette carrier systems for ocular diseases are recombinant viral vector-based. Other potential strategies are the use of exosomes/liposomes, antisense oligonucleotides (AONs), electroporation of naked DNA/RNA, or application of nanoparticles [12,13]. In most clinical retinal gene therapy studies, the vector of choice is the rAAV gene expression vector [14]. Two genes that do not fit in a conventional rAAV gene cassette (*MYO7A* linked to Usher syndrome Type 1B and *ABCA4* to Stargardt disease) have

been delivered to the retina by recombinant lentiviral expression vectors [15–18]. *CEP290*-mutations linked to LCA has been rescued in patients by AONs correcting the mRNA transcript (QR-110 for LCA with *CEP290*; QR-421a for LCA with *USH2A*) [19]. Finally, the therapeutic product is administered to the target cells by either subretinal or intravitreal injection. Subretinal injections can target a focal area (e.g., macula), favoring high vector delivery to the RPE and photoreceptors. Intravitreal injections efficiently target the ganglion cell layer and spread the rAAV to the whole retina in rodents but not in the primate retina due to the properties of the inner limiting membrane. Figure 1 describes the considerations for choosing a gene therapy strategy.

1.2. rAAV gene therapy for ocular diseases – Advantages & disadvantages

rAAV DNA carrier systems have been used successfully because (1) they express the transgene within days or weeks and might reach full level expression after 4-6 weeks *in vivo* [20,21]. (2) rAAV DNA carrier systems allow long-term treatment for at least ten years in large animals [22], (3) and primarily deliver their gene cassette in episomal concatemers into the nucleus [23]. (4) rAAV DNA carrier systems do spread well within tissues to target large retinal areas [24]. (5) The capsid composition can be adjusted to fit one's goals [25], to achieve (6) low serious adverse events (SAE) in clinical trials [26]. rAAVs, similar to other viral strategies, have limitations such as (1) a small gene cassette capacity (up to 4.5 kb + 2x145 bp ITRs), (2) instability of the inverted terminal repeats (ITRs), (3) the need for high viral load for transgene expression, (4) and the occurrence of humoral immune reactions such as neutralizing antibodies that reduce the number of capsids reaching the target cells, the innate immune pathways silencing the gene cassette within the host cell, and the cell-mediated T-cell immune response against foreign protein expression [27]. It is important to outweigh the advantages of using rAAVs over other attractive strategies (Figure 1). Here, we describe how successful gene cassettes (vectors) have been designed for AAV gene therapies that could be potentially also explored for other viral gene therapies (*vectorology*).

2. Ocular rAAV vector-based therapies in clinical trials

Inherited retinal dystrophies (IRDs) and inherited optic neuropathies (IONs) are chronic and disabling disorders of the visual function affecting 1/2000 to 1/4000 people worldwide. They display considerable genetic, symptomatic, and anatomical heterogeneity (Figure 2A; [28–30]). More than 250 genes can cause IRDs and IONs [31]. IRDs include pigmentary retinopathies, maculopathies, and stationary retinopathies. Patients with pigmentary retinopathies regularly suffer from night blindness, tunnel vision, and photophobia. Maculopathies affect color vision and accurate vision. Some IRDs are syndromic. The most common syndromic retinopathies are ciliary or mitochondrial retinopathies. Common ciliary retinopathies are Usher syndrome, Bardet-Biedl syndrome, and Senior-Løken syndrome [32–34]. Lastly, IONs affect the ganglion cells transmitting the visual signal from the retina

through the optic nerve to the cortex. IONs progressively degenerate the optic nerve leading to vision loss.

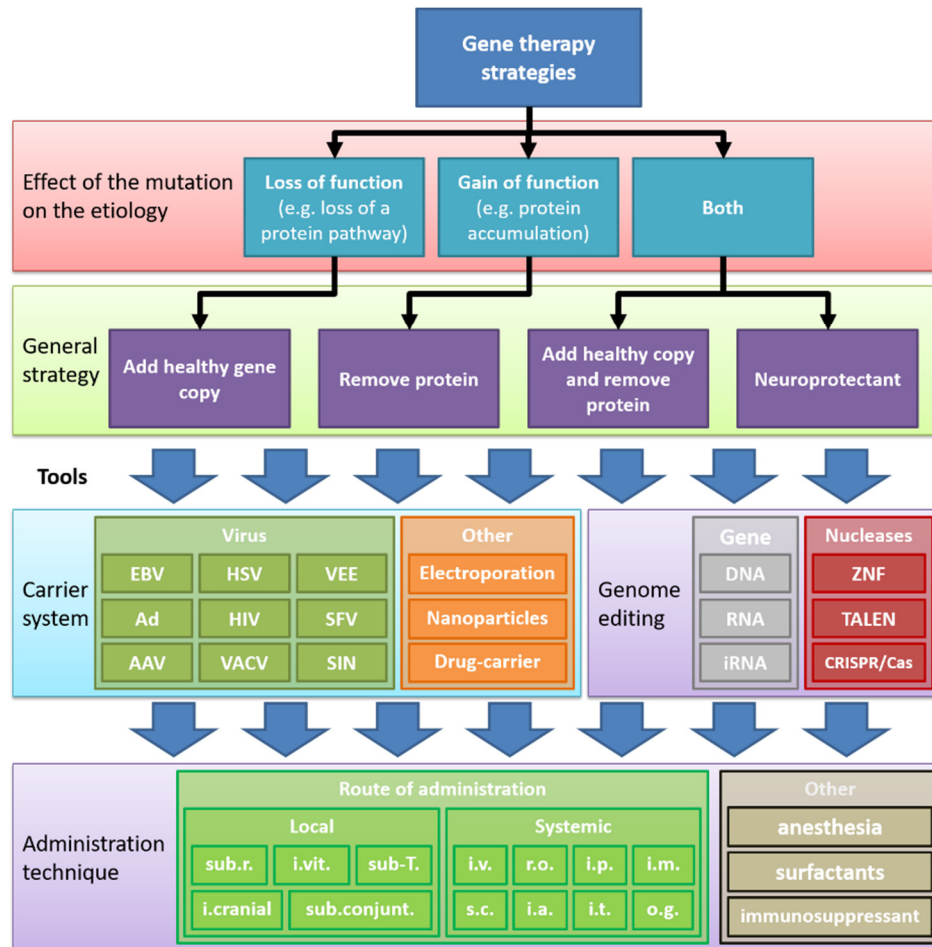


Figure 1. An overview of retinal gene therapy strategies. The effects of the gene variations determine the gene therapy rescue strategy to be applied. Physical DNA delivery includes electroporation, sonoporation, magnetofection, and bioballistic (gene gun) methods. Viruses: AAV, Adeno-associated virus; Ad, Adenovirus; alpha, alphavirus; Epstein-Barr virus (EBV); FV, Foamy virus; HSV, Herpes simplex virus; HIV, Human immunodeficiency virus; VACV, Vaccinia virus. Nucleases: ZNF, Zinc-finger nuclease; TALEN, transcription activator-like effector nuclease; CRISP/Cas, clustered regulatory interspaced short palindromic repeat (CRISPR)/Cas-based RNA-guided DNA endonuclease. Route of administration: i.cranial, intracranial; i.a., intraarterial; i.m., intramuscular; i.v., i.t., intrathecal; intravenous (e.g. tail vein or facial vein); i.vit, intravitreous; o.g., oral gavage; r.o., retro-orbital; sub.r, subretinal; sub-T, sub-Tenon; sub.conjunt, sub conjunctiva; s.c., subcutaneous.

rAAVs are one of the most promising gene augmentation tools for the treatment of inherited ocular diseases. The FDA approved in December 2017 the first rAAV-based retinal gene therapy (voretigene neparvovec-rzyl; Spark Therapeutics). More than 32 rAAV gene therapies have been delivered to clinical trials (Table 1). A wild-type copy of the gene is supplemented by rAAV delivery to RPE or photoreceptor cells for 13 genes causing inherited retinal diseases (Figure 2A). Two inverted terminal repeats of the AAV serotype 2 (ITR2) flank the gene cassette of conventional rAAVs. Many rAAV gene cassettes consist of a promoter, a wild-type copy of the cDNA of the gene-of-interest, other enhancers or transcript stabilizing elements, an intron, and a polyadenylation sequence. The promoter can be of viral origin, shortened-native, or synthetic. Many new promoters incorporate conserved transcription factor binding sites (TFBS), called enhancers, to boost transcription. Also, many additional sequences can be added to a gene cassette, including fluorescent probes, linkers, base editors, nuclear localization signals, or short-hairpin RNAs (See Figure 2B and section 3).

The first ocular rAAV clinical trial for *RPE65* was initiated in 2007. Over the years, five different AAV-*RPE65* products were tested in a total of 13 clinical trials by Applied Genetic Technologies Corporation (AGTC; Alachua, USA), Hadassah Medical Organization (Jerusalem, Israel), Spark Therapeutics (Philadelphia, USA), University of Pennsylvania (Philadelphia, USA), MeiraGTx (London, UK), Nantes University Hospital (Nantes, France), and University College London (London, UK). The clinical trial results led to the first and only retinal gene therapy (so far) approved by the FDA in December 2017 and EMA in November 2018 (AAV-*hRPE65v2*; voretigene neparvovec-rzyl, LUXTURN A; Spark Therapeutics). The five different strategies delivered the *RPE65* gene to RPE cells by subretinal administration of the rAAV2, rAAV4, and rAAV5 (Table 1). Administration of rAAV2/2-*hRPE65* at a high dose of 10^{12} viral genomes (vg) resulted in transient inflammation [35]. Switching to rAAV5 resulted in increased transduction of RPE cells. Shortening of the 1.6 kb long native *RPE65* promoter to 750 bp (NA65p) and other modifications (SV40 intron; Kozak sequence; codon optimization) resulted in an even more potent and cell-specific expression of *hRPE65*. The resulting product (rAAV2/5-OPTIRPE65) seems to be at least as efficient as the AAV2/2-*hRPE65v2* in *RPE65*-deficient mouse retinal pigment epithelium [36]. The search for the best product demonstrates the complexity of implementing native promoters ([long]RPE65, NA65) over ubiquitous strong promoters (CAG, CB-SB) in transcription regulation over different animal models and disease states (see also section 3.4 retina-specific promoters).

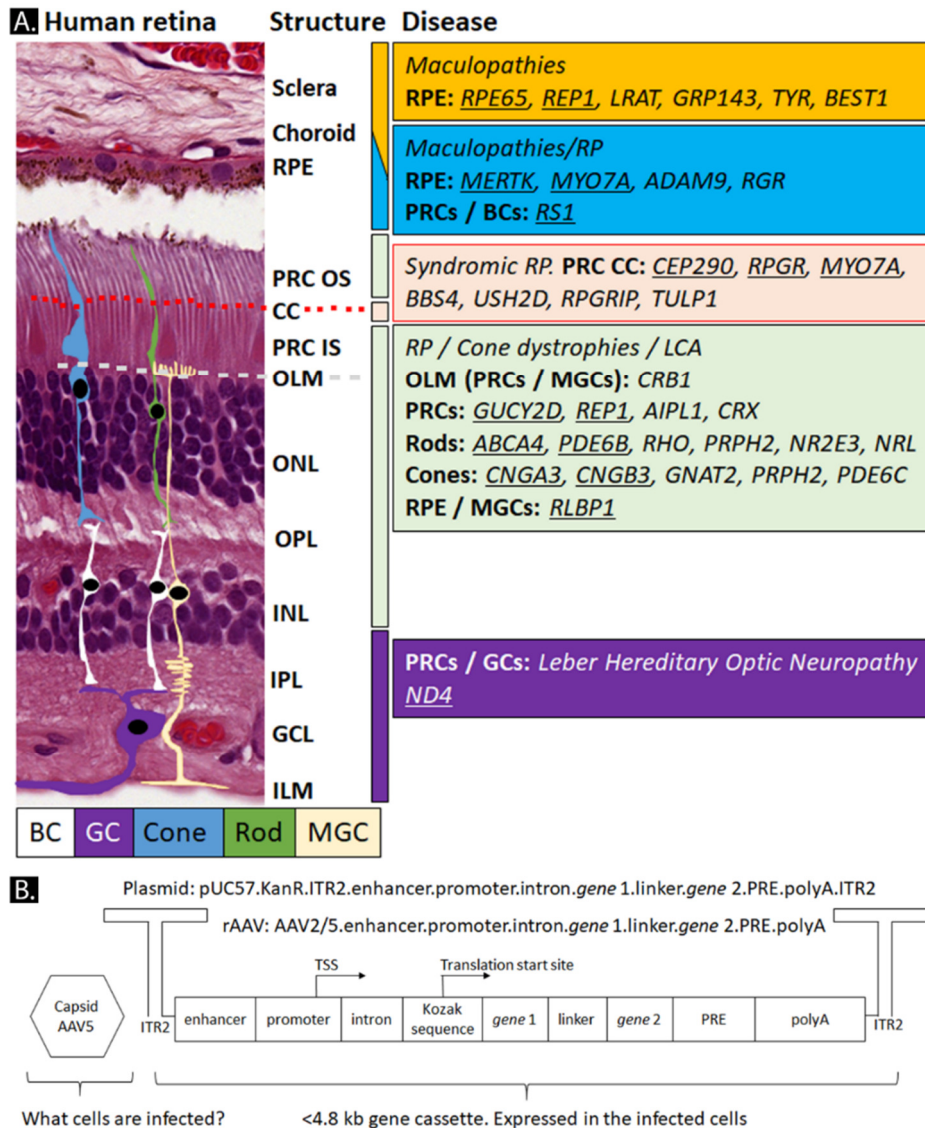


Figure 2. The development of recombinant AAV vectors targeting ocular diseases. (A) Main location (arrow) of frequent gene products (genes indicated) causing retinal diseases (color), and rAAV-gene supplementation therapy genes (in clinical trials; underlined genes). (B) Hypothetical rAAV gene cassette and the corresponding plasmid. AAV5, adeno-associated viral vector serotype 5; BC, bipolar cell; Cone, cone photoreceptor; CC, connecting cilium; GC, ganglion cell; GCL, Ganglion Cell Layer; ILM, Inner Limiting Membrane; IPL, Inner Plexiform Layer; ITR, inverted terminal repeat; KanR, kanamycin resistance gene; LCA, Leber congenital amaurosis; MGC, Müller glial cell; ONL, outer nuclear layer; OPL, Outer Plexiform Layer; PRC IS, photoreceptor inner segment; PRC OS, photoreceptor outer segment; polyA, polyadenylation sequence; PRE, post-transcriptional gene regulatory element; RP, retinitis pigmentosa; RPE, retinal pigment epithelium; rod, rod photoreceptor; TSS, transcription start site.

Many clinical trials are still far away from FDA / EMA approval. But many more clinical trials for hereditary ocular diseases, including *CRBI*-related retinitis pigmentosa, will be initiated. Numerous breakthrough clinical phase I/II trials were already initiated over the recent years (see Figure 2A and Table 1). ProQR was able to move from clinical trial phase I/II to II/III within one year (Product: AON QR-110 for *CEP290* mRNA). GenSight Biologics (GS010, rAAV2/2-*ND4*) was able to move to clinical trial phase III within four years for the treatment of Leber Hereditary Optic Neuropathy (LHON). NightstaRx Ltd initiated a clinical trial phase I/II with a linked clinical trial phase III for Usher's syndrome in which 200 patients in the XOLARIS study phase I/II might become included in the follow-up clinical trial phase III study (rAAV2/8-*RPGR*-ORF15). AMD might be treated either by monthly administration of aflibercept (Product ProCon consists of *sFLT01*, an antibody-like product; Regeneron Pharmaceuticals) or by potential long-lasting rAAV-*sFLT01* expression from transduced cells (Product: AAV2-*sFLT01*; Sanofi / Genzyme). Other exciting ocular therapies are displayed in Figure 2A and Table 1. All clinical trial identifiers, clinical trial start dates, and products can be found in Table S1.

Upon studying the rAAV capsids that have been administered to patients, we observed yet minimal clinical use of the various available serotypes. Only rAAV2 (and rAAV2 variants rAAV2-tYF and rAAV2-7m8), AAV5, and AAV8 have been injected into the eye compared to the vast and large number of novel capsids that have been developed over the past years. More clinical studies will follow evidently with the sharp increase in rAAV clinical trial initiations since 2017 and diversification of capsid use (Figure 3A). Also, rAAV products moved from the initial use of only the RPE65 promoter and ubiquitous promoter system to a more diverse pool of photoreceptor-specific promoters (Figure 3B). Large promoters, such as the CBA/CAG (1661 bp), are less common in recent clinical trial products. New products contain relatively small ubiquitous promoters such as CAG / CMV promoter versions of less than 1 kb (smCBA; CB-SB; CMV; CB7), or photoreceptor (PRC) / Müller glial cell (MGC) cell-specific promoters of less than 600 bp.

Apart from the promoter and capsid, we looked at a less documented area of described rAAV vectors, including enhancers, stabilizing elements (e.g., introns, splice donor/acceptors, WPRE), polyadenylation sequences, pro-viral plasmid backbones, and production platforms. The main enhancers used were the cytomegalovirus (CMV) enhancer that is present in CMV and the CBA/CAG promoters. The interphotoreceptor retinoid-binding protein (IRBP) enhancer was used in front of the hRS1 promoter (clinical trial NCT02317887). Common synthetic introns apart from native introns in the gene are rabbit β -globin intron with splice donor/splice acceptor (SD/SA; in CAG promoter), SV40 intron with SD/SA, human β -globin intron, and synthetic introns (e.g., 5'-splice donor of the first human β -globin intron and the 3'-splice acceptor of an intron of the immunoglobulin gene heavy chain variable region; Gene product: ADVN-022).

Table 1 rAAV gene therapy products registered on clinicaltrials.gov

Disease	Year	Product	Capsid	Promoter	Intron	Other	Gene	PolyA	Production			
LCA	2007	hRPE65v2	AAV2	CAG			RPE65	bGH	HEK293			
LCA	2007	AAV-RPE65	AAV2	CB-SB			RPE65	SV40	HEK293			
LCA	2008	tgAAG76	AAV2	hRPE65			RPE65	bGH	B50, helper adenovirus			
LCA	2011	HORA-RPE65	AAV4	hRPE65			RPE65	bGH	HEK293			
LCA	2016	OPTIRPE	AAV5	NA65	SV40		RPE65	SV40	HEK293			
AMD	2009	sFLT01	AAV2	CAG			sFLT01	bGH	HEK293			
AMD	2011	OXB-201	EIAV	CMV		IRES + WPRE	Endo+ Angio	SIN-LTR	?			
AMD	2011	AAV.sFlt-1	AAV2	CMV		Chimeric intron	sFlt-1	SV40	HEK293			
AMD	2017	RGX-314	AAV8	CAG/CB7			aVEGFfabH.F2 A	rabbit β-globin	?			
AMD	2018	HMR59	AAV2	CAG			.aVEGFfabL sCD59	bGH	?			
AMD	2018	ADVM-022	AAV2-7m8	CMV			β-globin ^{SD/SA} β-globin ^{SD} Ig ^{SA}	TLP-eMLP	Sf9			
AMD	2019	GT005	AAV2	CBA			β-globin	WPRE	CFI			
LHON	2010	AAV2-ND4	AAV2	CMV			5'UTR COX10	3'UTR COX10(MT S)	ND4	bGH	HEK293, HSV1-re/ΔUL2	
LHON	2011	scAAV2-P1ND4v2	AAV2-tYF	smCBA			ATP1(MTS); WPRE	ND4	bGH	HEK293		
LHON	2014	GSO10	AAV2	CMV			β-globin	COX10(MT S)	ND4	3'COX10	HEK293	
Stargardt	2011	SAR422459	EIAV	CMV			ABCA4	SIN-LTR	HEK293			
CHM	2011	AAV2.REP1	AAV2	CAG			β-globin ^{SD/SA}	WPRE	CHM	bGH	HEK293	
CHM	2015	AAV2.REP1	AAV2	CAG			β-globin		CHM	bGH	HEK293	
RP	2011	AAV2.MERTK	AAV2	hVMD2			SV40 ^{SD/SA}		MERTK	SV40.	bGH	HEK293
Usher	2012	UshStat	EIAV	CMV				WPRE	MYO7A	SIN-LTR	HEK293	
Usher	2018	QR-421a						AON-USH2A			Synthetic	
LCA	2019	EDIT-101	AAV5	U6; hGRK1			SV40 ^{SD/SA}	gRNA-CEP290	SaCas9	Synthetic	HEK293	
LCA	2019	AAV5.GUCY2D	AAV5	hGRK1			SV40 ^{SD/SA}		GUCY2D	bGH	HeLaS3	
XLR	2015	AAV2-tYF.RS1	AAV2-tYF	smCB			β-globin ^{SD/SA}	WPRE	RS1	SV40	rHSV/sBHK	
XLR	2017	scAAV8-RS1	AAV8	hRS1			RS1	IRBP enhancer	RS1	Human β-globin	HEK293	
ACHM	2015	AAV2-tYF.CNGB3	AAV2-tYF	PR1.7			SV40 ^{SD/SA}		CNGB3	SV40	rHSV/sBHK	
ACHM	2015	AAV.CNGA3	AAV8	hCAR				WPREm	CNGA3	bGH	?	
ACHM	2016	AAV8.CNGA3	AAV8	hG1.7					CNGA3	SV40	HEK293	
ACHM	2016	AAV8.CNGB3	AAV8	hCAR					CNGB3	SV40	HEK293	
ACHM	2019	AGTC-402	AAV2-tYF	PR1.7			SV40 ^{SD/SA}		CNGA3	SV40	rHSV/sBHK	
RP	2017	AAV8.RPGR	AAV8	hGRK1					RPGRco-ORF15	bGH	HEK293	
RP	2017	AAV-RPGR	AAV5	hGRK1			SV40 ^{SD/SA}		RPGRco-ORF15-Long	SV40	HEK293	
RP	2017	AGTC-501	AAV2-tYF	hGRK1			SV40 ^{SD/SA}		RPGRco-ORF15	SV40	rHSV/sBHK	
RP	2017	RST-001	AAV2	CAG			β-globin ^{SD/SA}	WPRE	Chop2/ChR2	bGH	HEK293	
RP	2017	GS030	AAV2-7m8	CAG					ChrimsonR-tdT	bGH	?	
RP	2020	BSO1	AAV?	?					Chr90-FP	?	?	
RP	2017	AAV5.PDE6B	AAV5	hGRK1					PED6B	bGH	HEK293	
RP	2017	CPK850	scAAV8	sRLBP1			mSV40 ^{SD/SA}		RLBP1	SV40	HEK293	

Ordered on registration date (year) and disease. Full description, size (bp) of elements, and citations can be found in Table S1.

The regulatory element Woodchuck Hepatitis Virus (WHP) Posttranscriptional Regulatory Element (WPRE) was included in 8 products (RST-001; scAAV2-P1ND4v2; GT005; rAAV2-REP1; RetinoStat; rAAV.hCNGA3; UshStat; rAAV2tYF-CB-hRS1; See also section 3.6).

The main choice for polyadenylation (polyA) sequences are the effective bovine growth hormone (bGH) and the late SV40 polyA sequences (Figure 3C). New short (synthetic)

polyadenylation sequences are needed to allow CRISPR/*Cas9* constructs to fit in a single rAAV such as in the clinical trial product of Allergan / Editas Medicine Inc to correct the *CEP290* gene in patients (product: AGN-151587 / EDIT-101). We and others have employed a (modified) synthetic polyadenylation sequence [37–39]. Many clinical trial initiators exist today, with some companies acquiring efficient new potential therapies such as MeiraGTx and HORAMA (Figure 3D). A list of the pro-viral plasmids of clinical trials can be found in Table S1. Most rAAVs were produced in HEK293(T) cells without the use of helper viruses except for the products tgAAG76 (B50 cell line and helper adenovirus; [40]), rAAV2/2-*ND4* (HEK293 infected by HSV1-*rc/ΔUL2*; [41]), rAAV2tYF-CB-hRS1/rAAV2tYF-PR1.7-*hCNGB3/rAAV2tYF-GRK1-RPGR* (sBHK cells infected with rHSV; [42–44]), and ADVM-022 (Baculovirus Sf9; [42]). The choice of the production cell line might influence the tropism and potency of the rAAV vector. rAAV capsids have post-translational modifications such as glycosylations that depend on the species origin of the production cell [45]. Further, rAAVs produced in a human cell line (HEK293T) compared to baculovirus-*Sf9* produced rAAVs were more potent in transfecting the liver in mice *in vivo* and *in vitro* (HEK293T, Huh7, hiPSCs, primary human fibroblasts, mouse C2C12 cells). A more detailed description of pro-viral plasmids for the production of rAAVs for clinical trials is needed to move towards safer plasmids (more information in section 4.4.1: Production and Table S1).

3. Discovery of cell-specific promoters for ocular gene therapy

3.1. Core promoters and chromatin-association of rAAV-vectors

Eukaryotic RNA-polymerase II-dependent promoters consist of a core promoter and cis-acting regulatory elements that can include enhancers and silencer motifs [46]. In humans, the cis-acting regulatory domains and core promoters frequently contain cytosine-phosphate-guanosine islands (C:G ratio >60% for >200 bp). Recent studies indicated that the reduction of CpG islands in rAAV vectors increased transgene expression and reduced TLR9-mediated innate immune detection [47,48].

Minimal/core promoters require a transcription start site (TSS), a sequence motif for general transcription factors (e.g., TATA-binding protein or TFIIB) directing the binding of the RNA-polymerase II (e.g., ~35-bp upstream positioned TATA/CAAT/GC-box sequence) [46]. Many genes have more than only one TSS that are differentially active in tissue and at various developmental stages. Core promoters of strong ubiquitous promoters (e.g., core CMV [30 bp], SV40mini [106 bp], SCP3 [81 bp]. Table 2) can be linked with cell-specific enhancers and suppressors to generate strong cell-specific promoters [49–51].

Chromatin-modifying proteins have been extensively studied but are viewed as less relevant for rAAV vectors because rAAV vector DNA resides mainly in a concatemeric-episomal conformation in the nucleus, therefore potentially less regulated by epigenetics [23,52]. But chromatin immunoprecipitation did pull down rAAV concatemer vectors after treatment with

promoter/rabbit β -globin intron (CAG or CAGGS or CBA), the human phosphoglycerate kinase (PGK) promoter, and the elongation factor-1 alpha (EF-1 α) promoter [57–61]. Ubiquitous promoters transcribe relatively stable expression of transgenes. The CAG, CMV, and CBA promoters outperform the EF-1 α and PGK in total expression in the retina [60]. Smaller derivatives of the promoters have been developed with comparable expression patterns in some but not all tissues, such as the CMV/CBA-derivative CMV early enhancer with the chicken β -actin promoter with a chimeric chicken β -actin minute virus of mice (MVM) viral capsid protein (VP1) intron (CBh; ~800 bp), the CBA-derived CMV early enhancer with the chicken β -actin promoter and a truncated SV40 late 16S intron (CBA aka CB7, ~800 bp), and the minimal CMV promoter (~260 bp [24]; see Table 2). However, several ubiquitous promoters are silenced in specific cell types and tissues. For example, the CMV promoter had a sharp onset of expression but was silenced compared to the CBh promoter over ten weeks when expressed in the hippocampus, the spinal cord, or the substantia nigra. In contrast, the CMV promoter was not silenced in the striatum [60,62–64]. The role of CMV cis-regulatory silencing in the retina is less established. Administration of CMV.*eGFP* DNA incorporated into nanoparticles showed robust expression in the retina after two days, but the expression was not detectable after two weeks [65]. We have found protein expression (GFP, CRB1, or CRB2) in photoreceptors after one to three months of subretinal or intravitreal injection of rAAV9-CMV(min) or ShH10-Y445F.CMV(min) vectors in wild-type and *CRB1*-related retinitis pigmentosa mouse models [24,66]. *SpCas9* was also detected in retinal flat mounts in mice two weeks post-subretinal injection of the rAAV-CMV.*spCas9* [67]. Similarly, the expression of GFP was detected after two to four weeks in human iPSC-derived retinal organoids transduced with AAV5-, AAV9- or ShH10-Y445F.CMV.*eGFP* vector [68]. The studies indicate that the ubiquitous CBA and CMV promoters are most likely less affected by the retinal disease state or cellular differentiation status [36].

3.3. Bicistronic and tricistronic promoters in rAAV-vectors

Expression of two or more genes in a gene therapy vector can be achieved with an Internal Ribosomal Entry Sequence (IRES; non-read through linker), or otherwise, at least two different promoters could be used. The promoters could drive the expression of multiple genes with a fusion protein linker (e.g. (Gly₄ Ser)₂ spacers (~30 bp; read through linker), or a sequence encoding self-cleaving peptides (T2A, P2A, E2A, F2A; ~30-75 bp; read-through linkers) between the gene sequences. Fusion proteins can, however, alter the function of some of the proteins. The cleavage efficiency of genes connected with self-cleaving peptide sequences varies. Also, self-cleaving peptide sequences add additional amino acids that stay attached to the protein product. Also, several genes from one promoter connected with a linker generally reduce the expression of each subsequent gene. Nevertheless, researchers demonstrated the feasibility to mediate expression by a single promoter of three different genes (for example, *Oct4*, *Sox2*, and *Klf4*) connected with self-cleaving peptide sequences in

a rAAV9 expression vector upon transduction of ganglion cells. The rAAV9-*Oct4/Sox2/Klf4* expression vector rescued ganglion cell survival in an optic nerve crush mouse model [77].

The interspersing IRES (572 bp) or minimum IRES (436 bp) allows efficient expression of independent genes into cap-independent RNA transcripts [78]. Yet, studies indicate a decrease in protein production of the protein-coding DNA located behind the IRES compared to the use of a conventional promoter. Adding a spacer (~30-90 bp) in the inter-cistronic sequence can enhance the IRES-dependent translation of the second gene [79,80]. Many different IRES exist that have been extracted from different viruses, such as in the family of the picornaviridae. Placing two promoters in opposing directions next to each other also allows efficient bicistronic gene expression from one gene cassette [81]. Bi- or tricistronic rAAV gene cassettes are especially useful where the protein of interest (e.g., *Cre*-recombinase) is expressed in a specific cell type together with an internal marker (e.g., for reporter gene assays), or when studying retinal circuits (e.g., by calcium imaging), or when performing rAAV-retrograde labeling [58,82–85].

Bicistronic rAAV gene cassettes hold the key to supplement a wild-type transgene and removing disease-causing variant proteins in an all-in-one rAAV vector therapy. For example, in autosomal recessive retinal disease, ocular gene augmentation therapies express a functional gene in retinal cells that lack a functional copy of that same gene. However, in autosomal dominant (e.g., rhodopsin) or X-linked dominant (e.g., some variations in *RPGR*) retinal diseases, the allele bearing the dominant-negative variation needs to be specifically inactivated. Such inactivation can be achieved, for example, by gene editing or small interfering RNA to allow gene augmentation therapy to work. In the latter case, to prevent inhibition of the newly introduced gene, codon-optimization of the transgene might prevent inactivation by the gene-editing or siRNA tools used [86]. Here, an rAAV vector expressing a wild-type *RPGR* transgene and downregulation of the mutant *RPGR* transgene could benefit patients.

Similarly, many inherited retinal diseases benefit from the administration of cell survival factors [87–91]. The expression of cell survival factors, such as the basic fibroblast growth factor (*bFGF*; 470 bp), ciliary neurotrophic factor (*CNTF*; 600 bp), glial cell line-derived neurotrophic factor (*GDNF*; 511 bp), and brain-derived neurotrophic factor (*BDNF*; 750 bp) could be expressed concomitantly with the gene-of-interest boosting the treatment effect. Combining a gene supplementation therapy with a supporting factor expressed from one rAAV vector is very promising for future treatments.

3.4. Retina-specific promoters

The retina and surrounding tissue consist of several different cell types including bipolar cells, ganglion cells, horizontal cells, amacrine cells, cone photoreceptor cells, rod photoreceptor cells, Müller glial cells, RPE cells, vasculature cells (pericytes, endothelial

cells, smooth muscle cells, fibroblasts), immune-related cells (microglia, macrophages, dendritic cells), oligodendrocytes around the optic nerve, lens cells and the ciliary body (ciliary nerves, ciliary muscles, ciliary ganglion). Tissue-specific promoters restrict the expression to the specific cell type(s) and, therefore, potentially increase the safety of the product. Also, a native promoter of a gene of interest with all the essential promoter elements, enhancers, and silencers might allow for a more normalized expression. The use of these native occurring regulatory sequences may actively modulate transcription and thereby preventing overexpression. A native promoter could, therefore, potentially reduce toxicity due to overexpression of the transgene. Cellular toxicity can, for example, be observed in rAAV shRNA overexpression studies in which ubiquitous promoters were used that caused saturation of cellular miRNA pathways [92].

Table 2 Common ubiquitous promoters for rAAV-based ocular gene therapies.

Ubiquitous promoters	Size (bp)	Origin, cell expression, strength	References
CAGGS aka CBA or CAG	1,600	Ubiquitous, +++. Cytomegalovirus immediate-early enhancer, chicken β -actin promoter, chimera between introns from chicken β -actin and rabbit β -globin. pDRIVE CAG plasmid (Invivogen, San Diego, Calif.; having 100% sequence homology with the pCAGGS). The University of Pennsylvania considers CBA and CAGGS the same.	[69]
mini CAG (SV40 Intron)	800	Ubiquitous, +++	[70]
Mini CAG no intron	250	chicken β -actin promoter, Ubiquitous, +	[63]
CBA/CB7	800	Ubiquitous, ++	[71]
smCBA	953	Ubiquitous, ?	[72]
CBh	800	CBA.MVM Ubiquitous, ++	[60,73]
MeCP2	229	ubiquitous	[74]
CMV	800	Ubiquitous, ++, prone to silencing	[60]
shCMV	220	Ubiquitous, ++	[24]
CMVd2	52	Low basal activity. Ubiquitous, Promega, +	[75] Cat.: pFN23A Halo Tag CMV d2
core CMV	30	Not active without enhancers	[49]
SV40mini	106	SV40 minimal promoter	[49,50]
SCP3	81	Super core promoter. (TATA box, Inr, MTE and DPE)	[49]
EF1- α	2500	Ubiquitous, ++	[57,76]
PGK	426	Ubiquitous, ++	[59]
UbC	403	Ubiquitous, ++	[76]

The relative strength (+ being the weakest and +++ being the strongest). Adapted from [63].

Many retinal cell-type-specific promoters have been developed (Table 3). The selection and validation of tissue-specific promoters can be complicated and time-consuming. Many tissue-specific promoters in mice turned out to be less specific in human or non-human primates [51]. Further, many tissue-specific promoters drive much lower gene expression compared to the CBA/CMV/CAG ubiquitous promoters. Nevertheless, many tissue-specific promoters are very potent: NA65p (RPE cells), Nefh (ganglion cells), hGRK1 (rod and cone photoreceptor cells), hRLBP1 (Müller glial cells and RPE cells) and others [24,36,93–95]. For an extensive list, see Table 3. Codon-optimization, introns (e.g., MVM, SV40), and enhancers (e.g., CMVe, IRBPe, Grm6e) to tissue-specific promoters can substantially increase their potency. For example, the NA65p promoter is derived from the hRPE65p but now has a 150x higher potency than the CBA and 300x higher potency than the hRPE65 promoters (clinical trial NCT02946879) [36]. Many viral promoters evolved to maximize the survival of the virus in different cellular contexts. Several viral promoters exhibit ubiquitous expression in many cell types in various cell “states” (stressed, developmental state, cell cycling) or in animal tissues, indicating that the promoter activity is less affected by (temporal) cellular-specific transcriptional factor changes compared to native promoters. Adding viral enhancers to native promoters might decrease the susceptibility to gene silencing of the rAAV gene cassette. Nevertheless, the testing of synthetic and native promoters needs to be closely monitored on disease-related and species-related cell profiles.

Still, many tissue-specific promoters are too large to fit into rAAV vectors. Fitting depends on the size of the gene of interest, which is why many promoters are further shortened and optimized for cell-type-specific expression. We reduced the length of a Müller glial cell-specific CD44 promoter from 1775 bp to 363 bp but then abandoned the shortened CD44 promoter because of a substantial loss of expression *in vivo* [24,96]. The full-length glial fibrillary acidic protein (GFAP) promoter (2789 bp) showed excellent Müller glial specific gene expression in human retinal organoids and human retinal explants [24,68]. Furthermore, a shortened version of the GFAP promoter called gfaABC1D (686 bp) showed similar expression strength in neurons (brain), whereas the gfaABC1D promoter maintained Müller glial cell-specific expression in the retina [97,98].

3.5. Small nuclear RNA (snRNA) promoters

RNA polymerase (RNAP)-dependent regulatory promoters (U1, U2, U6, U7, H1; ~250 bp) can be used to drive short hairpin RNAs (shRNAs). The human U6 promoter is a potent promoter that has been widely used for the expression of shRNAs. However, the relatively large size, the requirement that the transcript starts with a G or A, the sometimes too active transcription, and the sensitivity to specific cellular profiles make the human U6 promoter a less versatile promoter [131–133]. RNA polymerase III promoters also have been re-engineered with CMV enhancers [134] or tissue-specific enhancers (heart, muscle) for siRNA expression [135]. The tissue-specific enhancers increased expression but were less

tissue-specific. Single guide RNAs (gRNA) are typically expressed by a U3 or U6 RNA promoter in rAAV gene cassettes. Relative tissue-specific expression of two gRNAs for CRISPR/Cas gene editing in myotubes was achieved by linking a muscle-specific MHCK7 promoter (pol II) with gRNA-linked self-cleaving ribozyme sequences derived of Hepatitis delta virus (HDV) and a Hammerhead (HH) sequence [135–138].

3.6. WPRE, introns, miRNAs and other elements in an rAAV-gene cassette

Post-transcriptional regulatory elements (PRE) can substantially increase gene expression. Woodchuck posttranscriptional regulatory element (WPRE; 600 bp) or Hepatitis B Virus Posttranscriptional Regulatory Element (HPRE; 533 bp) increase the transgene expression up to 6-9 times [63]. The addition of a WPRE also protects from silencing in human ES cells and the brain. To validate the use of WPRE for retinal gene therapy, rAAV2/2.CMV.eGFP.pA vectors with or without WPRE were applied to human retinal explants or injected in mouse eyes [139]. A shorter version of the WPRE (WPRE3; 247 bp) showed only a 15% drop in expression in hippocampal neuron cultures or GFP expression in rAAV infected hippocampal CA1 region in the mouse brain [140]. A modified WPRE version that removed any viral protein expression has been patented for retinal use [141]. WPRE might be redundant if used in combination with a promoter containing introns such as found in the CAG or EF-1 α promoters [81,142]. Inclusion of natively occurring or synthetic introns can strongly boost protein expression, especially for vectors with low efficiency of gene splitting sites [143]. Many introns have been developed for rAAV gene cassettes that can enhance the gene expression (Table 4). Especially, the strong MVM intron-1 of the viral capsid protein (*VP-1*) of only 67-to-97 bp can increase the transcript expression by 10x [144]. Also, the development of minicircle rAAVs has contributed to novel introns that are placed in the backbone of pro-viral plasmids to boost production yield. This strategy will be discussed further under section production [145].

Adding microRNAs (miRNA, ~18-25 bp) can alternatively be used to prevent the ectopic expression of the transgene in ocular gene therapy. Adding 4x the complementary sequence of miRNA204 to a rAAV2/5.CMV.eGFP.WPRE.4xmiRNA204T significantly reduced eGFP expression in RPE cells after subretinal injection in mice and pigs. Similarly, adding 4x the complementary sequence of miR-124 removed the expression in photoreceptors [146]. Also, a dual-acting rAAV2/5 vector expressed the miRNA (5, B, 7), against Vascular endothelial growth factor A (VEGFA) and antiangiogenic protein pigment endothelial-derived factor (PEDF) driven by an RPE-specific Bestrophin 1 (VMD2) promoter, to suppress choroidal neovascularization in a wet-AMD mouse model [147]. However, the oversaturation of the cognate miRNA needs to be considered when using miRNAs, because they can decrease the function of native miRNAs in the cell. 4x miRNA placed in an rAAV-CMV expression cassette generally is sufficient for miRNA expression without inducing side-effects [146]. Others have used miRNAs to inhibit transgene expression in antigen-presenting cells (APCs)

with miR-142-3p [148]. Still, short hairpin DNA sequences need to be placed at least proximal to the second ITR and be tested for possible rAAV genome truncation for proper expression of the short hairpin RNA (shRNA). Short-hairpin DNA can effectively truncate rAAV genomes during production and produce non-intact shRNA expression cassettes [149]. A more detailed review of miRNAs can be found here [150]. Moreover a rAAV vector-based microRNA (miRNA) sensor array (*Asensor*) has been developed [151]. The *Asensor* is based on the principle that rAAV vectors are relatively stable at +4°C so that 96-well plates can be coated with live rAAV vectors. Then, the plate is loaded with the cells of interest that are infected by the rAAV vector-based microRNA (miRNA) sensor that starts to express luciferase. The miRNA activity is subsequently measured on a microplate luminometer for high-throughput microRNA profiling.

3.7. Polyadenylation sequences in rAAV-gene cassette

To allow for efficient pre-mRNA processing, an efficient polyadenylation sequence needs to be included behind the transgene to form a proper poly(A) tail at the RNA's 3' end. Polyadenylation sequences in rAAVs gene cassettes are for example SV40 late (135 bp; +++), bGHpolyA (250 bp; ++), synthetic polyadenylation (spA) + 2x SV40 late upstream elements (100 bp, ++, +), 2x sNRP1 (34 bp, +/++), synthetic polyA (spA; 49-60 bp, +), hGHpolyA (624 bp, +), 1x sNRP1 (17 bp, +), and adenovirus L3 (21 bp, +) polyadenylation sites [63,167] (Table 5).

Recent developments allow for shorter and more potent expression cassettes. The SV40 late polyadenylation signal upstream element and the SV40 late polyadenylation signal combined with the WPRE3 (420 bp), decrease the length to less than half compared to the commonly used WPRE-bGHpolyA gene cassette (919 bp) but maintain a similar expression profile [140]. The removal of a WPRE sequence reduced the expression by 80%. But using a synthetic polyadenylation sequence (49 bp) + 2x SV40 late upstream elements (50 bp), increased the GFP expression compared to the use of a robust bGHpolyA sequence. Interestingly, the interplay of the polyadenylation sequence with transcriptional regulation enhancers can increase transcript levels, such as pairing a CMV β enhancer with an SV40 polyA. But the effect was lost when the CMV β enhancer was paired with a bGHpolyA [152]. Also, the rAAV gene cassette for hemophilia B was tested with different polyadenylation sequences. The bGHpolyA was the strongest for the *FIX* gene expression, outperforming the synthetic polyA, mouse β -globin pA, rabbit β -globin pA, and H4-based pA [144]. Studying polyadenylation sequences can be very valuable for rAAV gene cassette size reduction. Notably, a 17-bp soluble neuropilin-1 (sNRP-1) polyA sequence efficiently expressed transgenes on infection of an rAAV vector. When the sequence was used twice (2x sNRP-1 polyA), then the potency was as efficient as an SV40polyA sequence [167,168]. Yet, the 2x sNRP-1 polyA was less suitable for specific transcripts compared to bGHpolyA or spA [169]. The effects of polyadenylation sequences for specific transcripts are still less well

understood. For example, whereas polyA's increase transcript stability/expression, certain polyadenylation sequences can also reduce viral titers during rAAV particle production [170]. Thus, different polyadenylation sequences should be tested for optimal gene expression and virus production.

3.8. rAAV vector cassettes and inducible promoters

Many gene supplementation therapies rely on constant overexpression of the therapeutic gene. The constant active expression increases the risk that the rescue vector itself becomes toxic to the cell. Stress (GFAP promoter) or hypoxia-driven GFAP promoter (HRSE-6xHRE-GfaABC1D) have been generated that might be safer for cells that are sensitive to continuous overexpressed artificial gene vectors [97,98,100,101,103]. Other inducible On/Off gene expression systems have been described: Tetracycline (Ptet), dihydrofolate reductase (DHFR) protein destabilizing domains, riboswitches, metal activated promoters (metallothionein-Ia; MT-1), and hormone-activated promoters (dexamethasone, MMTV LTR. Table 6) [175–178]. All but the riboswitches require the expression of an exogenous

Table 3 Retina cell-specific promoters in rAAVs for ocular gene therapy

Müller glial cells	Size (bp)	Origin, cell expression, strength	References
CHX10	164	Retinal progenitor cells	[99]
GFAP	2600	Müller glial cells,	[100,101]
GFAP	2200	Müller glial cells (Novartis)	[102]
GfaABC1D	686	Müller glial cells	[97,98]
HRSE-6xHRE-GfaABC1D	~820	Hypoxia-induced reactive MGC promoter. HRE is (A/G)CGT(G/C)C. HRSE from metallothionein II promoter (90 bps)	[98,103]
RLBP1	2789	Müller glial cells	[24,93]
Short RLBP1	581	Müller glial cells	[102]
Murine CD44	1775	Müller glial cells	[24,96]
Murine shCD44	363	Müller glial cells	[24,104]
ProB2	592	Müller glial cells	[51]
Photoreceptor cells	Size (bp)	Origin, cell expression, strength	References
Mouse RHO	1400	Rod PRCs	[105]
Human RHO (rhodopsin)	800	Rod PRCs	[106]
Human RHO	520	Rod- PRCs	[24]
Mouse rod opsin mOp500	500	Rod- PRCs -385/+86	[107]
Mouse rod opsin	221	Rod- PRCs	[108]
Human Rhodopsin kinase (RHOK/GRK1)	294	Rod and cone PRCs. AY327580.1: bp 1,793–2,087 (-112 to +180). More efficient than IRBP in NHP for cone transduction	[24,95,109–111]
Human blue opsin HB570	570	S-cone and subset of M-cones PRCs	[112]
Human blue opsin HB569	569	blue cone opsin PRCs	[107,113]
PR0.5	496	Red cone PRCs	[107]
PR1.7	1700	Red cone PRCs	[107]
PR2.1	2,100	Red cone PRCs	[107]
3LCR-PR0.5	~600	Red cone PRCs	[107]
Mouse blue opsin (mBP500)	500	Mouse S opsin	[114]
Human interphotoreceptor retinoid binding protein (hIRBP)	235	Cone & rod PRCs X53044.1, bp 2,603–2,837	[115]

IRBPε/GNAT2	500	Cone PRCs	[116]
Mouse CAR / ARR3	500	Cone PRCs, some rods, and RPE	[116]
Human CAR / ARR3	500	Cone PRCs, some rods, and RPE cells	[116]
CAR / ARR3	215	Cone PRC	[117]
Human red opsin	2,100	Human red cone opsin	[118]
Human green red opsin (G1.7p)	1700	Cone PRCs. Core green opsin promoter including a mutation (0.5 kb) + Locus Control Region (LCR; 1.2 kb) upstream of the red opsin gene	[119–121]
Crx2kb	2000	Cone & rod PRCs	[122]
ProA1	2000	cone PRCs	[51]
ProA4	2000	cone PRCs	[51]
ProC1	731	Cone & rod PRCs	[51]
ProA6,ProB5,ProC22,ProC32,ProD2,ProD3,ProD4,ProD5,ProD6	1229,619,774, 814,366, 691,552, 321,448	rod PRCs	[51]
Synp161	150	Mouse CD47 enhancer + SV40-mini promoter. Rod PRCs	[50]
Bipolar cells	Size (bp)	Origin, cell expression, strength	References
Mouse metabotropic glutamate receptor 6 (mGrm6)	200	On-bipolar cells	[99]
4x mGRM6e+SV40	1,000	On-bipolar cells. 203 bp SV40 minimal promoter	[123]
Grm6e-Chx10-Cabp5	809	200 bp Grm6 + 164 bps Chx10 enhancer + 445 bp Cabp5 promoter. Wide overlapping bipolar expression	[99]
Grm6-SV40	400	Grm6=mGluR6. 200 bp mGluR6 enhancer + SV40 promoter. On-Bipolar cells	[99]
Cabp5	445	Bipolar cells	[99]
Chx10-SV40	364	164 bp Chx10 enhancer + 200 bp SV40 promoter. Bipolar cells and Müller Glial cells	[99]
Grm6-mGluR500P	700	On-bipolar cells.	[124]
In4s-In3e- Grm6-mGluR500P	1997	690 bp shortend Intron 4s + 807 bp Intron 3 + 500 bp mGluR500P	[124]
ProB4	1317	Off-bipolar cells	[51]
Amacrine cells	Size (bp)	Origin, cell expression, strength	References
ProC2	964	All amacrine cells + few MGCs	[51]
ProB1	394	Amacrine cells with processes in one stratum	[51]
Horizontal cells	Size (bp)	Origin, cell expression, strength	References
ProC3	694	Some off-target in amacrine and ganglion cells	[51]
Retinal Ganglion cells	Size (bp)	Origin, cell expression, strength	References
Syn1	495	Off target amacrine, strength: ++	[125]
Nefh	2251	Strength: +++	[94]
hSNCGp	948	Human SNCG promoter (−785 to +163 region)	[126]
ProA3	2000	Synthetic	[51]
Ple344	801	Gene TUBB3. GCL & corneal nerves. ++	[127]
Ple345	2693	Gene NEFL. +++ (stronger than smCBA)	[127]
RPE	Size (bp)	Origin, cell expression, strength	References
hRPE65p	1383	Chr1.68449936-68451318. RPE+ some PRC infection	[128]
NA65p	1383	Codon optimized hRPE65p+SV40 intron+Kozak seq, 150x more efficient than CBA and 300x more efficient than hRPE65p	[36]
VMD2	646	NG_009033.1, bp 4,870–5,516	[126,129]
Synpiii	1317	+ SV40 mini promoter	[130]

The relative strength (+ being the weakest and +++ being the strongest). Adapted from [63].

Table 4 Other elements in rAAV vectors: A. Introns, PRE, and enhancers. B. Miscellaneous

Introns & PRE & enhancers	Size	Description, strength	References
CE (CMV early enhancer)	431	+++; 1.5-67x increase; -118/-522 TSS pCMV β / 5'CMV enhancer	[152]
IRBPe	235	human interphotoreceptor retinoid-binding protein proximal enhancer. – 1619 to – 141 IRBP	[116]
metabotropic glutamate receptor 6 enhancer (Grm6e)	200	Grm6 proximal enhancer	[99]
Woodchuck Hepatitis Virus PRE (WPRE)	600	+++; 6-10x increase	[140,153]
Hepatitis B Virus PRE (HPRE)	533	+++; 6-10x increase	[153]
WPRE3	247	++, 6x increase	[140]
MVM	67-97	+++; minute virus of mice, 10x increase	[144]
chCMV.HBB2	~506	Chimeric CMV (146 bp) + human β -globulin intron 2 (340 bp) + exon 3 20 bp incl SA/SD	[154]
Hybrid adenovirus SD [#] / IgG Sa*	230	+++; pAd β , 2x increase to synthetic polyA	[152]
SV40 late SD [#] / Sa* (19S/16S)	180	+, pCMV β (Promega; 1.6x increase)	[152]
Modified SV40 SD [#] / Sa*	157	modSV40 SA/SD= modified SV40 splice acceptor/donor intron, 157 bp in length, nucleotides 502–561 and 1,410–1,497 of SV40 genomic sequence (NC_001669.1) + connecting sequence CGGATCCGG between two fragments.	[102,155]
Mini SV40 SD [#] / Sa*	100	Mini SV40 SD [#] / Sa* intron	[44,156,157]
Human β -globin intron 2 SD [#] / Sa*	875	0.5-86-fold increase. pZac2.1	[140,158–160]
F.IX truncated intron1	300	+, human factor IX (100x)	[144,161]
Miscellaneous	Size	Description	References
2A	75	Self-cleaving linker	[162]
internal ribosomal entry site (IRES)	600	Ubiquitous. Placed between two genes. The second gene is transcribed without a promoter (at a lower expression compared to the first gene)	[163]
SPTP	154	Synthetic polyA signal/transcriptional pause site frp, pGL4.25	[164]
PolII miR-155	~500	Block-iT PolII miR vector system based on miR-155 expressing artificial miRNAs engineered to a target sequence resulting in target cleavage	Cat.: K493600 ThermoFisher Scientific
shRNA-YB1	N/A	7-to-45 fold AAV production increase in physical titer	[165]
MIP backbone	N/A	mini-intronic plasmid (MIP) backbones for AAV production increased transgene expression by 40-100 fold <i>in vivo</i>	[145]
R6K	545	+ (~40x),pUC + prokaryotic RNA-OUT antibiotic-free, minicircle AAVs	[145]
OIPR	1300	+ (~40x),pUC + prokaryotic RNA-OUT antibiotic-free, minicircle AAVs	[145]
Shorter OIPR	500	+ (~5x),pUC + prokaryotic RNA-OUT antibiotic-free, minicircle AAVs	[145]

The relative strength (+ being the weakest and +++ being the strongest). Adapted from [7,63,166].

Table 5 Polyadenylation sequences

Polyadenylation	Size	Description, strength	References
SV40 late	135	+++	[140]
2x SV40 late	100	+/+++	[171]
bGHpolyA	250	++	[152]
2x sNRP1	34	+/++	[169]
Rabbit gbpA	56	Rabbit β -globin	[152]
spA	49	+/++ (7x lower than bGHpolyA, 3x lower than SV40 late)	[140,152]
hGHpolyA	624	+	[42,172,173]
1x sNRP1	17	+	[169]
HSV TK poly(A)	48	herpes simplex virus (HSV) thymidine kinase (TK) polyadenylation signal. Generally used for NeoR and KanR genes	[174]
Adenovirus (L3) USE	21	+	[171]

The relative strength (+ being the weakest and +++ being the strongest). Modified from [7,63,166].

(bacterial) protein. The TET-system is activated by an antibiotic (tetracycline or doxycycline), making it suboptimal for human use. An example of an efficient TET-off rAAV system is an rAAV expression cassette that includes 6x the mutated tetracycline response elements (TRE; ~200 bp) placed in front of a minimal promoter (CMV; ~40 bp; total cistronic size: ~270 bp). The full rAAV plasmid (Addgene #35625) demonstrates the possibility of expressing it from rAAV gene cassettes. Upon rAAV infection of the cell, then the ubiquitous promoter UbC will drive the transactivator reverse tetracycline transactivator 3 (rtTA3), making it a Tet-on system. Upon Cre recombinase expression, the rtTA3 is floxed-out, rendering the plasmid to a Tet-off system. The rtTA3 binds to the TRE in the presence of doxycycline, starting the expression of the TurboRFP open reading frame (ORF) that allows tracking of the target mRNA knockdown because the miR-30 sequences induce the Drosha and Dicer processing of the expressed target sequence. The promoter drives the microRNA adapted short hairpin RNA. If the Drosha/Dicer degradation complex recognizes the target sequence specified by the shRNA, then the transcript of the target sequence and the TurboRFP transcript is degraded. The construct allows fast testing of the efficiency of shRNAs [179].

Riboswitches have gained considerable attention for rAAV ocular therapies because of their small size (100 bp cis-acting RNA sequence), adaptability to ligands, and the development of synthetic riboswitches [175,180,181]. The riboswitch is encoded downstream of the polyadenylation sequence in the rAAV-vector. It encodes for a ligand-sensing aptamer, a communication module (linker), and an effector domain (ribozyme) that depending on the presence of the ligand, cleaves the mRNA of the gene expression cassette. A *proof-of-concept-study* for anti-VEGF expression by the activating ligand tetracycline in a wet AMD mouse model demonstrated the feasibility of the riboswitch in ocular gene therapy [181].

Table 6 Inducible promoters

Inducible promoters	Size (bp)	Origin, cell expression, strength	References
MT-1	13200	Zinc, cadmium or copper-inducible sheep metallothionine-Ia promoter	[176]
MMTV LTR	792	dexamethasone (Dex)-inducible mouse mammary tumor virus. Active when glucocorticoids or progestins present	[177,178]
Ptet	270	tetracycline On or Off system promoters (Ptet). 6x mutated TRE (~200 bp) core CMV (~40 bps)	[179]
T7lac	42	T7 bacteriophage promoter (17 bp) requires T7 RNA polymerase and lac operator (25 bp). Induces expression by IPTG	[182]
Riboswitches	~100	ligand-sensing aptamer, a communication module (linker), and an effector domain (ribozyme)	[175,180,181]

Adapted from [63]

4. Optimizing genes for rAAV vector therapies (minigenes, dual/triple rAAV-vector, ITRs)

4.1. Intron removal, exon removal and finding surrogates for large genes

rAAV gene cassettes only allow expression of small genes because of the limited packaging size of around 4.5-4.6 kb (excluding the two ITRs). It has been challenging to fit large genes into rAAV vectors. Introns and sometimes exons are truncated to allow proper packaging. Thus, many large cDNAs in AAV gene cassettes do not contain any or contain only a few native introns (see Table 1, and Table S1). Introns can serve many functions, for example, to increase mRNA stability, modulate RNA synthesis rate, introduce alternative splicing, and decrease DNA damage on highly expressed genes. Also, an intron can dictate the mRNA export mechanism from the nucleus to the endoplasmic reticulum [183,184]. Removal of introns in rAAV gene cassettes might further alter the intrinsic gene regulation apart from artificial promoters and rAAV expression system. For example, the CRB1 protein (UniProtKB P82279-1) consists of 1406 amino acids and is encoded on 210,251 bp (GRCh37 197,237,334-197,447,585. ENSG00000134376). The exon-coding sequence alone is 4221 bp, including the 3' stop codon, whose size is close to the maximum packaging capacity of the rAAV. Nevertheless, we achieved an efficient expression of CRB1 in retinal cell types by making use of short promoters (<300 bp) and 50 bp synthetic polyadenylation sequences [66].

Shortened versions of proteins (exon truncation) are generally not advised because many shortened proteins lose their functionality. For example, many shortened versions of the Duchenne muscular dystrophy gene (*DMD*; 2.3 Mb; 79-exons; 3685 amino acids; 11,055 bp) do not rescue the Duchenne muscular dystrophy phenotype in muscle cells except for the micro-dystrophin for which was reported a milder clinical phenotype [185,186]. Nevertheless, the micro-dystrophin rescue in patients in clinical trials has been at least

suboptimal and needs further optimization [187]. We also tried a native occurring short version of the CRB1 protein encoded by a *CRB1* cDNA lacking exons 3 and 4, but whereas the short *CRB1* (*sCRB1*) was expressed, it also caused retinal degeneration upon subretinal injection of the AAV9-CMV-*sCRB1* or AAV9-hGRK1-*sCRB1* [24]. Instead of employing a shortened protein, one can also apply a surrogate protein such as utrophin for dystrophin [187,188]. We also developed a surrogate gene therapy for patients with *CRB1*-related retinal dystrophy by employing the Crumbs homolog 2 (*CRB2*; 3.8 kb). However, such a strategy can only be performed if the proteins of interest execute similar functions in cells, which is the case for CRB1 and CRB2 [68,189–202]. The rAAV-CMV-*CRB2* rescued the loss of CRB1 function in mouse Müller glial cells [66]. Interestingly, mice lacking CRB1 or mouse retinas lacking CRB2 develop the same phenotype as observed in human iPSC-derived retinal organoids lacking CRB1 [68]. Surrogate proteins might be less immunogenic than the native protein - like utrophin over dystrophin - because the surrogate protein is already expressed in the body. Surrogate proteins could have great potential for many rAAV gene therapies.

4.2. Lentiviral and dual/triple rAAV vectors

Retroviral 3rd generation lentivirus-based systems have a larger packaging size of ~8.5 kb compared to 4.5 kb in rAAV [203]. They can infect both dividing and nondividing cells and integrate into the genome. Equine infectious anemia virus (EIAV) 3rd generation lentivirus-based gene therapies for the *MYO7A* gene (6645 bp; 2215 amino acid) and the *ABCA4* gene (6819 bp; 2273 amino acids) delivered to photoreceptors are in clinical trials (NCT01367444; NCT01505062) since 2011/2012. Though the clinical trial ended (May/June 2019), no data has been published since the start of the trial.

Dual and triple rAAV vectors are another strategy to circumvent the small capacity of rAAVs. Nicked ITRs (Δ ITRs) have been used that allow for annealing of two or three different rAAV gene cassettes. An update on dual and triple rAAV vectors can be found here [204]. A dual AAV vector system rescued the *ABCA4* gene in *Abca4* knockout mice [205,206]. The first generation of dual rAAV vector cassettes resulted in a high ratio of truncated gene expression. Adjustments, such as 200-300 bp of specific compatible overhangs, have resulted in normal concatemerization of independent gene cassettes such as the hybrid dual rAAV approach [204].

4.3. rAAV-vectors expressing CRISPR/Cas

Staphylococcus aureus CRISPR associated protein 9 (SaCas9) is an RNA-guided endonuclease enzyme associated with the CRISPR (type II prokaryotic Clustered Regularly Interspaced Short Palindromic Repeats) complex. Cas9 unwinds, checks, binds, and finally cuts in the DNA (causing a double-stranded DNA break [DBS]) complementary to the annealed 20-nucleotide genome-specific part of the single guide RNA (gRNA). The genome-specific part of the gRNA anneals proximal to the 3-bp protospacer adjacent motif (PAM). The guide RNA can be adjusted to target the whole genome as long as a PAM sequence is

found close by (for *S. aureus*: NGG). Many Cas protein homologs and orthologs have been described with the most significant ones for rAAV gene-editing cassettes being Cas9, Cas12a (Cpf1), Cpf1, SpCas9, SaCas9 [207]. The large Cas9 (*SpCas9*, 4100 bp) or type-V Cas system (*AsCpf1*, 3921 bp; *LbCpf1*, 3684 bp) together with the gRNA cassette generally do not fit smoothly in a single rAAV gene cassette. The new generation of *SaCas9*, *CjCas9*, and *NmCas9* (2.9-3.3 bp) allows the packaging of both Cas9 and gRNA in a single AAV vector. CRISPR/Cas gene editing can inactivate the dominant-negative effect or can regulate positively or negatively the transcription of genes. However, if left active in cells, functional rAAV-CRISPR/Cas9 systems do increase the number of off-target integration events into the genome [208].

The large *SpCas9* (4100 bp) would require a dual rAAV system to incorporate all elements, including the gRNA cassette. A dual rAAVs system (rAAV.RKp.*SpCas9*; rAAV.U7.gRNA-*Nrl*) rescued vision in three mouse lines of rod retinal degeneration (*Crx-Nrl*^{-/-}; rd10 or *Pde6b*^{-/-}; *Rho*^{-/-}) by knocking out *Nrl* in one or both alleles [209]. The *Nrl*-knockout pushed rod photoreceptors to a more cone-like state helping in the survival of the remaining photoreceptors. Similar results have been reported in a second independent study [210]. The mutant rhodopsin gene encoding a dominant-negative form of rhodopsin (*Rho*^{P23H/P23H}) was also silenced by gene editing in a mouse model of retinal degeneration (*Rho*^{P23H/P23H}) by a dual rAAV-vector administration (rAAV2/8(Y733F)-sCMV-*SpCas9*.spA and rAAV2/8(Y733F)-U6.gRNA1gRNA2(*mRho*).mRho.h*RHO*.SV40-polyA) rescuing retinal degeneration [67].

A shorter Cas protein, *CjCas9* (2950 bp), allows expression from a single rAAV vector. Intravitreal injection of a single rAAV2/9-vector at P0 in mice efficiently downregulated angiogenesis genes (rAAV-gRNA against *Vegfa:Hif1a.CjCas9-T2A-GFP*) protected mice of visual loss when the mice were challenged by a laser inducing wet age-related macular degeneration at P42 causing choroidal neovascularization [211]. Their follow-up paper showed that 14-months post-injection, the *CjCas9* is still active but does not affect the retinal function as measured by electroretinogram (ERG), indicating that the therapy might be safe [212].

Cas proteins can also be altered and fused to other proteins. For example, the 3200 bp cDNA encoding a nonfunctional nuclease-activity-dead *S. aureus* ortholog Cas9 (dCas9) can be fused with a cDNA encoding a transactivation domain such as VP64 fused to the two transcription factors p65 and Rta (*dCas9-VPR*). The cDNAs encoding VP64, p65, and Rta are 150 bp, 357 bp, and 570 bp in length, respectively. Because of the relatively large size of 4277 bp of *dCas9-VPR* cDNA, the authors used a dual rAAV system to express the *dCas9-VPR* and gRNA expression cassettes [213,214]. Recently, a single rAAV expression vector has been developed driving the gRNA by a U6 promoter (360 bp) and a shortened but 3x less active *VPR* (500 bp) and *dSaCas9* (3200 bp) from an SCPI promoter (80 bp) attached to 2x-

sNRP-1 polyA signal (34 bp). A modified rAAV-vector version with a full-length CMV promoter and the bGHpolyA efficiently upregulated a gene (*Actc1*, *Neurog2*, or *Hbb*) upon infection of N2A neuron derived cells by 50-150x *in vitro* [169]. A single rAAV vector expressing dCas9 fusion protein, as well as a sgRNA, shows excellent potential for positive or negative regulation of transcription in many genetic pathways involved in retinal diseases. Several other exciting *Cas9* gene cassettes in rAAVs will most definitely be developed. A recent review reported an rAAV-CRISPR vector that can self-inactivate its Cas9 protein by encoding an anti-Cas9 gRNA on the same construct that harbors the Cas9 itself [150]. Nevertheless, single guide RNAs (*sgRNA*) comprise short hairpin sequences that potentially cause truncation of the rAAV production similar to short-hairpin RNAs (shRNA). Placing the gRNAs close to the second ITR might increase the production yield and increase proper vector expression upon infection of the target cells [149].

4.4. Production and rAAV vector integration

4.4.1 Production: The backbones and bacterial resistance genes

Impurities in rAAV products hinder the release of pharmaceutical products but might also negatively impact the potency of the expression vector. During the rAAV production, the gene therapy vector is packaged in the rAAV capsids. However, under suboptimal conditions, the capsids do also package other sequences such as vector plasmid backbones (~3%), helper plasmids (~0.05%), and even human genome sequences (~0.15%) [215]. Increasing the size of the vector plasmid backbone to above 5 kb considerably reduced inappropriate packaging and also reduced the number of empty capsids. But larger plasmids give lower DNA plasmid yields in bacterial culture and are somewhat harder to transfect efficiently into cell lines. Jean Bennett's group enhanced safety and maximized the therapeutic effect by adding a stuffer sequence for rAAV product hRPE65v2 [40,216]. The global health agencies (FDA, EMA, WHO) also discourage the use of β -lactams (i.e., ampicillin, penicillin) and streptomycin resistance genes in plasmids for gene therapy [217]. Kanamycin and neomycin are both members of the aminoglycoside antibiotic class. These antibiotics are tolerated but switching to antibiotic-free systems or minimizing the use of antibiotics is preferred. Some researchers use, therefore, minicircle DNA vectors devoid of prokaryotic and antibiotic DNA sequences for their AAV production [218]. No differences were found for minicircle single-stranded rAAV2.*eGFP* production. For the self-complementary rAAV2.*GFP* vector, the plasmid backbone was packaged 30 times less into capsids. Also, the use of minicircle plasmids during rAAV production allowed for high transduction titers of rAAV vectors on HeLa cells [219].

Pro-viral plasmids can also include short-hairpin RNAs to downregulate host cell proteins that hinder rAAV capsid assembly during production. Downregulating the Y-box binding protein 1 (YB1) in HEK293T cells did increase the physical titer by 47x for rAAV2, yet it failed to improve the yield for rAAV5 [165].

4.4.2 Production: ITR stabilization

An ITR consists of an A-A', RBE-RBE', B-B', C-C', D, and terminal resolution site (trs) sequence (Figure 4A). The AAV Rep78 and Rep68 proteins expressed by the pHelper plasmid induce a nick on the trs site on the ITR [220]. The RBE-RBE' initiates the binding of Rep78 and Rep68 proteins, and the B-B' further stabilizes the proteins so the Rep78 and Rep68 can efficiently induce DNA replication during the rAAV production cycle [221]. The D sequence is the packaging signal, is important for the AAV replication, and can bind the double-stranded D sequence binding protein (ds-D-BP) [222–224]. When high copy numbers of a D sequence expression vector are present in HEK293 cells, then the the interferon-λ-mediated activation of the major histocompatibility complex class II (MHC-II) is dampened, potentially by the binding of the ds-D-BP protein with the D-sequence instead of the the X-box (RFX) regulator [225]. rAAV can be produced with only one ITR if the other ITR has large deletions. Also, ITR deletions can be recovered during production [223,226]. Also, replacing the 5' ITR with a U-shaped hairpin allows rAAV production and episomal concatemerization [149]. A systematical study into ITR mutations (deleting B-B and C-C' regions) indicated a reduced yield (4-8x fold) but a 4-fold increased transgene expression in HEK293 cells 72 hours post-infection [227]. The deletion of the BC region caused an ITR change from a T-shape to a U-shape hairpin (similar to short hairpin RNA). The authors postulated that the 2x34bp ITR deletions might allow larger packaging of rAAV gene cassettes.

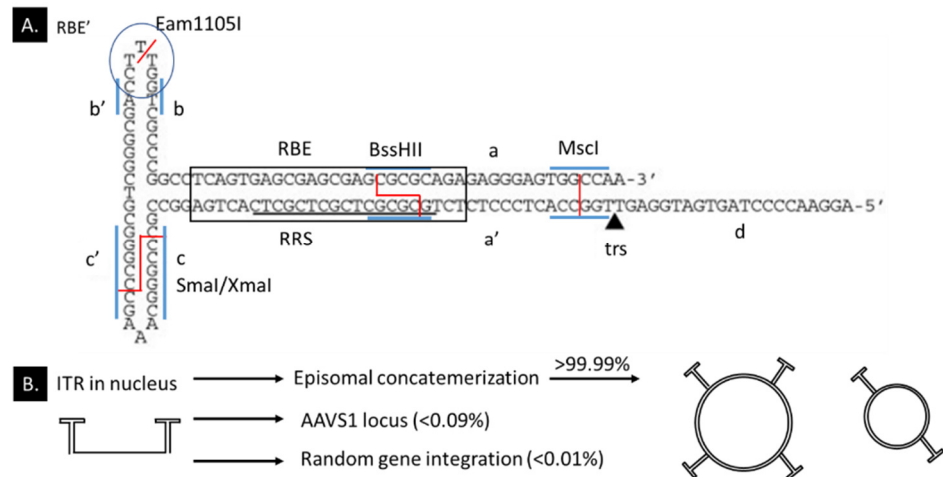


Figure 4. How to assess Inverted Terminal Repeats (ITRs) of rAAV and how they allow concatemerization. (A.) Restriction enzyme sites in the AAV serotype 2 ITR in the flop configuration. RBE'/RBE binds Rep68 (RBE, Rep-binding element) and initiates the Rep helicase. The Rep helicase nicks the trs (trs, terminal resolution site). Restriction enzyme recognition site indicated in blue and the actual cut in red. Figure adapted from [228]. (A) (B.) ITR structure in the nucleus after second-strand DNA synthesis in dividing cells favoring homologous recombination. Most rAAV-vectors form episomal concatemeric circular double-stranded DNA.

Recombinant AAV plasmids can lose/damage ITRs in many *E. coli* cells during plasmid production or rAAV production. We also noticed an almost complete loss of one ITR within one production cycle of a pro-viral plasmid in bacterial GeneHog cells (Invitrogen) (TMB & JW, unpublished data). We validated the loss in the pro-viral plasmids by restriction enzyme digestion with XmaI at the C-C', BssHII for the RBE, and Eam1105I for the RBE' region. ITR Sanger sequencing has been intricate on circular DNA. We sequenced the whole ITR by first linearizing the plasmid by Eam1105I digestion at the RBE', and then Sanger sequenced the pro-viral plasmid from both directions. The method allows us to use similar functional ITR ratios between batches (Figure 4A).

4.4.3 rAAV vector integration in the host genome

Integration of rAAV in the genome is unwanted because it might be genotoxic and lead to oncogenesis, especially in dividing cells and nontarget cells. The rAAV gene cassettes only harbor the palindromic inverted terminal repeats (ITR) of the original wild-type AAV. All other AAV wild-type sequences are lost during the rAAV production. The ITRs are part of the Long Terminal Repeats (LTRs) family. The LTRs are extensively exploited by retrotransposons or the pro-viral DNA of retroviral RNA. ITRs, similar to LTRs, are essential to allow AAV genome integration or episomal concatemerization. The ITR hairpin structures allow self-priming (primase independent synthesis of double-stranded DNA). The ITR-gene cassette stays as a monomeric episomal form in the nucleus at low multiplicity-of-infection (MOI). High MOIs, the ITRs form head-to-tail end-to-end joining, essentially making circularized DNA (>12kb). Further, the 5'LTR generally has a promoter function, and the 3'LTR can act as a termination sequence. Each of the ITRs of the AAV serotype 2 (ITR2) is only 145 bp long and lacks the promoter and termination functions (Figure 2B).

rAAVs lack viral proteins for efficient genome integration. Integration of foreign DNA (rAAV gene cassettes) into the mammalian genome is related to the amount of double-stranded DNA (dsDNA) breaks and the DNA repair pathway that is active in the cell. Integration events can be increased by increasing dsDNA breaks *in vitro* by adding intron-encoded endonuclease I-SceI, etoposide, or γ -irradiation [229]. Dividing cells favor the homologous recombination (HR) DNA repair pathway during the cell cycle S-phase that requires a DNA template to guide repair such as a viral gene cassette. However, quiescent cells, such as retinal and RPE cells, favor the nonhomologous end-joining (NHEJ) pathway ligating the ends directly without the insertion of a template.

The safety profile of the rAAV relies on that upon intravenous injection, more than 85-95% of rAAV vector genomes remain episomal in the dividing hepatocytes in the mouse liver (Figure 4B; [230]). The study might have overestimated integration events in hepatocytes. Others estimate the AAV integration events closer to 0.1-1% [231]. Yet, follow-up studies indicated that 53-62% of rAAV integrations in the liver fused into actively-transcribed genes, and 3-8 % into ribosomal DNA [232]. rAAV genome integration into mouse muscle tissue

DNA compared to hepatocyte DNA was hard to detect or not present, indicating that the integration frequency also depends on the cell type [23]. Integration of wtAAV compared to rAAV for human cardiomyocytes at high MOI (50,000 viral particles per cell) was 5.6x higher with both AAVs integrating into mitochondrial DNA [233]. A recent study looked at integration events in nonhuman primates and patient DNA in clinical trials (liver biopsy) that received the rAAV2/5-*cohPBGD* and found 10^{-3} to 10^{-5} integration events per cell or 0.04–9% integration events [234]. Very little information is available for rAAV vector genome integration events into retinal tissue. A recent CRISPR/Cas9 study indicated that Cas9 breaks caused >1-20% insertion events of the rAAV cassette (EDIT-101) into the dsDNA break in the CEP290 intron in human retinal explant DNA, not counting integrations in other regions of the genome [38]. The insertion of the rAAV was higher when more indels, deletions, and inversions were detected (over 25 independent samples). The results indicate, as expected, that rAAV integrations events in photoreceptor cells correlate to the rAAV dosage. rAAV integration studies in the retina is an underrepresented research field. Almost no rAAV study specifically investigated rAAV integration events.

The integration of rAAV vectors at ribosomal DNA (rDNA) can be exploited by adding 1 kb homology arms of the rDNA locus adjacent to the ITRs. The homology arms increased the integration frequency in dividing cells favoring homologous recombination by 10-30x from a baseline of 0.001-5% AAV vector integrations per 100 cells (depending on the vector dose). Further, many rAAV gene cassette integrations caused deletions in the genome [235].

The unique T-shape AAV serotype 2 ITR-DNA (ITR2) conformation enables even gene editing. A defective eGFP reporter plasmid in dividing cells was rescued (gene-edited) by adding only the ITR2-*eGFP*part(165 bp)-ITR2 with 40 bp *eGFP* homology arms adjacent to the ITR2 [236]. Nevertheless, the rAAV gene expression from integration events is generally silenced within eight passages. Also, wild-type AAV integrates preferentially at 94% at the AAVS1 locus on chromosome 19 (Chr19) because the ITR sequence is homologous to the AAVS1 locus, but this requires the AAV integrases Rep78 and Rep68 that have been removed in rAAVs. Thus, rAAVs do not integrate at the AAVS1 locus. Interestingly, very little to no rAAV integration has been found in the genome of CRISPR/Cas9 gene-edited quiescent cells suggesting that off-target editing requires cell division. Unmistakably, many successful AAV gene therapies in mice and >130 rAAV clinical trials in humans, have indirectly demonstrated that the genome integration / genotoxic events are of a lesser concern [234].

4.5. Codon optimization and self-complementary rAAVs

The final rAAV gene cassette could be codon-optimized to improve the optimal expression of the transgene in the target cell and organism. Essentially, codon-optimization is primarily looking at codon frequencies that might rate limit the transcription of the gene in the target cell, such as favoring the codon GUG over GUU for valine in humans. The codon

optimization of rAAVs should prevent the inclusion of potential hairpin structures, repeats, extreme GC content, alternative open reading frames (ORF), and cryptic splice sites. Different codon optimizations have been tested for the rAAV gene therapy for Crigler-Najjar syndrome that increased the *FIX* transgene expression by 4-10-fold [237]. Also, the codon-optimization (humanized; removal of cryptic splice sites; elimination of alternative ORFs) of rAAV2/5.hRPE65.hRPE65 to rAAV2/5.OPTIRPE65 could theoretically reduce the vector dose 300-fold in mice [36]. The authors claimed that the future use of codon optimization for human cells might further improve the potency to 1800-fold in humans. The final lower rAAV administration might reduce temporal capsid-mediated toxicity found in their earlier studies [36]. For the rAAV vector AGTC-501 expressing the human *RPGR-ORF15* gene, the Codon Adaptation Index (CAI) of human codon-usage frequency was increased from 0.73 to 0.87, and the Frequency of Optimal Codons (Fop) was increased from 32% to 57%. Further, the GC content was increased, and the maximum repeat size decreased. Such adaptations in the AGTC-501 vector resulted in reduced frequency of alternative splicing and increased mRNA stability [44,111]. Interestingly, the same stabilized RPGR sequence of the AGTC-501 produced a full-length RPGR-and a truncated form of RPGR-ORF15 in the retina of mice *in vivo*. But when applied to HEK293T cells *in vitro*, then the AGTC-501 vector produced only the full-length RPGR-ORF15 protein. The different products produced from the same *RPGR* expression cassette indicated species differences in the regulation of gene transcription or RNA splicing or differences between *in vitro* versus *in vivo* transgene expression systems. Transgene expression cassettes for clinical retina studies should, therefore, be tested in cultured human cells and preferentially in human retinal organoids or human RPE cells.

Recombinant self-complementary AAV (scAAV) vectors are more potent to express high levels of transgenes than recombinant single-stranded AAV (ssAAV) vectors. Once the cell is infected by the scAAV and the scAAV becomes decapsidated, the rate-limiting step to create double-stranded DNA is overcome more efficiently in scAAV than in single-stranded rAAV. A major disadvantage of scAAV is however the reduced packaging capacity of the gene expression cassette from up to 4.9 kb to a maximum of 2.5 kb, including the two ITRs. Transgene expression could be enhanced by 5 up to 140 fold *in vitro* [238]. Deleting the terminal resolution site sequence from one ITR (ITR2 Δ) increased the yield of dimeric genomes by 90% [239]. When compared to ssDNA, lowered rAAV doses of scAAV gene therapy vector can be used to reach similar transgene expression levels in the retina *in vivo* [102,155,240,241]. ScAAVs can also have significant effects on the promoter choice. The rescue by subretinal injection of scAAV8-sRLBP1p.*RLBP1* rescued the rate of dark adaptation measured by electroretinography (ERG) in *Rlbp1* knockout mice [102,155]. The transcription of hRLBP1 by a short RLBP1 promoter increased 50-fold at a low dose (1×10^8 viral genome) and 6.4 fold at a high dose (1×10^9 viral genome) in cynomolgus monkey retina. The scAAV might be especially beneficial when weak promoters are required or if low viral

doses are desired to prevent capsid toxicity of specific target cells. A more specific review on scAAV can be found here [239].

5. Transgene & bioactivity assays in ocular tissue

Quality control is essential in rAAV production. Quality control includes testing the rAAV production on safety (sterility, viral contaminants, mycoplasma, endotoxins, bacterial & fungistatic activity), appearance, pH, osmolarity, potency (viral genome titer, infectivity, expression), purity, and vector genome identity [242]. Here, we focus on the rAAV potency: infectivity and *in vitro* & *in vivo* expression.

5.1. *In vitro* immortalized epithelial cell lines for transgene and bioactivity assays

The most straight forward, high-throughput, fast, cheap, robust, but less predictive transgene expression assays are still monoculture systems *in vitro*. The ideal system would allow a fast characterization of the transduction profile, including rAAV capsid-specific infection, promoter expression profiling (mRNA level), and protein-of-interest expression. Such an assay would allow fast screening of different gene cassettes in research development but also validating the gene therapy products and batches in the clinical-grade production cycle.

rAAV transfection efficiency (potency: infectivity) and transgene expression (potency: *in vitro* expression) has been tested on rAAV epithelial production cell lines (for example: HEK293T, HER911, HeLa-E1, Per.C6). One can measure the rAAV infection or functional titers measured in transducing units per mL (TU/mL) by two common assays: (1.) Median tissue culture infective dose (TCID₅₀) based on rAAV-vector (MOI 20,000 viral genome/cell) infecting HeLaRC32 (HeLa AAV rep-cap expressing cell line) and concomitant adenovirus type 5 (Ad5; 500 IUs/cell) infection (Outcome: vector genome quantification). (2.) Infectious center assay (ICA) based on HeLaRC32 and Ad5 (500 IUs/cell) infection (Outcome measure: hybridization of a probe to the rAAV gene cassette). The HeLaRC32 cells allow rAAV replication if the rAAV gene cassette can enter the nucleus [243].

Spark Therapeutics also developed an *in vitro* potency assay for rAAV-*RPE65* vectors. Here, modified HEK293 cells constitutively expressing lecithin-retinol acyltransferase (LRAT) are transduced by the rAAV-*RPE65* at different MOIs. Then, 72 hours later, the cells are lysed by adding lysis buffer, and the lysate is incubated with all-trans-retinol and CRALBP for 2 hours in the dark to assess the enzymatic activity of RPE65 (an isomerohydrolase) to convert all-trans-retinol to 11-cis-retinol [244]. The rAAV-*REP1* for the treatment of choroideremia is assessed on *in vitro* prenylation of RAB6A in HEK293 cells [245]. The directly injectable dose can also be assayed. The potency of the residual diluted vector (rAAV2-*REP1*) from the syringe used to inject patients was applied to the REP1-deficient cell line HT1080 for REP1 expression [246]. An endothelial-like Human Trabecular Meshwork (HTM) immortalized

cell line is currently explored for glaucoma gene therapy. Still, the surrogate cell line might also be interesting for studying the off-target effects of rAAV vectors injected intravitreally [247,248]. However, it is not always possible to develop informative assays on epithelial cells, especially for large screens for novel retinal-specific capsids or retinal specific promoters. For example, rAAV5 vectors infect very poorly HEK293 cells, HeLa cells, and BJ fibroblasts [249] but infect RPE cells and human retinal organoids efficiently [68,250]. Consequently, if a rAAV5-CAG vector does not express a gene product in a HEK293 assay, then the vector might still express the gene in human RPE or human retinal organoids.

5.2. *In vitro* immortalized ocular cell lines for transgene and bioactivity assays

Researchers can also use various human retinal cell lines to achieve improved infection and expression of retinal specific capsids or promoters. Promising ocular cell lines are the 661W mouse photoreceptor cell line / retinal ganglion precursor-like cell line (a surrogate for cone photoreceptors), the Adult Retinal Pigment Epithelial cell line-19 (ARPE-19; a surrogate for RPE cells), hTERT RPE-1 (ATCC® CRL-4000™), human astrocytes and the MIO-M1 (surrogates for Müller glial cells).

661W cells express *Opn1SW*, *Opn1mw*, *Rbpms*, *Brn3b*, *Brn3c*, *Thy1*, γ -synuclein, nestin, NeuN, *Map2C*, *Map2D*, and β -III tubulin. GFAP is not expressed in the 661W cell line. The 661W cells are light-sensitive but do not have visible outer segments [251,252]. 661W and ARPE-19 cells allow for screening of RPE-specific (*mCARpro*, *MOPS500*, *VMD2*) and ubiquitous (*smCBA*) promoters for most rAAV serotypes [253]. The 661W cell line has been further modified to achieve improved transfection by overexpression of the universal adeno-associated virus receptor (AAVR) or more stably express key photoreceptor genes such as *GRK1* and *CAR* by rAAV-VPR-*dCas9* vector infection [254]. Two major drawbacks to immortalized ocular cell lines are that most tend to be very heterogeneous, some of the cell lines express multiple cell-type-specific markers such as for retinal ganglion cells (*Brn3*) as well as for cones (*Opn1mw*) in addition to neuronal cell markers (*Nestin*, *NeuN*). And none of the cell lines have mature photoreceptor outer segments. Another RPE cell line (hTERT RPE1; ATCC® CRL-4000™) was used for liposome co-flotation assays expressing a biological active truncated CEP290 (1-580 amino acid) protein (rAAV-*CEP290^{1-580aa}*) in the primary cilium [255]. A *CEP290* knockout hTERT RPE1 line was constructed, showing the cilia-related CEP290-phenotype [256].

Human primary astrocytes have been successfully employed to select for novel rAAV capsid variants that are specific for (Müller) glial cells. An example is the rAAV6 variant ShH10-Y445F that efficiently infects rat, mouse, and human Müller glial cells [66,68,257]. Human astrocytes also express common Müller glial cell markers such as *SOX9*, *GFAP*, *GLAST*, *GS*, *Kir4.1*, and *S100 β* [258,259]. A human Müller glial-like cell line (MIO-M1) expresses the proteins *GLUL*, *VIM*, low *GFAP* (but found on mRNA level), *RLBP1*, *GLAST*, *EGFR*, *SLCA1*, *AQP4*, *Kir4.1*, *THY1*, *NEFH*, *MAP2*, *NEUROD1*, *NEUN*, *Nestin*,

SOX2, Chx10, PAX6, NOTCH1, β III tubulin. But the Müller glial-like cell line also contains mRNA for the following opsins or visual cycle-related proteins: OPN1SW, OPN2, OPN3, OPN4, OPN5, RRH, GNAZ, GNAT1, and GNAT2 [260,261]. The MIO-M1 cell line has been successfully used to screen for rAAV infectivity, rAAV, and lentivirus cell-specific promoter expression [262]. The hypoxia-Müller glial specific promoter (scAAV2.HRSE.6xHRE.GfaABC1D.*luciferase*) is active in MIO-M1 cells under hypoxic conditions. The hypoxia-induced Müller glial specific promoter showed no luciferase expression in HEK293, C6, HT22, and ARPE19 cells [98].

All described cell lines hold great promise for further rAAV studies. One needs to be cautious of the results because (1.) changes in culture condition can strongly affect the “cell-specific” gene expression, (2.) cell contamination has been found in several lines such as the rat ganglion cell line 5 (RGC-5) being a subclone of the 661W cell line, (3) multiple cell-type-specific gene markers expressed for example in 661W, and (4) the overall lower biologically relevance compared to 2D and 3D cell or *in vivo* studies.

5.3. In vitro differentiation of human induced pluripotent stem cells (hiPSCs) to retinal pigment epithelium (RPE) cells

Human patient induced pluripotent stem cells (hiPSCs) can be differentiated to photoreceptors [263]. 2D differentiation of hiPSCs to photoreceptors peaks at 45 days of differentiation, but it declines fast, making rAAV studies difficult because of the short time window and the inherent instability of inner/outer segments.

Human patient induced pluripotent stem cells (hiPSCs) can also be differentiated to monolayers of RPE. rAAV-*REPI* vector transduction of patient hiPSC-derived *CHM*-RPE rescued the biochemical phenotype [264]. The patient hiPSC-derived RPE can be efficiently used for testing the AAV-*CHM* vector for rescuing prenylation, phagocytosis, and protein trafficking [265]. Also, a *proof-of-concept* for dominant retinitis pigmentosa due to haploinsufficiency rescued phagocytosis and cilia formation by AAV2/*Anc80-PRPF31* in hiPSC-derived *PRPF31*^{+/-} RPE cells [266]. Spark Therapeutics filed a patent application for a potency assay of rAAV-CHM on hiPSC-derived RPE cells lacking CHM expression [267].

5.4. In vitro differentiation of human induced pluripotent stem cells (hiPSCs) to retinal organoids for transgene and bioactivity assays

We and others used human retinal organoids to study rAAV transduction and potency [68,250,268,269]. In summary, photoreceptors are transduced by rAAVs such as rAAV2, rAAV2-7m8, rAAV5, rShH10, rShH10-Y445F, rAAV8, rAAV8T(Y733F), and rAAV9 albeit at different transduction efficacies. The rAAV2-7m8, rAAV5, rShH10, and rShH10Y-445F capsids infect photoreceptors efficiently. Interestingly, (early) radial retinal progenitor cells in retinal organoids or common cell lines can be efficiently infected by rAAV6, the rAAV6 variants (ShH10 and ShH10Y-445F), and the AAV2-7m8 [21,68,250,269]. For

example, rAAV6 and rAAV-derived vectors (ShH10; ShH10-Y445F) can efficiently infect hiPSCs and hiPSC-derived RPE cells [21,68,250]. The rAAV2-7m8 and rAAV5 also efficiently infected RPE cells [250,269].

Many challenges still lay ahead. For example, the quality of the starting material (hiPSCs) and the differentiation method can significantly affect the success in differentiation to retinal organoids [270,271]. Also, the medium composition altering the extracellular matrix can influence rAAV infection. For example, the fibroblast growth factor receptors (FGFRs) are important for the stabilization of the heparan sulfate proteoglycans (HSPGs) on the extracellular matrix of the cell [272]. FGF-2 binds with low affinity to the heparin sulfate chains of HSPGs and the FGFRs [273]. It can be found in many medium compositions as supplement or in fetal bovine serum (FBS; 8-45 pg/mL) [274]. Many AAV capsids require the HSPGs, the universal AAV receptor (AAVR), and the FGFRs for efficient cell entry. For example, rAAV2 requires FGFR1 receptor that can be blocked by FGF-2 supplementation [275]. But other rAAV serotypes, such as AAV4 derivatives are less dependent on the HSPGs and FGFRs for rAAV capsid cell entry [272]. Thus, the FGF-2 concentration in the medium needs to be defined for rAAV potency assays. Not all co-receptors for rAAV entries have been discovered yet, adding to the uncertainty of rAAV potency assay data.

Other limitations are the loss of ganglion cells in long-term culture, improper lamination of the ganglion cell layer including astrocytes, no innervation of the optic nerve that is required for proper foveal development, no vascularization of retinal organoids (therefore no pericytes), no sclera & Bruch's-membrane (blood-brain-barrier), no immune cells (macrophages, microglia, dendritic cells), and no integration with other organs (brain, heart, liver, kidney). More sophisticated models are currently in development. For example, human iPSC-derived retinal organoids and RPE-sheets can be cultured in a microfluidic chip system that enhances photoreceptor maturation and stabilization *in vitro* [276].

5.5. Human *ex vivo* retinal culture for transgene and bioactivity assays

We and others have also demonstrated that rAAVs can be tested on *ex vivo* cadaveric human retinas [38,51,68,277–281]. *Ex vivo* studies have especially become more attractive since the advent of more efficient medium compositions with better inner-outer photoreceptor segment (IS/OS) quality and ganglion cell survival that allow for longer rAAV-transgene expression. rAAV1, rAAV2[*MAX*], rAAV2(*quad Y-F*), rAAV2-7m8, rAAV4, rAAV5, rAAV6 and to a lesser degree rAAV2 and rAAV9 can efficiently infect photoreceptors on *ex vivo* human cadaveric retinas. We have shown that rAAV5, rAAV6 variants ShH10 and ShH10-Y445F can efficiently infect both human photoreceptors and Müller glial cells *ex vivo* [66,68]. rAAV2(*quad Y-F*) and rAAV2-7m8 also infected Müller glial cells and some rod photoreceptor cells *ex vivo* [278,279]. rAAV2/8BP2 infected photoreceptors, Müller glial cells, amacrine cells, ganglion cells, and horizontal cells *ex vivo* [51]. Also, the hRLBP1 promoter (2.6 kb) can restrict expression to Müller glial cells and RPE [66]. Recently,

rAAV5.GRK1.*SaCas9* vector particles were added to retinal explants that were subsequently cultured for 28 days. The human photoreceptor-specific rhodopsin kinase (GRK1) promoter directed Cas9 expression specifically in human photoreceptors [38]. We have also shown that the GRK1 promoter can limit expression to photoreceptor cells in *ex vivo* cadaveric human retinas [282].

We have previously shown that mouse retinal explants at P0 can be cultured longer than adult retinal explants [283]. Likewise, human fetal retinae can be cultured for three weeks, with preservation of the general morphology preserved and only the loss of ganglion cells [284]. More astonishingly, fetal retinal tissue that maintained some photoreceptor morphology has been cultured for 293 days *in vitro* [284]. However, the access to and quality of the donor human fetal material limits the application for many researchers [68,285,286]. We observed that efficient transduction of photoreceptors by rAAVs required the presence of well-developed inner/outer segments of photoreceptors. Interestingly, rAAVs infected Müller glial cells more efficiently in explants that showed retinal degeneration [68,279].

5.6. In vivo studies for transgene and bioactivity assays

5.6.1 Developmental stage and rAAV infection

Many adult mouse rAAV potency studies have been performed and are reviewed elsewhere [2,7]. It is interesting to note that rAAV infection can differ depending on the developmental stage of the ocular tissue. Mouse fetal retina (embryonic day 13; subretinal injection) can be transduced well by rAAV5 but not by rAAV1 and rAAV2. But rAAV1, rAAV2, and rAAV5 transduce photoreceptors well at P30 [286]. Mouse photoreceptor cells at postnatal day 0 can be efficiently targeted by subretinal injection of rAAV1, rAAV5, rAAV9, and rAAV11 [122]. However, AAV1 transduces mainly RPE cells at the adult stage [2,7]. Also, rAAV8-CMV-*GFP* transduces photoreceptors and Müller glial cells at postnatal day six but only transduces photoreceptors at postnatal day 0 [287]. Here, the rAAV vector containing the CAG promoter compared to the CMV promoter showed expression in more cells (photoreceptors, horizontal cells, amacrine cells, and retinal ganglion cells vs. only photoreceptors) at postnatal day 0. The difference in the infection efficiency at early development compared to more mature retinas has been linked to rAAV receptors and co-receptors important for rAAV cell entry [269]. The main universal AAV receptor (AAVR) was present already in 44-day-old human retinal organoids. However, the poor transfection efficiency of rAAV9 of retinal organoids [250,288] was linked to the low abundance of N-linked-galactose at early retinal developmental stages [269]. It points to the importance of describing the receptor composition and medium composition accurately at the time of infection to make meaningful comparisons between the infectivity of different rAAV capsids.

5.6.2 rAAVs overcoming membranes in the retina and the retinal disease state

Delivery of rAAV gene supplementation to photoreceptors or RPE cells is generally done by subretinal injection because many rAAVs cannot penetrate through the inner limiting

membrane (ILM) when injected intravitreally. The ILM is close to the ganglion cells and the Müller glial endfeet with a thickness varying between 100 nm up to 2000 nm in nonhuman primates [289]. The rAAV subretinal injection creates a fluid bleb between the retina and the RPE layer causing temporal retinal detachment and infection of cells at foci. Intravitreal injections target a larger retinal area. Intravitreal injections of empty rAAV capsids can induce a temporary immune inflammation of the aqueous and the vitreous [290]. Enzymatic digestion (proteasome inhibitors) of the ILM or ILM/OLM or disruptions of the ILM/OLM by the disease can alter rAAV infection and allow rAAV infection deeper into the retina [100,279,291,292]. Applying a low trans-ocular electric current also allowed efficient transduction of RPE and photoreceptors by rAAV8 upon intravitreal injection in adult mice [293]. Finally, the application of tyrosine kinase inhibitors might improve the passage of rAAV through the ILM or OLM [294]. The novel methods might make the intravitreal injection more common for photoreceptor and Müller glial cell infection. Intravitreal injection of some rAAVs might result in the transduction of a larger pool of off-target cells, such as the ciliary body and iris epithelium [66].

Disease-induced changes to the retinal morphology do impact the rAAV infectivity. In many retinal diseases, for example in *Crb1* retinitis pigmentosa mouse models, we first find that Müller glial cells express stress markers (gliosis), the outer limiting membrane (OLM) which contains adherens junctions between photoreceptors and Müller glial cells disrupts at foci, the inner/outer segments of photoreceptors shrink, some of the photoreceptors die, macrophages and microglial cells are activated and assemble in the photoreceptor segment layers, the outer and inner nuclear layers mix and thin out, and neovascularization takes place [68,189–202]. Likewise, transgenic rats overexpressing rhodopsin variants causing autosomal dominant retinitis pigmentosa show an early (P20), intermediate (P30), and advanced stages of retinal degeneration (P60). rAAV1 or rAAV5 intravitreally injected in rats showed no accumulation of AAV particles at the ILM [291]. But under the disease condition or enzymatic digestion of the ILM, all rAAV (1, 2, 5, 8, and 9) traversed, most likely via Müller glial cells, to RPE cells through the retina [100,291,295]. rAAV2-7m8 vectors infected a wide range of cells in the degenerate retina of rd1 mice (*Pde6b^{rd1/rd1}*) with little differences found in tropism when the vector was injected subretinally or intravitreally [279]. The potency to infect the degenerate photoreceptors by subretinal injection of *Abca4^{KO}* mice compared to wild-type mice was lower for four different rAAVs (rAAV2, rAAV5, rAAV2rec2, rAAV2rec3) while the potency to infect INL cells was increased in *Pde6b^{rd1/rd1}* mice at least for rAAV5, rAAV2/Rec2 [296]. Intravitreal injection of rAAVrh-10 shifted infection from mainly INL cells towards photoreceptor and RPE cells in *Rsl^{KO}* and *Rho^{KO}* mice (XLRS and RP models, respectively) compared to wild-type mice [297,298]. The studies indicate that disease models allow deeper penetration of rAAVs in disease state compared to healthy retinas with generally lower photoreceptor infection. How well changes

in the OLM and ILM impacts rAAV infection needs to be determined separately for each type of retinal disease (Figure 5).

The changes in rAAV vector transduction and expression can be linked to the differentiation stage of cells and cellular stress. Nondividing terminally differentiated cells allow efficient expression from rAAV gene therapy vectors because the cells downregulate proteins of the DNA damage response [299]. In AMD and retinitis pigmentosa, retinal

cells might show an increase in DNA damage response, including more double-stranded DNA breaks and impaired (decreased) autophagy leading to increased cell size, granularity, and protein accumulation [300–302]. How the increase in DNA-damage sensors or the decrease of terminal differentiation is linked to rAAV vector transgene expression needs to be further evaluated. Cell stress-induced expression was observed upon induction of gliosis, by light or application of ciliary neurotrophic factor (*CNTF*), in *Crb1*-deficient retina injected intravitreally with rAAV.GFAP.*eGFP* [100].

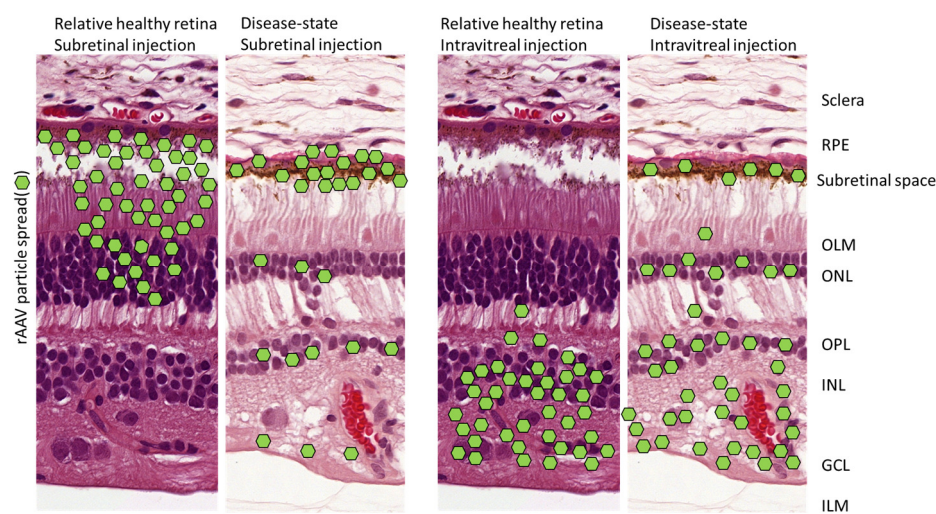


Figure 5. A hypothetical model of the spread of rAAV capsids (serotypes 1, 2, 5, 8, and 9) after intravitreal or subretinal injection in disease or non-disease mouse retinas *in vivo* based on the studies [100,279,291,293,295,296]. RPE, retinal pigment epithelium; OLM, outer limiting membrane, ONL, outer nuclear layer; OPL, outer plexiform layer; INL, inner nuclear layer; GCL, ganglion cell layer; ILM, Inner Limiting Membrane.

5.6.3 Nonhuman primate studies and rAAV infection

Several rAAV serotypes are studied for safety/toxicological assessment in retinas of nonhuman primates (NHP) before entering clinical trials. Some information on tropism and promoter cell specificity has been acquired. Subretinal injection (ubiquitous promoter): rAAV1, rAAVrh64R1, rAAV2, rAAV2-7m8, rAAV5, rAAVrh8R, rAAV7, rAAV8, rAAV8BP2, rAAV9, rAnc80L65 infect rod photoreceptors and RPE cells [265,278,303–

307]. rAAV8BP2, rAAV9 and rAAV5 infect cone photoreceptors more efficiently than rAAV2 [305,306,308]. Novel AAV capsids, such as the rAAV7m8 and rAAV8BP2, also infected some INL cells and ganglion cells [51,306]. High titer rAnc80L65 and rAAV5 might infect some NHP Müller glial cells [309]. Intravitreal injection (ubiquitous promoter): rAAV2 infects Müller glial cells and ganglion cells [310]. rAAV2-7m8 infects well Müller glial cells and retinal ganglion cells, whereas rAAV8BP2 infects ganglion cells. Self-complementary rAAV2tYF infects Müller glial cells, at least if the ILM is peeled off before injection [311]. rAAVrh-10 showed promise in transducing the whole rabbit retina and patches of RPE cells, including photoreceptors [297].

Different cell-type-specific promoters have been tested by subretinal or intravitreal injection in NHPs with surprising results. The hGRK1 promoter expressed GFP specifically in rod- and cone photoreceptors [308]. The strong cone-specific promoters in mice (mCAR, PR2.1, and PR1.7) all showed some rod expression and strong cone expression. However, the mouse cone arrestin promoter (mCAR) also expressed eGFP in rods, inner nuclear layer cells, and ganglion cells [278]. A large scale study compared novel synthetic cell-specific promoters using previously described rAAV serotypes (AAV8, AAV9, AAV8BP2) between mice, NHPs, and human retinal explants [51]. Unsurprisingly, NHP and human retinal explants matched closer (correlation $r=0.66-0.67$) compared to mouse/NHP or mouse/human ($r=0.34-0.38$; $r=0.24-0.32$). But a predictive value mean correlation of 0.3 demands that rAAVs and cell-specific promoters need to be tested in human systems. Nevertheless, if an rAAV vector expressed well in human retinal explants and NHP, then it is more likely (conditional probability = 0.12-0.14) that the rAAV vector works as well in the mouse retina. The results suggest, therefore, that mouse retina can be used to pre-screen rAAV vectors for cell-type specificity.

5.6.4 *Cis-regulatory toxicity of rAAV vectors in vivo?*

AAV retinal-specific promoters were compared by subretinal injection at P0 for cis-regulatory sequence toxicity in the CD-1 albino mouse line [312]. This CD-1 mouse line is prone to hearing and vision loss, whereas albino mice are more susceptible to light-induced retinal damage [313]. The encapsidated rAAV vectors containing cis-regulatory ubiquitous promoters (CMV, CAG) or the RPE-specific promoter (hBEST1) showed higher dose-dependent toxicity to the RPE and photoreceptors than photoreceptor-specific promoters (Rho; RedO, CAR, GRK1). The ubiquitous UbC promoter showed no toxicity to the mouse RPE [312]. Interestingly, C57BL/6J mouse retinas injected with AAV8- or AAV5-CMV-*GFP* at P0 and subsequently analyzed at P30 showed RPE aberrations by SD-OCT but no ERG or OKT differences at 3×10^9 vector genome copies [312]. However, stronger rAAV vectors such as the ones that contain a CMV promoter and a WPRE element such as the vector rAAV2/8.CMV.*eGFP*.WPRE.bGHpolyA caused retinal degeneration in mice at 5×10^{10} vg (ONL reduction and ERG) [314].

Interestingly, photoreceptor cells that were infected by rAAVs carrying a non-coding gene cassette (rAAV-flox vector) that is floxed out in Cre recombinase expressing cells also caused toxicity 1×10^{11} vg or above, indicating that the rAAV-capsid can cause toxicity [314]. Further, the ubiquitous CAG promoter caused more toxicity than the rhodopsin specific promoter. Thus, further studies on how promoters might activate the innate immune system by TLR2 or TLR-9 activation, what sequence motifs are more prone to induce toxicity, or what time points are especially sensitive are of great importance. However, antigen-presenting cells can take up capsids and express the antigens on MHC class II receptors that can activate CD4⁺ T-helper cells releasing cytokines that stimulate CD8⁺ T-cells. This immune cascade model might explain why re-administration in patients could become difficult, and why the administration of rAAVs in patients with high neutralizing antibodies (nAbs) are generally not included in clinical trials [315]. However, the innate, humoral, and cell-mediated immune response might contribute to vector toxicity. For example, intravitreally injected empty rAAV capsids can induce a transient inflammation of the aqueous and the vitreous body [290]. Most importantly, cis-regulatory-sequence, rAAV-capsid, and transgene-related toxicity need to be investigated in the retinal degeneration model. Further, the more efficient gene expression cassettes might allow a rescue strategy at lower rAAV titers, thereby causing less toxicity and lower transient inflammation [290].

6. Concluding Remarks and Future Prospects

The tools for modulating rAAV gene therapy vectors are expanding rapidly. Novel rAAV capsids, production platforms, (short) promoters, stabilizing introns, and polyadenylation sequences are continuously published. However, many papers on rAAV ocular trials do not sufficiently describe the used pro-viral plasmids, especially on the backbone side (origin and bacterial selection marker). The vast expanse and the poor description make a fair comparison of rAAV vector elements very challenging because large scale comparative rAAV element studies are missing. Nevertheless, recent studies indicate that:

- (1) The use of tyrosine-mutated rAAV2 capsids (AAV2-tYF; AAV2-7m8) increases retinal penetration and infection potentially replacing wild-type capsids (Section 2, 5.6)
- (2) The strong viral promoter CAG expresses the transgenes in the RPE for many years without being silenced [22] (section 2, 3, 5.6)
- (3) Native promoters are more prone to differ in expression in disease models, different species, and *in vivo/in vitro/ex vivo* models (section 3.4, 5)
- (4) Inducible promoters (riboswitches and dead-Cas9) offer exciting opportunities to control protein expression (section 3.8)
- (5) Surrogate (homolog/ortholog or synthetic) gene supplementation might circumvent cellular immunogenicity (Section 4.1)
- (6) The rAAV production cell line might influence the transduction efficiency [45] (section 2 and 4.4)

- (7) The inverted terminal repeats of rAAVs are essential for high production yields but less critical for the efficient transgene expression (section 4.4.2)
- (8) Genome integrations of rAAV vectors and the potential cell-toxic effect of genome integrations are insufficiently studied in retinal tissue (section 4.4.3)
- (9) Differences in medium composition, culturing techniques/protocols, and the developmental stage influence rAAV infection and transgene expression (section 5.6.1)
- (10) The disease state strongly influences rAAV-vector penetration, potency, and tropism of the retina (section 5.6.2)

A large panel of models are available for studying retinal diseases. However, all models have inherent drawbacks. Improved models will become available, allowing more rapid screening of promoters and rAAV capsids in human systems with high biological relevance (Figure 6. Section 5.1-5.6).

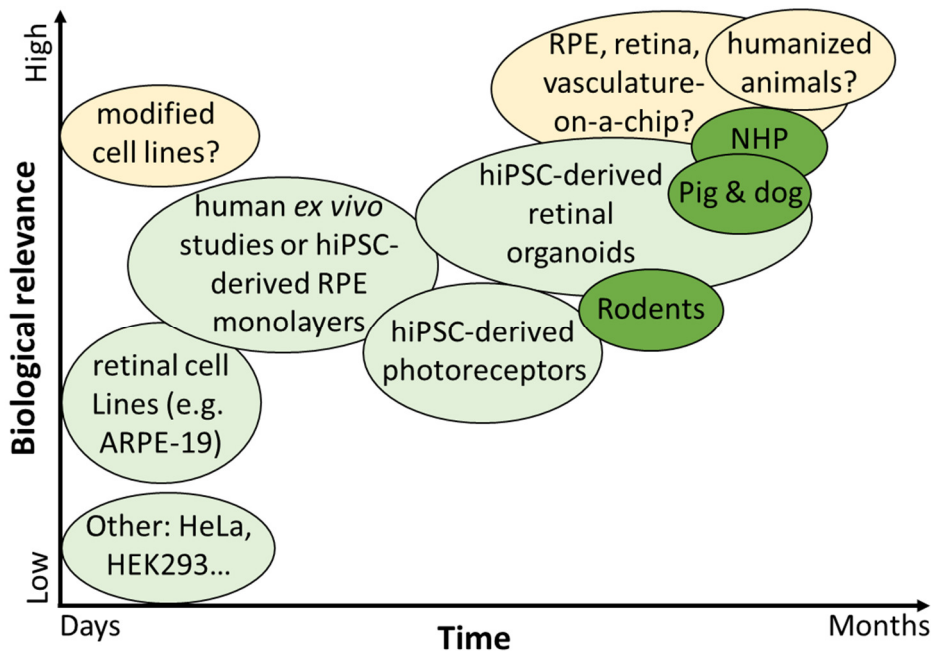


Figure 6. Qualitative assessment of biological relevance and time of assay for retina-specific rAAV potency assay models. hiPSC, human induced pluripotent stem cell; NHP, non-human primates; RPE, retinal pigment epithelium.

7. Methods

A meta-analysis on pro-viral plasmids and production platforms for ocular rAAV therapies in clinical trials (Table 1 & S1)

We analyzed current reviews on gene therapy on clinical trial identifiers. Then, we searched for the keywords (AAV, gene therapy, retinitis pigmentosa, RP, Leber congenital amaurosis, LCA, AMD, CHM) on <https://clinicaltrials.gov/> (last date 01-April-2020). We limited the search to gene therapies expressing the gene-of-interest in the eye. We further cross-checked the results with reported clinical trials in the news and current reviews. If sequences or rAAV production platforms were insufficiently reported in research papers the search was widened: (1.) Patents based on researchers and companies involved; (2.) Ph.D. thesis; (3.) Company registration documents; (4.) Company websites; (5.) Company-provided presentations; (6.) Posters on international conferences; (7.) Abstracts on international conferences. All related information was gathered in the supplementary word document. All clinical trial identifiers were added to each unique rAAV product to identify the unique products. Lentiviral products, cell therapy products, antibodies, and antisense oligonucleotide (AONs) products were removed. The unique ocular gene therapy products were then analyzed on prokaryotic plasmid backbone, inverted terminal repeat AAV serotype, enhancers, promoters, introns, genes, codon-optimization, human or other species-related sequences, post-transcriptional stabilizing sequences, polyadenylation sequences, and rAAV production platform. Not present information was indicated as “UntoldR”.

Conflict of interest statement

The LUMC is owner of a pending patent on the use of *CRB2* gene therapy vectors (WO2015020522A1) and received license income and research funds from HORAMA. JW is full-term employee of LUMC and acts for LUMC as temporary consultant for HORAMA. JW is mentioned as an inventor on the patent application. TMB declares no conflict of interest.

Acknowledgments

We would like to thank Nanda Boon and Timo Oosenbrug for their input. This research was funded by Foundation Fighting Blindness [TA-GT-0715-0665-LUMC], The Netherlands Organization for Health Research and Development [43200004], Million Dollar Bike Ride Grant Program [MDBR-19-131-CRB1] and [MDBR-20-112-CRB1].

1.3 Aim and outline of this thesis

Chapter 1 reviews (a) the origin and models of *CRB1*-associated retinal dystrophy, (b) the current recombinant adeno-associated viral (rAAV) plasmid vectors in ocular clinical trials, (c) ubiquitous and retinal cell-specific promoters, (d) bioactivity assays, and (e) transgene assays.

Chapter 2 describes (a) the morphological phenotype and visual deficits of the *Crb1^{KO}Crb2^{LowMGC}* mouse (a *CRB1*-like retinitis pigmentosa mouse model) in which one *Crb2* allele is made nonfunctional in Müller glial cells on a *Crb1*-null genetic background and compared to *Crb1^{KO}* littermates, (b) a novel DL-AAA Müller glial-cell stress-induced *CRB1*-like RP mouse model, and (c) how rAAV-h*CRB2* and rAAV-h*CRB1* therapy to Müller cells protects against retinal degeneration but only rAAV-h*CRB2* protecting against vision deficits in the DL-AAA exposed *CRB1*-like retinitis pigmentosa mouse model.

In **Chapter 3** we developed and describe an assay where one can screen more than eight rAAV vectors in parallel from one human cadaver neuroretina which can be kept viable for 21 days *ex vivo*. Several rAAV-vectors require 3-4 weeks of incubation for maximal transgene expression but *ex vivo* human neuroretinal material tends to degenerate quickly. The described transgene expression assay can evaluate the tropism and potency on human tissue and provides tips&tricks in assay setup (such as controlling for photoreceptor outer segment presence during rAAV infection).

In **Chapter 4** we describe how CRB proteins are expressed in the developing human retina (foetal explants and human retinal organoids). We differentiated three human control induced pluripotent (hiPSC) lines and three *CRB1*-RP patient hiPSC lines to mature retinal organoids. The three patient lines developed vulcanic cell eruptions similar as seen in *CRB1*-like RP mouse models. We also screened three different rAAV capsids on tropism and potency on human retinal organoids *in vitro* and human cadaver neuroretinas *ex vivo*. The rAAV-vector potency assay indicated that rAAV serotype 5 capsids can efficiently infect the target cells of a rAAV-based gene supplementation therapy (human photoreceptors and Müller glial cells) outperforming rAAV9. Further, we show that the loss of outer segments may decrease the photoreceptor rAAV-infectivity.

Chapter 5 describes the development of isogenic hiPSC lines of two patient *CRB1* RP lines and how the *CRB1* RP phenotype develops in *CRB1*-RP retinal organoids over time after the onset of *CRB1* expression at the outer limiting membrane. We hypothesized that CRB1 variant protein may aggregate or be less efficiently shuttled to the outer limiting membrane. Interestingly, we found little variant CRB1 protein throughout the neuroretina in patient-derived retinal organoids. We show that (a) the decrease of CRB1 protein upregulates degradative protein markers (p62, LC3, LAMP1, ARL8A/B), (b) that the extracellular domain of CRB1 can interact with NOTCH1 which by large is lost in *CRB1* patient organoids, (c) a strong decrease of recycling endosomal marker RAB11A and an increase of early endosomes (EEA1+ particles), and (d) an increase of WDFY1 protein at the OLM/ONL. We propose that the decrease of CRB1 at the outer limiting membrane reduces the turnover of receptor recycling shifting early/late endosomes maturation towards degradation (lysosomes, autophagosomes).

Chapter 6 is a discussion of the thesis. **Chapter 7** includes a summary and the Nederlandse samenvatting, acknowledgements, curriculum vitae of the author of this thesis and a list of publications.

REFERENCES

1. Rodrigues, G.A.; Shalaev, E.; Karami, T.K.; Cunningham, J.; Slater, N.K.H.; Rivers, H.M. Pharmaceutical Development of AAV-Based Gene Therapy Products for the Eye. *Pharm. Res.* **2019**, *36*.
2. Boye, S.E.; Boye, S.L.; Lewin, A.S.; Hauswirth, W.W. A comprehensive review of retinal gene therapy. *Mol. Ther.* **2013**, *21*, 509–19.
3. Vandenberghe, L.H.; Wilson, J.M.; Gao, G. Tailoring the AAV vector capsid for gene therapy. *Gene Ther.* **2009**, *16*, 311–9.
4. Wang, D.; Tai, P.W.L.; Gao, G. Adeno-associated virus vector as a platform for gene therapy delivery. *Nat. Rev. Drug Discov.* **2019**, *18*, 358–378.
5. Cheever, T.R.; Berkley, D.; Braun, S.; Brown, R.H.; Byrne, B.J.; Chamberlain, J.S.; Cwik, V.; Duan, D.; Federoff, H.J.; High, K.A.; et al. Perspectives on Best Practices for Gene Therapy Programs. *Hum. Gene Ther.* **2015**, *26*, 127–133.
6. Lipinski, D.M.; Thake, M.; Maclaren, R.E. Clinical applications of retinal gene therapy. *Prog. Retin. Eye Res. Clin. Appl. Retin. gene Ther.* **2013**, *32*, 22–47.
7. McClements, M.E.; Maclaren, R.E. Gene therapy for retinal disease. *Transl. Res.* **2013**, *161*, 241–54.
8. Smith, A.J.; Bainbridge, J.W.; Ali, R.R. Prospects for retinal gene replacement therapy. *Trends Genet.* **2009**, *25*, 156–65.
9. Bainbridge, J.W.B.; Tan, M.H.; Ali, R.R. Gene therapy progress and prospects: the eye. *Gene Ther.* **2006**, *13*, 1191–7.
10. Duncan, J.L.; Pierce, E.A.; Laster, A.M.; Daiger, S.P.; Birch, D.G.; Ash, J.D.; Iannaccone, A.; Flannery, J.G.; Sahel, J.A.; Zack, D.J.; et al. Inherited retinal degenerations: Current landscape and knowledge gaps. *Transl. Vis. Sci. Technol.* **2018**, *7*.
11. Fahim, A.T.; Daiger, S.P.; Weleber, R.G. Nonsyndromic Retinitis Pigmentosa Overview Available online: <http://www.ncbi.nlm.nih.gov/pubmed/20301590> (accessed on Apr 14, 2020).
12. Waehler, R.; Russell, S.J.; Curriel, D.T. Engineering targeted viral vectors for gene therapy. *Nat. Rev. Genet.* **2007**, *8*, 573–87.
13. Ma, Y.; Bao, J.; Zhang, Y.; Li, Z.; Zhou, X.; Wan, C.; Huang, L.; Zhao, Y.; Han, G.; Xue, T. Mammalian Near-Infrared Image Vision through Injectable and Self-Powered Retinal Nanoantennae. *Cell* **2019**, *177*, 243–255.e15.
14. Ziccardi, L.; Cordeddu, V.; Gaddini, L.; Matteucci, A.; Parravano, M.; Malchiodi-Albedi, F.; Varano, M. Gene therapy in retinal dystrophies. *Int. J. Mol. Sci.* **2019**, *20*.
15. Zallocchi, M.; Binley, K.; Lad, Y.; Ellis, S.; Widdowson, P.; Iqbal, S.; Scripps, V.; Kelleher, M.; Loader, J.; Miskin, J.; et al. EIAV-based retinal gene therapy in the shaker1 mouse model for usher syndrome type 1B: Development of UshStat. *PLoS One* **2014**, *9*.
16. Truran, R.; Buckley, R.; Radcliffe, P.; Miskin, J.; Mitrophanous, K. Virus purification. Patent US9169491B2 2008, 1–18.
17. Payne, S.L.; Rausch, J.; Rushlow, K.; Montelaro, R.C.; Issel, C.; Flaherty, M.; Perry, S.; Sellon, D.; Fuller, F. Characterization of infectious molecular clones of equine infectious anaemia virus. *J. Gen. Virol.* **1994**, *75*, 425–429.
18. Kong, J.; Kim, S.-R.R.; Binley, K.; Pata, I.; Doi, K.; Mannik, J.; Zernant-Rajang, J.; Kan, O.; Iqbal, S.; Naylor, S.; et al. Correction of the disease phenotype in the mouse model of Stargardt disease by lentiviral gene therapy. *Gene Ther.* **2008**, *15*, 1311–20.
19. Vázquez-Domínguez, I.; Garanto, A.; Collin, R.W.J. Molecular Therapies for Inherited Retinal Diseases-Current Standing, Opportunities and Challenges. *Genes (Basel)*. **2019**, *10*.
20. Aschauer, D.F.; Kreuz, S.; Rumpel, S. Analysis of Transduction Efficiency, Tropism and Axonal Transport of AAV Serotypes 1, 2, 5, 6, 8 and 9 in the Mouse Brain. *PLoS One* **2013**, *8*.
21. Duong, T.T.; Lim, J.; Vasireddy, V.; Papp, T.; Nguyen, H.; Leo, L.; Pan, J.; Zhou, S.; Chen, I.; Bennett, J.; et al. Comparative AAV-EGFP transgene expression using vector serotypes 1–9, 7M8, and 8b in human pluripotent stem cells, RPEs, and human and rat cortical neurons. *Stem Cells Int.* **2019**, *2019*.
22. Gardiner, K.L.; Cideciyan, A. V.; Swider, M.; Dufour, V.L.; Sumaroka, A.; Komáromy, A.M.; Hauswirth, W.W.; Iwabe, S.; Jacobson, S.G.; Beltran, W.A.; et al. Long-term Structural Outcomes of Late-stage RPE65 Gene Therapy. *Mol. Ther.* **2020**, *28*, 266–278.
23. Schnepf, B.C.; Clark, K.R.; Klemanski, D.L.; Pacak, C.A.; Johnson, P.R. Genetic Fate of Recombinant Adeno-Associated Virus Vector Genomes in Muscle. *J. Virol.* **2003**, *77*, 3495–3504.
24. Pellissier, L.P.; Hoek, R.M.; Vos, R.M.; Aartsen, W.M.; Klimczak, R.R.; Hoyng, S.A.; Flannery, J.G.; Wijnholds, J. Specific tools for targeting and expression in Müller glial cells. *Mol. Ther. — Methods Clin. Dev.* **2014**, *1*, 14009.
25. Koerber, J.T.; Klimczak, R.; Jang, J.-H.H.; Dalkara, D.; Flannery, J.G.; Schaffer, D. V. Molecular evolution of adeno-associated virus for enhanced glial gene delivery. *Mol. Ther.* **2009**, *17*, 2088–95.
26. Pleticha, J.; Heilmann, L.F.; Evans, C.H.; Asokan, A.; Samulski, R.J.; Beutler, A.S. Preclinical toxicity evaluation of AAV for pain: Evidence from human AAV studies and from the pharmacology of analgesic drugs. *Mol. Pain* **2014**, *10*.

27. Calcedo, R.; Wilson, J.M. Humoral Immune Response to AAV. *Front. Immunol.* **2013**, *4*.
28. Tan, M.H.; Smith, A.J.; Pawlyk, B.; Xu, X.; Liu, X.; Bainbridge, J.B.; Basche, M.; McIntosh, J.; Tran, H.V.; Nathwani, A.; et al. Gene therapy for retinitis pigmentosa and Leber congenital amaurosis caused by defects in AIPL1: effective rescue of mouse models of partial and complete Aipl1 deficiency using AAV2/2 and AAV2/8 vectors. *Hum. Mol. Genet.* **2009**, *18*, 2099–114.
29. Francis, P.J. Genetics of inherited retinal disease. *J. R. Soc. Med.* **2006**, *99*, 189–91.
30. den Hollander, A.I.; Black, A.; Bennett, J.; Cremers, F.P.M. Lighting a candle in the dark: advances in genetics and gene therapy of recessive retinal dystrophies. *J. Clin. Invest.* **2010**, *120*, 3042–53.
31. Daiger, S.; Sullivan, L.; Bowne, S. RetNet Available online: <https://sph.uth.edu/retnet/sum-dis.htm#A-genes>.
32. Schachat, A.P.; Maumenee, I.H. Bardet-Biedl Syndrome and Related Disorders. *Arch. Ophthalmol.* **1982**, *100*, 285–288.
33. Bocquet, B.; Lacroux, A.; Surget, M.-O.; Baudoin, C.; Marquette, V.; Manes, G.; Hebrard, M.; Sénéchal, A.; Delettre, C.; Roux, A.-F.; et al. Relative frequencies of inherited retinal dystrophies and optic neuropathies in Southern France: assessment of 21-year data management. *Ophthalmic Epidemiol.* **2013**, *20*, 13–25.
34. Lei, B.; Zhang, K.; Yue, Y.; Ghosh, A.; Duan, D. Retinal Degenerative Diseases. **2010**, *664*, 671–678.
35. Bainbridge, J.W.B.; Smith, A.J.; Barker, S.S.; Robbie, S.; Henderson, R.; Balaggan, K.; Viswanathan, A.; Holder, G.E.; Stockman, A.; Tyler, N.; et al. Effect of gene therapy on visual function in Leber's congenital amaurosis. *N. Engl. J. Med.* **2008**, *358*, 2231–2239.
36. Georgiadis, A.; Duran, Y.; Ribeiro, J.; Abelleira-Hervas, L.; Robbie, S.J.; Sünkel-Laing, B.; Fourali, S.; Gonzalez-Cordero, A.; Cristante, E.; Michaelides, M.; et al. Development of an optimized AAV2/5 gene therapy vector for Leber congenital amaurosis owing to defects in RPE65. *Gene Ther.* **2016**, *23*, 857–862.
37. Maeder, M.L.; Bumcrot, D.A.; Shen, S. CRISPR/CAS-related methods and compositions for treating Leber's Congenital Amaurosis 10 (LCA10). Patent US10253312B 2014, 1–298.
38. Maeder, M.L.; Stefanidakis, M.; Wilson, C.J.; Baral, R.; Barrera, L.A.; Bounoutas, G.S.; Bumcrot, D.; Chao, H.; Ciulla, D.M.; DaSilva, J.A.; et al. Development of a gene-editing approach to restore vision loss in Leber congenital amaurosis type 10. *Nat. Med.* **2019**, *25*, 229–233.
39. Pellissier, L.P.; Quinn, P.M.; Henrique Alves, C.; Vos, R.M.; Klooster, J.; Flannery, J.G.; Alexander Heimel, J.; Wijnholds, J. Gene therapy into photoreceptors and Müller glial cells restores retinal structure and function in CRB1 retinitis pigmentosa mouse models. *Hum. Mol. Genet.* **2015**, *24*, 3104–3118.
40. Bennett, J. Gene Therapy for Leber's Congenital Amaurosis Due to RPE65 Mutations. In *Gene- and Cell-Based Treatment Strategies for the Eye*; Rakoczy, E.P., Ed.; Springer, Berlin, Heidelberg, 2015; pp. 9–25 ISBN 978-3-662-45187-8.
41. Yang, S.; Ma, S. qi; Wan, X.; He, H.; Pei, H.; Zhao, M. jian; Chen, C.; Wang, D. wen; Dong, X. yan; Yuan, J. jia; et al. Long-term outcomes of gene therapy for the treatment of Leber's hereditary optic neuropathy. *EBioMedicine* **2016**, *10*, 258–268.
42. Grishanin, R.; Vuilleminot, B.; Sharma, P.; Keravala, A.; Greengard, J.; Gelfman, C.; Blumenkrantz, M.; Lawrence, M.; Hu, W.; Kiss, S.; et al. Preclinical Evaluation of ADVDM-022, a Novel Gene Therapy Approach to Treating Wet Age-Related Macular Degeneration. *Mol. Ther.* **2019**, *27*, 118–129.
43. Ye, G.; Budzynski, E.; Sonnentag, P.; Nork, T.M.; Miller, P.E.; Sharma, A.K.; Ver Hoeve, J.N.; Smith, L.M.; Arndt, T.; Calcedo, R.; et al. Safety and Biodistribution Evaluation in Cynomolgus Macaques of rAAV2tYF-PR1.7-hCNGB3, a Recombinant AAV Vector for Treatment of Achromatopsia. *Hum. Gene Ther. Clin. Dev.* **2016**, *27*, 37–48.
44. Song, C.; Conlon, T.J.; Deng, W.T.; Coleman, K.E.; Zhu, P.; Plummer, C.; Mandapati, S.; Van Hoosear, M.; Green, K.B.; Sonnentag, P.; et al. Toxicology and pharmacology of an AAV vector expressing codon-optimized RPGR in RPGR-deficient Rd9 mice. *Hum. Gene Ther. Clin. Dev.* **2018**, *29*, 188–197.
45. Rumachik, N.G.; Malaker, S.A.; Poweleit, N.; Maynard, L.H.; Adams, C.M.; Leib, R.D.; Cirolia, G.; Thomas, D.; Stamnes, S.; Holt, K.; et al. Methods Matter -- Standard Production Platforms For Recombinant AAV Can Produce Chemically And Functionally Distinct Vectors. *bioRxiv* **2019**, 640169.
46. Smale, S.T.; Kadonaga, J.T. The RNA Polymerase II Core Promoter. *Annu. Rev. Biochem.* **2003**, *72*, 449–479.
47. Chanda, D.; Hensel, J.A.; Higgs, J.T.; Grover, R.; Kaza, N.; Ponnazhagan, S. Effects of cellular methylation on transgene expression and site-specific integration of adeno-associated virus. *Genes (Basel)*. **2017**, *8*.
48. Faust, S.M.; Bell, P.; Cutler, B.J.; Ashley, S.N.; Zhu, Y.; Rabinowitz, J.E.; Wilson, J.M. CpG-depleted adeno-associated virus vectors evade immune detection. *J. Clin. Invest.* **2013**, *123*, 2994–3001.
49. Even, D.Y.; Kedmi, A.; Basch-Barzilay, S.; Ideses, D.; Tikotzki, R.; Shir-Shapira, H.; Shefi, O.; Juven-Gershon, T. Engineered promoters for potent transient overexpression. *PLoS One* **2016**, *11*.
50. Hartl, D.; Schübeler, D.; Roska, B.; Krebs, A.; Jüttner, J. Synp161, a promoter for the specific expression of genes in rod photoreceptors. Patent WO2017093935A1 2015, 1–26.
51. Jüttner, J.; Szabo, A.; Gross-Scherf, B.; Morikawa, R.K.; Rompani, S.B.; Hantz, P.; Szikra, T.; Esposti, F.; Cowan, C.S.; Bharioke, A.; et al. Targeting neuronal and glial cell types with synthetic promoter AAVs in mice, non-human primates and humans. *Nat. Neurosci.* **2019**, *22*, 1345–1356.

52. Crémisi, C.; Pignatti, P.F.; Yaniv, M. Random location and absence of movement of the nucleosomes on SV 40 nucleoprotein complex isolated from infected cells. *Biochem. Biophys. Res. Commun.* **1976**, *73*, 548–554.
53. Okada, T.; Uchibori, R.; Iwata-Okada, M.; Takahashi, M.; Nomoto, T.; Nonaka-Sarukawa, M.; Ito, T.; Liu, Y.; Mizukami, H.; Kume, A.; et al. A histone deacetylase inhibitor enhances recombinant adeno-associated virus-mediated gene expression in tumor cells. *Mol. Ther.* **2006**, *13*, 738–46.
54. Crémisi, C.; Chestier, A.; Yaniv, M. Preferential association of newly synthesized histones with replicating SV40 DNA. *Cell* **1977**, *12*, 947–951.
55. Mano, M.; Ippodrino, R.; Zentilin, L.; Zacchigna, S.; Giacca, M. Genome-wide RNAi screening identifies host restriction factors critical for in vivo AAV transduction. *Proc. Natl. Acad. Sci. U. S. A.* **2015**, *112*, 11276–11281.
56. Provost, N.; Le Meur, G.; Weber, M.; Mendes-Madeira, A.; Podevin, G.; Cherel, Y.; Colle, M.A.; Deschamps, J.Y.; Moullier, P.; Rolling, F. Biodistribution of rAAV vectors following intraocular administration: Evidence for the presence and persistence of vector DNA in the optic nerve and in the brain. *Mol. Ther.* **2005**, *11*, 275–283.
57. Xu, L.; Daly, T.; Gao, C.; Flotte, T.R.; Song, S.; Byrne, B.J.; Sands, M.S.; Parker Ponder, K. CMV-beta-actin promoter directs higher expression from an adeno-associated viral vector in the liver than the cytomegalovirus or elongation factor 1 alpha promoter and results in therapeutic levels of human factor X in mice. *Hum. Gene Ther.* **2001**, *12*, 563–73.
58. Miyazaki, M.; Ikeda, Y.; Yonemitsu, Y.; Goto, Y.; Sakamoto, T.; Tabata, T.; Ueda, Y.; Hasegawa, M.; Tobimatsu, S.; Ishibashi, T.; et al. Simian lentiviral vector-mediated retinal gene transfer of pigment epithelium-derived factor protects retinal degeneration and electrical defect in Royal College of Surgeons rats. *Gene Ther.* **2003**, *10*, 1503–11.
59. Gilham, D.E.; Lie-A-Ling, M.; Taylor, N.; Hawkins, R.E. Cytokine stimulation and the choice of promoter are critical factors for the efficient transduction of mouse T cells with HIV-1 vectors. *J. Gene Med.* **2010**, *12*, 129–136.
60. Gray, S.J.; Foti, S.B.; Schwartz, J.W.; Bachaboina, L.; Taylor-Blake, B.; Coleman, J.; Ehlers, M.D.; Zylka, M.J.; McCown, T.J.; Samulski, R.J. Optimizing promoters for recombinant adeno-associated virus-mediated gene expression in the peripheral and central nervous system using self-complementary vectors. *Hum. Gene Ther.* **2011**, *22*, 1143–53.
61. Ohlfest, J.R.; Frandsen, J.L.; Fritz, S.; Lobitz, P.D.; Perkinson, S.G.; Clark, K.J.; Nelsestuen, G.; Key, N.S.; McIvor, R.S.; Hackett, P.B.; et al. Phenotypic correction and long-term expression of factor VIII in hemophilic mice by immunotolerization and nonviral gene transfer using the Sleeping Beauty transposon system. *Blood* **2005**, *105*, 2691–8.
62. McCown, T.J.; Xiao, X.; Li, J.; Breese, G.R.; Samulski, R.J. Differential and persistent expression patterns of CNS gene transfer by an adeno-associated virus (AAV) vector. *Brain Res.* **1996**, *713*, 99–107.
63. Powell, S.K.; Rivera-Soto, R.; Gray, S.J. Viral expression cassette elements to enhance transgene target specificity and expression in gene therapy. *Discov. Med.* **2015**, *19*, 49–57.
64. Klein, R.L.; Meyer, E.M.; Peel, A.L.; Zolotukhin, S.; Meyers, C.; Muzyczka, N.; King, M.A. Neuron-specific transduction in the rat septohippocampal or nigrostriatal pathway by recombinant adeno-associated virus vectors. *Exp. Neurol.* **1998**, *150*, 183–94.
65. Farjo, R.; Skaggs, J.; Quiambao, A.B.; Cooper, M.J.; Naash, M.I. Efficient non-viral ocular gene transfer with compacted DNA nanoparticles. *PLoS One* **2006**, *1*.
66. Pellissier, L.P.; Quinn, P.M.; Henrique Alves, C.; Vos, R.M.; Klooster, J.; Flannery, J.G.; Alexander Heimel, J.; Wijnholds, J. Gene therapy into photoreceptors and Müller glial cells restores retinal structure and function in CRB1 retinitis pigmentosa mouse models. *Hum. Mol. Genet.* **2015**, *24*, 3104–3118.
67. Tsai, Y.T.; Wu, W.H.; Lee, T.T.; Wu, W.P.; Xu, C.L.; Park, K.S.; Cui, X.; Justus, S.; Lin, C.S.; Jauregui, R.; et al. Clustered Regularly Interspaced Short Palindromic Repeats-Based Genome Surgery for the Treatment of Autosomal Dominant Retinitis Pigmentosa. *Ophthalmology* **2018**, *125*, 1421–1430.
68. Quinn, P.M.; Buck, T.M.; Mulder, A.A.; Ohonin, C.; Alves, C.H.; Vos, R.M.; Bialecka, M.; van Herwaarden, T.; van Dijk, E.H.C.C.; Talib, M.; et al. Human iPSC-Derived Retinas Recapitulate the Fetal CRB1 CRB2 Complex Formation and Demonstrate that Photoreceptors and Müller Glia Are Targets of AAV5. *Stem Cell Reports* **2019**, *12*, 906–919.
69. Niwa, H.; Yamamura, K.; Miyazaki, J. Efficient selection for high-expression transfectants with a novel eukaryotic vector. *Gene* **1991**, *108*, 193–199.
70. Wang, Z.; Ma, H.-I.; Li, J.; Sun, L.; Zhang, J.; Xiao, X. Rapid and highly efficient transduction by double-stranded adeno-associated virus vectors in vitro and in vivo. *Gene Ther.* **2003**, *10*, 2105–11.
71. Sawicki, J.A.; Morris, R.J.; Monks, B.; Sakai, K.; Miyazaki, J. SHORT NOTE A Composite CMV-IE Enhancer / \square - Actin Promoter Is Ubiquitously Expressed in Mouse Cutaneous Epithelium. **1998**, *369*, 367–369.
72. Koilkonda, R.; Yu, H.; Talla, V.; Porciatti, V.; Feuer, W.J.; Hauswirth, W.W.; Chiodo, V.; Erger, K.E.; Boye, S.L.; Lewin, A.S.; et al. LHON gene therapy vector prevents visual loss and optic neuropathy induced by G11778A mutant mitochondrial DNA: Biodistribution and toxicology profile. *Investig. Ophthalmol. Vis. Sci.* **2014**, *55*, 7739–7753.
73. Bobo, R.H.; Laske, D.W.; Akbasak, a; Morrison, P.F.; Dedrick, R.L.; Oldfield, E.H. Convection-enhanced delivery of macromolecules in the brain. *Proc. Natl. Acad. Sci. U. S. A.* **1994**, *91*, 2076–80.

74. Rastegar, M.; Hotta, A.; Pasceri, P.; Makarem, M.; Cheung, A.Y.L.; Elliott, S.; Park, K.J.; Adachi, M.; Jones, F.S.; Clarke, I.D.; et al. MECP2 isoform-specific vectors with regulated expression for Rett syndrome gene therapy. *PLoS One* **2009**, *4*, e6810.
75. Li, C.; Hirsch, M.; Carter, P.; Asokan, A.; Zhou, X.; Wu, Z.; Samulski, R.J. A small regulatory element from chromosome 19 enhances liver-specific gene expression. *Gene Ther.* **2009**, *16*, 43–51.
76. Gill, D.R.; Smyth, S.E.; Goddard, C.A.; Pringle, I.A.; Higgins, C.F.; Colledge, W.H.; Hyde, S.C. Increased persistence of lung gene expression using plasmids containing the ubiquitin C or elongation factor 1alpha promoter. *Gene Ther.* **2001**, *8*, 1539–46.
77. Lu, Y.; Krishnan, A.; Brommer, B.; Tian, X.; Meer, M.; Vera, D.L.; Wang, C.; Zeng, Q.; Yu, D.; Bonkowski, M.S.; et al. Reversal of ageing- and injury-induced vision loss by Tet-dependent epigenetic reprogramming. *bioRxiv* **2019**, 710210.
78. Bochkov, Y.A.; Palmenberg, A.C. Translational efficiency of EMCV IRES in bicistronic vectors is dependent upon IRES sequence and gene location. *Biotechniques* **2006**, *41*, 283–292.
79. Attal, J.; Theron, M.C.; Puissant, C.; Houdebine, L.M. Effect of intercistronic length on internal ribosome entry site (IRES) efficiency in bicistronic mRNA. *Gene Expr.* **1999**, *8*, 299–309.
80. Al-Allaf, F.A.; Abduljaleel, Z.; Athar, M.; Taher, M.M.; Khan, W.; Mehmet, H.; Colakogullari, M.; Apostolidou, S.; Bigger, B.; Waddington, S.; et al. Modifying inter-cistronic sequence significantly enhances IRES dependent second gene expression in bicistronic vector: Construction of optimised cassette for gene therapy of familial hypercholesterolemia. *Non-coding RNA Res.* **2019**, *4*, 1–14.
81. Fagoe, N.D.; Eggers, R.; Verhaagen, J.; Mason, M.R.J. A compact dual promoter adeno-associated viral vector for efficient delivery of two genes to dorsal root ganglion neurons. *Gene Ther.* **2014**, *21*, 242–52.
82. Osakada, F.; Takahashi, M. Challenges in retinal circuit regeneration: Linking neuronal connectivity to circuit function. *Biol. Pharm. Bull.* **2015**, *38*, 341–357.
83. Tervo, D.G.R.; Hwang, B.Y.; Viswanathan, S.; Gaj, T.; Lavzin, M.; Ritola, K.D.; Lindo, S.; Michael, S.; Kuleshova, E.; Ojala, D.; et al. A Designer AAV Variant Permits Efficient Retrograde Access to Projection Neurons. *Neuron* **2016**, *92*, 372–382.
84. Dana, H.; Sun, Y.; Mohar, B.; Hulse, B.K.; Kerlin, A.M.; Hasseman, J.P.; Tsegaye, G.; Tsang, A.; Wong, A.; Patel, R.; et al. High-performance calcium sensors for imaging activity in neuronal populations and microcompartments. *Nat. Methods* **2019**, *16*, 649–657.
85. Nickells, R.W.; Schmitt, H.M.; Maes, M.E.; Schlamp, C.L. AAV2-mediated transduction of the mouse retina after optic nerve injury. *Investig. Ophthalmol. Vis. Sci.* **2017**, *58*, 6091–6104.
86. Garanto, A. RNA-Based Therapeutic Strategies for Inherited Retinal Dystrophies. *Adv. Exp. Med. Biol.* **2019**, *1185*, 71–77.
87. Ren, R.; Li, Y.; Liu, Z.; Liu, K.; He, S. Long-term rescue of rat retinal ganglion cells and visual function by AAV-mediated BDNF expression after acute elevation of intraocular pressure. *Investig. Ophthalmol. Vis. Sci.* **2012**, *53*, 1003–1011.
88. LeVaillant, C.J.; Sharma, A.; Muhling, J.; Wheeler, L.P.; Cozens, G.S.; Hellström, M.; Rodger, J.; Harvey, A.R. Significant changes in endogenous retinal gene expression assessed 1 year after a single intraocular injection of AAV-CNTF or AAV-BDNF. *Mol. Ther. - Methods Clin. Dev.* **2016**, *3*, 16078.
89. Lau, D.; McGee, L.H.; Zhou, S.; Rendahl, K.G.; Manning, W.C.; Escobedo, J. a; Flannery, J.G. Retinal degeneration is slowed in transgenic rats by AAV-mediated delivery of FGF-2. *Invest. Ophthalmol. Vis. Sci.* **2000**, *41*, 3622–33.
90. Leaver, S.G.; Cui, Q.; Plant, G.W.; Arulpragasam, A.; Hisheh, S.; Verhaagen, J.; Harvey, A.R. AAV-mediated expression of CNTF promotes long-term survival and regeneration of adult rat retinal ganglion cells. *Gene Ther.* **2006**, *13*, 1328–1341.
91. Dalkara, D.; Kolstad, K.D.; Guerin, K.I.; Hoffmann, N. V.; Visel, M.; Klimczak, R.R.; Schaffer, D. V.; Flannery, J.G. AAV mediated GDNF secretion from retinal glia slows down retinal degeneration in a rat model of retinitis pigmentosa. *Mol. Ther.* **2011**, *19*, 1602–8.
92. Grimm, D.; Streetz, K.L.; Jopling, C.L.; Storm, T.A.; Pandey, K.; Davis, C.R.; Marion, P.; Salazar, F.; Kay, M.A. Fatality in mice due to oversaturation of cellular microRNA/short hairpin RNA pathways. *Nature* **2006**, *441*, 537–541.
93. Vázquez-Chona, F.R.; Clark, A.M.; Levine, E.M. Rlbp1 promoter drives robust Müller glial GFP expression in transgenic mice. *Invest. Ophthalmol. Vis. Sci.* **2009**, *50*, 3996–4003.
94. Hanlon, K.S.; Chadderton, N.; Palfi, A.; Fernandez, A.B.; Humphries, P.; Kenna, P.F.; Millington-Ward, S.; Farrar, G.J. A novel retinal ganglion cell promoter for utility in AAV vectors. *Front. Neurosci.* **2017**, *11*.
95. Khani, S.C.; Pawlyk, B.S.; Bulgakov, O. V.; Kasperek, E.; Young, J.E.; Adamian, M.; Sun, X.; Smith, A.J.; Ali, R.R.; Li, T. AAV-mediated expression targeting of rod and cone photoreceptors with a human rhodopsin kinase promoter. *Invest. Ophthalmol. Vis. Sci.* **2007**, *48*, 3954–61.
96. Hebbard, L.; Steffen, A.; Zawadzki, V.; Fieber, C.; Howells, N.; Moll, J.; Ponta, H.; Hofmann, M.; Sleeman, J. CD44 expression and regulation during mammary gland development and function. *J. Cell Sci.* **2000**, *113* (Pt 14), 2619–30.

97. Su, M.; Hu, H.; Lee, Y.; D'Azzo, A.; Messing, A.; Brenner, M. Expression Specificity of GFAP Transgenes. *Neurochem. Res.* **2004**, *29*, 2075–93.
98. Prentice, H.M.; Biswal, M.R.; Dorey, C.K.; Blanks, J.C. Hypoxia-regulated retinal glial cell-specific promoter for potential gene therapy in disease. *Invest. Ophthalmol. Vis. Sci.* **2011**, *52*, 8562–70.
99. Kim, D.S.; Matsuda, T.; Cepko, C.L. A core paired-type and POU homeodomain-containing transcription factor program drives retinal bipolar cell gene expression. *J. Neurosci.* **2008**, *28*, 7748–7764.
100. Aartsen, W.M.; van Cleef, K.W.R.R.; Pellissier, L.P.; Hoek, R.M.; Vos, R.M.; Blits, B.; Ehlert, E.M.E.E.; Balaggan, K.S.; Ali, R.R.; Verhaagen, J.; et al. GFAP-driven GFP expression in activated mouse Müller glial cells aligning retinal blood vessels following intravitreal injection of AAV2/6 vectors. *PLoS One* **2010**, *5*, e12387.
101. Dorrell, M.I.; Aguilar, E.; Jacobson, R.; Yanes, O.; Gariano, R.; Heckenlively, J.; Banin, E.; Ramirez, G.A.; Gasmi, M.; Bird, A.; et al. Antioxidant or neurotrophic factor treatment preserves function in a mouse model of neovascularization-associated oxidative stress. *J. Clin. Invest.* **2009**, *119*, 611–623.
102. Choi, V.; Bigelow, C.E.; Dryja, T.P.; Reddy POLICE, S. Viral vectors for the treatment of retinal dystrophy. Patent US9163259B2 2012, 1–173.
103. Dougherty, C.J.; Smith, G.W.; Dorey, C.K.; Prentice, H.M.; Webster, K.A.; Blanks, J.C. Robust hypoxia-selective regulation of a retinal pigment epithelium-specific adeno-associated virus vector. *Mol. Vis.* **2008**, *14*, 471–80.
104. Foster, L.C.; WIESEL, P.; HUGGINS, G.S.; PAÑARES, R.; CHIN, M.T.; PELLACANI, A.; PERRELLA, M.A. Role of activating protein-1 and high mobility group-I(Y) protein in the induction of CD44 gene expression by interleukin-1 β in vascular smooth muscle cells. *FASEB J.* **2000**, *14*, 368–378.
105. Ichsan, A.M.; Kato, I.; Yoshida, T.; Takasawa, K.; Hayasaka, S.; Hiraga, K. Rhodopsin promoter-EGFP fusion transgene expression in photoreceptor neurons of retina and pineal complex in mice. *Neurosci. Lett.* **2005**, *379*, 138–143.
106. Allocchio, M.; Mussolino, C.; Garcia-Hoyos, M.; Sanges, D.; Iodice, C.; Petrillo, M.; Vandenberghe, L.H.; Wilson, J.M.; Marigo, V.; Surace, E.M.; et al. Novel adeno-associated virus serotypes efficiently transduce murine photoreceptors. *J. Virol.* **2007**, *81*, 11372–80.
107. Komáromy, a M.; Alexander, J.J.; Cooper, a E.; Chiodo, V.A.; Glushakova, L.G.; Acland, G.M.; Hauswirth, W.W.; Aguirre, G.D. Targeting gene expression to cones with human cone opsin promoters in recombinant AAV. *Gene Ther.* **2008**, *15*, 1049–55.
108. Quiambao, A.B.; Peachey, N.S.; Mangini, N.J.; Röhlich, P.; Hollyfield, J.G.; Al-Ubaidi, M.R. A 221-bp fragment of the mouse opsin promoter directs expression specifically to the rod photoreceptors of transgenic mice. *Vis. Neurosci.* **1997**, *14*, 617–25.
109. Young, J.E. A Short, Highly Active Photoreceptor-Specific Enhancer/Promoter Region Upstream of the Human Rhodopsin Kinase Gene. *Invest. Ophthalmol. Vis. Sci.* **2003**, *44*, 4076–4085.
110. Sun, X.; Pawlyk, B.; Xu, X.; Liu, X.; Bulgakov, O. V.; Adamian, M.; Sandberg, M. a; Khani, S.C.; Tan, M.-H.; Smith, A.J.; et al. Gene therapy with a promoter targeting both rods and cones rescues retinal degeneration caused by AIP1L1 mutations. *Gene Ther.* **2010**, *17*, 117–31.
111. Beltran, W.A.; Cideciyan, A. V; Boye, S.E.; Ye, G.-J.; Iwabe, S.; Dufour, V.L.; Marinho, L.F.; Swider, M.; Kosyk, M.S.; Sha, J.; et al. Optimization of Retinal Gene Therapy for X-Linked Retinitis Pigmentosa Due to RPGR Mutations. *Mol. Ther.* **2017**, *25*, 1866–1880.
112. Pang, J.; Deng, W.-T.; Dai, X.; Lei, B.; Everhart, D.; Umino, Y.; Li, J.; Zhang, K.; Mao, S.; Boye, S.L.; et al. AAV-mediated cone rescue in a naturally occurring mouse model of CNGA3-achromatopsia. *PLoS One* **2012**, *7*, e35250.
113. Glushakova, L.G.; Timmers, A.M.; Pang, J.; Teusner, J.T.; Hauswirth, W.W. Human blue-opsin promoter preferentially targets reporter gene expression to rat s-cone photoreceptors. *Invest. Ophthalmol. Vis. Sci.* **2006**, *47*, 3505–13.
114. Michalakos, S.; Mühlfriedel, R.; Tanimoto, N.; Krishnamoorthy, V.; Koch, S.; Fischer, M.D.; Becirovic, E.; Bai, L.; Huber, G.; Beck, S.C.; et al. Restoration of cone vision in the CNGA3 $^{-/-}$ mouse model of congenital complete lack of cone photoreceptor function. *Mol. Ther.* **2010**, *18*, 2057–63.
115. Beltran, W.A.; Cideciyan, A. V; Lewin, A.S.; Iwabe, S.; Khanna, H.; Sumaroka, A. Gene therapy rescues photoreceptor blindness in dogs and paves the way for treating human X-linked retinitis pigmentosa. *PNAS* **2012**, *106*, 1–6.
116. Dyka, F.; Boye, S.; Ryals, R.; Chiodo, V.; Boye, S.; Hauswirth, W. Cone specific promoter for use in gene therapy of retinal degenerative diseases. *Adv Exp Med Biol* **2014**, *801*, 695–701.
117. Pickrell, S.W.; Zhu, X.; Wang, X.; Craft, C.M. Deciphering the contribution of known cis-elements in the mouse cone arrestin gene to its cone-specific expression. *Invest. Ophthalmol. Vis. Sci.* **2004**, *45*, 3877–84.
118. Li, Q.; Timmers, A.M.; Guy, J.; Pang, J.; Hauswirth, W.W. Cone-specific expression using a human red opsin promoter in recombinant AAV. *Vision Res.* **2008**, *48*, 332–8.
119. Georgiadis, A.; Matsuki, T.; Rizzi, M.; Hoke, J.; Gonzalez-Cordero, A.; Sampson, R.; Bainbridge, J.; Smith, A.; Ali, R. ARVO Annual Meeting Poster A197 Development and efficacy assessment of AAV2/8-hG1.7p.coCNGA3, a CNGA3 gene therapy vector. *Invest. Ophthalmol. Vis. Sci.* **2019**, *60*, 3426.

120. Rizzi, M.; Ali, R.; Smith, A.; Nishiguchi, K. Gene therapy to improve vision. Patent US20180030477A1 2015, 1–66.
121. Forbes, A. *United States Securities and exchange commission (SEC) Form S-1 registration statement MeiraGTx Holdings plc*; Washington, D.C. 2018;
122. Watanabe, S.; Sanuki, R.; Ueno, S.; Koyasu, T.; Hasegawa, T.; Furukawa, T. Tropisms of AAV for Subretinal Delivery to the Neonatal Mouse Retina and Its Application for In Vivo Rescue of Developmental Photoreceptor Disorders. *PLoS One* **2013**, *8*.
123. Horsager, A.; Smith, A.; Matteo, B.C. Modulation neural pathways 2010, 1–44.
124. Lu, Q.; Ganjawala, T.H.; Ivanova, E.; Cheng, J.G.; Troilo, D.; Pan, Z.H. AAV-mediated transduction and targeting of retinal bipolar cells with improved mGluR6 promoters in rodents and primates. *Gene Ther.* **2016**, *23*, 680–689.
125. Glover, C.P.J.; Bienemann, A.S.; Heywood, D.J.; Cosgrave, A.S.; Uney, J.B. Adenoviral-mediated, high-level, cell-specific transgene expression: A SYN1-WPRE cassette mediates increased transgene expression with no loss of neuron specificity. *Mol. Ther.* **2002**, *5*, 509–516.
126. Dalkara, D.; Picaud, S.; Desrosiers, M.; Sahel, J.-A.; Duebel, J.; Bemelmans, A.; Roska, B. Promoters and uses thereof. Patent US2018035534A1 2015, 1–37.
127. Simpson, E.M.; Korecki, A.J.; Fomes, O.; McGill, T.J.; Cueva-Vargas, J.L.; Agostinone, J.; Farkas, R.A.; Hickmott, J.W.; Lam, S.L.; Mathelier, A.; et al. New MiniPromoter Ple345 (NEFL) drives strong and specific expression in retinal ganglion cells of mouse and primate retina. *Hum. Gene Ther.* **2019**, *30*, 257–272.
128. Ali, R.R.; Bainbridge, J.W.B.; Smith, A.J. Devices and methods for delivering polynucleotides into retinal cells of the macula and fovea. Patent US20100081707A1 2008, 1–58.
129. Maddalena, A.; Tornabene, P.; Tiberi, P.; Minopoli, R.; Manfredi, A.; Mutarelli, M.; Rossi, S.; Simonelli, F.; Naggert, J.K.; Cacchiarelli, D.; et al. Triple Vectors Expand AAV Transfer Capacity in the Retina. *Mol. Ther.* **2018**, *26*, 524–541.
130. Jüttner, J.; Krol, J.; Roska, B. Synpiii, a promoter for the specific expression of genes in retinal pigment epithelium. Patent WO2019106035A1 2017, 1–30.
131. Mäkinen, P.I.; Koponen, J.K.; Kärkkäinen, A.M.; Malm, T.M.; Pulkkinen, K.H.; Koistinaho, J.; Turunen, M.P.; Ylä-Herttuala, S. Stable RNA interference: Comparison of U6 and H1 promoters in endothelial cells and in mouse brain. *J. Gene Med.* **2006**, *8*, 433–441.
132. Gao, Z.; Harwig, A.; Berkhout, B.; Herrera-Carrillo, E. Mutation of nucleotides around the +1 position of type 3 polymerase III promoters: The effect on transcriptional activity and start site usage. *Transcription* **2017**, *8*, 275–287.
133. Grimm, D.; Streetz, K.L.; Jopling, C.L.; Storm, T.A.; Pandey, K.; Davis, C.R.; Marion, P.; Salazar, F.; Kay, M.A. Fatality in mice due to oversaturation of cellular microRNA/short hairpin RNA pathways. *Nature* **2006**, *441*, 537–541.
134. Ong, S.T.; Li, F.; Du, J.; Tan, Y.W.; Wang, S. Hybrid cytomegalovirus enhancer-h1 promoter-based plasmid and baculovirus vectors mediate effective RNA interference. *Hum. Gene Ther.* **2005**, *16*, 1404–12.
135. Eckenfelder, A.; Tordo, J.; Babbs, A.; Davies, K.E.; Goyenvalle, A.; Danos, O. The Cellular Processing Capacity Limits the Amounts of Chimeric U7 snRNA Available for Antisense Delivery. *Mol. Ther. Nucleic Acids* **2012**, *1*, e31.
136. Salva, M.Z.; Hameda, C.L.; Tai, P.W.; Nishiuchi, E.; Gregorevic, P.; Allen, J.M.; Finn, E.E.; Nguyen, Q.G.; Blankinship, M.J.; Meuse, L.; et al. Design of tissue-specific regulatory cassettes for high-level rAAV-mediated expression in skeletal and cardiac muscle. *Mol. Ther.* **2007**, *15*, 320–9.
137. LaVail, M.M.; Yasumura, D.; Matthes, M.T.; Drenser, K. a; Flannery, J.G.; Lewin, a S.; Hauswirth, W.W. Ribozyme rescue of photoreceptor cells in P23H transgenic rats: long-term survival and late-stage therapy. *Proc. Natl. Acad. Sci. U. S. A.* **2000**, *97*, 11488–93.
138. Xu, L.; Zhao, L.; Gao, Y.; Xu, J.; Han, R. Empower multiplex cell and tissue-specific CRISPR-mediated gene manipulation with self-cleaving ribozymes and tRNA. *Nucleic Acids Res.* **2017**, *45*.
139. Patrício, M.I.; Barnard, A.R.; Orlans, H.O.; McClements, M.E.; MacLaren, R.E. Inclusion of the Woodchuck Hepatitis Virus Posttranscriptional Regulatory Element Enhances AAV2-Driven Transduction of Mouse and Human Retina. *Mol. Ther. - Nucleic Acids* **2017**, *6*, 198–208.
140. Choi, J.-H.; Yu, N.-K.; Baek, G.-C.; Bakes, J.; Seo, D.; Nam, H.J.; Baek, S.H.; Lim, C.-S.; Lee, Y.-S.; Kaang, B.-K. Optimization of AAV expression cassettes to improve packaging capacity and transgene expression iChoi J-H, Yu N-K, Baek G-C, Bakes J, Seo D, Nam HJ, Baek SH, Lim C-S, Lee Y-S, Kaang B-K. 2014. Optimization of AAV expression cassettes to improve packaging . *Mol. Brain* **2014**, *7*, 17.
141. Michalakis, S.; Biel, M.; Seeliger, M.; Schoen, C. Gene therapy for the treatment of a retinal degeneration disease. Patent US20180353620A1 2016, 1–20.
142. Ramezani, A.; Hawley, T.S.; Hawley, R.G. Lentiviral vectors for enhanced gene expression in human hematopoietic cells. *Mol. Ther.* **2000**, *2*, 458–469.
143. Lai, Y.; Yue, Y.; Liu, M.; Duan, D. Synthetic intron improves transduction efficiency of trans-splicing adeno-associated viral vectors. *Hum. Gene Ther.* **2006**, *17*, 1036–42.

144. Wu, Z.; Sun, J.; Zhang, T.; Yin, C.; Yin, F.; Van Dyke, T.; Samulski, R.J.; Monahan, P.E. Optimization of self-complementary AAV vectors for liver-directed expression results in sustained correction of hemophilia B at low vector dose. *Mol. Ther.* **2008**, *16*, 280–289.
145. Lu, J.; Williams, J.A.; Luke, J.; Zhang, F.; Chu, K.; Kay, M.A. A 5' noncoding exon containing engineered intron enhances transgene expression from recombinant AAV vectors in vivo. *Hum. Gene Ther.* **2017**, *28*, 125–134.
146. Karali, M.; Manfredi, A.; Puppo, A.; Marrocco, E.; Gargiulo, A.; Allocca, M.; de Corte, M.; Rossi, S.; Giunti, M.; Bacci, M.L.; et al. MicroRNA-Restricted transgene expression in the retina. *PLoS One* **2011**, *6*.
147. Askou, A.L.; Alsing, S.; Benckendorff, J.N.E.; Holmgaard, A.; Mikkelsen, J.G.; Aagaard, L.; Bek, T.; Corydon, T.J. Suppression of Choroidal Neovascularization by AAV-Based Dual-Acting Antiangiogenic Gene Therapy. *Mol. Ther. - Nucleic Acids* **2019**, *16*, 38–50.
148. Brown, B.D.; Cantore, A.; Annoni, A.; Sergi, L.S.; Lombardo, A.; Della Valle, P.; D'Angelo, A.; Naldini, L. A microRNA-regulated lentiviral vector mediates stable correction of hemophilia B mice. *Blood* **2007**, *110*, 4144–52.
149. Xie, J.; Mao, Q.; Tai, P.W.L.; He, R.; Ai, J.; Su, Q.; Zhu, Y.; Ma, H.; Li, J.; Gong, S.; et al. Short DNA Hairpins Compromise Recombinant Adeno-Associated Virus Genome Homogeneity. *Mol. Ther.* **2017**, *25*, 1363–1374.
150. Domenger, C.; Grimm, D. Next-generation AAV vectors—do not judge a virus (only) by its cover. *Hum. Mol. Genet.* **2019**, *28*, R3–R14.
151. Tian, W.; Dong, X.; Liu, X.; Wang, G.; Dong, Z.; Shen, W.; Zheng, G.; Lu, J.; Chen, J.; Wang, Y.; et al. High-Throughput Functional MicroRNAs Profiling by Recombinant AAV-Based MicroRNA Sensor Arrays. *PLoS One* **2012**, *7*, e29551.
152. Yew, N.S.; Wysokenski, D.M.; Wang, K.X.; Ziegler, R.J.; Marshall, J.; McNeilly, D.; Cherry, M.; Osburn, W.; Cheng, S.H. Optimization of plasmid vectors for high-level expression in lung epithelial cells. *Hum. Gene Ther.* **1997**, *8*, 575–84.
153. Donello, J.E.; Loeb, J.E.; Hope, T.J. Woodchuck hepatitis virus contains a tripartite posttranscriptional regulatory element. *J. Virol.* **1998**, *72*, 5085–92.
154. Ronzitti, G.; Collaud, F.; Bortolussi, G.; Charles, S.; Vidal, P.; Sola, M.S.; Muro, A.; Mingozzi, F. Cryptic ATG Removal from Synthetic Introns Increase the Therapeutic Efficacy of AAV Vector Mediated Gene Transfer. *Mol. Ther.* **2016**, *24*, S62.
155. Choi, V.W.; Bigelow, C.E.; McGee, T.L.; Gujar, A.N.; Li, H.; Hanks, S.M.; Vrovljanis, J.; Maker, M.; Leehy, B.; Zhang, Y.; et al. AAV-mediated RLBPI gene therapy improves the rate of dark adaptation in Rlbp1 knockout mice. *Mol. Ther. - Methods Clin. Dev.* **2015**, *2*, 15022.
156. Beltran, W.A.; Aguirre, G.D.; Jacobson, S.G.; Cideciyan, A. V.; Lewin, A.S.; Boye, S.L.; Hauswirth, W.W.; Deng, W.-T. AAV-mediated gene therapy for RPGR X-linked retinal degeneration. Patent US9770491B2 2012, 1–40.
157. Xu, D.H.; Wang, X.Y.; Jia, Y.L.; Wang, T.Y.; Tian, Z.W.; Feng, X.; Zhang, Y.N. SV40 intron, a potent strong intron element that effectively increases transgene expression in transfected Chinese hamster ovary cells. *J. Cell. Mol. Med.* **2018**, *22*, 2231–2239.
158. MacLaren, R.E.; Groppe, M.; Barnard, A.R.; Cottrill, C.L.; Tolmachova, T.; Seymour, L.; Reed Clark, K.; During, M.J.; Cremers, F.P.M.; Black, G.C.M.; et al. Retinal gene therapy in patients with choroideremia: Initial findings from a phase 1/2 clinical trial. *Lancet* **2014**, *383*, 1129–1137.
159. Jacobson, S.G.; Cideciyan, A. V.; Ratnakaram, R.; Heon, E.; Schwartz, S.B.; Roman, A.J.; Peden, M.C.; Aleman, T.S.; Boye, S.L.; Sumaroka, A.; et al. Gene therapy for leber congenital amaurosis caused by RPE65 mutations: safety and efficacy in 15 children and adults followed up to 3 years. *Arch. Ophthalmol. (Chicago, Ill. 1960)* **2012**, *130*, 9–24.
160. Lam, B.L.; Davis, J.L.; Gregori, N.Z.; MacLaren, R.E.; Girach, A.; Verriotto, J.D.; Rodriguez, B.; Rosa, P.R.; Zhang, X.; Feuer, W.J. Choroideremia Gene Therapy Phase 2 Clinical Trial: 24-Month Results. *Am. J. Ophthalmol.* **2019**, *197*, 65–73.
161. Kurachi, S.; Hitomi, Y.; Furukawa, M.; Kurachi, K. Role of intron I in expression of the human factor IX gene. *J. Biol. Chem.* **1995**, *270*, 5276–81.
162. Kim, J.H.; Lee, S.R.; Li, L.H.; Park, H.J.; Park, J.H.; Lee, K.Y.; Kim, M.K.; Shin, B.A.; Choi, S.Y. High cleavage efficiency of a 2A peptide derived from porcine teschovirus-1 in human cell lines, zebrafish and mice. *PLoS One* **2011**, *6*.
163. Urabe, M.; Hasumi, Y.; Ogasawara, Y.; Matsushita, T.; Kamoshita, N.; Nomoto, A.; Colosi, P.; Kurtzman, G.J.; Tobita, K.; Ozawa, K. A novel dicistronic AAV vector using a short IRES segment derived from hepatitis C virus genome. *Gene* **1997**, *200*, 157–62.
164. Eggermont, J.; Proudfoot, N.J. Poly(A) signals and transcriptional pause sites combine to prevent interference between RNA polymerase II promoters. *EMBO J.* **1993**, *12*, 2539–48.
165. Satkunanathan, S.; Wheeler, J.; Thorpe, R.; Zhao, Y. Establishment of a novel cell line for the enhanced production of recombinant adeno-associated virus vectors for gene therapy. *Hum. Gene Ther.* **2014**, *25*, 929–941.
166. VectorBuilder Inc. [Vectorbuilder.com/learning-center/vector-component/promoter](https://en.vectorbuilder.com/learning-center/vector-component/promoter) Available online: <https://en.vectorbuilder.com/learning-center/vector-component/linker.html> (accessed on Jan 13, 2020).

167. Martinez-Lopez, A.; Encinas, P.; García-Valtanen, P.; Gomez-Casado, E.; Coll, J.M.; Estepa, A. Improving the safety of viral DNA vaccines: Development of vectors containing both 5' and 3' homologous regulatory sequences from non-viral origin. *Appl. Microbiol. Biotechnol.* **2013**, *97*, 3007–3016.
168. McFarland, T.J.; Zhang, Y.; Atchaneeyaskul, L. ongsri; Francis, P.; Stout, J.T.; Appukuttan, B. Evaluation of a novel short polyadenylation signal as an alternative to the SV40 polyadenylation signal. *Plasmid* **2006**, *56*, 62–67.
169. Vora, S.; Cheng, J.; Xiao, R.; VanDusen, N.J.; Quintino, L.; Pu, W.T.; Vandenberghe, L.H.; Chavez, A.; Church, G. Rational design of a compact CRISPR-Cas9 activator for AAV-mediated delivery. *bioRxiv* **2018**, *9*, 298620.
170. Hager, S.; Frame, F.M.; Collins, A.T.; Burns, J.E.; Maitland, N.J. An internal polyadenylation signal substantially increases expression levels of lentivirus-delivered transgenes but has the potential to reduce viral titer in a promoter-dependent manner. *Hum. Gene Ther.* **2008**, *19*, 840–850.
171. Schambach, A.; Galla, M.; Maetzig, T.; Loew, R.; Baum, C. Improving transcriptional termination of self-inactivating gamma-retroviral and lentiviral vectors. *Mol. Ther.* **2007**, *15*, 1167–73.
172. Ostedgaard, L.S.; Rokhlina, T.; Karp, P.H.; Lashmit, P.; Afione, S.; Schmidt, M.; Zabner, J.; Stinski, M.F.; Chiorini, J.A.; Welsh, M.J. A shortened adeno-associated virus expression cassette for CFTR gene transfer to cystic fibrosis airway epithelia. *Proc. Natl. Acad. Sci. U. S. A.* **2005**, *102*, 2952–7.
173. Kumar-Singh, R.; Leaderer, D.; Cashman, S. Compositions, kits and methods for treatment of complement-related disorders. Patent US20170209535A1 2017, 1–45.
174. Cole, C.N.; Stacy, T.P. Identification of sequences in the herpes simplex virus thymidine kinase gene required for efficient processing and polyadenylation. *Mol. Cell. Biol.* **1985**, *5*, 2104–2113.
175. Lipinski, D.M. A Comparison of Inducible Gene Expression Platforms: Implications for Recombinant Adeno-Associated Virus (rAAV) Vector-Mediated Ocular Gene Therapy. In *Advances in Experimental Medicine and Biology*; Bowes Rickman, C., Grimm, C., Anderson, R., Ash, J., LaVail, M., Hollyfield, J.G., Eds.; Springer: Cham, 2019; Vol. 1185, pp. 79–83.
176. Peterson, M.G.; Mercer, J.F.B. Structure and regulation of the sheep metallothionein-Ia gene. *Eur. J. Biochem.* **1986**, *160*, 579–585.
177. Grimm, S.L.; Nordeen, S.K. Mouse mammary tumor virus sequences responsible for activating cellular oncogenes. *J. Virol.* **1998**, *72*, 9428–35.
178. Yamamoto, K.R. Steroid Receptor Regulated Transcription of Specific Genes and Gene Networks. *Annu. Rev. Genet.* **1985**, *19*, 209–252.
179. Naughton, B.J.; Han, D.D.; Gu, H.H. Fluorescence-based evaluation of shRNA efficacy. *Anal. Biochem.* **2011**, *417*, 162–4.
180. Strobel, B.; Spöring, M.; Klein, H.; Blazevic, D.; Rust, W.; Sayols, S.; Hartig, J.S.; Kreuz, S. High-throughput identification of synthetic riboswitches by barcode-free amplicon-sequencing in human cells. *Nat. Commun.* **2020**, *11*, 714.
181. Reid, C.A.; Nettesheim, E.R.; Connor, T.B.; Lipinski, D.M. Development of an inducible anti-VEGF rAAV gene therapy strategy for the treatment of wet AMD. *Sci. Rep.* **2018**, *8*.
182. Peränen, J.; Rikonen, M.; Hyvönen, M.; Kääriäinen, L. T7 vectors with modified T7lac promoter for expression of proteins in Escherichia coli. *Anal. Biochem.* **1996**, *236*, 371–3.
183. Cenik, C.; Chua, H.N.; Zhang, H.; Tarnawsky, S.P.; Akef, A.; Derti, A.; Tasan, M.; Moore, M.J.; Palazzo, A.F.; Roth, F.P. Genome analysis reveals interplay between 5'UTR introns and nuclear mRNA export for secretory and mitochondrial genes. *PLoS Genet.* **2011**, *7*, e1001366.
184. Bonnet, A.; Grosso, A.R.; Elkaoutari, A.; Coleno, E.; Presle, A.; Sridhara, S.C.; Janbon, G.; Géli, V.; de Almeida, S.F.; Palancade, B. Introns Protect Eukaryotic Genomes from Transcription-Associated Genetic Instability. *Mol. Cell* **2017**, *67*, 608–621.e6.
185. Duan, D. Systemic AAV Micro-dystrophin Gene Therapy for Duchenne Muscular Dystrophy. *Mol. Ther.* **2018**, *26*, 2337–2356.
186. England, S.B.; Nicholson, L. V.; Johnson, M.A.; Forrest, S.M.; Love, D.R.; Zubrzycka-Gaam, E.E.; Bulman, D.E.; Harris, J.B.; Davies, K.E. Very mild muscular dystrophy associated with the deletion of 46% of dystrophin. *Nature* **1990**, *343*, 180–2.
187. Davies, K.E.; Chamberlain, J.S. Surrogate gene therapy for muscular dystrophy. *Nat. Med.* **2019**, *25*, 1473–1474.
188. Song, Y.; Morales, L.; Malik, A.S.; Mead, A.F.; Greer, C.D.; Mitchell, M.A.; Petrov, M.T.; Su, L.T.; Choi, M.E.; Rosenblum, S.T.; et al. Non-immunogenic utrophin gene therapy for the treatment of muscular dystrophy animal models. *Nat. Med.* **2019**, *25*, 1505–1511.
189. van Rossum, A.G.S.H.; Aartsen, W.M.; Meuleman, J.; Klooster, J.; Malysheva, A.; Versteeg, I.; Arsanto, J.P.; Le Bivic, A.; Wijnholds, J. Pals1/Mpp5 is required for correct localization of Crb1 at the subapical region in polarized Müller glia cells. *Hum. Mol. Genet.* **2006**, *15*, 2659–2672.

190. Pellissier, L.P.; Alves, C.H.; Quinn, P.M.; Vos, R.M.; Tanimoto, N.; Lundvig, D.M.S.; Dudok, J.J.; Hooibrink, B.; Richard, F.; Beck, S.C.; et al. Targeted ablation of CRB1 and CRB2 in retinal progenitor cells mimics Leber congenital amaurosis. *PLoS Genet.* **2013**, *9*, e1003976.
191. Pellissier, L.P.; Lundvig, D.M.S.; Tanimoto, N.; Klooster, J.; Vos, R.M.; Richard, F.; Sothilingam, V.; Garcia Garrido, M.; Le Bivic, A.; Seeliger, M.W.; et al. CRB2 acts as a modifying factor of CRB1-related retinal dystrophies in mice. *Hum. Mol. Genet.* **2014**, *23*, 3759–71.
192. Quinn, P.M.; Mulder, A.A.; Henrique Alves, C.; Desrosiers, M.; de Vries, S.I.; Klooster, J.; Dalkara, D.; Koster, A.J.; Jost, C.R.; Wijnholds, J. Loss of CRB2 in Müller glial cells modifies a CRB1-associated retinitis pigmentosa phenotype into a Leber congenital amaurosis phenotype. *Hum. Mol. Genet.* **2019**, *28*, 105–123.
193. Kantardzhieva, A.; Gosens, I.; Alexeeva, S.; Punte, I.M.; Versteeg, I.; Krieger, E.; Neeffjes-Mol, C. a; den Hollander, A.I.; Letteboer, S.J.F.; Klooster, J.; et al. MPP5 recruits MPP4 to the CRB1 complex in photoreceptors. *Invest. Ophthalmol. Vis. Sci.* **2005**, *46*, 2192–201.
194. Talib, M.; van Schooneveld, M.J.; van Genderen, M.M.; Wijnholds, J.; Florijn, R.J.; ten Brink, J.B.; Schallij-Delfos, N.E.; Dagnelie, G.; Cremers, F.P.M.; Wolterbeek, R.; et al. Genotypic and Phenotypic Characteristics of CRB1-Associated Retinal Dystrophies: A Long-Term Follow-up Study. *Ophthalmology* **2017**, *124*, 884–895.
195. Alves, C.H.; Sanz, A.S.; Park, B.; Pellissier, L.P.; Tanimoto, N.; Beck, S.C.; Huber, G.; Murtaza, M.; Richard, F.; Sridevi Gurubaran, I.; et al. Loss of CRB2 in the mouse retina mimics human retinitis pigmentosa due to mutations in the CRB1 gene. *Hum. Mol. Genet.* **2013**, *22*, 35–50.
196. Alves, C.H.; Boon, N.; Mulder, A.A.; Koster, A.J.; Jost, C.R.; Wijnholds, J. CRB2 Loss in Rod Photoreceptors Is Associated with Progressive Loss of Retinal Contrast Sensitivity. *Int. J. Mol. Sci.* **2019**, *20*, 4069.
197. van de Pavert, S. a; Meuleman, J.; Malysheva, A.; Aartsen, W.M.; Versteeg, I.; Tonagel, F.; Kamphuis, W.; McCabe, C.J.; Seeliger, M.W.; Wijnholds, J. A single amino acid substitution (Cys249Trp) in Crb1 causes retinal degeneration and deregulates expression of pituitary tumor transforming gene Pttg1. *J. Neurosci.* **2007**, *27*, 564–73.
198. Alves, C.H.; Bossers, K.; Vos, R.M.; Essing, A.H.W.; Swagemakers, S.; van der Spek, P.J.; Verhaagen, J.; Wijnholds, J. Microarray and morphological analysis of early postnatal CRB2 mutant retinas on a pure C57BL/6J genetic background. *PLoS One* **2013**, *8*, e82532.
199. Alves, C.H.; Pellissier, L.P.; Vos, R.M.; Garcia Garrido, M.; Sothilingam, V.; Seide, C.; Beck, S.C.; Klooster, J.; Furukawa, T.; Flannery, J.G.; et al. Targeted ablation of Crb2 in photoreceptor cells induces retinitis pigmentosa. *Hum. Mol. Genet.* **2014**, *23*, 3384–401.
200. Quinn, P.M.; Alves, C.H.; Klooster, J.; Wijnholds, J. CRB2 in immature photoreceptors determines the superior-inferior symmetry of the developing retina to maintain retinal structure and function. *Hum. Mol. Genet.* **2018**, *27*, 3137–3153.
201. Van De Pavert, S.A.; Sanz, A.S.; Aartsen, W.M.; Vos, R.M.; Versteeg, I.; Beck, S.C.; Klooster, J.; Seeliger, M.W.; Wijnholds, J. Crb1 is a determinant of retinal apical Müller glia cell features. *Glia* **2007**, *55*, 1486–1497.
202. van de Pavert, S. a; Kantardzhieva, A.; Malysheva, A.; Meuleman, J.; Versteeg, I.; Levelt, C.; Klooster, J.; Geiger, S.; Seeliger, M.W.; Rashbass, P.; et al. Crumbs homologue 1 is required for maintenance of photoreceptor cell polarization and adhesion during light exposure. *J. Cell Sci.* **2004**, *117*, 4169–77.
203. Lundstrom, K. Viral Vectors in Gene Therapy. *Diseases* **2018**, *6*, 42.
204. Trapani, I. Adeno-Associated Viral Vectors as a Tool for Large Gene Delivery to the Retina. *Genes (Basel)*. **2019**, *10*, E287.
205. Trapani, I.; Toriello, E.; de Simone, S.; Colella, P.; Iodice, C.; Polishchuk, E. V; Sommella, A.; Colecchi, L.; Rossi, S.; Simonelli, F.; et al. Improved dual AAV vectors with reduced expression of truncated proteins are safe and effective in the retina of a mouse model of Stargardt disease. *Hum. Mol. Genet.* **2015**, *24*, 6811–25.
206. McClements, M.E.; Barnard, A.R.; Singh, M.S.; Charbel Issa, P.; Jiang, Z.; Radu, R.A.; MacLaren, R.E. An AAV Dual Vector Strategy Ameliorates the Stargardt Phenotype in Adult Abca4^{-/-} Mice. *Hum. Gene Ther.* **2019**, *30*, 590–600.
207. Kumar, N.; Stanford, W.; de Solis, C.; Aradhana; Abraham, N.D.; Dao, T.M.J.; Thaseen, S.; Sairavi, A.; Gonzalez, C.U.; Ploski, J.E. The development of an AAV-based CRISPR SaCas9 genome editing system that can be delivered to neurons in vivo and regulated via doxycycline and Cre-recombinase. *Front. Mol. Neurosci.* **2018**, *11*.
208. Hanlon, K.S.; Kleinstiver, B.P.; Garcia, S.P.; Zaborowski, M.P.; Volak, A.; Spirig, S.E.; Muller, A.; Sousa, A.A.; Tsai, S.Q.; Bengtsson, N.E.; et al. High levels of AAV vector integration into CRISPR-induced DNA breaks. *Nat. Commun.* **2019**, *10*.
209. Yu, W.; Mookherjee, S.; Chaitankar, V.; Hiriyanna, S.; Kim, J.W.; Brooks, M.; Ataeijannati, Y.; Sun, X.; Dong, L.; Li, T.; et al. Nrl knockdown by AAV-delivered CRISPR/Cas9 prevents retinal degeneration in mice. *Nat. Commun.* **2017**, *8*.
210. Zhu, J.; Ming, C.; Fu, X.; Duan, Y.; Hoang, D.A.; Rutgard, J.; Zhang, R.; Wang, W.; Hou, R.; Zhang, D.; et al. Gene and mutation independent therapy via CRISPR-Cas9 mediated cellular reprogramming in rod photoreceptors. *Cell Res.* **2017**, *27*, 830–833.
211. Kim, E.; Koo, T.; Park, S.W.; Kim, D.; Kim, K.; Cho, H.Y.; Song, D.W.; Lee, K.J.; Jung, M.H.; Kim, S.; et al. In vivo genome editing with a small Cas9 orthologue derived from *Campylobacter jejuni*. *Nat. Commun.* **2017**, *8*, 14500.

212. Jo, D.H.; Koo, T.; Cho, C.S.; Kim, J.H.; Kim, J.-S.; Kim, J.H. Long-Term Effects of In Vivo Genome Editing in the Mouse Retina Using *Campylobacter jejuni* Cas9 Expressed via Adeno-Associated Virus. *Mol. Ther.* **2019**, *27*, 130–136.
213. Perez-Pinera, P.; Kocak, D.D.; Vockley, C.M.; Adler, A.F.; Kabadi, A.M.; Polstein, L.R.; Thakore, P.I.; Glass, K.A.; Ousterout, D.G.; Leong, K.W.; et al. RNA-guided gene activation by CRISPR-Cas9-based transcription factors. *Nat. Methods* **2013**, *10*, 973–976.
214. Konermann, S.; Brigham, M.D.; Trevino, A.E.; Joung, J.; Abudayyeh, O.O.; Barcena, C.; Hsu, P.D.; Habib, N.; Gootenberg, J.S.; Nishimasu, H.; et al. Genome-scale transcriptional activation by an engineered CRISPR-Cas9 complex. *Nature* **2015**, *517*, 583–588.
215. Lecomte, E.; Tournaire, B.; Cogné, B.; Dupont, J.B.; Lindenbaum, P.; Martin-Fontaine, M.; Broucque, F.; Robin, C.; Hebben, M.; Merten, O.W.; et al. Advanced characterization of DNA molecules in rAAV vector preparations by single-stranded virus next-generation sequencing. *Mol. Ther. - Nucleic Acids* **2015**, *4*, e260.
216. Bencicelli, J.; Wright, J.F.; Komaromy, A.; Jacobs, J.B.; Hauck, B.; Zelenia, O.; Mingozi, F.; Hui, D.; Chung, D.; Tonia, S.; et al. Reversal of Blindness in Animal Models of Leber Congenital Amaurosis Using Optimized AAV2-mediated Gene Transfer. *Mol. Ther.* **2010**, *16*, 458–465.
217. Mignon, C.; Sodoyer, R.; Werle, B. Antibiotic-free selection in biotherapeutics: Now and forever. *Pathogens* **2015**, *4*, 157–181.
218. Kay, M.A.; He, C.Y.; Chen, Z.Y. A robust system for production of minicircle DNA vectors. *Nat. Biotechnol.* **2010**, *28*, 1287–1289.
219. Schnödt, M.; Schmeer, M.; Kracher, B.; Krüsemann, C.; Espinosa, L.E.; Grünert, A.; Fuchsluger, T.; Rischmüller, A.; Schleaf, M.; Büning, H. DNA Minicircle Technology Improves Purity of Adeno-associated Viral Vector Preparations. *Mol. Ther. - Nucleic Acids* **2016**, *5*, e355.
220. Bishop, B.M.; Santin, A.D.; Quirk, J.G.; Hermonat, P.L. Role of terminal repeat GAGC trimer, the major Rep78 binding site, in adeno-associated virus DNA replication. *FEBS Lett.* **1996**, *397*, 97–100.
221. Ryan, J.H.; Zolotukhin, S.; Muzyczka, N. Sequence requirements for binding of Rep68 to the adeno-associated virus terminal repeats. *J. Virol.* **1996**, *70*, 1542–53.
222. Zhou, X.; Zeng, X.; Fan, Z.; Li, C.; McCown, T.; Samulski, R.J.; Xiao, X. Adeno-associated virus of a single-polarity DNA genome is capable of transduction in vivo. *Mol. Ther.* **2008**, *16*, 494–499.
223. Wang, X.S.; Ponnazhagan, S.; Srivastava, A. Rescue and replication of adeno-associated virus type 2 as well as vector DNA sequences from recombinant plasmids containing deletions in the viral inverted terminal repeats: selective encapsidation of viral genomes in progeny virions. *J. Virol.* **1996**, *70*, 1668–77.
224. Wang, X.S.; Qing, K.; Ponnazhagan, S.; Srivastava, A. Adeno-associated virus type 2 DNA replication in vivo: mutation analyses of the D sequence in viral inverted terminal repeats. *J. Virol.* **1997**, *71*, 3077–3082.
225. Kwon, H.-J.; Qing, K.; Ponnazhagan, S.; Wang, X.-S.; Markusic, D.M.; Gupte, S.; Boye, S.; Srivastava, A. AAV D-sequence-mediated suppression of expression of a human major histocompatibility class II gene: Implications in the development of AAV vectors for modulating humoral immune response. *Hum. Gene Ther.* **2020**, hum.2020.018.
226. Samulski, R.J.; Srivastava, A.; Berns, K.I.; Muzyczka, N. Rescue of adeno-associated virus from recombinant plasmids: Gene correction within the terminal repeats of AAV. *Cell* **1983**, *33*, 135–143.
227. Zhou, Q.; Tian, W.; Liu, C.; Lian, Z.; Dong, X.; Wu, X. Deletion of the B-B' and C-C' regions of inverted terminal repeats reduces rAAV productivity but increases transgene expression. *Sci. Rep.* **2017**, *7*.
228. McAlister, V.J.; Owens, R.A. Substitution of adeno-associated virus Rep protein binding and nicking sites with human chromosome 19 sequences. *Virol. J.* **2010**, *7*, 218.
229. Miller, D.G.; Petek, L.M.; Russell, D.W. Adeno-associated virus vectors integrate at chromosome breakage sites. *Nat. Genet.* **2004**, *36*, 767–73.
230. Nakai, H.; Yant, S.R.; Storm, T.A.; Fuess, S.; Meuse, L.; Kay, M.A. Extrachromosomal recombinant adeno-associated virus vector genomes are primarily responsible for stable liver transduction in vivo. *J. Virol.* **2001**, *75*, 6969–76.
231. Colella, P.; Ronzitti, G.; Mingozi, F. Emerging Issues in AAV-Mediated In Vivo Gene Therapy. *Mol. Ther. - Methods Clin. Dev.* **2018**, *8*, 87–104.
232. Nakai, H.; Montini, E.; Fuess, S.; Storm, T.A.; Grompe, M.; Kay, M.A. AAV serotype 2 vectors preferentially integrate into active genes in mice. *Nat. Genet.* **2003**, *34*, 297–302.
233. Ceiler, J.; Afzal, S.; Leuchs, B.; Fronza, R.; Lulay, C.; Büning, H.; Schmidt, M.; Gil-Farina, I. Wild-Type and Recombinant AAV Integration in Human Cardiomyocytes: Focus on Mitochondrial Genome. In Proceedings of the AAV Vector Biology; Molecular Therapy - Cell Press, 2017; Vol. 5, p. 1.
234. Gil-Farina, I.; Fronza, R.; Kaeppl, C.; Lopez-Franco, E.; Ferreira, V.; D'Avola, D.; Benito, A.; Prieto, J.; Petry, H.; Gonzalez-Aseguinolaza, G.; et al. Recombinant AAV Integration Is Not Associated With Hepatic Genotoxicity in Nonhuman Primates and Patients. *Mol. Ther.* **2016**, *24*, 1100–1105.

235. Wang, Z.; Lisowski, L.; Finegold, M.J.; Nakai, H.; Kay, M.A.; Grompe, M. AAV vectors containing rDNA homology display increased chromosomal integration and transgene persistence. *Mol. Ther.* **2012**, *20*, 1902–1911.
236. Hirsch, M.L. Adeno-associated virus inverted terminal repeats stimulate gene editing. *Gene Ther.* **2015**, *22*, 190–195.
237. Ronzitti, G.; Bortolussi, G.; van Dijk, R.; Collaud, F.; Charles, S.; Leborgne, C.; Vidal, P.; Martin, S.; Gjata, B.; Sola, M.S.; et al. A translationally optimized AAV-UGT1A1 vector drives safe and long-lasting correction of Crigler-Najjar syndrome. *Mol. Ther. - Methods Clin. Dev.* **2016**, *3*, 16049.
238. McCarty, D.M.; Monahan, P.E.; Samulski, R.J. Self-complementary recombinant adeno-associated virus (scAAV) vectors promote efficient transduction independently of DNA synthesis. *Gene Ther.* **2001**, *8*, 1248–54.
239. McCarty, D.M. Self-complementary AAV vectors; advances and applications. *Mol. Ther.* **2008**, *16*, 1648–1656.
240. Koilkonda, R.D.; Chou, T.H.; Porciatti, V.; Hauswirth, W.W.; Guy, J. Induction of rapid and highly efficient expression of the human ND4 complex I subunit in the mouse visual system by self-complementary adeno-associated virus. *Arch. Ophthalmol.* **2010**, *128*, 876–883.
241. Yokoi, K.; Kachi, S.; Zhang, H.S.; Gregory, P.D.; Spratt, S.K.; Samulski, R.J.; Campochiaro, P.A. Ocular gene transfer with self-complementary AAV vectors. *Investig. Ophthalmol. Vis. Sci.* **2007**, *48*, 3324–3328.
242. Wright, J.F.; Zeleniaia, O. Vector characterization methods for quality control testing of recombinant adeno-associated viruses. *Methods Mol. Biol.* **2011**, *737*, 247–78.
243. François, A.; Bouzelha, M.; Lecomte, E.; Broucque, F.; Pénau-Budloo, M.; Adjali, O.; Moullier, P.; Blouin, V.; Ayuso, E. Accurate Titration of Infectious AAV Particles Requires Measurement of Biologically Active Vector Genomes and Suitable Controls. *Mol. Ther. - Methods Clin. Dev.* **2018**, *10*, 223–236.
244. Couto, L.; Buchlis, G.; Farjo, R.; High, K.A. Poster C0048 ARVO: Potency Assay for AAV Vector Encoding Retinal Pigment Epithelial 65 Protein. *Invest. Ophthalmol. Vis. Sci.* **2016**, *57*, 1.
245. Patrício, M.I.; Barnard, A.R.; Cox, C.I.; Blue, C.; MacLaren, R.E. The Biological Activity of AAV Vectors for Choroideremia Gene Therapy Can Be Measured by In Vitro Prenylation of RAB6A. *Mol. Ther. - Methods Clin. Dev.* **2018**.
246. MacLaren, R.E.; Groppe, M.; Barnard, A.R.; Cottrill, C.L.; Tolmachova, T.; Seymour, L.; Clark, K.R.; During, M.J.; Cremers, F.P.M.M.; Black, G.C.M.M.; et al. Retinal gene therapy in patients with choroideremia: initial findings from a phase 1/2 clinical trial. *Lancet* **2014**, *383*, 1129–37.
247. Wang, L.; Xiao, R.; Andres-Mateos, E.; Vandenbergh, L.H. Single stranded adeno-associated virus achieves efficient gene transfer to anterior segment in the mouse eye. *PLoS One* **2017**, *12*.
248. Borrás, T.; Xue, W.; Choi, V.W.; Bartlett, J.S.; Li, G.; Samulski, R.J.; Chisolm, S.S. Mechanisms of AAV transduction in glaucoma-associated human trabecular meshwork cells. *J. Gene Med.* **2006**, *8*, 589–602.
249. Ellis, B.L.; Hirsch, M.L.; Barker, J.C.; Connelly, J.P.; Steininger, R.J.; Porteus, M.H. A survey of ex vivo/in vitro transduction efficiency of mammalian primary cells and cell lines with Nine natural adeno-associated virus (AAV1-9) and one engineered adeno-associated virus serotype. *Virol. J.* **2013**, *10*, 74.
250. Gonzalez-Cordero, A.; Goh, D.; Kruczek, K.; Naeem, A.; Fernando, M.; Kleine Holthaus, S.M.; Takaaki, M.; Blackford, S.J.I.; Kloc, M.; Agundez, L.; et al. Assessment of AAV Vector Tropisms for Mouse and Human Pluripotent Stem Cell-Derived RPE and Photoreceptor Cells. *Hum. Gene Ther.* **2018**, *29*, 1124–1139.
251. Sayyad, Z.; Sirohi, K.; Radha, V.; Swarup, G. 661W is a retinal ganglion precursor-like cell line in which glaucoma-associated optineurin mutants induce cell death selectively. *Sci. Rep.* **2017**, *7*.
252. Tan, E.; Ding, X.-Q.; Saadi, A.; Agarwal, N.; Naash, M.I.; Al-Ubaidi, M.R. Expression of cone-photoreceptor-specific antigens in a cell line derived from retinal tumors in transgenic mice. *Invest. Ophthalmol. Vis. Sci.* **2004**, *45*, 764–8.
253. Ryals, R.C.; Boye, S.L.; Dinculescu, A.; Hauswirth, W.W.; Boye, S.E. Quantifying transduction efficiencies of unmodified and tyrosine capsid mutant AAV vectors in vitro using two ocular cell lines. *Mol. Vis.* **2011**, *17*, 1090–1102.
254. McDougald, D.S.; Duong, T.T.; Palozola, K.C.; Marsh, A.; Papp, T.E.; Mills, J.A.; Zhou, S.; Bennett, J. CRISPR Activation Enhances In Vitro Potency of AAV Vectors Driven by Tissue-Specific Promoters. *Mol. Ther. - Methods Clin. Dev.* **2019**, *13*, 380–389.
255. Drivas, T.G.; Bennett, J. Compositions and methods for treatment of disorders related to CEP290. Patent US10301366B2 2013, 1–105.
256. Katoh, Y.; Michisaka, S.; Nozaki, S.; Funabashi, T.; Hirano, T.; Takei, R.; Nakayama, K. Practical method for targeted disruption of ciliarelated genes by using CRISPR/Cas9-mediated, homology-independent knock-in system. *Mol. Biol. Cell* **2017**, *28*, 898–906.
257. Klimczak, R.R.; Koerber, J.T.; Dalkara, D.; Flannery, J.G.; Schaffer, D. V. A novel adeno-associated viral variant for efficient and selective intravitreal transduction of rat Müller cells. *PLoS One* **2009**, *4*, e7467.
258. Zhang, Z.; Ma, Z.; Zou, W.; Guo, H.; Liu, M.; Ma, Y.; Zhang, L. The Appropriate Marker for Astrocytes: Comparing the Distribution and Expression of Three Astrocytic Markers in Different Mouse Cerebral Regions. *Biomed Res. Int.* **2019**, *2019*, 1–15.

259. Vecino, E.; Rodriguez, F.D.; Ruzafa, N.; Pereiro, X.; Sharma, S.C. Glia-neuron interactions in the mammalian retina. *Prog. Retin. Eye Res.* **2016**, *51*, 1–40.
260. Lawrence, J.M.; Singhal, S.; Bhatia, B.; Keegan, D.J.; Reh, T.A.; Luthert, P.J.; Khaw, P.T.; Limb, G.A. MIO-M1 Cells and Similar Müller Glial Cell Lines Derived from Adult Human Retina Exhibit Neural Stem Cell Characteristics. *Stem Cells* **2007**, *25*, 2033–2043.
261. Limb, G.A.; Salt, T.E.; Munro, P.M.G.; Moss, S.E.; Khaw, P.T. In vitro characterization of a spontaneously immortalized human Müller cell line (MIO-M1). *Invest. Ophthalmol. Vis. Sci.* **2002**, *43*, 864–9.
262. Koch, P.; Greef, S. de; Chtarto, A.; Kemp, T.; Bockstae, O.; Velu, T.; Caspers, L.; Tenenbaum, L. ARVO abstract: In vitro comparison of AAV-mediated eGFP gene transfer on Müller cells and ARPE cells. *Invest. Ophthalmol. Vis. Sci.* **2004**, *45*.
263. Mellough, C.B.; Sernagor, E.; Moreno-Gimeno, I.; Steel, D.H.W.; Lako, M. Efficient stage-specific differentiation of human pluripotent stem cells toward retinal photoreceptor cells. *Stem Cells* **2012**, *30*, 673–86.
264. Cereso, N.; Pequignot, M.O.; Robert, L.; Becker, F.; De Luca, V.; Nabholz, N.; Rigau, V.; De Vos, J.; Hamel, C.P.; Kalatzis, V. Proof of concept for AAV2/5-mediated gene therapy in iPSC-derived retinal pigment epithelium of a choroideremia patient. *Mol. Ther. - Methods Clin. Dev.* **2014**, *1*, 14011.
265. Duong, T.T.; Vasireddy, V.; Ramachandran, P.; Herrera, P.S.; Leo, L.; Merkel, C.; Bennett, J.; Mills, J.A. Use of induced pluripotent stem cell models to probe the pathogenesis of Choroideremia and to develop a potential treatment. *Stem Cell Res.* **2018**, *27*, 140–150.
266. Brydon, E.M.; Bronstein, R.; Buskin, A.; Lako, M.; Pierce, E.A.; Fernandez-Godino, R. AAV-mediated gene augmentation therapy restores critical functions in mutant iPSC-derived PRPF31^{+/−} cells. *bioRxiv* **2019**, 729160.
267. Wright, J.F.; Sumaroka, M. Rab escort protein potency assay. Patent US201662418637P 2016, 1–16.
268. Garita-Hernandez, M.; Guibbal, L.; Toualbi, L.; Routet, F.; Chaffiol, A.; Winckler, C.; Harinquet, M.; Robert, C.; Fouquet, S.; Bellow, S.; et al. Optogenetic light sensors in human retinal organoids. *Front. Neurosci.* **2018**, *12*.
269. Garita-Hernandez, M.; Routet, F.; Guibbal, L.; Khabou, H.; Toualbi, L.; Riancho, L.; Reichman, S.; Duebel, J.; Sahel, J.A.; Goureau, O.; et al. AAV-mediated gene delivery to 3D retinal organoids derived from human induced pluripotent stem cells. *Int. J. Mol. Sci.* **2020**, *21*.
270. Capowski, E.E.; Samimi, K.; Mayerl, S.J.; Phillips, M.J.; Pinilla, I.; Howden, S.E.; Saha, J.; Jansen, A.D.; Edwards, K.L.; Jager, L.D.; et al. Reproducibility and staging of 3D human retinal organoids across multiple pluripotent stem cell lines. *Dev.* **2019**, *146*.
271. Mellough, C.B.; Collin, J.; Queen, R.; Hilgen, G.; Dorgau, B.; Zerti, D.; Felemban, M.; White, K.; Sernagor, E.; Lako, M. Systematic Comparison of Retinal Organoid Differentiation from Human Pluripotent Stem Cells Reveals Stage Specific, Cell Line, and Methodological Differences. *Stem Cells Transl. Med.* **2019**, *8*, 694–706.
272. Dudek, A.M.; Pillay, S.; Puschnik, A.S.; Nagamine, C.M.; Cheng, F.; Qiu, J.; Carette, J.E.; Vandenberghe, L.H. An Alternate Route for Adeno-associated Virus (AAV) Entry Independent of AAV Receptor. *J. Virol.* **2018**, *92*.
273. Akl, M.R.; Nagpal, P.; Ayoub, N.M.; Tai, B.; Prabhu, S.A.; Capac, C.M.; Gliksman, M.; Goy, A.; Suh, K.S. Molecular and clinical significance of fibroblast growth factor 2 (FGF2/bFGF) in malignancies of solid and hematological cancers for personalized therapies. *Oncotarget* **2016**, *7*, 44735–44762.
274. ThermoScientific Growth Factors in HyClone Cell Culture Serum Available online: <https://static.thermoscientific.com/images/D22225~.pdf> (accessed on Mar 31, 2020).
275. Qing, K.; Mah, C.; Hansen, J.; Zhou, S.; Dwarki, V.; Srivastava, A. Human fibroblast growth factor receptor 1 is a co-receptor for infection by adeno-associated virus 2. *Nat. Med.* **1999**, *5*, 71–77.
276. Achberger, K.; Haderspeck, J.C.; Kleger, A.; Liebau, S. Stem cell-based retina models. *Adv. Drug Deliv. Rev.* **2019**, *140*, 33–50.
277. Wiley, L.A.; Burnight, E.R.; Kaalberg, E.E.; Jiao, C.; Riker, M.J.; Halder, J.A.; Luse, M.A.; Han, I.C.; Russell, S.R.; Sohn, E.H.; et al. Assessment of Adeno-Associated Virus Serotype Tropism in Human Retinal Explants. *Hum. Gene Ther.* **2018**, *29*, 424–436.
278. Khabou, H.; Garita-Hernandez, M.; Chaffiol, A.; Reichman, S.; Jaillard, C.; Brazhnikova, E.; Bertin, S.; Forster, V.; Desrosiers, M.; Winckler, C.; et al. Noninvasive gene delivery to foveal cones for vision restoration. *JCI insight* **2018**, *3*.
279. Hickey, D.G.; Edwards, T.L.; Barnard, A.R.; Singh, M.S.; de Silva, S.R.; McClements, M.E.; Flannery, J.G.; Hankins, M.W.; MacLaren, R.E. Tropism of engineered and evolved recombinant AAV serotypes in the rd1 mouse and ex vivo primate retina. *Gene Ther.* **2017**, *24*, 787–800.
280. Buck, T.M.; Pellissier, L.P.; Vos, R.M.; van Dijk, E.H.C.; Boon, C.J.F.; Wijnholds, J. AAV serotype testing on cultured human donor retinal explants. In *Methods in Molecular Biology*; Wijnholds, J., Ed.; Humana Press: New York, NY, 2018; pp. 275–288 ISBN 978-1-4939-7522-8.
281. Reid, C.A.; Ertel, K.J.; Lipinski, D.M. Improvement of photoreceptor targeting via intravitreal delivery in mouse and human retina using combinatory rAAV2 capsid mutant vectors. *Investig. Ophthalmol. Vis. Sci.* **2017**, *58*, 6429–6439.

282. Buck, T.M.; Quinn, P.M.; Celso Alves, H.; Van Dijk, E.; Ohonin, C.; Boon, C.J.F.; Wijnholds, J. Potency assay for AAV-gene vectors in human iPSCs-derived retinas and donor retinas | IOVS | ARVO Journals. *Invest. Ophthalmol. Vis. Sci.* **2017**, *58*, 4093.
283. van Rossum, A.G.S.H.S.H.; Aartsen, W.M.; Meuleman, J.; Klooster, J.; Malysheva, A.; Versteeg, I.; Arsanto, J.-P.P.; Le Bivic, A.A.; Wijnholds, J. Pals1/Mpp5 is required for correct localization of Crb1 at the subapical region in polarized Müller glia cells. *Hum. Mol. Genet.* **2006**, *15*, 2659–2672.
284. Singh, H.P.; Wang, S.; Stachelek, K.; Lee, S.; Reid, M.W.; Thornton, M.E.; Craft, C.M.; Grubbs, B.H.; Cobrinik, D. Developmental stage-specific proliferation and retinoblastoma genesis in RB-deficient human but not mouse cone precursors. *Proc. Natl. Acad. Sci. U. S. A.* **2018**, *115*, E9391–E9400.
285. Petit, L.; Ma, S.; Cheng, S.-Y.; Gao, G.; Punzo, C. Rod Outer Segment Development Influences AAV-Mediated Photoreceptor Transduction After Subretinal Injection. *Hum. Gene Ther.* **2017**, *28*, 464–481.
286. Surace, E.M.; Auricchio, A.; Reich, S.J.; Glover, E.; Pineles, S.; Tang, W.; O'Connor, E.; Lyubarsky, A.; Savchenko, A.; Pugh, E.N.; et al. Delivery of Adeno-Associated Virus Vectors to the Fetal Retina: Impact of Viral Capsid Proteins on Retinal Neuronal Progenitor Transduction. *J. Virol.* **2003**, *77*, 7957–7963.
287. Xiong, W.; Cepko, C. Distinct Expression Patterns of AAV8 Vectors with Broadly Active Promoters from Subretinal Injections of Neonatal Mouse Eyes at Two Different Ages. *Adv. Exp. Med. Biol.* **2016**, *854*, 501–7.
288. Quinn, P.M.; Buck, T.M.; Mulder, A.A.; Ohonin, C.; Alves, C.H.; Vos, R.M.; Bialecka, M.; van Herwaarden, T.; van Dijk, E.H.C.; Talib, M.; et al. Human iPSC-Derived Retinas Recapitulate the Fetal CRB1 CRB2 Complex Formation and Demonstrate that Photoreceptors and Müller Glia Are Targets of AAV5. *Stem Cell Reports* **2019**, *12*, 906–919.
289. Matsumoto, B.; Blanks, J.C.; Ryan, S.J. Topographic variations in the rabbit and primate internal limiting membrane. | IOVS | ARVO Journals. *Invest. Ophthalmol. Vis. Sci.* **1984**, *2*, 71–82.
290. Timmers, A.M.; Newmark, J.A.; Turunen, H.T.; Farivar, T.; Liu, J.; Song, C.; Ye, G.J.; Pennock, S.; Gaskin, C.; Knop, D.R.; et al. Ocular Inflammatory Response to Intravitreal Injection of Adeno-Associated Virus Vector: Relative Contribution of Genome and Capsid. *Hum. Gene Ther.* **2020**, *31*, 80–89.
291. Dalkara, D.; Kolstad, K.D.; Caporale, N.; Visel, M.; Klimczak, R.R.; Schaffer, D. V.; Flannery, J.G. Inner limiting membrane barriers to aav-mediated retinal transduction from the vitreous. *Mol. Ther.* **2009**, *17*, 2096–2102.
292. Cehajic-Kapetanovic, J.; Milosavljevic, N.; Bedford, R.A.; Lucas, R.J.; Bishop, P.N. Efficacy and Safety of Glycosidic Enzymes for Improved Gene Delivery to the Retina following Intravitreal Injection in Mice. *Mol. Ther. - Methods Clin. Dev.* **2018**, *9*, 192–202.
293. Song, H.; Bush, R.A.; Zeng, Y.; Qian, H.; Wu, Z.; Sieving, P.A. Trans-ocular Electric Current In Vivo Enhances AAV-Mediated Retinal Gene Transduction after Intravitreal Vector Administration. *Mol. Ther. - Methods Clin. Dev.* **2019**, *13*, 77–85.
294. Dias, M.S.; Araujo, V.G.; Vasconcelos, T.; Li, Q.; Hauswirth, W.W.; Linden, R.; Petrs-Silva, H. Retina transduction by rAAV2 after intravitreal injection: comparison between mouse and rat. *Gene Ther.* **2019**, *26*, 479–490.
295. Kolstad, K.D.; Dalkara, D.; Guerin, K.; Visel, M.; Hoffmann, N.; Schaffer, D. V.; Flannery, J.G. Changes in adeno-associated virus-mediated gene delivery in retinal degeneration. *Hum. Gene Ther.* **2010**, *21*, 571–8.
296. Charbel Issa, P.; de Silva, S.R.; Lipinski, D.M.; Singh, M.S.; Mouravlev, A.; You, Q.; Barnard, A.R.; Hankins, M.W.; During, M.J.; MacLaren, R.E. Assessment of Tropism and Effectiveness of New Primate-Derived Hybrid Recombinant AAV Serotypes in the Mouse and Primate Retina. *PLoS One* **2013**, *8*, 1–12.
297. Zeng, Y.; Qian, H.; Wu, Z.; Marangoni, D.; Sieving, P.A.; Bush, R.A. AAVrh-10 transduces outer retinal cells in rodents and rabbits following intravitreal administration. *Gene Ther.* **2019**, *26*, 386–398.
298. Giove, T.J.; Sena-Esteves, M.; Eldred, W.D. Transduction of the inner mouse retina using AAVrh8 and AAVrh10 via intravitreal injection. *Exp. Eye Res.* **2010**, *91*, 652–659.
299. Lovric, J.; Mano, M.; Zentilin, L.; Eulalio, A.; Zacchigna, S.; Giacca, M. Terminal differentiation of cardiac and skeletal myocytes induces permissivity to AAV transduction by relieving inhibition imposed by DNA damage response proteins. *Mol. Ther.* **2012**, *20*, 2087–97.
300. Moreno, M.L.; Mérida, S.; Bosch-Morell, F.; Miranda, M.; Villar, V.M. Autophagy dysfunction and oxidative stress, two related mechanisms implicated in retinitis pigmentosa. *Front. Physiol.* **2018**, *9*, 1008.
301. Blasiak, J.; Piechota, M.; Pawlowska, E.; Szatkowska, M.; Sikora, E.; Kaamiranta, K. Cellular senescence in age-related macular degeneration: Can autophagy and DNA damage response play a role? *Oxid. Med. Cell. Longev.* **2017**, 2017.
302. D'Adda Di Fagagna, F. Living on a break: Cellular senescence as a DNA-damage response. *Nat. Rev. Cancer* **2008**, *8*, 512–522.
303. Lotery, A.J.; Yang, G.S.; Mullins, R.F.; Russell, S.R.; Schmidt, M.; Stone, E.M.; Lindbloom, J.D.; Chiorini, J.A.; Kotin, R.M.; Davidson, B.L. Adeno-Associated Virus Type 5: Transduction Efficiency and Cell-Type Specificity in the Primate Retina. *Hum. Gene Ther.* **2003**, *14*, 1663–1671.

304. Gao, G.-P.; Auricchio, A.; Wang, L.; Johnston, J.; Hammill, D.; Raper, S.E.; Grant, R.; Bennett, J.; Wilson, J.M.; Gao, G.-P.; et al. 561. Evaluation of AAV Vectors Based on Serotypes 1,2 and 5 in Non-Human Primate Muscle, Liver and Retina. *Mol. Ther.* **2002**, *5*, S184.
305. Vandenberghe, L.H.; Bell, P.; Maguire, A.M.; Xiao, R.; Hopkins, T.B.; Grant, R.; Bennett, J.; Wilson, J.M. AAV9 targets cone photoreceptors in the nonhuman primate retina. *PLoS One* **2013**, *8*, e53463.
306. Ramachandran, P.S.; Lee, V.; Wei, Z.; Song, J.Y.; Casal, G.; Cronin, T.; Willett, K.; Huckfeldt, R.; Morgan, J.I.W.; Aleman, T.S.; et al. Evaluation of Dose and Safety of AAV7m8 and AAV8BP2 in the Non-Human Primate Retina. *Hum. Gene Ther.* **2017**, *28*, 154–167.
307. Carvalho, L.S.; Xiao, R.; Wassmer, S.J.; Langsdorf, A.; Zinn, E.; Pacouret, S.; Shah, S.; Comander, J.I.; Kim, L.A.; Lim, L.; et al. Synthetic Adeno-Associated Viral Vector Efficiently Targets Mouse and Nonhuman Primate Retina in Vivo. *Hum. Gene Ther.* **2018**, *29*, 771–784.
308. Boye, S.E.; Alexander, J.J.; Boye, S.L.; Witherspoon, C.D.; Sandefer, K.J.; Conlon, T.J.; Erger, K.; Sun, J.; Ryals, R.; Chiodo, V.A.; et al. The Human Rhodopsin Kinase Promoter in an AAV5 Vector Confers Rod- and Cone-Specific Expression in the Primate Retina. *Hum. Gene Ther.* **2012**, *23*, 1101–1115.
309. Carvalho, L.S.; Xiao, R.; Wassmer, S.J.; Langsdorf, A.; Zinn, E.; Pacouret, S.; Shah, S.; Comander, J.I.; Kim, L.A.; Lim, L.; et al. Synthetic Adeno-Associated Viral Vector Efficiently Targets Mouse and Nonhuman Primate Retina in Vivo. *Hum. Gene Ther.* **2018**, *29*, 771–784.
310. Yin, L.; Greenberg, K.; Hunter, J.J.; Dalkara, D.; Kolstad, K.D.; Masella, B.D.; Wolfe, R.; Visel, M.; Stone, D.; Libby, R.T.; et al. Intravitreal injection of AAV2 transduces macaque inner retina. *Invest. Ophthalmol. Vis. Sci.* **2011**, *52*, 2775–83.
311. Takahashi, K.; Igarashi, T.; Miyake, K.; Kobayashi, M.; Yaguchi, C.; Iijima, O.; Yamazaki, Y.; Katakai, Y.; Miyake, N.; Kameya, S.; et al. Improved Intravitreal AAV-Mediated Inner Retinal Gene Transduction after Surgical Internal Limiting Membrane Peeling in Cynomolgus Monkeys. *Mol. Ther.* **2017**, *25*, 296–302.
312. Xiong, W.; Wu, D.M.; Xue, Y.; Wang, S.K.; Chung, M.J.; Ji, X.; Rana, P.; Zhao, S.R.; Mai, S.; Cepko, C.L. AAV cis-regulatory sequences are correlated with ocular toxicity. *Proc. Natl. Acad. Sci. U. S. A.* **2019**, *116*, 5785–5794.
313. Peirson, S.N.; Brown, L.A.; Potheary, C.A.; Benson, L.A.; Fisk, A.S. Light and the laboratory mouse. *J. Neurosci. Methods* **2018**, *300*, 26–36.
314. Khabou, H.; Cordeau, C.; Pacot, L.; Fisson, S.; Dalkara, D. Dosage Thresholds and Influence of Transgene Cassette in Adeno-Associated Virus-Related Toxicity. *Hum. Gene Ther.* **2018**, *29*, 1235–1241.
315. Mingozzi, F.; High, K.A. Therapeutic in vivo gene transfer for genetic disease using AAV: progress and challenges. *Nat. Rev. Genet.* **2011**, *12*, 341–55.

Supplementary information

Table S1 Description of clinical trial rAAV gene therapy products in ophthalmology*Sponsor – Product – Clinical trial phase – Gene*

Achromatopsia (ACHM)
<p>MeiraGTx – AAV-CNGA3 – I/II – CNGA3</p> <p>Clinical trial start date (clinical trial identifier): 29-Nov-2018 (NCT03758404)</p> <p>rAAV: AAV2/8.hG1.7p.hCNGA3co.SV40polyA</p> <p>Proviral plasmid: pAAV.untoldR.ITR2.hG1.7p.hCNGA3co.SV40polyA.ITR2</p> <p>hG1.7p=Novel synthetic cone specific promoter. Core green opsin promoter including a mutation (0.5 kb) + Locus Control Region (LCR; 1.2 kb) upstream of the red opsin gene. Production platform: HEK293.</p> <p>Citation: [1–3]</p>
<p>STZ Eyetrial – rAAV.hCNGA3 – I/II – CNGA3</p> <p>Clinical trial start date (clinical trial identifier): 20-Nov-2015 (NCT02610582)</p> <p>rAAV: AAV2/8.hCAR.hCNGA3</p> <p>Proviral plasmid: pSub.KanR.ITR2.hCARp.hCNGA3co.WPREm.bGHpolyA</p> <p>hCAR= human cone arrestin (aka hArr3) 405 bp</p> <p>CNGA3= 2085 bp full-length human CNGA3 cDNA</p> <p>WPREm= WPRE is a mutated WPRE (WPREm) comprising non-expressible woodchuck hepatitis virus X protein (WHX) open reading frame (WHX OR). 543 bp</p> <p>bGHpolyA= bovine growth hormone 207 bp</p> <p>Production platform: AAV cis (pSub-hArr3-hCNGA3-WPREm-KanR) and trans (pDP8-KanR) in HEK293 cells. Citation: [4,5]</p>
<p>Applied Genetic Technologies Corp. (AGTC) – AGTC-402 – I/II – CNGA3</p> <p>Clinical trial start date (clinical trial identifier): 17-Oct-2019 (NCT02935517)</p> <p>rAAV: AAV2tYF.PR1.7p.SV40 SD/SA.hCNGA3co.SV40polyA</p> <p>Proviral plasmid: pAAV.untoldR.ITR2.PR1.7.SV40 SD/SA.hCNGA3co.SV40polyA.ITR2</p> <p>AAV2tYF=AAV serotype 2 with surface-exposed tyrosine mutations: Y275F, Y733F, Y447F.</p> <p>Production: (rHSV) complementation system in suspension-cultured baby hamster kidney (sBHK) cells</p> <p>Citation: [6,7]</p>
<p>Applied Genetic Technologies Corp. (AGTC) – rAAV2tYF-PR1.7-hCNGB3 – I/II – CNGB3</p> <p>Clinical trial start date (clinical trial identifier): 9-Nov-2015 (NCT02599922)</p> <p>rAAV: AAV2tYF.PR1.7.SV40 SD/SA.hCNGB3co.SV40polyA</p> <p>Proviral plasmid: pAAV.untoldR.ITR2.PR1.7p.SV40 SD/SA.hCNGB3co.SV40polyA.ITR2</p> <p>AAV2tYF= AAV serotype 2 with surface-exposed tyrosine mutations: Y275F, Y733F, Y447F.</p> <p>Production: (rHSV) complementation system in suspension-cultured baby hamster kidney (sBHK) cells</p> <p>Citation: [6–8]</p>
<p>MeiraGTx – either AAV-CNGB3 or AAV-CNGA3 – I/II – CNGB3/CNGA3</p> <p>Clinical trial start date (clinical trial identifier): 23-Dec-2016 (NCT03001310); 12-Sept-2017 (NCT03278873)</p> <p>rAAV: AAV2/8.hCARp.hCNGB3.SV40polyA or AAV2/8.hG1.7p.hCNGA3co.SV40polyA</p> <p>Proviral plasmid: pAAV.untoldR.ITR2.hCARp.hCNGB3.SV40polyA.ITR2 + pAAV.untoldR.ITR2.hG1.7p.hCNGA3co.SV40polyA.ITR2</p> <p>Production platform: HEK293. Citation: [1–3]</p>

Wet Age-Related Macular Degeneration (wet AMD)**Sanofi Genzyme – AAV2-sFLT01 – I/II**

Clinical trial start date (clinical trial identifier): 3-Dec-2009 (NCT01024998)

rAAV: rAAV2/2.CAGp.sFLT01.bGHpolyA

Proviral plasmid: pAAVSP70.untoldR.ITR2.CBA.sFLT01.bGHpolyA.ITR2

CBA: hybrid CMV/CBA promoter, derived from the pDRIVE CAG plasmid (Invivogen, San Diego, Calif.; having 100% sequence homology with the pCAGGS) with an upstream extension of about 49 nucleotides of CMV enhancer (1661 bp). CBA= proximal chicken β actin promoter and human beta-globin exon 1 and intron 1. The University of Pennsylvania considers CBA and CAGGS the same.

pAAVSP70 derived from pAV1 derived from pBR322. Citation: [9–14]

Adverum Biotechnologies – ADVM-022 - I

Clinical trial start date (clinical trial identifier): 21-Nov-2018 (NCT03748784)

rAAV: AAV2/7m8.eCMV.CMVp.sFLT01.hSAR.hGHpolyA

Proviral plasmid: pBAC-AAV.untoldR.ITR2.eCMV.pCMV.TLP.eMPL.SyntheticIntron.Kozak.sFLT01co.hSAR.hGHpolyA.ITR2

Production: Baculovirus, Sf9. (plasmids: rBAC-AAV. rBAC-RepCap)

eCMV = human early CMV enhancer. pCMV = human CMV promoter. TLP = adenovirus tripartite leader sequence. eMPL = major late promoter. SI = synthetic intron. pSI chimeric intron. 5 -donor site from the first intron of the human β -globin gene and the branch and 3 -acceptor site from the intron that lies between the leader and the body of an immunoglobulin gene heavy chain variable region [15]

sFLT01co = codon-optimized aflibercept (recombinant chimeric protein consisting of the vascular endothelial growth factor (VEGFA) binding portion of human VEGFR-1 (domain 2) and VEGFR-2 (domain 3 or KDR) fused to the Fc portion of human IgG1 immunoglobulin.). hSAR = human scaffold attachment region.

Citation: [15–17]

Oxford BioMedica – OXB-201 / RetinoStat – I

Clinical trial start date (clinical trial identifier): 23-Feb-2011 (NCT01301443); 5-Sept-2012 (NCT01678872)

Lenti: EIAV.CMVp.hEndo.IRES.hAngio.WPRE.LTR. Citation: [18]

Lions Eye Institute (Perth, Western Australia, Australia) / Adverum Biotechnologies – rAAV.sFlt-1 – I/II

Clinical trial start date (clinical trial identifier): 19-Dec-2011 (NCT01494805)

rAAV: AAV2/2.CMVp.chimericIntron.sFlt-1.SV40polyA

Proviral plasmid: pSSV9.untoldRAmpR.ITR2.CMV.ChimericIntron.sFlt-1.SV40polyA.ITR2

sFlt-1 = full-length soluble fms-like tyrosine kinase 1 (non-membrane associated splice variant of VEGF receptor 1 [sVEGFR-1]). Citation: [19–22]

Hemera Biosciences – AAVCAGsCD59 (HMR59) – I

Clinical trial start date (clinical trial identifier): 13-Jul-2018 (NCT03585556)

rAAV: AAV2/2.CAGp.sCD59.hGHpolyA

Proviral plasmid: pUC.untoldR.MCS(Stratagene).ITR2.CAG.sCD59.hGHpolyA.ITR2

sCD59 = soluble CD59 antigen binds C5b678 terminal complement protein complex and prevents incorporation of multiple C9 molecules (blockage of the Membrane attack complex [MAC] in the alternative complement cascade/pathway). Citation: [23,24]

Regenxbio – RGX-314 – I

Clinical trial start date (clinical trial identifier): 28-Feb-2017 (NCT03066258)

rAAV: AAV2/8.ITR.CB7p.aVEGFAfabH.(F)/F2A.aVEGFfabL.r β -globin-polyA.ITR

Proviral plasmid: pAAV.untoldR.ITR2.CAG/CB7.aVEGFAfabH.(F)/F2A.aVEGFfabL.r β -globin-polyA.ITR2

aVEGFAfabH = anti-VEGFA Heavy chain. Self-cleaving furin (F)/F2A linker. aVEGFAfabL = anti-VEGFA Light chain. r β -globin-polyA = rabbit β -globin polyA. Citation: [25]

Dry Age-Related Macular Degeneration (dry AMD) incl. Geographic Atrophy**Hemera Biosciences – AAVCAGsCD59 (HMR59) – I**

Clinical trial start date (clinical trial identifier): 9-May-2017 (NCT03144999)

rAAV: AAV2/2.CAGp.sCD59.hGHPolyA

Proviral plasmid: pUC.untoldR.MCS(Stratagene).ITR2.CAG.sCD59.hGHPolyA.ITR2

sCD59 = soluble CD59 antigen binds C5b678 terminal complement protein complex and prevents incorporation of multiple C9 molecules (blockage of the Membrane attack complex [MAC] in the alternative complement cascade/pathway). Citation: [23,24]

Gyroscope Therapeutics – GT005 – I/II

Clinical trial start date (clinical trial identifier): 19-Feb-2019 (NCT03846193)

rAAV: rAAV2/2.CBAP.hCFIco.WPRE.bGHPolyA

Proviral plasmid: pBR322.UntoldR.ITR2.CBA.CFI.WRPE.bGHPolyA.ITR2

hCFIco= human complement factor I codon-optimized (C3b/C4b inactivator). Increases the level of C3b-inactivating and iC3b-degradation activity in the RPE. Citation: [26,27]

Choroideremia**Biogen / Nightstar Therapeutics / University of Oxford (Oxford, OFE, UK) / University of Miami (Miami, FL, USA) / University of Alberta (Edmonton, AB, Canada) / STZ eyetrial (Tübingen, BW, Germany) – rAAV2-REP1 – I/II; II – CHM**

Clinical trial start date (clinical trial identifier): 28-Oct-2011 (NCT01461213); 4-Mar-2014 (NCT02077361); 3-Apr-2015 (NCT02407678); 17-Sept-2015 (NCT02553135); 2-Feb-2016 (NCT02671539); 25-Apr-2018 (NCT03507686); 12-Apr-2018 (NCT03496012); 12-Jul-2018 (NCT03584165);

rAAV: rAAV2/2.CBA.rabbit β-globin SD/SA.hCHM.WPRE.bGHPolyA

Proviral plasmid: pAAV.untoldR.ITR2.CBA.rabbit β-globin SD/SA.hCHM.WPRE.bGHPolyA.ITR2

Production: Triple co-transfection of HEK293 cells (AAV2 rep-cap helper plasmid; adenovirus helper plasmid containing E2A, E4ORF6, and VA RNA ORFs; pAAV). Citation: [28–30]

Spark Therapeutics – AAV2-REP1 – I/II – CHM

Clinical trial start date (clinical trial identifier): 19-Jan-2015 (NCT02341807)

rAAV: AAV2/2.CBAP.hCHM.bGHPolA.

Proviral plasmid: pAAV.Stuffer.KanR.ITR2.CBA.hCHM.bGHPolA.ITR2. Citation: [31]

Leber Congenital Amaurosis**Allergan / Editas Medicine Inc– AGN-151587 (EDIT-101) – I/II – LCA10 – CEP290**

Clinical trial start date (clinical trial identifier): 13-Mar-2019 (NCT03872479)

rAAV: AAV2/5.U6.CEP290gRNAs323/U6.CEP290gRNAs64.hGrk1.Kozak.SV40

SA/SD.SaCas9.NLS.spA

Proviral plasmid: pAAV.untoldR.ITR2.U6.CEP290gRNAs323/U6.CEP290gRNAs64.hGrk1p.Kozak.SV40

SA/SD.SaCas9.NLS.SyntheticPolyA.ITR2

CEP290 rescue= in intron 26 of CEP290 (IVS26 c.2991+1655 A>G) gene editing (removal) of the mutation (p.Cys998X). Modified synthetic polyA sequence: (bold+underlined=synthetic polyA sequence. 60 bp).

TAGC**ATAAAGGATCGTTTATTTTCATTGGAAGCGTGTGTTGGTTTTTTGATCAGGCGCG**

Production: HEK293. Citation: [32,33]

ProQR – QR-110 – I/II & II/III – LCA10 – CEP290

AON technology. p.Cys998X mutation correction on mRNA level

Clinical trial start date (clinical trial identifier): 20-Sept-2018 (NCT03140969); 12-Apr-2019

(NCT03913143); 2-Aug-2019 (NCT03913130). Citation: [34]

Genzyme / Sanofi - SAR439483 – I/II – GUCY2D

Clinical trial start date (clinical trial identifier): 18-Apr-2019 (NCT03920007)

rAAV: AAV2/5.hGRK1p.SV40 SA/SD.GUCY2D.bGHPolyA

Proviral plasmid: pAAV.puromycinR.ITR2.hGRK1p.SV40 SA/SD.GUCY2D.bGHPolyA.ITR2

Production platform: HeLaS3. Citation: [35,36]

Spark Therapeutics – AAV2-RPE65 (hRPE65v2) – III – RPE65 *FDA & EMA approved

Clinical trial start date (clinical trial identifier): 15-Aug-2007 (NCT00516477); 24-Sep-2010 (NCT01208389); 26-Mar-2018 (NCT00999609); 24-Jul-2018 (NCT03597399); 27-Jul-2018 (NCT03602820);

rAAV: AAV2/2.CBAp.hRPE65.bGHpolA

CBA: hybrid CMV/CAG promoter, derived from the pDRIVE CAG plasmid (Invivogen, San Diego, Calif.; having 100% sequence homology with the pCAGGS) with an upstream extension of about 49 nucleotides of CMV enhancer (1661 bp). CBA= proximal chicken β -actin promoter and human β -globin exon 1 and intron 1. The University of Pennsylvania considers CBA and CAGGS the same.

Proviral plasmid: pAAV.Stuffer.KanR.ITR2.CBA.hRPE65.bGHpolA.ITR2. Citation: [37]

Applied Genetic Technologies Corp (AGTC) / Hadassah Medical Organization (Jerusalem, Israel) / University of Pennsylvania (Pennsylvania, USA) – AAV2-CBSB-RPE65 – I + I/II – RPE65

Clinical trial start date (clinical trial identifier): 1-Jun-2007 (NCT00481546); 13-Jan-2009 (NCT00821340); 10-Sept-2008 (NCT00749957);

rAAV: AAV2/2.CB-SBp.hRPE65.SV40polyA

Proviral plasmid: pAAV.KanR.ITR2.CB-SBp.hRPE65.SV40polyA.ITR2. CB-SB: 152 bp-shortened CBA promoter on CMV enhancer 5' end. Production: HEK293 cells, two-plasmid system. Citation: [38,39]

MeiraGTx – AAV2/5-OPTIRPE65 – I/II - RPE65

Clinical trial start date (clinical trial identifier): 27-Okt-2016 (NCT02946879) 24-May-2016 (NCT02781480)

rAAV: AAV2/5.NA65p.SV40Intron.hRPE65co.SV40polyA

Proviral plasmid: pAAV.untoldR.ITR2.NA65p.SV40Intron.hRPE65co.SV40polyA.ITR2

NA65p= optimized human RPE65 promoter stronger than CBA

Production: HEK293T cells, three-plasmid system. Citation: [40]

Nantes University Hospital (Nantes, France) – rAAV-2/4hRPE65 – I/II - RPE65

Clinical trial start date (clinical trial identifier): 21-Dec-2011 (NCT01496040)

rAAV: AAV2/4.hRPEp.hRPE65.bGHpolyA

Proviral plasmid: pAAV.untoldR.ITR2.hRPE65p.hRPE65.bGHpolyA.ITR2

Production: HEK293T cells, two-plasmid system (pDP4-Kana helper plasmid)

Citation: [41]

University College (London, UK) – tgAAG76 (rAAV 2/2.hRPE65p.hRPE65) – I/II - RPE65

Clinical trial start date (clinical trial identifier): 26-Mar-2008 (NCT00643747)

rAAV: AAV2/2.hRPE65p.hRPE65.bGHpolyA

Proviral plasmid: pAAV.untoldR.ITR2.hRPE65p.hRPE65.bGHpolyA.ITR2

hRPE65p= 1.6 kb human RPE65 promoter

Production: B50 cell line utilizing helper adenovirus. Citation: [42]

Leber Hereditary Optic Neuropathy (LHON)**GenSight Biologics – GSO10 – III – G11778A mtDNA**

Clinical trial start date (clinical trial identifier): 17-Feb-2014 (NCT02064569); 12-Jan-2016 (NCT02652780); 12-Jan-2016 (NCT02652767); 26-Sept-2017 (NCT03293524); 23-Jan-2018 (NCT03406104); 17-Sep-2018 (NCT03672968)

rAAV: AAV2/2.ND4

Proviral plasmid: pAAV2.untoldR.ITR.CMVp.HBB2.MTS-COX10.hND4.3'COX10.ITR

HBB2=human β -globulin intron

Production: HEK293 cells. Citation: [43–46]

University of Miami (Miami, FL, USA) – scAAV2-P1ND4v2 – I – G11778A mtDNA

Clinical trial start date (clinical trial identifier): 11-Jun-2011 (NCT02161380);
rAAV: scAAV2/2-tyF.smCMVp. ATP1mt(MTS).hND4.bGHpolA
Proviral plasmid: pBS.UntoldR.ITR2Δ.Sc-trs.smCMVp.ATP1mt(MTS).hND4.WPRE.bGHpolA .ITR2
(P1ND4v2). smCBA= a truncated chimeric CMV/CBA promoter (953 bp)
MTS=ATP1-based mitochondrial targeting sequence
AAV2-tyF= AAV2 mutated capsids Y444F+Y500F+Y730F
Production: HEK293 cells. Citation: [47,48]

Huazhong University of Science and Technology (Huazhong, Hubei Sheng, China) – rAAV2-ND4– not applicable – G11778A mtDNA

Clinical trial start date (clinical trial identifier): 28-Dec-2010 (NCT01267422); 15-May-2017
(NCT03153293); 9-Feb-2018 (NCT03428178)
rAAV: AAV2/2.CMVp.COX10(5'UTR).ND4.COX10(3'UTR).bGHpolyA
Proviral plasmid: pSNAV.neoR.ITR2.CMV.COX10(5'UTR).ND4.COX10(3'UTR).bGHpolyA.ITR2
COX10(5'UTR)= mitochondrial targeting sequence
Production: HEK293 + HSV1-rc/ΔUL2. Beijing FivePlus Molecular Medicine Institute. Citation: [49–51]

Retinitis Pigmentosa

Allergan / RetroSense Therapeutics – RST-001 – I/II – advanced RP

Clinical trial start date (clinical trial identifier): 22-Sep-2015 (NCT02556736)
rAAV: AAV2/2.CBAp.Chop2/ChR2.WPRE.bGHpolyA
Proviral plasmid: pAAV.untoldR.ITR2.CBAp.Chop2/ChR2.WPRE.bGHpolyA.ITR2
Chop2/ChR2= Microbial type rhodopsins. Light-gated cation-selective membrane channel rhodopsin-2
CBA= hybrid CMV/CBA promoter, derived from the pDRIVE CAG plasmid (Invivogen, San Diego, Calif.;
having 100% sequence homology with the pCAGGS) with an upstream extension of about 49 nucleotides of
CMV enhancer (1661 bp). THE CBA= proximal chicken β actin promoter and human beta-globin exon 1
and intron 1. The University of Pennsylvania considers CBA and CAGGS the same.
Production: HEK293. Citation: [12,52–54]

jCyte, Inc – jCell – I, II – RP

Clinical trial start date (clinical trial identifier): 19-Dec-2014 (NCT02320812); 5-Mrt-2017 (NCT03073733)
Single intravitreal injection of 0.5 - 3.0 million human retinal progenitor cells (hRPC). Citation: [55,56]

ReNeuron Limited – hRPCRP– I/II – RP

Clinical trial start date (clinical trial identifier): 8-Jun-2015 (NCT02464436)
Participants will undergo vitrectomy surgery and subretinal implantation of human retinal progenitor cells
(hRPC) in the study eye.

GenSight Biologics– rAAV2.7m8-CAG-ChrimsonR-tdTomato (GS030) – I/II – non-syndromic

Clinical trial start date (clinical trial identifier): 31-Oct-2017 (NCT03326336)
rAAV: rAAV2/7m8.CAGp.ChrimsonR-tdTomato.bGHpolyA
Proviral plasmid: pAAV.KanR.ITR2.CAG.ChrimsonR-tdTomato.bGHpolyA.ITR2
AAV2 7m8= AAV serotype 2 mutated capsid variant AAV2-⁵⁸⁸LALGETTRP. No sialic acid dependence.
Lower heparin affinity. Expression of Channelrhodopsin in retinal ganglion cells. Citation: [57–59]

Bionic Sight LLC / Applied Genetic Technologies Corp (AGTC) – BSO1 – I/II

Clinical trial start date (clinical trial identifier): 06-Feb-2020 (NCT04278131)
rAAV: AAV(untold).untold.ChronosFP(Chr90-fluorescent protein).untold. Proviral plasmid: untold
Expression of channelrhodopsin variant chronos (fast acting) in retinal ganglion cells

Horama SA – AAV2/5-hPDE6B – I/II – PDE6B

Clinical trial start date (clinical trial identifier): 1-Nov-2017 (NCT03328130)
rAAV: rAAV2/5.hGRK1p.hPED6B.bGHpolyA
Proviral plasmid: pAAV.untoldR.ITR2.hGRK1.hPED6B.bGHpolyA.ITR2. Citation: [60,61]

King Khaled Eye Specialist Hospital (Riyadh, Saudi Arabia) – rAAV2-VMD2-hMERTK – I/II – MERTK

Clinical trial start date (clinical trial identifier): 30-Nov-2011 (NCT01482195)
 rAAV: rAAV2/2.hVMD2p.SV40 SD/SD.hMERTK.SV40polyA.bGHPolyA
 Proviral plasmid: pTR.ColE1ori.untoldR.F1(+).ori.ITR2.hVMD2p.SV40 SD/SD.hMERTK.SV40polyA.bGHPolyA.ITR2
 hVMD2p= human VMD2 promoter (- 585 to + 38 bp region. 623 bp)
 Production: HEK293 co-transfection (pTR-VMD2-hMerTK and pDG-KanR). Citation: [62]

Novartis – CPK850 AAV8 – I/II – RLBPI

Clinical trial start date (clinical trial identifier): 15-Dec-2017 (NCT03374657)
 rAAV: scAAV2/8.sRLBP1p.modSV40.hRLBPI.SV40polyA
 Proviral plasmid: pAAV.untoldR.ITR2Δ.sRLBP1p.modSV40 SA/SD.hRLBPI.SV40polyA.ITR2 modSV40 SA/SD= modified SV40 splice acceptor/donor intron, 157 bp in length, nucleotides 502–561 and 1,410–1,497 of SV40 genomic sequence (NC_001669.1) + connecting sequence CCGATCCGG between two fragments.
 Production: AAV293 in CellSTACK (HEK293 subclone; Stratagene). Triple-plasmid transfection (pHelper, pRep2Cap8, pAAV). Citation: [63,64]

Applied Genetic Technologies Corp. (AGTC)/Biogen-rAAV2tYF-GRK1-RPGR (AGTC-501/BIIB088)-I/II-RPGR

Clinical trial start date (clinical trial identifier): 20-Oct-2017 (NCT03316560)
 rAAV: AAV2/2tYF.hGRK1p.SV40 SA/SD.hRPGR/co-ORF15.SV40polyA
 Proviral plasmid: pAAV.untoldR.ITR2.hGRK1p.SV40 SA/SD.hRPGR/co-ORF15.SV40polyA.ITR2
 hGRK1p= 292 bp human GRK1 promoter (positions 1793-2087)
 SV40 SA/SD= 100 bp mini SV40 splice donor/acceptor intron
 hRPGR/co = Based on GenBank reference mRNA sequence NM_001034853 hRPGR isoform C. Codon optimized based on human codon usage, reduced tandem repeats, adjusted G/C content
 2tYF= AAV2 triple YF mutations
 Production: recombinant herpes simplex virus (HSV) complementation system in suspension-cultured baby hamster kidney (sBHK) cells
 Citation: [65,66]

MeiraGTx UK II Ltd / Janssen – AAV-RPGR – I/II – RPGR

Clinical trial start date (clinical trial identifier): 17-Aug-2017 (NCT03252847)
 rAAV: AAV2/5.hGRK1p.SV40 SD/SA.hRPGR-ORF15-L.SV40polyA
 Proviral plasmid: pAAV.untoldR.ITR2.hGRK1.SV40 SD/SA.hRPGR-ORF15-L.SV40polyA.ITR2
 hRPGR-ORF15-L= small-deletion human hRPGR-ORF15 'long form' (codons 862-988del) expresses a human RPGR-ORF15 protein of ~170 kD
 Citation: [67,68]

Nightstar Therapeutics / Biogen - AAV-RPGR – II/III – RPGR

Clinical trial start date (clinical trial identifier): 14-Apr-2017 (NCT03116113)
 rAAV: AAV2/8.hGRK1p.hRPGRco-ORF15co.bGHPolyA
 Proviral plasmid: pAAV.untoldR.ITR2.hGRK1.hRPGRco-ORF15.bGHPolyA.ITR2 (AAV2.CBA.eGFP cat. 7072 Vector Biolabs)
 Production: HEK293T Hyperflask. Two-plasmid co-transfection: pDP8.ape (PlasmidFactory) + pAAV
 Citation: [69,70]

Usher syndrome

ProQR - QR-421a (STELLAR) – I/II – USH2A Exon 13

Clinical trial start date (clinical trial identifier): 19-Dec-2018 (NCT03780257)

RNA therapies antisense oligonucleotide exon-13 skipping

Citation: [34]

Sanofi / Oxford Biomedical - EIAV-CMV-MYO7A (UshStat) – I/II – Usher syndrome type 1B / MYO7A

Clinical trial start date + #: 6-Jan-2012 (NCT01505062); 17-Feb-2014 (NCT02065011)

Lenti: EIAV.SIN-LTR.NeoR.CMVp.hMYO7A.WPRE.SIN-LTR

Production: HEK293T co-transfection pHCMVG, pESynGP, pONY8-EIAV.CMV.hMYO7A.LTR (based on pLG338-SPORT).

Citation: [71–73]

Stargardt disease

Sanofi / Oxford Biomedical - EIAV-ABCA4 (SAR422459) – I/II – ABCA4

Clinical trial start date (clinical trial identifier): 7-Jun-2011 (NCT01367444); 29-Nov-2012 (NCT01736592)

Lenti: EIAV.CMVp.ABCA4.LTR

Plasmid: pONY8-EIAV.SIN-LTR.NeoR.CMVp.hABCA4.SIN-LTR

Production: HEK293T co-transfection pHCMVG, pESynGP, pONY8-EIAV.CMV.ABCA4.LTR (based on pONY4.0Z and pLG338-SPORT).

Citation: [72–74]

X-linked retinoschisis

Applied Genetic Technologies Corp. (AGTC) / Biogen - rAAV2tYF-CB-hRS1 – I/II – RSI

Clinical trial start date (clinical trial identifier): 15-Apr-2015 (NCT02416622)

rAAV: AAV2tYF.CBp.hRS1.WPRE.SV40polyA

Proviral plasmid: pTR-AAV.untoldR.ITR2.smCB.hRS1.WPRE.SV40polyA.ITR2

smCB= 953 bp chimeric CMV-chicken β -actin promoter (shortened hybrid chicken β -actin/rabbit β -globin intron)

tYF= AAV serotype 2 with surface-exposed tyrosine mutations: Y275F, Y733F, Y447F.

Production: rHSV + sBHK cells. Two-plasmid co-transfection system (pAAV,

pHelper(AAV2rep.AAV2tYFCap)

Citation: [75–77]

National Eye Institute (Washington DC, USA) - AAV8-RS1 – I/II – RSI

Clinical trial start date (clinical trial identifier): 17-Dec-2017 (NCT02317887)

rAAV: scAAV2/8.IRBPe.hRS1p.hRS1.hBGpolyA

Proviral plasmid: pAAV.untoldR.ITR2 Δ .IRBPe.hRS1p.hRS1.hBGpolyA.ITR2

IRBPe= interphotoreceptor retinoid-binding protein (IRBP) enhancer element

hRS1p= modified tissue-selective human retinoschisin promoter

hRS1=an intact human retinoschisin cDNA with a truncated first intron located in its authentic position between the exon 1 and 2 sequences

hBGpolyA= human β -globin 3' UTR and polyadenylation site

Production: triple co-transfection of HEK293 cells

Citation: [78–80]

UntoldR, not reported in the primary literature

Supplementary information references

1. Georgiadis, A.; Matsuki, T.; Rizzi, M.; Hoke, J.; Gonzalez-Cordero, A.; Sampson, R.; Bainbridge, J.; Smith, A.; Ali, R. ARVO Annual Meeting Poster A197 Development and efficacy assessment of AAV2/8-hG1.7p.coCNGA3, a CNGA3 gene therapy vector. *Invest. Ophthalmol. Vis. Sci.* **2019**, *60*, 3426.
2. Rizzi, M.; Ali, R.; Smith, A.; Nishiguchi, K. Gene therapy to improve vision. Patent US20180030477A1 2015, 1–66.
3. Forbes, A. *United States Securities and exchange commission (SEC) Form S-1 registration statement MeiraGTx Holdings plc*; Washington, D.C, 2018;
4. Michalakakis, S.; Biel, M.; Seeliger, M. Gene therapy to improve vision. Patent US20180353619A1 2016, 1–23.
5. Michalakakis, S.; Mühlfriedel, R.; Tanimoto, N.; Krishnamoorthy, V.; Koch, S.; Fischer, M.D.; Becirovic, E.; Bai, L.; Huber, G.; Beck, S.C.; et al. Restoration of cone vision in the CNGA3^{-/-} mouse model of congenital complete lack of cone photoreceptor function. *Mol. Ther.* **2010**, *18*, 2057–63.
6. Ye, G.-J. Promoters, expression cassettes, vectors, kits, and methods for the treatment of achromatopsia and other diseases. Patent US201361824071P 2013.
7. Gootwine, E.; Ofri, R.; Banin, E.; Obolensky, A.; Averbukh, E.; Ezra-Elia, R.; Ross, M.; Honig, H.; Rosov, A.; Yamin, E.; et al. Safety and Efficacy Evaluation of rAAV2(YF-PR1.7-hCNGA3 Vector Delivered by Subretinal Injection in CNGA3 Mutant Achromatopsia Sheep. *Hum. Gene Ther. Clin. Dev.* **2017**, *28*, 96–107.
8. Ye, G.; Budzinski, E.; Sonnentag, P.; Nork, T.M.; Miller, P.E.; Sharma, A.K.; Ver Hoeve, J.N.; Smith, L.M.; Arndt, T.; Calcedo, R.; et al. Safety and Biodistribution Evaluation in Cynomolgus Macaques of rAAV2(YF-PR1.7-hCNGA3), a Recombinant AAV Vector for Treatment of Achromatopsia. *Hum. Gene Ther. Clin. Dev.* **2016**, *27*, 37–48.
9. Scaria, A. Compositions and methods for treating and preventing macular degeneration. Patent US20170007719A1 2014, 1–61.
10. Ziegler, R.J.; Lonning, S.M.; Armentano, D.; Li, C.; Souza, D.W.; Cherry, M.; Ford, C.; Barbon, C.M.; Desnick, R.J.; Gao, G.; et al. AAV2 vector harboring a liver-restricted promoter facilitates sustained expression of therapeutic levels of alpha-galactosidase A and the induction of immune tolerance in Fabry mice. *Mol. Ther.* **2004**, *9*, 231–40.
11. Laughlin, C.A.; Tratschin, J.D.; Coon, H.; Carter, B.J. Cloning of infectious adeno-associated virus genomes in bacterial plasmids. *Gene* **1983**, *23*, 65–73.
12. Bennett, J. Taking Stock of Retinal Gene Therapy: Looking Back and Moving Forward. *Mol. Ther.* **2017**, *25*, 1076–1094.
13. Pechan, P.; Rubin, H.; Lukason, M.; Ardinger, J.; DuFresne, E.; Hauswirth, W.W.; Wadsworth, S.C.; Scaria, A. Novel anti-VEGF chimeric molecules delivered by AAV vectors for inhibition of retinal neovascularization. *Gene Ther.* **2009**, *16*, 10–6.
14. Heier, J.S.; Kherani, S.; Desai, S.; Dugel, P.; Kaushal, S.; Cheng, S.H.; Delacono, C.; Purvis, A.; Richards, S.; Le-Halpere, A.; et al. Intravitreal injection of AAV2-sFLT01 in patients with advanced neovascular age-related macular degeneration: a phase 1, open-label trial. *Lancet (London, England)* **2017**, *390*, 50–61.
15. Bothwell, A.L.M.; Paskind, M.; Reth, M.; Imanishi-Kari, T.; Rajewsky, K.; Baltimore, D. Heavy chain variable region contribution to the NPb family of antibodies: somatic mutation evident in a $\gamma 2a$ variable region. *Cell* **1981**, *24*, 625–637.
16. Grishanin, R.; Vuilleminot, B.; Sharma, P.; Keravala, A.; Greengard, J.; Gelfman, C.; Blumenkrantz, M.; Lawrence, M.; Hu, W.; Kiss, S.; et al. Preclinical Evaluation of ADVDM-022, a Novel Gene Therapy Approach to Treating Wet Age-Related Macular Degeneration. *Mol. Ther.* **2019**, *27*, 118–129.
17. Chalberg, T.W.; Neitz, J.; Neitz, M. Compositions and methods for enhanced gene expression in cone cells. Patent US20150259395A1 2015, 1–154.
18. Parker, M.; Bellec, J.; McFarland, T.; Scripps, V.; Appukuttan, B.; Hartzell, M.; Yeager, A.; Hady, T.; Mitrophanous, K.A.; Stout, T.; et al. Suppression of neovascularization of donor corneas by transduction with equine infectious anemia virus-based lentiviral vectors expressing endostatin and angiostatin. *Hum. Gene Ther.* **2014**, *25*, 408–18.
19. Lai, C.-M.; Estcourt, M.J.; Wikstrom, M.; Himbeck, R.P.; Barnett, N.L.; Brankov, M.; Tee, L.B.G.; Dunlop, S. a; Degli-Esposti, M. a; Rakoczy, E.P. rAAV.sFlt-1 gene therapy achieves lasting reversal of retinal neovascularization in the absence of a strong immune response to the viral vector. *Invest. Ophthalmol. Vis. Sci.* **2009**, *50*, 4279–87.
20. Rakoczy, E.P.; Lai, C.-M.; Magno, A.L.; Wikstrom, M.E.; French, M.A.; Pierce, C.M.; Schwartz, S.D.; Blumenkrantz, M.S.; Chalberg, T.W.; Degli-Esposti, M.A.; et al. Gene therapy with recombinant adeno-associated vectors for neovascular age-related macular degeneration: 1 year follow-up of a phase 1 randomised clinical trial. *Lancet (London, England)* **2015**, *386*, 2395–403.
21. Constable, I.J.; Pierce, C.M.; Lai, C.M.; Magno, A.L.; Degli-Esposti, M.A.; French, M.A.; McAllister, I.L.; Butler, S.; Barone, S.B.; Schwartz, S.D.; et al. Phase 2a Randomized Clinical Trial: Safety and Post Hoc Analysis of Subretinal rAAV.sFLT-1 for Wet Age-related Macular Degeneration. *EBioMedicine* **2016**, *14*, 168–175.
22. Constable, I.J.; Rakoczy, E.P.; Lai, C.-M.; Chalberg, T.W.J. Treatment of amd using aav sflt-1. Patent US20140341977A1 2014, 1–127.

23. Cashman, S.M.; Ramo, K.; Kumar-Singh, R. A non membrane-targeted human soluble CD59 attenuates choroidal neovascularization in a model of age related macular degeneration. *PLoS One* **2011**, *6*.
24. Kumar-Singh, R.; Leaderer, D.; Cashman, S. Compositions, kits and methods for treatment of complement-related disorders. Patent US20170209535A1 2017, 1–45.
25. Liu, Y.; Fortmann, S.D.; Shen, J.; Wielechowski, E.; Tretiakova, A.; Yoo, S.; Kozarsky, K.; Wang, J.; Wilson, J.M.; Campochiaro, P.A. AAV8-anti-VEGF Fab Ocular Gene Transfer for Neovascular Age-Related Macular Degeneration. *Mol. Ther.* **2018**, *26*, 542–549.
26. Groendahl, C.; Funnell, T.; Hollowood, C. Gene Therapy. Patent US20190255193A1 2015, 1–53.
27. Buchberger, A. PhD thesis: The therapeutic utility of Factor I in the treatment of complement dependent pathophysiological processes, University of Leicester, 2016.
28. MacLaren, R.E.; Groppe, M.; Barnard, A.R.; Cottrill, C.L.; Tolmachova, T.; Seymour, L.; Reed Clark, K.; During, M.J.; Cremers, F.P.M.; Black, G.C.M.; et al. Retinal gene therapy in patients with choroideremia: Initial findings from a phase 1/2 clinical trial. *Lancet* **2014**, *383*, 1129–1137.
29. Jacobson, S.G.; Cideciyan, A. V.; Ratnakaram, R.; Heon, E.; Schwartz, S.B.; Roman, A.J.; Peden, M.C.; Aleman, T.S.; Boye, S.L.; Sumaroka, A.; et al. Gene therapy for leber congenital amaurosis caused by RPE65 mutations: safety and efficacy in 15 children and adults followed up to 3 years. *Arch. Ophthalmol. (Chicago, Ill. 1960)* **2012**, *130*, 9–24.
30. Lam, B.L.; Davis, J.L.; Gregori, N.Z.; MacLaren, R.E.; Girach, A.; Verriotto, J.D.; Rodriguez, B.; Rosa, P.R.; Zhang, X.; Feuer, W.J. Choroideremia Gene Therapy Phase 2 Clinical Trial: 24-Month Results. *Am. J. Ophthalmol.* **2019**, *197*, 65–73.
31. Wright, J.F.; Sumaroka, M. Rab escort protein potency assay. Patent US201662418637P 2016, 1–16.
32. Maeder, M.L.; Stefanidakis, M.; Wilson, C.J.; Baral, R.; Barrera, L.A.; Bounoutas, G.S.; Bumcrot, D.; Chao, H.; Ciulla, D.M.; DaSilva, J.A.; et al. Development of a gene-editing approach to restore vision loss in Leber congenital amaurosis type 10. *Nat. Med.* **2019**, *25*, 229–233.
33. Maeder, M.L.; Bumcrot, D.A.; Shen, S. CRISPR/CAS-related methods and compositions for treating Leber's Congenital Amaurosis 10 (LCA10). Patent US10253312B 2014, 1–298.
34. Vázquez-Domínguez, I.; Garanto, A.; Collin, R.W.J. Molecular Therapies for Inherited Retinal Diseases-Current Standing, Opportunities and Challenges. *Genes (Basel)*. **2019**, *10*.
35. Nass, S.A.; Mattingly, M.A.; Woodcock, D.A.; Burnham, B.L.; Ardinger, J.A.; Osmond, S.E.; Frederick, A.M.; Scaria, A.; Cheng, S.H.; O'Riordan, C.R. Universal Method for the Purification of Recombinant AAV Vectors of Differing Serotypes. *Mol. Ther. - Methods Clin. Dev.* **2018**, *9*, 33–46.
36. Boye, S.E.; Boye, S.L.; Pang, J.; Ryals, R.; Everhart, D.; Umino, Y.; Neeley, A.W.; Besharse, J.; Barlow, R.; Hauswirth, W.W. Functional and behavioral restoration of vision by gene therapy in the guanylate cyclase-1 (GC1) knockout mouse. *PLoS One* **2010**, *5*, e11306.
37. Bennett, J. Gene- and Cell-Based Treatment Strategies for the Eye. In *Essentials in Ophthalmology*; Rakoczy, E.P., Ed.; Springer, Berlin, Heidelberg: Berlin Heidelberg, 2015; pp. 9–25 ISBN 978-3-662-45187-8.
38. Banin, E.; Bandah-Rozenfeld, D.; Obolensky, A.; Cideciyan, A. V.; Aleman, T.S.; Marks-Ohana, D.; Sela, M.; Boye, S.; Sumaroka, A.; Roman, A.J.; et al. Molecular anthropology meets genetic medicine to treat blindness in the North African Jewish population: Human gene therapy initiated in Israel. *Hum. Gene Ther.* **2010**, *21*, 1749–1757.
39. Jacobson, S.G.; Acland, G.M.; Aguirre, G.D.; Aleman, T.S.; Schwartz, S.B.; Cideciyan, A. V.; Zeiss, C.J.; Komaromy, A.M.; Kaushal, S.; Roman, A.J.; et al. Safety of Recombinant Adeno-Associated Virus Type 2-RPE65 Vector Delivered by Ocular Subretinal Injection. *Mol. Ther.* **2006**, *13*, 1074–1084.
40. Georgiadis, A.; Duran, Y.; Ribeiro, J.; Abelleira-Hervas, L.; Robbie, S.J.; Sünkel-Laing, B.; Fourali, S.; Gonzalez-Cordero, A.; Cristante, E.; Michaelides, M.; et al. Development of an optimized AAV2/5 gene therapy vector for Leber congenital amaurosis owing to defects in RPE65. *Gene Ther.* **2016**, *23*, 857–862.
41. Le Meur, G.; Lebranchu, P.; Billaud, F.; Adjali, O.; Schmitt, S.; Béziau, S.; Péréon, Y.; Valabregue, R.; Ivan, C.; Darmon, C.; et al. Safety and Long-Term Efficacy of AAV4 Gene Therapy in Patients with RPE65 Leber Congenital Amaurosis. *Mol. Ther.* **2018**, *26*, 256–268.
42. Bainbridge, J.W.B.; Mehat, M.S.; Sundaram, V.; Robbie, S.J.; Barker, S.E.; Ripamonti, C.; Georgiadis, A.; Mowat, F.M.; Beattie, S.G.; Gardner, P.J.; et al. Long-term effect of gene therapy on Leber's congenital amaurosis. *N. Engl. J. Med.* **2015**, *372*, 1887–1897.
43. Cwerman-Thibault, H.; Augustin, S.; Lechaue, C.; Ayache, J.; Ellouze, S.; Sahel, J.A.; Corral-Debrinski, M. Nuclear expression of mitochondrial ND4 leads to the protein assembling in complex I and prevents optic atrophy and visual loss. *Mol. Ther. - Methods Clin. Dev.* **2015**, *2*, 15003.
44. Lemanssier, S.; Brovedani, F. *2017 Registration document including the annual financial report the management report and the corporate governance report*; Paris, France, 2018;
45. Katz, B. *Innovation Showcase - GenSight: OIS @ American Society of Cataract and Refractive Surgery (ASCRS)*; San Diego, CA, USA, 2019;

46. Biologics, G. Summary notification information format for the release of genetically modified organisms other than higher plants in accordance with article 11 of directive 2001/18/EC Available online: <https://gmoinfo.jrc.ec.europa.eu/bsnifs-gmo/B-FR-13-GT05.pdf>.
47. Koilkonda, R.; Yu, H.; Talla, V.; Porciatti, V.; Feuer, W.J.; Hauswirth, W.W.; Chiodo, V.; Erger, K.E.; Boye, S.L.; Lewin, A.S.; et al. LHON gene therapy vector prevents visual loss and optic neuropathy induced by G11778A mutant mitochondrial DNA: Biodistribution and toxicology profile. *Investig. Ophthalmol. Vis. Sci.* **2014**, *55*, 7739–7753.
48. Koilkonda, R.D.; Chou, T.H.; Porciatti, V.; Hauswirth, W.W.; Guy, J. Induction of rapid and highly efficient expression of the human ND4 complex I subunit in the mouse visual system by self-complementary adeno-associated virus. *Arch. Ophthalmol.* **2010**, *128*, 876–883.
49. Yang, S.; Ma, S. qi; Wan, X.; He, H.; Pei, H.; Zhao, M. jian; Chen, C.; Wang, D. wen; Dong, X. yan; Yuan, J. jia; et al. Long-term outcomes of gene therapy for the treatment of Leber's hereditary optic neuropathy. *EBioMedicine* **2016**, *10*, 258–268.
50. Wu, Z.; Wu, X.; Cao, H.; Dong, X.; Wang, H.; Hou, Y. A novel and highly efficient production system for recombinant adeno-associated virus vector. *Sci. China, Ser. C Life Sci.* **2002**, *45*, 96–104.
51. Xiaobing, W.(吴小兵); Wenhong, T.(田文洪); Zheyue, D.(董哲岳); Xiaoyan, D.(董小岩) AAV vector-based high-throughput miRNA activity detection method, and applications thereof. Patent CN102719556A 2011.
52. Zhang, Z.; Feng, J.; Wu, C.; Lu, Q.; Pan, Z.H. Targeted expression of channelrhodopsin-2 to the axon initial segment alters the temporal firing properties of retinal ganglion cells. *PLoS One* **2015**, *10*.
53. Rodrigues, G.A.; Shalaev, E.; Karami, T.K.; Cunningham, J.; Slater, N.K.H.; Rivers, H.M. Pharmaceutical Development of AAV-Based Gene Therapy Products for the Eye. *Pharm. Res.* **2019**, *36*.
54. Pan, Z.-H. AAV-mediated subcellular targeting of heterologous rhodopsins in retinal ganglion cells. Patent US9968689B2 2010, 1–101.
55. Tucker, B.A.; Park, I.-H.; Qi, S.D.; Klassen, H.J.; Jiang, C.; Yao, J.; Redenti, S.; Daley, G.Q.; Young, M.J. Transplantation of adult mouse iPS cell-derived photoreceptor precursors restores retinal structure and function in degenerative mice. *PLoS One* **2011**, *6*, e18992.
56. Wiley, L.A.; Burnight, E.R.; Deluca, A.P.; Anfinson, K.R.; Cranston, C.M.; Kaalberg, E.E.; Penticoff, J.A.; Affatigato, L.M.; Mullins, R.F.; Stone, E.M.; et al. CGMP production of patient-specific iPSCs and photoreceptor precursor cells to treat retinal degenerative blindness. *Sci. Rep.* **2016**, *6*, 22–24.
57. Douar, A.M.; Bouquet, C.; Pruneau, D.; Chavas, J.; Dalkara, D.; Duebel, J.; Benosman, R.; Chenegros, G.; Picaud, S.; Sahel, J.; et al. 268. Optogenetic Engineering of Retinal Ganglion Cells with AAV2.7m8-ChrimsonR-tdTomato (GS030-DP) Is Well Tolerated and Induces Functional Responses to Light in Non-Human Primates. *Mol. Ther.* **2016**, *24*, S106–S107.
58. Dalkara, D.; Byrne, L.C.; Klimczak, R.R.; Visel, M.; Yin, L.; Merigan, W.H.; Flannery, J.G.; Schaffer, D. V In Vivo-Directed Evolution of a New Adeno-Associated Virus for Therapeutic Outer Retinal Gene Delivery from the Vitreous. *Sci. Transl. Med.* **2013**, *5*, 189ra76–189ra76.
59. Dalkara, D.; Picaud, S.; Desrosiers, M.; Sahel, J.-A.; Duebel, J.; Bemelmans, A.; Roska, B. Promoters and uses thereof. Patent US20180355354A1 2015, 1–37.
60. Pichard, V.; Provost, N.; Mendes-Madeira, A.; Libeau, L.; Hulin, P.; Tshilenge, K.T.; Biget, M.; Ameline, B.; Deschamps, J.Y.; Weber, M.; et al. AAV-mediated gene therapy halts retinal degeneration in PDE6 β -deficient dogs. *Mol. Ther.* **2016**, *24*, 867–876.
61. Petit, L.; Lh riteau, E.; Weber, M.; Le Meur, G.; Deschamps, J.-Y.; Provost, N.; Mendes-Madeira, A.; Libeau, L.; Guihal, C.; Colle, M.-A.; et al. Restoration of vision in the pde6 β -deficient dog, a large animal model of rod-cone dystrophy. *Mol. Ther.* **2012**, *20*, 2019–30.
62. Conlon, T.J.; Deng, W.-T.T.; Erger, K.; Cossette, T.; Pang, J. jing; Ryals, R.; Cl ment, N.; Cleaver, B.; McDoom, I.; Boye, S.E.S.L.; et al. Preclinical potency and safety studies of an AAV2-mediated gene therapy vector for the treatment of MERTK associated retinitis pigmentosa. *Hum. Gene Ther. Clin. Dev.* **2013**, *24*, 23–8.
63. Choi, V.W.; Bigelow, C.E.; McGee, T.L.; Gujar, A.N.; Li, H.; Hanks, S.M.; Vrouvlianis, J.; Maker, M.; Leehy, B.; Zhang, Y.; et al. AAV-mediated RLBP1 gene therapy improves the rate of dark adaptation in Rlbp1 knockout mice. *Mol. Ther. - Methods Clin. Dev.* **2015**, *2*, 15022.
64. Choi, V.; Bigelow, C.E.; Dryja, T.P.; Reddy POLICE, S. Viral vectors for the treatment of retinal dystrophy. Patent US9163259B2 2012, 1–173.
65. Song, C.; Conlon, T.J.; Deng, W.T.; Coleman, K.E.; Zhu, P.; Plummer, C.; Mandapati, S.; Van Hoosear, M.; Green, K.B.; Sonnentag, P.; et al. Toxicology and pharmacology of an AAV vector expressing codon-optimized RPGR in RPGR-deficient Rd9 mice. *Hum. Gene Ther. Clin. Dev.* **2018**, *29*, 188–197.
66. Beltran, W.A.; Aguirre, G.D.; Jacobson, S.G.; Cideciyan, A. V; Lewin, A.S.; Boye, S.L.; Hauswirth, W.W.; Deng, W.-T. AAV-mediated gene therapy for RPGR X-linked retinal degeneration. Patent US9770491B2 2012, 1–40.

67. Deng, W.T.; Dyka, F.M.; Dinculescu, A.; Li, J.; Zhu, P.; Chiodo, V.A.; Boye, S.L.; Conlon, T.J.; Erger, K.; Cossette, T.; et al. Stability and Safety of an AAV Vector for Treating RPGR-ORF15 X-Linked Retinitis Pigmentosa. *Hum. Gene Ther.* **2015**, *26*, 593–602.
68. Smith, A.; Georgiadis, A.; Hoke, J.; Ribeiro, J.; Basche, M.; Robbie, S.; Gonzalez-Cordero, A.; Ovando-Roche, P.; Naylor, S.; Bainbridge, J.; et al. Efficacy and safety of AAV2/5-hRKp.RPGR to treat X-linked retinitis pigmentosa. ESGCT XXV Anniversary Congress 2017, 1.
69. Fischer, M.D.; McClements, M.E.; Martinez-Fernandez de la Camara, C.; Bellingrath, J.S.; Daultbekov, D.; Ramsden, S.C.; Hickey, D.G.; Barnard, A.R.; MacLaren, R.E. Codon-Optimized RPGR Improves Stability and Efficacy of AAV8 Gene Therapy in Two Mouse Models of X-Linked Retinitis Pigmentosa. *Mol. Ther.* **2017**, *25*, 1854–1865.
70. Bellingrath, J.-S.E. PhD thesis: Optimising Gene Therapy for X-linked Retinitis Pigmentosa, Universität Tübingen, 2019.
71. Zallocchi, M.; Binley, K.; Lad, Y.; Ellis, S.; Widdowson, P.; Iqbal, S.; Scripps, V.; Kelleher, M.; Loader, J.; Miskin, J.; et al. EIAV-based retinal gene therapy in the shaker1 mouse model for usher syndrome type 1B: Development of UshStat. *PLoS One* **2014**, *9*.
72. Turan, R.; Buckley, R.; Radcliffe, P.; Miskin, J.; Mitrophanous, K. Virus purification. Patent US9169491B2 2008, 1–18.
73. Payne, S.L.; Rausch, J.; Rushlow, K.; Montelaro, R.C.; Issel, C.; Flaherty, M.; Perry, S.; Sellon, D.; Fuller, F. Characterization of infectious molecular clones of equine infectious anaemia virus. *J. Gen. Virol.* **1994**, *75*, 425–429.
74. Kong, J.; Kim, S.-R.R.; Binley, K.; Pata, I.; Doi, K.; Mannik, J.; Zernant-Rajang, J.; Kan, O.; Iqbal, S.; Naylor, S.; et al. Correction of the disease phenotype in the mouse model of Stargardt disease by lentiviral gene therapy. *Gene Ther.* **2008**, *15*, 1311–20.
75. Ye, G.J.; Budzynski, E.; Sonnentag, P.; Miller, P.E.; Sharma, A.K.; Ver Hoeve, J.N.; Howard, K.; Knop, D.R.; Chulay, J.D. Safety and Biodistribution Evaluation in Cynomolgus Macaques of rAAV2tYF-CB-hRS1, a Recombinant Adeno-Associated Virus Vector Expressing Retinoschisin. *Hum. Gene Ther. Clin. Dev.* **2015**, *26*, 165–176.
76. Thomas, D.L.; Wang, L.; Niamke, J.; Liu, J.; Kang, W.; Scotti, M.M.; Ye, G.; Veres, G.; Knop, D.R. Scalable rAAV Production Using rHSV Co-infection of Suspension-Adapted Mammalian Cells. *Hum. Gene Ther.* **2009**, *20*, 861–870.
77. Boye, S.L.; Hauswirth, W.W.; Byrne, B.J. Self-complementary adeno-associated virus having a truncated CMV-chicken β -actin promoter. Patent US8298818B2 2006, 1–28.
78. Cukras, C.; Wiley, H.E.; Jeffrey, B.G.; Sen, H.N.; Turriff, A.; Zeng, Y.; Vijayasathay, C.; Marangoni, D.; Ziccardi, L.; Kjellstrom, S.; et al. Retinal AAV8-RS1 Gene Therapy for X-Linked Retinoschisis: Initial Findings from a Phase I/IIa Trial by Intravitreal Delivery. *Mol. Ther.* **2018**, *26*, 2282–2294.
79. Wright, J.F. Transient transfection methods for clinical adeno-associated viral vector production. *Hum. Gene Ther.* **2009**, *20*, 698–706.
80. Marangoni, D.; Bush, R.A.; Zeng, Y.; Wei, L.L.; Ziccardi, L.; Vijayasathay, C.; Bartoe, J.T.; Palyada, K.; Santos, M.; Hiriyantha, S.; et al. Ocular and systemic safety of a recombinant AAV8 vector for X-linked retinoschisis gene therapy: GLP studies in rabbits and Rs1-KO mice. *Mol. Ther. Methods Clin. Dev.* **2016**, *5*, 16011.

Chapter 2

AAV-CRB2 protects against vision loss in an inducible *CRB1* retinitis pigmentosa mouse model

T.M. Buck, R.M. Vos, C.H. Alves, and J. Wijnholds

Molecular Therapy: Methods & Clinical Development, 2021, 20, 423-441

Abstract

Loss of CRB1 or CRB2 proteins in Müller cells or photoreceptors in the mouse retina results in a CRB-dose-dependent retinal phenotype. Here, we present a novel Müller cell-specific *Crb1*^{KO}*Crb2*^{LowMGC} retinitis pigmentosa mouse model (Complete loss of CRB1 and reduced levels of CRB2 specifically in Müller cells). The *Crb* double mutant mice showed deficits in electroretinography, optokinetic head tracking, and retinal morphology. Exposure of retinas to low levels of DL- α -aminoadipate acid induced gliosis and retinal disorganization in *Crb1*^{KO}*Crb2*^{LowMGC} but not in wild-type or *Crb1*-deficient retinas. *Crb1*^{KO}*Crb2*^{LowMGC} mice showed a substantial decrease in inner/outer photoreceptor segments length and optokinetic head-tracking response. Intravitreal application of rAAV vectors expressing human *CRB2* in Müller cells of *Crb1*^{KO}*Crb2*^{LowMGC} mice subsequently exposed to low levels of DL- α -aminoadipate acid prevented loss of vision, whereas rAAV vectors expressing human *CRB1* did not. Both rAAV-vectors partially protected the morphology of the retina. The results suggest that human *CRB* expression in Müller cells is vital for control of retinal cell adhesion at the outer limiting membrane, and that the rAAV-CMV-h*CRB2* vector is more potent than the rAAV-CMVmin-h*CRB1* in protection against loss of vision.

Introduction

Mutations in the Crumbs homolog-1 (*CRB1*) gene are associated with retinitis pigmentosa (RP), Leber congenital amaurosis (LCA), cone-rod dystrophies, and sporadically found in foveal retinoschisis and macular dystrophy [1–3]. The human and nonhuman primate retina express and localize CRB1 and CRB2 proteins in Müller glial cells (MGCs) and photoreceptors (PRCs) at the outer limiting membrane (OLM) [4–6]. The mouse retina also expresses and localizes the CRB2 protein at the OLM in Müller glial cells and photoreceptor cells (PRCs). However, whereas the mouse retina does express and localize the CRB1 protein at the OLM in MGCs and retinal progenitor cells, the mouse retina does not express the CRB1 protein in PRCs. The human and nonhuman primate retina express a CRB1 protein of 1406 aa, whereas the mouse retina expresses a CRB1 protein of 1405 aa [7–9]. Loss of the CRB1 or the CRB2 protein in the retina results in loss of adhesion between MGCs, between PRCs, and amongst MGCs and PRCs [5,8,10–12]. No therapy is available for the treatment of *CRB1*-related retinal dystrophies. Recombinant adeno-associated viral (rAAV) vector-mediated gene supplementation may provide a lasting therapy to *CRB1* RP patients. We previously showed that CRB2 can rescue retinas lacking CRB1 or CRB2 proteins from retinal degeneration in two fast-progression RP-mouse models by increasing the levels of CRB2 into both MGCs and PRCs [13]. However, rescue at mid-stage retinal disease could not be achieved with *CRB1* cDNA supplementation, or by supplementation of *CRB2* cDNA only in PRCs or only in MGCs. Here, we developed a sensitive RP MGC-specific mouse model to test for protection at early-stage retinal disease by rAAV-h*CRB* gene therapy vectors.

We also investigated the development of the mouse retinal phenotype to explore the window-of-opportunity for rAAV-h*CRB* gene therapy. Previously, we analyzed *Crb*-related retinal degeneration mouse models: (1) The knockout of the *Crb1* gene (*Crb1*^{KO}) ablates the expression of the CRB1 protein in Müller glial cells and retinal precursor cells, and resulted in slow progression of retinal disorganization and degeneration from postnatal day 14 [8,12,14]. (2) In *Crb1*^{KO} mice, retinal degeneration occurs at foci in the inferior temporal quadrant of the retina. (3) Cell-type specific ablation of CRB1 in MGCs, or of CRB2 in MGCs, suggested that CRB proteins execute important overlapping roles in MGCs. Loss of CRB1 protein in mouse MGCs, or the loss of CRB2 in MGCs, results in disruptions at the outer limiting membrane, protrusion of rows of photoreceptor nuclei into the photoreceptor inner and outer segment layers, and ingressions of rows of photoreceptor nuclei into the outer plexiform layer. These retinas mimic retinitis pigmentosa in which the retinal degeneration process remains slow over the period of one year [5,6,11,15,16]. (4) Most importantly, the complete loss of CRB2 in MGCs in *Crb1*^{KO} mice worsened the retinal phenotype from a RP-like to LCA-like phenotype [5,9,16]. These *Crb1*^{KO}*Crb2*^{ΔMGC} retinas lacking CRB1 and CRB2 specifically in MGCs show in addition to protrusion of photoreceptor nuclei into the segment layers, also an intermingling of photoreceptors with inner retinal cells. The *CRB1*

RP and *CRB2* MGC-specific RP models are not suitable for testing gene therapy vectors since the onset of retinal degeneration is too slow, whereas the *Crb1^{KO}Crb2^{AMGC}* MGC-knockout LCA model is not suitable to test gene therapy vectors because the onset of retinal degeneration occurs during retinal development and is too fast. Here, we analyzed a novel mouse model by reducing endogenous mouse CRB2 (mCRB2) expression in MGCs from one instead of two *Crb2* alleles in *Crb1^{KO}* mice (*Crb1^{KO}Crb2^{LowMGC}*). Compared to littermate control *Crb1^{KO}Crb2^{Flox/wt}*, the *Crb1^{KO}Crb2^{LowMGC}* showed a worsened retinal phenotype, therefore we used these mice to test rAAV h*CRB1* and h*CRB2* gene therapy vectors that specifically target the MGCs.

Many underlying diseases show a nominal phenotype until a stressor triggers an escalation. DL- α -amino adipate acid (DL-AAA)-mediated MGC-specific stress causes disruptions at the OLM and protrusion of photoreceptor nuclei into the segment layers [17]. DL-AAA is a cystine/glutamate-specific antiporter inhibitor, decreasing the reserve pool of cysteine and glutathione (GSH) in MGCs [18]. Low doses of DL-AAA disrupts the distal Müller glial sealing at the OLM by downregulation of the adherens junction-associated protein ZO-1 [19]. The decrease in adhesion mediated by DL-AAA intravitreal injection is linked to photoreceptor nuclei protrusions in control mice and S334ter-line-3 rat model of retinitis pigmentosa [17,19]. First, a decrease of GFAP was found 3 days post intravitreal injection of DL-AAA in the S334ter-line-3 rat model of retinitis pigmentosa, followed by an upregulation of GFAP two weeks later [19]. Subretinal injection of DL-AAA to nonhuman primates caused a reduction in photoreceptor nuclei and a decrease in the ERG response [20]. The long-term effects of low doses of DL-AAA on vision-guided behavior in RP models have not been thoroughly investigated.

Here, we studied the effects of DL-AAA on retinas with decreased levels of CRB2 in MGCs lacking CRB1 (*Crb1^{KO}Crb2^{LowMGC}*) compared to retinas with normal levels of CRB2 in MGCs lacking CRB1 (*Crb1^{KO}Crb2^{Flox/wt}*). We challenged the following mice on a 99.9% C57BL/6JolaHsd genetic background to DL-AAA: *Crb2^{Flox/Flox}* control mice that do not express Cre recombinase, and two RP-mouse models (*Crb1^{KO}Crb2^{Flox/wt}* not expressing Cre recombinase, and *Crb1^{KO}Crb2^{LowMGC}* that express Cre recombinase specifically in MGCs to ablate one allele of *Crb2*). Our data suggest that *Crb1^{KO}Crb2^{Flox/wt}* and *Crb2^{Flox/Flox}* retinas are less sensitive to DL-AAA than *Crb1^{KO}Crb2^{LowMGC}*, suggesting that raising the levels of CRB2 by rAAV gene therapy targeting *Crb1^{KO}Crb2^{LowMGC}* MGCs might prevent against the adverse effects of the glial toxin DL-AAA.

In summary, we demonstrate that (1) low levels of CRB2 in *Crb1^{KO}Crb2^{LowMGC}* MGCs lacking CRB1, with normal levels of CRB2 expressed at the OLM in photoreceptors (see cartoon in Figure S1 on CRB protein expression in the mouse model), results in a RP retinal phenotype with foci of retinal disorganization mostly in the inferior retina. Interestingly, our previous studies showed that complete loss of CRB2 in MGCs lacking CRB1 resulted in a

LCA retinal phenotype throughout the entire retina [5]. (2) Reduction of CRB2 protein levels worsens the retinal phenotype in the inferior quadrants as found in *Crb1*^{KO} mice, (3) *Crb1*^{KO}*Crb2*^{LowMGC} RP mice are more susceptible to stress on Müller glial cells than *Crb1*^{KO}*Crb2*^{Flox/wt} and *Crb2*^{Flox/Flox} mice, and (4) rAAV-hCRB2 therapy protects *Crb1*^{KO}*Crb2*^{LowMGC} retinas against loss of vision due to exposure to DL-AAA.

Results

Reduction of CRB2 and loss of CRB1 in Müller glial cells leads to ERG and OKT deficits

We expressed *Cre* under control of the *Pdgfra*-promoter in MGCs to ablate *Crb2* expression of one floxed allele (*Crb1*^{KO}*Crb2*^{LowMGC} = *Crb1*^{-/-}*Crb2*^{Floxed/Wildtype} *PdgfraCre*^{Tg/+}; Figure S1). High levels of *Cre* recombinase expression in photoreceptors and other neuronal cells can cause toxicity impairing neuronal function.[21,22] We assessed if *Cre* expression in *Crb1*^{KO} MGCs (*Crb1*^{-/-}*PdgfraCre*^{Tg/+}) has an impact on retinal morphology, retinal transmission (ERG responses), or vision-guided optokinetic head-tracking thresholds (OKT response). No adverse effects were found (Figure S2).

Next, we measured flash-ERGs and OKT responses in 1-, 3-, 6-, 9-, and 12-month-old *Crb1*^{KO}*Crb2*^{LowMGC} mice and age-matched littermate controls (*Crb1*^{KO}*Crb2*^{Flox/wt}; Figure 1A-J; Figure S3). One-month-old *Crb1*^{KO}*Crb2*^{LowMGC} mice showed normal ERG responses (scotopic, photopic, flicker) and OKT thresholds (visual acuity [VA] thresholds; contrast sensitivity thresholds) compared to age-matched littermate controls (Figure S3 A+B, H). Three-months-old dark-adapted *Crb1*^{KO}*Crb2*^{LowMGC} mice showed a reduced a- and b-wave response (Figure 1A-D) and a reduced ERG flicker response (0.5 Hz; Figure S3M) compared to *Crb1*^{KO}*Crb2*^{Flox/wt} mice, suggesting a reduced rod photoreceptor retinal function. The ERG dark-adapted a- and b-wave response worsened over time in *Crb1*^{KO}*Crb2*^{LowMGC} and *Crb1*^{KO}*Crb2*^{Flox/wt} mice (6-, 9-, 12-month-old mice; Figure 1 A+E-G; Figure S3). The a-wave and b-wave amplitudes were proportionally lower (Figure 1 H+I) but the b-/a-wave ratio of the scotopic ERG was not affected (Figure 1J), indicating that the overall retinal transmission (b-wave) and the photoreceptor response (a-wave) were impeded.

Vision-guided OKT responses (Figure 1K) were assessed on visual acuity (spatial frequency) and contrast sensitivity measurements.[23–25] The spatial frequency threshold (visual acuity) was lower in 12-month-old *Crb1*^{KO}*Crb2*^{LowMGC} mice compared to *Crb1*^{KO}*Crb2*^{Flox/wt} littermates (Figure 1L). The contrast sensitivity threshold was markedly lower already at 6- and 12-months at a wide range of spatial frequencies measured (Figure 1M). Effects on contrast sensitivity threshold differences were detected with a higher statistical significance level at the spatial frequencies 0.064 and 0.092 cycles/degree (c/d; Figure 1M) suggesting that these spatial frequencies are most informative for hCRB gene therapy studies.

Reduction of CRB2 in Müller glial cells results in a more severe CRB1 phenotype in the inferior part of the retina

We analyzed the morphological phenotype on mouse eyes on plastic sections. We included a wild-type-like mouse with a similar genetic background ($Crb2^{Floxed/Floxed}$) because ectopic cell counts and inner/outer photoreceptor segment length quantification compared to $Crb1^{KO}Crb2^{Flox/wt}$ mice on plastic sections had not been done previously on mice with 99.9% C57BL/6J0laHsD genetic background. At 3-months-of-age, in $Crb1^{KO}Crb2^{LowMGC}$ retinas compared to littermate control $Crb1^{KO}Crb2^{Flox/wt}$ retinas, disorganization of the retinal layering at foci was detected in the two inferior quadrants of the retina (Figure 2A-E; Symbols: arrows=protrusions; triangle=loss of photoreceptor inner/outer segments; asterisk=neovascularization). These disorganizations at foci included protrusions of photoreceptor nuclei into the photoreceptor segment layers, ingression of photoreceptor nuclei into the outer plexiform layer, disruptions at the OLM, and intermingling of photoreceptor cells with inner retinal cells. Interestingly, outside the foci of retinal disorganization the layering of the retina remained intact. At 12-months-of-age the severity and number of retinal disorganization at foci increased. Retinal disorganization could also be observed in the littermate control $Crb1^{KO}Crb2^{Flox/wt}$ retinas, but outside of the affected foci the retinal layering remained intact (Figure 2F-J). In the superior retina of the $Crb1^{KO}Crb2^{LowMGC}$ but not the $Crb1^{KO}Crb2^{Flox/wt}$ mice at 3-months-of-age, sporadic protrusions of photoreceptor nuclei at foci could also be detected (Fig 2D), and sporadic at 12 months in $Crb1^{KO}Crb2^{LowMGC}$ retinas as well as in littermate control $Crb1^{KO}Crb2^{Flox/wt}$ retinas (Fig 2I, 2G). At 12-months-of age, we observed that 4 out of 5 $Crb1^{KO}Crb2^{LowMGC}$ retinas, and 1 out of 5 in the littermate $Crb1^{KO}Crb2^{Flox/wt}$ control retinas, developed focal neovascularization in the inferior quadrants (Figure 2J asterisk).

We generated retinal spidergrams for retinal thickness, outer nuclear layer (ONL) thickness, inner nuclear layer (INL) thickness, number of rows of photoreceptor nuclei in the ONL, photoreceptors' inner/outer segment (IS/OS) length, ectopic cells in the subretinal space, and ectopic cells in the outer plexiform layer (OPL). In 12-month-old mice, the retinal thickness, the number of rows of photoreceptor nuclei in the ONL, and the ONL thickness were decreased compared to $Crb1^{KO}Crb2^{Flox/wt}$ mice (Figure 2L+M+O). No major difference was found in the INL thickness in 12-month-old mice (Figure 1 N). $Crb1^{KO}Crb2^{LowMGC}$ mice displayed many displaced retinal cells (at 1-, 3-, and 6-months of age. Figure 2E+P-R). Most of the ectopic nuclei were found in the OPL and some at the subretinal space (compare Figure 2S and Figure 2Q). The photoreceptor inner/outer segment length in the inferior quadrants of $Crb1^{KO}Crb2^{LowMGC}$ retinas was shorter compared to $Crb1^{KO}Crb2^{Flox/wt}$ retinas at 3-months, and both mouse lines had similar but shorter inner/outer segments in the inferior quadrants compared to the superior quadrants at 6-months of age (Figure T-U).

We also assessed the morphology on protein expression by immunohistochemistry in 3-month-old mice for gliosis, Müller glial microvilli, inner/outer segments of photoreceptors, synapses at the OPL and IPL, and OLM disruptions (Figure 3). More GFAP-positive stress fibers extending from the ILM-to-OLM were observed in the inferior and superior quadrants of *Crb1*^{KO}*Crb2*^{LowMGC} compared to *Crb1*^{KO}*Crb2*^{Flox/wt} mouse littermate retinas (Figure 3A-E). When further looking at Müller glial morphology, also shortened and collapsed microvilli (CD44⁺) were observed in *Crb1*^{KO}*Crb2*^{LowMGC} compared to *Crb1*^{KO}*Crb2*^{Flox/wt} retinas (Figure F-J). This matches our previous TEM observation that the CRB levels from photoreceptors at the OLM and here in MGCs are important for MGC microvilli extensions [11,12]. Also, the outer segments of photoreceptors (labeled with cone arrestin for cones and rhodopsin for rods) were lost at foci in the inferior and partially in the superior quadrants of *Crb1*^{KO}*Crb2*^{LowMGC} compared to *Crb1*^{KO}*Crb2*^{Flox/wt} retinas (Figure 3K-O). Similarly, the internalization of rhodopsin around the cell nucleus was found in photoreceptor ingressions (Figure 3 L+M+O asterisks). The IPL synapses (sublamina-a OFF-bipolar cell synapses; sublamina-b ON-bipolar cell synapses) were relatively unaffected shown by the synaptic marker PMCA1, but the OPL synapses (PKC α /PMCA1 markers) were disrupted in the superior and inferior quadrants of the retina of *Crb1*^{KO}*Crb2*^{LowMGC} compared to *Crb1*^{KO}*Crb2*^{Flox/wt} retinas (Figure 3 P-T asterisk=OPL disruption).[26] We also found many more OLM disruptions and a lower CRB2 expression at the OLM in *Crb1*^{KO}*Crb2*^{LowMGC} compared to *Crb1*^{KO}*Crb2*^{Flox/wt} and wildtype-like (*Crb2*^{Flox/Flox}) retinas (Figure 3 U-Y. The asterisks indicate OLM disruptions).

We previously hypothesized that the loss of mouse CRB2 (mCRB2) protein expression at the OLM determines the retinal phenotype in *Crb1*^{KO} mice, but it was not clear on how much mCRB2 is contributed by MGCs and PRCs.[6] Here, we semi-quantified mCRB2 protein expression (on fluorescence intensity) at the OLM and the number of OLM breaks in 3-month-old *Crb2*^{Floxed/Floxed} (wild-type-like), *Crb2* ^{Δ Rods} (ablation of *Crb2* in rods), *Crb1*^{KO}*Crb2*^{Flox/wt}, *Crb1*^{KO}*Crb2*^{LowMGC}, and *Crb1*^{KO}*Crb2* ^{Δ Rods} mice. We validated our previous results, indicating that the OLM mCRB2 protein expression in the inferior retina compared to the superior retina was similar to the previous mixed genetic background of *Crb1*^{KO} mice.[27] The CRB2 protein expression was decreased at the OLM by 49 \pm 3(SEM)% in *Crb2* ^{Δ Rods} (n=3 mice), 34 \pm 10% in *Crb1*^{KO}*Crb2*^{LowMGC} (n=5 mice) and 62 \pm 12% in *Crb1*^{KO}*Crb2* ^{Δ Rods} (n=3 mice) compared to *Crb1*^{KO}*Crb2*^{Flox/wt} retinas (n=7), suggesting that MGCs contribute about half of the total CRB2 protein levels to the outer limiting membrane (OLM; Figure 3 Z). CRB2 protein expression between the peripheral (27 \pm 6 AU [arbitrary fluorescence unit] and 15 \pm 4 AU; n=5 mice) and central retina (21 \pm 1 AU and 14 \pm 5 AU) was not statistically different in *Crb1*^{KO}*Crb2*^{Flox/wt} (p=0.08) or *Crb1*^{KO}*Crb2*^{LowMGC} mice (p=0.30. Data not shown).

The adherens junctions and the subapical region are located at the outer limiting membrane. We and others have previously investigated the recruitment of adherens junction markers (e.g., cadherins or catenins) by the Crumbs complex at the subapical region.[8] The Crumbs complex consists of the CRB protein family (CRB1 and CRB2), the PALS1(MPP5)-PATJ-MUPP1 protein complex, and the PAR6-PAR3-aPKC-CDC42 protein complex [28–31]. Disruption of the Crumbs complex leads to loss of polarity and loss of adhesion in many *Crb* mouse models [5,7,8,12,16,27,32,33]. Semi-quantification of p120-catenin, an adherens junction marker, showed a 28 ± 3 (SEM)% decrease in *Crb2*^{ΔRods} compared to wild-type and a 45 ± 7 % reduction in *Crb1*^{KO}*Crb2*^{ΔRods} compared to *Crb1*^{KO}*Crb2*^{Flox/wt} mice (Figure 3 AA). No statistical difference in p120-catenin expression were found between *Crb1*^{KO}*Crb2*^{Flox/wt} and *Crb1*^{KO}*Crb2*^{LowMGC} mice (Figure 3 AA).

Further, the level of CRB1 and CRB2 proteins at the OLM determined the number of OLM breaks. More OLM breaks were found in mice with less CRB protein expression at the OLM (Figure 3BB). We further validated our previous results that the loss of CRB1 or CRB2 reduces the p120-catenin protein localization at the OLM, subsequently destabilizing the OLM and reducing adhesion between MGCs and photoreceptors, causing OLM breaks, and finally facilitating photoreceptor loss in the form of protrusion of photoreceptor nuclei through the OLM into the layer of the inner segments.[27] Finally, the morphological data at 3-months-of-age suggests that the *Crb1*^{KO}*Crb2*^{LowMGC} retinas show more degeneration in the superior as well as inferior retinal quadrants compared to *Crb1*^{KO}*Crb2*^{Flox/wt} retinas. In the next paragraph, we will describe studies on the hypothesis whether or not the MGCs in *Crb1*^{KO}*Crb2*^{LowMGC} retinas are more sensitive to the glial toxin DL-AAA than littermate control *Crb1*^{KO}*Crb2*^{Flox/wt} retinas.

Exposure to DL-AAA causes lasting retinal damage and worsened sight

A low dose of 100 μg DL-AAA injected intravitreally in wild-type mice was shown by others to disrupt the OLM causing photoreceptor nuclei protrusions into the photoreceptor segment layers that were resolved over 48 hours.[17,34] Here, we examined whether retinas with reduced levels of CRB2 proteins in *Crb1*^{KO}*Crb2*^{LowMGC} MGCs are more sensitive to DL-AAA than retinas expressing normal levels of CRB2 proteins in *Crb1*^{KO}*Crb2*^{Flox/wt} MGCs.

We challenged 2-months-old wild-type-like (*Crb2*^{Flox/Flox}), and the RP *Crb1*^{KO}*Crb2*^{Flox/wt} and *Crb1*^{KO}*Crb2*^{LowMGC} mice with different doses of DL-AAA (100 μg, 150 μg, or 200 μg) and analyzed the retinal morphology, the retinal transmission (ERG), and vision-guided behavior (OKT) one-month post-intravitreal injection (3-months-old-mice. Figure 4A). No effect was seen on OKT and ERG when we injected PBS as a control (Figure 4B-I). An overall dosage-effect of DL-AAA on retinal transmission (ERG) and vision-guided behavior (OKT) was found for all mouse lines (Figure 4B-I). 100 μg DL-AAA markedly decreased the retinal transmission for the scotopic a- and b-wave (Figure 4C-E) and the OKT thresholds (Figure F-I) in the *Crb1*^{KO}*Crb2*^{LowMGC} but not in *Crb2*^{Flox/Flox} and *Crb1*^{KO}*Crb2*^{Flox/wt} mice.

No effect was seen on morphology when we injected PBS as a control (Figure 4K-N). Very little effect on morphology was found at 100 μ g DL-AAA except for the *Crb1*^{KO}*Crb2*^{LowMGC} retinas (Figure 4O-S). The *Crb1*^{KO}*Crb2*^{LowMGC} retinas had an overall worsened retinal phenotype on the superior as well as the inferior retina indicated by the ingressions (asterisk) and protrusions (arrow) in the retina (Figure 4R-S). 150 and 200 μ g DL-AAA caused irreversible retinal damage on morphology in all mouse lines (Figure 4T-CC). The decrease in ERG/OKT and worse retinal morphology indicates that *Crb1*^{KO}*Crb2*^{LowMGC} retina might be more sensitive to OLM disruptions induced by DL-AAA. In the next paragraph we investigated whether or not the increased sensitivity could be alleviated by hCRB1 or hCRB2 gene supplementation therapy.

Recombinant AAV-hCRB protects retinal morphology, OKT and ERG response in the DL-AAA-challenged Crb1^{KO}Crb2^{LowMGC} RP mouse model

We previously determined the tropism and potency of the ShH10^{Y445F} capsid (and the cell-specific expression of the CMV and CMVmin promoter) and the human *CRB1* codon-optimized or the human *CRB2* codon-optimized cDNA delivery to Müller glial cells by intravitreal of the rAAVs in wildtype mice. We previously showed that the ShH10^{Y445F} capsid can effectively infect and efficiently express GFP in more than 40% of all mouse MGCs by intravitreal injection [35,36]. We also previously showed that subretinal injected rAAV2/9.CMVmin.hCRB1co.spA or intravitreal rAAV2/ShH10^{Y445F}.CMVmin.hCRB1co.spA can express hCRB1 protein at the OLM in *Crb1*^{KO} mice. Finally, we previously demonstrated that we can express human CRB2 protein at the OLM by intravitreal delivery of rAAV2/ShH10^{Y445F}.CMV.hCRB2co.spA in *Crb2* cKO retinas [13].

Recombinant AAV2/ShH10^{Y445F}.CMVmin.hCRB1co.spA (rAAV-hCRB1) or AAV2/ShH10^{Y445F}.CMV.hCRB2co.spA (rAAV-hCRB2) was injected intravitreally into one eye of *Crb1*^{KO}*Crb2*^{LowMGC} mice at postnatal day 21. Then, 2-months-old retinas were challenged by intravitreal injection of 100 μ g DL-AAA in both eyes. ERG, OKT, SD-OCT, and retinal morphology were assessed in 3-month-old mice (Figure 5 A).

The overall retinal morphology improved with both rAAV vectors (Figure 5B-G). Retinas receiving the rAAV-hCRB treatment had more rows of photoreceptor nuclei in the ONL (Figure 5H). The expression of human CRB in mouse Müller glial cells protected against the protrusion of photoreceptor nuclei into the subretinal space and outer plexiform layer (Figure 5I). In the central-inferior retina of *Crb1*^{KO}*Crb2*^{LowMGC} mice, the photoreceptor inner/outer segment length was 33 \pm 6 μ m (See also Figure 2P), 21 \pm 6 μ m in 100 μ g DL-AAA treated mice, 41.7 \pm 5 μ m in 100 μ g DL-AAA+[rAAV-hCRB1] treated mice, and 40 \pm 22 μ m in 100 μ g AAA+[rAAV-hCRB2] treated mice (Figure 5J), indicating a significant protection against loss of photoreceptor segment lengths in the central area for rAAV-hCRB injected eyes. We then investigated the retinal morphology by SD-OCT (Figure 5K-M). We found retinal

degeneration in the central inferior quadrants at around 0.5-0.9 mm from the optic nerve head on the Volume Intensity Projection (VIP) in the ONL comparable to changes found on plastic sections (Figure 5H+J). More extensive disruptions in the OPL/ONL/OLM of control mice (100 µg DL-AAA only) were found in the inferior and superior retinal quadrants (red arrows Figure 5K-M). Interestingly, some mice injected with rAAV-h*CRB1* showed many vitreous infiltrating cells (Asterisks; Figure 5L).

We measured ERG and OKT visual acuity and contrast sensitivity in these mice. We analyzed the differences between the rAAV-h*CRB* treated eye against the eye not receiving the rAAV treatment (control eye) because the variation between mice was considerable, and comparison on an individual mouse reduces variation and permits a pairwise comparison reducing the number of mice needed to show effects (see Figure 6 and Figure S4 absolute values). The retinal function measured by scotopic and photopic ERG was significantly higher in rAAV-h*CRB2* treated eyes, but no significant changes were found in rAAV-h*CRB1* treated eyes compared to the control eye (Figure 6A-C. See also Figure S4). The visual acuity improved for rAAV-h*CRB2* treated eyes but not for rAAV-h*CRB1* treated eyes (Figure 6D). The contrast sensitivity threshold (spatial frequency: 0.032, 0.064, and 0.092) was significantly increased upon delivering h*CRB2* cDNA but not for h*CRB1* cDNA to MGCs (Figure 6E-G. Figure S4N-O). The tracking at 0.092 cycles per degree was significantly worse for rAAV-h*CRB1* injected eyes compared to control eyes (Figure 6G. Figure S4N-O).

Recombinant AAV-hCRB therapy reduces gliosis and protects Müller cell microvilli & photoreceptor inner/outer segments

Müller glial cells extend from the endfeet at the inner limiting membrane (ILM) up to the apical villi above the OLM and support maintain retinal homeostasis and retinal integrity. Long Müller glial stress fibers (GFAP-positive) extended through the retina in the inferior-central retinal areas of *Crb1*^{KO}*Crb2*^{LowMGC} mice injected with 100 µg DL-AAA (Figure 7A; arrows=stress fibers). But eyes treated by rAAV-h*CRB* showed shortened and less GFAP-positive stress fibers extending into the ONL (Figure 7B-C; arrows=stress fibers). Similarly, shortened and thickened Müller microvilli were observed in the retina of eyes injected with DL-AAA without rAAV-h*CRB* treatment. But retinas with rAAV-h*CRB* treatment displayed less severely affected Müller microvilli in the inferior retinal quadrants (Figure 7E-F).

Crb1^{KO}*Crb2*^{LowMGC} retinas exposed to DL-AAA mediated loss of adhesion had long stretches of no inner/outer photoreceptor segments in the inferior retinal quadrants stained by rhodopsin and cone arrestin (Figure 7G arrows). Also, more ectopic nuclear rhodopsin expression in photoreceptor ingressions was observed (Figure 7G asterisks=ingressions). The most affected inferior-central retinal quadrants frequently had some outer photoreceptor segments left in rAAV-h*CRB* treated eyes compared to the control eyes (Figure 7G-I).

Retinas of *Crb1*^{KO}*Crb2*^{LowMGC} mice injected with DL-AAA had more ectopic synapses and loss of horseshoe-shaped synapses (Figure 7G). Retinas treated with rAAV-hCRB showed smaller disruptions of horseshoe-shaped synapses at the OPL (Figure 7G-I. See also 5K-M arrows). Also, DL-AAA-induced retinal stress may induce synaptic changes in the IPL but no differences between the previously described conditions without DL-AAA (Figure 3P-T), with 100 µg DL-AAA, or DL-AAA with rAAV-hCRB treatment were observed (Figure 7J-L, asterisks indicate photoreceptor [synaptic] ingressions).

Neovascularization, activated microglial cells, ectopic hCRB1 expression, and ciliary body changes related to rAAV-hCRB1 intravitreal injections

rAAV-hCRB1 treatment produced human CRB1 protein at the OLM (Figure S5A-E) but it was also found in the ciliary body (Figure S5D). Similarly, CRB2 was found at the OLM in rAAV-hCRB2 of nontreated retinas (Figure S5G). The benefit of the rAAV-hCRB2 over rAAV-hCRB1 therapy on ERG retinal transmission and OKT behavior outcome measures (see Figure 6 and Figure S4) compared to similar benefits on retinal morphology (Figure 5) prompted us to further investigate if one of these vectors increases neovascularization events or microglial activation.

First, we characterized the background of neovascularization and microglial activation in the inferior-central quadrants of 3-month-old *Crb2*^{Flox/Flox}, *Crb1*^{KO}*Crb2*^{Flox/wt}, *Crb1*^{KO}*Crb2*^{LowMGC} mice injected with DL-AAA (100 µg) against the noninjected control eye (Figure S5H-M). A strong increase in neovascularization events was detected, in the degenerate inferior retinal quadrants of *Crb1*^{KO}*Crb2*^{LowMGC} mice injected with DL-AAA (100 µg), upon immunohistochemical staining for Plasmalemma Vesicle-Associated Protein (PLVAP; a marker for early vascular leakage[37,38]) or activated microglial cells (CD11b-positive microglial cell dendrites and migration to the ONL and GCL) (Figure S5M). Neovascularization was not observed in the RPE, ONL, or INL when rAAV-hCRB1 or rAAV-hCRB2 was administered to *Crb1*^{KO}*Crb2*^{LowMGC} mice (Figure S5N-O) matching the proper retinal lamination seen in 4 eyes on plastic section and 5-6 eyes per rAAV-vector on SD-OCT morphology (Figure 5). However, we also observed many PLVAP-positive ectopic cells in the lower part of the ganglion cell layer / nerve-fiber layer (GCL/NFL) intermingled with activated microglial cells (CD11b-positive) in 3 out of 6 eyes on immunohistochemistry when rAAV-hCRB1 was injected in *Crb1*^{KO}*Crb2*^{LowMGC} mice (Figure S5N arrows = PLVAP-positive cells; asterisk = microglial activation in the GCL. See also Figure 5L SD-OCT image arrows = massive cell infiltration in the vitreous body). Neovascularization events were only seen in one eye out of four eyes and no microglial activation in four eyes sampled on immunohistochemistry of *Crb1*^{KO}*Crb2*^{LowMGC} mice injected with rAAV-hCRB2 (data not shown). No thickened GCL/NFL with PLVAP-positive cell nuclei were found in control eyes injected with DL-AAA (100 µg) in *Crb1*^{KO}*Crb2*^{LowMGC} (Figure S5M) indicative that the rAAV-hCRB1 may increase neovascularization events in the GCL/NFL. We also found

double-positive-labeled PLVAP and VE-cadherin-expressing vascular cells in the ciliary body of *Crb1*^{KO}*Crb2*^{LowMGC} mice treated with rAAV-h*CRB1* but not in the rAAV-h*CRB2* treatment group (Figure S5P-S). rAAV-vector contaminations could explain the neovascularization events seen in the rAAV-h*CRB1* treatment group. But we did not detect major protein contaminants in two independently produced rAAV batches used in the study (Figure S5T).

In summary, we observed more neovascularization events on immunohistochemistry in the ONL/OPL/INL when 100 µg DL-AAA was injected intravitreally in *Crb1*^{KO}*Crb2*^{LowMGC} mice compared to noninjected *Crb1*^{KO}*Crb2*^{LowMGC} mice (Figure S5L-M). Less neovascularization events in the ONL/OPL/INL were observed on immunohistochemistry and SD-OCT in the rAAV-h*CRB2* treatment group or rAAV-h*CRB1* treatment group compared to the control eye. But we observed in the treatment groups of rAAV-h*CRB2* compared to rAAV-h*CRB1* less GFAP-positive stress fibers (Figure 6B-C) and less neovascularization events in the GCL/NFL (Figure S5H-O). Additionally, the rAAV-h*CRB1* treatment group showed consistent neovascularization at the ciliary body that was not found in control eyes (100 µg DL-AAA injected) or in rAAV-h*CRB2* treated eyes. Neovascularization at the ciliary body was previously observed after 4.5 M post-intravitreal injection of rAAV-h*CRB1* but not by rAAV-h*CRB2* in *Crb1*^{KO}*Crb2*^{Flox/wt}Chx10*CreGFP*^{Tg/+} retinas [13].

Discussion

In this study, we show that (a) in *Crb1*^{KO}*Crb2*^{LowMGC} mice, a minimum of half of the endogenous mouse CRB2-levels in MGCs lacking CRB1 (with normal levels of CRB2 expressed at the OLM in photoreceptors) results in a RP retinal phenotype. Interestingly, in previous studies we showed that complete loss of CRB2 in MGCs lacking CRB1 resulted in a LCA retinal phenotype [5]. (b) Mice with reduced levels of CRB2 protein in MGCs lacking CRB1 in MGCs (*Crb1*^{KO}*Crb2*^{LowMGC}) showed increased sensitivity to OLM disruptions upon exposure to DL-AAA. (c) rAAV-h*CRB2* therapy to MGCs protects against OLM disruptions, decrease of ERG responses, and loss of OKT contrast sensitivity in *Crb1*^{KO}*Crb2*^{LowMGC} mice.

CRB1-related RP patients have a nonfunctional or less-functional CRB1 protein in MGCs and photoreceptors [4]. We have shown that we can model the *CRB* phenotype in human retinal organoids *in vitro* [4] and mice *in vivo*. Here, we further explore the effect of ablating *CRB* in late-born retinal cells, such as MGC. Previously, we showed that the full ablation of *Crb1* and *Crb2* in MGCs (*Crb1*^{KO}*Crb2*^{ΔMGC}) caused a severe LCA-like retinal phenotype with no ERG response already in 1-month-old mice [5]. Previously, we showed that full ablation of *Crb2* specifically in MGCs (*Crb2*^{ΔMGC}) causes a slow progressing RP-like phenotype with sporadic disruptions at the OLM with protrusion of photoreceptor nuclei into the photoreceptor segment layer, similar as previously observed in retinas lacking CRB1, without effects on the ERG response [5]. Here, we show that *Crb1*^{KO}*Crb2*^{LowMGC} mice

develop a more severe RP-like phenotype than *Crb1*^{KO} or *Crb2*^{ΔMGC} with clear effects on ERG and OKT response and retinal morphology, suggesting similar functions of CRB1 and CRB2 proteins in MGCs.

Mice are housed under standard low light conditions that do not resemble the retinal stress that RP patients undergo in their regular life. We have shown previously that light exposure can worsen the *CRB1* RP mouse phenotype [8,12]. Bright light exposure causes prolonged inflammation, neovascularization, and retinal damage in RP mouse models. Blue light exposure induces retinal degeneration, oxidative stress, and neuroinflammatory activity similar to dry-age age-related macular degeneration (AMD). Here, we explored intravitreal DL-AAA injections that act on glial cells such as MGCs, causing disruptions at foci at the OLM. Since exposure of DL-AAA to the mouse retina, or loss of CRB1 or loss of CRB2 proteins in the mouse retina, cause disruptions at foci at the OLM we examined whether mice with decreased levels of CRB proteins in MGCs are more sensitive to DL-AAA exposure than retinas with higher levels of CRB proteins in MGCs. The outer limiting membrane disruptions caused by low doses of DL-AAA are reversible in wild-type mice.[17] The phenotype described indicated some similarities like photoreceptor nuclei protrusions into the photoreceptor segment layer that we previously observed in *Crb1* RP mouse models. But it was not known how the DL-AAA could affect the visual tracking thresholds (OKT), the retinal function (ERG), quantitative retinal morphology, or on mouse models with reduced cell adhesion. West *et al* (2008) showed that low levels of DL-AAA (100 μg) did not affect the gross retinal morphology in wild-type mouse retinas [17]. Here, we first demonstrated that mice expressing normal levels of endogenous CRB2 proteins in MGCs (*Crb2*^{Flox/Flox} or *Crb1*^{KO}*Crb2*^{Flox/wt}) are less sensitive to exposure of 100 μg DL-AAA than mice with reduced levels of endogenous CRB proteins in MGCs (*Crb1*^{KO}*Crb2*^{LowMGC}). Subsequently, we demonstrated that increasing the levels of recombinant human CRB2 in MGCs in *Crb1*^{KO}*Crb2*^{LowMGC} retinas prior to the exposure to DL-AAA decreased the sensitivity to DL-AAA exposure. We applied the rAAV-hCRB gene therapy vectors at postnatal day 21 (P21), and it could have been more effective to apply rAAV-hCRB at earlier time points. Here, we show that rAAV-hCRB2 applied at P21 to *Crb1*^{KO}*Crb2*^{LowMGC} MGCs at early-stage retinal disease effectively prevents against the adverse effects of exposure of DL-AAA. The *Crb1*^{KO}*Crb2*^{LowMGC} mice pre-treated intravitreally with rAAV-hCRB2 and subsequently exposed to DL-AAA showed significant fewer disruptions at the OLM, fewer protrusions of photoreceptor nuclei in the photoreceptor segment layers, less loss of photoreceptors, an improved contrast sensitivity as measured by OKT and an improved retinal function as measured by ERG.

Intravitreal injection of rAAV vectors is more efficient in supplementing cDNA to MGCs compared to subretinal injections. For example, we have shown that rAAV2/ShH10^{Y445F} can effectively infect and efficiently express GFP in more than 40% of all mouse MGCs [35,36].

Yet, intravitreal injections increase the risk of alternate rAAV vector biodistribution and ectopic vector expression [13]. Others have indicated a transient inflammation of the aqueous and the vitreous body by empty rAAV capsids and rAAV supplementation vectors at high doses [39]. Here, we re-assessed the effect of rAAV-h*CRB1* and rAAV-h*CRB2* to the vitreous body, ciliary body and the neuroretina. We previously found that rAAV-h*CRB1* applied at postnatal day 14 causes ectopic CRB1 expression within the epithelium of the ciliary body and the iris epithelia affecting the corneal thickness, the eyeball perimeter, and CD11b & CD3-positive infiltrating cells to the ciliary body [13]. We find similar ectopic rAAV-h*CRB1* expression at 3-months-of-age in the *Crb1*^{KO}*Crb2*^{LowMGC} mouse model injected at P21 with rAAV-h*CRB1* and at 2 months-of-age with DL-AAA injected. Interestingly, cDNA supplementation of h*CRB1* to MGCs (by rAAV capsids) improved the retinal morphology, such as a decrease in ectopic cells in the OPL/subretinal space and the maintenance of the number of rows of photoreceptor nuclei in ONL in the central retina.

We hypothesize that human CRB1 applied to Müller cells can protect against loss of OLM integrity, but OKT visual behavioral and ERG electrical transmission studies suggest that the neural network is not sufficiently restored, whereas morphological studies of the treated eyes suggest that there are adverse effects upon ectopic expression of CRB1. Potentially, the neovascularization events seen in the GCL/NFL of the inferior mouse retinas and the poor ERG/OKT responses measured in the rAAV-h*CRB1* but not in the rAAV-h*CRB2* treated eyes may be linked to differences of h*CRB2* over h*CRB1* (over-)expression in (a) MGCs, (b) astrocytes, (c) protein-protein interactions, or (d) immunogenic properties of hCRB1 protein in a *Crb1*^{KO} mouse. We will discuss the points below.

(a) MGCs contribute to the maintenance & rigidity of the retina layers (i.e. tensile strength), regulate blood flow & maintain the retina-blood-barrier (e.g. release VEGF), ensheath the synapses in IPL and the OPL, guide light rays to the segment layer, and remove waste products [40–42]. Mouse *Crb1* and *Crb2* expression in MGCs is linked to the intermediate capillary plexus development by suppressing the angiogenic growth factor *VEGFA* [43] and promoting *MMP-3* expression (extracellular matrix remodeling) [44]. Human *CRB1* expression protected MGCs less than h*CRB2* from gliosis. (b) Astrocytes wrap around retinal endothelial cells and pericytes of the superficial capillary plexus at the GCL/NLF. The astrocytic foot processes may release angiogenic growth factors (e.g. VEGF) during retinal development and disease altering the expression of tight junction proteins in retinal endothelial cells (blood-retinal barrier; ZO-1/Occludin/VE-cadherin proteins) [45–47]. VEGF suppression speeds up programmed capillary regression during development [48]. The AAV6 capsid variant ShH10^{Y445F} used in our study efficiently infects astrocytes [49]. We found only neovascularization events in the GCL/NFL with rAAV-h*CRB1* that may be linked to differences of h*CRB1* over h*CRB2* expression in DL-AAA stressed astrocytes. (c) The protective function of h*CRB2* over h*CRB1* protein may also be explained by not known

differences in the intracellular protein function (both have a short intracellular FERM/PDZ/ERLI domains [9,14]) or differences in human CRB homo-/heteromerization of extracellular human/mouse CRB protein at the OLM. But both vectors rescued the retinal morphology at the OLM where we would expect that the homo-heteromerization takes place. (d) The *Crb1*^{KO}*Crb2*^{LowMGC} mice are naïve for any CRB1 protein but potentially not for hCRB2 (*Crb2* is in this model expressed in e.g. RPE cells, the choroid, lung tissue, and the brain [5,50–52]) and the expression of human CRB1 on a *Crb1*^{KO} background may induce an immune reaction especially in a *CRB1*-RP model with a leaky blood-retina-barrier (partially aggravated by DL-AAA) allowing more infiltration of immune cells. More research is needed to delineate the effects of hCRB1 overexpression in MGCs or astrocytes on retinal vasculature in the healthy, degenerate, and *Crb1*^{KO} retina.

Nevertheless, the additive effect of DL-AAA on *Crb1*^{KO}*Crb2*^{LowMGC} MGCs may model the exudative vasculopathy seen in RP-*CRB1* patients[1] and help to better understand what therapies on MGC-regulated vasculopathy may be beneficial for RP-*CRB1* patients. Coats'-like exudative vasculopathy (also called idiopathic retinal telangiectasia) is strongly associated with the RP-*CRB1* phenotype seen in clinics [1]. We observed (early) vascular leakage (PLVAP) in the inner retina in this study but also previous studies found neovascularization (VEGF, vWF, FA-cSLO) in RP-*CRB1* mouse and rat models [5,8,12,15,27,44,53]. Subretinal injection of a high dose of DL-AAA induces MGC injuries that can develop into vascular telangiectasis and hemorrhages of the inner retinal vasculature in rats, rabbits and nonhuman primates [20,54,55]. Thus, a (pan-)*CRB1*-therapy may need to address not only the cell-cell adhesion at the OLM but also regulating glial cells on retinal vasculature signaling and overall retinal maintenance.

We show that rAAV-h*CRB2* does not cause adverse changes at the ciliary body or the GCL/NFL. Further, rAAV-h*CRB2* protected against loss of retinal and visual function and retinal morphology. Our study suggests that expression of human CRB2 does not cause adverse effects in mouse retinas and that it can significantly increase retinal adhesion in a new cell-adhesion *CRB1* RP mouse model. The study further strengthens the hypothesis that rAAV-h*CRB2* retinal gene therapy might be of benefit for RP patients with mutations in the *CRB1* gene.

Materials and Methods

Mice

Procedures concerning animals were performed according to the Dutch Central Commission Animal Experimentation (CCD) license number AVD1160020172924, the working protocols (OZP number: PE.18.016.002; PE.18.016.006; PE.18.016.007; PE.18.016.010) approved by the local ethical committee (Instantie voor Dierenwelzijn, IvD) of the Leiden University Medical Center, and the ARVO statement for the use of animals in ophthalmic

and vision research. All mice used were maintained on a 99.9% C57BL/6JOLA_{Hsd} genetic background with a 12 h day-night cycle (standard low light housing condition ~10-20 lux) and supplied with food and water *ad libitum*. All experiments were carried out in male and female mice. All mouse strains below were confirmed to be *Crb1*^{rd8} negative, *Nnt(exon 7-11)*^{WT/WT}, *Mmrn1(Exon8)*^{-/-}, α -Synuclein(Exon-6)^{-/-}, and *Pde6b*^{WT/WT}, thus similar to the genetic background of C57BL/6JOLA_{Hsd} mice.

Crb1^{KO}*Crb2*^{Floxed/Floxed} mice were crossed with a *Crb1*^{KO}*Pdgfra-Cre*^{Tg/+} to produce *Crb1*^{-/-}*Crb2*^{Floxed/wt}*Pdgfra-Cre*^{Tg/+} mice (*Crb1*^{KO}*Crb2*^{LowMGC}) and *Crb1*^{-/-}*Crb2*^{Floxed/wt} mice.[5][27] The *Crb1*^{KO}*Crb2*^{LowMGC} mice lack CRB1 in radial glial progenitor cells and MGCs and reduced CRB2 protein expression in MGCs during early retinal development.[5] The *Crb1*^{-/-}*Crb2*^{Floxed/wt}*Pdgfra-Cre*^{Tg/+} mice contain a *Pdgfra-Cre* transgene (C57BL/6-Tg(*Pdgfra-cre*)1Clc/J) driving the *Cre* gene specifically in Müller glial cells [5,56]. We determined the *Cre* mosaicism in a reporter mouse line (ROSA^{mT/mG}). We found that 95% of all Müller glial cells to have excised membrane-targeted enhanced green fluorescent protein (mG) by *Pdgfra-Cre*-mediated recombination [5]. Mouse *Crb2* protein is expressed by Müller glial cells and photoreceptor cells at the OLM. The *Cre* mice used express the *Cre* recombinase specifically in MGCs generating hemizygote *Crb2* MGCs. Assuming that 49±3(SEM)% of *Crb2* is localized at the OLM within photoreceptors (Figure 3Z), we estimate that 51% of *Crb2* is localized at the OLM in control *Crb1*^{KO}*Crb2*^{Flox/wt} MGCs. Since the total levels of *Crb2* at the OLM of *Crb1*^{KO}*Crb2*^{LowMGC} are reduced by 34±10(SEM)% compared to the reference littermate control *Crb1*^{KO}*Crb2*^{Flox/wt} (*Crb1*^{KO}) retina (Figure 3Z), we estimate that the levels at the OLM of *Crb2* in *Crb1*^{KO}*Crb2*^{Flox/wt} MGCs dropped from 100% to 33% ((51-34%)/51%*100=33%) specifically in *Crb1*^{KO}*Crb2*^{LowMGC} MGCs. The *Crb2*^{ARods} and *Crb1*^{KO}*Crb2*^{ARods} were previously described [11]. The mice contained a *Rho-iCre* transgene ablating the *Crb2* gene in developing rod photoreceptors. Chromosomal DNA isolation and genotyping were performed as previously described [5]. All mice were euthanized using CO₂/O₂. The experimental and control mice were collected at the same time at 5-8 hours within the day time cycle to have comparable lengths of the inner/outer segments of photoreceptors.

Electroretinography

Dark and light-adapted electroretinographies (ERGs) were performed under dim red light using an Espion E2 (Diagnosys, LLC, MA). ERGs were performed on 1-month-old (1M), 3M, 6M, 9M, and 12M *Crb1*^{KO}*Crb2*^{LowMGC} and *Crb1*^{KO} mice. The ERG values of the right and left eye were averaged for the analysis in Figure 1 and Figure S2. One eye was used for analysis for other experiments (treatment vs control eye). Mice were anesthetized using 100 mg/kg ketamine and 10 mg/kg xylazine intraperitoneally, and the pupils were dilated using atropine drops (5 mg/mL). ERGs were recorded as previously described [16]. Scotopic recordings were obtained at: -4, -3, -2, -1, 0, 1, 1.5, 1.9 log cd s/m² light intensity. Flicker

recordings were obtained at 0.5 log cd s/m² fixed light intensity at the frequencies: 0.5, 1, 2, 3, 5, 7, 10, 12, 15, 18, 20, and 30 Hz. Photopic recordings were obtained at 30 cd/m² background light at: -2, -1, 0, 1, 1.5, 1.9 log cd s/m² light intensity. The ERG tests were performed consecutively: 1) Scotopic, 2) Flicker, 3) 10 min light exposure (30 cd s/m² light intensity), 4) photopic.

SD-Optical coherence tomography imaging

Mice were anesthetized using 100 mg/kg ketamine and 10 mg/kg xylazine intraperitoneally, and the pupils were dilated using atropine drops (5 mg/mL). The mouse was placed on a rodent alignment system with a bit bar (AIM-RAS, Bioptigen, USA). The optic nerve was aligned to the center of the image on an SD-Optical coherence tomography (SD-OCT) imaging device with a mouse retina lens with a 50-degree field of view (Bioptigen Envisu R2210 VHR; Bioptigen, USA). The eyes were kept moisturized with eye drops (Systance Ultra, Alcon) and an eye gel (Vidisic carbogen, Bausch+Lomb). The following protocols (a-scan x b-scan x frame) for both eyes were run: (1) Linear B-scan 1.0mm 1000 x 2 x 24 (Fast Fundus); (2) Rectangular 1.8mm x 1.8mm 1000 x 100 x 6 x 1 (High resolution volume); (3) Rectangular 1.8mm x 1.8mm 400 x 400 x 4 x 1 (Square pixel volume), and (4) Radial 1.8mm x 1.8mm 1000 x 100 x 6 x 1 (High resolution radial volume). The frames were averaged on the InVivoVue Reader (Software, Bioptigen, USA) and analyzed on the Diver 3.4.4 (Software, Bioptigen, USA) for the Volume Intensity projection for the ONL.

Optokinetic head-tracking response

Optokinetic head-tracking response (OKT) was measured as previously described [11,23,24]. The testing was performed in awake and non-restrained mice. Mice were placed on a pedestal surrounded by four displays that create a visual drum for the mice. The grating was set at 12 degrees/second (spatial frequency). The tracking was recorded in a clockwise (CW) or counterclockwise (CCW) direction. The drum rotation was random from trial to trial, and the experimenter made a forced-choice decision between CW and CCW rotation. The maximum spatial frequency capable of driving head tracking was determined first (Visual acuity threshold). The contrast sensitivity was measured at 0.032, 0.064, 0.092, 0.103, 0.192, 0.272 cycles per degree (spatial frequency). The recording was done twice per mouse. Mice were measured at 1-month-of-age (1M), 3M, 6M, 9M, and 12M at random and blinded for the experimenter. The eyes of mice measured in DL-AAA, PBS, and rAAV-hCRB injected experiments were recorded separately (treatment vs. nontreated eye).

Morphological and immunohistochemical analysis

Eyes were collected at the time points of 1-month-old (1M), 3M, 6M, 9M, and 12M. Mice injected with DL-AAA, PBS and/or rAAV-CRB were collected at 3M. Mouse eyes were compared to (age-matched) littermates or the nontreated eye of the same animal. The eyes were marked on the superior side with a dye for superior-inferior orientation [57]. For

morphological analysis, eyes were enucleated and fixed at room temperature with 4% paraformaldehyde in PBS for 25 minutes. Then, the eyes were dehydrated for 30 min in 30, 50, 70, 2x 90, 2x 100% Ethanol, 50:50 Ethanol:Technovit 7100 (Kulzer, Wehrheim, Germany), and finally in 100% Technovit 7100 overnight at +4°C.[57] The eyes were sectioned (2 μ m), stained with 1% Toluidine blue, and mounted with Entellan. The sections were imaged on 51x native resolution (brightfield) on a slidescanner (3DHistech Panoramic 250). For immunohistochemistry, we dehydrated the eyes for 30 min in 15% sucrose in PBS, followed by 30% sucrose in PBS (30 min). A detailed immunohistochemistry protocol is described in Buck *et al.* [58]. Cryosections (7 μ m) were rehydrated in PBS, blocked (1 hour), stained with the primary antibody overnight at 4°C, washed in PBS thrice (10 min), stained with the secondary antibody (Alexa488, Alexa555, Alexa647, cy3, or cy5. 1 hour), 3x washed in PBS (10 min), and mounted with Vectashield HardSet mounting medium containing DAPI (Vector Laboratories). A Leica TCS SP8 confocal microscope was used for image acquisition. Image analysis was done in Leica X, Fiji ImageJ, and Adobe Photoshop CC2018.

Antibodies

The following primary antibodies were used: Glutamine synthetase (1:250 BD Biosciences), Rhodopsin (1:500; Millipore); Cone Arrestin (1:500; Millipore); PKC α (1:250; BD Biosciences); MPP4 AK4 (1:200; homemade [33]), CRB1 AK2 pH 1.5 (1:200; homemade [8]), CRB2 (1:200 [8]), p120-catenin (1:100; BD Biosciences), GFAP (1:200; Dako), CD11b (1:100; BD Biosciences); PLVAP (1:200; BD Pharmingen), VE-cadherin (1:100 BD Biosciences).

DL- α -aminoadipate preparation

DL- α -aminoadipate (DL-AAA) preparations were prepared on the day of injections. DL-AAA in PBS was dissolved/deprotonated by dropwise addition 10M NaOH. Then, the pH was raised to 7.3 by adding hydrochloric acid (37% w/v fuming) dropwise. The volume was adjusted with PBS to 100 μ g/ μ L, 150 μ g/ μ L, or 200 μ g/ μ L. The final solution was filter-sterilized (0.22 μ m). A volume of 1 μ L DL-AAA or PBS was injected intravitreally in one eye corresponding to 0 μ g (PBS), 100 μ g, 150 μ g, or 200 μ g DL-AAA.

Generation and purification of recombinant adeno-associated viral vectors

The pAAV2-AmpR-ITR-CMVmin-h*CRB1*co-SpA-ITR or pAAV-AmpR-ITR-CMV-h*CRB2*co-SpA-ITR plasmids consist of the flanking ITRs of AAV serotype 2, the minimal CMV promoter (for *CRB1* expression), the full-length CMV promoter (for *CRB2* expression), the human codon-optimized *CRB1* or *CRB2* cDNA, and a 48 bp synthetic polyadenylation sequence [13]. The plasmid DNA was produced in Sure-2 cells and extracted on an anion exchange column (Endotoxin range: 1-10 EU/ μ g). Endotoxin levels were not measured and potential endotoxins were not removed from plasmid preps. The human *CRB1*

and CRB2 coding sequence used in our rAAV-vectors are highly similar to the mouse CRB1 or CRB2 coding sequence protein. Human/mouse CRB1 (1406 aa; 1405 aa. UniProtKB: P82279; Q8VHS2, respectively) or human/mouse CRB2 (1285 aa; 1282 aa. UniProtKB: Q5IJ48; Q80YA8, respectively) protein expressed at the OLM are similar in protein size and have similar protein domains (signal peptide, EGF-like, LamG, transmembrane, FERM, PDZ ERLI) [9,14]. The pAAV-hCRB plasmid, the pHelper, the pXX2-ShH10F were co-transfected in 10x 15-cm dishes of 80% confluent HEK293T cells to generate rAAV2/ShH10^{Y445F}.CMV.hCRB2_{co}.spA or rAAV2/ShH10^{Y445F}.CMVmin.hCRB1_{co}.spA viral particles. After benzonase treatment, the lysates were ultracentrifuged onto an iodixanol density gradient. The purified rAAV stock was filter-sterilized and then concentrated on an amplicon spin column (100,000 NMWL). All viral titers were determined by quantitative PCR. The final rAAV preparation was stored in 0.001% Pluronic® F-68 in PBS at -80°C. No major contaminants were found for the rAAV-ShH10^{Y445F}.CMVmin.hCRB1_{co} when a 10¹⁰ viral genome (vg) rAAV sample was denatured by lithium dodecyl sulfate (LDS) sample buffer, dithiothreitol (DTT; reducing agent), and heat (96°C; 5 min) and loaded on a SDS PAGE gel (NuPAGE Bis-Tris Mini gel) and protein-stained (Pierce Silver Stain Kit. See Figure S5T).

Recombinant AAV and AAA injection

Mice were anesthetized with 100 mg/kg ketamine and 5 mg/mL xylazine intraperitoneally, and the pupils were dilated using atropine drops (5 mg/mL). The pain was blocked locally by topically applying lidocaine (10 mg/mL) on a cotton swap to the eye and surrounding tissue. rAAV-hCRB1 or rAAV-hCRB2 was injected intravitreally in one eye (around 50/50 right vs. left eye) at postnatal day 21 (P21)-old mice (1 μ L; 10¹⁰ viral genomes). AAA-DL or PBS was injected intravitreally in one eye in 2-month-old (2M) mice (1 μ L). A Hamilton 10 μ L needle was used for AAA, PBS, and rAAV-hCRB injections. The injected and noninjected eyes were washed with Hypo-mellose (3 Mg/mL) drops, covered with chloramphenicol (TEVA, 10 mg/g), and placed on a heating mat for recovery.

Quantification and measurement for spidergrams

The thickness of the retina (ILM-to-OLM) was measured on plastic sections at 0.5, 1.0, 1.5, and 2.0 mm distance to the optic nerve head (ONH), as previously described.[16,57] Three measurements on three different sections were averaged per mouse. Brightfield images were taken on a slide scanner (3DHistech Pannoramic 250) at 51x native resolution.

Normalized CRB2 protein and p120-catenin quantification and OLM breaks

We stained against nuclei (DAPI), CRB2 (2nd antibody: anti-rabbit-cy3) and p120-catenin (2nd antibody: anti-mouse-Alexa488) using a master mix at the same time with one *Crb1*^{KO}*Crb2*^{Flox/wt} and *Crb1*^{KO}*Crb2*^{LowMGC} eye on each glass slide (Total 6 slides. Total animals: n=6 *Crb1*^{KO}; n=6 *Crb1*^{KO}*Crb2*^{LowMGC} mice). Three sections per eye were imaged

with the same laser and gain settings (12 images per mouse. >1 mm retinal length analyzed for periphery and central area). Two images in the periphery and two images in the central area (inferior and superior; four images per section). The confocal microscopy was done in one run (Total 144 images, 12 animals). An additional group of *Crb2^{Flox/Flox}*, *Crb2^{ΔRods}*, *Crb1^{KO}Crb2^{ΔRods}*, *Crb1^{KO}*, and additional *Crb1^{KO}Crb2^{Flox/wt}* retinas were similarly analyzed in one immunohistochemical and microscopy session but normalized to the previous *Crb1^{KO}Crb2^{Flox/wt}* fluorescence intensity values. The OLM area was defined as an area of ~2.5 μm above and 2.5 μm below the OLM. The fluorescence intensity was measured on gray-scale images. The mean gray intensity per pixel over the OLM area was calculated. One OLM disruption was defined as an area without p120-catenin OLM expression ≥1 photoreceptor nuclei column (2.5 μm). The OLM disruptions were normalized over 100 μm retinal length. The concomitant values were averaged per section, then averaged per mouse, and then averaged over the genotype group (n=6 mice per group). The images were blinded for the investigator before analysis.

Statistical analysis

All statistical analyses were performed using GraphPad Prism version 7 (GraphPad software). Normality was tested by the Kolmogorov-Smirnov test. We performed the following statistical analysis for group comparisons: A two-way ANOVA with a Bonferroni post hoc test (averaging right and left eye of a mouse; Figure 1 B-J; Figure S2; Figure S3), a two-way ANOVA / Mixed model with matched values across columns test with a Bonferroni post hoc test (comparing the treated eye vs the control eye within the same mouse. Figure S5), a one-way ANOVA (Kruskal-Wallis) with a Bonferroni post hoc test (Figure S4), unpaired t-test (Figure 1 L+M; Figure 2+3+5), or paired t-test (comparing the treated eye vs the control eye within the same mouse. Figure 6) [59]. All values are expressed as mean ±SEM if not otherwise indicated. Statistically significant values: *P<0.05, **P<0.01, ***P<0.001.

Conflict of interest statement

The authors declare that the research was conducted without any commercial or financial relationship that could be construed as a potential conflict of interest. The LUMC is the holder of patent number PCT/NL2014/050549, which describes the potential clinical use of CRB2; JW is listed as co-inventor of this patent, and JW is an employee of the LUMC.

Author contribution

Conceptualization, T.M.B. and J.W.; Methodology, T.M.B and J.W.; Investigation, T.M.B., R.M.V.; Formal Analysis, T.M.B. and J.W.; Writing – Original Draft, T.M.B.; Writing – Review & Editing, T.M.B., C.H.A. and J.W.; Funding Acquisition, C.H.A., J.W.; Resources, R.M.V., J.W.; Supervision, J.W.

Acknowledgments

The authors also thank Ilse Voshart, Ariadna Rocha Sierra, Martijn Koomen, Charlotte A. Andriessen, Annelies Boonzaier-van der Laan for technical assistance, and all Wijnholds Lab members for advice on the manuscript.

Funding

Foundation Fighting Blindness (TA-GT-0715-0665-LUMC, to JW), the Netherlands Organization for Health Research and Development (ZonMw grant 43200004, to JW), and the Dutch blindness funds (Uitzicht 2013-13 to JW, Uitzicht 2018-6 to CHA and JW): Rotterdamse Stichting Blindenbelangen, MaculaFonds, Stichting Blindenhulp, Landelijke Stichting voor Blinden en Slechtzienden, Algemene Nederlandse Vereniging ter Voorkoming van Blindheid, Stichting Blinden-Penning.

REFERENCES

1. Talib, M., van Schooneveld, M.J., van Genderen, M.M., Wijnholds, J., Florijn, R.J., ten Brink, J.B., Schalijs-Delfos, N.E., Dagnelie, G., Cremers, F.P.M., Wolterbeek, R., et al. (2017). Genotypic and Phenotypic Characteristics of CRB1-Associated Retinal Dystrophies: A Long-Term Follow-up Study. *Ophthalmology* *124*, 884–895.
2. Vincent, A., Ng, J., Gerth-Kahlert, C., Héon, E., Maynes, J.T., Wright, T., Tiwari, A., Tumber, A., Li, S., Hanson, J.V.M., et al. (2016). Biallelic mutations in CRB1 underlie autosomal recessive familial foveal retinoschisis. *Investig. Ophthalmol. Vis. Sci.* *57*, 2637–2646.
3. Tsang, S.H., Burke, T., Oil, M., Yzer, S., Lee, W., Xie, Y.A., and Allikmets, R. (2014). Whole Exome Sequencing Identifies CRB1 Defect in an Unusual Maculopathy Phenotype. *Ophthalmology* *121*, 1–10.
4. Quinn, P.M., Buck, T.M., Mulder, A.A., Ohonin, C., Alves, C.H., Vos, R.M., Bialecka, M., van Herwaarden, T., van Dijk, E.H.C.C., Talib, M., et al. (2019). Human iPSC-Derived Retinas Recapitulate the Fetal CRB1 CRB2 Complex Formation and Demonstrate that Photoreceptors and Müller Glia Are Targets of AAV5. *Stem Cell Reports* *12*, 906–919.
5. Quinn, P.M., Mulder, A.A., Henrique Alves, C., Desrosiers, M., de Vries, S.I., Klooster, J., Dalkara, D., Koster, A.J., Jost, C.R., and Wijnholds, J. (2019). Loss of CRB2 in Müller glial cells modifies a CRB1-associated retinitis pigmentosa phenotype into a Leber congenital amaurosis phenotype. *Hum. Mol. Genet.* *28*, 105–123.
6. Pellissier, L.P., Lundvig, D.M.S., Tanimoto, N., Klooster, J., Vos, R.M., Richard, F., Sothilingam, V., Garcia Garrido, M., Le Bivic, A., Seeliger, M.W., et al. (2014). CRB2 acts as a modifying factor of CRB1-related retinal dystrophies in mice. *Hum. Mol. Genet.* *23*, 3759–3771.
7. van Rossum, A.G.S.H., Aartsen, W.M., Meuleman, J., Klooster, J., Malysheva, A., Versteeg, I., Arsanto, J.-P.P., Le Bivic, A.A., and Wijnholds, J. (2006). Pals1/Mpp5 is required for correct localization of Crb1 at the subapical region in polarized Müller glia cells. *Hum. Mol. Genet.* *15*, 2659–2672.
8. van de Pavert, S.A., Kantardzhieva, A., Malysheva, A., Meuleman, J., Versteeg, I., Levelt, C., Klooster, J., Geiger, S., Seeliger, M.W., Rashbass, P., et al. (2004). Crumbs homologue 1 is required for maintenance of photoreceptor cell polarization and adhesion during light exposure. *J. Cell Sci.* *117*, 4169–4177.
9. Quinn, P.M., Pellissier, L.P., and Wijnholds, J. (2017). The CRB1 complex: Following the trail of Crumbs to a feasible gene therapy strategy. *Front. Neurosci.* *11*, 175.
10. van de Pavert, S.A., Meuleman, J., Malysheva, A., Aartsen, W.M., Versteeg, I., Tonagel, F., Kamphuis, W., McCabe, C.J., Seeliger, M.W., and Wijnholds, J. (2007). A single amino acid substitution (Cys249Trp) in Crb1 causes retinal degeneration and deregulates expression of pituitary tumor transforming gene Pttg1. *J. Neurosci.* *27*, 564–573.
11. Alves, C.H., Boon, N., Mulder, A.A., Koster, A.J., Jost, C.R., and Wijnholds, J. (2019). CRB2 Loss in Rod Photoreceptors Is Associated with Progressive Loss of Retinal Contrast Sensitivity. *Int. J. Mol. Sci.* *20*, 4069.
12. Van De Pavert, S.A., Sanz, A.S., Aartsen, W.M., Vos, R.M., Versteeg, I., Beck, S.C., Klooster, J., Seeliger, M.W., and Wijnholds, J. (2007). Crb1 is a determinant of retinal apical Müller glia cell features. *Glia* *55*, 1486–1497.
13. Pellissier, L.P., Quinn, P.M., Henrique Alves, C., Vos, R.M., Klooster, J., Flannery, J.G., Alexander Heimel, J., and Wijnholds, J. (2015). Gene therapy into photoreceptors and Müller glial cells restores retinal structure and function in CRB1 retinitis pigmentosa mouse models. *Hum. Mol. Genet.* *24*, 3104–3118.

14. Boon, N., Wijnholds, J., and Pellissier, L.P. (2020). Research Models and Gene Augmentation Therapy for CRB1 Retinal Dystrophies. *Front. Neurosci.* *14*, 860.
15. Alves, C.H., Sanz, A.S., Park, B., Pellissier, L.P., Tanimoto, N., Beck, S.C., Huber, G., Murtaza, M., Richard, F., Sridevi Gurubaran, I., et al. (2013). Loss of CRB2 in the mouse retina mimics human retinitis pigmentosa due to mutations in the CRB1 gene. *Hum. Mol. Genet.* *22*, 35–50.
16. Quinn, P.M., Alves, C.H., Klooster, J., and Wijnholds, J. (2018). CRB2 in immature photoreceptors determines the superior-inferior symmetry of the developing retina to maintain retinal structure and function. *Hum. Mol. Genet.* *27*, 3137–3153.
17. West, E.L., Pearson, R.A., Tschernutter, M., Sowden, J.C., MacLaren, R.E., and Ali, R.R. (2008). Pharmacological disruption of the outer limiting membrane leads to increased retinal integration of transplanted photoreceptor precursors. *Exp. Eye Res.* *86*, 601–611.
18. Kato, S., Ishita, S., Sugawara, K., and Mawatari, K. (1993). Cystine/glutamate antiporter expression in retinal Müller glial cells: implications for DL-alpha-aminoacidopate toxicity. *Neuroscience* *57*, 473–482.
19. Yu, W.Q., Eom, Y.S., Shin, J.A., Nair, D., Grzywacz, S.X.Z., Grzywacz, N.M., Craft, C.M., and Lee, E.J. (2016). Reshaping the cone-mosaic in a rat model of retinitis Pigmentosa: Modulatory role of ZO-1 expression in dl-alpha-aminoacidopate reshaping. *PLoS One* *11*, e0151668.
20. Shen, W., Zhang, J., Chung, S.H., Hu, Y., Ma, Z., and Gillies, M.C. (2011). Submacular DL- α -aminoacidopate eradicates primate photoreceptors but does not affect luteal pigment or the retinal vasculature. *Invest. Ophthalmol. Vis. Sci.* *52*, 119–127.
21. Jimeno, D., Feiner, L., Lillo, C., Teofilo, K., Goldstein, L.S.B., Pierce, E.A., and Williams, D.S. (2006). Analysis of kinesin-2 function in photoreceptor cells using synchronous Cre-loxP knockout of Kif3a with RHO-Cre. *Investig. Ophthalmol. Vis. Sci.* *47*, 5039–5046.
22. Murray, S.A., Eppig, J.T., Smedley, D., Simpson, E.M., and Rosenthal, N. (2012). Beyond knockouts: Cre resources for conditional mutagenesis. *Mamm. Genome* *23*, 587–599.
23. Prusky, G.T., West, P.W.R., and Douglas, R.M. (2000). Behavioral assessment of visual acuity in mice and rats. *Vision Res.* *40*, 2201–2209.
24. Prusky, G.T. (2004). Rapid Quantification of Adult and Developing Mouse Spatial Vision Using a Virtual Optomotor System. *Invest. Ophthalmol. Vis. Sci.* *45*, 4611–4616.
25. Prusky, G.T., and Douglas, R.M. (2004). Characterization of mouse cortical spatial vision. *Vision Res.* *44*, 3411–3418.
26. Krizaj, D., Demarco, S.J., Johnson, J., Strehler, E.E., and Copenhagen, D.R. (2002). Cell-specific expression of plasma membrane calcium ATPase isoforms in retinal neurons. *J. Comp. Neurol.* *451*, 1–21.
27. Pellissier, L.P., Alves, C.H., Quinn, P.M., Vos, R.M., Tanimoto, N., Lundvig, D.M.S., Dudok, J.J., Hooibrink, B., Richard, F., Beck, S.C., et al. (2013). Targeted ablation of CRB1 and CRB2 in retinal progenitor cells mimics Leber congenital amaurosis. *PLoS Genet* *9*, e1003976.
28. Bazellières, E., Aksenova, V., Barthélémy-Requin, M., Massey-Harroche, D., and Le Bivic, A. (2018). Role of the Crumbs proteins in ciliogenesis, cell migration and actin organization. *Semin. Cell Dev. Biol.* *81*, 13–20.
29. Bulgakova, N. a, and Knust, E. (2009). The Crumbs complex: from epithelial-cell polarity to retinal degeneration. *J. Cell Sci.* *122*, 2587–96.
30. Margolis, B. (2018). The Crumbs3 polarity protein. *Cold Spring Harb. Perspect. Biol.* *10*, a027961.
31. Assémat, E., Crost, E., Ponsérre, M., Wijnholds, J., Le Bivic, A., and Massey-Harroche, D. (2013). The multi-PDZ domain protein-1 (MUPP-1) expression regulates cellular levels of the PALS-1/PATJ polarity complex. *Exp. Cell Res.* *319*, 2514–2525.
32. Alves, C.H., Pellissier, L.P., Vos, R.M., Garcia Garrido, M., Sothilingam, V., Seide, C., Beck, S.C., Klooster, J., Furukawa, T., Flannery, J.G., et al. (2014). Targeted ablation of Crb2 in photoreceptor cells induces retinitis pigmentosa. *Hum. Mol. Genet.* *23*, 3384–3401.
33. Kantardzhieva, A., Gosens, I., Alexeeva, S., Punte, I.M., Versteeg, I., Krieger, E., Neeffjes-Mol, C.A., Den Hollander, A.I., Letteboer, S.J.F.F., Klooster, J., et al. (2005). MPP5 recruits MPP4 to the CRB1 complex in photoreceptors. *Investig. Ophthalmol. Vis. Sci.* *46*, 2192–2201.
34. Pearson, R.A., Barber, A.C., West, E.L., MacLaren, R.E., Duran, Y., Bainbridge, J.W., Sowden, J.C., and Ali, R.R. (2010). Targeted disruption of outer limiting membrane junctional proteins (Crb1 and ZO-1) increases integration of transplanted photoreceptor precursors into the adult wild-type and degenerating retina. *Cell Transplant.* *19*, 487–503.
35. Pellissier, L.P., Hoek, R.M., Vos, R.M., Aartsen, W.M., Klimczak, R.R., Hoyng, S.A., Flannery, J.G., and Wijnholds, J. (2014). Specific tools for targeting and expression in Müller glial cells. *Mol. Ther. — Methods Clin. Dev.* *1*, 14009.
36. Klimczak, R.R., Koerber, J.T., Dalkara, D., Flannery, J.G., and Schaffer, D. V. (2009). A novel adeno-associated viral variant for efficient and selective intravitreal transduction of rat Müller cells. *PLoS One* *4*, e7467.
37. Klaassen, I., Van Noorden, C.J.F., and Schlingemann, R.O. (2013). Molecular basis of the inner blood-retinal barrier and its breakdown in diabetic macular edema and other pathological conditions. *Prog. Retin. Eye Res.* *34*, 19–48.

38. Wisniewska-Kruk, J., Van Der Wijk, A.E., Van Veen, H.A., Gorgels, T.G.M.F., Vogels, I.M.C., Versteeg, D., Van Noorden, C.J.F., Schlingemann, R.O., and Klaassen, I. (2016). Plasmalemma vesicle-associated protein has a key role in blood-retinal barrier loss. *Am. J. Pathol.* *186*, 1044–1054.
39. Timmers, A.M., Newmark, J.A., Turunen, H.T., Farivar, T., Liu, J., Song, C., Ye, G.J., Pennock, S., Gaskin, C., Knop, D.R., et al. (2020). Ocular Inflammatory Response to Intravitreal Injection of Adeno-Associated Virus Vector: Relative Contribution of Genome and Capsid. *Hum. Gene Ther.* *31*, 80–89.
40. Newman, E., and Reichenbach, A. (1996). The Müller cell: a functional element of the retina. *Trends Neurosci.* *19*, 307–312.
41. Franze, K., Grosche, J., Skatchkov, S.N., Schinkinger, S., Foja, C., Schild, D., Uckermann, O., Travis, K., Reichenbach, A., and Guck, J. (2007). Müller cells are living optical fibers in the vertebrate retina. *Proc. Natl. Acad. Sci. U. S. A.* *104*, 8287–8292.
42. Newman, E.A. (2015). Glial cell regulation of neuronal activity and blood flow in the retina by release of gliotransmitters. *Philos. Trans. R. Soc. B Biol. Sci.* *370*, 1–9.
43. Witmer, A.N., Blaauwgeers, H.G., Weich, H., Alitalo, K., Vrensen, G., and Schlingemann, R. (2002). Altered expression patterns of VEGF receptors in human diabetic retina and in experimental VEGF-induced retinopathy in monkey. *Invest. Ophthalmol. Vis. Sci.* *43*, 849–857.
44. Son, S., Cho, M., and Lee, J. (2019). Crumbs proteins regulate layered retinal vascular development required for vision. *Biochem. Biophys. Res. Commun.* *521*, 939–946.
45. Kim, J.H., Kim, J.H., Yu, Y.S., Kim, D.H., and Kim, K.-W. (2009). Recruitment of pericytes and astrocytes is closely related to the formation of tight junction in developing retinal vessels. *J. Neurosci. Res.* *87*, 653–659.
46. Gardner, T.W., Lieth, E., Khin, S.A., Barber, A.J., Bonsall, D.J., Leshner, T., Rice, K., and Brennan, W.A. (1997). Astrocytes increase barrier properties and ZO-1 expression in retinal vascular endothelial cells. *Investig. Ophthalmol. Vis. Sci.* *38*, 2423–2427.
47. Witmer, A.N., Vrensen, G.F.J.M., Van Noorden, C.J.F., and Schlingemann, R.O. (2003). Vascular endothelial growth factors and angiogenesis in eye disease. *Prog. Retin. Eye Res.* *22*, 1–29.
48. Meeson, A.P., Argilla, M., Ko, K., Witte, L., and Lang, R.A. (1999). VEGF deprivation and capillary regression. *Development* *126*, 1407–1415.
49. Koerber, J.T., Klimczak, R., Jang, J.-H.H., Dalkara, D., Flannery, J.G., and Schaffer, D. V. (2009). Molecular evolution of adeno-associated virus for enhanced glial gene delivery. *Mol. Ther.* *17*, 2088–2095.
50. Xiao, Z., Patrakka, J., Nukui, M., Chi, L., Niu, D., Betsholtz, C., Pikkarainen, T., Vainio, S., and Tryggvason, K. (2011). Deficiency in Crumbs homolog 2 (Crb2) affects gastrulation and results in embryonic lethality in mice. *Dev Dyn.* *240*, 2646–2656.
51. Hurk, J.J. van den, Rashbass, P., Roepman, R., Davis, J., Voesenek, K., Arends, M., Zonneveld, M.N., Roekel, M.V. van, Cameron, K., Rohrschneider, K., et al. (2005). Characterization of the Crumbs homolog 2 (CRB2) gene and analysis of its role in retinitis pigmentosa and Leber congenital amaurosis. *Mol. Vis.* *11*, 263–273.
52. Dolón, J.F., Paniagua, A.E., Valle, V., Segurado, A., Arévalo, R., Velasco, A., and Lillo, C. (2018). Expression and localization of the polarity protein CRB2 in adult mouse brain: a comparison with the CRB1rd8 mutant mouse model. *Sci. Rep.* *8*, 11652.
53. Zhao, M., Andrieu-Soler, C., Kowalczyk, L., Cortés, M.P., Berdugo, M., Dernigoghossian, M., Halili, F., Jeanny, J.C., Goldenberg, B., Savoldelli, M., et al. (2015). A new CRB1 rat mutation links Müller glial cells to retinal telangiectasia. *J. Neurosci.* *35*, 6093–6106.
54. Shen, W., Li, S., Chung, S.H., and Gillies, M.C. (2010). Retinal vascular changes after glial disruption in rats. *J. Neurosci. Res.* *88*, 1485–1499.
55. Li, Y., Busoy, J.M., Zaman, B.A.A., Tan, Q.S.W., Tan, G.S.W., Barathi, V.A., Cheung, N., Wei, J.J.Y., Hunziker, W., Hong, W., et al. (2018). A novel model of persistent retinal neovascularization for the development of sustained anti-VEGF therapies. *Exp. Eye Res.* *174*, 98–106.
56. Roesch, K., Jadhav, A.P., Trimarchi, J.M., Stadler, M.B., Roska, B., Sun, B.B., and Cepko, C.L. (2008). The transcriptome of retinal Müller glial cells. *J. Comp. Neurol.* *509*, 225–38.
57. Alves, C.H., and Wijnholds, J. (2018). AAV gene augmentation therapy for CRB1-associated retinitis pigmentosa. In *Methods in Molecular Biology*, C. J. F. Boon and J. Wijnholds, eds. (New York, NY: Humana Press Inc.), pp. 135–151.
58. Buck, T.M., Pellissier, L.P., Vos, R.M., van Dijk, E.H.C.C., Boon, C.J.F., and Wijnholds, J. (2018). AAV serotype testing on cultured human donor retinal explants. In *Methods in Molecular Biology*, C. J. F. Boon and J. Wijnholds, eds. (New York, NY: Humana Press Inc.), pp. 275–288.
59. Heynen, S.R., Meneau, I., Caprara, C., Samardzija, M., Imsand, C., Levine, E.M., and Grimm, C. (2013). CDC42 Is Required for Tissue Lamination and Cell Survival in the Mouse Retina. *PLoS One* *8*, e53806.
60. de Souza, C.F., Nivison-Smith, L., Christie, D.L., Polkinghorne, P., McGhee, C., Kalloniatis, M., and Acosta, M.L. (2016). Macromolecular markers in normal human retina and applications to human retinal disease. *Exp. Eye Res.* *150*, 135–148.

61. Chakarova, C.F., Khanna, H., Shah, A.Z., Patil, S.B., Sedmak, T., Murga-Zamalloa, C.A., Papaioannou, M.G., Nagel-Wolfrum, K., Lopez, I., Munro, P., et al. (2011). TOPORS, implicated in retinal degeneration, is a cilia-centrosomal protein. *Hum. Mol. Genet.* *20*, 975–987.
62. Aartsen, W.M., Arsanto, J.P., Chauvin, J.P., Vos, R.M., Versteeg, I., Cardozo, B.N., Bivic, A.L., and Wijnholds, J. (2009). PSD95 β regulates plasma membrane Ca(2+) pump localization at the photoreceptor synapse. *Mol. Cell. Neurosci.* *41*, 156–165.

Figures

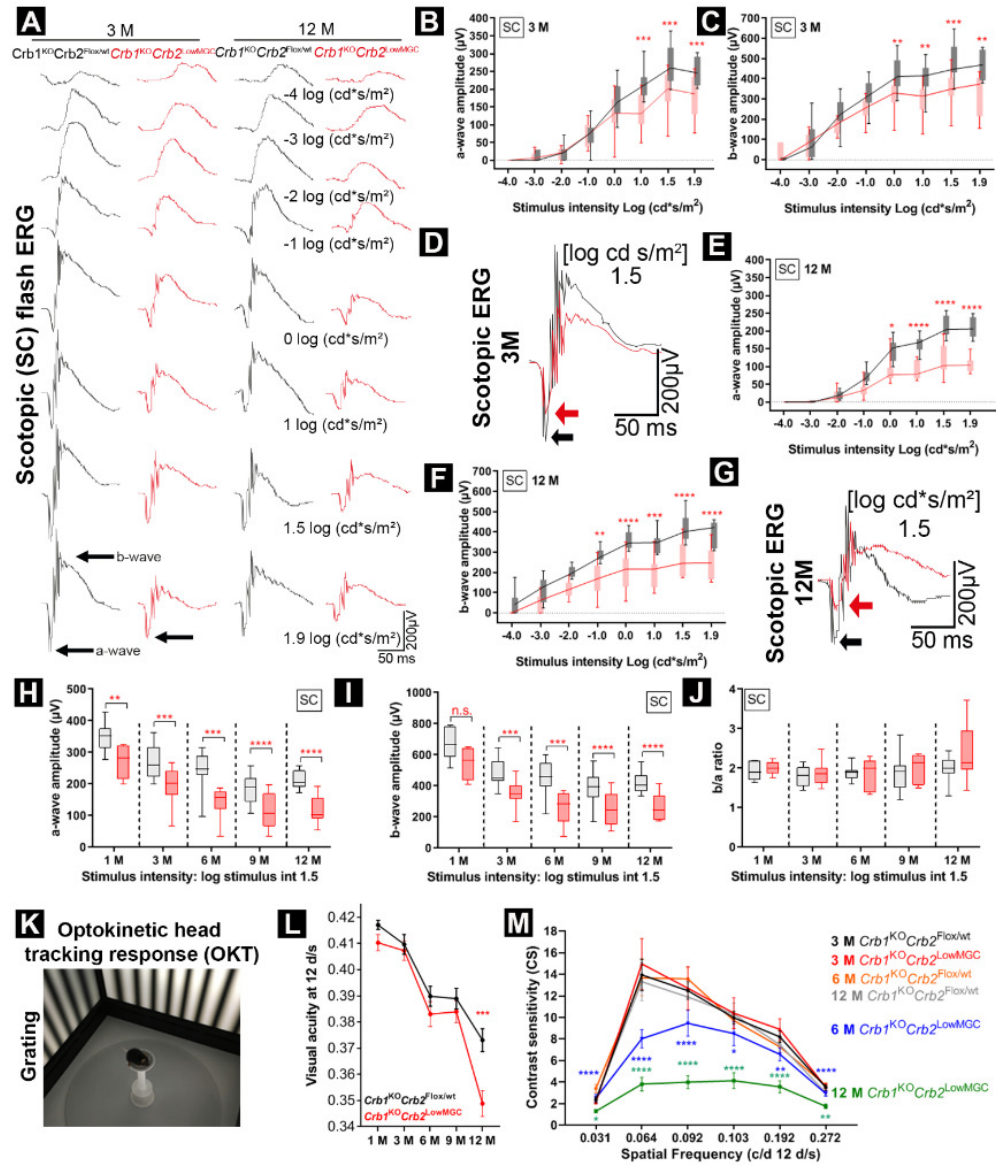


Figure 1. Decreased retinal function and vision-guided behavior in *Crbl^{KO}Crb2^{LowMGC}* compared to *Crbl^{KO}Crb2^{Flox/wt}* age-matched littermates. *Crbl^{KO}Crb2^{LowMGC}* measurements are indicated in red (experimental group) and *Crbl^{KO}Crb2^{Flox/wt}* age-matched littermates with a similar genetic background in black (control group). Electroretinographic analysis of the retinal function: (A) Scotopic single-flash intensity series (-4, -3, -2, -1, 0, 1, 1.5, 1.9 log cd s/m² light intensity) ERG from representative animals at 3-months (n=14 control group and n=12 experimental group) and 12-months of age (n=8 per group). Quantitative evaluation of the scotopic single-flash ERG intensity series of the a-wave (B+E+H), b-wave (C+F+I). Superimposed scotopic single-flash ERG traces at 1.5 log cd s/m² intensity from representative animals at 3-months and 12-months (D-G). Quantitative evaluation of the scotopic a-wave, b-wave, and b/a-wave ratio at 1.5 log cd s/m² intensity (H-J). Boxes indicate the 25 and 75% quantile range, whiskers indicate the 5 and 95% quantiles, and the intersection of line and error bar indicates the median of the data (box-and-whisker plot). Optokinetic head tracking response at 1-, 3-, 6-, and 12-month-old mice (mean±SEM; K-M). (L) Spatial frequency threshold (visual acuity. Number of animals (control vs experimental): 1-month (n=13; n=17); 3-months (n=23; n=20); 6-month (n=23; n=16); 9-month (n=26; n=17); 12-month (n=22; n=16). (M) Contrast sensitivity threshold at different spatial frequencies (mean ±SEM. Number of animals (Control vs. experimental): 3-months (N=11; n=11); 6-month (n=10; n=11); 9-months (n=11; n=8); 12-months (n=20; n=11). *P<0.05; **p<0.01, ***P<0.001. See also Figure S3.

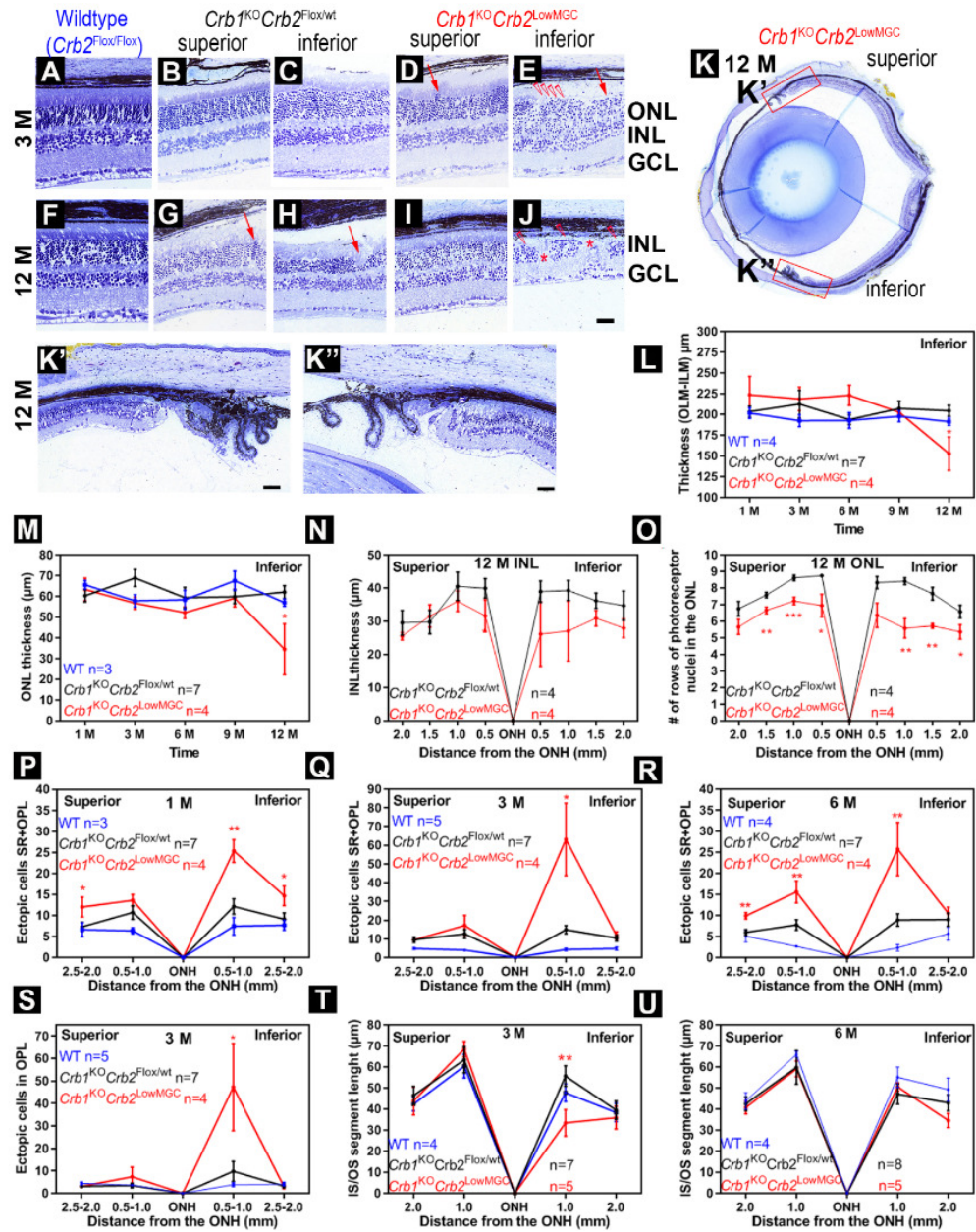


Figure 2. Removal of CRB1 and low levels of CRB2 in Müller glial cells leads to abnormal layering in the inferior quadrants. (A-K'') Toluidine-stained light microscopy of retinal sections from control ($Crb2^{Flox/Flox}$, $Crb1^{KO}Crb2^{Flox/wt}$, and $Crb1^{KO}Crb2^{LowMGC}$ mice at 3- and 12-month-of-age. Representative morphological changes: Protrusions (red arrow downward), ingressions, neovascularization (asterisks), and loss of inner/outer segments of photoreceptors (red triangles). (K-K'') Representative 12-month-old retina of a $Crb1^{KO}Crb2^{LowMGC}$ mouse indicates photoreceptor layer presence in periphery and superior quadrants of the retina. (L-U) Spidergrams of the retina of wild-type (WT; $Crb2^{Flox/Flox}$), $Crb1^{KO}Crb2^{Flox/wt}$, $Crb1^{KO}Crb2^{LowMGC}$ mice. (L-M) Decrease of retinal thickness (outer limiting membrane to the inner limiting membrane) and ONL thickness at 1 mm distance on the inferior retina in 1-, 3-, 6-, 9- and 12-month-old mice. (N-O) INL thickness and the number of rows of photoreceptor nuclei in the ONL of 12-month-old mice. (P-S) Total number of ectopic cells at 1-, 3-, and 6-months. (S) Most ectopic cells are in the Outer Plexiform Layer at 3-months-of-age. (T-U) Inner/outer segment length of photoreceptors in the periphery (2.0 mm) and central (1.0 mm) from the optic nerve head (ONH). Scale bar: 50 μ m. Data are presented as mean \pm SEM. Statistical significance: * $P < 0.05$, ** $P < 0.01$, *** $P < 0.001$.

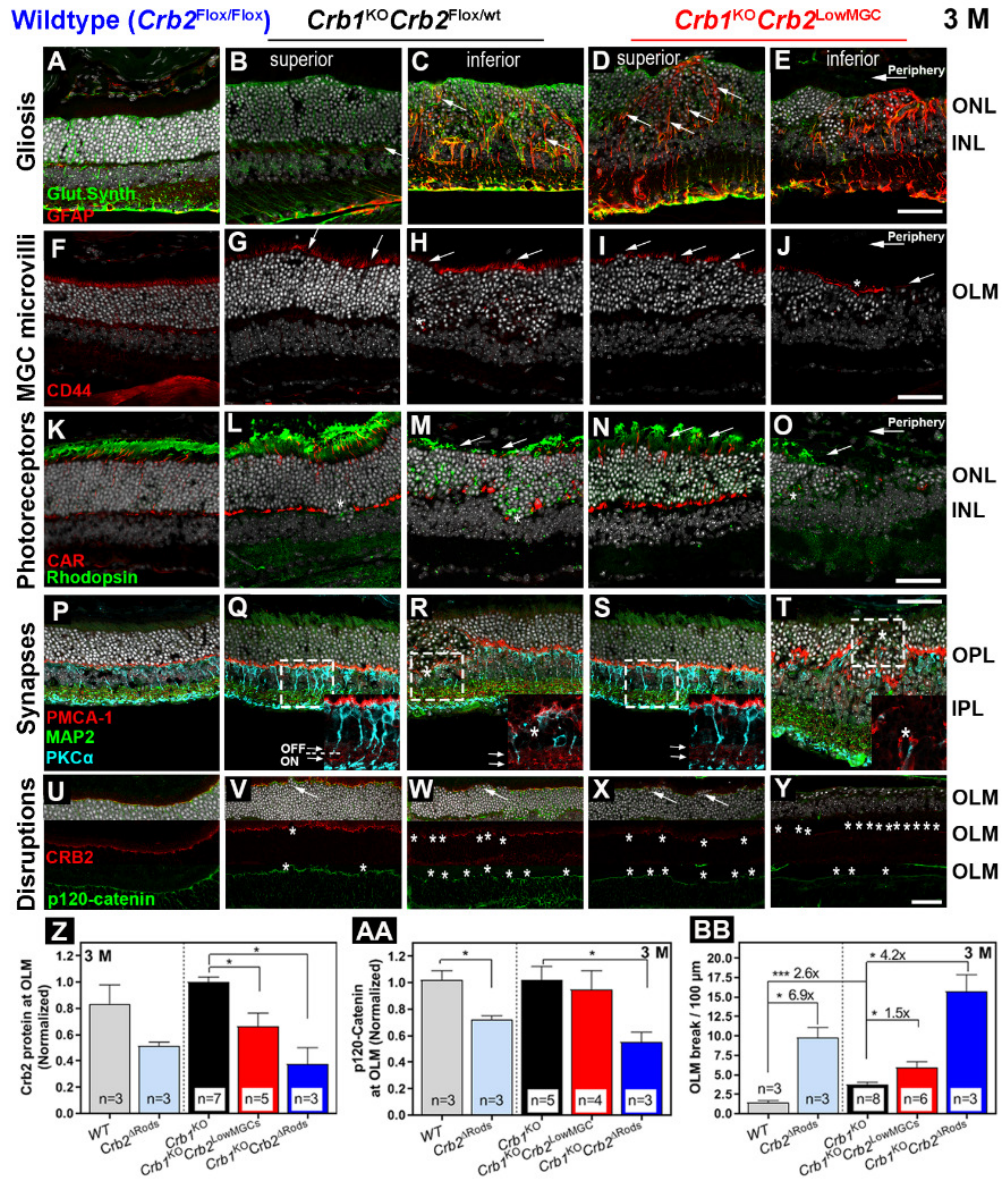


Figure 3. *Crb1*^{KO}*Crb2*^{LowMGC} retinas compared to *Crb1*^{KO}*Crb2*^{Flox/wt} retinas show more disruptions at the outer limiting membrane. Immunohistochemistry of 3-month-old mice. A representative image is shown of 3-6 retinas per group analyzed. Sections were stained for: (A-E) Glutamine synthetase (green) for Müller glial cells and Glial Fibrillary Acidic Protein (GFAP; red) for MGC stress fibers. (F-J) CD44 (red) for Müller glial microvilli processes; (K-O) cone arrestin (CAR; red) for cone photoreceptor segments and rhodopsin for rod photoreceptor outer segments (green). (P-T) MAP2 (green) for ganglion cells and synapses in the inner plexiform layer (IPL)⁶⁰, PMCA1 (red) for pre-synapses of photoreceptors at the outer plexiform layer (OPL) and lamina a-/b- in the IPL²⁶, and PKC α (light blue) for bipolar cells and bipolar post-synapses at the OPL. (I-P) subapical region marker CRB2 (red) and the adherens junction marker p120-catenin (green). (Z-BB) The decrease in CRB proteins and p120-catenin proteins at the OLM increases breaks at the OLM in 3-month-old wild-type (WT), *Crb2* ^{Δ Rods}, *Crb1*^{KO}*Crb2*^{Flox/wt}, *Crb1*^{KO}*Crb2*^{LowMGC}, and *Crb1*^{KO}*Crb2* ^{Δ Rods} mice. (Z) Normalized CRB2 protein expression to *Crb1*^{KO} mice (Fluorescence). (AA) Normalized p120-catenin protein expression to *Crb1*^{KO}*Crb2*^{Flox/wt}. (BB) OLM breaks per 100 μ m retinal length. ONL, outer nuclear layer; INL, Inner Nuclear Layer; GCL, Ganglion Cell Layer; MAP2, microtubule-associated protein 2; OPL, Outer Plexiform Layer; wt, Wildtype; OLM, Outer Limiting Membrane. Inserts 50 μ m. Scale bar: 50 μ m. Data are presented as mean \pm SEM. Statistical significance: *P<0.05, **P<0.01, ***P<0.001.

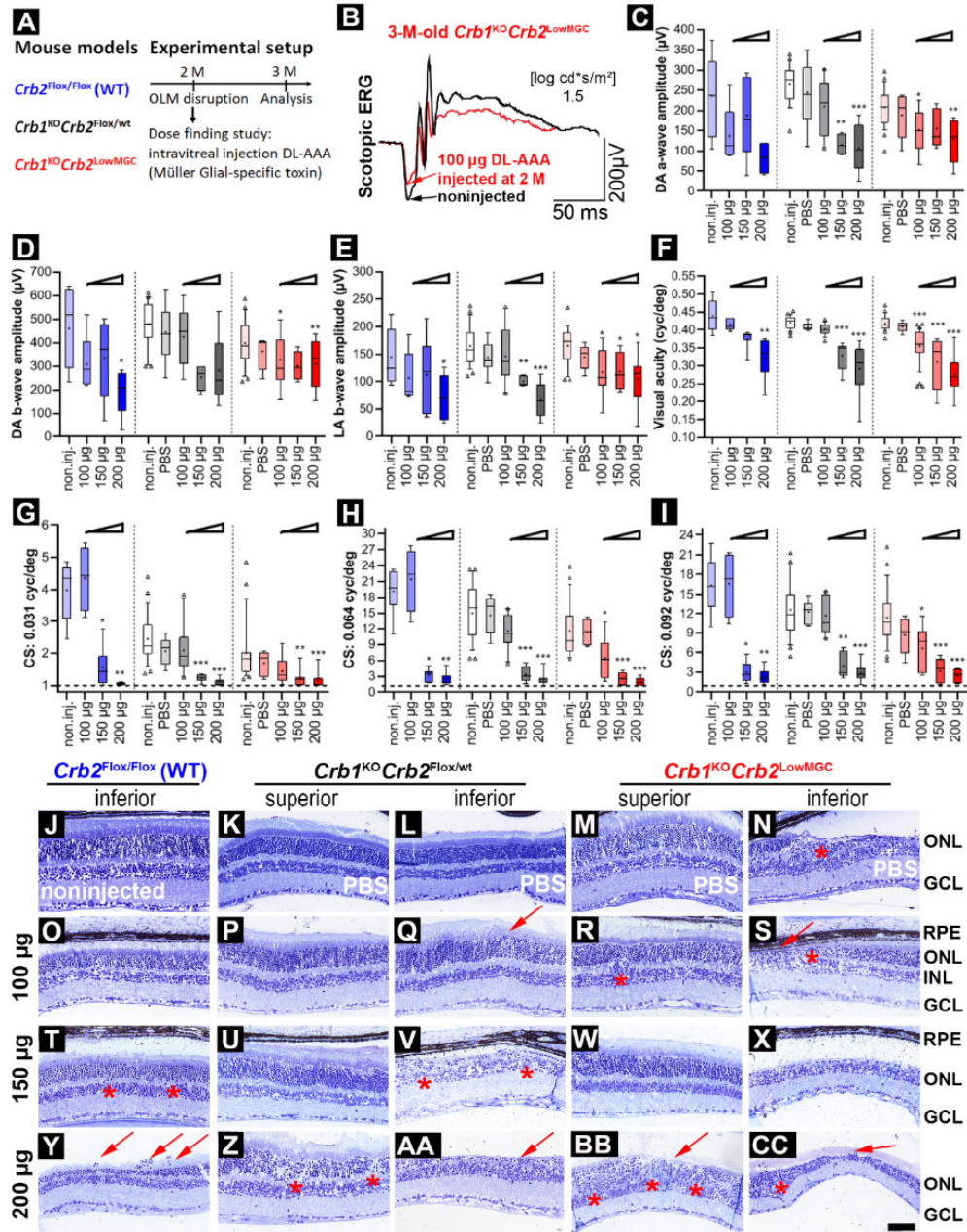


Figure 4. Intravitreal injection of DL-AAA worsens retinal morphology, retinal transmission, and vision-guided behavior. (A) Mouse models ($Crb2^{Fllox/Fllox}$; $Crb1^{KO}Crb2^{Fllox/wt}$; $Crb1^{KO}Crb2^{LowMGC}$) are exposed to OLM disruptions by DL-AAA intravitreal injection of DL-AAA at 2-months and the effect measured at 3-months (ERG; OKT; morphology). (B) Single-flash scotopic ERG traces at 1.5 log cd s/m² intensity for a $Crb1^{KO}Crb2^{LowMGC}$ mouse (black traces=noninjected; red trace 100 μg DL-AAA injected). (C-E) $Crb2^{Fllox/Fllox}$ = blue boxplots; $Crb1^{KO}Crb2^{Fllox/wt}$ = grey boxplots; $Crb1^{KO}Crb2^{LowMGC}$ = red boxplots: (C) scotopic a-wave (μV) at 1.5 log cd s/m², (D) scotopic b-wave (μV) and photopic b-wave (μV) at 1.5 log cd s/m² Number of animals for ERG (C-E): $Crb2^{Fllox/Fllox}$: noninjected n=8; 100 μg n=5; 150 μg 200 μg n=5 per group. $Crb1^{KO}Crb2^{Fllox/wt}$: noninjected n=23; PBS n=7; 100 μg n=10; 150 μg n=4; 200 μg n=6. $Crb1^{KO}Crb2^{LowMGC}$: noninjected n=24; PBS n=5; 100 μg n=9; 150 μg n=5; 200 μg n=7). (F-I) Optokinetic head tracking responses (OKT): (F) Spatial frequency threshold (visual acuity). (G-I) Contrast sensitivity threshold at 0.031, 0.064, and 0.092 spatial frequency (cycles/degree). Number of animals for OKT (F-I): $Crb2^{Fllox/Fllox}$: noninjected n=6; 100 μg n=4; 150 μg n=8; 200 μg n=8. $Crb1^{KO}Crb2^{Fllox/wt}$: noninjected n=25; PBS n=7; 100 μg n=10; 150 μg n=6; 200 μg n=7. $Crb1^{KO}Crb2^{LowMGC}$: noninjected n=25; PBS n=4; 100 μg n=9; 150 μg n=7; 200 μg n=8). (J-CC) Toluidine-stained light microscopy of retinal sections from 3-month-old mice. ONL, outer nuclear layer; INL, Inner Nuclear Layer; GCL, Ganglion Cell Layer; wt, Wildtype. Scale bar: 50 μm. Data presented as box plots (10-90%) and outliers (triangles). Mean indicated as a plus sign (+). An ANOVA followed by Bonferroni post-hoc test was performed to determine statistical significance comparing the noninjected (non.inj.) values to PBS, 100 μg, 150 μg, and 200 μg DL-AAA injected mouse values. Statistical significance: *P<0.05, **P<0.01, ***P<0.001.

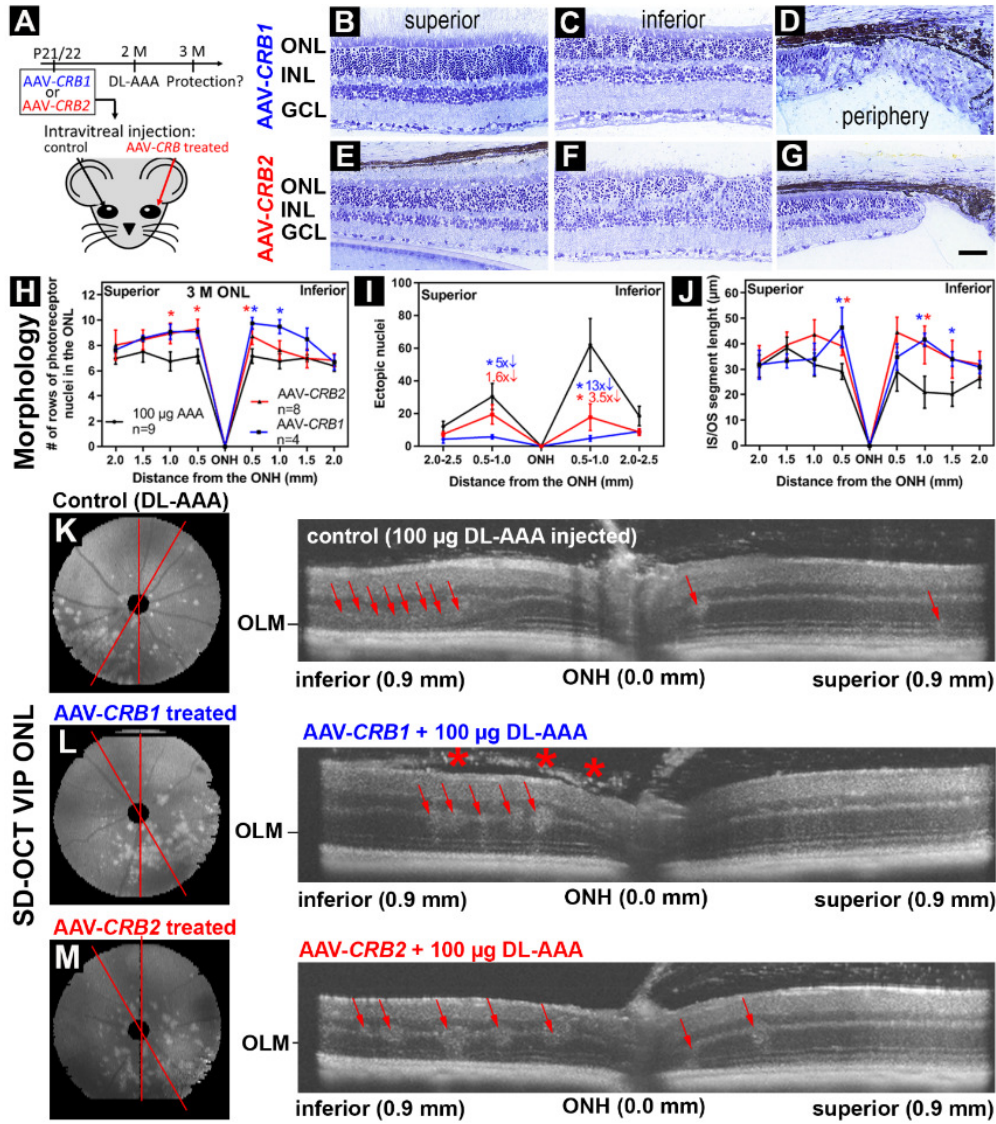


Figure 5. rAAV-hCRB2 protects against retinal disorganization and degeneration in the AAA-challenged *Crb1*^{KO}*Crb2*^{LowMGC} mice. (A) Retinitis pigmentosa model: rAAV-hCRB was injected in one eye vs noninjected eye (control) at postnatal day 21/22. Both eyes were then injected with a MGC-specific OLM stressor (100 µg DL-AAA) at the 2-month time point. The potential rAAV-therapy protective effect was measured at 3 months. (B-G) Toluidine-stained light microscopy of retinal sections from 3-month-old *Crb1*^{KO}*Crb2*^{LowMGC} mice that were treated with (B-D) rAAV2/ShH10^{Y445F}.CMVmin.hCRB1 or treated with (E-G) rAAV2/ShH10^{Y445F}.CMV.hCRB2. (H-J) Spidergrams of the retina of *Crb1*^{KO}*Crb2*^{LowMGC} mice (100 µg AAA injected, n=9; rAAV-hCRB1 injected n=4 and rAAV-hCRB2 injected n=8). (I) rAAV-hCRB treated retinas had more rows of photoreceptor nuclei in the ONL (H), less ectopic photoreceptor cell nuclei in the subretinal space and outer plexiform layer (I), and longer inner/outer segments of photoreceptors (J). (K-M) Representative spectral domain optical coherence tomography (SD-OCT) images indicate the phenotype in inferior-temporal quadrant in the Volume Intensity Projection (VIP) of the ONL and a representative radial SD-OCT averaged stacks (150°-180° or 180°-210° see red lines) of superior-inferior retina indicates more retinal damage in eyes not supplemented with hCRB1 or hCRB2 cDNA (Number of animals: rAAV-hCRB1 n=5; rAAV-hCRB2 n=6; untreated n=11. Arrows indicate ingressions. The asterisk indicates infiltrating vitreous cells). ONL, outer nuclear layer; INL, Inner Nuclear Layer; GCL, Ganglion Cell Layer; ONH, Optic Nerve Head; IS/OS, inner/outer segments of photoreceptors; OLM, Outer Limiting Membrane. Scale bar: 50 µm. Data are presented as mean±SEM. Statistical significance: *P<0.05, **P<0.01, ***P<0.001.

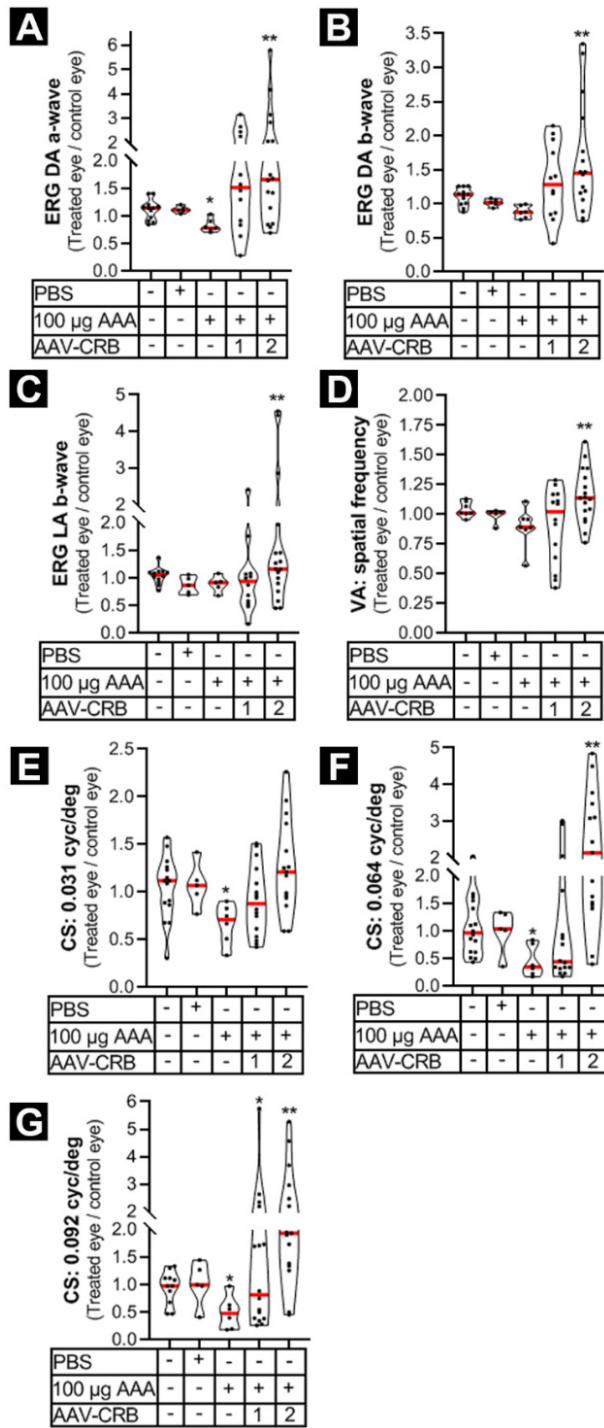


Figure 6. rAAV-hCRB2 protects against loss of ERG and OKT response in the AAA-challenged *Crb1*^{KO}*Crb2*^{lowMGC} mice. Group comparisons (e.g. rAAV-treated eye divided by control eye value) in violin plots in columns 1-5: (1) overall control: left eye value divided by the right eye value. (2) One eye injected with PBS divided by one eye not injected; (3) One eye injected with DL-AAA 100 µg divided by one eye not injected; (4-5) P21/22 injection of rAAV-hCRB in one eye, 100 µg DL-AAA injected at 2-month in both eyes, and protection against retinal damage analyzed at 3-month (rAAV-treated divided by control eye). (A-C) Single-flash ERG traces at 1.5 log cd s/m² intensity for the (A) scotopic a-wave, (B) scotopic b-wave, and (C) photopic b-wave. (D-G) Optokinetic head tracking responses (OKT): (D) Spatial frequency threshold (visual acuity); (E-G) Contrast sensitivity threshold at 0.031, 0.064, and 0.092 spatial frequency (cycles/degree). The probability distribution is presented in a violin plot. The median is given in red. Dots in graphs represent the values obtained for each mouse. For statistical comparison, a paired *t*-test on the total value of the rAAV-treated eye against total value of the eye not receiving the *CRB1* or *CRB2* cDNA (control eye) was performed. Mice tested are represented as black dots in figures. Statistical significance: **P*<0.05, ***P*<0.01, ****P*<0.001. See also Figure S4.

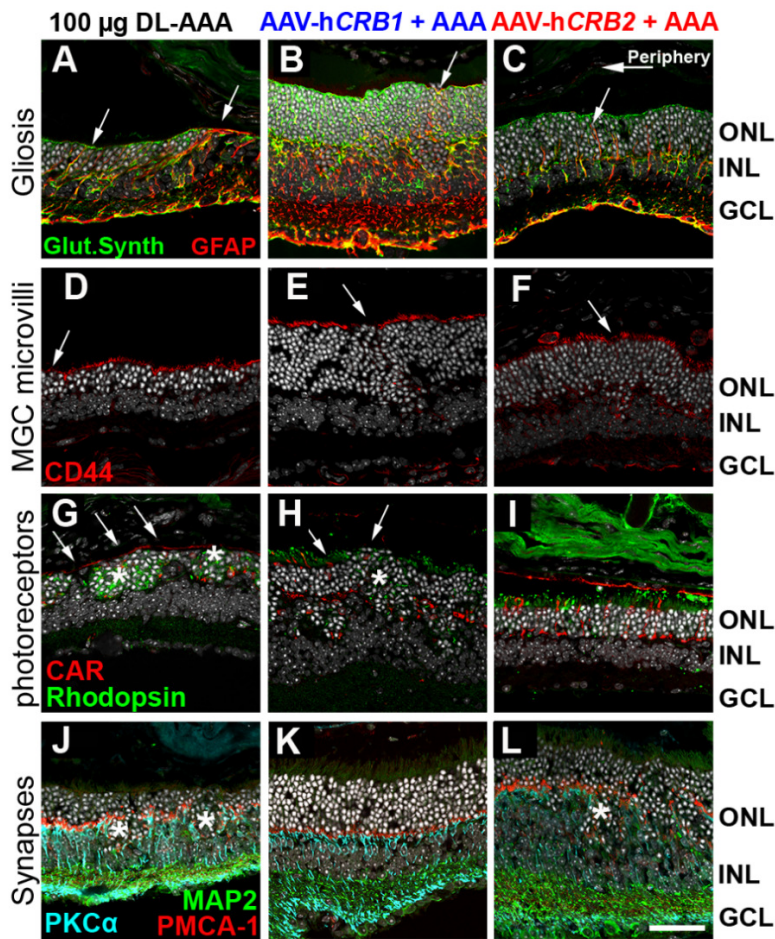


Figure 7. Intravitreal injection of rAAV-hCRB in the AAA-challenged *Crb1*^{KO}*Crb2*^{LowMGC} mouse model protects against loss of Müller glial microvilli length. Immunohistochemistry on the inferior retinal quadrants of 3-month-old mice that received an intravitreal injection of rAAV-hCRB in one of the two eyes at postnatal day 21, and subsequently at 2 months-of-age intravitreal injections of 100 µg DL-AAA in both eyes. Sections were stained for: (A-C) Glutamine synthetase (green) for Müller glial processes and Glial Fibrillary Acidic Protein (GFAP; red) for stress fibers (arrows); (D-F) CD44 (red) for Müller glial microvilli processes subapical region marker (arrow indicates loss / decrease of villi); (G-I) cone arrestin (CAR; red) for cone photoreceptor segments and rhodopsin for rod photoreceptors (green; arrows indicate loss/decrease in length of inner/outer photoreceptor segments. Asterisk indicate intracellular rhodopsin expression in stressed rod photoreceptors); and (J-L) MAP2 (green) for ganglion cells, synapses in the inner plexiform layer (IPL) as well as PRC inner segments;^{60,61} PMCA1 (red) for synaptic elements of photoreceptors at the outer plexiform layer (OPL) and lamina a-/b- in the IPL;^{26,62} and PKCα (light blue) for pre-synaptic elements of bipolar cells (asterisk indicate decrease in horseshoe-shaped synapse at OPL). Scale bar=50 µm. Inserts 50 µm. ONL, outer nuclear layer; INL, inner nuclear layer; GCL, ganglion cell layer; OPL, outer plexiform layer. 3-4 eyes per group were analyzed.

Supplementary material

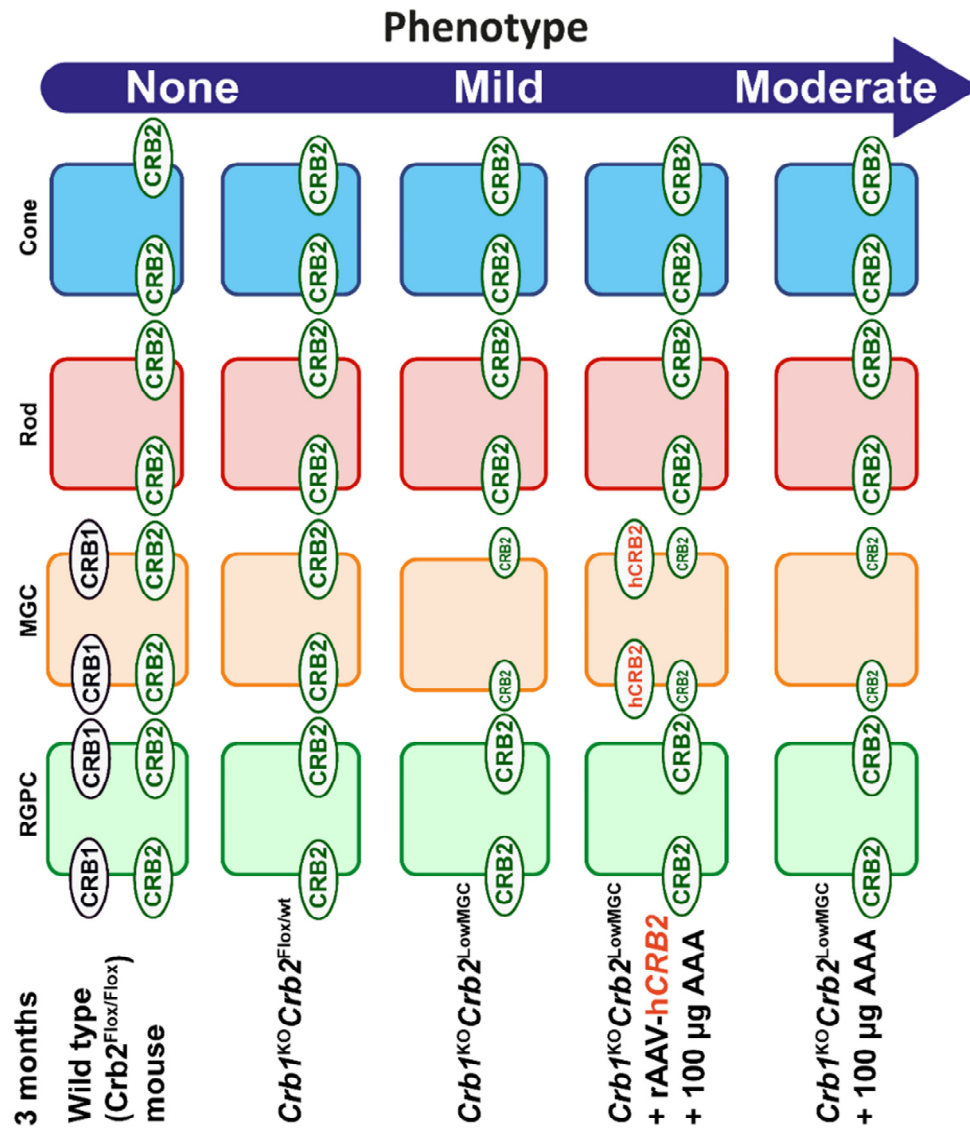


Figure S1. Graphical schematic representation of CRB localization and the severity of the phenotype in 3-month-old mice. Graphical schematic representation of CRB1 and CRB2 in radial glial progenitor cells (RGPC), Müller glial cells (MGC), rod and cone photoreceptors in wildtype (*Crb2^{Flox/Flox}*), *Crb1^{KO}Crb2^{Flox/Flox}* (Control to *Crb1^{KO}Crb2^{LowMGC}*), *Crb1^{KO}Crb2^{LowMGC}*, *Crb1^{KO}Crb2^{LowMGC}* + 100 µg DL-AAA intravitreally (i.vit) injected at 2 months (Control to rAAV-CRB2 injected mice), and *Crb1^{KO}Crb2^{LowMGC}* + rAAV-hCRB2 i.vit injected at postnatal day 21 + 100 µg DL-AAA i.vit injected at 2 months. rAAV, recombinant adeno-associated viral vector; i.vit., intravitreal. Modified from [5].

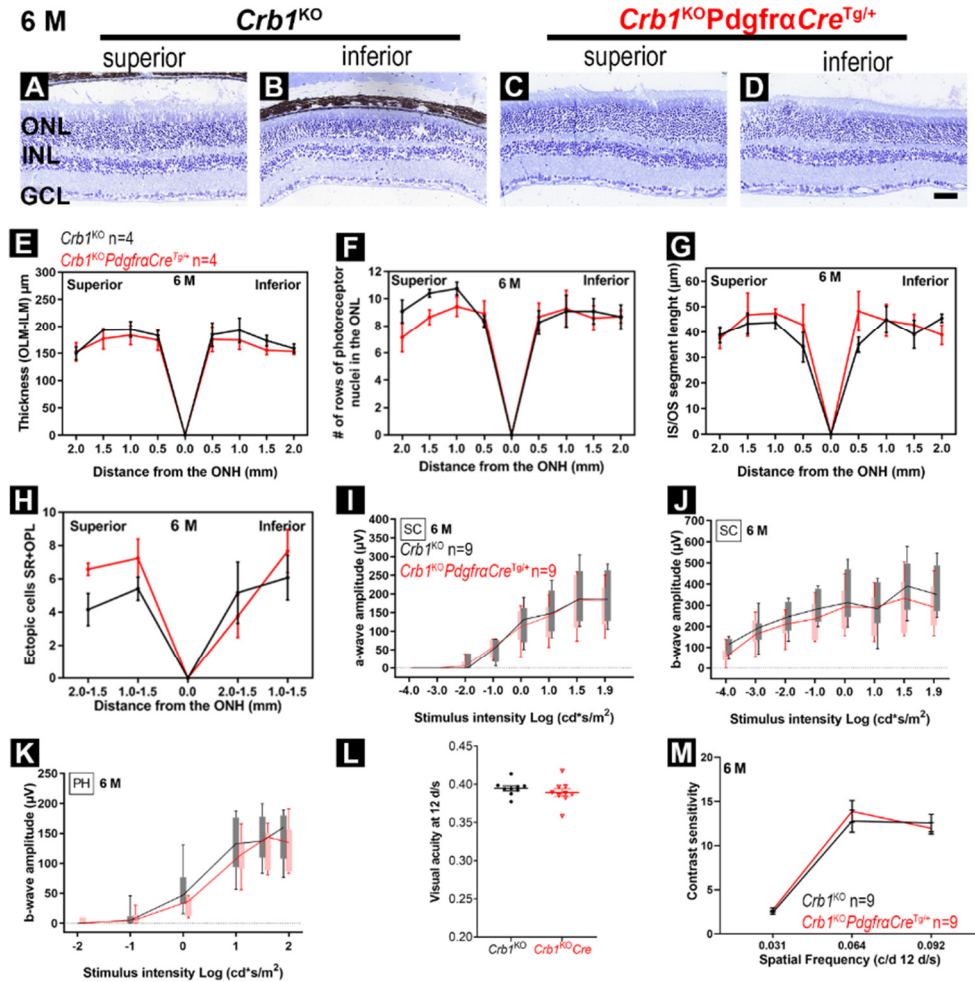


Figure S2. Cre-expression in Müller glial cells does not affect retinal morphology, ERG responses, and OKT responses. Toluidine-stained light microscopy of retinal sections from control (*Crb1*^{KO}; A-B) and *Crb1*^{-/-}*PdgfraCre*^{Tg/+} (C-D) mice at 6-month-of-age. Spidergrams for (E) Retinal thickness, (F) number of photoreceptors per row, (G) inner/outer segments of photoreceptor length, and (H) ectopic cells in the subretinal space and outer plexiform layer. Quantitative evaluation of the scotopic single-flash intensity series of the a-wave (I), b-wave (J), and photopic b-wave (K) amplitudes in 6-month-old mice. Boxes indicate the 25 and 75% quantile range, whiskers indicate the 5 and 95% quantiles, and the intersection of line and error bar indicates the median of the data (box-and-whisker plot). (L-M) Optokinetic head tracking response at 6-month-old mice. (L) Spatial frequency threshold (visual acuity). (M) Contrast sensitivity threshold at different spatial frequencies. *P<0.05; **p<0.01, ***P<0.001.

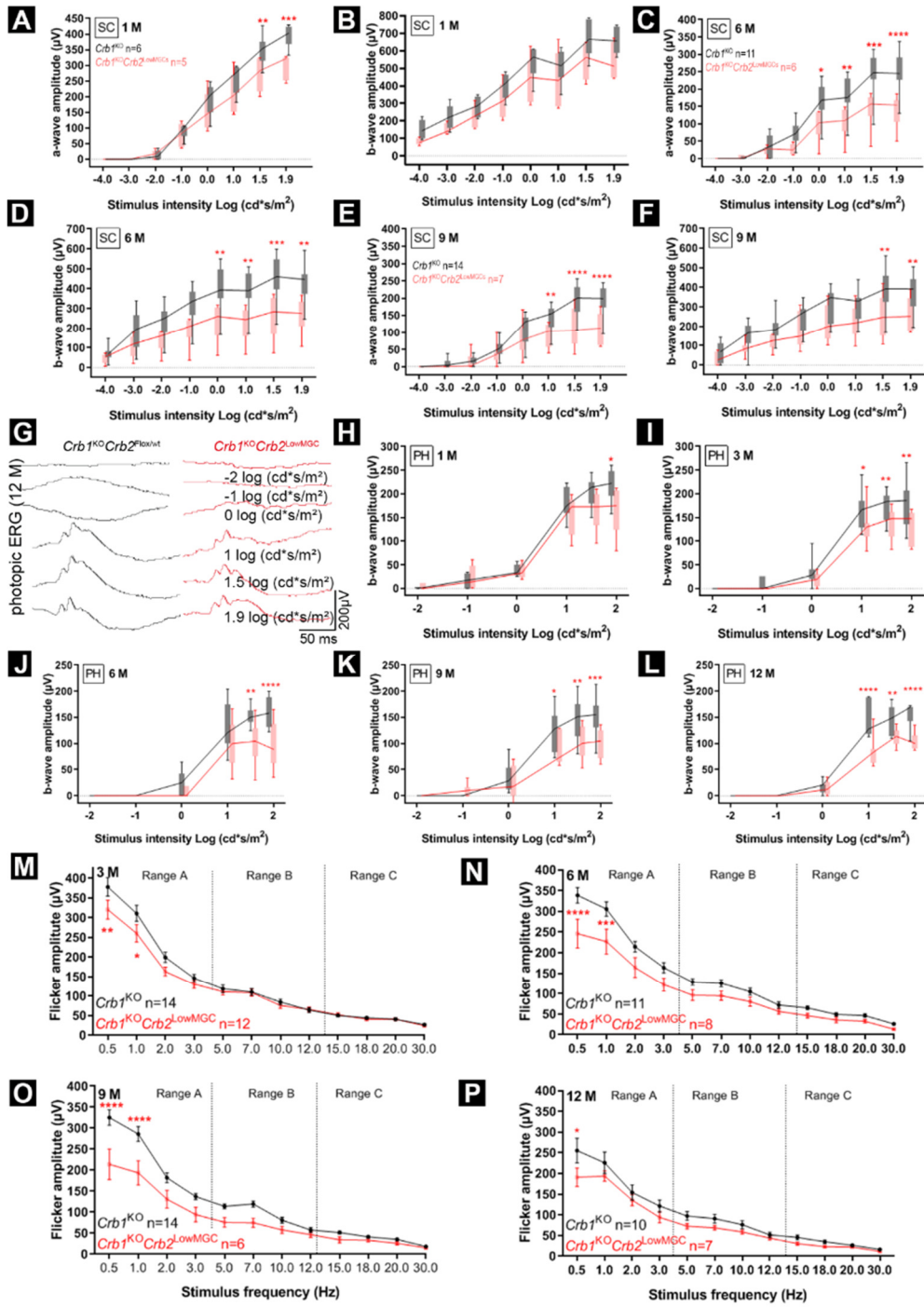


Figure S3. Decreased retinal function and vision- behavior in $Crb1^{KO}Crb2^{LowMGC}$ compared to $Crb1^{KO}Crb2^{Flox/wt}$ age-matched littermates. $Crb1^{KO}Crb2^{LowMGC}$ measurements are indicated in red (experimental) and $Crb1^{KO}Crb2^{Flox/wt}$ age-matched littermates in black (control). Electroretinographic analysis of the retinal function: (A-F) Scotopic [SC] single-flash intensity series ERG from representative animals at 1-, 6-, 9-month-old mice of age. (G-L) Photopic [PH] single-flash ERG at different light intensities (-2, -1, 0, 1, 1.5, 1.9 log cd s/m² light intensity at 30 cd/m² background light): (G) Photopic ERG traces of representative 12-month-old animals. (H-L) Photopic b-wave amplitudes at 1-, 3-, 6-, 9-, and 12-month-old mice (H-L). No statistical analysis was performed for (A-L). (M-P) Time course of flicker response amplitudes from 3-, 6-, 9-, and 12-month-old mice (Mean±SEM; M-P; *P<0.05; **p<0.01, ***P<0.001). Animal numbers (control vs. experimental): 1-month (n=6; n=6), 3-month (n=14; n=12), 6-month (n=11; n=6), 9-month (n=12; n=7), 12-month (n=7; n=8).

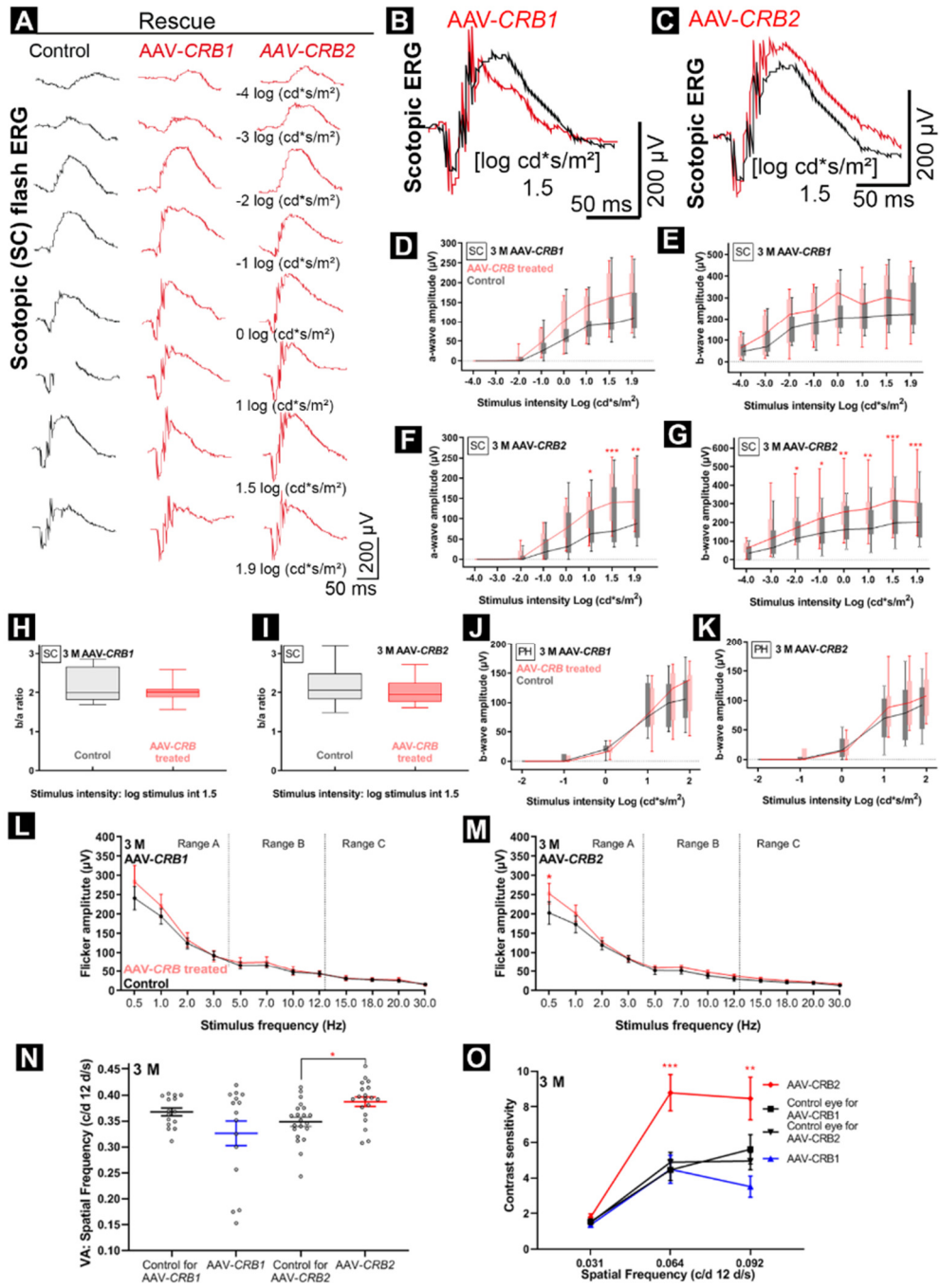


Figure S4. Retinal function (ERG) and visual-guided head tracking (OKT) in rAAV-hCRB treated *Crb1*^{KO}*Crb2*^{LowMGC} compared to control eyes. Both eyes received a 100 μ g DL-AAA treatment at 2-months. Eyes were measured at three months. The ERG traces of the rAAV treated eye (rAAV-hCRB injected at postnatal day 21) are indicated in red (experimental group) and compared to the control eye (Not treated) not receiving the AAV therapy (black trace, control group). Electroretinographic analysis of the retinal function: (A-C) Scotopic [SC] single-flash intensity series (-4, -3, -2, -1, 0, 1, 1.5, 1.9 log cd s/m² light intensity) ERG from representative animals in 3-month old mice. (B-C) Superimposed scotopic [SC] single-flash ERG traces at 1.5 log cd s/m² intensity from representative animals. (D) Scotopic a-wave of rAAV-hCRB1 injected mice vs. the control eye. (E) Scotopic b-wave of rAAV-hCRB1 injected mice vs. control eye. (F) Scotopic a-wave of rAAV-hCRB2 injected mice vs. control eye. (G) Scotopic b-wave of rAAV-hCRB2 injected mice vs. control eye. (H-I) b-wave/a-wave ratio of AAV-hCRB1 or AAV-hCRB2 at single-flash ERG traces at 1.5 log cd s/m² intensity. (J-K) Photopic b-wave amplitudes in 3-month-old mice injected with rAAV-hCRB1 or rAAV-hCRB2 vs. control eye. No statistical analysis was performed (A-K). (L-M) Flicker response amplitudes from 3-month-old mice injected with rAAV-hCRB1 or rAAV-hCRB2 vs. the control eye. Number of animals (Control vs experimental): rAAV-hCRB1 (n=16; n=14). rAAV-hCRB2 (n=18; n=16). (N-P) Optokinetic head tracking response: (N) Visual acuity (animals indicates as black circles); contrast sensitivity OKT (Number of animals: rAAV-hCRB1 n=16; rAAV-hCRB2: n=21). Mean \pm SEM; M-P; *P<0.05; **p<0.01, ***P<0.001.

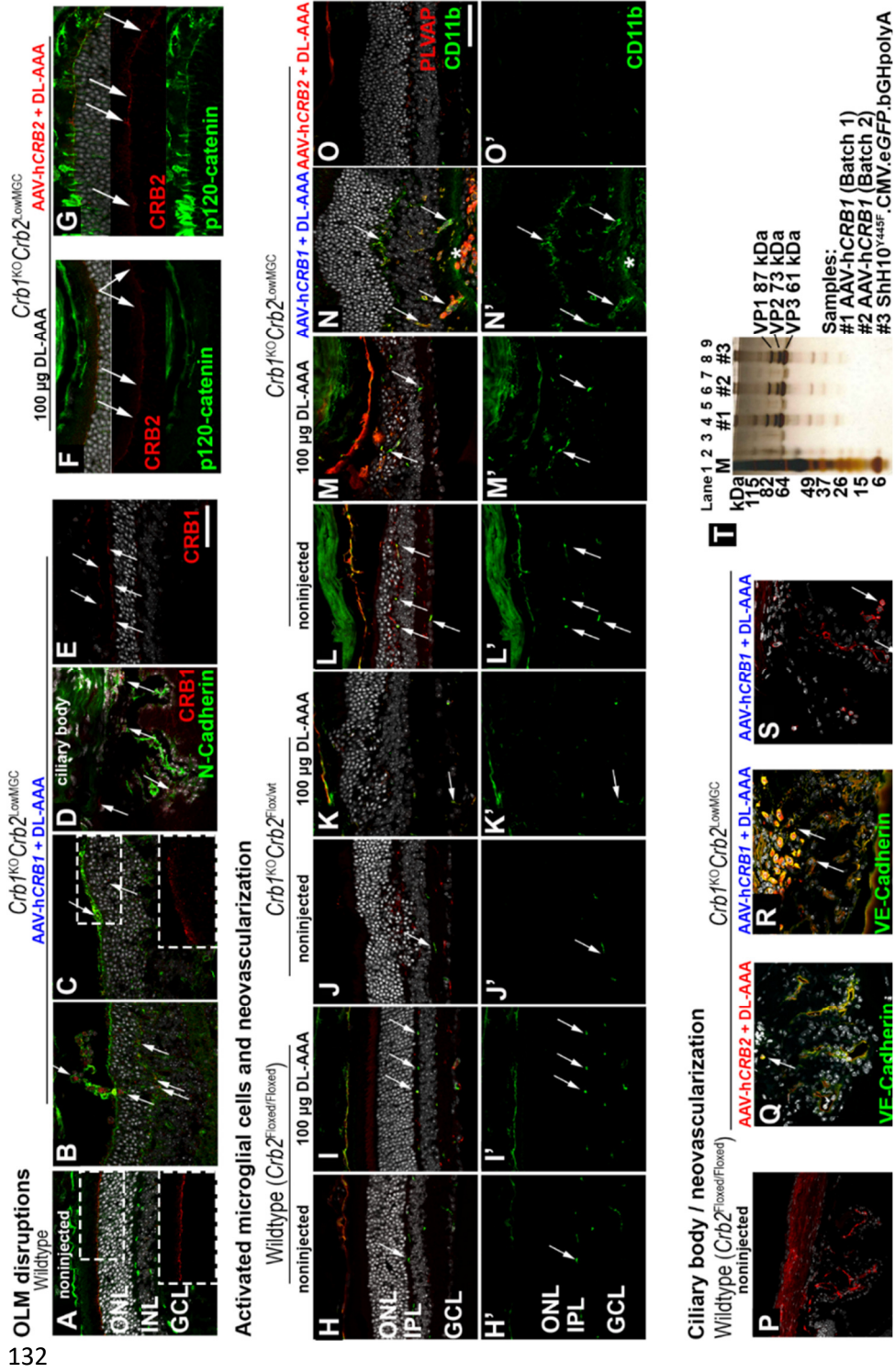


Figure S5. AAV-hCRB1 increases neovascularization in the ciliary body. Immunohistochemistry of 3-month-old mice. Sections were stained for: (A-E) CRB1 protein (red) at the subapical region and N-cadherin (green) at the adherens junction in (A) wildtype and (B-E) *Crb1*^{KO}*Crb2*^{LowMGC} mice injected with rAAV-hCRB1 and 100 µg DL-AAA (arrows indicate CRB1 protein expression). (F-G) CRB2 protein (red) at the subapical region and p120-catenin (green) at the adherens junction in (F) *Crb1*^{KO}*Crb2*^{LowMGC} mice injected with 100 µg DL-AAA and (G) *Crb1*^{KO}*Crb2*^{LowMGC} mice injected with 100 µg DL-AAA and rAAV-hCRB2 (arrows = CRB2 protein expression at OLM). (H-O) PLVAP (red) for (neo-)vascularization and CD11b (green) for microglial activation (arrows). (H'-O') Puncta-like CD11b-positive microglia cells in IPL are dormant and activated CD11b-positive microglia cells in ONL and GCL (arrows). (P-S) The ciliary body of (P) wildtype control mice or *Crb1*^{KO}*Crb2*^{LowMGC} mice injected with (Q) rAAV-hCRB2 or (R-S) rAAV-hCRB1. PLVAP (red) and VE-cadherin (green) are vascularization markers. (Neo-)vascularization indicated by arrows in Q-S. (T) 1x10¹⁰ viral genomes (vg) of two batches of rAAV2/ShH10^{Y445F}.CMVmin.hCRB1 vector preparation and one batch of 1x10¹⁰ vg of rAAV2/ShH10^{Y445F}.CMV.GFP were analysed by silver nitrate staining to detect capsid proteins VP1, VP2, VP3. Note that the silver stained SDS-PAGE gel was overstained (for marker and capsid proteins) to allow evaluation of capsid degradation products and contaminants. Lane 1, protein marker. Lanes 4 and 6, two independent samples of rAAV2/ShH10^{Y445F}.hCRB1 used in this study. Lane 8, a sample of rAAV2/ShH10^{Y445F}.GFP. Note that lanes 2, 3, 5, 7 and 9 contain overflow from adjacent sample wells. Scale bar=50 µm. Inserts 50 µm height. PLVAP, plasmalemma vesicle associated protein; ONL, outer nuclear layer; INL, inner nuclear layer; GCL, ganglion cell layer. 3-4 eyes per group were analyzed.

Chapter 3

AAV serotype testing on cultured human donor retinal explants

T.M. Buck, R. Vos, E.H.C. van Dijk, C.J.F. Boon, and J. Wijnholds

Methods Mol Biol, 2018; 1715, 275-288

Abstract

This protocol details on a screening method for infectivity and tropism of different serotypes of Adeno-associated viruses (AAVs) on human retinal explants with cell-type specific or ubiquitous green fluorescent protein (*GFP*) expression vectors. Eyes from deceased adult human donors are enucleated and the retinas are isolated. Each retina is punched into eight to ten 6-mm equal pieces. Whatman™ paper punches are placed on the retinas and the stack is transferred onto 24-well culture inserts with the photoreceptors facing the membrane. AAVs are applied on the retinal explant punches to allow transduction for 48 hours. Retinas are nourished by a serum-free Neurobasal®-A based medium composition that allows extended culturing of explants containing photoreceptor inner and outer segments. The protocols include quality control measurements and histological staining for retina cells. The cost and time effective procedure permits AAV transgene expression assays, RNAi knockdown, and pharmacological intervention on human retinas for 21 days *ex vivo*.

1 Introduction

The first recombinant adeno-associated viral (rAAV) gene rescue therapies have been administered to patients in clinical trials [1, 2]. Preliminary clinical results are promising, but these still have to be converted into medication. Though, for the AAV gene therapy product Glybera (UniQure, Amsterdam, The Netherlands), for lipoprotein lipase deficiency, European market approval has been obtained. The prediction of the cell tropism of different rAAV serotypes and variants on human retinas has been a hurdle. rAAV transduction information of mice has little predictive value for human tissue because the distribution and specificity of receptors hijacked by rAAVs to infect cells differ between species. Yet, information on rAAV serotype infection and both onset and levels of expression in human retinal cell types is limited because adult retinas rapidly lose their morphology during *ex vivo* culturing. Generally, the gene therapy vector protein expression is detectable a week after infection [3, 4] -- provided the AAV particles applied has a sufficient titer -- and peaks at around five weeks [5, 6]. Currently, a fair comparison of cell tropism and infectivity of AAV serotypes and variants with different promoter strengths and onset of expression can only be assessed in monkey studies. Here, we provide a technique to screen rAAVs on cell tropism and infectivity on human retinal explants. This technique can also be employed for neurodegeneration, neuroprotection, and cell transplantation assays.

Many variables influence the success of a retina culture. Differences of the maximum days in culture depends on the species and the age of retina. For example, cultured organotypic neonate mouse retinas last up to 27 days [7,16]. Young adulthood retinas of rats and neonate retinas of chickens have been cultured for up to 7 days [8-10]. However, adult mammalian material, such as human, mouse, and pig retinas have only been cultured for short-term (up to 10 days) [10-14]. This is because many cell, molecular, and morphological changes take place once the retina is cultured *ex vivo*. Changes include the deactivation of the shedding and regeneration of the outer segments (OS) of photoreceptors (PRCs), loss of cells with a successive retinal thinning, collapse of the outer plexiform layer (OPL), and Müller glia stress as identified by the upregulation of glial fibrillary acidic protein (GFAP) [12,13]. The health of the retina needs to be thoroughly monitored and recorded. This can be achieved at the end by immunohistochemistry (retina cells, cell apoptosis, and cell cycling, *see Table 1*), morphological description (retinal layer thickness), and comparing it to control samples at the day of dissection; but also by inspecting it for tissue shrinkage and medium usage.

Diverse techniques can be employed to reduce retinal degeneration and culture intervariability, such as to use only fresh tissue (<72 hours post-mortem), to keep the tissue until dissection in Phosphate buffered saline (PBS) or Hanks' Balanced Salt Solution (HBSS) buffers at 4 °C (<24 hours), to minimally manipulate the retina during dissection, to use serum-free medium compositions with supplements similar to *in vivo* retina environments, to change medium conditionally and frequently, to set the incubator to the optimal temperature

(34 °C-37 °C) and air composition (oxygen: ambient or reduced oxygen to 3 %), and to work clean [11–14]. The only two serum-free medium for retina cultures described are R-16 and Neurobasal®-A medium [12,14,15].

2 Materials

2.1 Solutions and media

1. Explant medium: 300 µL 50X B-27 Supplement (Invitrogen), 150 µL 100X N-2 Supplement (Invitrogen), 30 µL 50 mM Taurine, 120 µL 200 mM L-glutamine, 150 µL 100 mM sodium pyruvate, 18,45 µL 1 mM N-Acetyl-L-cysteine, 150 µL 100X antibiotic–antimycotic (10,000 units/mL penicillin, 10,000 µg/mL streptomycin, 25 µg/mL Amphotericin B) in a final volume of 15 mL Neurobasal®-A medium (Invitrogen). Aliquot into 5 mL and store at 4 °C and use up within 5 days. Warm up aliquots only once.
2. Hanks' Balanced Salt Solution (HBSS). HBSS liquid containing Ca²⁺ and Mg²⁺
3. Sterile distilled water.
4. MilliQ autoclaved water.
5. Phosphate buffered saline (PBS): 2.6 mM KH₂PO₄, 26 mM Na₂HPO₄, 145 mM NaCl, 7.0 - 7.2.
6. Dulbecco's Phosphate buffered saline with Ca²⁺ and Mg²⁺ (DPBS): 0.9 mM CaCl₂, 0.49 mM MgCl₂·6·H₂O, 2.67 mM KCl, 1.47 mM KH₂PO₄, 137.93 mM NaCl, 8.6 mM Na₂HPO₄·7·H₂O, pH 7.0 - 7.2
7. 4 % Paraformaldehyde (PFA) in PBS.
8. 5 % Sucrose in PBS.
9. 30 % Sucrose in PBS.
10. Cryo-embedding media, Tissue-Tek® O.C.T. compound.
11. 1% Sodium dodecyl sulfate (SDS).
12. Ethanol absolute 99.99 %.
13. 70 % ethanol in milliQ water (70 % EtOH): 70 mL Ethanol absolute, 30 mL milliQ water.
14. 10 % Poloxamer-188 surfactant solution, sterile.
15. 0.001 % Poloxamer-188 in DPBS. Filter-sterilized. Stored in 1 mL aliquots at -20 °C.

2.2 Materials and supplies

1. 12 mm filter diameter; 0.4 µm pore Hydrophilic Polytetrafluoroethylene (PTFE) Millicell Cell Culture Inserts (Millipore; catalogue number PICM01250).
2. Whatman™ 3MM Chr Chromatography Paper. Clean a 2-hole punch with warm water and soap, and 70 % ethanol. Punch the Whatman™ 3MM paper. Autoclave the 6-mm punches.

AAV serotype testing on cultured human donor retinal explants

- 24-well culture plates, flat bottom.
- Surgical instruments: Lancet. 11 cm Iris Scissor, curved. 18 cm Operating scissor, sharp/blunt, curved. Dressing forceps. Tissue forceps. 6 mm Surgical punch with adapter (*see Note 1*).
- P1000, P200, P20, P10 pipette tips and single-channel pipette set.
- Standard pipette gun and serological pipettes.
- 37 °C 5 % CO₂ incubator.
- Parafilm.
- Sucrose.
- Superfrost Plus microscope slides.
- 15 mL conical tubes.
- 9 cm petridish.
- 10 x 10 x 5 mm Cryomold® biopsy, square.
- Dry-ice.
- Cryostat.
- 70 mm thickness Antirroll glass.
- Carbon steel microtome blades C-35 pfm.
- 20 % Bovine Serum Albumin (BSA) dissolved in PBS.
- Triton X-100.
- (Goat) Serum.
- Blocking Buffer: to prepare 10 mL, mix 1 mL normal goat serum, 0.04 mL Triton X-100, 0.5 mL 20 % BSA, and 8.46 mL PBS.
- First Antibody Buffer: to prepare 10 mL, mix 0.03 mL (goat) serum, 0.04 mL Triton X-100, 0.5 mL 20 % BSA, 9.43 mL PBS, and first Antibody.
- Second Antibody Buffer: to prepare 10 mL, mix 0.5 mL 20 % BSA, 9.5 mL PBS, and second Antibody.
- VECTASHIELD HardSet Antifade Mounting Medium with 4',6-Diamidin-2-phenylindol (DAPI; Vector Labs).
- Protective equipment: gloves, safety goggles, lab coat, Biosafety level 2 laboratory, and laminar flow hood.

2.3 Recombinant AAV with transgene expression cassette

- Recombinant AAV particles to be tested at a titer of $>10^{12}$ genomic copies, e.g. rAAV2.CMV.*EGFP*.WPRE.pA packaged into serotype AAV9 capsids. The expression vector contains e.g. the two inverted terminal repeats (ITRs) of AAV2, the ubiquitous immediate early CMV promoter (CMV), the cDNA for *EGFP*, the woodchuck hepatitis virus post-transcriptional regulatory element (WPRE), and a SV40 polyadenylation sequence (pA).

2. The virus was produced as previously reported [3]. In short, HEK293T cells were triple transfected by Ca-phosphate transfection method with the helper plasmid pAAV9 from the Vector Core University of Pennsylvania, the helper plasmid pAd Δ F6 [17], and a pAAV2.CMV.*EGFP*.WPRE.pA transfer plasmid. The cells were lysed and harvest 72 hours post-transfection. AAVs were purified by an iodixanol gradient and concentrated by amplicon-spin columns. AAVs were tested on purity by SDS-PAGE Silver Staining and the genomic copies per mL (titer) were measured against a standard by qPCR.

3 Methods

3.1 Culturing of post-mortem human retina

The tissue was collected in agreement with the guidelines of the ethics committee of the LUMC. Patient anonymity was strictly maintained. All tissue samples were handled in a coded fashion, according to Dutch national ethical guidelines (Code for Proper Secondary Use of Human Tissue, Dutch Federation of Medical Scientific Societies).

3.1.1 Dissecting out the eye

1. Within 24 hours after the death of a human donor, removal of the entire globe of the eye and its contents, with preservation of all other periorbital and orbital structures was performed.
2. The optic nerve was cut at 1 cm distance from the eye globe.
3. Eyes were transported and stored in HBSS at 4°C.
4. A suture was put through an eye muscle to differentiate right and left eyes (*see Note 2*).
5. The eye was stored in cold HBSS in the fridge (*see Note 3*).

3.1.2 Prepare medium and 24-well culture plate (>1 hour before dissection)

1. Prepare fresh medium and warm it up in a water bath (*see Note 4*).
2. Add 15 mL milliQ autoclaved water between 24 wells. Place in incubator (*see Note 5*).
3. Add 300 μ L medium to the 8 wells in the middle of the plate. Leave the outside wells empty.
4. Add the inserts.
5. Gently shake the plate until all the inserts are wet.
6. Place it back in the incubator for at least 30 min before adding the retina pieces (*see Note 6*).

3.1.2 Dissecting out a retina from a post-mortem human eye

1. Place the eye for 30 seconds in 70 % EtOH in a 50 mL tube or 6 cm dish to prevent infections.
2. Rinse off the EtOH with cold HBSS.
3. Place the eye in a 6 cm dish in cold HBSS (*see Note 7*).
4. Remove the extraocular tissue (such as muscles, epithelia layers, visible blood vessels) with the operating scissor and the tissue forceps until you only see the white sclera.
5. Fix the eye against the side of the dish with the help of a forceps (*see Note 8*).
6. Use the lancet or a surgical blade and slowly make a small cut around 0.5 cm below the lens slightly below the ciliary body (where you can see a colour difference (*see Note 9* and **Figure 1.a**)).
7. Subsequently cut around the eye with the Iris Scissor (*see Note 10* and **Figure 1.b**).
8. Cut the optic nerve preferably from the inside of the eye (between retinal pigment epithelium (RPE) and retina). If the retina is still attached then you can also cut the optic nerve from the outside (*see Note 11* and **Figure 1.c+d**).
9. Remove the lens with the vitreous attached.
10. Make three cuts spaced evenly from the edge to the optic nerve.
11. Carefully flatten the eye by pushing in the sides so they flip upwards. Now, the retina detaches slowly from the RPE (*see Figure 1.c+e*).
12. Remove the sclera with the RPE attached to another dish. The retina with the ganglion cell layer (GCL) facing up should float in clean cold HBSS solution (*see Note 12* and **Figure 1.e**).
13. Locate the fovea (yellowish dot, avascular zone, ~1.5 mm diameter, ~5 mm from the optic disc). Make punches starting from the fovea going outwards. You should be able to make 8-14 punches (*see Figure 1.g+h*).
14. Place the Whatman™ paper punches on each retina (*see Note 13* and **Figure 1.g+h**).
15. Take out the previously prepared 24 well plate with inserts and medium from the incubator.
16. Carefully place the retina pieces on the inserts (Whatman™ paper facing upwards, PRCs downwards) and put it back in the incubator (*see Note 14*).
17. Take retina pieces for control and process them: Fixate (cold 4 % PFA, 30 min), cryo-protect (cold 5 % sucrose in PBS, 30 min; then cold 30 % sucrose in PBS, 30 min) and freeze in O.C.T Tissue Tek on Dry-Ice (*see Note 15*).

3.1.3 Culturing retina punches

1. Conditionally change medium daily. Remove 150 µL and replace it with fresh 150 µL pre-warmed CO₂ equilibrated medium.
2. End the culture at desired endpoint (7-21 days) as described under **3.1.2.17**.

3.2 AAV infection of post-mortem donor retinas

3.2.1 Preparation of the virus (1 hour before infection)

1. Warm up 50 μ L medium per punch to be infected.
2. Centrifuge the concentrated virus suspension shortly and store on ice.
3. Prime the pipette tips in 0.001 % poloxamer-188 in PBS solution (*see Note 16*).
4. Prepare the 50 μ L infection mix: Add 3.4×10^{11} genome copies of AAV2/9.CMV.GFP to a final volume of 50 μ L pre-warmed medium (*see Note 17*).

3.2.2 AAV infection of post-mortem donor retinas (3 h after dissection)

1. Remove 150 μ L of each 24 well.
2. Pipette the 50 μ L infection mix on top of the WhatmanTM paper in the inserts.
3. Incubate the retina with the AAVs for 48 hours.
4. Remove medium and add 300 μ L fresh pre-warmed equilibrated medium
5. Conditionally change the medium every day as described at **3.1.3.1**, and end the culture at the desired endpoint as described at **3.1.2.17**.

3.3 Workflow: Tissue processing of post-mortem donor retinas

1. Prepare a fresh 24-well plate. Add 300 μ L of PFA, PBS, 5 % sucrose, and 30 % of sucrose to the wells (horizontally).
2. Lift off the retinas with the WhatmanTM paper attached from the insert (*see Note 18*).
3. Wash/dip the insert in the PBS well.
4. Move it to the 4 % PFA in PBS well for 30 min (continue as described in **3.1.2.17** and in **Figure 2**; *see Note 19*). Then quickly wash it in PBS.
5. Set the cryostat to -18/20 °C. Temperate the blade, antiroll glass (70 mm), the sample(s) at least for 1 hour before cutting in the cutting chamber to -18/20 °C. And set the cutting thickness to 8 μ m.
6. In the meantime, label 1-15 Superfrost slides per 2 samples. (Initials, date, experiment, slide number).
7. Freeze the sample on a freezing block on the thin edge as depicted (*see Figure 2*)
8. Orientate the block horizontally (*see Figure 2*).
9. Cut as described e.g. in Fischer et al. [18]. In short: cut one section and move in on slide #1. Cut one section and move it on slide #2. (*see Figure 2*).
10. Dry sections between 1 to 18 hours before storing them at -20 °C or -80 °C (*see Note 20*).
11. Staining guideline: air dry glasses for 1 hour.
12. Wash 1x in PBS.
13. Incubate in a blocking buffer with a serum of the second antibody (but not raised against it) for 30-60 min. Dip off medium. Incubate with 150-200 μ L / slide of first

AAV serotype testing on cultured human donor retinal explants

antibody buffer with the appropriate first antibody dilution (*see Table 1*). Incubate in a humid chamber at 4°C overnight. Wash 3x for 15 min in PBS. Add 200-300 µL of the second Antibody buffer with the appropriate second antibody dilution for 40-60 min (*see Note 21*). Wash 3x for 15 min in PBS. Dip off excess PBS and mount with 1 drop (30 µL) of VECTASHIELD HardSet Antifade Mounting Medium with DAPI. Harden at room temperature for 3 hours or at 4 °C for >48 hours (storage condition).

14. Image on a confocal (or fluorescent) microscope at >20x magnification (*see Figure 3 and Note 22*).

Notes

1. Clean surgical tools with warm water, soap and then 70 % EtOH.
2. Eye should be enucleated within 24 hours after death, to obtain the best results.
3. Retina should be dissected out within 36 hours after dissection.
4. You can also warm up the medium by placing it in the incubator with unscrewed cap. This allows activation of the sodium bicarbonate buffer in a 5 % CO₂ environment.
5. This ensures that the plate is an evenly humid chamber for all retinas.
6. If the dissection is in another room with incubator than your standard culture room then take the prepared 24-well plate wrapped in parafilm to the dissection room and place it there in the incubator. Don't move a dissected retina in a 6 cm plate. It will shear off all the OS of the retinas.
7. HBSS medium provides the glucose to cells while keeping the pH in check under atmospheric conditions.
8. A second person can support the fixation with an additional forceps.
9. Cutting below the ciliary body helps to remove the vitreous body and the RPE from the retina.
10. Make large cuts to minimize the physical shearing on the retina during dissection.
11. The older the material and human donor, the stickier the retina. Cold HBSS (without Magnesium, Calcium) can help detaching the retina from the RPE.
12. You can conditionally replace the medium to keep the temperature low.
13. The punches should easily attach to each piece. Autoclaving the punches can cause punches to stick to each other. Use forceps to take only one punch at a time.
14. Try to minimize pressure and area touched with the forceps. Work quick (<5 min) so the medium stays warm and the pH of the medium stays intact (*see Figure 1*).
15. See Figure 1 for detailed tissue processing steps.
16. This helps to prevent AAV attachment to the plastic tip.
17. Different AAVs are differently effective in infecting retinal cells. Other AAVs can infect as low as 10⁷ genome copies per infection mix. Limit the amount added to the medium to 15 µL added not to diluting the medium to much.

18. The retinas never attached to the inserts so cutting out the inserts is not necessary. When handling retinas, minimize the contact (touch only sides). You can also select Whatman™ punches where not the complete retina is attached to so you can manipulate on areas where no retina is attached to it.
19. After the cryopreserving step in 30 % sucrose and the tissue dropped to the bottom, then you can store it for a few days in the fridge. We always continued immediately by freezing it. At this step you can also peel off the Whatman™ paper. Yet, we did not find a difference in staining if it was carefully peeled off or not. We decided not to peel it off anymore to have less artefacts introduced by the peeling off.
20. It is a good practice to stain one section directly after cutting with 1 % toluidine blue in milliQ water or anti-fade mounting medium with DAPI to quickly assess the tissue morphology under a light or fluorescent microscope.
21. If not enough liquid is on the slide then you can place parafilm or a cover slide on top of it. It helps to get even distribution of the second antibody on the slide.
22. Compare the OS of PRCs after dissection and at the time of harvest with e.g. PNA and Rhodopsin staining (*see Figure 3*). We observed that OS seem to be relevant in the AAV infection pathway to photoreceptors (unpublished).

4 REFERENCES

1. Kumar SR, Markusic DM, Biswas M, et al. (2016) Clinical development of gene therapy: results and lessons from recent successes. *Mol Ther Methods Clin Dev* 3:16034.
2. Carvalho LS, Vandenbergh LH (2015) Promising and delivering gene therapies for vision loss. *Vision Research*. 111:124–133.
3. Pellissier LP, Hoek RM, Vos RM et al (2014) Specific tools for targeting and expression in Müller glial cells. *Mol Ther Methods Clin Dev* 1:14009.
4. Van Wyk M, Hulliger EC, Girod L et al (2017) Present Molecular Limitations of ON-Bipolar Cell Targeted Gene Therapy. *Frontiers Neurosci* 11: (in press)
5. Wu Z, Asokan A, Samulski RJ (2006) Adeno-associated virus serotypes: vector toolkit for human gene therapy. *Mol Ther*. 14:316–327.
6. Thomas CE, Storm TA, Huang Z et al (2004) Rapid uncoating of vector genomes is the key to efficient liver transduction with pseudotyped adeno-associated virus vectors. *Journal of Virology*. 78:3110–3122.
7. van Rossum AG, Aartsen WM, Meuleman J et al (2006) Pals1/Mpp5 is required for correct localization of Crb1 at the subapical region in polarized Müller glia cells, *Hum Mol Genet* 15:2659–2672.
8. Barr-Nea L, Barishak RY (1970) Tissue culture studies of the embryonal chicken retina. *Invest Ophthalmol* 9:447–457.
9. Aartsen WM, Arsanto JP, Chauvin JP et al (2009) PSD95 β regulates plasma membrane Ca(2+) pump localization at the photoreceptor synapse *Mol and Cell Neurosci* 41:156–165.
10. Johnson TV, Bull ND, Martin KR (2011) Organotypic explant culture of adult rat retina for in vitro investigations of neurodegeneration, neuroprotection and cell transplantation. *Protocol Exchange* 1–28. doi:10.1038/protex.2011.215
11. Fernandez-Bueno I, Fernandez-Sanchez L, Gayoso MJ et al (2012) Time course modifications in organotypic culture of human neuroretina. *Exp Eye Res* 104:26–38.
12. Johnson TV, Martin KR (2008) Development and characterization of an adult retinal explant organotypic tissue culture system as an in vitro intraocular stem cell transplantation model *Invest Ophthalmol Vis Sci* 49:3503–3512.
13. Bull ND, Johnson TV, Welsapar G et al (2011) Use of an adult rat retinal explant model for screening of potential retinal ganglion cell neuroprotective therapies, *Invest Ophthalmol Vis Sci* 52:3309–3320.
14. Wang J, Kolomeyer AM, Zarbin M et al (2011) Organotypic culture of full-thickness adult porcine retina. *J Vis Exp* 49:2655. doi:10.3791/2655.
15. Romijn HJ (1988) Development and advantages of serum-free, chemically defined nutrient media for culturing of nerve tissue. *Biol Cell*. 63:263–268.

16. Caffé AR, Ahuja P, Holmqvist B et al (2001) Mouse retina explants after long-term culture in serum free medium, *J Chem Neuroanat.* 22:263–273.
17. Gao G.-P, Alvira MR, Wang L et al (2002) Novel adeno-associated viruses from rhesus monkeys as vectors for human gene therapy. *Proc Nat Acad Sci USA* 99:11854–11859.
18. Fischer AH, Jacobson KA, Rose J et al (2008) Cryosectioning tissues. *Cold Spring Harbor Protocols* 3:8–10.

Acknowledgement

This work was supported by the Foundation Fighting Blindness USA project TA-GT-0715-0665-LUMC and ZonMw project 43200004. The funding organizations had no role in the design or conduct of this research. This study was presented in part at The Association for Research in Vision and Ophthalmology (ARVO) Meeting, Baltimore, MD, USA, May 2017. We wish to thank PM Quinn for his technical support, his help in designing the experiment and our fruitful discussions on how to improve the culture system.

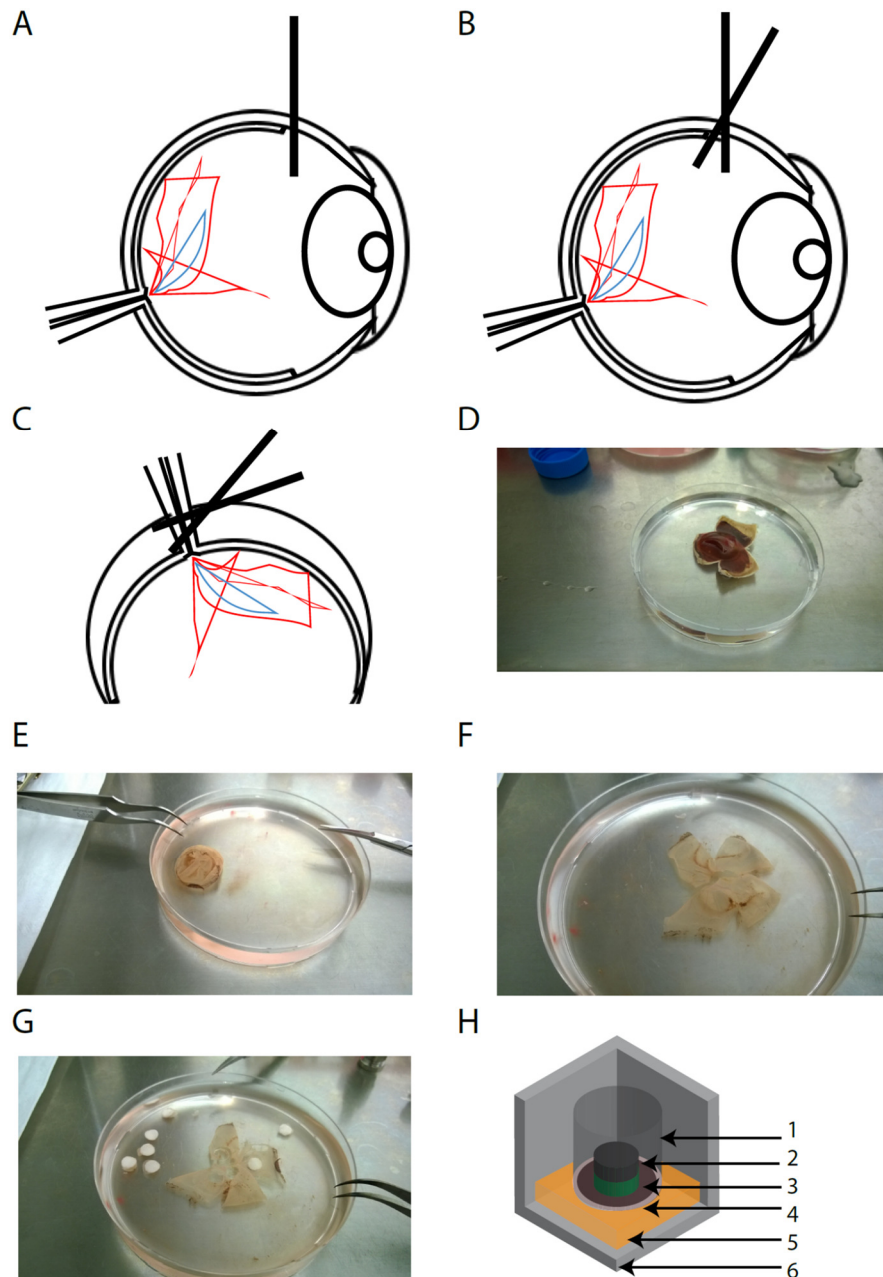


Figure 1. Dissecting out a human retina and placement of the retina on the insert. A) Stance at the border of the retina and the ciliary body. You can see color change from black to white. 2) Make long cuts with a scissor. 3) Cut off the optic nerve to free the retina. 4) Eye with the retina removed. You can see the retinal pigmented epithelium in black. 5) The retina without retinal pigmented epithelium. F) Flattened out retina. G) Punches made from the Ganglion cell layer side and Whatman paper placed on the top. H) Culture system. AAVs are applied on the Whatman™ paper from the top and the PRCs face on the membrane.

AAV serotype testing on cultured human donor retinal explants

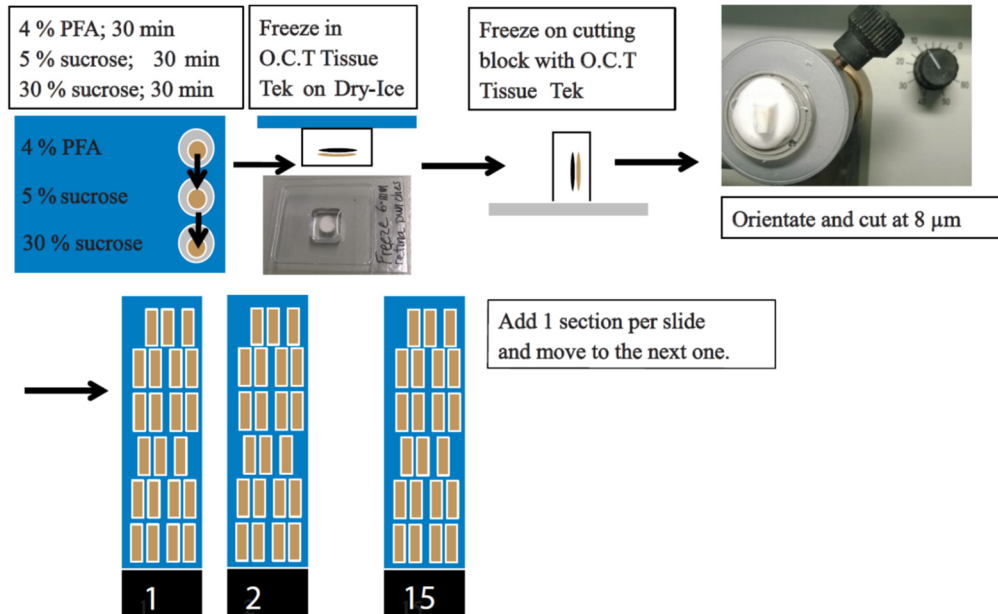


Figure 2. Workflow for tissue processing. A) Fixing process and cryopreservation. B) Freeze in a cryomold for better orientation. C) Flip the block and then freeze it on the cutting block (see image) to get all retina layers on one section. D) Add one section per slide and then move to the next slide. You can add two samples per slide to have an internal control for immunohistochemistry staining.

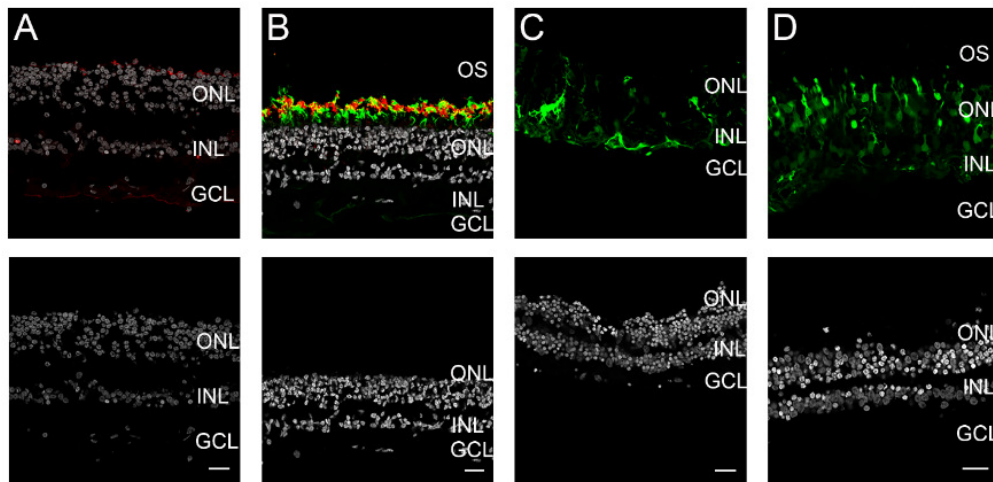


Figure 3. Expected results. A) Poor dissection or tissue without outer segments present (stained with PNA in red). B) Good dissection and tissue with outer segments present (stained with Rhodopsin in red and PNA in green). C) Retinal explant infected by AAV2/9.CMV.EGFP, 21 days after infection (GFP in green). D) Retinal explant infected with AAV2/9.CMV.EGFP, 14 days after infection (GFP in green). Retinal layers: Outer Nuclear Layer (ONL), Inner Nuclear Layer (INL), Ganglion Cell Layer (GCL). Nuclear staining (DAPI) in gray. Scale bar: 25 μ m.

Table 1. List of antibodies for immunohistochemistry.

Antibody	anti-	dilution	Company	Staining property
Calbindin	rabbit	1/250	AnaSpec	Strongly horizontal cells/INL-OPL; lower amacrine/INL
Calretinin	rabbit	1/500	Chemicon	Amacrine/INL; displaced amacrine and ganglion cells/GCL
CRB1	rabbit	1/250	Home made	Subapical region
Cone arrestin	rabbit	1/500	Millipore BD	Cone photoreceptors
PKC α	mouse	1/250	Biosciences	Rod bipolar cells Stressed Müller glial cells and gliosis
GFAP	rabbit	1/200	DAKO BD	
Glutamine Synthetase	mouse	1/200	Biosciences	Müller glial cells Müller glial cells and cell cycle
p27 ^{kip1}	rabbit	1/150	Millipore	inhibitor protein Müller glial nuclei/INL; astrocyte nuclei/GCL; RPE nuclei
SOX9	rabbit	1/250	Millipore	
Recoverin	rabbit	1/500	Chemicon	Rod and cone somas and segments Outer segment and weakly soma of rods
Rhodopsin	mouse	1/250	Millipore	Activated microglia or macrophage/monocyte lineage cells
CD45	mouse	1/250	Emelca Bioscience	
Rhodamine PNA	N/A	1/200	Vector	Outer segments. Added with second Antibody Buffer.
Caspase 3 (cleaved)	rabbit	1/250	Cell Signaling	Cell apoptosis
Phospho- Histone H3	rabbit	1/100	Millipore	Mitosis Marker

Chapter 4

Human iPSC-Derived Retinas Recapitulate the Fetal CRB1 CRB2 Complex Formation and Demonstrate that Photoreceptors and Müller Glia Are Targets of AAV5

P.M. Quinn*, **T.M. Buck***, A.A. Mulder, C. Ohonin, C.H. Alves, R.M. Vos, M. Bialecka, T.v Herwaarden, E.H.C.v. Dijk, M. Talib, C. Freund, H.M.M. Mikkers, R.C. Hoeben, M.J. Goumans, C.J.F. Boon, A.J. Koster, S.M. Chuva de Sousa Lopes, C.R. Jost, and J. Wijnholds

***These authors contributed equally to this work (co-first authors)**

Stem Cell Reports, 2019,12(5),906-919

Abstract

Human retinal organoids from induced pluripotent stem cells (hiPSCs) can be used to confirm the localisation of proteins in retinal cell types and to test transduction and expression patterns of gene therapy vectors. Here, we compared the onset of CRB protein expression in human fetal retina to human iPSC-derived retinal organoids. We show that CRB2 protein precedes the expression of CRB1 in the developing human retina. Our data suggest the presence of CRB1 and CRB2 in human photoreceptors and Müller glial cells. Thus the fetal CRB complex formation is replicated in hiPSC-derived retina. *CRB1* patient iPSC retinal organoids showed disruptions at the outer limiting membrane as found in *Crb1* mutant mice. Furthermore, AAV serotype 5 (AAV5) is potent in infecting human Müller glial cells and photoreceptors in hiPSC-derived retinas and retinal explants. Our data suggest that human photoreceptors can be efficiently transduced by AAVs in the presence of photoreceptor segments.

INTRODUCTION

Mutations in the Crumbs homolog-1 (*CRBI*) gene are linked to an array of retinal dystrophies that exhibit high phenotypic variability and affect approximately 80,000 patients worldwide with an estimated prevalence in the US of 1/86,500 [1–3]. A meta-analysis has found that mutations in the *CRBI* gene account for 2.7% and 10.1% of autosomal recessive retinitis pigmentosa (RP) and Leber congenital amaurosis (LCA) cases, respectively [4]. LCA is an early onset disease with newborns being blind around birth. However, we are yet to understand the localisation of the CRB complex in early human fetal retinal development. No treatment is currently available for *CRBI*-associated retinal dystrophy in patients, but *proof-of-concept* gene supplementation studies have shown both morphological and functional rescue in *CRBI* retinitis pigmentosa mouse models [5]. A retrospective cohort study of patients with *CRBI*-associated retinitis pigmentosa has shown that gene therapeutic intervention is most likely required within the first three decades of life, but clinical endpoint criteria for a clinical trial need to be established from natural history studies [2]. Preclinical considerations to be evaluated include the choice of adeno-associated virus (AAV) serotype for delivery of the clinical vector, in terms of potency, tropism, safety and biodistribution.

Some retinal gene therapies are using a serotype of AAV as delivery vector in clinical trials [6–8] because they restrict vector tropism to specific retinal sub-populations, improve the efficiency of gene delivery, have low immunogenicity and long transgene expression. Cross-species differences in vector tissue tropism between mice and non-human primates have been previously highlighted and must be sufficiently addressed before moving towards clinical trials [9,10]. We previously showed proof of concept for *CRBI* gene therapy in *Crb1*-retinitis pigmentosa-like mice by subretinal application of an AAV9-CMV-*CRB2* gene therapy vector, thereby demonstrating the need of transgene expression in both photoreceptors and Müller glial cells [5]. Upon subretinal application, AAV9 and the AAV6 variant serotype ShH10Y445F are able to efficiently infect in mouse photoreceptors, Müller glial cells and retinal pigment epithelium, whereas AAV5 does not efficiently infect and express in mouse Müller glial cells [11,12]. AAV tropism differs between species, therefore the AAV serotype for clinical *CRBI*-gene therapy in both photoreceptors and Müller glial cells needs to be validated. AAV5 and AAV9 infect non-human primate rod and cone photoreceptors [13,14]. Human induced pluripotent stem cell (hiPSC)-derived retinal organoids, although *in vitro*, are a promising alternative or additional/pre-screening tool to animal models for evaluating transgene expression and biological activity [15]. As previously demonstrated by others and ourselves hiPSC-derived retinal organoids and photoreceptors are amenable for the testing of AAV serotype/promoter combinations [15–17]. However, for this purpose the hiPSC-derived retinal organoids should suitably recapitulate the human retina and the onset of expression of its proteins.

The core Crumbs complex in mammals is comprised of CRB1-3, PALS1 (also called MPP5), MUPP1 and PATJ. The prototypic CRB protein has a large extracellular domain with EGF-like domains and laminin-A globular domains adjacent to a single transmembrane domain. A short C-terminus of 37 amino acids contains a FERM protein-binding domain juxtaposing the single transmembrane domain. At the C-terminal end, there is a PDZ protein-binding motif of 4 amino acids (ERLI) that allow interaction with adaptor proteins such as PALS1 and PAR6 [18–21]. In non-human primates, CRB1 and CRB2 proteins localize to the subapical region adjacent to adherens junctions in Müller glial cells and photoreceptors [22]. Similarly, in two-days-old human adult cadaveric retina, both CRB1 and CRB2 are located at the subapical region in Müller glial cells. However, in photoreceptors, the CRB1 protein is detectable at the subapical region near to the outer limiting membrane, but CRB2 is not. Additionally, both CRB1 and CRB2 are detected at vesicles in the photoreceptor inner segments at a distance from the outer limiting membrane [5,23]. Thus far, the localisation of the CRB complex in early human fetal retinal development is unknown.

In this study, we show the recapitulation of the CRB complex between the human fetal retina and cultured hiPSC-derived retinal organoids. These studies highlight that CRB2, but not CRB1, is present at the subapical region in human fetal retina during the 1st trimester of pregnancy. CRB1 is expressed only at later time points from the 2nd trimester onwards concurring with the birth of differentiated cell types such as photoreceptors and Müller glial cells. These data suggest role(s) for CRB2 but not CRB1 in the 1st trimester in the earliest human retinal radial glial progenitor cells. The data also suggest that *CRB1* patient iPSC-derived retinal organoids develop a retinal phenotype as found in *Crb1^{KO}* and *Crb1^{KO/C249W}* mice [24–26].

Additionally, we show higher efficacy of AAV5 and ShH10Y445F over AAV9 serotypes for infection of photoreceptors in cultured human donor retinal explants. We also show the preference of AAV5 and ShH10Y445F over AAV9 to infect Müller glial cells in hiPSC-derived retinal organoids. Overall, our results suggest that the AAV5 serotype combined with CMV-promoter mediated expression is suitable for gene therapy of *CRB* genes into human Müller glial cells and rod and cone photoreceptors.

RESULTS

Retinal architecture in the human fetal retina and iPSC retinal organoids

The human fetal retina, as it transitions from the 1st to the 2nd trimester of pregnancy, gives rise to all adult retinal cell types as the retina moves from a mitotic to post-mitotic state [27]. We examined 1st (week 11-13) and 2nd Trimester (weeks 16-18) fetal retina and compared these with early (differentiation day 30 (DD30)) and late (DD120 -DD240) healthy hiPSC retinal organoids. The retinal architecture in the human fetal retina recapitulated the retinal architecture as found in hiPSC retinal organoids (Figures S1 and S2).

The CRB complex in the human fetal retina and iPSC retinal organoids

We undertook immunohistochemistry studies to delineate the onset of expression of CRB1 and CRB2 in 1st and 2nd trimester human fetal retina and in early and late stage differentiated retinal organoids. In week 9 human fetal retina we did not detect the typical puncta-like CRB1⁺ immunostaining at the subapical region adjacent to the adherence junction marker β -catenin (Figures S3A-C). However, at week 11 we observed a gradient of CRB1 immunostaining located at the outer limiting membrane (OLM) (Figure 1A). In week 9 and 11 the human fetal retina stained positive for CRB2 at the subapical region adjacent to the adherence junctions as marked by anti-p120-catenin (Figures 1B, S3D-F). Furthermore, in the 1st trimester fetal retina at week 9 (Figures S3G-I), we found PATJ at the OLM and additionally in a subset of anti-Ki67⁺ cells; this was also seen in the developing mouse retina [28]. In week 19 the human fetal retina expressed CRB1 (Figure 1E) and CRB2 (Figure 1F) with their prototypic puncta immunostaining pattern. Immunostaining for CRB complex members PALS1, MUPP1, PAR3 and the adherens junction markers β -catenin, p120-catenin and N-cadherin were detected in both 1st and 2nd trimester human fetal retina (Figure 1).

Similarly, In DD28 and DD80 retinal organoids we did not detect typical CRB1⁺ puncta-like immunostaining (Figures 1I and S3J). Its family member CRB2 was present at DD28 and DD80 (Figures 1J and S3K). PALS1 and MUPP1 were present at the subapical region in DD28 hiPSC-derived retinal organoids (Figures S3L and S3M). Moreover, in retinal organoids at DD30 (Figures S3N-P) we found PATJ at the OLM and additionally in a subset of anti-Ki67⁺ cells. However, a typical and clear puncta-like staining pattern for CRB1 was detected at DD160 subapical of adherens junctions marker β -catenin (Figure 1K). CRB complex members CRB2, PALS1, MUPP1 and PAR3 and adherens junction markers p120-catenin and N-cadherin were also detected in DD160 retinal organoids (Figures 1L-O). CRB1 and CRB2 localisation in retinal organoids was also confirmed in two other hiPSC lines: LUMC0080iCTRL12 (Figures S3Q, S3R, S3S), LUMC0044iCTRL44 (Figures 5E-H, 6E-H).

Ultra-localisation of CRB1 and CRB2 in the human fetal retina and in iPSC retinal organoids

We performed immuno-EM studies to analyse at ultra-high resolution the localisation of CRB1 and CRB2 in PRCs and MGCs in 1st and 2nd trimester human fetal retina and in retinal organoids. Immuno-EM for CRB1 in the 1st trimester fetal retina showed occasional and limited staining at putative inner segments (Figure 2A) and apical villi (Figure 2B) of radial glial progenitor cells. However, in the 2nd trimester CRB1 labelling could be clearly detected at the subapical region adjacent to adherens junctions between putative photoreceptor inner segments (Figure 2C) and in the apical villi of radial glial progenitor cells/ MGCs (Figure 2D). Immuno-EM for CRB2 showed pronounced labelling in 1st (Figures 3E and 3F) and 2nd trimester (Figures 2G and 2H) fetal retina. CRB2 labelling localised at the plasma membrane and at the subapical region adjacent to adherens junctions between putative photoreceptor

inner segments (Figures 2E and 2G) and in the apical villi of radial glial progenitor cells/ MGCs (Figures 2F and 2H).

Similarly to 1st trimester human fetal retina, immuno-EM performed on retinal organoids showed sporadic and limited CRB1 labelling at the subapical region adjacent to adherens junctions between putative photoreceptor inner segments (Figure 3A) and in the apical villi of radial glial progenitor cells/ MGCs (Figure 3B) in early retinal organoids. However, in late retinal organoids CRB1 labelling localised at the plasma membrane and at the subapical region adjacent to adherens junctions between putative photoreceptor inner segments (Figure 3C) and in the apical villi of radial glial progenitor cells/ MGCs (Figure 3D). Immuno-EM for CRB2 showed pronounced labelling in early (Figures 3E and 3F) and late (Figures 3G and 3H) retinal organoids. CRB2 labelling localised at the plasma membrane and at the subapical region adjacent to adherens junctions between putative photoreceptor inner segments (Figures 3E and 3G) and in the apical villi of radial glial progenitor cells/ MGCs (Figures 3F and 3H).

Taken together, these data suggest that CRB1 is not required for the localisation of CRB2, PALS1, MUPP1 or PATJ in the first trimester of human retinal development. The onset of CRB protein expression in human fetal retina is recapitulated in retinal organoids.

Disruptions at the outer limiting membrane in retinal organoids from CRB1 retinitis pigmentosa (RP) patients

We generated three hiPSC lines (LUMC0116iCRB; LUMC0117iCRB; LUMC0128iCRB) from *CRB1* RP patients. As with healthy iPSCs (Figure S4A), patient iPSCs were validated via immunostaining with pluripotent and germ layer markers (Figure S4B). LUMC0116iCRB has c.3122T>C p.(Met1041Thr) homozygote missense mutations. LUMC0117iCRB has 2983G>T p.(Glu995*) and c.1892A>G, p.(Tyr631Cys) mutations. LUMC0128iCRB has c.2843G>A p.(Cys948Tyr) and c.3122T>C p.(Met1041Thr) missense mutations. The *CRB1* gene mutations were re-confirmed in the established iPSCs (Figure S4C).

CRB1 patient iPSCs were able to differentiate to DD180 retinal organoids and were compared to healthy retinal organoids (Figure 4). The patient retinal organoids had pH3⁺ mitotic cells apically at the OLM, with Ki67⁺ cycling cells less tightly restricted to the middle of the NBL (Figure 4I, M, Q). The *CRB1* patient iPSCs retinal organoids developed all three retinal layers: a GCL marked by Tuj1⁺ dendrites (Figure 4J, N, R), a NBL marked by SOX9⁺ retinal progenitor cells/MGCs (Figure 4K, O, S) and an ONL marked by recoverin⁺ PRCs (Figure 4L, P, T). However, frequent ectopic cells were found above the OLM (Figure 4I-T). We observed many areas of funnel-shaped outward protruding recoverin⁺ PRCs (Figures 4L, P, T) and sporadically SOX9⁺ cells above the OLM (Figure 4O).

All retinal organoids from the three different *CRB1* patient lines developed small but frequent disruptions of CRB complex members at the OLM that were not detected in control lines (Figure 5). The adherens junction proteins N-Cadherin, p120-catenin, β -catenin and the subapical region proteins CRB2, PALS1, PAR3, MUPP1 were localized as in healthy retinal organoids at DD180 (Figure 5). Interestingly, CRB1 variant protein localized similar as the wild type CRB1 protein at the subapical region above the adherens junctions but showed a curved and broadened expression pattern (Figure 5I, M, Q, U) compared to the healthy control lines (Figure 5A, E). CRB1 variant protein was also mislocalized in the apical area of the NBL and in the ONL (Figure 5I, M, Q). The mislocalized PRCs above the OLM resided at areas of OLM disruptions (Figure 5V, W, X). In conclusion, the data from *CRB1* patient hiPSC retinal organoids suggest a retinal degeneration phenotype similar as previously found in mice lacking CRB1 or expressing variant CRB1^{C249W} [24–26].

Transduction of human iPSC retinal organoids with AAV5, AAV9 and ShH10Y445F

Human iPSC-derived retinal organoids are a promising tool for evaluating transgene expression and biological activity [15]. We have shown the need in *Crb1*-retinitis pigmentosa like mice to direct *CRB* gene therapy to both photoreceptors and Müller glial cells [5]. Choosing the optimal promoter and AAV serotype for the therapeutic vector is therefore crucial to achieving expression in photoreceptors and Müller glial cells. Here, we transduced the hiPSC-derived retinal organoids with AAV9-CMV-*GFP*, AAV5-CMV-*GFP*, ShH10Y445F-CMV-*GFP* and ShH10Y445F-RLBP1-*GFP* at 10¹⁰ genome copies (gc). The CMV promoter drives expression of GFP in multiple cell types, whereas the hRLBP1 promoter drives expression in Müller glial cells and retinal pigment epithelial cells [11]. When analysed at the same laser intensity settings (Figures S5A-D) AAV5-CMV-*GFP*, ShH10Y445F-CMV-*GFP* and ShH10Y445F-hRLBP1-*GFP* significantly outperformed AAV9-CMV-*GFP* at transducing DD220 hiPSC-derived retinal organoids collected 14 days after infection (Figures 6E and 6F). We quantified both the number of GFP⁺ cells per total cells (Figure 6E) and the mean grey value (Figure 6F) for each vector. The GFP⁺ nuclei were mainly located in the inner retina and exhibited radial projections. The GFP⁺ nuclei co-localised with anti-LHX2 (Figures 6A-D, inserts) and anti-SOX2 (Figures S5E-H and S5E'-H') both transcription factors required for Müller glial cell development. Further proof of Müller glial specific transduction is also seen with the use of ShH10Y445F-RLBP1-*GFP* (Figure 6D) which drives GFP in Müller glial cells in rat and mouse retinas [11,29]. We additionally stained with anti-recoverin and found occasional co-localisation between the photoreceptor marker and GFP⁺ nuclei (Figures S5I-L and S5I'-L'). In conclusion, these results indicate that AAV5 and ShH10Y445F serotypes are more potent transducers of Müller glial cells than AAV9 in hiPSC-derived retinal organoids.

Transduction of adult post-mortem human retinal explants with serotypes AAV5, AAV9 and ShH10Y445F

To verify the results of our transduction studies on hiPSC-derived retinal organoids we also tested AAV9-, AAV5- and ShH10Y445F-CMV-*GFP* on human adult retinal explants. Initially, a titration study for AAV9 (Figure S6A-C), AAV5 (Figure S6D-F), and ShH10Y445F (Figure S6G-I) was undertaken to determine what genome copies (gc) level is required to infect photoreceptors and Müller glial cells efficiently. Analysis for total infection (Figures S6P and S6Q), infection per retinal layer (Figures S6R and S6S) and tropism (Figure S6T) in donor 1 indicated 3×10^{10} gc as a suitable level. Similar transduction patterns were found in donor 1 (Figures 6H-K, 6L-N, S6B, D, G), donor 2 (Figures S6J-L) and donor 3 (Figures S6M-O) at 3×10^{10} gc. With individual analysis for total infection (Figures S6U, S6V, S6Y and S6Z), infection per retinal layer (Figures S6W and S6AA) and tropism (Figures S6X and S6BB) also done for donors 2 and 3 at 3×10^{10} gc. Donors 1-3 had similar retinal layer thickness (Figure S6CC) and cells per retinal layer (Figure S6DD). In the INL, GFP co-labelled with Müller glial cell marker anti-SOX9 (Figures 6G-J); and in the ONL, GFP co-labelled with photoreceptor marker anti-recoverin (Figures 6K-N). When analysing donors 1-3 together, AAV5 showed the higher efficacy of transducing retinal cell types than AAV9 ($14 \pm 5\%$ vs $3 \pm 1\%$; Figure 6O), and AAV5 and ShH10Y445F showed higher potency in transduction of photoreceptors in the ONL than AAV9 ($11 \pm 3\%$ and $5 \pm 1\%$ vs $3 \pm 1\%$; Figures 6P and 6Q). Interestingly, we noticed that the photoreceptors of cadaveric human retinal explants were only efficiently infected by AAV9 (Figure S7A, B) or AAV5 (Figure S7C) or ShH10Y445F (Figure S7D) in the presence of intact photoreceptor segments (Figure S7E-G). This suggests an important role for the segments in the photoreceptor uptake of AAV particles. In conclusion, transduction of AAV serotypes in human cadaveric retina was more successful at targeting both photoreceptors and Müller glial cells than in hiPSC-derived retinal organoids. AAV5 at 3×10^{10} gc significantly outperformed AAV9 in the transduction of photoreceptor cells.

CRB2 is located in the apical membrane of iPSC-derived and fetal retinal pigment epithelium

CRB2 but not CRB1 immunostaining was detected in 1st trimester human fetal RPE (Figures S3D'-F'). This was confirmed by immuno-EM in 1st and 2nd trimester human fetal RPE (Figures 7A and 7B). CRB2 labelling was located above the adherens junctions at and above the tight junctions in the apical membrane and microvilli of human fetal RPE. Spheroids of hiPSC-derived RPE are also generated during the differentiation method used [15,30,31]. These RPE spheroids initially attach to the periphery of the retinal organoids but can detach during culturing (Figures 7C, 7D and 7D'). CRB1 could not be detected apically of β -catenin (Figure 7C) in hiPSC-derived RPE, but CRB2 was found apically of the adherens junction marker p120-catenin in DD160 hiPSC-derived RPE (Figure 7D). This pattern of localisation was also found in hiPSC-derived RPE derived from hiPSC lines LUMC0080iCTRL12

(Figures 7E and S7F) and LUMC0044iCTRL44 (Figures 7G and 7H). Immuno-EM of iPSC-derived RPE confirmed the apical staining for CRB2 above adherens junctions at and above the tight junctions in the apical membrane and microvilli. Aspecific staining was detected within melanin granules due to the presence of endogenous peroxidase in these structures (Figures 7I and 7I'). Electron microscopy of hiPSC-derived RPE also showed the presence of melanosomes with pigments, basally located mitochondria and basement membrane (Figure 7J, insert) and fibrous long-spacing collagen (FLSC) (Figures 7J and 7J'). RPE cells were also infected by AAV9, AAV5 and ShH10Y445F (Figures S7H-K).

DISCUSSION

In this study, we showed (i) that in human fetal retina during the 1st trimester of pregnancy CRB2 is the predominant CRB family member in radial glial progenitor cells. And that CRB1 onset of expression at the subapical region coincides with the maturation of the retina during the 2nd trimester. (ii) CRB2 but not CRB1 is expressed in the fetal RPE. (iii) The onset of CRB protein expression in human fetal retina and RPE is recapitulated in hiPSC-derived retinal organoids and RPE. (iv) *CRB1* RP patient retinal organoids develop disruptions at the OLM with misplaced photoreceptors. (v) AAV5 and ShH10Y445F serotypes are more potent than AAV9 serotype in infecting cultured retinal organoids. (vi) AAV5-CMV-*GFP* is more efficient than AAV9-CMV-*GFP* to express GFP in PRCs in cultured human donor retinal explants. (vii) Human PRCs are efficiently transduced only in the presence of photoreceptor segments.

In the human fetal retina, we found that CRB2 is the predominant CRB effector protein in the 1st trimester of pregnancy. *CRB2* is a gene expressed in several tissues, including the cerebral cortex [32], with a crucial role during early development in both mice and humans. Mice lacking *Crb2* are embryonic lethal with a crucial role for the CRB2 protein during gastrulation in the epithelial-to-mesenchymal transition [33]. CRB2 protein variants in humans have been linked to a syndromic phenotype causing kidney and brain dysfunctions and lethality [34,35] as well as to retinitis pigmentosa [36]. In the 2nd trimester, CRB1 and CRB2 localised at the subapical region in apical villi of radial glial progenitor cells/MGCs and at the subapical region above the adherens junctions in the inner segments of PRCs. During the 2nd trimester, the retina undergoes the birth of all adult cell types, and the retina is transitioning from a mitotic to post-mitotic state [27,37]. Retinal organoids go from an early highly-cell-cycling state, in which Ki67 marks the entire NBL at DD28, towards a moderate-cell-cycling state, in which Ki67 becoming restricted to the mid-NBL at DD120.

Interestingly, here we showed that the onset of CRB1 protein expression coincided with the maturation of the retinal organoids, and this finding is recapitulated in the human fetal retina. In early-stage retinal organoids, we found as in the 1st trimester fetal retina CRB2 but little CRB1 protein expression at the subapical region. In later stage hiPSC-derived retinal organoids we found CRB2 and CRB1 protein expression at the subapical region as in 2nd

trimester fetal retina. We also found a recapitulation of CRB2 expression when comparing 1st trimester fetal RPE with hiPSC-derived RPE.

We present here the generation and characterization of *CRB1*-patient-derived hiPSCs differentiated to retinal organoids. We demonstrate that patient retinal organoids give rise to a morphological significant phenotype even though variant CRB1 protein and its interaction partners (MUPP1, PALS1, CRB2) are detected at the OLM. The data suggests disruptions at the OLM resulting in loss of adhesion between photoreceptors and Müller glial cells. Decreased levels of CRB1 and CRB2 proteins at the OLM exacerbated retinal degeneration in mouse models [28,38,39]. Also, the volcanic-like cell protrusions and OLM disruptions in the patient retinal organoids show striking similarities to the morphological phenotype found in 3 month-old *Crb1*^{KO} and 8 month-old *Crb1*^{KO/C249W} RP mice [24–26]. Further studies are needed to elucidate the underlying effects of the variant CRB1 proteins on protein-protein interactions and downstream cell signalling pathways.

We hypothesise that retinal organoids could be a good model for evaluating transgene expression and biological activity due to their close mimicking of human fetal retinal development [15]. Our transduction studies on cadaveric human retinal explants showed a higher potency for AAV5 over AAV9 for transduction of photoreceptors. Also, the data suggest the higher efficacy of AAV5-CMV-*GFP* than AAV9-CMV-*GFP* or ShH10Y445F-CMV-*GFP* to express in PRCs and MGCs. In the absence of photoreceptor segments in the human retinal explants, AAV5-CMV-*GFP*, ShH10Y445F-CMV-*GFP* and AAV9-CMV-*GFP* showed higher efficacy to express in MGCs than in PRCs. The latter tropism and expression potency data in cultured cadaveric human retinal explants are reproduced in retinal organoids that recapitalise 2nd trimester fetal retina.

Previous subretinal injection studies in which AAV5 was administered in mice at postnatal day 0 (P0) or 30 (P30) have shown preferred transduction of P0 cone PRC and MGCs but only of P30 rod and cone PRCs [40]. We hypothesise that this preference in transduction patterns of PRC and MGCs in immature versus mature retina is due to the presence or absence of matured photoreceptor segments. In mice, photoreceptor segments seem to be required for the efficient transduction of photoreceptor cells with AAV vectors [41]. A very interesting and clinically relevant finding is that photoreceptors in cultured cadaveric human retinal explants are only efficiently transduced when they have photoreceptor segments. Retinal organoids represent immature fetal retina that contain PRCs but with yet very immature segments. We hypothesise that PRCs are transduced by AAV5, AAV9 and ShH10Y445F once the PRC segments are formed in sufficient number and size. In the absence of PRC segments, however, there is increased bioavailability of AAV vectors to target less abundant/preferred receptors for AAV uptake, e.g. on MGCs. Interestingly, dependency on the presence of photoreceptor segments for photoreceptor transduction was observed for all three AAV serotypes (AAV5, AAV9 and ShH10Y445F), suggesting a putative common

mechanism of active AAV uptake into photoreceptors. The inner segments are a putative site of receptor-dependent or independent clathrin- and caveolae-mediated endocytosis [42].

Our data suggest that for clinical gene therapy with AAV5, AAV9 or ShH10Y445F the target PRCs should have intact photoreceptors to become efficiently transduced. It also implies that the AAV vector particles should be able to reach the PRC segments during clinical surgical application. This condition of accessibility of PRC inner segments in human retina *in vivo* is met upon subretinal injection as suggested by AAV5 or AAV9 infection of PRCs in non-human-primate retinas [14,43]. Our mice lacking CRB1 as well as the mice with reduced levels of CRB2 showed a compromised outer limiting membrane. We further hypothesise from our previous studies in mice that the retinas of human patients with loss of CRB1, or expressing non-functional CRB1 variants, have a compromised outer limiting membrane that allows increased passage of AAV viral particles across the adherence junctions to reach the AAV-receptor molecules on MGCs [44].

MATERIALS AND METHODS

Experimental Procedures

See further details in the Supplemental Experimental Procedures.

Fetal human retinal tissue

The use and collection of the material was approved by the Medical Ethics Committee of the Leiden University Medical Center (P08.087).

Adult human retinal tissue

Tissue was collected in agreement with the guidelines of the ethics committee of the LUMC. Informed consent was obtained on the basis of the Declaration of Helsinki (World Medical Association).

Cell Culture and Retinal Organoid Differentiation

Human iPSCs (LUMC0004iCTRL10 (Dambrot et al., 2014), LUMC0044iCTRL44 (Chen et al., 2017), LUMC0080iCTRL12 (Figure S4A), LUMC0116iCRB09, LUMC0117iCRB01, LUMC0128iCRB01 (Figure S4B)) were maintained on Matrigel (BD) coated plates in mTeSR medium (STEMCELL Technologies) and passaged mechanically. Retinal organoid differentiation was carried out as previously reported (Quinn et al., 2018a; Zhong et al., 2014).

Electron microscopy

Immuno-electron microscopy was performed as previously described (Klooster et al., 2011). In brief, Sections were incubated with first antibody for 48 h, then incubated with appropriate secondary peroxidase anti-peroxidase (PAP) for 2h, then developed in a 2,2-

diaminobenzidine solution for 4 min and then the gold substitute silver peroxidase method applied.

Generation and purification of the viral vectors

The pAAV2-*eGFP* plasmids were generated previously and consist of the flanking inverted terminal repeats (ITRs) of AAV2, the full-length CMV promoter, or the human RLBP1 promoter, the *eGFP* cDNA, the Woodchuck posttranscriptional regulatory element (WPRE) and the bovine growth hormone poly(A) (bGHpoly(A)) (Aartsen et al., 2010; Alves et al., 2014b; Pellissier et al., 2014a).

In vitro transduction of human donor retina and human induced pluripotent stem cell derived retinal organoids

In vitro transduction protocols for 1) human donor retina and 2) hiPSC-derived retinal organoids have been described (Buck et al., 2018; Quinn et al., 2018a).

Statistical method

All statistical analyses were performed using GraphPad Prism version 7 (GraphPad Software). All values are expressed as mean \pm SEM. Multiple t-tests were performed with the analysed number of samples indicated in the figure legends. Immunohistochemistry was performed on iPSC-derived retinal organoids from 3 independent healthy and 3 independent *CRBI*-patient iPSC lines from 2 or more differentiations, with 3-6 sections examined per organoid. Immunohistochemistry was performed on at least 2 independent human fetal eyes per time point, with 3-6 sections examined per eye. Immuno-EM was performed on at least 2 independent human fetal eyes, iPSC-derived retinal organoids and RPE for each time point. For AAV transduction studies between 3-6 different sections from at least three different human donor retina or hiPSC-derived retinal organoids (1-2 organoids from 2 independent differentiations analysed) were used for quantification. Between 3-5 images per organoid and 10 images per adult donor retina were analysed.

Author contributions

P.M.Q., T.M.B. and J.W. conceived and designed the experiments. P.M.Q., T.M.B., C.O., C.H.A., A.A.M., performed the experiments. R.V. produced virus stocks. M.B., T.v.H., E.H.C.v.D., M.T., collected study material. H.M.M., C.F., R.C.H., M-J.G., C.J.F.B., A.J.K. and S.M.C.d.S.L. provided study material and/or access to facilities. P.M.Q. and T.M.B. assembled data. P.M.Q., T.M.B., A.A.M., C.R.J. and J.W. analysed and interpreted the data. P.M.Q., T.M.B. and J.W. wrote the manuscript. All authors reviewed the manuscript. J.W. provided funding acquisition, supervision and final approval of manuscript.

Acknowledgments

The Wijnholds Laboratory would like to thank Yacintha van Doorn and Hind Almushattat for differentiation of retinal organoids, André Le Bivic for providing PATJ antibodies, Maaïke Nieveen and Fang Wang for collecting study materials, Annelies van der Laan and Joop Wiegant from the LUMC microscope facility, and Anke 't Jong from the LUMC iPSC facility for advice. We would like to thank the abortion clinic Gynaikon in Rotterdam for the collection of the fetal material. We would also like to thank all our supporters, which include the Foundation Fighting Blindness USA (TA-GT-0313-0607-NIN and TA-GT-0715-0665-LUMC), the Netherlands Organization for Health Research and Development (ZonMw grant 43200004), the Curing Retinal Blindness Foundation (CRBF), Stichting Retina Nederland Fonds, Landelijke Stichting voor Blinden en Slechtzienden (LSBS), Rotterdamse Stichting Blindenbelangen (RSB), Stichting Blindenhulp, Stichting Blinden-Penning, Algemene Nederlandse Vereniging ter Voorkoming van Blindheid (ANVVB), Gelderse Blinden Stichting (GBS), and MaculaFonds. The LUMC is the holder of patent number PCT/NL2014/050549, which describes the potential clinical use of CRB2; JW is listed as inventor on this patent, and JW is an employee of the LUMC. The authors declare that the research was conducted without any commercial or financial relationships that could be construed as a potential conflict of interest.

REFERENCES

- Alves, C.H.; Pellissier, L.P.; Wijnholds, J. The CRB1 and adherens junction complex proteins in retinal development and maintenance. *Prog. Retin. Eye Res.* **2014**, *40*, 35–52.
- Talib, M.; van Schooneveld, M.J.; van Genderen, M.M.; Wijnholds, J.; Florijn, R.J.; ten Brink, J.B.; Schalijs-Delfos, N.E.; Dagnelie, G.; Cremers, F.P.M.; Wolterbeek, R.; et al. Genotypic and Phenotypic Characteristics of CRB1-Associated Retinal Dystrophies: A Long-Term Follow-up Study. *Ophthalmology* **2017**, *124*, 884–895.
- Stone, E.M.; Andorf, J.L.; Whitmore, S.S.; DeLuca, A.P.; Giacalone, J.C.; Streb, L.M.; Braun, T.A.; Mullins, R.F.; Scheetz, T.E.; Sheffield, V.C.; et al. Clinically Focused Molecular Investigation of 1000 Consecutive Families with Inherited Retinal Disease. *Ophthalmology* **2017**, *124*, 1314–1331.
- Bujakowska, K.; Audo, I.; Mohand-Saïd, S.; Lancelot, M.-E.; Antonio, A.; Germain, A.; Léveillard, T.; Letexier, M.; Saraiva, J.-P.; Lonjou, C.; et al. CRB1 mutations in inherited retinal dystrophies. *Hum. Mutat.* **2012**, *33*, 306–315.
- Pellissier, L.P.; Quinn, P.M.; Henrique Alves, C.; Vos, R.M.; Klooster, J.; Flannery, J.G.; Alexander Heimel, J.; Wijnholds, J. Gene therapy into photoreceptors and Müller glial cells restores retinal structure and function in CRB1 retinitis pigmentosa mouse models. *Hum. Mol. Genet.* **2015**, *24*, 3104–3118.
- Reichel, F.F.; Peters, T.; Wilhelm, B.; Biel, M.; Ueffing, M.; Wissinger, B.; Bartz-Schmidt, K.U.; Klein, R.; Michalakakis, S.; Fischer, M.D.; et al. Humoral Immune Response After Intravitreal But Not After Subretinal AAV8 in Primates and Patients. *Invest. Ophthalmol. Vis. Sci.* **2018**, *59*, 1910–1915.
- Maguire, A.M.; Simonelli, F.; Pierce, E.A.; Pugh, E.N.; Mingozzi, F.; Bencicelli, J.; Banfi, S.; Marshall, K.A.; Testa, F.; Surace, E.M.; et al. Safety and efficacy of gene transfer for Leber's congenital amaurosis. *N. Engl. J. Med.* **2008**, *358*, 2240–2248.
- MacLaren, R.E.; Groppe, M.; Barnard, A.R.; Cottrill, C.L.; Tolmachova, T.; Seymour, L.; Reed Clark, K.; During, M.J.; Cremers, F.P.M.; Black, G.C.M.; et al. Retinal gene therapy in patients with choroideremia: Initial findings from a phase 1/2 clinical trial. *Lancet* **2014**, *383*, 1129–1137.
- Asokan, A.; Schaffer, D. V.; Jude Samulski, R. The AAV Vector Toolkit: Poised at the Clinical Crossroads. *Mol. Ther.* **2012**, *20*, 699–708.
- Ramachandran, P.S.; Lee, V.; Wei, Z.; Song, J.Y.; Casal, G.; Cronin, T.; Willett, K.; Huckfeldt, R.; Morgan, J.I.W.; Aleman, T.S.; et al. Evaluation of Dose and Safety of AAV7m8 and AAV8BP2 in the Non-Human Primate Retina. *Hum. Gene Ther.* **2017**, *28*, 154–167.

11. Pellissier, L.P.; Hoek, R.M.; Vos, R.M.; Aartsen, W.M.; Klimczak, R.R.; Hoyng, S.A.; Flannery, J.G.; Wijnholds, J. Specific tools for targeting and expression in Müller glial cells. *Mol. Ther. — Methods Clin. Dev.* **2014**, *1*, 14009.
12. Aartsen, W.M.; van Cleef, K.W.R.R.; Pellissier, L.P.; Hoek, R.M.; Vos, R.M.; Blits, B.; Ehler, E.M.E.E.; Balaggan, K.S.; Ali, R.R.; Verhaagen, J.; et al. GFAP-driven GFP expression in activated mouse Müller glial cells aligning retinal blood vessels following intravitreal injection of AAV2/6 vectors. *PLoS One* **2010**, *5*, e12387.
13. Vandenberghe, L.H.; Bell, P.; Maguire, A.M.; Xiao, R.; Hopkins, T.B.; Grant, R.; Bennett, J.; Wilson, J.M. AAV9 targets cone photoreceptors in the nonhuman primate retina. *PLoS One* **2013**, *8*, e53463.
14. Boye, S.E.; Alexander, J.J.; Boye, S.L.; Witherspoon, C.D.; Sandefer, K.J.; Conlon, T.J.; Erger, K.; Sun, J.; Ryals, R.; Chiodo, V.A.; et al. The Human Rhodopsin Kinase Promoter in an AAV5 Vector Confers Rod- and Cone-Specific Expression in the Primate Retina. *Hum. Gene Ther.* **2012**, *23*, 1101–1115.
15. Quinn, P.M.; Buck, T.M.; Ohonin, C.; Mikkers, H.M.M.M.; Wijnholds, J. Production of iPS-derived human retinal organoids for use in transgene expression assays. In *Methods in Molecular Biology*; Humana Press Inc., 2018; Vol. 1715, pp. 261–273.
16. Wiley, L.A.; Burnight, E.R.; Drack, A. V.; Banach, B.B.; Ochoa, D.; Cranston, C.M.; Madumba, R.A.; East, J.S.; Mullins, R.F.; Stone, E.M.; et al. Using Patient-Specific Induced Pluripotent Stem Cells and Wild-Type Mice to Develop a Gene Augmentation-Based Strategy to Treat *CLN3* -Associated Retinal Degeneration. *Hum. Gene Ther.* **2016**, *27*, 835–846.
17. Khabou, H.; Garita-Hernandez, M.; Chaffiol, A.; Reichman, S.; Jaillard, C.; Brazhnikova, E.; Bertin, S.; Forster, V.; Desrosiers, M.; Winckler, C.; et al. Noninvasive gene delivery to foveal cones for vision restoration. *JCI insight* **2018**, *3*.
18. Bulgakova, N.A.; Knust, E. The Crumbs complex: from epithelial-cell polarity to retinal degeneration. *J. Cell Sci.* **2009**, *122*, 2587–96.
19. Bachmann, A.; Schneider, M.; Theilenberg, E.; Grawe, F.; Knust, E. Drosophila Stardust is a partner of Crumbs in the control of epithelial cell polarity. *Nature* **2001**, *414*, 638–643.
20. Lemmers, C.; Michel, D.; Lane-Guermontprez, L.; Delgrossi, M.-H.; Médina, E.; Arsanto, J.-P.; Bivic, A. Le CRB3 Binds Directly to Par6 and Regulates the Morphogenesis of the Tight Junctions in Mammalian Epithelial Cells. *Mol. Biol. Cell* **2004**, *15*, 1324.
21. Roh, M.H.; Makarova, O.; Liu, C.-J.; Shin, K.; Lee, S.; Laurinec, S.; Goyal, M.; Wiggins, R.; Margolis, B. The Maguk protein, Pals1, functions as an adapter, linking mammalian homologues of Crumbs and Discs Lost. *J. Cell Biol.* **2002**, *157*, 161–72.
22. Quinn, P.M.; Mulder, A.A.; Henrique Alves, C.; Desrosiers, M.; de Vries, S.I.; Klooster, J.; Dalkara, D.; Koster, A.J.; Jost, C.R.; Wijnholds, J. Loss of CRB2 in Müller glial cells modifies a CRB1-associated retinitis pigmentosa phenotype into a Leber congenital amaurosis phenotype. *Hum. Mol. Genet.* **2019**, *28*, 105–123.
23. Pellissier, L.P.; Lundvig, D.M.S.; Tanimoto, N.; Klooster, J.; Vos, R.M.; Richard, F.; Sothilingam, V.; Garcia Garrido, M.; Le Bivic, A.; Seeliger, M.W.; et al. CRB2 acts as a modifying factor of CRB1-related retinal dystrophies in mice. *Hum. Mol. Genet.* **2014**, *23*, 3759–3771.
24. van de Pavert, S.A.; Sanz, A.S.; Aartsen, W.M.; Vos, R.M.; Versteeg, I.; Beck, S.C.; Klooster, J.; Seeliger, M.W.; Wijnholds, J. Crb1 is a determinant of retinal apical Müller glia cell features. *Glia* **2007**, *55*, 1486–1497.
25. van de Pavert, S.A.; Kantardzhieva, A.; Malysheva, A.; Meuleman, J.; Versteeg, I.; Levelt, C.; Klooster, J.; Geiger, S.; Seeliger, M.W.; Rashbass, P.; et al. Crumbs homologue 1 is required for maintenance of photoreceptor cell polarization and adhesion during light exposure. *J. Cell Sci.* **2004**, *117*, 4169–4177.
26. van de Pavert, S.A.; Meuleman, J.; Malysheva, A.; Aartsen, W.M.; Versteeg, I.; Tonagel, F.; Kamphuis, W.; McCabe, C.J.; Seeliger, M.W.; Wijnholds, J. A single amino acid substitution (Cys249Trp) in Crb1 causes retinal degeneration and deregulates expression of pituitary tumor transforming gene Pttg1. *J. Neurosci.* **2007**, *27*, 564–573.
27. Provis, J.M.; van Driel, D.; Billson, F.A.; Russell, P. Development of the human retina: patterns of cell distribution and redistribution in the ganglion cell layer. *J. Comp. Neurol.* **1985**, *233*, 429–451.
28. Alves, C.H.; Sanz, A.S.; Park, B.; Pellissier, L.P.; Tanimoto, N.; Beck, S.C.; Huber, G.; Murtaza, M.; Richard, F.; Sridevi Gurubaran, I.; et al. Loss of CRB2 in the mouse retina mimics human retinitis pigmentosa due to mutations in the CRB1 gene. *Hum. Mol. Genet.* **2013**, *22*, 35–50.
29. Klimczak, R.R.; Koerber, J.T.; Dalkara, D.; Flannery, J.G.; Schaffer, D. V. A novel adeno-associated viral variant for efficient and selective intravitreal transduction of rat Müller cells. *PLoS One* **2009**, *4*, e7467.
30. Zhong, X.; Gutierrez, C.; Xue, T.; Hampton, C.; Vergara, M.N.; Cao, L.-H.; Peters, A.; Park, T.S.; Zambidis, E.T.; Meyer, J.S.; et al. Generation of three-dimensional retinal tissue with functional photoreceptors from human iPSCs. *Nat. Commun.* **2014**, *5*, 4047.
31. Liu, S.; Xie, B.; Song, X.; Zheng, D.; He, L.; Li, G.; Gao, G.; Peng, F.; Yu, M.; Ge, J.; et al. Self-Formation of RPE Spheroids Facilitates Enrichment and Expansion of hiPSC-Derived RPE Generated on Retinal Organoid Induction Platform. *Invest. Ophthalmol. Vis. Sci.* **2018**, *59*, 5659–5669.
32. Dudok, J.J.; Murtaza, M.; Henrique Alves, C.; Rashbass, P.; Wijnholds, J. Crumbs 2 prevents cortical abnormalities in mouse dorsal telencephalon. *Neurosci. Res.* **2016**, *108*, 12–23.

33. Ramkumar, N.; Omelchenko, T.; Silva-Gagliardi, N.F.; McGlade, C.J.; Wijnholds, J.; Anderson, K.V. Crumbs2 promotes cell ingression during the epithelial-to-mesenchymal transition at gastrulation. *Nat. Cell Biol.* **2016**, *18*, 1281–1291.
34. Ebarasi, L.; Ashraf, S.; Bierzynska, A.; Gee, H.Y.; McCarthy, H.J.; Lovric, S.; Sadowski, C.E.; Pabst, W.; Vega-Warner, V.; Fang, H.; et al. Defects of CRB2 cause steroid-resistant nephrotic syndrome. *Am. J. Hum. Genet.* **2015**, *96*, 153–61.
35. Slavotinek, A.; Kaylor, J.; Pierce, H.; Cahr, M.; DeWard, S.J.; Schneidman-Duhovny, D.; Alsadah, A.; Salem, F.; Schmajuk, G.; Mehta, L. CRB2 mutations produce a phenotype resembling congenital nephrosis, Finnish type, with cerebral ventriculomegaly and raised alpha-fetoprotein. *Am. J. Hum. Genet.* **2015**, *96*, 162–9.
36. Chen, X.; Jiang, C.; Yang, D.; Sun, R.; Wang, M.; Sun, H.; Xu, M.; Zhou, L.; Chen, M.; Xie, P.; et al. CRB2 mutation causes autosomal recessive retinitis pigmentosa. *Exp. Eye Res.* **2018**, *180*, 164–173.
37. Lee, T.C.; Almeida, D.; Claros, N.; Abramson, D.H.; Cobrinik, D. Cell cycle-specific and cell type-specific expression of Rb in the developing human retina. *Investig. Ophthalmol. Vis. Sci.* **2006**, *47*, 5590–5598.
38. Pellissier, L.P.; Alves, C.H.; Quinn, P.M.; Vos, R.M.; Tanimoto, N.; Lundvig, D.M.S.; Dudok, J.J.; Hooibrink, B.; Richard, F.; Beck, S.C.; et al. Targeted ablation of CRB1 and CRB2 in retinal progenitor cells mimics Leber congenital amaurosis. *PLoS Genet* **2013**, *9*, e1003976.
39. Quinn, P.M.; Alves, C.H.; Klooster, J.; Wijnholds, J. CRB2 in immature photoreceptors determines the superior-inferior symmetry of the developing retina to maintain retinal structure and function. *Hum. Mol. Genet.* **2018**, *27*, 3137–3153.
40. Surace, E.M.; Auricchio, A.; Reich, S.J.; Rex, T.; Glover, E.; Pineles, S.; Tang, W.; O'Connor, E.; Lyubarsky, A.; Savchenko, A.; et al. Delivery of Adeno-Associated Virus Vectors to the Fetal Retina: Impact of Viral Capsid Proteins on Retinal Neuronal Progenitor Transduction. *J. Virol.* **2003**, *77*, 7957–7963.
41. Petit, L.; Ma, S.; Cheng, S.-Y.; Gao, G.; Punzo, C. Rod Outer Segment Development Influences AAV-Mediated Photoreceptor Transduction After Subretinal Injection. *Hum. Gene Ther.* **2017**, *28*, 464–481.
42. Fuchs, M.; Brandstätter, J.H.; Regus-Leidig, H. Evidence for a Clathrin-independent mode of endocytosis at a continuously active sensory synapse. *Front. Cell. Neurosci.* **2014**, *8*, 1–13.
43. Vandenberghe, L.H.; Bell, P.; Maguire, A.M.; Cearley, C.N.; Xiao, R.; Calcedo, R.; Wang, L.; Castle, M.J.; Maguire, A.C.; Grant, R.; et al. Dosage thresholds for AAV2 and AAV8 photoreceptor gene therapy in monkey. *Sci. Transl. Med.* **2011**, *3*, 88ra54.
44. Pearson, R.A.; Barber, A.C.; West, E.L.; MacLaren, R.E.; Duran, Y.; Bainbridge, J.W.; Sowden, J.C.; Ali, R.R. Targeted disruption of outer limiting membrane junctional proteins (Crb1 and ZO-1) increases integration of transplanted photoreceptor precursors into the adult wild-type and degenerating retina. *Cell Transplant.* **2010**, *19*, 487–503.
45. Dambrot, C.; Buermans, H.P.J.; Varga, E.; Kosmidis, G.; Langenberg, K.; Casini, S.; Elliott, D.A.; Dinnyes, A.; Atsma, D.E.; Mummery, C.L.; et al. Strategies for rapidly mapping proviral integration sites and assessing cardiogenic potential of nascent human induced pluripotent stem cell clones. *Exp. Cell Res.* **2014**, *327*, 297–306.
46. Chen, X.; Janssen, J.M.; Liu, J.; Maggio, I.; 't Jong, A.E.J.; Mikkers, H.M.M.; Gonçalves, M.A.F. V In trans paired nicking triggers seamless genome editing without double-stranded DNA cutting. *Nat. Commun.* **2017**, *8*, 657.
47. Klooster, J.; Blokker, J.; ten Brink, J.B.; Unmehopa, U.; Fluiter, K.; Bergen, A.A.B.; Kamermans, M. Ultrastructural localization and expression of TRPM1 in the human retina. *Investig. Ophthalmol. Vis. Sci.* **2011**, *52*, 8356–8362.
48. Alves, C.H.; Pellissier, L.P.; Vos, R.M.; Garcia Garrido, M.; Sothilingam, V.; Seide, C.; Beck, S.C.; Klooster, J.; Furukawa, T.; Flannery, J.G.; et al. Targeted ablation of Crb2 in photoreceptor cells induces retinitis pigmentosa. *Hum. Mol. Genet.* **2014**, *23*, 3384–3401.
49. Buck, T.M.; Pellissier, L.P.; Vos, R.M.; van Dijk, E.H.C.C.; Boon, C.J.F.; Wijnholds, J. AAV serotype testing on cultured human donor retinal explants. In *Methods in Molecular Biology*; Boon, C.J.F., Wijnholds, J., Eds.; New York, NY: Humana Press; New York, NY, 2018; Vol. 1715, p. pp 275-288 ISBN 978-1-4939-7522-8.

FIGURES

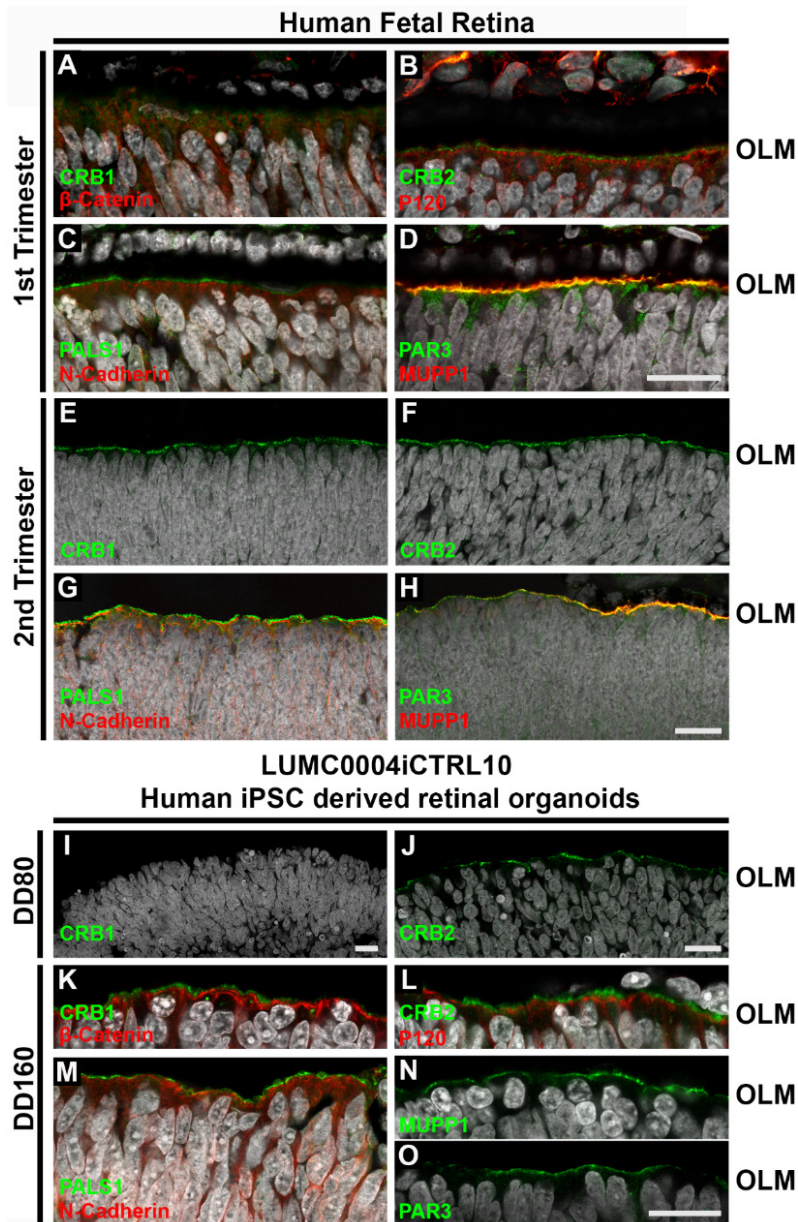


Figure 1. Localization of the CRB complex at the outer limiting membrane in human fetal and iPSC-derived human retina. Immunohistochemistry pictures of 1st (A-D) and 2nd (E-H) trimester human fetal retina and early (I, J) and late (K-O) LUMC0004iCTRL10 hiPSC-derived retinal organoids. Sections were stained for subapical region markers: CRB1 (A, E, I, K), CRB2 (B, F, J, L), PALS1 (C, G, M), PAR3 (D, H, O), MUPP1 (D, H, N) and for adherens junction markers: β -catenin (A, K), p120-catenin (B, L), N-cadherin (C, G, M). OLM, outer limiting membrane. Scale bars: (A-0), 20 μ m. See also Figure S1 and S2.

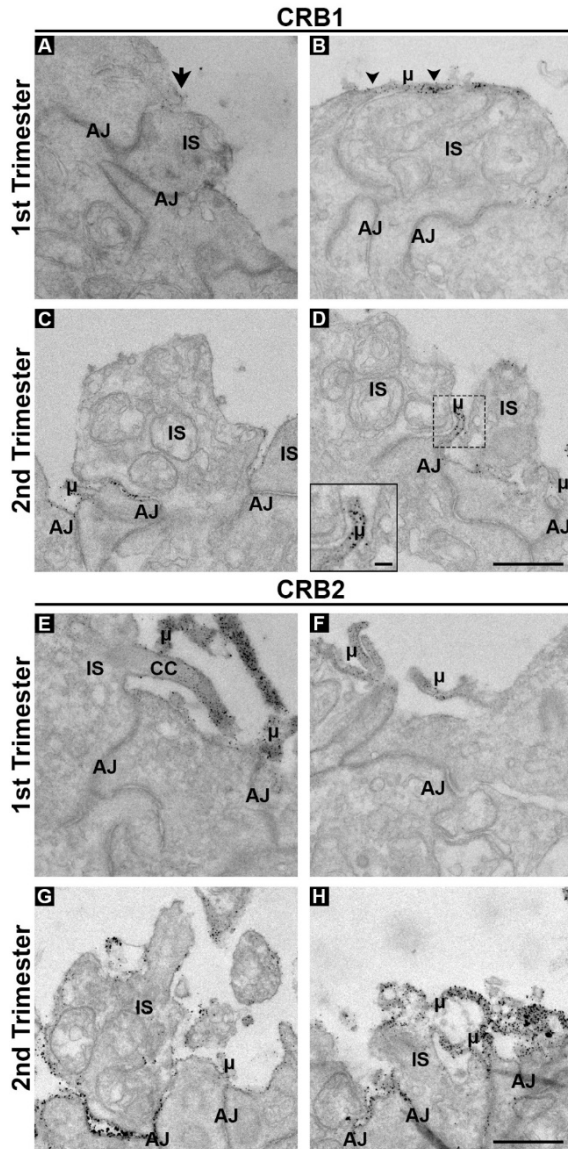


Figure 2. CRB1 and CRB2 are located at the outer limiting membrane in Müller glial cells and photoreceptors of 1st and 2nd Trimester human fetal retina. Immun-EM staining showing the localisation of CRB1 (A-D) and CRB2 (E-H) in 1st (A, B, E, F) and 2nd (C, D, G, H) trimester human fetal retina. CRB1 was sporadically detected in the 1st trimester but being found subapically of adherens junctions adjacent to photoreceptor inner segments (A, arrow) and in Müller glial cell apical villi (B, arrowheads). In the 2nd trimester, CRB1 was found consistently throughout the outer limiting membrane of human fetal retina subapically of adherens junctions of photoreceptors and Müller glial cells (C, D). CRB2 was localised in both 1st and 2nd trimester retina subapically of adherens junctions being located in photoreceptor inner segments and apical villi of Müller glial cells. At least two independent samples were analysed per time point. CC, connecting cilium; AJ, adherens junction; μ , microvilli; IS, inner segment. Scale bar: 1 μ m, insets: 500nm.

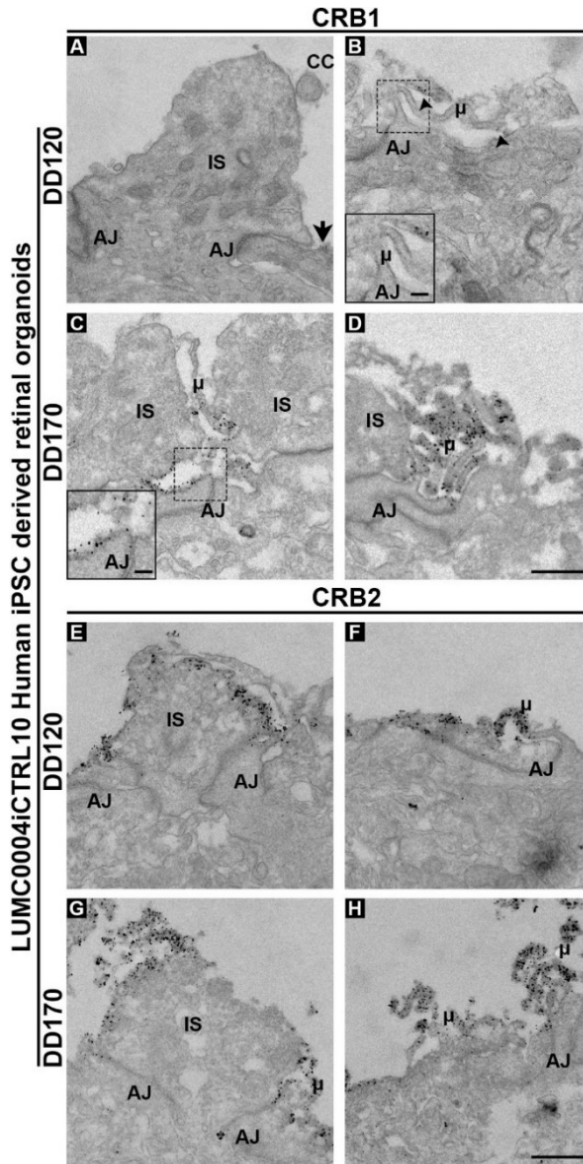


Figure 3. CRB1 and CRB2 are located at the outer limiting membrane in Müller glial cells and photoreceptors of human iPSC-derived retinal organoids. Immun-EM staining showing the localisation of CRB1 (A-D) and CRB2 (E-H) in DD120 (A, B, E, F) and DD170 (C, D, G, H) LUMC0004iCTRL10 human iPSC-derived retinal organoids. CRB1 was lowly and sporadically detected at DD120 but being found subapically of adherens junctions adjacent to photoreceptor inner segments (A, arrow) and in Müller glial cell apical villi (B, arrowheads). At DD170 CRB1 was found consistently throughout the outer limiting membrane of human iPSC-derived retinal organoids subapically of adherens junctions of photoreceptors and Müller glial cells (C, D). CRB2 was localised at both DD120 and DD170 subapically of adherens junctions being located in photoreceptor inner segments and apical villi of Müller glial cells. At least two independent samples were analysed per time point. CC, connecting cilium; AJ, adherens junction; μ , microvilli; IS, inner segment. Scale bar: $1\mu\text{m}$, inserts: 500nm .

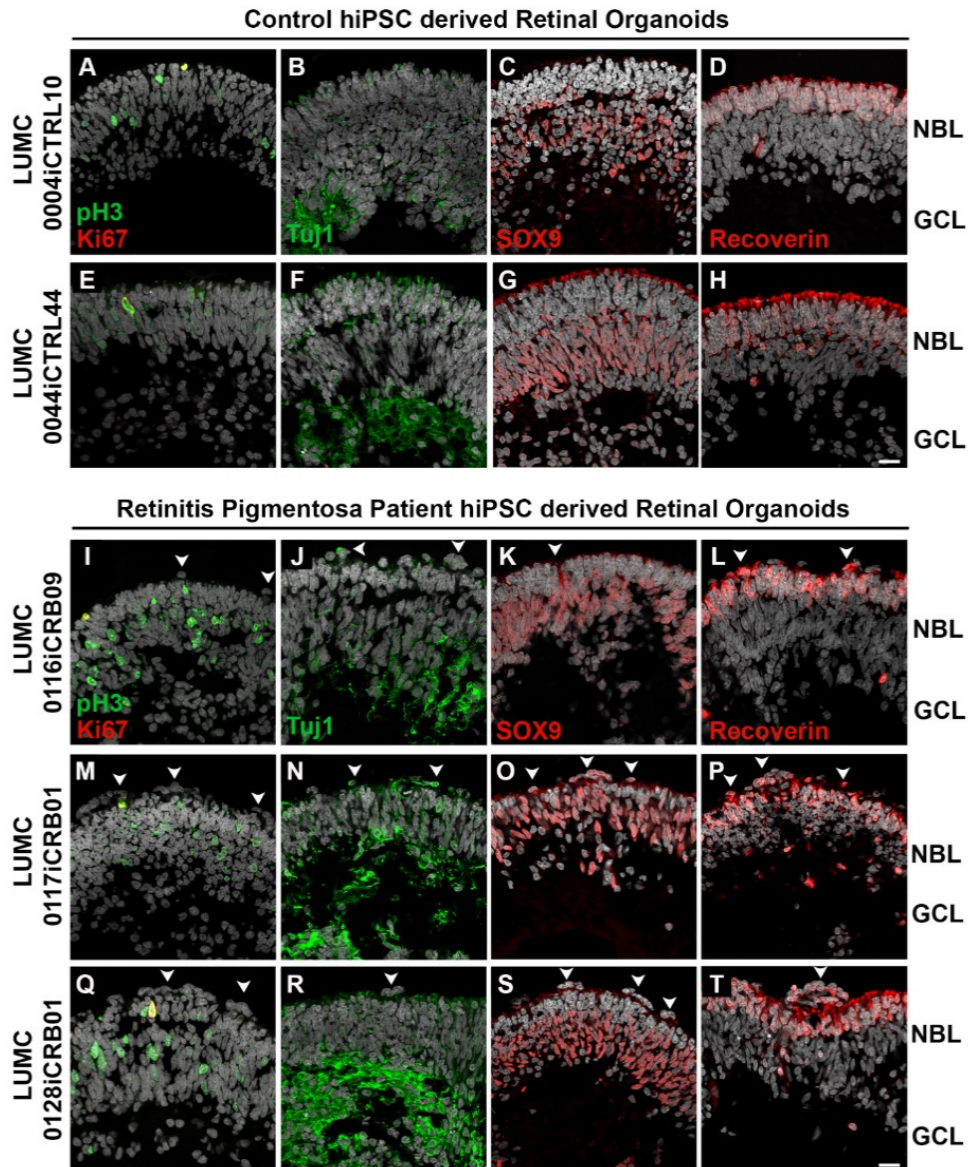


Figure 4. *CRBI* patient retinal organoids develop proper lamination. Immunohistochemistry pictures of healthy (LUMC0004iCTRL10; LUMC0044iCTRL44) vs *CRBI* patient (LUMC0116iCRB09, LUMC0117iCRB01, LUMC0128iCRB01) retinal organoids at DD180. Sections were stained for pH3⁺ mitotic cells and Ki67⁺ cycling cells (A, E, I, M, Q); Tuj1⁺ dendrites marking the GCL (B, F, J, N, R); SOX9⁺ NBL cells (C, G, K, O, S); and recoverin⁺ PRCs marking the ONL (D, H, L, P, T). Experiments were validated in two differentiations for retinal organoids. NBL, neurobasal layer; GCL, ganglion cell layer. Scale bars: (A-0), 20 μ m. See also Figure S4.

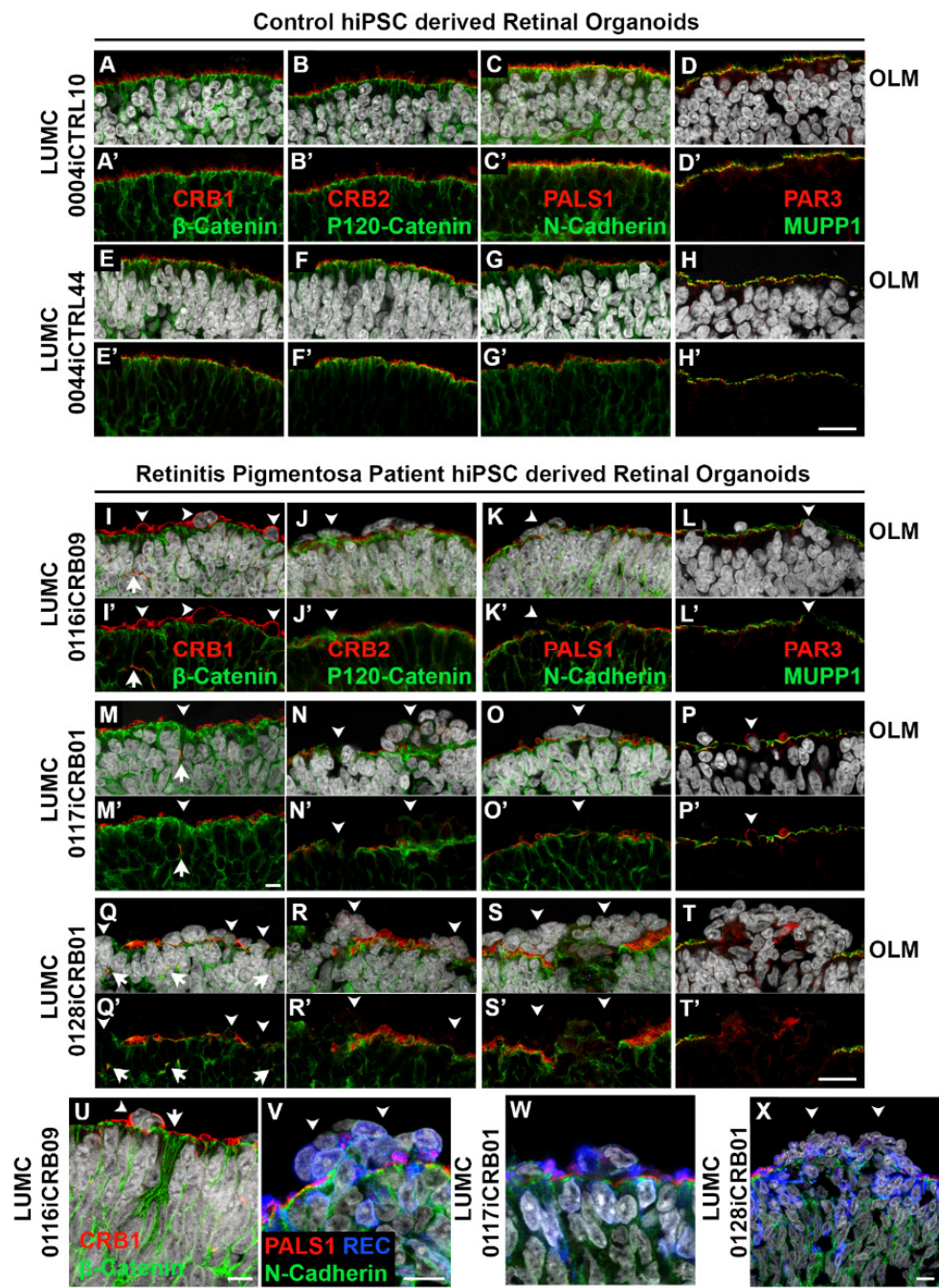


Figure 5. *CRB1* patient organoids develop retinal degeneration. Immunohistochemistry pictures of healthy (LUMC0004iCTRL10 (A-D, A'-D'); LUMC0044iCTRL44 (E-H, E'-H')) and *CRB1* patient (LUMC0116iCRB09 (I-L, I'-L', U, V), LUMC0117iCRB01 (M-P, M'-P', W), LUMC0128iCRB01 (Q-T, Q'-T, X)) retinal organoids at DD180. Sections were stained for subapical region markers: CRB1 (A, E, I, M, Q, U), CRB2 (B, F, J, N, R), PALS1 (C, G, K, O, S, V, W, X), PAR3 (D, H, L, P, T), MUPP1 (D, H, L, P, T) and for adherens junction markers: β -catenin (A, E, I, M, Q, U), p120-catenin (B, F, J, N, R), N-cadherin (C, G, K, O, S, V). Disruptions of the OLM are seen in patient retinal organoids (I-T, I'-T') with recoverin⁺ photoreceptors found displaced (V-X). A-X counterstained with DAPI. Experiments were validated in two differentiations for retinal organoids. OLM, outer limiting membrane; NBL, neurobasal layer. Scale bars: (A-0), 20 μ m. See also Figure S4.

LUMC0004iCTRL10 Human iPSC derived retinal organoids

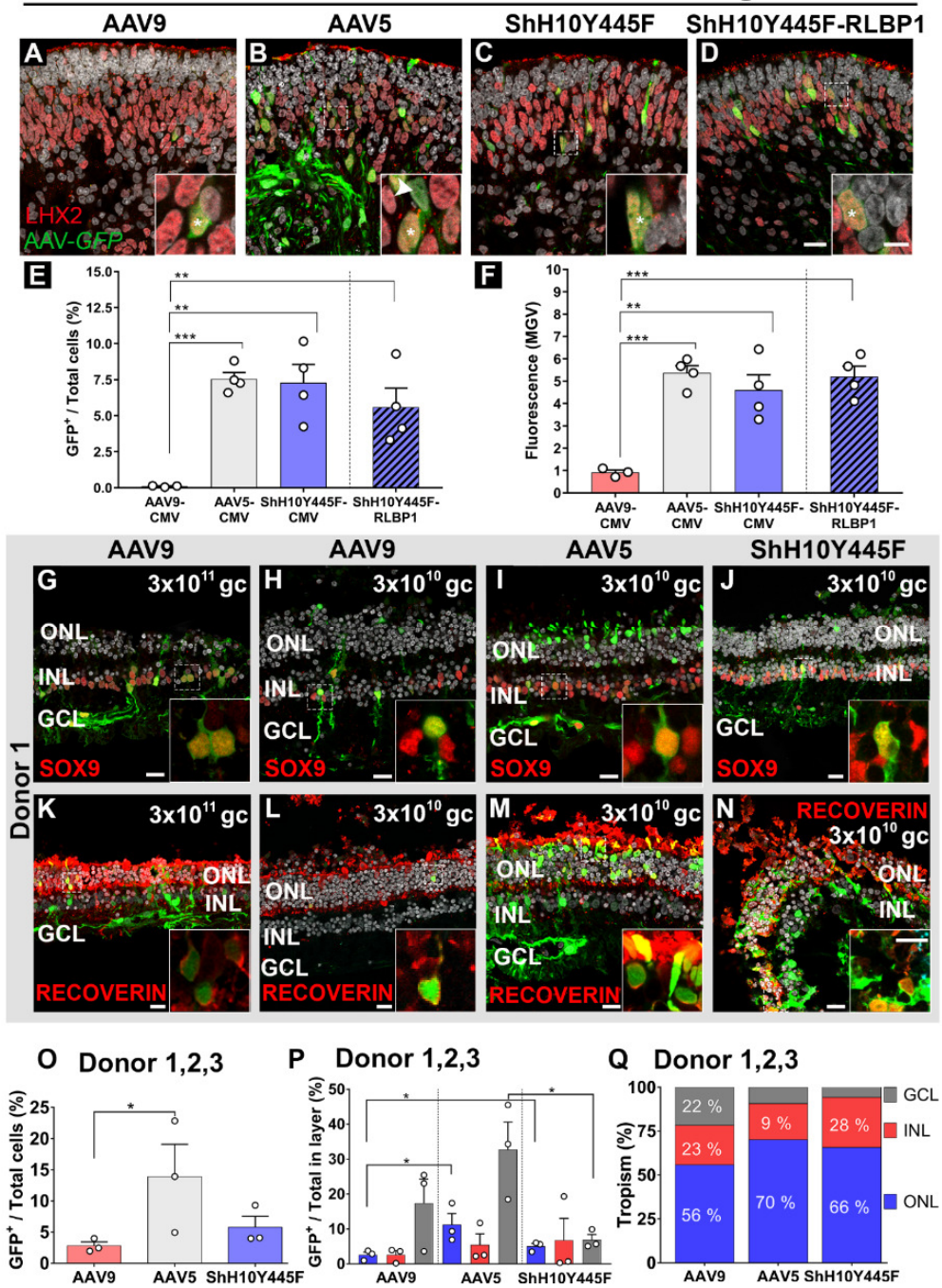


Figure 6. AAV5 and ShH10Y445F efficiently infect Müller glial cells in human iPSC retinal organoids and photoreceptors and Müller glial cells in the human adult retina. Infection of 7.5-month-old LUMC0004iCTRL10 hiPSC retinal organoids at 10^{10} gc with AAV9-CMV-*GFP* (A), AAV5-CMV-*GFP* (B), ShH10Y445F-CMV-*GFP* (C) and ShH10Y445F-RLBP1-*GFP* (D) and co-staining with the Müller glial cell marker LHX2, the majority of LHX2⁺ cells were also GFP⁺ (asterisk). Efficacy of transducing retinal cell types was quantified by measuring the number of GFP⁺ cells in the total cell population (E) and fluorescence (MGV) (F). AAV5 and ShH10Y445F showed the higher efficacy of transducing retinal cell types at 10^{10} gc than AAV9, which showed lower efficacy. 10^{10} gc applied per 2 organoids, two independent differentiations used, 3-4 organoids analysed per vector. Infection of human retinal explants with AAV9-CMV-*GFP* at 3×10^{11} gc (G, K) and 3×10^{10} gc (H, L), AAV5-CMV-*GFP* at 3×10^{10} gc (I, M) and ShH10Y445F-CMV-*GFP* at 3×10^{10} gc (J, N). Co-staining showed the presence of GFP⁺/Sox9⁺ Müller glial cells with AAV9 (G, H), AAV5 (I), and ShH10Y445F (J). Co-staining showed the presence of GFP⁺/recoverin⁺ photoreceptors AAV9 (K, L), AAV5 (M), and ShH10Y445F (N). Efficacy of transducing retinal cell types at 3×10^{10} gc was quantified by measuring the number of GFP⁺ cells in the total cell population (O). When compared for 3 donors at 3×10^{10} gc, AAV5 showed higher efficacy of transducing retinal cell types than AAV9. The potency of AAV serotypes was compared by analysing transduction of cell types in each of the ONL, INL and GCL (P). AAV5 and ShH10Y445F showed higher potency in transduction of photoreceptors in the ONL than AAV9. All serotypes transduced cells in all layers at 3×10^{10} gc (Q). Each dot represents the average of an individual donor (O, P), 10 images were analysed per donor (O-Q) ONL, outer nuclear layer; INL, inner nuclear layer; GCL, ganglion cell layer; gc, genome copies; MGV, mean grey value. Scale bar: (A-N), 20µm; (G-N) inserts 10µm. Data are presented as mean ± SEM. * $p < 0.05$. See also Figure S5, S6 and S7.

Supplementary Figures and Legends

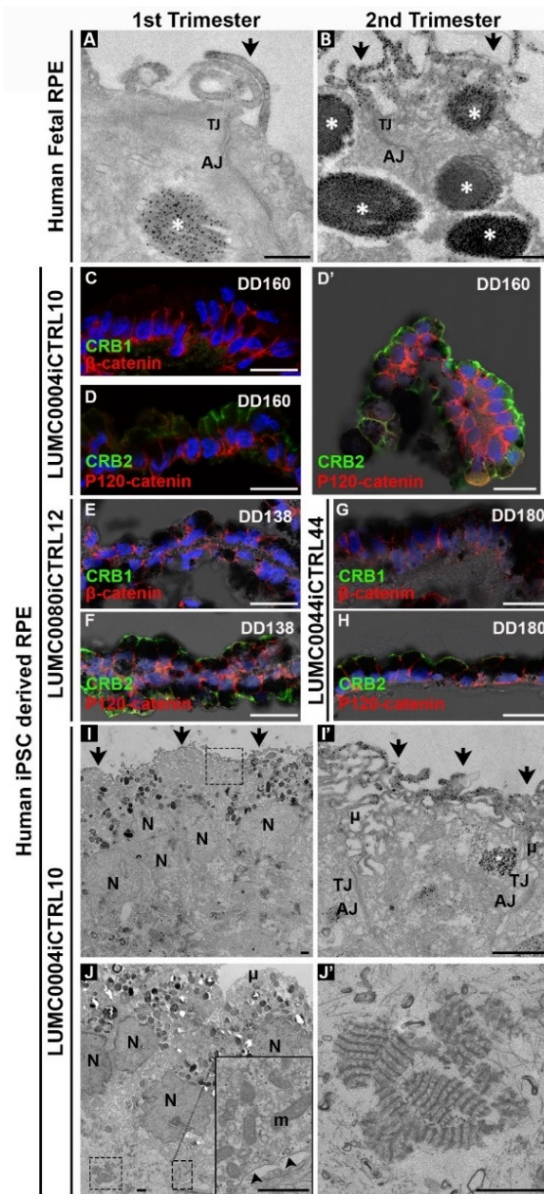


Figure 7. Human iPSC retinal pigment epithelium localise CRB2 at and above tight junctions in the apical membrane and microvilli. Immuno-EM showed staining for CRB2 above adherens junctions at and above tight junctions in the apical membrane and in the microvilli in 1st (A) and 2nd (B) trimester in human fetal RPE. A specific staining was detected within melanosomes (A and B, asterisk). Immunohistochemistry did not detect CRB1 apically of β -catenin (C) in hiPSC RPE, but CRB2 was found apically of p120-catenin in LUMC0004iCTRL10 (D, D'). LUMC0080iCTRL12 (E, F) and LUMC0044iCTRL44 (G, H) human iPSC-derived RPE. RPE spheroids were found either attached to retinal organoids or became independent, detached spheroids (D'). Immuno-EM confirmed apical staining for CRB2 above adherens junctions at and above tight junctions in the apical membrane and in the microvilli (I and I', arrows). Aspecific staining was detected within pigmented melanosomes (I', asterisk). Electron microscopy of hiPSC-derived RPE also showed basally located mitochondria (J, insert) and basement membrane (J, insert arrowheads) and fibrous long-spacing collagen (FLSC) (J and J'). AJ, adherens junction; N, nuclei; μ , microvilli; TJ, tight junction; m, mitochondria. Scale bars: (A, B, B', E, F, G, H) 20 μ m, (C, C', D, D', insert D) 1 μ m.

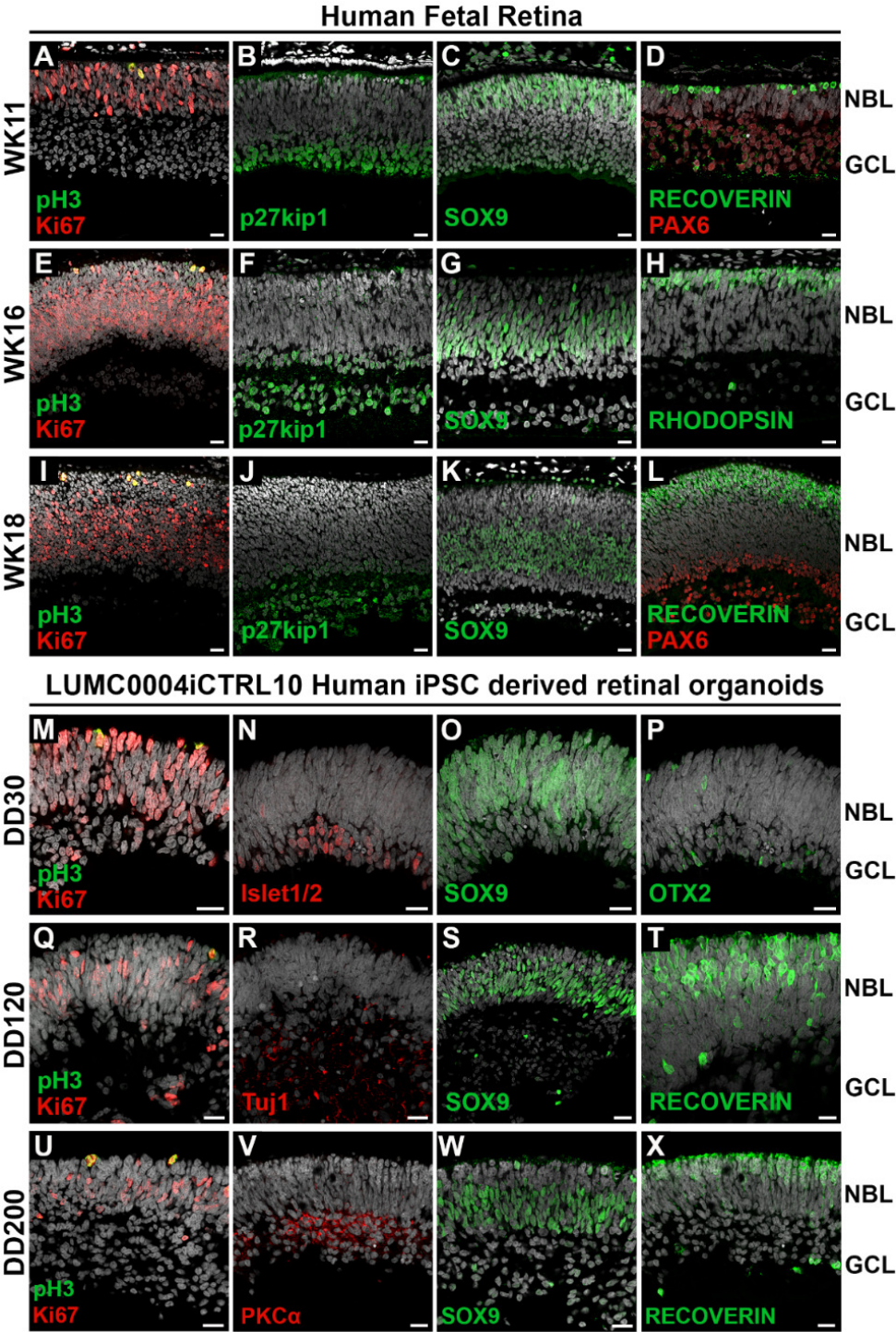


Figure S1. Retinal architecture in the human fetal retina and human iPSC retinal organoids. Related to Figure 1. Immunohistochemistry pictures of WK11 (A-D), WK16 (E-H) and WK18 (I-L) human fetal retina and DD30 (M-P), DD120 (Q-T) and D200 (U-X) LUMC0004iCTRL10 hiPSC-derived retinal organoids. Sections were stained with antibodies against: Ki67 (A, E, I, M, Q, U), pH3 (A, E, I, M, Q, U), p27^{kip1} (B, F, J), SOX9 (C, G, K, O, S, W), Recoverin (D, L, T, X), PAX6 (D, L), Rhodopsin (H), Islet1/2 (N), Tuj1 (R), PKC α (V), OTX2 (P). In human fetal retina at week 11 in the 1st trimester of pregnancy we observed cycling cells that stained positive for anti-Ki67 and spanned the thickness of the neuroblast layer (NBL). The mitotic cells located most apically and stained positive for pH3 (A). Inner retinal cells as marked by p27^{kip1} and PAX6 were restricted to the ganglion cell layer and a subset of cells in the NBL (B and D). The cells that exited the cell cycle were marked with p27^{kip1}, whereas the ganglion cells, amacrine cells and migrating retinal progenitors were marked with PAX6. Radial glial progenitor cell nuclei spanned the thickness of the NBL and stained positive for anti-SOX9 (C). Newborn cone photoreceptors marked positive for anti-recoverin (D (See also Figure S2A and S2B)). In the human fetal retina at weeks 16 and 18 in the 2nd trimester of pregnancy, we observed the localisation of anti-pH3-positive mitotic cells most apically within the NBL (E and I). However, the cycling anti-Ki67-positive cells became mostly restricted to the middle NBL cells but also labelled occasional outer NBL cells (E and I). Both p27^{kip1}- and PAX6-positive cells restricted to the inner NBL and the ganglion cell layer (F, J, L). SOX9-positive cell nuclei localised in the middle NBL and occasionally the outer NBL, marking at this stage of development both the maturing Müller glial cells and radial glial progenitor cells (G (See also Figure S2C)). The outer NBL showed an increase in recoverin-positive photoreceptors at weeks 16 and 18 compared to week 11 (H and L). Rhodopsin-positive staining indicated the presence of rod photoreceptors whose basal processes extended from the outer NBL to the bottom of the inner NBL (H). In early DD30 hiPSC retinal organoids we observed that Ki67-positive cycling cells spanned the thickness of the NBL with pH3-positive mitotic cells located most apically (M). Ki67-positive cycling cells were also detected in the ganglion cell layer (GCL). Islet1/2-positive cells were found mostly restricted to the GCL with sporadic cells in the NBL (Figure 1N). SOX9-positive radial glial progenitor cell nuclei spanned the thickness of the NBL but were also seen occasionally in the GCL (Figure 1O). Immature photoreceptors that stained positive for anti-OTX2 could be found in both the NBL and GCL (Figure 1P). In later DD120 and DD200 hiPSC-derived retinal organoids Ki67-positive cycling cells restricted mostly to the middle NBL but occasionally were detected in the outer NBL and in the GCL, whereas pH3-positive mitotic cells located apically (Q and U). In the inner retina Tuj1-positive ganglion cell axons (R) and PKC α -positive bipolar cells (V) were detected. SOX9-positive cell nuclei became more restricted to the middle NBL but occasionally were detected in the outer NBL and the GCL (S and W (See also Figure S2D)). Recoverin-positive photoreceptor cells were mostly restricted to the outer NBL. Some recoverin-positive cells were detected within the NBL and occasional recoverin-positive cells were detected in the GCL (T and X). At least two independent differentiations/samples were analysed, 3-6 sections examined per organoid or fetal eye. Scale bars: (A-X), 20 μ m.

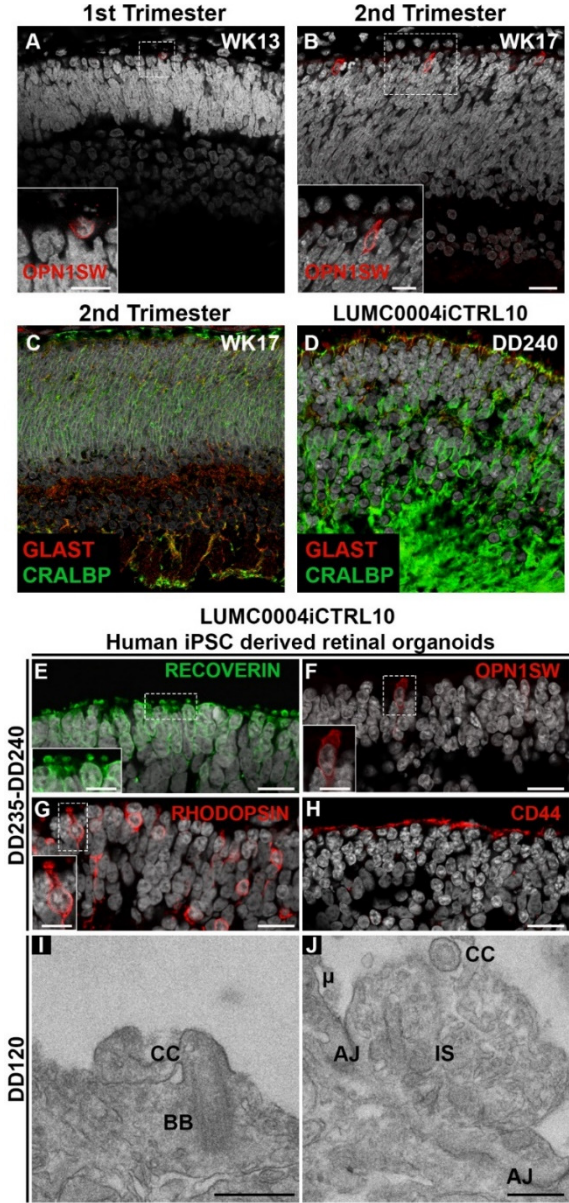


Figure S2. Long-term maturation of fetal retinas and human iPSC retinal organoids. Related to Figures 1 and S1. Immunohistochemistry pictures of 1st and 2nd trimester fetal retina (A-C) and LUMC0004iCTRL10 human iPSC-derived retinal organoids (D-J). Sections were stained for OPN1SW (A, B, F), RLBPI and GLAST (C, D), Recoverin (E), Rhodopsin (G), and CD44 (H). Human fetal retina had cones in the 1st (A) and 2nd trimester (B) and Müller glial cells in the 2nd trimester (D). Immature photoreceptor segments were detected in human iPSC retinal organoid (E) with the presence of both cones (F) and rods (G). Additionally, staining of CRALBP, GLAST and CD44 suggested the presence of Müller glial cells (D, H). Electron microscopy at DD120 confirmed a number of retinal structures including: basal bodies (I), connecting cilium (I,J), inner segment (J), adherens junction (J), microvilli (J). At least two independent differentiations/samples were analysed, 3-6 sections examined per organoid or fetal eye. CC =connecting cilium; IS = inner segment; BB =basal body; AJ =adherens junction; μ= microvilli. Scale bars: (A, B, E, F, G) 10 μm, (I, J) 500nm.

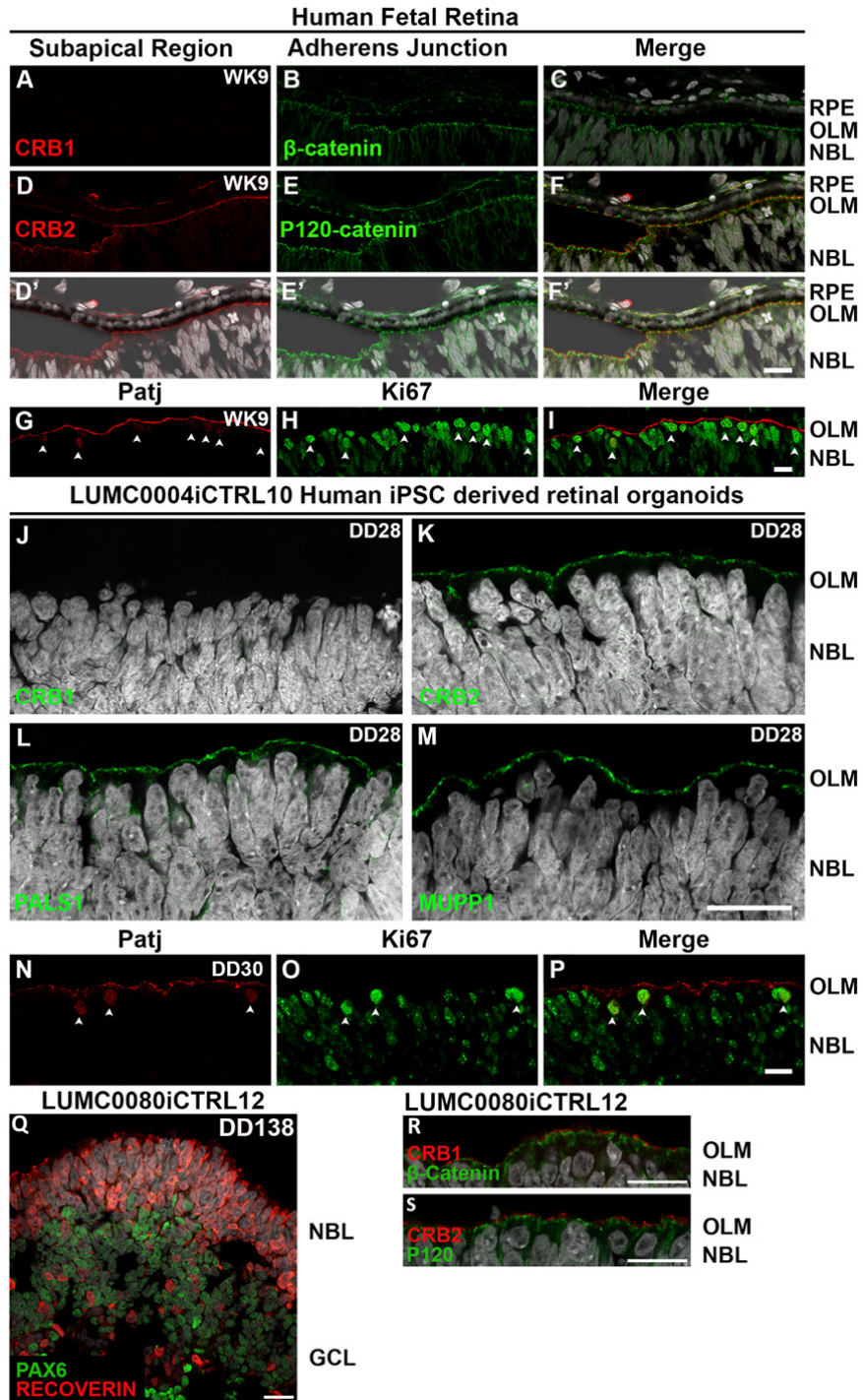


Figure S3. Localisation of CRB complex in the 1st trimester fetal retina and early and late human iPSC retinal organoids. Related to Figure 1, 4 and 5. Immunohistochemistry pictures of week 9 1st Trimester human fetal retina (A-I), DD28 LUMC0004iCTRL10 human iPSC-derived retinal organoids (J-P) and retinal organoids derived from hiPSC lines LUMC0080iCTRL12 (Q, R, S). Sections were stained with antibodies against: CRB1 and β -catenin (A-C), CRB2 and p120-catenin (D-F, D'-F'), PATJ and Ki67 (G-I) in week 9 human fetal retina. Sections were stained with antibodies against: CRB1 (J), CRB2 (K), PALS1 (L), MUPP1 (M), PATJ and Ki67 (N-P) in DD28-30 human iPSC-derived retinal organoids. Sections were stained with antibodies against: Recoverin and PAX6 (Q), CRB1 and β -catenin (R), CRB2 and p120-catenin (S) from retinal organoids derived from hiPSC lines LUMC0080iCTRL12. CRB1 was not found subapically of β -catenin (A-C) but CRB2 was found subapically of p120-catenin (D-F, D'-F') in week 9 human fetal retina. CRB2 was detected in week 9 fetal retinal pigment epithelium (D'-F'). PATJ was observed at the outer limiting membrane and also co-stained a subset of Ki67-positive cells (G-I, arrowheads) in week 9 human fetal retina. In DD28 human iPSC-derived retinal organoids CRB1 was not found at the subapical region (J) but CRB2 (K), PALS1 (L) and MUPP1 (M) were. PATJ also co-stained a subset of Ki67-positive cells in DD28 human iPSC-derived retinal organoids (N-P, arrowheads). Human iPSC lines LUMC0080iCTRL12 formed retinal organoids (Q). CRB1 was found subapically of β -catenin (R) and CRB2 was found subapically of p120-catenin (S). At least two independent differentiations/samples were analysed, 3-6 sections examined per organoid or fetal eye. RPE, retinal pigment epithelium; OLM, outer limiting membrane; NBL, neuroblast layer. Scale bars: 20 μ m (A-S).

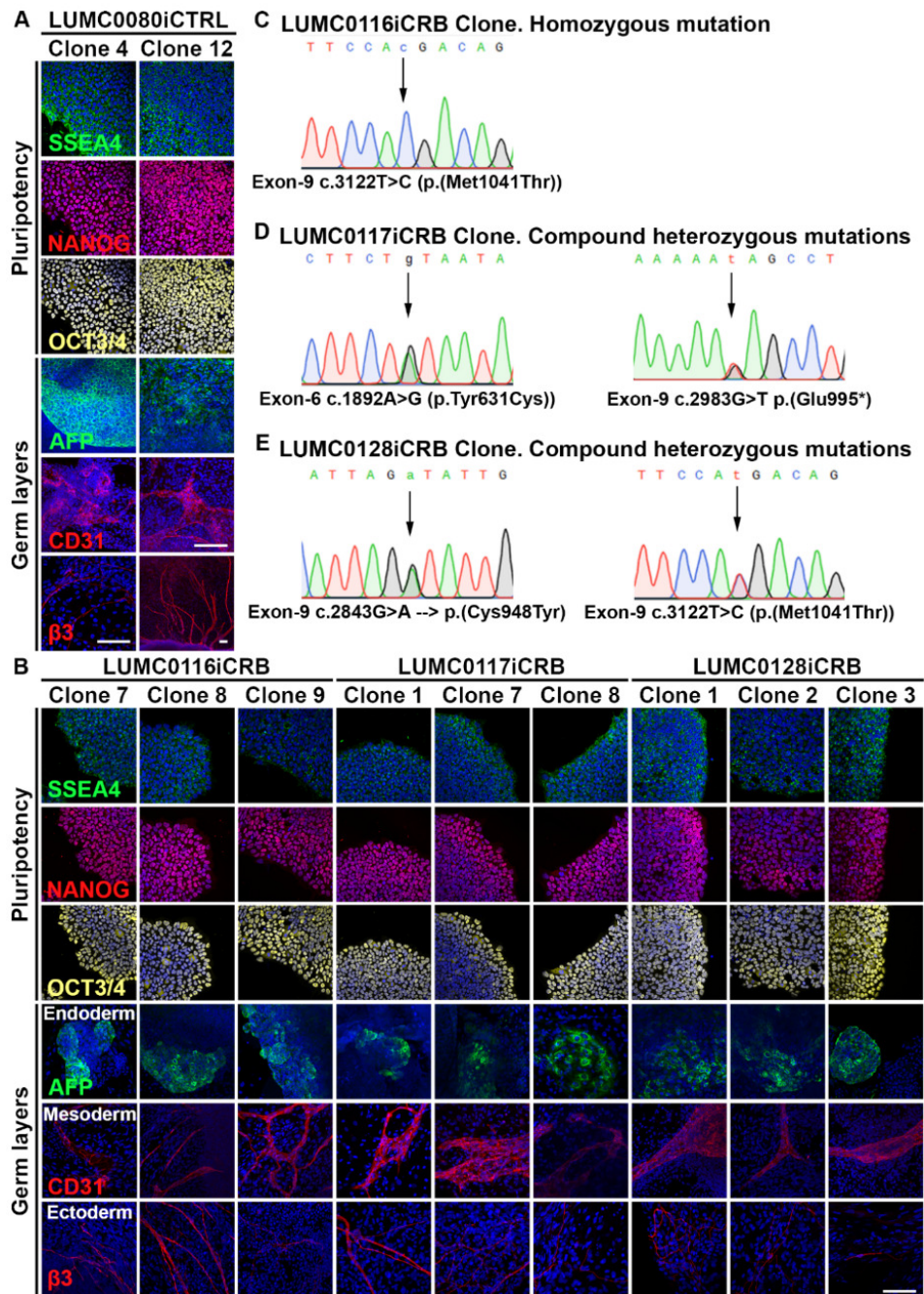


Figure S4. Generation of human iPSC lines of *CRBI*-related retinitis pigmentosa patients. Related to Figures 4 and 5. Immunohistochemistry pictures of the characterization and validation of human iPSCs for pluripotency (SSEA4, NANOG, OCT3/4) and germ layers (AFP, CD31, β 3). LUMC0080iCTRL clones 4 and 12 (A); LUMC0080iCTRL clones 4 and 12 (A); LUMC0116iCRB clones 7, 8, 9 (B); LUMC0117iCRB clones 1, 7, 8 (B); LUMC0128iCRB clones 1, 2, 3 (B). *CRBI* gene exon 6 and 9 was forward and reverse Sanger sequenced for patient lines (LUMC0116iCRB09, C; LUMC0117iCRB01, D; LUMC0128iCRB01, E) and healthy line LUMC0004iCTRL10 (not shown). The mutation in LUMC0116iCRB09 was validated as c.3122T>C (Effect: p(Met1041Thr)) (C). The mutations in LUMC0117iCRB01 was validated as heterozygous mutations with allele 1 being c.1892A>G (Effect: p.Tyr631Cys) and allele 2 being c.2983G>T (Effect: p.(Glu995*)) (D). The mutations in LUMC0128iCRB01 was validated as heterozygous mutations with allele 1 being c.2843G>A (Effect: p.(Cys948Tyr)) and allele 2 being c.3122T>C (Effect: p(Met1041Thr)) (E). All Scale Bars: 20 μ m.

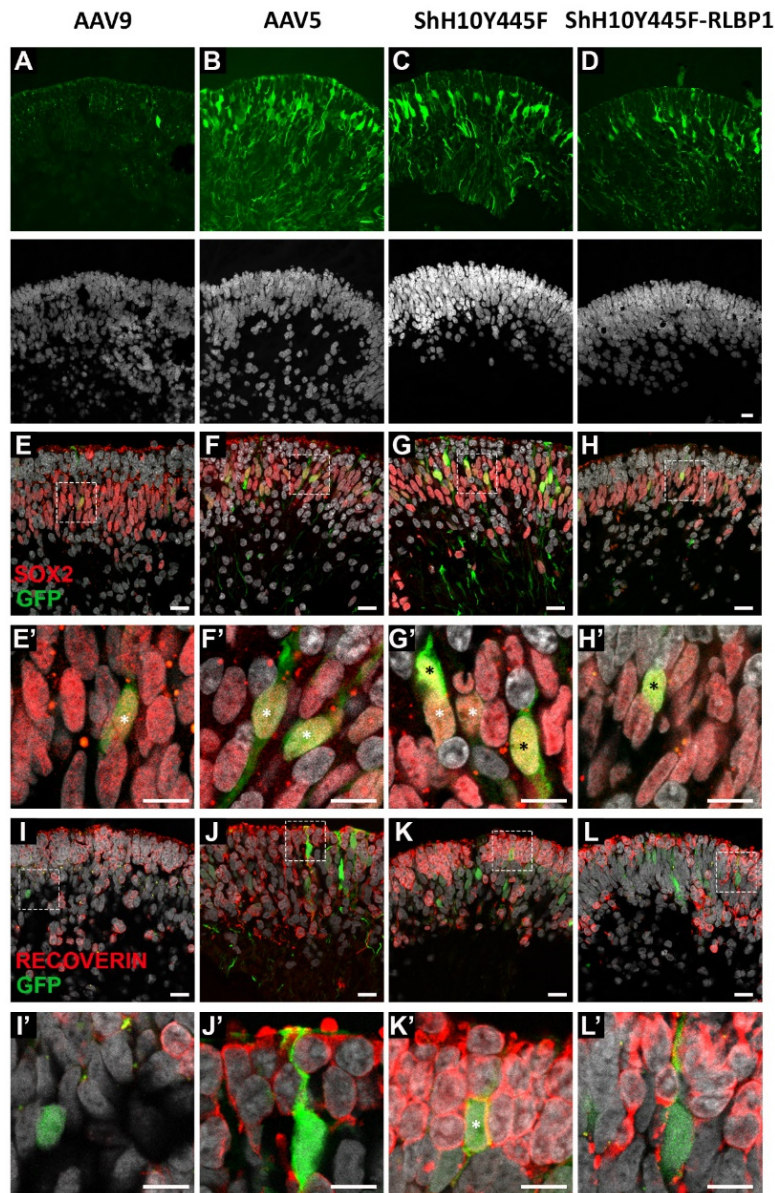


Figure S5. AAV9, AAV5 and ShH10Y445F infect Müller glial cells. Related to Figure 5. Infection of 7.5-month-old LUMC0004iCTRL10 human iPSC-derived retinal organoids at 10^{10} gc with AAV9-CMV-*GFP* (A, E, E', I, I'), AAV5-CMV-*GFP* (B, F, F', J, J'), ShH10Y445F-CMV-*GFP* (C, G, G', K, K') and ShH10Y445F-RLBP1-*GFP* (D, H, H', L, L'). High laser intensity images of AAV9- (A), AAV5- (B), ShH10Y445F-CMV-*GFP* (C) and ShH10Y445F-RLBP1-*GFP* (D). Infection with AAV9- CMV-*GFP*, AAV5- CMV-*GFP*, ShH10Y445F-CMV-*GFP* and ShH10Y445F-RLBP1-*GFP* showed co-staining with Müller glial marker SOX2 (E, F, G, H and inserts E', F', G', H') but not with photoreceptor marker Recoverin (I, J, K, L and inserts I', J', L'). Occasional GFP/recoverin-positive cells were detected (K'). Two independent differentiations of the hiPSC line LUMC0004iCTRL10 were used, 3-6 sections examined per organoid. Scale Bars: 20 μ m (A-L), inserts 10 μ m (E'-L').

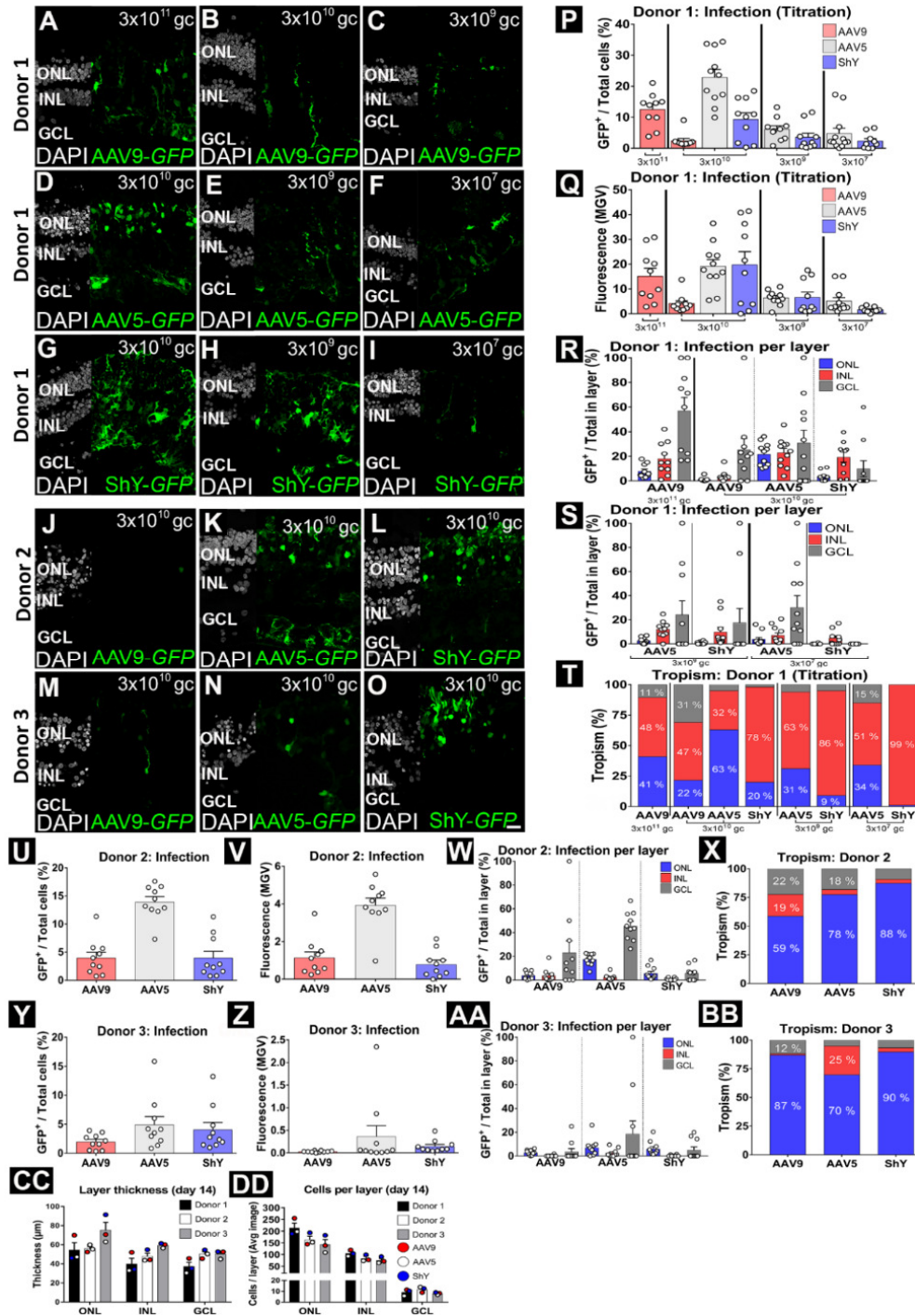
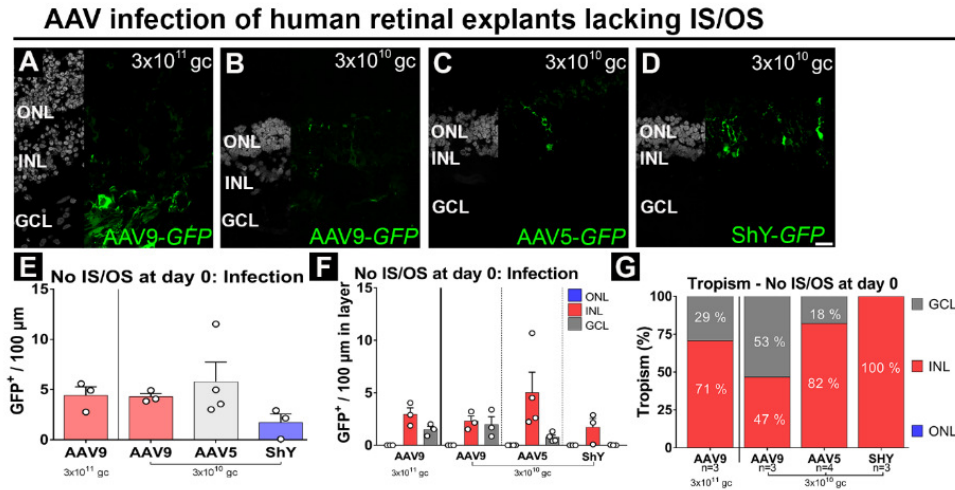


Figure S6. Titration of AAV serotypes on human donor 1 retina and independent repeats on donor 2 and 3. Related to Figure 6. Transduction of AAV9- (A-C, J, M), AAV5- (D-F, K, N) and ShH10Y445F (G-I, L, O) on human adult donor retina at 3×10^{11} gc (A), 3×10^{10} gc (B, D, G, J-O), 3×10^9 gc (C, E, H), 3×10^7 gc (F, I). AAV infection by total GFP-positive cells / Total cells infected for donor 1 (P). Infection measured by GFP-fluorescence for donor 1 (Q). GFP-positive cells per total cells in layer for donor 1 (R, S). Tropism: GFP-positive cells in layer per Total GFP-positive cells for donor 1 (T). Human adult donor retina 2 (J-L) and 3 (M-O). AAV potency measured by total GFP-positive cells / Total cells infected for donor 2 (U) and 3 (Y). Infection measured by GFP-fluorescence for donor 2 (V) and 3 (Z). GFP-positive cells per total cells in layer for donor 2 & 3 (W, AA). Tropism (GFP-positive cells in layer per Total GFP-positive cells) for donor 2 and 3 (X, BB). Retinal thickness between donors 1-to-3 at day 14 in culture (CC). Cells per layer in averaged image (DD). Each dot represents an individual image (P-BB). 90 images analysed donor 1, 30 images analysed donors 2 and 3 (CC and DD). ShY, ShH10Y445F; ONL, outer nuclear layer; INL, inner nuclear layer; GCL, ganglion cell layer; gc, genome copies. Scale bar: $20 \mu\text{m}$ (A-O). Data are presented as mean \pm SEM.



LUMC0004iCTRL10 Human iPSC derived retinal pigment epithelium

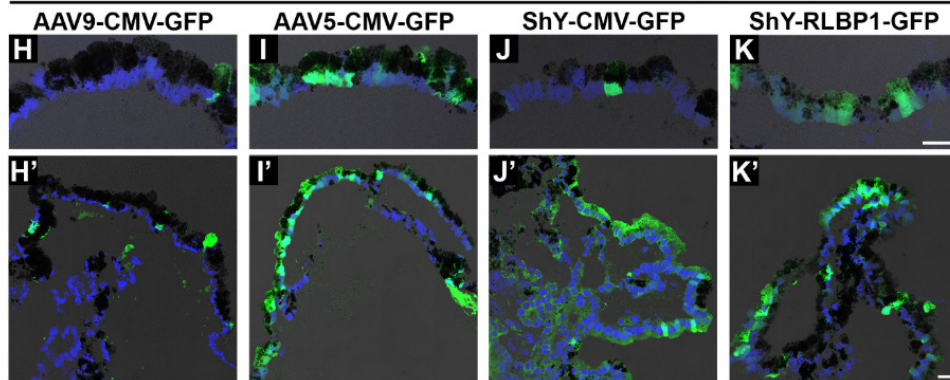


Figure S7. Human retinal explants lacking outer segments show no photoreceptor transduction. Related to Figure 6. Infection of human retinal explants missing outer segments with AAV9-CMV-GFP at 3×10^{11} gc (A) and 3×10^{10} gc (B), AAV5-CMV-GFP at 3×10^{10} gc (C) and ShH10Y445F-CMV-GFP at 3×10^{10} gc (D). Efficacy of transduction of retinal cell types was quantified by measuring the number of GFP-positive cells per 100 μm retinal length (E). GFP-positive cells per 100 μm retinal length in each layer (F). INL cells were mostly infected, and no photoreceptors were transduced by AAV9, AAV5 or ShH10Y445F (G). AAV9 at 3×10^{10} gc, 3×10^{11} gc and AAV5 at 3×10^{10} gc showed infection in the GCL. DAPI=grey. AAV-GFP=green. Each dot represents an individual donor (E, F), 10 images were analysed per donor (E-G). AAVs infect human iPSC derived retinal pigment epithelium. Related to Figure 7. LUMC0004iCTRL10 human derived retinal pigment epithelium is transduced at 10^{10} gc by AAV9-CMV-GFP (H, H'), AAV5-CMV-GFP (I, I'), ShH10Y445F-CMV-GFP (J, J') and ShH10Y445F-RLBP1-GFP (K, K'). DAPI=blue. Pigment=black. AAV-GFP=green. ShY, ShH10Y445F; ONL, outer nuclear layer; INL, inner nuclear layer; GCL, ganglion cell layer; gc, genome copies. Scale bar: (A-D, H-K, H'-K'), $20 \mu\text{m}$. Data are presented as mean \pm SEM.

Table S1. Antibody list and dilution used for immunohistochemistry and EM. Related to All Figures.

Antibody	Dilution	Manufacture	Catalogue Numbers
pH3	1:100	Millipore	06-570
Ki67	1:100	BD Biosciences	550609
p27kip1	1:200	Millipore	06-445
SOX9	1:250	Millipore	AB5535
Recoverin	1:500	Millipore	AB5585
Rhodopsin	1:500	Millipore	MAB5356
PAX6	1:100	DSHB	AB_528427
Islet1/2	1:200	DSHB	AB_2314683
Tuj1	1:200	Biologend	801201
PKCa	1:250	BD Biosciences	610107
OTX2	1:200	Proteintech Europe	13497-1-AP
CRB1 AK2	1:200	Homemade	N/A
CRB2 EP13	1:200	gift from Pen Rashbass	N/A
CRB2 SK11	1:200	gift from Pen Rashbass	N/A
PALS1 SN47	1:200	Homemade	N/A
PAR3	1:100	Millipore	07-330
MUPP1	1:200	BD Biosciences	M98820
β-catenin	1:200	BD Biosciences	610153
p120-catenin	1:200	BD Biosciences	610134
N-Cadherin	1:250	BD Biosciences	610920
LHX2	1:200	Santa Cruz	sc-19344
peanut agglutinin (PNA)	1:200	Vector Lab	RL-1072
CD44	1:400	BD Biosciences	553132
PATJ	1:200	gift from André Le Bivic	N/A
SOX2	1:200	Santa Cruz	sc-17319
EAAT1 (GLAST)	1:100	Abcam	ab416
CRALBP	1:200	Abcam	ab15051
OPN1SW	1:200	Millipore	AB5407

Supplemental Experimental Procedures

Fetal human retinal tissue

Human fetal eyes at gestational age week 9 to 19 were collected from elective abortion material (vacuum aspiration) without medical indication, with signed informed consent and provided anonymised. In this study, “weeks of gestation” was used as determined by the last menstrual period (LMP).

Adult human retinal tissue

Patient anonymity was strictly maintained. All tissue samples were handled in a coded fashion, according to Dutch national ethical guidelines (Code for Proper Secondary Use of Human Tissue, Dutch Federation of Medical Scientific Societies). Post-mortem adult human

donor eye (from 56 to 88 years-old donors) were acquired within the LUMC and were processed within 24 hours after death.

Cell Culture and Retinal Organoid Differentiation

Three healthy lines (LUMC0004iCTRL10, LUMC0044iCTRL44, LUMC0080i CTRL12) and three male *CRB1* RP patient lines (LUMC0116iCRB09, LUMC0117iCRB01, LUMC0128iCRB01) were derived from skin fibroblast using polycistronic Lentiviral vectors [1]. The *CRB1* RP patient line LUMC0117iCRB01 also had the variant c.1892A>G (p.(His631Arg)) in the *RPGRIP1* gene, which was classified as a variant of unknown significance.

In brief, human iPSCs were collected and incubated with (\pm)blebbistatin in mTeSR medium overnight and transitioned from mTeSR/NIM-1 (3:1), to (1:1), and to (0:1) over the subsequent three days to form Embryoid Bodies (EBs) in floating culture. Floating EBs were plated onto Matrigel-coated wells from differentiation day (DD) 7 till DD28, with a change from NIM-1 to NIM-2 medium at DD16. At DD28 neuroepithelial rosettes are flushed loose from the matrigel using a P1000 pipet and are kept in floating culture in agarose coated plates from this point onwards. NIM-2 is used till DD41, RLM is used from DD42 to DD48, RLM-1 from DD49 to DD97, and RLM-2 from DD98 for long-term culture. Medium is changed as required, typically every other day from DD3 till DD33 and typically twice a week from DD41 onwards. Plates were checked for possible medium changes every other day. Neural Induction Medium 1 (NIM-1): 48.95 mL DMEM/F12 supplemented with 0.5 mL 100x N2 supplement, 0.5 mL 100x Minimum Essential Media-Non Essential Amino Acids (MEM NEAAs), 10 μ L 10 mg/mL Heparin (Sigma). Neuronal Induction Medium 2 (NIM-2): 96 mL DMEM/F12 (3:1) supplemented with 2 mL 50x B27 Supplement, 1 mL 100x NEAA, 1 mL 100x antibiotic-antimycotic (10,000 units/mL of penicillin, 10,000 μ g/mL of streptomycin, 25 μ g/mL of amphotericin B). Retinal Lamination Medium (RLM): 107.25 mL DMEM/F12 (3:1) supplemented with 12.5 mL embryonic stem cell-qualified FBS, 2.5 mL 50x B27 Supplement, 1.25 mL 100x MEM NEAAs, 1.25 mL 100x antibiotic-antimycotic (10,000 units/mL of penicillin, 10,000 μ g/mL of streptomycin, 25 μ g/mL of Amphotericin B), 0.25 mL taurine (100 μ M final concentration). Retinal Lamination Medium 1 (RLM-1): RLM supplemented with 0.1 μ L 10 mM retinoic acid (1 μ M final concentration) per mL. Retinal Lamination Medium 2 (RLM-2): RLM supplemented with 0.05 μ L 10 mM retinoic acid (0.5 μ M final concentration) per mL.

Sequence validation on patient mutations in the *CRB1* gene

DNA of retinal cells were extracted with the DNeasy Blood & Tissue Kit (QIAGEN) from *CRB1* RP patient retinal organoids (LUMC0116iCRB09, LUMC0117iCRB01, LUMC0128iCRB01). Exon 6 was PCR amplified (Forward primer: TTTGAGGGCGATGGCTTCCT. Reverse primer: TGAGGCATGGCACTCCTAGC).

Exon 9 was PCR amplified (Forward primer: TGAACAAAATTACTTAAATTCTG TGAG. Reverse primer: TCCTCCATGCAAACAGGGGT). The samples were then purified (QIAquick PCR Purification) and then Sanger sequenced. Exon 6 was Sanger sequenced in forward and reverse direction:

Forward primer: TAATCAGTCAAAGGTGCTTCTGTT

Reverse primer: CTCTCAGACAGTTGGGGCCT

Exon 9 was sequenced in forward and reverse direction:

Forward primer: TGAACAAAATTACTTAAATTCTGTGAG

Reverse primer: TGACTTAGACACCCTTGACG)

The electropherograms were analysed in Snapgene Viewer (Version 3.2) and aligned to Exon 6 and Exon 9 extracted from the *CRB* gene region chromosome 1: 197,268,278-197,478,455 (ENSG00000134376 GRCh38).

Immunohistochemical analysis

Adult human donor retina, human fetal retina, hiPSC-derived retinal organoids were incubated for 30 minutes in 4% paraformaldehyde in PBS for fixation and 15% and then 30% sucrose in PBS for cryo-protection. Finally, retina were orientated, embedded in Tissue-Tek, frozen and stored at -20°C. Sections of 8-10 µm were made with a Leica CM1900 cryostat (Leica Microsystems). Sections for immunohistochemistry were blocked for 1 hour in 10% normal goat serum, 0.4% Triton X-100 and 1% bovine serum albumin (BSA) in PBS, incubated in a moist-chamber overnight at 4°C (Table S1) diluted in 0.3% normal goat serum, 0.4% Triton X-100 and 1% BSA in PBS. After rinsing in PBS, the sections were incubated for 1 hour with complementary conjugated secondary antibodies (Table 1) and rinsed in PBS again. Sections were mounted in Vectashield HardSet DAPI mounting media (Vector Laboratories). A Leica TCS SP8 confocal microscope were used for Image acquisition. Image analysis and processing were carried out using ImageJ and Adobe Photoshop CC2014, respectively.

Electron microscopy

In brief, 40 µm thick sections were incubated with the appropriate first antibody for 48 h (Table 1), then incubated with appropriate secondary (anti-Rabbit or anti-Mouse) peroxidase anti-peroxidase (PAP) for 2h, then developed in a 2,2-diaminobenzidine solution containing 0.03% H₂O₂ for 4 min and then the gold substitute silver peroxidase method applied. Sections were embedded in epoxy resin, ultrathin sections made and examined with an electron microscope (Microscope: FEI Tecnai T12 Twin Fei Company, Eindhoven, The Netherlands; Camera: OneView, Gatan) operating at 120 kV. Overlapping images were collected and stitched together into separate images as previously described [2]. At least two independent

samples were analysed per time point for human fetal eyes and human iPSC-derived retinal organoids and RPE.

Generation and purification of the viral vectors

Briefly, pAAV2-*eGFP* plasmids were co-transfected with the pHelper and pAAV9, pXX2-ShH10Y445F, or pDP5rs capsid plasmid into HEK293T cells to generate AAV9, ShH10Y445F or AAV5 viral particles. After benzonase treatment, the lysates were ultracentrifuged onto an iodixanol density gradient and concentrated on Amplicon spin columns (100 kDa, Millipore). All viral titers were determined by quantitative PCR and all viral stocks with titers around 1×10^{13} genome copies per ml were stored at -80°C .

In vitro transduction of human donor retina and human induced pluripotent stem cell derived retinal organoids

1) In brief, 3-6 6 mm punches of human donor retina were dissected in cold HBSS (Sigma) within 24 hours after death. Whatman™ paper was placed on the ganglion cell side of each punch. Punches were then placed, photoreceptor side down, on Millicell Cell culture Inserts (Millipore, PICM01250) and placed into a 24 well plate with 300 μL of explant medium per well. After that, 50 μL of explant medium with the desired titre of a viral vector (3×10^7 , 3×10^9 , 3×10^{10} or 3×10^{11} gc) was added to Whatman™ paper for 48 hours, and medium changed every other day until day 14. Explant medium: 300 μL 50X B-27 Supplement (Invitrogen), 150 μL 100X N-2 Supplement (Invitrogen), 30 μL 50 mM Taurine, 120 μL 200 mM L-glutamine, 150 μL 100 mM sodium pyruvate, 18.45 μL 1 mM N-Acetyl-L-cysteine, 150 μL 100X antibiotic-antimycotic (10,000 units/mL penicillin, 10,000 $\mu\text{g}/\text{mL}$ streptomycin, 25 $\mu\text{g}/\text{mL}$ Amphotericin B) in a final volume of 15 mL Neurobasal®-A medium (Invitrogen). 2) In brief, two retinal organoids were placed in 1%-agarose coated wells of a 96-well plate, and 50 μL of RLM-2 containing the 10^{10} gc of the AAV vector was added for 24 hours. A further 50 μL of RLM-2 only was added to the well for another 24 hours. The organoids were washed three times in PBS and replated in RLM-2 in a 24-well plate. The medium was then changed twice a week for 14 days post infection. Tissues were fixed, cryo-protected and frozen for further processing as described in: Immunohistochemical analysis.

Quantitative analysis of GFP fluorescence intensity and cell number

Quantitative analysis of GFP expression allowed for assessment of both AAV potency and tropism in human donor retina and hiPSC-derived retinal organoids. For the quantitative analysis of GFP expression, images were taken using a Leica TCS SP8 confocal microscope (Leica). Images were obtained at 40x magnification using identical acquisition settings, including laser intensity, and were saved at a resolution of 1024x1024 pixels. GFP expression profiles were measure in three ways: 1) GFP positive cells per total cells, 2) Mean grey value (Transduction profiles were analyzed by defining a region of interest (ROI) for the outer

nuclear layer, inner nuclear layer and ganglion cell layer for human donor material and a top nuclear layer and bottom nuclear layer for the hiPSC-derived retinal organoids), and 3) GFP-positive cells in layer per cells in layer. Tropism was measured as GFP-positive cells in layer (ONL, INL or GCL/Nerve Fiber Layer) per total GFP-positive cells. The Cell Counter plugin for ImageJ was used to quantify total cell number (counterstain: DAPI, LHX2, and SOX2) and total GFP positive cell number for each ROI. The number of GFP positive cells for each ROI was divided by the total number of cells for each ROI to obtain the percentage of transduced cells. Fluorescence images were also analysed by calculating the mean grey value (MGV), corrected for area and background levels of fluorescence, for each ROI using ImageJ software. 6-mm harvested retinal explant punches were sectioned at 90 degree angle [3]. This allows to assess the AAV transfection on the whole retina stretch of 6-mm retinal explant punch. Edges or otherwise damaged areas were not used for image acquisition. Between 3-6 different sections from at least three different human donor retina or hiPSC-derived retinal organoids were used for quantification of mean grey value or cell counting's (>900 μm in retinal length. 3-5 images per organoid and 10 images for adult donor retina).

Supplemental References

1. Warlich, E.; Kuehle, J.; Cantz, T.; Brugman, M.H.; Maetzig, T.; Galla, M.; Filipczyk, A.A.; Halle, S.; Klump, H.; Schöler, H.R.; et al. Lentiviral vector design and imaging approaches to visualize the early stages of cellular reprogramming. *Mol. Ther.* **2011**, *19*, 782–789.
2. Faas, F.G.A.; Cristina Avramut, M.; van den Berg, B.M.; Mieke Mommaas, A.; Koster, A.J.; Ravelli, R.B.G. Virtual nanoscopy: Generation of ultra-large high resolution electron microscopy maps. *J. Cell Biol.* **2012**, *198*, 457–469.
3. Buck, T.M.; Pellissier, L.P.; Vos, R.M.; van Dijk, E.H.C.C.; Boon, C.J.F.; Wijnholds, J. AAV serotype testing on cultured human donor retinal explants. In *Methods in Molecular Biology*; Boon, C.J.F., Wijnholds, J., Eds.; New York, NY: Humana Press: New York, NY, 2018; Vol. 1715, p. pp 275-288 ISBN 978-1-4939-7522-8.

Chapter 5

CRB1 is required for the recruitment of NOTCH1 and proper recycling by RAB11A+ vesicles in human retinal organoids

Thilo M. Buck, Peter M.J. Quinn, Lucie P. Pellissier, Aat A. Mulder, Aldo Jongejan, Daniëlle, Koot, Hind Almushattat, Christiaan H. Arendzen, Rogier M. Vos, Edward J. Bradley, Christian Freund, Harald M.M. Mikkers, Camiel J.F. Boon, Perry D. Moerland, Frank Baas, Abraham J. Koster, Jacques Neefjes, Ilana Berlin, Carolina R. Jost, Jan Wijnholds.

Submitted

Abstract

Mutations in the *CRB1* gene are a leading cause of monogenetic early-onset blindness in children. Recapitulating human *CRB1* phenotypes in animal models has proven challenging; necessitating the development of alternatives. We have generated human iPSC-derived retinal organoids of patients with retinitis pigmentosa caused by biallelic *CRB1* mutations and evaluated them against autologous gene-corrected hiPSCs and hiPSCs from healthy individuals. We find that patient organoids suffer loss of cell adhesion, photoreceptors and CRB1 & NOTCH1 expression. Using a proximity ligation assay, we show that CRB1 and NOTCH1 can interact on the extracellular domain. *CRB1* patient organoids also feature large EEA1- and WDFY1-positive vesicles, fewer RAB11A+ recycling endosomes and more degradative endolysosomal compartments relative to their normal counterparts. Taken together, our data demonstrate that patient-derived retinal organoids enable modelling of retinal degeneration and highlights the importance of CRB1 in early endosome maturation receptor recycling in the neuroretina.

Introduction

In mammals, the Crumbs (CRB) protein family consists of CRB1, CRB2, and CRB3A, the latter lacking a large extracellular domain [1]. Mutations in the *CRB1* gene are responsible for retinal diseases such as retinitis pigmentosa (RP), Leber congenital amaurosis (LCA) and macular dystrophy [2–6]. Cell adhesion and cell polarity protein complexes at the retinal outer limiting membrane (OLM), such as adherens junctions and CRB complexes play a critical role in the proliferation of retinal progenitor cells (RPCs) [7,8] as well as in cell adhesion [9–11]. The CRB complex is located at the subapical region adjacent to the adherens junctions between RPCs in the developing retina and at the subapical regions of Müller glial cells (MGCs), photoreceptor cells (PRCs), PRCs-PRCs, and PRCs-MGCs [10,12,13]. Retinal cell generation and retinal maturation in the mouse occurs from embryonic day (E) 11 to postnatal day (P) 10. In humans, the same process takes place from fetal gestation week 14 to the first year of life in men [14] and early retinal development can be mimicked in human induced pluripotent stem cell (hiPSC)-derived retinal organoids [12].

We have previously described that the CRB protein levels at the apical membrane in PRCs and MGCs are a major determinant of the severity of the retinal phenotype in *Crb1*^{KO} and *Crb1*^{KO}*Crb2*^{cKO} (cKO, conditional knockout) mice compared to controls [7–11,15,16]. Interestingly, only knocking out *Crb1* [10,11] or expressing a variant *Crb1* (natural occurring *Crb1*^{rd8}) in mice [17] or rat [18,19] did not result in an early developmental phenotype as seen in LCA-*CRB1* patients [2,20], pointing to interspecies differences. Such discrepancy may be due to the restriction of murine *Crb1* protein expression to MGCs, while human and non-human-primate CRB1 is expressed in both PRCs and MGCs [12,13,21]. In contrast to CRB1, CRB2 protein is present in PRCs as well as MGCs in both species [9]. Finally, little is known about expression or localization of proteins harbouring disease-causing amino-acid variations in CRB1. Previous mouse and fruit fly studies have identified *Crb* variant-related gain-/loss-of-function phenotypes [22,23]. We showed that the RP *CRB1* patient-derived retinal organoids expressing different variant CRB1 proteins (*CRB1*^{M1041T/ M1041T}; *CRB1*^{Y631C/E995*}; *CRB1*^{M1041T/C948Y}) have little cell polarity and cell adhesion markers at differentiation day (DD) 180, permitting local displacement of photoreceptor cell columns [12]. Loss of apical polarity has been previously linked to the dysregulation of the endolysosomal system [24–27]. The membrane vesicle trafficking system has been associated with many diseases but, to our knowledge, has not been studied in detail in human retinal organoids.

Numerous reports have previously demonstrated a link between loss of the CRB complex and activation of the Notch signal pathway [7,28,29]. We specifically focused on NOTCH1 because it regulates the retinal progenitor cells (RPCs) population and the differentiation of RPCs into early-born cone PRCs and late-born rod PRCs in mice [30–34]. Additionally, a direct interaction between extracellular domains (ECD) of the Notch-Crb was observed in

fruit fly and zebrafish models. The ECD of Crb in fruit fly or Crumbs2 in zebrafish stabilizes the Notch receptor at the apical membrane [26,35–37]. Furthermore, *Drosophila* Crb mutant protein (*crb*^{P13A9}) decreases Notch receptor localization at the plasma membrane, increases Notch intracellular domain (ICD) concentrations which activates the Notch pathway, and expands the number of lysosomes in rhabdomeres (a cluster of PRCs & support cells in flies) compared to controls [27].

In the present study, we first gather target genes governing the molecular mechanisms of the *CRB1* LCA-like phenotype in mice. We identify *Wdfy-1*, an overexpressed gene in the *CRB1* LCA-like mouse model, pointing to a misregulation of early endosomes [38]. We follow up on the endolysosomal system in human retinal organoids. First, we generate isogenic controls for patient hiPSCs and validate the evolution of the human RP-*CRB1* phenotype in retinal organoids over time (DD90, 120, 150 and 180). We find a strong decrease of apical CRB1 variant & apical NOTCH1 proteins with a concomitant loss of photoreceptor cells at DD180. We then backtrace how the loss of CRB1 variant proteins appear by investigating the trafficking and degradation of CRB1 proteins. We find that the loss of CRB1 variant protein coincides with a repression of the maturation of early endosomes (EE) shown by an increase of WDFY1 and EEA1 in EE, a reduction of RAB11A+ recycling endosomes, and an increase in degradative endolysosomal compartments in patient organoids. This study suggests that (a) CRB1 is involved in EE/recycling endosome maturation and (b) patients with the common RP *CRB1*-associated mutations (*CRB1*^{Met1041Thr}; *CRB1*^{Cys948Tyr}) have little CRB1 in the neuroretina thus potentially benefiting from a gene supplementation therapy.

Results

Deletion of Crb1 and Crb2 in the developing mouse neuronal retina reveals molecular defect at the endolysosomal system using RNAseq data

To identify the developmental degradative molecular mechanisms in the neural retina lacking CRB1 and CRB2, we first examined the mouse phenotype of *Crb1*^{KO} (*Crb1*^{KO}*Crb2*^{Flox/Flox}) and *Crb1*^{KO}*Crb2*^{ARPC} conditional knockout (cKO) mice backcrossed into 100% C57BL/JOlaHsd. In agreement with previous findings on mixed genetic background [7], we show in *Crb1*^{KO}*Crb2*^{ARPC} mice at embryonic day 15.5 (E15.5), E17.5, postnatal day 1 (P1), 1 month (1M), 3M, 6M and 12M that CRB1 and CRB2 are essential for proper retinal development preventing disturbed retinal layering and loss of retinal function (Figure 1 A-B; Figure S1 and Figure S2). Of note, the 100% C57BL6/JOlaHsd genetic background against the 50% background show a slightly milder retinal phenotype at foci (Figure 1 C; Figure S1). Some regions in the retina mimic the previously described *Crb1*^{WT/KO}*Crb2*^{ARPC} cKO retinal phenotype, whereas other regions mimic the more severely affected *Crb1*^{KO}*Crb2*^{ARPC} retina on mixed genetic background [7]. The severity of the phenotype was still comparable to the mixed genetic background, considering retinal cell loss measured by retinal thickness (Figure S2 H) and the loss of the retinal response to light flashes measured by ERGs (Figure S2 I-K)

in 1-M-old mice [7]. Previous studies on developing *Crb1*^{KO}*Crb2*^{ARPC} retinas (<P1) on mixed genetic background showed a transiently thicker retina with an increased number and mislocalization of late-born cells (rod PRCs, bipolar cells, MGCs, late-born amacrine cells), increased cell proliferation and apoptosis, dysregulation of the cell cycle, which severely impairs retinal function in adult mice. It has been speculated that CRB1 and CRB2 suppress the cell proliferation of retinal progenitors by regulation of mitogenic signalling pathways such as Notch, YAP and Sonic Hedgehog [7]. We also found an upregulation of mitotic cells (pH3+ cells) at P1 and P5 (Figure 1 F) indicative of an increase in cell proliferation on the 100% C57BL/6JOLA^{Hsd} background.

We, therefore, performed RNAseq on mouse neuroretina to gain insights into these developmental changes at the transcriptional level. A comparison between *Crb1*^{KO}*Crb2*^{ARPC} and *Crb1*^{KO} retina, at E15.5, or E17.5, or P1 on 100% C57BL/6JOLA^{Hsd}, yielded only subtle persistent changes at the transcriptional level over time (Figure 1 G-I, respectively), despite significant differences in morphology. As internal positive control at E15.5, E17.5 and P1 we used ATP-binding cassette, sub-family D (ALD), member 4 (*Abcd4*), which is substantially upregulated in mouse retina expressing the *Cre* recombinase fused to the *Chx10* promoter, with the *Abcd4* gene immediately adjacent to the *Chx10Cre* locus in the mouse genome. The *Abcd4* expression and other genes were also validated by qPCR at P1 (Figure S2 L).

To further examine potential transcriptional changes at E15.5, we compared *Crb1*^{KO}*Crb2*^{ARPC} mice in 100% C57BL/6JOLA^{Hsd} genetic background against wild type C57BL/6JR^c^{Hsd} mice. In this setting, we observed 40 differentially expressed genes (DEGs) compared to the previously 0 DEGs (E15.5; adj. p-val < 0.01 & log₂FC > 1.5. See also Table S4). The *Crb1*^{KO}*Crb2*^{ARPC} mice on C57BL/6JOLA^{Hsd} genetic background, due to mutations in the synuclein alpha (*Snca*), multimerin-1 (*Mmrn1*), and *Crb1* gene, do not express *Snca*, *Mmrn1*, or *Crb1* gene transcripts, and express high levels of *Abcd4* due to the adjacent *Chx10Cre* transgene on chromosome 6. We made use of all 4 genes as negative and positive controls in the gene expression profiling, since the mice on C57BL/6JR^c^{Hsd} genetic background have no mutations in *Snca*, *Mmrn1* or *Crb1* and express low levels of *Abcd4* [39]. Analysis of the E15.5 data revealed upregulated expression of the WD repeat and FYVE domain-containing protein 1 (*Wdpy1*) gene also known as *FYVE domain-containing protein localized to endosomes (Fens-1)*, which encodes a phosphatidylinositol 3-phosphate binding protein that contains a FYVE zinc finger domain and multiple WD-40 repeat domains (Figure 1 J). These results are in line with the data from *Crb* fruit fly genetics [25–27] that imply changes in the *Crb* endolysosomal system at the OLM. The *CRB1* RP-like morphologic phenotype in mouse, and the surprisingly subtle differences on transcript levels (*Crb1*^{KO}*Crb2*^{ARPC} against wildtype mice) with the *Wdpy1* being upregulated and potential localizing on early

endosomes, prompted us to investigate if major CRB1 variant proteins affect early endosomes in *CRB1* RP-like human patient-derived retinal organoids (Figure 1 K).

Characterization of CRB1 patient retinal organoids

To investigate the disease-state in a human system, we first validated the *CRB1* RP retinal organoid model. We generated isogenic hiPSC controls to exclude that different genetic backgrounds were mediating the *CRB1* patient organoid phenotype. We generated them by homology directed repair (HDR) of the *CRB1*^{M1041T} variant using CRISPR/Cas9 (Figure S3; Table S1). At DD90, all hiPSC lines developed retinal organoids with an outer nuclear layer with PRCs (ONL, OTX2+ nuclei layer) and an inner retina with ganglion cells (BRN3A+ nuclei; Figure 2 A-E; Figure S4 A-C). This indicates that the induction took place for the eyefield development, the optic vesicle regionalization, followed by the retinal neurogenesis. We found a significant decrease in ONL thickness in patient retinal organoids compared to their isogenic controls (Figure 2 F), as well as a decrease in the number of OTX2+ nuclei in the ONL (Figure 2 G) and an increase in the number of PR nuclei above the OLM at DD180 (Figure 2 H). Subsequently, we validated expression of wild type CRB1 and variant CRB1 proteins (encoded by *CRB1*^{M1041T/M1041T}, *CRB1*^{M1041T/C948Y} or *CRB1*^{Y631C/E995*}) by monitoring fluorescence over time using two different antibodies recognizing either an epitope on the short intracellular domain (ICD) of CRB1 or the first EGF-like domains of the ECD. The CRB1-ECD/CRB1-ICD antibodies have a high CRB1-antigen specificity with little background observed on immuno-EM and IHC on human donor cadaveric retinas [13]. Both antibodies indicated a clear CRB1 expression in the isogenic and control organoids at 180 (Figure 2 F-G; Figure S4 D-E). No CRB1-ECD/ICD overlapping signal was found at DD90/DD120 (Figure S4 H-M) which is at the onset of CRB1 expression (DD120) previously found on TEM [12]. Very weak signal was observed at the OLM in the *CRB1* patient lines compared to the isogenic or control retinal organoids at DD180 (Figure 2 F-I; Figure S4 L+M). Thus, the *CRB1* RP organoid model permits comparative protein analysis and is not related to the differences in genetic backgrounds of the control organoids. Also, the reduction of CRB1 variant expression at the OLM suggests that patient-derived gene mutations may alter trafficking of CRB1-containing vesicles to the OLM or the CRB1 turnover at the OLM (cartoon Figure 1 K).

CRB1/NOTCH1-ECD interact and variant CRB1 reduces apical NOTCH1 expression

The retinal thickening seen in *CRB1* LCA-associated patients [2] might be associated with increased cell proliferation during development or a loss of cell adhesion and cell organization. Both has been found in previous *CRB1* LCA mouse studies [7–11,15,16]. An increase in number of retinal cells in patient retinal organoids during development was not found (Figure 2). Also, we found a strong reduction of adhesion markers at DD180 [12]. Interesting candidates bridging loss-of-adhesion with cell proliferation have been NOTCH receptors, especially NOTCH1. For example, mouse *Notch1* was shown as the driving force

behind the developmental shut down by downregulating the Notch pathway activity in RPCs in the mouse neuroretina [40]. *Notch1* is essential in maintaining the RPC population (cycling cells) in the developing retina. Conditional knockdown of *Notch1* restricts the RPC sub-population and confines the differentiation capacity of RPCs mainly to cone photoreceptors [30,33,34,41]. Also, the fruit fly Crb mutant protein (*crb*^{P13A9}) decreases Notch receptor localization [27].

NOTCH1 was expressed in the RPE at all time points serving as a positive control (Figure 3 A+C-D). We found, as expected, little NOTCH1 expression at the OLM in immature healthy human retinal organoids (DD90, Figure 3 B) or fetal retina (Figure 3 C). In developed retinas (DD180), NOTCH1 expression was almost exclusively limited to MGC-villi at the OLM (co-labelled with CD44-MGC-villi marker and not with the PRC/on-bipolar marker recoverin (Figure 3 E-F). This indicates that apical NOTCH1 expression is linked to the developmental stage in human retinal organoids. *CRB1* patient retinal organoids expressed little NOTCH1 at the OLM (Figure 3 G-I) and more NOTCH1 in the inner retina (Figure 3 G-I asterisks). Recently, a NOTCH-CRB interaction on the ECD was indicated by the proximity ligation assay (PLA) in fruit fly [26]. We observed an interaction of CRB1/NOTCH1-ECD by PLA on human retinal organoids in both patient and control retinal organoids (Figure 3 J-M). The interaction signal in patient retinal organoids was reduced at the OLM and increased in the ONL (Figure 3 J-M). The increase of interaction below the OLM may indicate that the CRB1 variants cannot efficiently traffick from RAB11+ endosomes to OLM or not efficiently recycle in RAB11+ vesicles causing CRB1 variant aggregation or altering the endolysosomes below the OLM.

More autophagy-lysosomal compartments in CRB1 retinal organoids

Loss of CRB increased Notch and Delta endocytosis in fruit fly [42] which increases ARL8-positive lysosomes in rhabdomeres compared to controls in a pre-disease state [26,27]. We next sought to determine what endolysosomal vesicles (size, morphology) are affected by the loss of apical CRB1 on transmission electron microscopy (TEM; Figure 4) and then identified & quantified on light microscopy (Figure 5) at DD180. On TEM, we found few electron-dense degradative compartments/vacuoles in control organoids (Figure 4 A-B; no arrowheads) compared to many in patient organoids (Figure 4 E-G; arrowheads) and, surprisingly, some in the heterozygote gene-corrected organoids (Figure 4 C-D; arrowheads). Additionally, the electron-dense adherens junction / subapical region appeared elongated in some patient organoids (Figure 4 E+G; red arrows indicate adherens junction / subapical regions). Furthermore, some cell disruptions were detected in the *CRB1*^{M1041T/C948Y} organoids (Figure 4 D; asterisks indicate nuclei above adherens junction) as seen on immunofluorescence (Figure 2 F''+G''+H''). Interestingly, we did not find definitive multivesicular bodies in any of the above specimens, suggesting that photoreceptors and Müller glial cells may not utilise them during the endosomal maturation.

The increase in electron-dense degradative compartments/vacuoles on TEM in patient retinal organoids was then semi-quantified on immunofluorescence signal on DD180 retinal organoids. We hypothesized that CRB1 variant is less efficiently shuttled from the ONL/INL to the OLM aggregating in degradative compartments or alternatively that the turnover of CRB1 variant protein at the OLM is higher. Yet, we found an increase of CRB1 variant in only one patient line (*CRB1*^{Met1041Thr}) in the INL/ONL (Figure S5 I), so indicating little overall aggregation. Also, we observed minimal co-labelling of CRB1 variant with the general endolysosomal marker LAMP1 in the ONL/OLM (Figure S5 A'-H'). We found more lysosomal LAMP1+ vesicles in the ONL but not close to the OLM in patient retinal organoids (Figure S5 K-L). Then, we assessed the co-labelling and expression of the small GTPase lysosome kinesin adaptor ARL8A/B with CRB1 (Figure 5). ARL8A/B is primarily found on late lysosomes [43]. Also, ARL8A/B takes part in the anterograde transport of mature lysosomes to the cell and co-mediates the transport of endocytic cargo to lysosomes [43,44]. Arl8+ lysosomes were previously indicated to accumulate Crb variant proteins in fruit fly [27]. We, however, also found little co-labelling of variant CRB1 with ARL8A/B (Figure 5 A-H). Similar to LAMP1, the area of the total ARL8A/B (lysosome/late endosome) punta was increased in the ONL of patient organoids (Figure 5 K-L), implying accumulation of degradative compartments but not an accumulation of CRB1 variant protein.

We also examined CRB1 variant protein being co-labelled with classical autophagy markers such as the ubiquitin-binding protein adapter p62 and the microtubule-associated proteins 1A/1B light chain 3B (LC3B) in the ONL/OLM. The autophagy cargo adapter p62 can transport substrates to the lysosome that have been tagged, e.g. by LIR (LC3-interacting motif for degradation) [45]. P62 provides an important role for selective autophagy of organelles and ubiquitinated misfolded/damaged proteins (here potentially the CRB1 variant protein). Further, p62 has been linked to selective stress-response-induced autophagy and proteostasis and extensively implicated in selective autophagy [45–47]. We found a strong increase in LC3B and p62 presence in *CRB1* patient retinal organoids in the ONL and at the OLM (Figure 6; Figure S6). The increase may be related to changes in the autophagic flux. We added BafA1 to inhibit acidification of endolysosomes by blocking the vacuole-ATPase (H⁺/Ca²⁺ antiporter), which is required for fusion of lysosomes with autophagosomes to form auto-lysosomes, and hence for degradation of proteins targeted to lysosomes. We incubated retinal organoids with BafA1 (500 nM) for 6 hours and extracted the lysate. BafA1 induced a robust block of lysosome-autophagosome fusion on individual organoids (Figure 6 I+J; Figure S6 C+D). We found more autophagosome markers (LC3-II) in *CRB1* patient retinal organoids and a decreased autophagic flux (Figure 6 J+K; Figure S6 G+H) pointing towards a blockage of autophagic vesicle removal. We also found little variant CRB1 expression and co-labelling of CRB1 with p62, LC3B or ARL8A/B. Accordingly, CRB1 variant protein might be either expressed at low levels (see also Figure 2+Figure S4), unstable, degraded in

the ONL/INL with little variant CRB1 reaching the OLM, or reach the OLM but show high turnover due to abnormal vesicle sorting.

Loss of CRB1 reduces the pool of recycling endosomes

To determine where the block of autophagic flux takes place, we investigated the expression of RAB11A. RAB11A is a small GTPase regulating the formation of transport vesicles, recycling endosomes and overall intracellular membrane trafficking [48]. The turnover of CRB and CRB membrane integration is also determined by RAB11 [49] (Figure 1 K). We found a strong signal of RAB11A co-labelling with F-actin in control organoids at the OLM (Figure 7 A+C. Figure S7 A-C). The RAB11A/F-actin co-labelling was strongly reduced in *CRB1* RP patient retinal organoids (Figure 7 B+D. Figure S7 D) with RAB11A yielding 50% less signal at the OLM (Figure 7 P). We further investigated the early endosomal population (EEA1+), late endolysosomal population (RAB7+), retromer-positive recycling compartments (RAB7+, VPS35+), and late endolysosomal population (RAB7+, ARL8A/B+). We found little difference in RAB7 expression between patient and control retinal organoids (Figure 7 E-H+I-L+M. Figure S7 E-H). However, less RAB7 co-labeled with VPS35 (Figure 7 E'''-H'''; Figure S7 E'''-H''') while co-labelling with ARL8A/B increased in patient retinal organoids (Figure 7 E''''-H''''; Figure S7 E''''-H'''). Furthermore, the early endosome population was increased in patient retinal organoids (Figure 7 I'-L'+N. Figure S7 I). Finally, we investigated the WDFY1 protein (also called *FYVE domain-containing protein localized to endosomes* [Fens-1]) expression on retinal organoids, which we found to be upregulated at the transcript level in *Crb1^{KO}Crb2^{ARPC}* compared to wildtype mouse retina (Figure 1 J). We found little co-labelling with early endosomes in control organoids and cross-validated the WDFY1 antibody with another WDFY1 antibody (Figure S8 A+B). Moreover, WDFY1 does not necessarily have to reside on early endosomes but could instead be located in the cytosol from where it is most likely scrapped by the phospholipid PtdIns(3)P, which is actively recruited by EEA1 [38,50]. We noted that early endosomes in patient organoids expressed more EEA1 (Figure S8 C-H) and co-localized with WDFY1/EEA1 (Figure S8 C'''-H'''), indicating that dysregulated early endosomes may recruit more WDFY1. An increase of WDFY1 fluorescence signal was found in the ONL and OLM (Figure S8 I+J). Interestingly, the isogenic retinal organoids that also potentially express CRB1 variant proteins from one allele (genotype: *CRB1^{M1041T/+}*) had an increase of WDFY1 when compared to the three control lines (expressing wildtype CRB1. Figure S8 I+J). Further research will be needed to determine the function of cytosolic WDFY1 and early endosome bound WDFY1, and if more WDFY1 prime early endosomes for degradation or block the autophagic flux.

Discussion

It is still challenging to predict the progression of the spectrum of *CRB1*-associated retinal dystrophy phenotypes in *CRB1* patients based on the identified genotype variants. A thorough

knowledge on the clinical spectrum, detailed phenotyping, the natural history studies [2,4], are important for optimal counselling and patient selection for interventional studies. Here we address three common RP *CRB1*-associated variants on (a) their protein expression profile in the neuroretina (variant *CRB1* being lost) and (b) the loss-of-function of the three *CRB1* variants on apical early endosome maturation. Both results have implications for the treatment (e.g. supporting early endosome maturation or *CRB* gene supplementation) and information for patients with one of the *CRB1* variants on understanding the etiology.

We started by investigating *CRB1*-associated disease determinants first at the transcriptional level in mice and subsequently ended at the protein level in a human retinal organoid disease model. We find a strong retinal morphological phenotype in the neuroretina of *Crb1^{KO}Crb2^{ARPC}* mice with little phenotype seen in *Crb1^{KO}* (comparable to wildtype mice). But, surprisingly, we find few differences on the transcriptional level in *Crb1^{KO}Crb2^{ARPC}* against *Crb1^{KO}* RNAseq data similar to a previous microarray study comparing *Crb2^{ARPC}* against wildtype mouse retina [29]. However, we do find a strong upregulation of *Wdfy1* in *Crb1^{KO}Crb2^{ARPC}* compared to wildtype mice. The function of *Wdfy1* is still elusive in many cell types but is linked to early endosomes [38]. We also find an upregulation of apical *WDFY1* protein in *CRB1* patient retinal organoids. Taken together, this indicates that loss of apical *CRB1* changes the apical endolysosomal system opening new avenues into rescue biomarkers for *CRB* gene supplementation and *CRB1* gene-editing approaches [51].

Little is still known how different *CRB1* variant proteins behave in human neuroretinas. We previously showed that *Crb1^{C249W/-}* mice (C249W corresponds to the human C250W) traffic and express *CRB1* at normal levels at the OLM [23]. Yet, when specific mutant *CRB* proteins (gene mutations on the central domain of the *Crb* gene) are introduced to a *Crb*-null fruit fly model then the *Crb*-null phenotype is exacerbated, the *CRB* mutant protein mislocalizes in rhabdomeres and aggregates constituting a gain-of-function phenotype [22]. Interestingly, some fruit fly *Crb* gene mutations (e.g. the *Crb^{C749W}* gene mutation somewhat comparable to the human *CRB1^{C250W}* variant) exhibited poor *CRB* protein expression, but is still able to partially rescue degeneration under light stress when introduced to a *Crb*-null fruit fly. Based on the Pellika and Tepass studies (2017), we initially expected that the three *CRB1* variants studied here in patient organoids have a gain-of-function related to *CRB1* variant aggregation as found in fruit flies because the mutations are similarly located on the *CRB1* gene affecting the transcription/translation of the *CRB1* central protein domain. However, we did find a strong reduction of the *CRB1* protein in patient organoids pointing towards a loss-of-function phenotype affecting potentially the turn-over of other apical proteins. We show that this is the case for the NOTCH1 receptor because NOTCH1 potentially stabilized by the here newly discovered *CRB1*/NOTCH1-ECD physical interaction.

The question remains to determine what controls the *CRB1* protein expression, localisation and turn-over rate at the OLM to determine the progression of retinal degeneration in *CRB1*-

associated retinal dystrophy phenotypes in *CRB1* patients. In the present study, we focused on the endolysosomal system because we find an increase of the endosome-associated *Wdfy1* gene expression in *Crb1^{KO}Crb2^{ARPC}* mice and the degradation-associated proteins on the endolysosomes (ARL8/LAMP1/p62/LC3 puncta) in patient retinal organoids. We paid particular attention to the retromer-positive and early recycling compartments. The retromer complex (SNX1/2, SNX5/6, VPS26, VPS29, and VPS35) on early/late endosomes and the budded off vesicles/recycling endosomes (e.g. RAB11A, TfR1) work in synergy for efficient protein recycling in cells [52], thus are potential essential parameters controlling CRB1 protein turn-over. What is more, the retromer proteins VPS26/VPS35 localize on early and late endosomes in fruit fly photoreceptors, and loss of VPS26 or VPS35 considerably increased degradative compartments [53]. Little has been studied in a human situation but more is already known on the mouse or zebrafish *Crb1* family member *Crb2(a)*. The recycling of CRB2 at the apical membrane is determined by binding of its intracellular domain to VPS35 of the retromer complex on early endosomes [25], a highly conserved 37-aa CRB2-ICD harbouring FERM (4.1, ezrin, radixin, moesin)-PDZ(ERLI) domains shared by the family members CRB1, CRB2, and CRB3A (reviewed in [54]). The CRB protein recycling also depends on RAB11 [49]. The ICD of CRB2A on RAB11A+ recycling endosomes takes part in regulating the cell cycle exit of RPCs and maintaining NOTCH1 at the OLM [55]. RAB11 is known to mediate the release of the early endosomal cargo (e.g. NOTCH1, CRB1) to the endocytic recycling compartment when peripheral early endosomes experience a temporary peak in PtdIns(3)P integration on their vesicular membrane [50,56]. Potential poor RAB11A-initiated release in *CRB1* patient retinal organoids may also amass WDFY1 mediated by its FYVE domain binding to PtdIns(3)P [38]. Further assays show that the presence of PtdIns(3)P in a membrane is vital for shifting WDFY1 from a soluble and cytosolic form to an early endosome or vesicle membrane-bound form. The actual function and normal equilibrium of cytosolic versus membrane-bound WDFY1 is not known. In line with this, our data on *CRB1* variant patient retinal organoids have reduced retromer-associated late endosomes (VSP35+/RAB7+), an increase in early endosomes destined for degradation (EEA1+/WDFY1+), a decrease of recycling endosomes (RAB11A+), and a concomitant expansion of degradative endolysosomal compartments (ARL8/LAMP1/LC3-II/p62+). We propose that in *CRB1* patient retinal organoids, the disturbed early endosomes are trafficked to degradative compartments lowering the CRB1 protein expression at the OLM.

Finally, we propose that – given the CRB1 loss-of-function phenotype in patient organoids and the phenotypic rescue from one allele (isogenics) as well as knowing that the amount of CRB correlates to the severity of retinal phenotype seen in *Crb1* mouse models [7–9,13,15,16,57] – few copies of *CRB1* or *CRB2* need to be delivered to the retina of RP *CRB1*-associated patients by recombinant adeno-associated viral vectors to have a therapeutic effect.

Materials and Methods

Mice

Procedures concerning animals were performed with permission of the ethical committee of the Leiden University Medical Center and the animal experimentation committee (DEC) of the Royal Netherlands Academy of Arts and Sciences (KNAW) under permit number NIN 12.105. All mice used were maintained on a 99.9% C57BL/6J0laHsd genetic background with a 12 h day-night cycle and supplied with food and water *ad libitum*. *Crb1^{KO}* (*Crb1^{-/-}*) mice [10] were crossed with a retinal *Crb2^{ΔRPC}* (*Crb2^{F/F}Chx10Cre^{Tg/+}* clone P1E9) mouse strain [58,59] to ablate both *Crb1* and *Crb2* during retinal development from retinal progenitor cells. *Cre* starts to be expressed around E9.5 in the retina [59]. The previously made *Chx10Cre* mice were generated by knocking in *GFP-Cre-IRES-AP* cDNA in exon-1 of the *Chx10* gene on a Bacterial Artificial Chromosomes (BAC; -55 kb *Chx10* of ATG to +22 kb off of the polyadenylation sequence) [59]. Interestingly, the last exon of the *Abcd4* gene is only ~7000 bp from the last exon of the *Chx10* gene thus was on the BAC. Others have shown that large BACS containing several genes can lead to overexpression of flanking genes [60,61]. We believe the integration of the cDNA in close proximity to the *Abcd4* gene and being both on the BAC may have led to the overexpression of the *Abcd4* gene in *Crb1^{KO}Crb2^{ΔRPC}* mice. *Crb1^{KO}Crb2^{ΔRPC}* mice were compared to littermate *Crb1^{KO}Crb2^{F/F}* mice not expressing *Cre*. C57BL/6J0laHsd mice have a 365 kb deletion ablating the *Mmrn1* and *Snca* and express low levels of *Abcd4* [39,62]. The C57BL/6J substrain (from the Jackson Laboratory) carries a 5-exon-spanning deletion in the *Nnt* gene but C57BL/6J0laHsd have a wildtype *Nnt* gene [63]. Analysis of the *Crb1^{KO}Crb2^{ΔRPC}* and *Crb1^{KO}Crb2^{F/F}* mice was carried out on males and females. Chromosomal DNA isolation and genotyping were performed as previously described [10,58].

Morphology and retinal thickness measurements on plastic mouse eyes

Eyes were collected of double-knockout and control littermate mice. After enucleation, the eyes were fixed in 4% paraformaldehyde in PBS (25 min) and dehydrated in an ethanol series (30 min each step; 30 % EtOH, 50 % EtOH, 70 % EtOH, 2x 90 % EtOH, 2x 100% EtOH). Then, the eyes were hardened in Technovit, sectioned (3 μm), stained (0.5% Toluidine blue), and mounted (Entellan) as previously described [64]. Consecutive brightfield images were taken. We generated spidergrams of the retinal thickness (ILM-to-OLM) for P14, 1 M and 3M-old-mice by measuring at 0.25, 0.5, 0.75, 1.0, 1.25, 1.5, 1.75, 2.0, 2.25, 2.5, and 2.75 mm distance to the optic nerve head (ONH) as previously described [64].

Electroretinography

Electroretinography's (ERGs) were done in dim light on an Espion E2 (Diagnosys, LLC, MA). 1-month-old (1M) mice were dark-adapted (>12 hours). The mice were anesthetized (100 mg/kg ketamine, 10 mg/kg xylazine, intraperitoneal injection) and the pupils were

dilated (atropine drops, 5 mg/mL). Scotopic flash series: -4, -3, -2, -1, 0, 1, 1.5, 1.9 log cd s/m² light intensity. Photopic flash series at 30 cd/m² background light: -2, -1, 0, 1, 1.5, 1.9 log cd s/m² light intensity. We first recorded the scotopic ERG, followed by a 10 min light exposure (30 cd s/m² light intensity) and then the photopic ERG.

RNA Sequencing

Sequencing was performed using Life Technologies SOLiD5500 with single-end, 50 bp reads. Two separate runs were performed. Run1 contained n=30 mice; n=5 *Crb1*^{KO}*Crb2*^{F/F} (*Crb1*^{KO}) and n=5 *Crb1*^{KO}*Crb2*^{ARPC} (Tg) per development timepoint of the mouse embryo at E15.5, E17.5 and P1. Run2 contained n=9 mice; n=4 *Crb1*^{KO}*Crb2*^{ARPC} mice (C57BL/6J0laHsd) and n=5 healthy mice (C57BL/6JRccHsd = wildtype, WT) at E15.5. Reads were aligned against mm10, using the 'whole.transcriptome.frag' workflow with bamgen.mqv.threshold set to 20 (Lifescopy v2.5). Counts were obtained using the GTF as supplied by Lifescopy (transformation of refGene.txt downloaded from UCSC at 25-06-2014) within this workflow.

Differential expression analysis

The analysis was performed as previously [7]. The two runs were analysed separately. Statistical analyses were performed using the edgeR [65] (and limma/voom [66] R/Bioconductor packages. One of the *Crb1*^{KO}*Crb2*^{ARPC} E15.5 samples in the first run was identified as an outlier and removed from the analysis. Genes with more than one count in five or more samples were retained. Count data were transformed to log₂-counts per million (logCPM), normalized by applying the trimmed mean of M-values method [67] and precision weighted using voom [68]. Differential expression was assessed using an empirical Bayes moderated t-test within limma's linear model framework including the precision weights estimated by voom. Resulting p-values were corrected for multiple testing using the Benjamini-Hochberg false discovery rate. Additional gene annotation was retrieved from Ensembl (release 90) using the biomaRt R/Bioconductor package. Analyses were performed using R v3.4.1 and Bioconductor v3.5.

Real-time quantitative PCR

RNA was isolated from 5 controls (*Crb1*^{KO}) and *Crb1*^{KO}*Crb2*^{ARPC} retinas using TRIZOL reagent (Gibco life technologies), according to the manufacturer manual, and after the final precipitation dissolved in RNase-free water. After genomic DNA degradation with RNase-free DNase I (New England Biolabs), 1 µg of total RNA was reverse transcribed into first-strand cDNA with Superscript III Plus RNase H-Reverse Transcriptase (Invitrogen) and 50 ng random hexamer primers, during 50 min at 50°C in a total volume of 20 µl. To the resulting cDNA sample, 14 µL of 10 mM Tris, 1 mM EDTA was added. From all samples, a 1:20 dilution was made and used for qPCR analysis. For this analysis, primer pairs were designed with a melting temperature of 60–62°C, giving rise to an amplicon of 80–110 bp. Real-time

qPCR was based on the real-time monitoring of SYBR Green I dye fluorescence on a ABI Prism 7300 Sequence Detection System (Applied Biosystems, Nieuwekerk a/d IJssel, The Netherlands). The PCR conditions were as follows: 12.5 μ L SYBR Green PCR 26mastermix (Applied Biosystems), 20 pmol of primers, and 2 μ L of the diluted cDNA (ca 3 ng total RNA input). An initial step of 50°C for 2 min was used for AmpErase incubation followed by 15 min at 95°C to inactivate AmpErase and to activate the AmpliTaq. Cycling conditions were as follows: melting step at 95°C for 1 min, annealing at 58°C for 1 min and elongation at 72°C, for 40 cycles. At the end of the PCR run, a dissociation curve was determined by ramping the temperature of the sample from 60 to 95°C while continuously collecting fluorescence data. Non template controls were included for each primer pair to check for any significant levels of contaminants. Values were normalized by the geometric mean of the 3 reference genes hypoxanthine-guanine phosphoribosyltransferase, elongation factor 1-alpha and ribosomal protein S27a.

Data repository

The RNA-Seq data have been deposited in the NCBI Gene Expression.

Cell Culture

We previously described the three male *CRBI* RP-patient human induced pluripotent stem cell (hiPSC) lines (Patient line 1-3: LUMC0116iCRB09, LUMC0117iCRB01, LUMC0128iCRB01) and three control lines (CTRL 1-3: LUMC0004iCTRL10 (hPSC^{reg} name: LUMCi029-B), LUMC0044iCTRL44, LUMC0080iCTRL12; see also Table S3; [12]). HiPSCs were maintained on mTeSR1 or mTeSR Plus on matrigel-coated plates and stored in mFreSR (STEMCELL Technologies) or CryoStor CS10 in liquid nitrogen for long-term storage. The pluripotency status and functional pluripotency was performed for at least 3 clones per line or repaired line (Figure S3 C). HiPSC clones were characterized on pluripotency by triple-staining dissociated single cells with OCT3/4, NANOG, and SSEA4 (1x10⁵ cells/sample; 1 hr at RT) and analyzed on FACS (Flow cytometer, Miltenyi-Vyb). HiPSCs were also differentiated into the three germ layers (STEMdiff Trilineage differentiation kit, Stem Cell Technologies) and stained on coverslips with the conjugated antibodies Nestin (ectoderm), PAX6 (ectoderm), FOXA2 (endoderm), GATA4 (endoderm), vimentin (mesoderm), CDX2 (mesoderm), Brachyury (mesoderm; blocking solution: 4% NSS/PBS with 0.1% Triton X-100; cells incubated with primary antibodies in 4%NSS/PBS for 1 hr at RT). Figure S3 F-G and see Table S2 antibody concentrations).

CRISPR/Cas9-based gene-repair of the hiPSC lines LUMC0116iCRB09 and LUMC0128iCRB01

The *CRBI* variant c.3122T>C (exon 9) was repaired by CRISPR/Cas9 ribonucleoprotein (RNP) mediated homologous recombination. Sequences of the sgRNA and the repair template (ssODN) are provided below. 1x10⁵ single cells were transfected using

electroporation (Neon System). The CRISPR/Cas9 RNP complex (crRNA:tracrRNA duplex (IDT); 10 pmol of crRNA/tracrRNA pre-annealed (IDT)) and the Cas9 V3 (1 µg; IDT) was transfected. Additionally, the homology directed (HRD) repair template (ssODN; 40 pmol) was added to correct the mutation. For screening of targeted clones, a restriction site is introduced via a silent mutation to avoid re-cutting after HDR (Figure S3 B). 3.6×10^5 cells in 27 µL were mixed with 6 µL ssODN (13.3 µM) and 3 µL Cas9/RNP complex (3.6 µg Cas9, 36 pmol pre-annealed crRNA:tracrRNA). Then, three times 10 µL (1.0×10^5 cells per tube. 30 µL and 3.0×10^5 cells in total per line) were electroporated (Neon System; Thermo Fisher Scientific; 1100V, 20 ms, 2 pulses), then plated on mTeSR-E8 + CloneR supplement (STEMCELL Technologies) into 12-well plates coated with Synthemax® II-SC substrate (Corning) and placed into an incubator (37°C, 5% CO₂, 20% O₂). Human iPSCs were seeded as single cells 5-7 days post-electroporation (1000 cells / 10-cm plate). Colonies were picked and gDNA isolated (QuickExtract) 8 days after seeding. Genomic DNA covering the variant region was amplified and targeting was analyzed using Taq1 (NEB; R0149) restriction of the PCR fragment. Successful targeting was confirmed by Sanger sequencing (*CRB1* gene exon 9. Figure S3 D-E).

Cas9 nuclease V3 (IDT #1081058); tracrRNA (IDT #1072532); crRNA (IDT, custom-made).

ssODN:

ACAAGTTTGCAGTCAGTGAATGATGGCACATGGCACGAAGTGACCCTTTTCGAT
GACAGACCCACTGTCCCAGACCTCCAGGTGGCAAATGGAAGTGGACA

Sequence of crRNA(s) used: CTGGGACAGTGGGTCTGTCTG

Sanger sequencing primers:

Fwd: ACCAGAGAACTCACCAATATCAC

Rev: CAATAGCTCTGTCTCCACATAA

Retinal Organoid Differentiation

The differentiation of the hiPSCs started at differentiation day (DD) 0 with floating single-cell hiPSCs that were self-aggregated to embryoid bodies in 10 µM (±)blebbistatin in mTeSR1 or mTeSR Plus medium (STEMCELL Technologies) on 1% agarose-coated (non-adhesive) plates overnight. The media was gradually changed from mTeSR to the Neural Induction Medium (NIM-1) over three days (mTeSR1/NIM-1: day 0, 1:0, day 1, 3:1; day 2, 1:1, day 3, 0:1). NIM-1 consists of DMEM/F12 supplemented with 1xN2 supplement, 1x Minimum Essential Media Non-Essential Amino Acids (MEM NEAAs) and 2 µg/mL Heparin (Sigma. See also [12]). The medium was changed every day until DD7. The embryoid bodies were plated at an approximate density of 20 aggregates per cm² onto Matrigel-coated wells on DD7 and lifted on DD22/28. NIM-1 was replaced every other day from DD7 to DD16, from DD16 medium was replaced each day with Neural induction

medium 2 (NIM-2). NIM-2: 1x B27 or NeuroCult SM1 without Vitamin A, 1x NEAA and 1x antibiotic-antimycotic in DMEM/F12(3:1). Subsequently, the lifted organoids were dislodged and kept in floating culture with NIM-2 on agarose-coated plates. At DD33 forebrain organoids were removed with a truncated P200 pipet tip. Medium was replaced three times a week from DD41 onwards. The medium was changed to Retinal Lamination Medium 1 (RLM-1) at DD42. RLM-1: 10% FBS, 1x B27 without Vitamin A (Gibco) or NeuroCult™ SM1 without Vitamin A (Stem Cell Technologies), 1x NEAA, 1x antibiotic-antimycotic, and 100 μ M taurine in DMEM/F12(3:1). The RLM-1 was supplemented with 1 μ M retinoic acid from DD49 to DD98. The long-term culture medium from DD98 onwards was Retinal Lamination Medium-2 (RLM-2) with low amounts of growth factors (N2 supplement instead of B27). RLM-2: 10% FBS, 1x N2, 1x NEAA, 1x antibiotic-antimycotic, and 100 μ M taurine in DMEM/F12(3:1) 0.5 μ M retinoic acid.

Fetal human retinal tissue

The use and collection of the material were approved by the Medical Ethics Committee of the Leiden University Medical Center (P08.087). Patient anonymity was strictly maintained. All tissue samples were handled in a coded fashion, according to Dutch national ethical guidelines (Code for Proper Secondary Use of Human Tissue, Dutch Federation of Medical Scientific Societies).

Fixation, sectioning and immunohistochemical staining

Retinal organoids were collected at the time points of differentiation day(DD)90, 120, 150, and 180. Prior to fixation, the organoids were washed shortly in PBS and then incubated for 30 minutes in 4% paraformaldehyde in PBS. Subsequently, the organoids were dehydrated in 15% sucrose in PBS (30 min) and 30% sucrose in PBS (30 min). After that, the retinal organoids were orientated and embedded in OCT Tissue-Tek cryo-embedding media. Finally, they were frozen on dry-ice and stored at -20°C. The retinal organoids were sectioned at 7 μ m using a Leica CM1900 cryostat (Leica Microsystems) and after 1 hour of air-drying stored at -20°C. The slides were rehydrated in PBS, blocked (1 hour, 0.1% BSA 0.04% Triton-X in PBS), stained with the primary antibody (in 0.1% BSA 0.04% Triton-X in PBS) overnight at 4°C or 3 hours at room temperature, washed three times in PBS (3x10 min), stained with the secondary antibody (1 hour), washed three times in PBS (3x10 min), and mounted with Vectashield® Vibrance® HardSet antifade mounting media containing DAPI (Vector Laboratories). For antibodies and dilutions see Table S2. A Leica TCS SP8 confocal microscope was used for image acquisition. Image analysis was done in Leica Application Suite X (Leica, LAS X), Fiji ImageJ, and Adobe Photoshop CC2018.

Fluorescence semi-quantification in ROIs

All organoids (7- μ m sectioned) imaged for fluorescence semi-quantification were stained (see Table S2) with the same antibody mix at the same time, imaged in one confocal

microscopy session, and included a negative control (no primary antibody added). At least six different organoids (generally 10-12) per line on generally three glass slides were analyzed per immunofluorescence staining. Several experiments were stained twice and analyzed twice showing overall high robustness of outcome parameters. The semi-quantification of CRB1 protein expression was done in triplicates with different secondary antibodies and incubation times (overnight at +4°C or 3 hours at RT) showing a strong reduction in patient organoids in all conditions. The analysis was done blinded. A 8-bit gray-scale raw image file was loaded into ImageJ. We manually defined three ROIs in the retina: ROI1, OLM (± 2.5 μm of OLM); ROI2, ONL (dense bright DAPI+ nuclei layer or OTX2+ nuclei layer below the ROI 1), ROI3, OPL/INL (nuclei layer below the ROI2 of spanning the neuroretina maximally 50 μm below ROI2). First, the mean gray value (MGV) per ROI was analysed. Then, we measured on each ROI the average particle size (area), the number of particles (counts), and the average intensity per spot (value between 0-255) using the ImageJ function “Analyze Particles”. We normalized the values to: counts per 100 μm^2 and the area of all spot sizes per ROI area (%).

Isolation of protein lysates and immunoblotting

Retinal organoids were collected at DD180. The RPE (dark parts) were dissected off with surgical scissors. Single neuroretinas were washed in cold 1xPBS and then lysed in cold RIPA buffer (#R0278, Sigma) including the protease inhibitor cocktail (cComplete, #11836153001, Roche). The single neuroretinas were mechanically disrupted by pipetting and incubated on ice for 2 hours. Then, the neuroretinas were vortexed and then sonicated in a pre-cooled +4°C water bath (Diagenode Biorupter Pico; Program: 15 sec ON, 30 sec OFF. 4 cycles; vortexed between 1st and 2nd cycle). The samples were then spun down (16000xg, 10 min, +4°C) and the supernatant was collected in a new pre-cooled tube. The protein concentration was measured by the Bradford assay (BCA Protein Assay Kit; ThermoFisher, #23227). The protein was then diluted to 1x Laemmli buffer with DTT (Bio-Rad, #1610737. Buffer: 0.12 M Tris-HCl, pH 6.8, 4% SDS, 20% glycerol, 10 mM DTT), boiled for 5 min (+95°C), and stored at -80°C. The protein lysates (20 μg per organoid per lane) were separated on a 4-20% SDS gel (Bio-Rad, #4561094) and transferred on PVDF (Bio-Rad Turbo transfer system. Protocol: mixed-molecular weight). The blots were blocked in 5% non-fatty milk in 1xPBS 0.1% Tween-20 (PBST; RT, 1 hour), incubated with the primary antibody (see Table S4 for concentrations; 5% milk in PBST), washed, incubated with the HRP-conjugated-antibody (RT, 1 hour 5% milk in PBST), and washed again. The signal was generated in ECL substrate (Bio-Rad, #1705061) and the chemiluminescence was imaged at three different exposure times (ChemiDoc MP Imaging System, Bio-Rad). The band intensity was measured (ImageJ, Gel analyzer) and averaged from three exposure times. Quantification was relative to GAPDH.

Transmission electron microscopy

Samples were washed in 1xPBS and then fixed in 1.5% glutaraldehyde in 0.1M cacodylate buffer at room temperature for 1 hour, stored in 0.5% PFA in 0.1M PHEM storage buffer until further processing. Samples were rinsed three times in 0.1 M cacodylate buffer and post-fixed in 1%OsO₄/1.5% potassium ferricyanide in 0.1M cacodylate buffer (1 hour on ice). Samples were rinsed again in 0.1M cacodylate buffer three times, and dehydrated in a series of ethanol, followed by a series of propylene oxide with EPON (LX112, Ladd research industries) and finally a step in 100% EPON. Organoids were put in a mould, those were filled up with EPON and polymerized at 70°C over two days. Ultrathin sections (90 nm) were created on a Reichert Ultracut S (Leica Microsystems) and after staining with uranylacetate and lead citrate, examined on an electron microscope (Microscope: FEI Tecnai T12 Twin Fei Company, Eindhoven, The Netherlands; Camera: OneView, Gatan) operating at 120 kV. Overlapping images were collected and stitched together into separate images as previously described [69].

Conjugation of NOTCH1 and CRB1 antibody to plus and minus oligonucleotide probes

We used the Duolink probemaker set (Sigma-Aldrich) to conjugate two same-species antibodies (mouse anti-NOTCH1 and mouse anti-CRB1 extracellular domain antibodies) to the plus or minus oligonucleotide probes as described in the protocol. In short: 20 µL of the primary antibody was mixed with 2 µL of the conjugation buffer. Subsequently, the antibodies were added to the Duolink In Situ Probemaker plus and minus vials for overnight incubation at room temperature. The next day, the stop reagent was added (incubation: 30 minutes, at RT), the storage solution was added and stored at +4°C.

Proximity ligation assay

For the proximity ligation assay the Duolink In Situ Detection Reagents kit green (Sigma-Aldrich) was used. Slides with sliced organoids were washed, and the tissue slices were circled with a hydrophobic pen. Slides were blocked with one drop of blocking solution from the Duolink PLA probe set per tissue slice and incubated for 1 hour at 37 °C in a humidity chamber. Blocking buffer was tapped off and the conjugated antibodies diluted in PLA probe diluent from the PLA probe kit were added for an overnight incubation at 4°C. After that the slides were washed twice in PLA wash buffer A (Sigma-Aldrich) for five minutes. For the ligation step the slides were incubated for 30 minutes at 37°C with ligase enzyme diluted (1:40) in 1x ligation buffer and were washed twice in wash buffer A again. Finally, the polymerase enzyme was diluted (1:80) in 1x amplification buffer and added to the slides and the slides were incubated in a humidity chamber (37 °C, 100 minutes). To one of the slides diluted amplification buffer was added without the polymerase, serving as a negative control. Subsequently, the slides were washed twice for 10 minutes in PLA wash buffer B and after that once for 1 minute in 0.01x wash buffer B. Wash buffer was tapped off and slides were

mounted by adding 5 μ L of Duolink In Situ Mounting Medium with DAPI with a 20 μ l pipet with truncated tip. Images were obtained using a Leica TCS SP8 confocal microscope.

Statistical analysis

The organoids were acquired from two or more differentiations and we aimed to obtain 3 images per organoid. Each image was analyzed on retinal length, thickness, total cells and total positive retinal cell population markers with ImageJ. Data were normalized per 100 μ m retinal length. For statistical analysis GraphPad Prism version 8 (GraphPad Software) was used. Shown values are expressed as mean \pm Standard error of the mean (SEM). Quantifications were tested for normality and if normally distributed unpaired T-tests assuming equal variance were used to compare patient and control lines. Measurements that did not show a normal distribution were tested with a Mann-Whitney test. Significance is indicated in graphs as $p < 0.05$ (*), $p < 0.01$ (**), and $p < 0.001$ (***)

Author contribution

Conceptualization: TMB, PMJQ, LPP, JW. Methodology retinal organoids and mouse morphology: TMB, PMJQ, LPP, AAM, DK. Generation hiPSC lines (patient) & repair (isogenic controls) and hiPSC characterization: CA, CF, HMM. Methodology/software/formal analysis/data curation of RNAseq data set: AJ, AvK, FB, PMJQ, JW. Formal analysis retinal organoids and mouse morphology: TMB, PMJQ, LPP. Investigation: TMB, PMJQ, LPP, JW. Writing – Original Draft: TMB and JW. Writing – Review & Editing: all authors. Visualization: TMB, PMJQ, LPP, JW. Resources: IB, JCN. Supervision: JW. Funding acquisition: JW.

Acknowledgments

We thank Marco Heuvelman and Yacintha van Doorn for their experimental work and the Wijnholds lab for their advice on experiments and reviewing the manuscript. We thank Annelies Boonzaier-van der Laan & Lennard M. Voortman for the technical assistance on microscopy & image analysis.

Funding

The Netherlands Organization for Health Research and Development (ZonMw grant 43200004, to JW), research grant MDBR-19-131-CRB1 from the University of Pennsylvania Orphan Disease Center in partnership with the Curing Retinal Blindness Foundation (to JW), research grant CRBF 2016-Aug-02 (to JW), and the Dutch blindness funds (Uitzicht 2015-22 to JW, Uitzicht 2020-01 to TMB and JW): Rotterdamse Stichting Blindenbelangen, OogFonds, Stichting Blindenhulp, Stichting Retina Fonds, Landelijke Stichting voor Blinden en Slechtzienden.

Conflict of interest statement

The authors declare that the research was conducted without any commercial or financial relationship that could be construed as a potential conflict of interest. The LUMC is the holder of patent number PCT/NL2014/050549, which describes the potential clinical use of CRB2; JW and LPP are listed as co-inventor of this patent, and JW is an employee of the LUMC.

REFERENCES

1. Quinn, P.M.; Pellissier, L.P.; Wijnholds, J. The CRB1 complex: Following the trail of Crumbs to a feasible gene therapy strategy. *Front. Neurosci.* **2017**, *11*, 175.
2. Talib, M.; van Schooneveld, M.J.; van Genderen, M.M.; Wijnholds, J.; Florijn, R.J.; ten Brink, J.B.; Schalij-Delfos, N.E.; Dagnelie, G.; Cremers, F.P.M.; Wolterbeek, R.; et al. Genotypic and Phenotypic Characteristics of CRB1-Associated Retinal Dystrophies: A Long-Term Follow-up Study. *Ophthalmology* **2017**, *124*, 884–895.
3. den Hollander, A.I.; Heckenlively, J.R.; van den Born, L.I.; de Kok, Y.J.; van der Velde-Visser, S.D.; Kellner, U.; Jurklics, B.; van Schooneveld, M.J.; Blankenagel, A.; Rohrschneider, K.; et al. Leber congenital amaurosis and retinitis pigmentosa with Coats-like exudative vasculopathy are associated with mutations in the crumbs homologue 1 (CRB1) gene. *Am. J. Hum. Genet.* **2001**, *69*, 198–203.
4. Nguyen, X.-T.-A.; Talib, M.; van Schooneveld, M.J.; Wijnholds, J.; van Genderen, M.M.; Schalij-Delfos, N.E.; Klaver, C.C.W.; Talsma, H.E.; Fiocco, M.; Florijn, R.J.; et al. CRB1-associated retinal dystrophies: a prospective natural history study in anticipation of future clinical trials. *Am. J. Ophthalmol.* **2021**.
5. Khan, K.N.; Robson, A.; Mahroo, O.A.R.; Arno, G.; Inglehearn, C.F.; Armengol, M.; Waseem, N.; Holder, G.E.; Carss, K.J.; Raymond, L.F.; et al. A clinical and molecular characterisation of CRB1-associated maculopathy. *Eur. J. Hum. Genet.* **2018**, *26*, 687–694.
6. Tsang, S.H.; Burke, T.; Oll, M.; Yzer, S.; Lee, W.; Xie, Y.A. (Angela); Allikmets, R. Whole Exome Sequencing Identifies CRB1 Defect in an Unusual Maculopathy Phenotype. *Ophthalmology* **2014**, *121*, 1–10.
7. Pellissier, L.P.; Alves, C.H.; Quinn, P.M.; Vos, R.M.; Tanimoto, N.; Lundvig, D.M.S.; Dudok, J.J.; Hooibrink, B.; Richard, F.; Beck, S.C.; et al. Targeted ablation of CRB1 and CRB2 in retinal progenitor cells mimics Leber congenital amaurosis. *PLoS Genet* **2013**, *9*, e1003976.
8. Alves, C.H.; Pellissier, L.P.; Vos, R.M.; Garcia Garrido, M.; Sothilingam, V.; Seide, C.; Beck, S.C.; Klooster, J.; Furukawa, T.; Flannery, J.G.; et al. Targeted ablation of Crb2 in photoreceptor cells induces retinitis pigmentosa. *Hum. Mol. Genet.* **2014**, *23*, 3384–3401.
9. Quinn, P.M.; Mulder, A.A.; Henrique Alves, C.; Desrosiers, M.; de Vries, S.I.; Klooster, J.; Dalkara, D.; Koster, A.J.; Jost, C.R.; Wijnholds, J. Loss of CRB2 in Müller glial cells modifies a CRB1-associated retinitis pigmentosa phenotype into a Leber congenital amaurosis phenotype. *Hum. Mol. Genet.* **2019**, *28*, 105–123.
10. van de Pavert, S.A.; Kantardzhieva, A.; Malysheva, A.; Meuleman, J.; Versteeg, I.; Levelt, C.; Klooster, J.; Geiger, S.; Seeliger, M.W.; Rashbass, P.; et al. Crumbs homologue 1 is required for maintenance of photoreceptor cell polarization and adhesion during light exposure. *J. Cell Sci.* **2004**, *117*, 4169–4177.
11. van de Pavert, S.A.; Sanz, A.S.; Aartsen, W.M.; Vos, R.M.; Versteeg, I.; Beck, S.C.; Klooster, J.; Seeliger, M.W.; Wijnholds, J. Crb1 is a determinant of retinal apical Müller glia cell features. *Glia* **2007**, *55*, 1486–1497.
12. Quinn, P.M.; Buck, T.M.; Mulder, A.A.; Ohonin, C.; Alves, C.H.; Vos, R.M.; Bialecka, M.; van Herwaarden, T.; van Dijk, E.H.C.C.; Talib, M.; et al. Human iPSC-Derived Retinas Recapitulate the Fetal CRB1 CRB2 Complex Formation and Demonstrate that Photoreceptors and Müller Glia Are Targets of AAV5. *Stem Cell Reports* **2019**, *12*, 906–919.
13. Pellissier, L.P.; Lundvig, D.M.S.; Tanimoto, N.; Klooster, J.; Vos, R.M.; Richard, F.; Sothilingam, V.; Garcia Garrido, M.; Le Bivic, A.; Seeliger, M.W.; et al. CRB2 acts as a modifying factor of CRB1-related retinal dystrophies in mice. *Hum. Mol. Genet.* **2014**, *23*, 3759–3771.

14. Quinn, P.M.J.; Wijnholds, J. Retinogenesis of the human fetal retina: An apical polarity perspective. *Genes (Basel)* **2019**, *10*, 987.
15. Buck, T.M.; Vos, R.M.; Alves, C.H.; Wijnholds, J. AAV-CRB2 protects against vision loss in an inducible CRB1 retinitis pigmentosa mouse model. *Mol. Ther. - Methods Clin. Dev.* **2021**, *20*.
16. Quinn, P.M.; Alves, C.H.; Klooster, J.; Wijnholds, J. CRB2 in immature photoreceptors determines the superior-inferior symmetry of the developing retina to maintain retinal structure and function. *Hum. Mol. Genet.* **2018**, *27*, 3137–3153.
17. Mehalow, A.K.; Kameya, S.; Smith, R.S.; Hawes, N.L.; Denegre, J.M.; Young, J. a; Bechtold, L.; Haider, N.B.; Tepass, U.; Heckenlively, J.R.; et al. CRB1 is essential for external limiting membrane integrity and photoreceptor morphogenesis in the mammalian retina. *Hum. Mol. Genet.* **2003**, *12*, 2179–89.
18. Boon, N.; Henrique Alves, C.; Mulder, A.A.; Andriessen, C.A.; Buck, T.M.; Quinn, P.M.J.; Vos, R.M.; Koster, A.J.; Jost, C.R.; Wijnholds, J. Defining phenotype, tropism, and retinal gene therapy using adeno-associated viral vectors (AAVs) in new-born brown norway rats with a spontaneous mutation in CRB1. *Int. J. Mol. Sci.* **2021**, *22*, 3563.
19. Zhao, M.; Andrieu-Soler, C.; Kowalczyk, L.; Cortés, M.P.; Berdugo, M.; Dernigoghossian, M.; Halili, F.; Jeanny, J.C.; Goldenberg, B.; Savoldelli, M.; et al. A new CRB1 rat mutation links Müller glial cells to retinal telangiectasia. *J. Neurosci.* **2015**, *35*, 6093–6106.
20. Motta, F.L.; Salles, M.V.; Costa, K.A.; Filippelli-Silva, R.; Martin, R.P.; Sallum, J.M.F. The correlation between CRB1 variants and the clinical severity of Brazilian patients with different inherited retinal dystrophy phenotypes. *Sci. Reports 2017 71* **2017**, *7*, 1–9.
21. van Rossum, A.G.S.H.; Aartsen, W.M.; Meuleman, J.; Klooster, J.; Malysheva, A.; Versteeg, I.; Arsanto, J.-P.P.; Le Bivic, A.A.; Wijnholds, J. Pals1/Mpp5 is required for correct localization of Crb1 at the subapical region in polarized Müller glia cells. *Hum. Mol. Genet.* **2006**, *15*, 2659–2672.
22. Pellikka, M.; Tepass, U. Unique cell biological profiles of retinal disease-causing missense mutations in the polarity protein Crumbs. *J. Cell Sci.* **2017**, *130*, 2147–2158.
23. van de Pavert, S.A.; Meuleman, J.; Malysheva, A.; Aartsen, W.M.; Versteeg, I.; Tonagel, F.; Kamphuis, W.; McCabe, C.J.; Seeliger, M.W.; Wijnholds, J. A single amino acid substitution (Cys249Trp) in Crb1 causes retinal degeneration and deregulates expression of pituitary tumor transforming gene Pttg1. *J. Neurosci.* **2007**, *27*, 564–573.
24. Zhou, B.; Wu, Y.; Lin, X. Retromer regulates apical-basal polarity through recycling crumbs. *Dev. Biol.* **2011**, *360*, 87–95.
25. Pocha, S.M.; Wassmer, T.; Niehage, C.; Hoflack, B.; Knust, E. Retromer Controls Epithelial Cell Polarity by Trafficking the Apical Determinant Crumbs. *Curr. Biol.* **2011**, *21*, 1111–1117.
26. Lattner, J.; Leng, W.; Knust, E.; Brankatschk, M.; Flores-Benitez, D. Crumbs organizes the transport machinery by regulating apical levels of pi (4,5)p2 in drosophila. *Elife* **2019**, *8*.
27. Kraut, R.S.; Knust, E. Changes in endolysosomal organization define a pre-degenerative state in the crumbs mutant Drosophila retina. *PLoS One* **2019**, *14*, e0220220.
28. Thompson, B.J.; Pichaud, F.; Röper, K. Sticking together the Crumbs - an unexpected function for an old friend. *Nat. Rev. Mol. Cell Biol.* **2013**, *14*, 307–14.
29. Alves, C.H.; Bossers, K.; Vos, R.M.; Essing, A.H.W.; Swagemakers, S.; van der Spek, P.J.; Verhaagen, J.; Wijnholds, J. Microarray and morphological analysis of early postnatal CRB2 mutant retinas on a pure C57BL/6J genetic background. *PLoS One* **2013**, *8*, e82532.
30. Chen, X.; Emerson, M.M. Notch signaling represses cone photoreceptor formation through the regulation of retinal progenitor cell states. *Sci. Reports 2021 111* **2021**, *11*, 1–18.
31. Mills, E.A.; Goldman, D. The Regulation of Notch Signaling in Retinal Development and Regeneration. *Curr. Pathobiol. Rep.* **2017**, *5*, 323–331.
32. Mizeracka, K.; Demaso, C.R.; Cepko, C.L. Notch1 is required in newly postmitotic cells to inhibit the rod photoreceptor fate. *Development* **2013**, *140*, 3188–3197.

33. Jadhav, A.P.; Cho, S.-H.; Cepko, C.L. Notch activity permits retinal cells to progress through multiple progenitor states and acquire a stem cell property. *Proc. Natl. Acad. Sci.* **2006**, *103*, 18998–19003.
34. Jadhav, A.P.; Mason, H.A.; Cepko, C.L. Notch 1 inhibits photoreceptor production in the developing mammalian retina. *Development* **2006**, *133*, 913–923.
35. Ohata, S.; Aoki, R.; Kinoshita, S.; Yamaguchi, M.; Tsuruoka-Kinoshita, S.; Tanaka, H.; Wada, H.; Watabe, S.; Tsuboi, T.; Masai, I.; et al. Dual Roles of Notch in Regulation of Apically Restricted Mitosis and Apicobasal Polarity of Neuroepithelial Cells. *Neuron* **2011**, *69*, 215–230.
36. Herranz, H.; Stamatakis, E.; Feiguin, F.; Milán, M. Self-refinement of notch activity through the transmembrane protein crumbs: Modulation of γ -secretase activity. *EMBO Rep.* **2006**, *7*, 297–302.
37. Nemetschke, L.; Knust, E. Drosophila Crumbs prevents ectopic Notch activation in developing wings by inhibiting ligand-independent endocytosis. *Development* **2016**, *143*, 4543–4553.
38. Ridley, S.H.; Kistakis, N.; Davidson, K.; Anderson, K.E.; Manifava, M.; Ellson, C.D.; Lipp, P.; Bootman, M.; Coadwell, J.; Nazarian, A.; et al. FENS-1 and DFPC1 are FYVE domain-containing proteins with distinct functions in the endosomal and Golgi compartments. *J. Cell Sci.* **2001**, *114*, 3991–4000.
39. Gajović, S.; Mitrečić, D.; Augustinčić, L.; Iaconcig, A.; Muro, A.F. Unexpected rescue of alpha-synuclein and multimerin1 deletion in C57BL/6JOLA^{Hsd} mice by beta-adducin knockout. *Transgenic Res.* **2006**, *15*, 255–259.
40. Ha, T.; Moon, K.H.; Dai, L.; Hatakeyama, J.; Yoon, K.; Park, H.-S.; Kong, Y.-Y.; Shimamura, K.; Kim, J.W. The Retinal Pigment Epithelium Is a Notch Signaling Niche in the Mouse Retina. *Cell Rep.* **2017**, *19*, 351–363.
41. Yaron, O.; Farhy, C.; Marquardt, T.; Applebury, M.; Ashery-Padan, R. Notch1 functions to suppress cone-photoreceptor fate specification in the developing mouse retina. *Development* **2006**, *133*, 1367–1378.
42. Richardson, E.C.N.; Pichaud, F. Crumbs is required to achieve proper organ size control during Drosophila head development. *Development* **2010**, *137*, 641–650.
43. Rosa-Ferreira, C.; Munro, S. Arl8 and SKIP Act Together to Link Lysosomes to Kinesin-1. *Dev. Cell* **2011**, *21*, 1171–1178.
44. Farfel-Becker, T.; Roney, J.C.; Cheng, X.T.; Li, S.; Cuddy, S.R.; Sheng, Z.H. Neuronal Soma-Derived Degradative Lysosomes Are Continuously Delivered to Distal Axons to Maintain Local Degradation Capacity. *Cell Rep.* **2019**, *28*, 51-64.e4.
45. Overhoff, M.; De Bruyckere, E.; Kononenko, N.L. Mechanisms of neuronal survival safeguarded by endocytosis and autophagy. *J. Neurochem.* **2021**, *157*, 263–296.
46. Pradhan, J.; Noakes, P.G.; Bellingham, M.C. The Role of Altered BDNF/TrkB Signaling in Amyotrophic Lateral Sclerosis. *Front. Cell. Neurosci.* **2019**, *13*, 368.
47. Babu, J.R.; Seibenhener, M.L.; Peng, J.; Strom, A.-L.; Kemppainen, R.; Cox, N.; Zhu, H.; Wooten, M.C.; Diaz-Meco, M.T.; Moscat, J.; et al. Genetic inactivation of p62 leads to accumulation of hyperphosphorylated tau and neurodegeneration. *J. Neurochem.* **2008**, *106*, 107–120.
48. Kakar-Bhanot, R.; Brahmabhatt, K.; Chauhan, B.; Katkam, R.R.; Bashir, T.; Gawde, H.; Mayadeo, N.; Chaudhari, U.K.; Sachdeva, G. Rab11a drives adhesion molecules to the surface of endometrial epithelial cells. *Hum. Reprod.* **2019**, *34*.
49. Aguilar-Aragon, M.; Fletcher, G.; Thompson, B.J. The cytoskeletal motor proteins Dynein and MyoV direct apical transport of Crumbs. *Dev. Biol.* **2020**, *459*, 126–137.
50. Gaullier, J.-M.; Simonsen, A.; D'Arrigo, A.; Bremnes, B.; Stenmark, H.; Aasland, R. FYVE fingers bind PtdIns(3)P. *Nat.* **1998**, *394*, 432–433.
51. Bellingrath, J.-S.; McClements, M.E.; Kaukonen, M.; Fischer, M.D.; MacLaren, R.E. In Silico Analysis of Pathogenic CRB1 Single Nucleotide Variants and Their Amenability to Base Editing as a Potential Lead for Therapeutic Intervention. *Genes* **2021**, *Vol. 12*, Page 1908 **2021**, *12*, 1908.
52. Trousdale, C.; Kim, K. Retromer: Structure, function, and roles in mammalian disease. *Eur. J. Cell Biol.* **2015**, *94*, 513–521.

53. Wang, S.; Tan, K.L.; Agosto, M.A.; Xiong, B.; Yamamoto, S.; Sandoval, H.; Jaiswal, M.; Bayat, V.; Zhang, K.; Charnig, W.-L.; et al. The Retromer Complex Is Required for Rhodopsin Recycling and Its Loss Leads to Photoreceptor Degeneration. *PLoS Biol.* **2014**, *12*, 1001847.
54. Boon, N.; Wijnholds, J.; Pellissier, L.P. Research Models and Gene Augmentation Therapy for CRB1 Retinal Dystrophies. *Front. Neurosci.* **2020**, *14*, 860.
55. Clark, B.S.; Miesfeld, J.B.; Flinn, M.A.; Collery, R.F.; Link, B.A. Dynamic Polarization of Rab11a Modulates Crb2a Localization and Impacts Signaling to Regulate Retinal Neurogenesis. *Front. Cell Dev. Biol.* **2021**, *8*, 608112.
56. Campa, C.C.; Margaria, J.P.; Derle, A.; Del Giudice, M.; De Santis, M.C.; Gozzelino, L.; Copperi, F.; Bosia, C.; Hirsch, E. Rab11 activity and PtdIns(3)P turnover removes recycling cargo from endosomes. *Nat. Chem. Biol.* **2018**, *14*, 801–810.
57. Pellissier, L.P.; Quinn, P.M.; Henrique Alves, C.; Vos, R.M.; Klooster, J.; Flannery, J.G.; Alexander Heimel, J.; Wijnholds, J. Gene therapy into photoreceptors and Müller glial cells restores retinal structure and function in CRB1 retinitis pigmentosa mouse models. *Hum. Mol. Genet.* **2015**, *24*, 3104–3118.
58. Alves, C.H.; Sanz, A.S.; Park, B.; Pellissier, L.P.; Tanimoto, N.; Beck, S.C.; Huber, G.; Murtaza, M.; Richard, F.; Sridevi Gurubaran, I.; et al. Loss of CRB2 in the mouse retina mimics human retinitis pigmentosa due to mutations in the CRB1 gene. *Hum. Mol. Genet.* **2013**, *22*, 35–50.
59. Rowan, S.; Cepko, C.L. Genetic analysis of the homeodomain transcription factor Chx10 in the retina using a novel multifunctional BAC transgenic mouse reporter. *Dev. Biol.* **2004**, *271*, 388–402.
60. Kolisnyk, B.; Guzman, M.S.; Raulic, S.; Fan, J.; Magalhães, A.C.; Feng, G.; Gros, R.; Prado, V.F.; Prado, M.A.M. Chat-ChR2-EYFP mice have enhanced motor endurance but show deficits in attention and several additional cognitive domains. *J. Neurosci.* **2013**, *33*, 10427–10438.
61. Ting, J.T.; Feng, G. Recombineering strategies for developing next generation BAC transgenic tools for optogenetics and beyond. *Front. Behav. Neurosci.* **2014**, *8*, 1–13.
62. Specht, C.G.; Schoepfer, R. Deletion of multimerin-1 in α -synuclein-deficient mice. *Genomics* **2004**, *83*, 1176–1178.
63. Huang, T.T.; Naeemuddin, M.; Elchuri, S.; Yamaguchi, M.; Kozy, H.M.; Carlson, E.J.; Epstein, C.J. Genetic modifiers of the phenotype of mice deficient in mitochondrial superoxide dismutase. *Hum. Mol. Genet.* **2006**, *15*, 1187–1194.
64. Alves, C.H.; Wijnholds, J. AAV gene augmentation therapy for CRB1-associated retinitis pigmentosa. In *Methods in Molecular Biology*; Boon, C.J.F., Wijnholds, J., Eds.; Humana Press Inc.: New York, NY, 2018; Vol. 1715, pp. 135–151 ISBN 9781493975211.
65. Robinson, M.D.; McCarthy, D.J.; Smyth, G.K. edgeR: a Bioconductor package for differential expression analysis of digital gene expression data. *Bioinformatics* **2010**, *26*, 139–140.
66. Ritchie, M.E.; Phipson, B.; Wu, D.; Hu, Y.; Law, C.W.; Shi, W.; Smyth, G.K. limma powers differential expression analyses for RNA-sequencing and microarray studies. *Nucleic Acids Res.* **2015**, *43*, e47–e47.
67. Robinson, M.D.; Oshlack, A. A scaling normalization method for differential expression analysis of RNA-seq data. *Genome Biol.* **2010**, *11*.
68. Law, C.W.; Chen, Y.; Shi, W.; Smyth, G.K. voom: Precision weights unlock linear model analysis tools for RNA-seq read counts. *Genome Biol.* **2014**, *15*.
69. Faas, F.G.A.; Cristina Avramut, M.; van den Berg, B.M.; Mieke Mommaas, A.; Koster, A.J.; Ravelli, R.B.G. Virtual nanoscopy: Generation of ultra-large high resolution electron microscopy maps. *J. Cell Biol.* **2012**, *198*, 457–469.

Figures

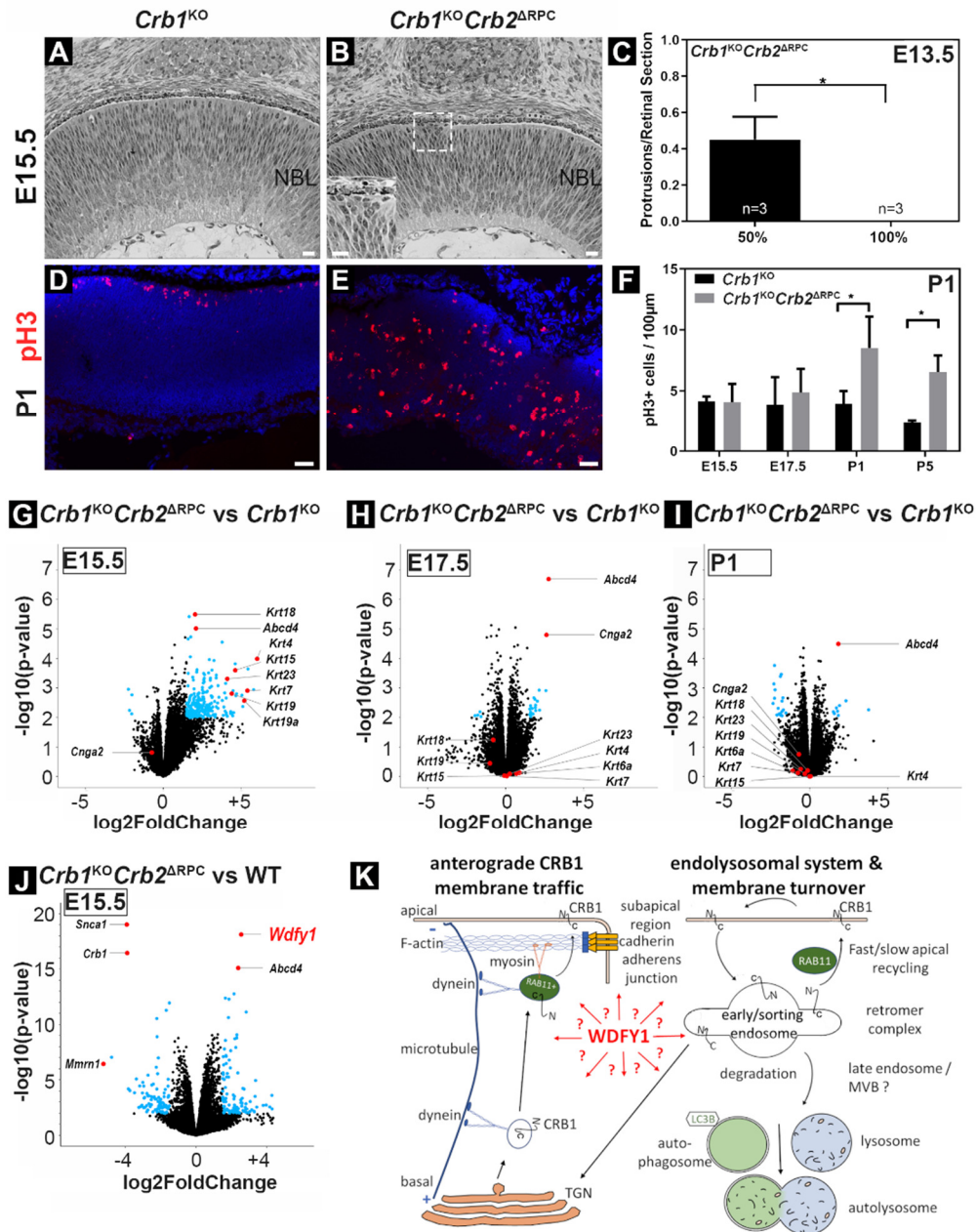


Figure 1. mRNA transcript levels are marginally different in *Crb1*^{KO}*Crb2*^{ARPC} against *Crb1*^{KO} neuroretina. (A-B) Retinal morphology on plastic sections of *Crb1*^{KO} and *Crb1*^{KO}*Crb2*^{ARPC} mice on 100% C57/B6 genetic background at E15.5. (A) *Crb1*^{KO} retinas appeared unaffected while (B) *Crb1*^{KO}*Crb2*^{ARPC} retinas had protrusions of NBL nuclei in the subretinal space (insert). (C) Protrusions per retinal section in 50% and 100% C57/B6 genetic background at E13.5. (D-J) 100% C57/B6 genetic background. (D-E) Immunofluorescence labelling of pH3+ nuclei (late G2 cell cycle and mitosis maker) at P1 in (D) *Crb1*^{KO} and (E) and *Crb1*^{KO}*Crb2*^{ARPC} retina. (F) Quantification of pH3+ cells at E15.5, E17.5, P1, and P5. (G-J) All changed genes indicated in blue circles (p-value < 0.01; log2fc > 1.5). (G-I) *Crb1*^{KO}*Crb2*^{ARPC} against *Crb1*^{KO} neuroretina transcripts (Run1) at embryonic day (E)15.5, E17.5, and P1. (J) *Crb1*^{KO}*Crb2*^{ARPC} compared to WT neuroretina transcripts at E15.5 (Run2). (K) Potential WDFY1 involvement in CRB1 protein trafficking (modified from [49]). Scale bar, 20 μm. WT, wildtype; TGN, trans golgi network; MVB, multivesicular body. See also Figure S1+S2.

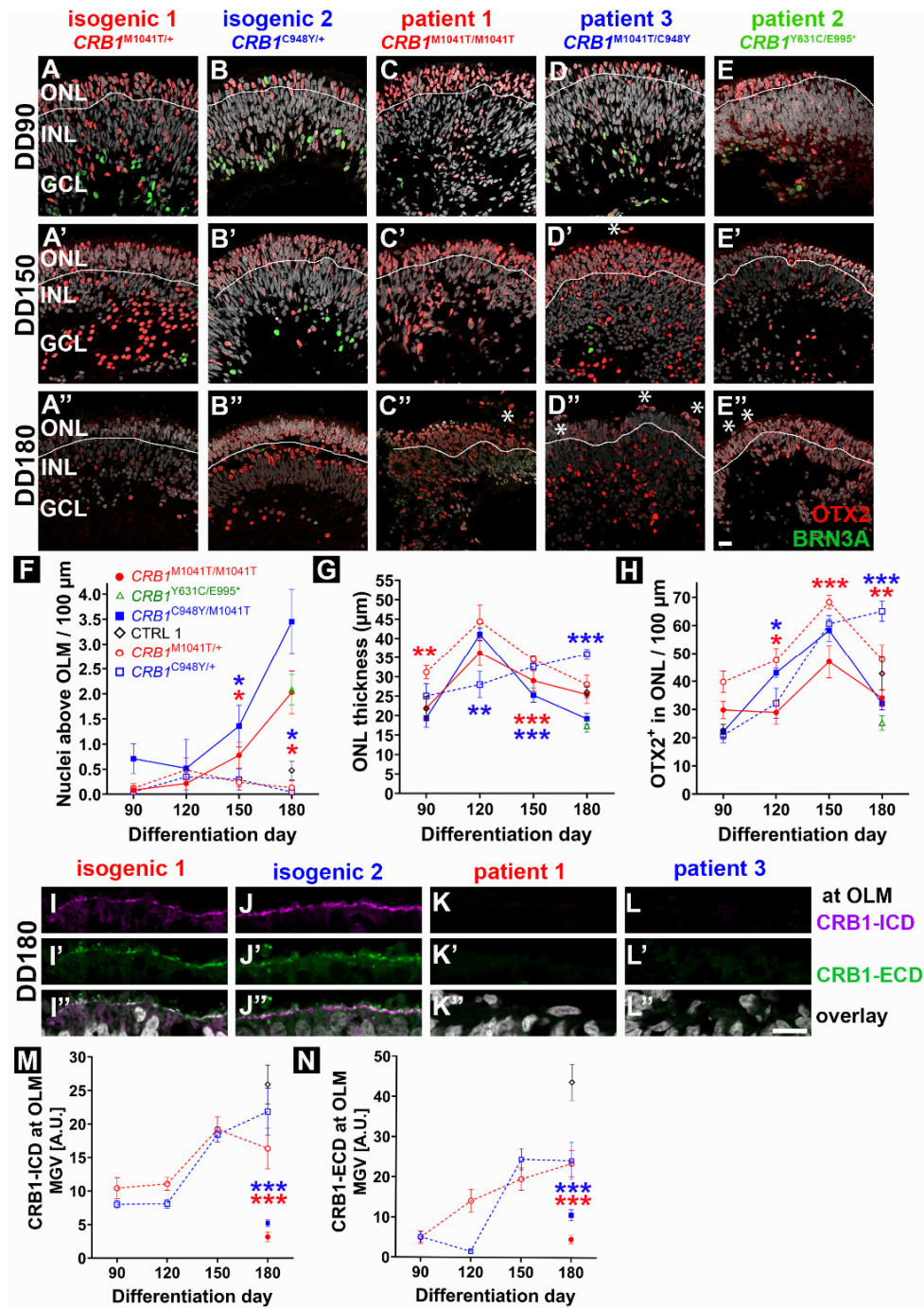


Figure 2. CRB1 patient organoids degenerate over time and express little CRB1 apically. (A-E) Nuclei stained for OTX2 (early photoreceptor cells) and BRN3A (Ganglion cells; scale bar, 50 μ m). (A-B) isogenic control, (C-E) CRB1 patient organoids at DD90 (A-E), DD150 (A'-E'), DD180 (A''-E''). Ectopic nuclei are indicated with an asterisk and ONL/INL border with a white line. (F) number of nuclei above the OLM over time, (G) number of ONL thickness over time (OTX2+/DAPI+ nuclei top layer), (H) OTX2+ photoreceptor loss over time (F-H: n=9-25). (I-L) CRB1 stained with an (I-L) intracellular (ICD) or (I'-L') extracellular domain (ECD) epitope antibodies at the OLM, and (I''-L'') overlay (scale bar, 10 μ m). (M-N) CRB1-Alexa conjugated fluorescence signal detected over time on ICD-(M) and ECD-(N) CRB1 antibodies (empty circles/dashed lines, isogenic controls; filled circles, patient lines; DD180, n=8; DD90-150, n=4-6 organoids per line). isogenic 1: CRB1Met1041Thr/+, iso03LUMC0116iCRB09; isogenic 2: CRB1Cys948Tyr/+, iso02LUMC0128iCRB01; Patient 1 to 3: CRB1Met1041Thr/ Met1041Thr, LUMC0116iCRB09; CRB1Tyr631Cys/Glu995*, LUMC0117iCRB01; CRB1Met1041Thr/Cys948Tyr, LUMC0128iCRB01. OLM, outer nuclear layer; MVG, mean gray value. See also Figure S3+S4.

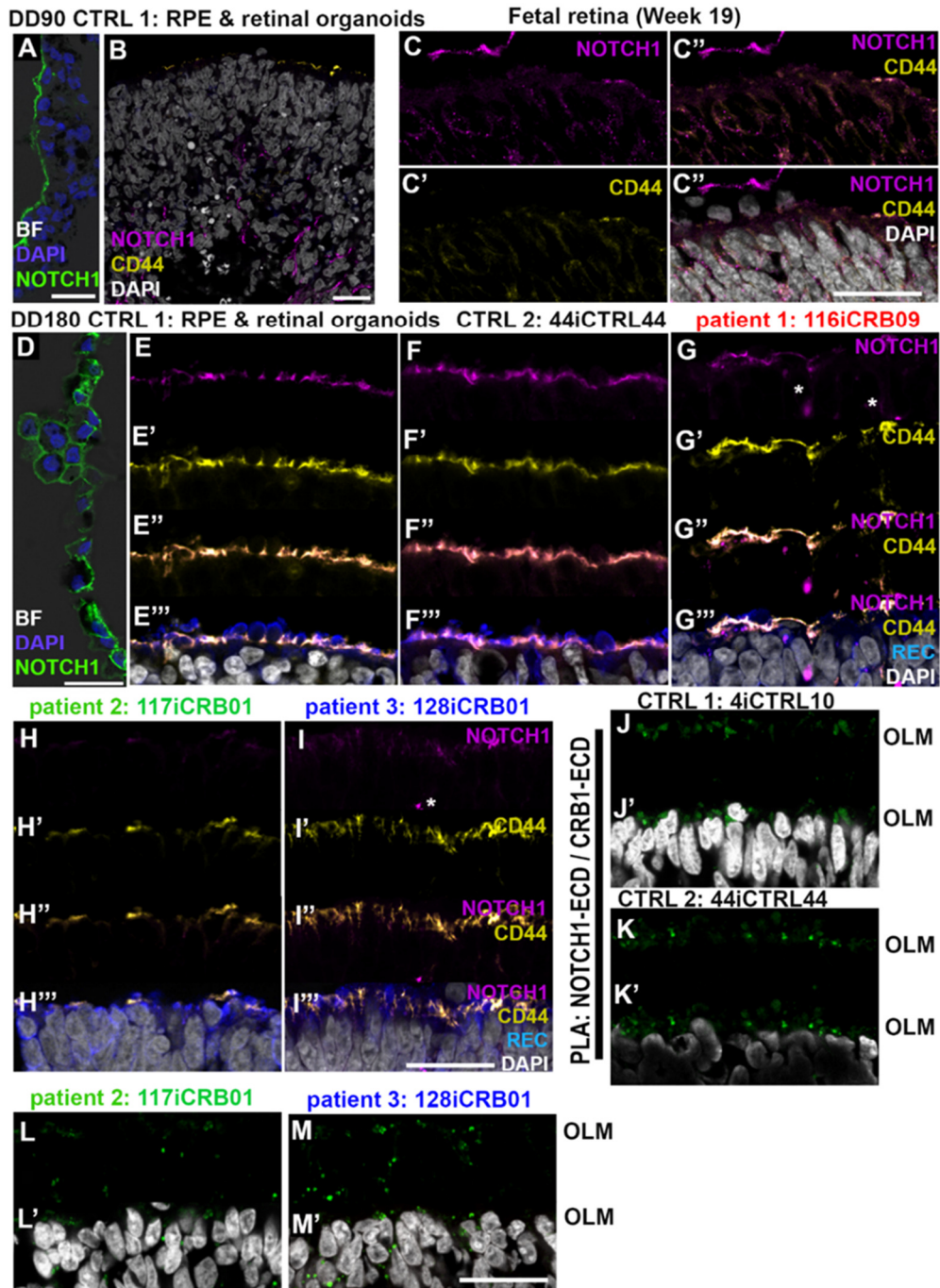


Figure 3. Apical NOTCH1 is lost in *CRB1* patient retinal organoids. (A+D) CTRL1 (LUMC004iCTRL10) RPE expresses NOTCH1 at DD90 and DD180. (B) Little NOTCH1 is expressed at the OLM in the CTRL1 DD90 retinal organoid. (C) NOTCH1 is expressed in the RPE and very little in the neuroretina at the OLM in human fetal retina (gestation week 19). (E) CTRL1, (F) CTRL2 (LUMC044iCTRL44), (G) patient 1 (LUMC0116iCRB09), (H) patient 2 (LUMC0117iCRB01), patient 3 (LUMC0128iCRB01). (E-I) NOTCH1 is expressed specifically in DD180 Müller glial apical villi (magenta, NOTCH1; yellow, CD44; blue, recoverin; gray, DAPI). (J-M) Proximity Ligation Assay of NOTCH1-ECD and CRB1-ECD (green signal) shows interaction at control OLM, but reduced interaction at patient OLM with increased localization in patient ONL. Scale bar, 25 μ m.

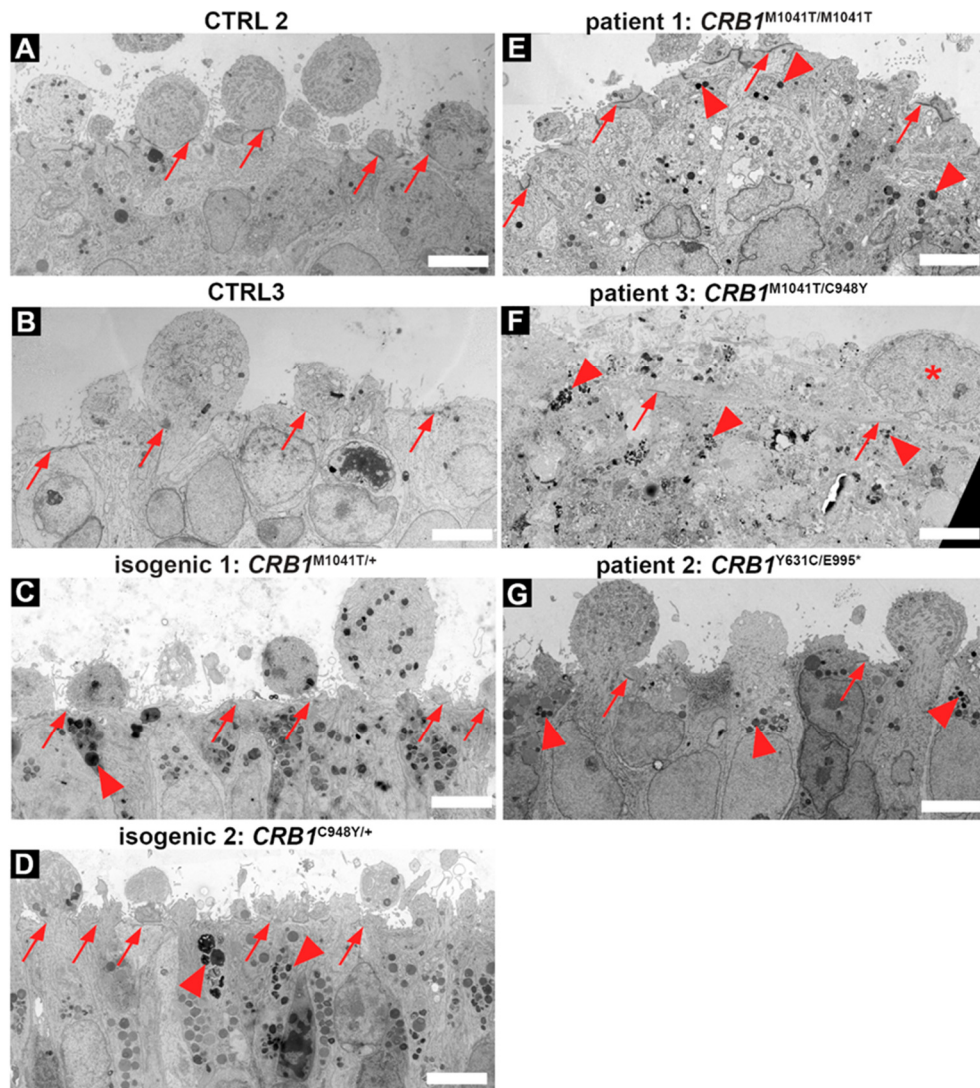
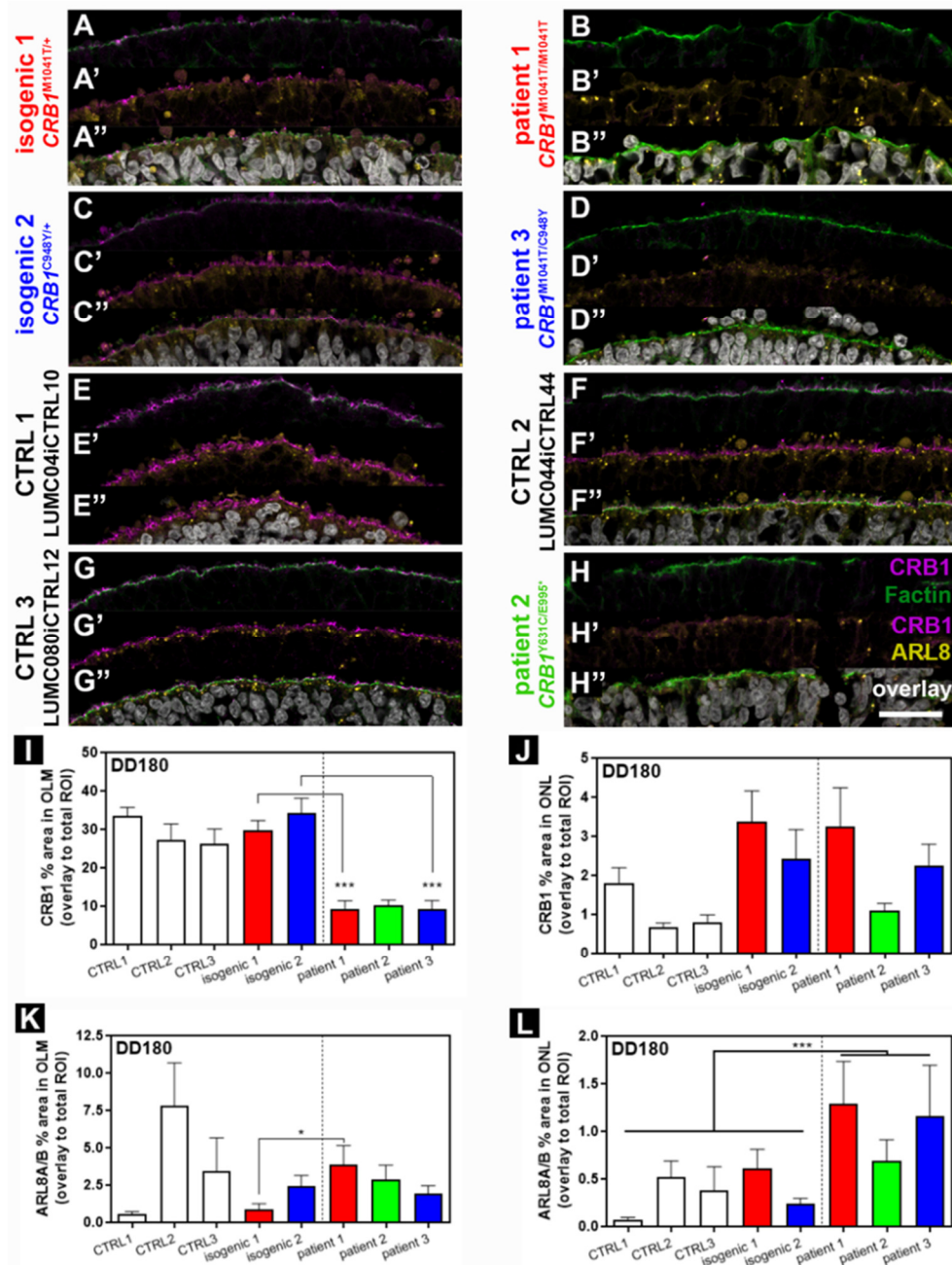


Figure 4. Transmission electron microscopy high resolution imaging of retinal organoids at DD180. Electron-dense outer limiting membrane (red arrows), electron-dense degradative compartments/vacuoles (arrowheads), and nuclei above OLM (asterisks). (A-B) control lines (LUMC0044iCTRL44; LUMC080iCTRL12), (C-D) gene corrected lines (iso3LUMC0116iCRB09; iso2LUMC0128iCRB01), and (E-G) patient lines (LUMC0116iCRB09; LUMC0117iCRB01; LUMC0128iCRB01). Scale bar, 5 μm.



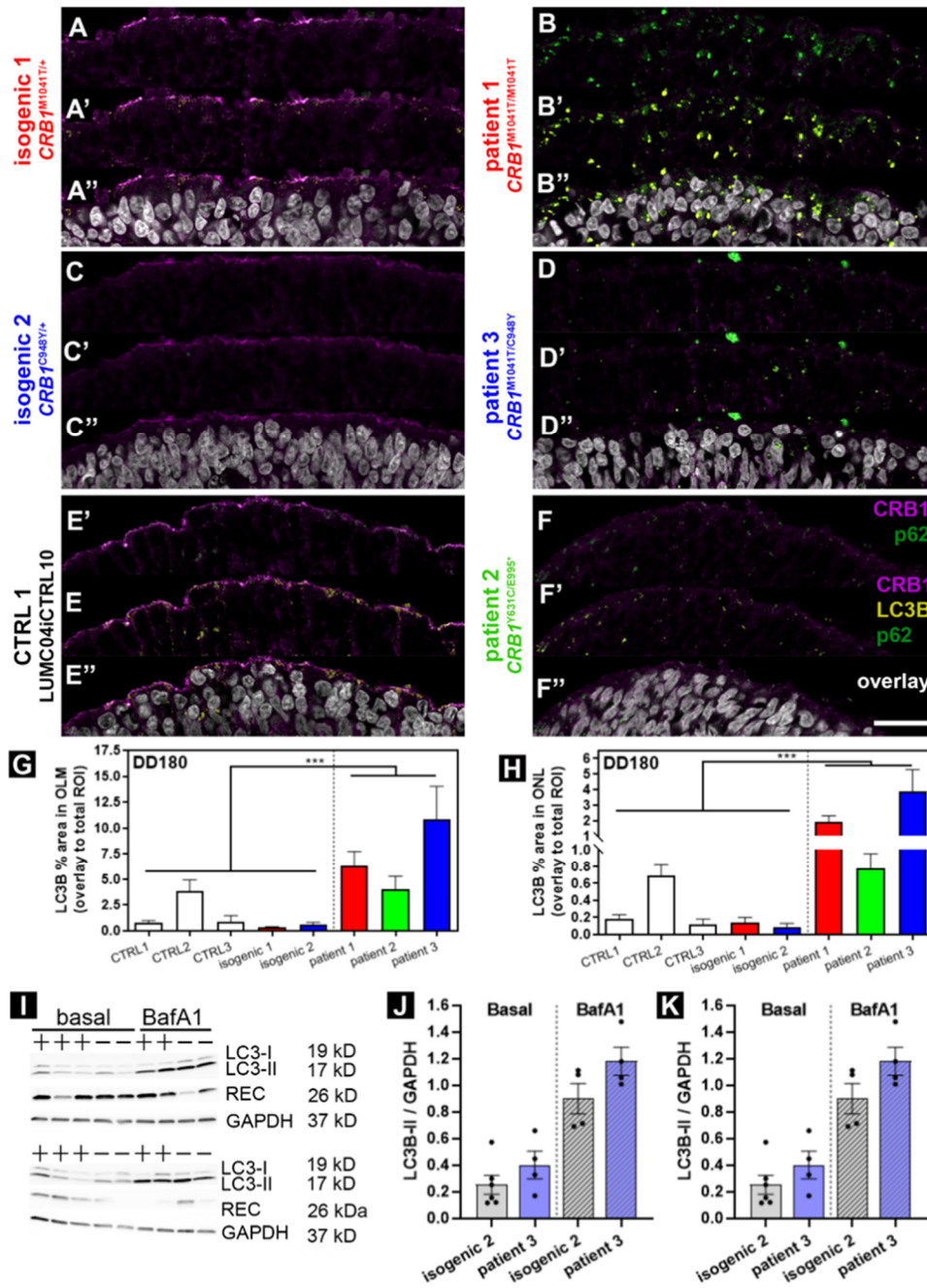


Figure 6. More degradative vesicles/compartments are present in *CRB1* patient retinal organoids. (A-F) Immunofluorescence triple staining CRB1 (magenta), p62 (green), and LC3B (yellow). (G-H) LC3B localized more in the ONL and OLM layers in *CRB1* RP retinal organoids. (I-K) Western blot of individual lysed organoids (plus symbol, isogenic 2 line (iso02-128iCRB01)); minus symbol, patient 3 (line LUMC0128CRB01) stained for LC3B (LC3-I and LC3-II; 19/17 kD); recoverin for photoreceptors (26 kD), and GAPDH (housekeeping control, 37 kD). The autophagic flux was decreased in *CRB1* patient organoids. Scale bar, 25 μ m.

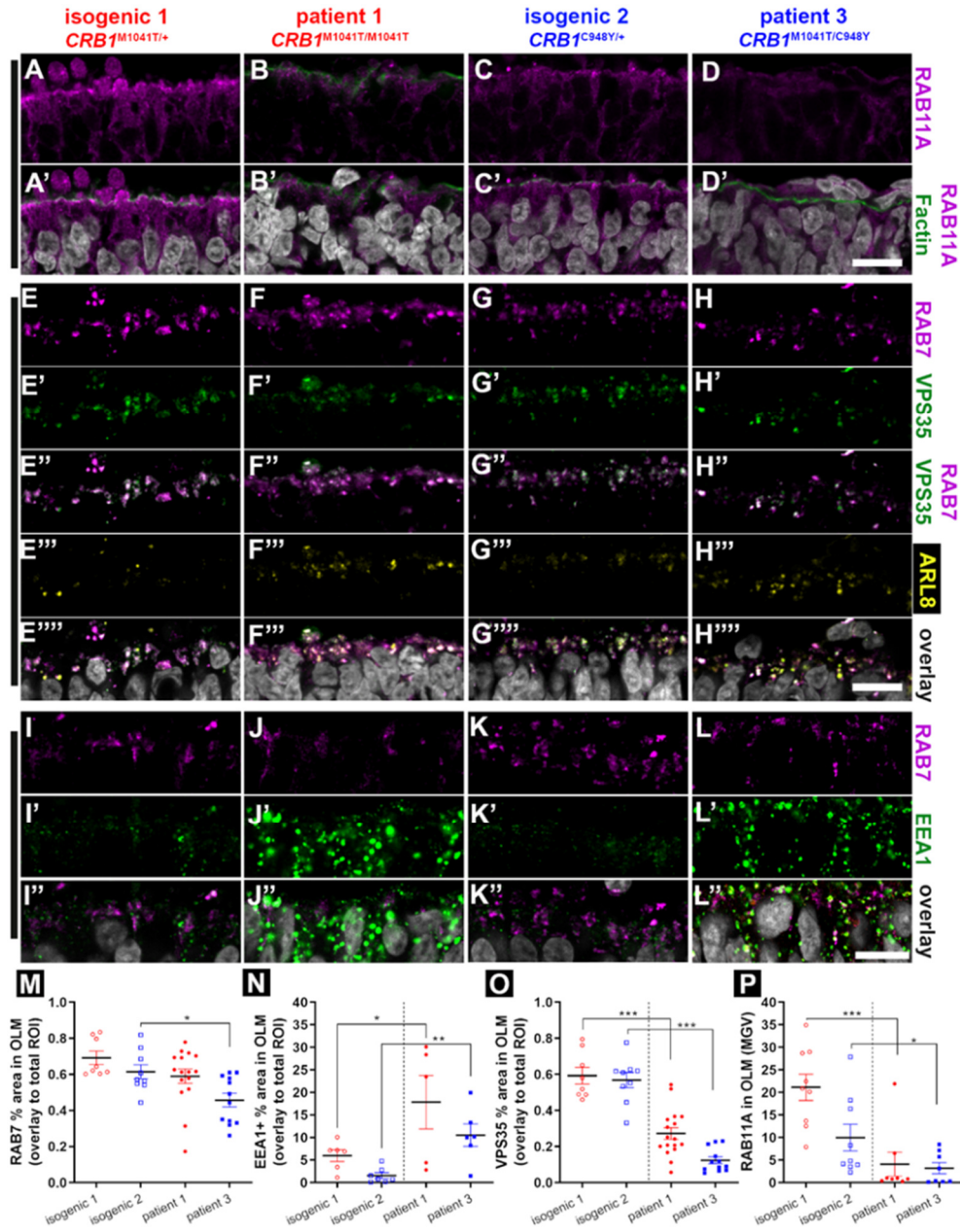


Figure 7. Dysregulation of the endolysosomal system in *CRB1* patient organoids. Immunofluorescence on isogenic control lines 1 and 2 (A+C; E+G; I+K) related to the patient lines 1 (LUMC0116iCRB09) and patient line 3 (LUMC0128iCRB01), and patient lines 1+3 (B+D; F+H; J-L). (A-D) recycling endosomes (RAB11A; magenta) and phalloidin (F-actin; green). (E-H) late endosomes (RAB7; magenta), retromer complex (VPS35; green), endolysosomes (ARL8A/B; yellow). (I-L) late endosomes (RAB7, magenta) and early endosomes (EEA1, green) and. (M-P) Quantification of fluorescence signal of early endosomes (EEA1), late endosomes (RAB7), retromer (VSP35), and recycling endosomes (RAB11A) in OLM. (M) RAB7 in OLM. (N) EEA1 in OLM. (O) VPS35 in OLM. (P) RAB11A in OLM. Scale bar, 10 μ m.

Supplemental Information

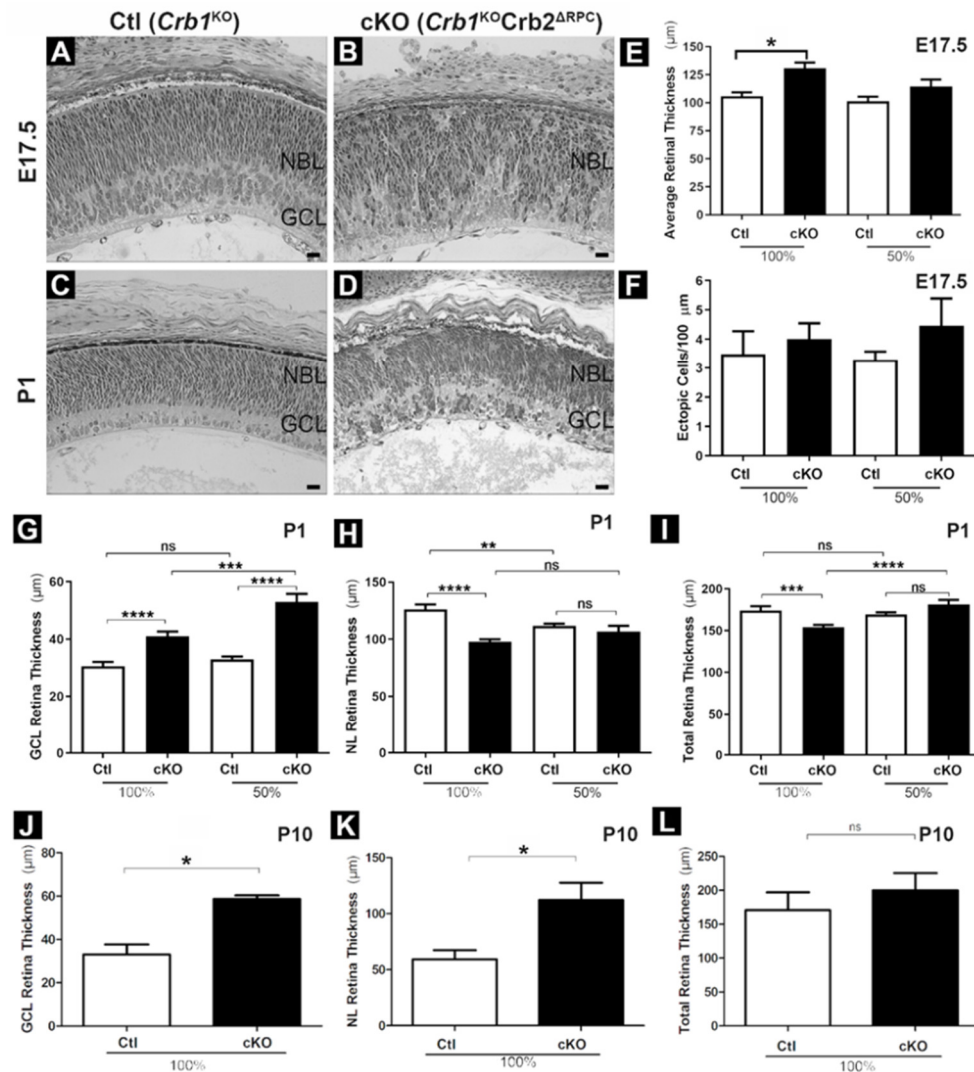


Figure S1. The retinal morphological phenotype is milder in *Crb1*^{KO}*Crb2*^{ARPC} on 100% C57/B6 genetic background than on 50% mixed genetic background. Related to Figure 1. (A-D) Retinal morphology on plastic sections of Ctl (*Crb1*^{KO}) and cKO (*Crb1*^{KO}*Crb2*^{ARPC}) mice on 100% C57/B6 genetic background at E17.5 and P1. (E-F) Ctl (*Crb1*^{KO}) and cKO (*Crb1*^{KO}*Crb2*^{ARPC}) mice on 50% and 100% C57/B6 genetic background. (E-F) Average retinal thickness and ectopic nuclei per 100 μm retinal length at E17.5. (G-I) Ganglion cell layer (GCL) thickness, neuroretina layer (NL) thickness, and retinal thickness (OLM-ILM) at P1. (J-L) GCL thickness, NL thickness, and retinal thickness in 100% C57/B6 genetic background at P10. Scale bar, 20 μm.

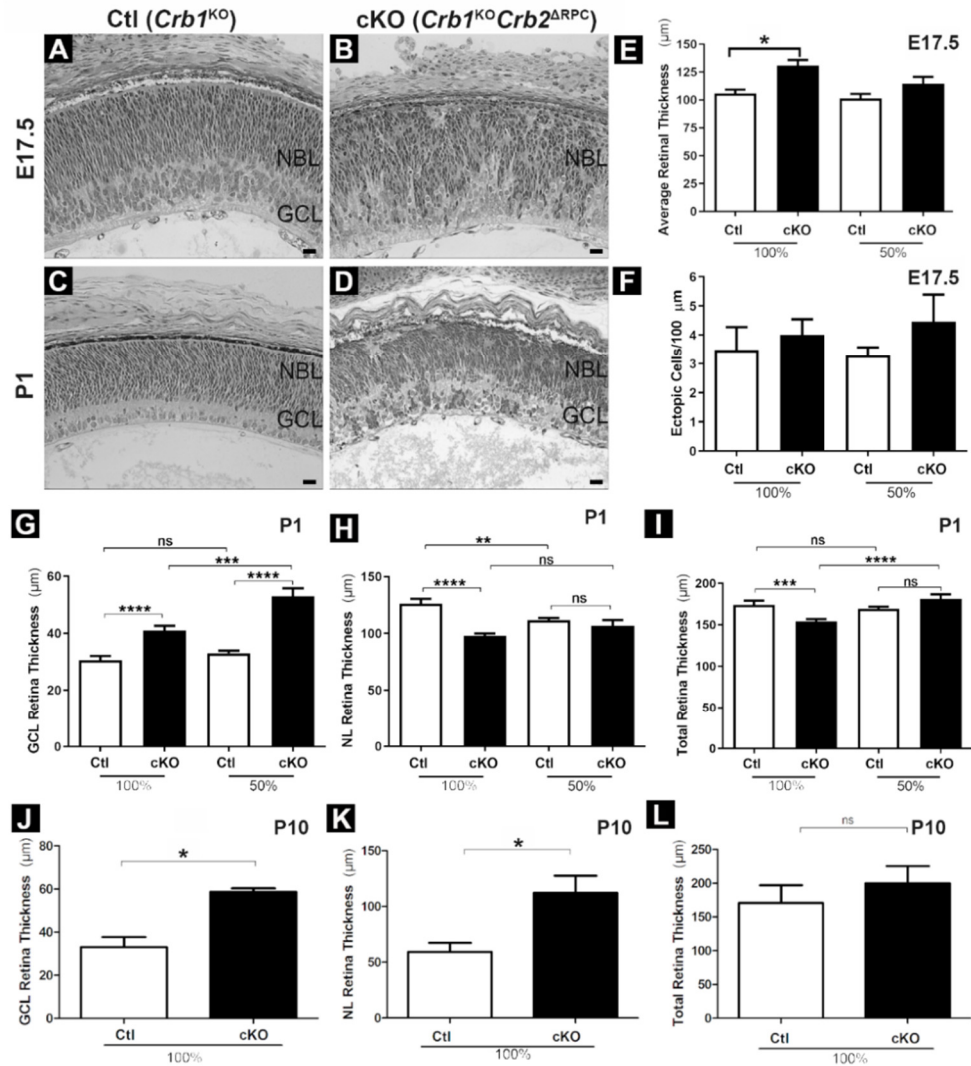


Figure S2. The *Crb1*^{KO}*Crb2*^{ARPC} mouse displays an LCA-like *CRB1* phenotype. Related to Figure 1. (A-F) Retinal morphology on plastic sections of Ctl (*Crb1*^{KO}) and cKO (*Crb1*^{KO}*Crb2*^{ARPC}) mice on 100% C57/B6 genetic background at P14, 1M, and 3M. (G-H) Retinal thickness (OLM-ILM) at P14, 1M, and 3M. (I-K) Electoretinographic (ERG) analysis of the retinal function at 1M. Conditional KOs are in red and Ctl age-matched littermates in gray: (L-M) Scotopic (SC) single-flash intensity series (-4, -3, -2, -1, 0, 1, 1.5, 1.9 log cd s/m² light intensity). (I) scotopic a-wave amplitudes. (J) scotopic b-wave amplitudes. (K) Photopic (PH) single-flash ERG at different light intensities (-2, -1, 0, 1, 1.5, 1.9 log cd s/m² light intensity at 30 cd/m² background light). Boxes indicate the 25 and 75% quantile range, whiskers indicate the 5 and 95% quantiles, and the intersection of line and error bar indicates the median of the data. (L) *Crb1*^{KO}*Crb2*^{ARPC} vs *Crb1*^{KO} neuroretina qPCR validation (n=5 retinas / group) of transcript changes at P1. Statistical significance calculated by a two-sided T-Test (p<0.05; 0.01; 0.001 shown as *, **, and *). Scale bar, 20 μm.**

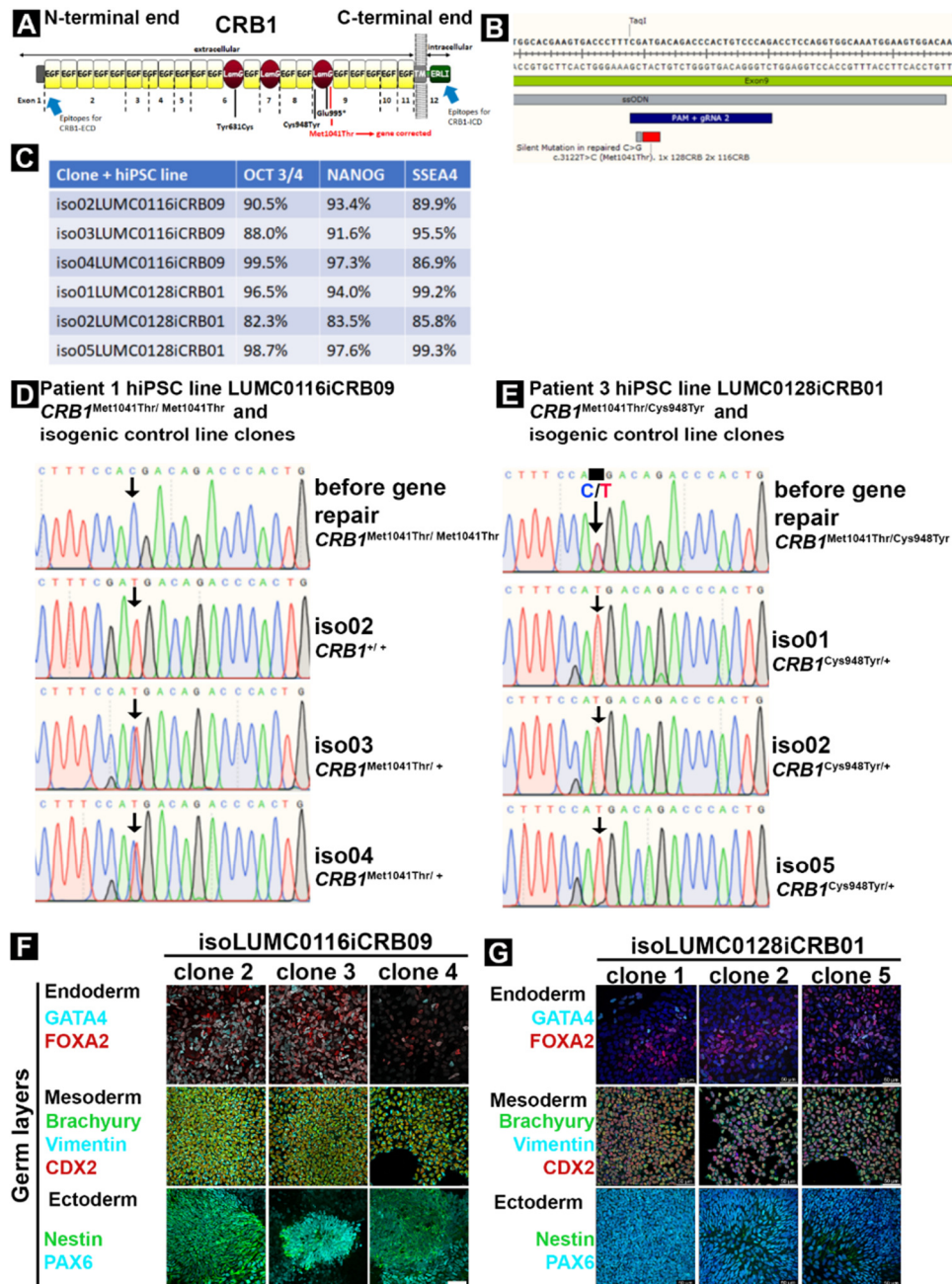


Figure S3. Validation of the isogenic control iPS cell lines. Related to Figure 2-7. (A) CRB1 protein domains and the corresponding exons, CRB1 patient variants, and the epitope of the CRB1-ICD and CRB-ECD antibodies. (B) Gene correction by single-stranded oligodeoxynucleotides (ssODN), gRNA, and nuclease Cas9 on locus c.3122T>C. (C) Flow cytometry sorted human iPSC clones indicating expression of pluripotency markers SSEA4, OCT3/4, and NANOG. (D-E) Sanger sequence validation of 3 clones per patient line. (G-H) human iPSC clones differentiated into the three germ layers. Scale bar, 50 μ m.

Table S1. Information on human iPSC lines. Related to Figure S3 and Figure 2-7.

Line code	Description	Gender
Control-derived and gene corrected (isogenic, iso) human iPSC line names		
LUMC0004iCTRL10	Control line 1 (CTRL 1)	male
LUMC0044iCTRL44	Control line 2 (CTRL 2)	female
LUMC0080iCTRL12	Control line 3 (CTRL 3)	male
iso01LUMC0116iCRB09	isogenic: Allele 1: c.3122T>C gene corrected to c.3122C>T. Allele 2: c.3122T>C. p.(Met1041Thr)	male
iso02LUMC0116iCRB09	isogenic 1: Allele 1: c.3122T>C gene corrected to c.3122C>T. Allele 2: c.3122T>C. p.(Met1041Thr)	male
iso03LUMC0116iCRB09	isogenic: Allele 1 and 2: Homozygous c.3122T>C gene corrected to c.3122C>T	male
iso01LUMC0128iCRB01	isogenic: Allele 1: c.2843G>A --> p.(Cys948Tyr). Allele 2: c.3122T>C gene corrected to c.3122C>T	male
iso02LUMC0128iCRB01	Isogenic 2: Allele 1: c.2843G>A. p.(Cys948Tyr). Allele 2: c.3122T>C gene corrected to c.3122C>T	male
iso03LUMC0128iCRB01	isogenic: Allele 1: c.2843G>A. p.(Cys948Tyr). Allele 2: c.3122T>C gene corrected to c.3122C>T	male
iso05LUMC0128iCRB01	isogenic: Allele 1: c.2843G>A. p.(Cys948Tyr). Allele 2: c.3122T>C gene corrected to c.3122C>T	male
Patient <i>CRB1</i> Retinitis pigmentosa-derived human iPSC lines		
LUMC0116iCRB09	Patient 1. Allele 1 and 2: homozygous c.3122T>C--> p.(Met1041Thr)	male
LUMC0117iCRB01	Patient 2. Allele 1: c.1892A>G (p.Tyr631Cys). Allele 2: c.2911G>T (p.(Glu995*))	male
LUMC0128iCRB01	Patient 3. Allele 1: c.2843G>A --> p.(Cys948Tyr). Allele 2: c.3122T>C --> p.(Met1041Thr)	male

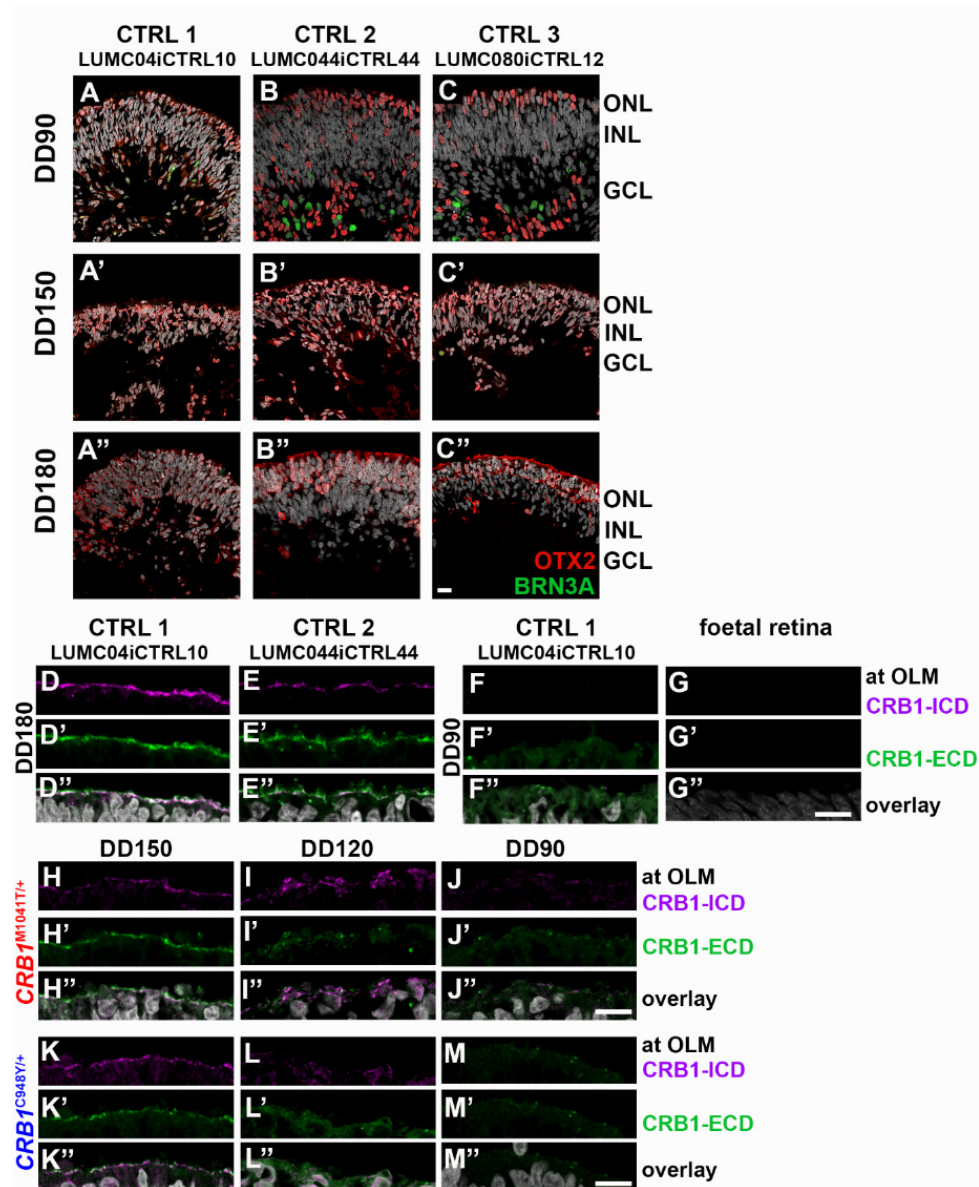


Figure S4. The onset of *CRB1* expression of *CRB1* at >DD120 coincides with a well-defined ONL layer. Related to Figure 2. (A-C) Nuclei stained for OTX2 (early photoreceptor cells) and BRN3A (Ganglion cells; scale bar, 50 μm). (A-C) control organoids of three independent donors at DD90 (A-C), DD150 (A'-C'), DD180 (A''-C''). (D-M) *CRB1* stained with an (D-M) intracellular (ICD) or (D'-M') extracellular domain (ECD) epitope antibodies at the OLM, and (D''-M'') overlay (scale bar, 10 μm) at DD180 (D-E; CTRL 1+2), DD90 (F: CTRL 1), human retina foetal gestation week 19 (G), DD150 (H+K; isogenic 1+2), DD120 (I+L; isogenic 1+2), and DD90 (J+M; isogenic 1+2). CTRL 1, LUMC04iCTRL10; CTRL2, LUMC044iCTRL44; isogenic 1, *CRB1^{M1041T/+}*; isogenic 2, *CRB1^{C948Y/+}*; OLM, outer limiting membrane; ICD, intracellular domain; ECD, extracellular domain; DD, differentiation day.

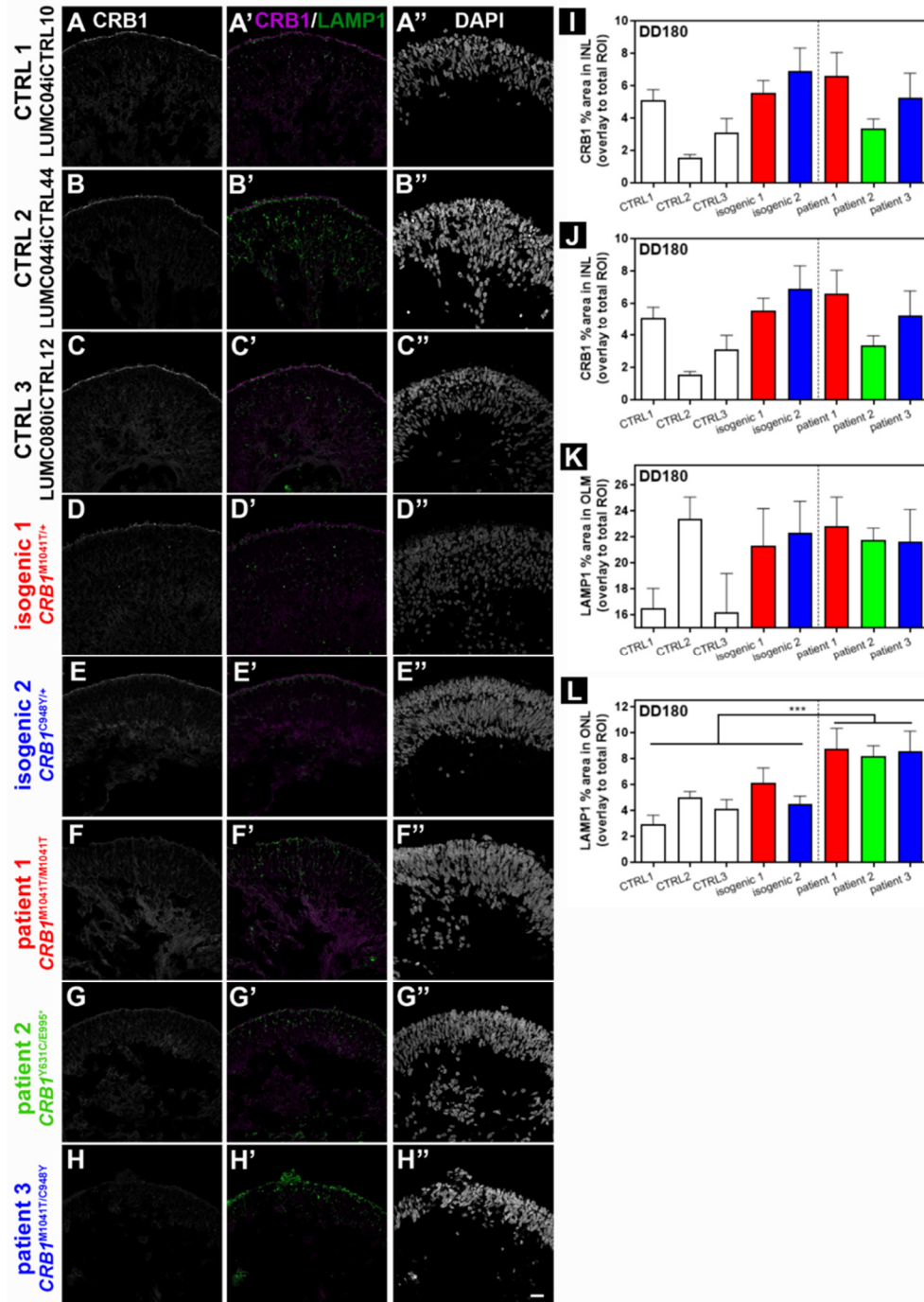


Figure S5. More lysosomes are present in *CRB1* patient retinal organoids. Related to Figure 4. Immunofluorescence CRB1 puncta (A-H; grayscale), co-labelling CRB1/LAMP1 (green/magenta in A'-H'), and nuclei (grayscale in A''-H'') in *CRB1* patient retinal organoids at DD180. (A-H) patient *CRB1* retinal organoids express little CRB1 protein throughout the neuroretina. (A'-H') Little co-labelling of CRB1 (magenta) and lysosomes (LAMP1+, green) were found. (A''-H'') Patient *CRB1* retinal organoids have more lysosomes at the ONL. (A'''-H''') Nuclei staining (DAPI, grayscale) showing overall morphology. (I) CRB1-fluorescence signal measured by puncta in the INL. (I) The average CRB1 puncta size measured on fluorescence signal. (J-K) LAMP1+ puncta measured in the OLM and ONL. N=8-13 organoids per line. Scale bar, 50 μ m.

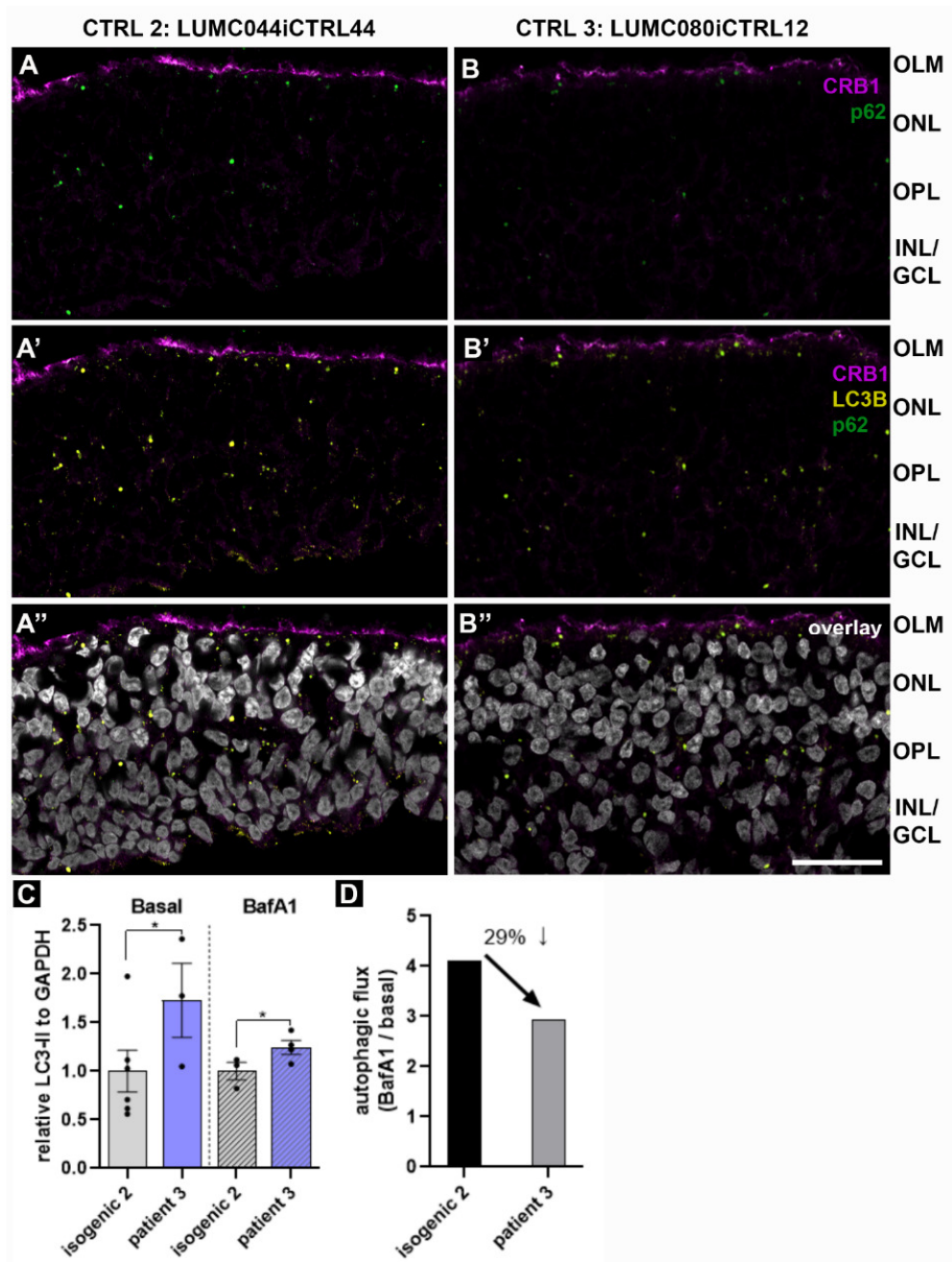


Figure S6. More degradative vesicles/compartments are present in *CRB1* patient retinal organoids. Related to Figure 5. (A-B) Immunofluorescence triple staining *CRB1* (magenta), p62 (green), and LC3B (yellow). (A-B) LC3B and p62 localized overall more in OLM layer, OPL layer and INL layer in control retinal organoids. Scale bar, 50 μm . (C-D) Iso02-128 is the isogenic control line related to the patient 3 line (LUMC0128iCRB01, here called RP *CRB1*). (C) Analysis of the protein band intensities of the western blot shown in Figure 6I of individual lysed organoids (depicted as dots) stained for LC3B (LC3-I and LC3-II; 19/17 kD), recoverin for photoreceptors (26 kD), and GAPDH (housekeeping control, 37 kD) but organoids lacking recoverin expression were removed from the analysis. (D) Western blot protein band intensities of the BafA1 condition divided by the basal condition showing a decrease in the autophagic flux in *CRB1* patient retinal organoids.

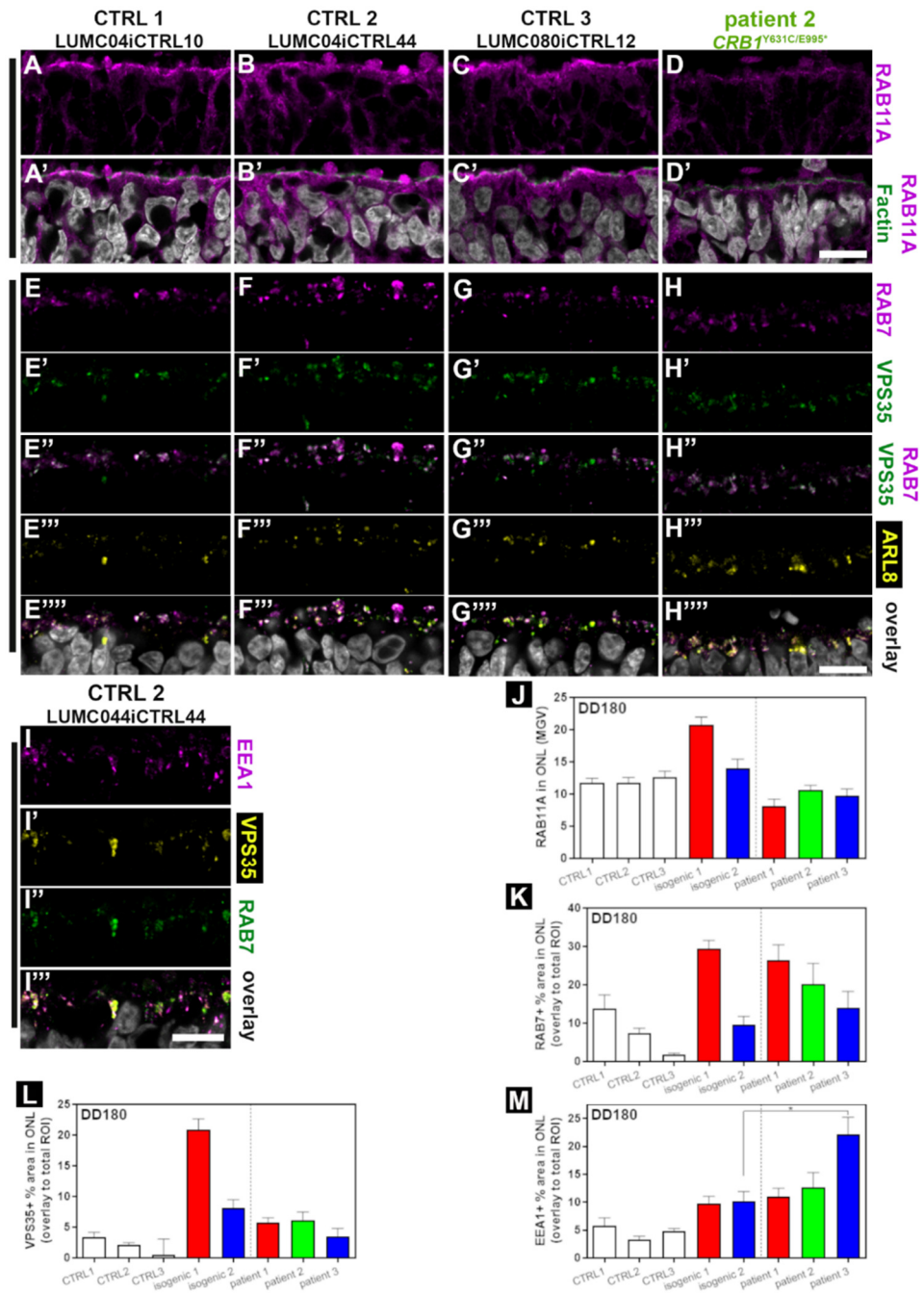


Figure S7. Dysregulation of the endolysosomal system in patient *CRBI* patient retinal organoids. Related to Figure 7. (A+E) CTRL 1 (LUMC04CTRL10) retinal organoids, (B+F+I) CTRL 2 (LUMC044iCTRL44) retinal organoids, (C+G) CTRL3 (LUMC080iCTRL12) retinal organoids, and (D+H) patient 2 (LUMC0117iCRB01) retinal organoids. (A-D) Immunofluorescence labelling of RAB11A (magenta), and phalloidin (F-actin; green). (E-H) Immunofluorescence labeling of RAB7 (magenta), VPS35 (green), and ARL8A/B (yellow). (E-H) Immunofluorescence labeling of EEA1 (magenta), RAB7 (green), and ARL8A/B (yellow). (I) Immunofluorescence labeling of EEA1 (magenta), RAB7 (green), and VPS35 (yellow). Overlay shown in white (E-I). (J-M) Semi-quantification of fluorescence signal. (J) RAB11A mean gray value (MVG) in ONL. (K) Total RAB7 particle area / total ONL area in %. (L) RAB11A mean gray value (MVG) in ONL. (K) Total VPS35 particle area / total ONL area in %. (M) RAB11A mean gray value (MVG) in ONL. (K) Total EEA1 particle area / total ONL area in %. All retinal organoids at DD180 collected. Scale bar, 10 μ m.

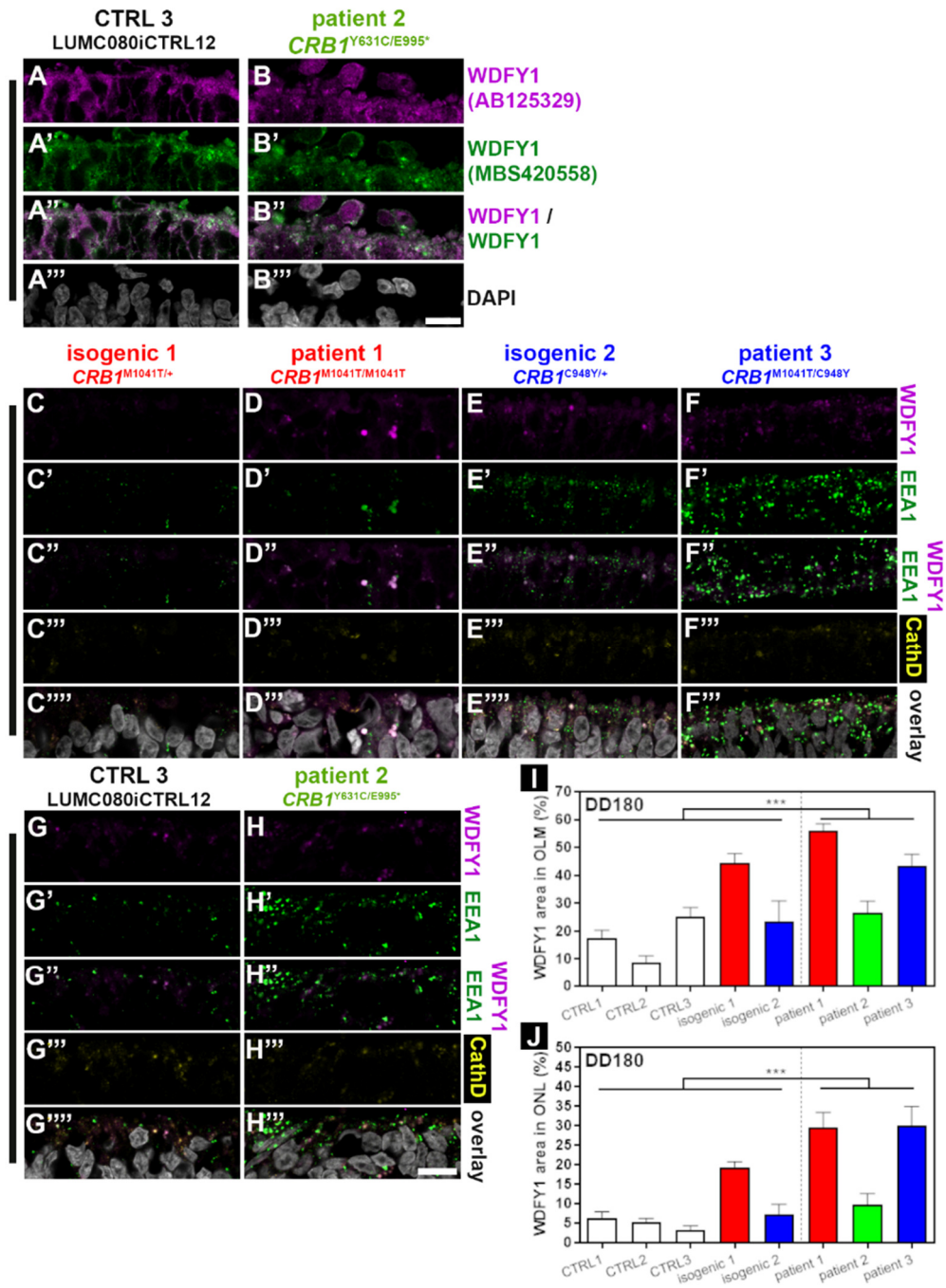


Figure S8. WDFY1 is more present in early endosomes in patient *CRB1* patient retinal organoids. Related to Figure 7. All organoids shown at DD180. (A-B) Immunofluorescence labelling of WDFY1 with two different antibodies (magenta / green) showing relative overlap. (C-H) Immunofluorescence labelling of WDFY1 (magenta; MBS420558 antibody), EEA1 (green), and Cathepsin D (yellow). Overlay shown in white (C-H). (I-J) Semi-quantification of fluorescence signal of WDFY1 (AB125329 antibody). (I) WDFY1 particle area / total OLM area in %. (J) WDFY1 particle area / total ONL area in %. CTRL3, wildtype line. Isogenic 1 and 2: isogenic control lines related to the patient line 1 (LUMC0116iCRB09) and patient line 3 (LUMC0128iCRB01). Scale bar, 10 μ m.

Table S2: Antibody list and dilution used for immunohistochemistry and western blots. Related to all figures.

Host; antibody	Dilution + procedure	Catalogue number
Primary antibodies		
Mouse anti-CRB1-ECD	1/200 IF, 1/300 PLA	H00023418-A01
Rabbit anti-CRB1-ICD (AK2)	1/100 IF	Home-made
Phalloidin-TRITC (<i>aka</i> F-actin)	1/250 IF	r-415
Rabbit anti-OTX2	1/200 IF	13497-1-AP
Mouse anti-BRN3A	1/100 IF	sc-8429
Mouse anti-LC3B	1/100 IF + WB 1/300	0231-100/LC-3-5F10
Rabbit anti-FENS1	1/200 IF	AB125329
Mouse anti-EEA1	1/100 IF	BD-610457
Mouse anti-LAMP1	1/100 IF	sc-20011
Rabbit anti-Cathepsin D	1/200 IF	IM16-100UG
Mouse anti-ARL8A/B	1/100 IF	sc-398635
Mouse anti-NOTCH1-ECD	1/300 IF + PLA	MA5-11961
Mouse anti-PIP2	1/200 IF	MA3-500
Rabbit anti-(pan-)cytokeratin	1/200 IF	AB9377
Rabbit anti-RCVRN	1/600 IF, 1/5000 WB	AB5585
Mouse anti-GAPDH	1/5000 WB	MAB374
Rabbit anti-RAB7	1/100 IF	CST9367S
Goat anti-VPS35 (retromer)	1/100 IF	Ab10099
Rabbit anti-VPS26 (retromer)	1/250 IF	Ab181352
Rabbit anti-RAB11a	1/100 IF	71-5300
Rat anti-CD44	1/100 IF	553132
Mouse anti-Oct3/4-BV421	1/25 FACS	565644
Mouse anti-NANOG-PE	1/5 FACS	560483
anti-SSEA4-FITC	1/25 FACS	130-098-371
Mouse anti-Nestin-Alexa488 CC	1/200 IF	CST; clone 10C2
Rabbit PAX6-Alexa647 c CC	1/200 IF	CST; clone D3A9V
Rabbit FOXA2-Alexa555 CC	1/500 IF	CST; clone D56D6
Rabbit GATA4-Alexa647 CC	1/200 IF	CST; clone D3A3M
Rabbit Vimentin-Alexa647 CC	1/400 IF	CST; clone D21H3
Rabbit CDX2-Alexa555 CC	1/500 IF	CST; clone D11D10
Rabbit Brachyury-Alexa488 CC	1/200 IF	CST; clone D2Z3J
Secondary antibodies		
Anti-rabbit-IgG-HRP	1/5000 WB	sc-2357
Anti-mouse-IgGc BP-HRP	1/5000 WB	sc-516102
Anti-rabbit Alexa647	1/1000 IF	Ab150083
Anti-mouse Alexa647	1/1000 IF	Ab150119
Anti-mouse Alexa488	1/1000 IF	Ab150113
Anti-chicken Alexa555	1/1000 IF	Ab150169
Anti-rabbit Alexa555	1/1000 IF	Ab150086
Anti-rat cy3 (50% glycerol added)	1/500 IF	712-165-153
Anti-rabbit cy3 (50% glycerol added)	1/500 IF	111-165-045

*IF, immunofluorescence; WB, western blot; PLA, Proximity ligation assay; CC, custom made conjugated

Table S3. RNAseq run-1. *Crb1*^{KO}*Crb2*^{ARPC} vs *Crb1*^{KO} at E15.5, E17.5, and P1.(A) *Crb1*^{KO}*Crb2*^{ARPC} vs *Crb1*^{KO} : E15.5

	Symbol	Description	logFC	adj.P.val
Upregulated				
1	Krt15	keratin 15	4,50	0,2
2	Abcd4	ATP-binding cassette, sub-family D, member 4	1,97	0,1
3	Col8a1	collagen, type VIII, alpha 1	1,85	0,3
4	9530091C08Rik	RIKEN cDNA 9530091C08 gene	1,69	0,2
5	Kcnq1ot1	KCNQ1 overlapping transcript 1	1,10	0,3
6	Fras1	Fraser extracellular matrix complex subunit 1	0,95	0,3
7	Col6a1	collagen, type VI, alpha 1	0,82	0,3
8	Zfp949	zinc finger protein 949	0,78	0,1
9	Dst	dystonin	0,53	0,2
10	Cacna1c	calcium channel, voltage-dependent, L type, alpha 1C subunit	0,48	0,3
Downregulated				
1	Pax2	paired box 2	-2,16	0,2
2	Pcp4l1	Purkinje cell protein 4-like 1	-0,59	0,2
3	Mthfd2	methylenetetrahydrofolate dehydrogenase (NAD+ dependent), methenyltetrahydrofolate cyclohydrolase	-0,50	0,3
4	Cldn12	claudin 12	-0,41	0,3
5	Tnfrsf21	tumor necrosis factor receptor superfamily, member 21	-0,36	0,3
6	Tgfb2	transforming growth factor, beta 2	-0,36	0,2
7	BC023829	NA	-0,35	0,2
8	Pea15a	phosphoprotein enriched in astrocytes 15A	-0,34	0,2
9	Fzd5	frizzled class receptor 5	-0,32	0,3
10	Mxra7	matrix-remodelling associated 7	-0,32	0,3

(B) *Crb1*^{KO}*Crb2*^{ARPC} vs *Crb1*^{KO} : E17.5

	Symbol	Description	logFC	adj.P.val
Upregulated				
1	Abcd4	ATP-binding cassette, sub-family D (ALD), member 4	2,84	0,0
2	Cd68	CD68 antigen	0,80	0,2
3	Dmpk	dystrophia myotonica-protein kinase	0,75	0,1
4	Csf2ra	colony stimulating factor 2 receptor, alpha, low-affinity (granulocyte-macrophage)	0,74	0,2
5	Ryr3	ryanodine receptor 3	0,66	0,2
6	Pcdh15	protocadherin 15	0,64	0,2
7	Flrt1	fibronectin leucine rich transmembrane protein 1	0,62	0,1
8	Zfp949	zinc finger protein 949	0,61	0,2
9	Lime1	Lck interacting transmembrane adaptor 1	0,57	0,1
10	Pank4	pantothenate kinase 4	0,52	0,1

Downregulated

1	Slc7a3	solute carrier family 7 (cationic amino acid transporter, y+ system), member 3	-1,29	0,0
2	Chac1	ChaC, cation transport regulator 1	-1,13	0,2
3	Atf5	activating transcription factor 5	-0,97	0,0
4	Rhod	ras homolog family member D	-0,90	0,2
5	Morf4l1	mortality factor 4 like 1	-0,88	0,0
6	Slc7a5	solute carrier family 7 (cationic amino acid transporter, y+ system), member 5	-0,88	0,0
7	Sesn2	sestrin 2	-0,86	0,1
8	Ajuba	ajuba LIM protein	-0,73	0,2
9	Etv4	ets variant 4	-0,65	0,2
10	Cldn12	claudin 12	-0,62	0,0

(C) *Crb1*^{KO}*Crb2*^{ARPC} vs *Crb1*^{KO}: P1

Upregulated

1	Abcd4	ATP-binding cassette, sub-family D (ALD), member 4	1,84	0,1
2	Taf13	TATA-box binding protein associated factor 13	1,00	0,1
3	Zic1	zinc finger protein of the cerebellum 1	0,86	0,2
4	Dram2	DNA-damage regulated autophagy modulator 2	0,86	0,2
5	Atg3	autophagy related 3	0,79	0,2
6	Srsf5	serine/arginine-rich splicing factor 5	0,70	0,2
7	Zfp422	zinc finger protein 422	0,64	0,2
8	Lipt2	lipoyl(octanoyl) transferase 2 (putative)	0,63	0,2
9	Syt4	synaptotagmin IV	0,57	0,2
10	Klf10	Kruppel-like factor 10	0,57	0,2

Downregulated

1	Neurog2	neurogenin 2	-0,62	0,2
2	Zfp773	zinc finger protein 773	-0,59	0,2
3	Zfp790	zinc finger protein 790	-0,51	0,2
4	Armex1	armadillo repeat containing, X-linked 1	-0,49	0,2
5	Reck	reversion-inducing-cysteine-rich protein with kazal motifs	-0,48	0,2
6	Rnf6	ring finger protein (C3H2C3 type) 6	-0,45	0,2
7	Parp11	poly (ADP-ribose) polymerase family, member 11	-0,45	0,2
8	Amotl2	angiomin-like 2	-0,44	0,2
9	Cln8	ceroid-lipofuscinosis, neuronal 8	-0,44	0,2
10	Cntrl	centriolin	-0,42	0,1

Table S4. RNAseq run-2. *Crb1*^{KO}*Crb2*^{ARPC} vs wildtype control at E15.5

	Symbol	Description	logFC	adj.P.Val
	Upregulated			
1	Gja8	gap junction protein, alpha 8	4,14	0,18
2	Igfbp7	insulin-like growth factor binding protein 7	3,43	0,21
3	Synpr	synaptoporin	2,75	0,00
4	Abcd4	ATP-binding cassette, sub-family D (ALD), member 4	2,50	0,00
5	Wdfy1	WD repeat and FYVE domain containing 1	2,47	0,00
6	Gfi1	growth factor independent 1	2,26	0,00
7	Tbx20	T-box 20	2,11	0,00
8	Chrn3	cholinergic receptor, nicotinic, beta polypeptide 3	2,04	0,00
9	Sparc11	SPARC-like 1	1,96	0,00
10	Sptb	spectrin beta, erythrocytic	1,93	0,00
	Downregulated			
1	Tmem181b-ps	transmembrane protein 181B, pseudogene crumbs family member 1, photoreceptor morphogenesis associated	-4,83	0,00
2	Crb1	associated	-4,15	0,00
3	Snca	synuclein, alpha	-3,91	0,00
4	Dusp9	dual specificity phosphatase 9	-2,12	0,00
5	Grm2	glutamate receptor, metabotropic 2	-2,10	0,00
6	Capn6	calpain 6	-1,88	0,19
7	Sfrp2	secreted frizzled-related protein 2	-1,62	0,00
8	Crabp1	cellular retinoic acid binding protein I	-1,47	0,00
9	Gpnmb	glycoprotein (transmembrane) nmb	-1,46	0,08
10	Sst	somatostatin	-1,33	0,18

Chapter 6

GENERAL DISCUSSION

T.M. Buck

Introduction: *CRBI*-associated retinal diseases and clinical spectrum

Inherited retinal dystrophies (IRDs) are chronic and disabling disorders of the visual function. The *CRBI* gene is one of more than 279 genes (316 loci & genes) associated with retinal dystrophies (RD) [1]. The RD-*CRBI* patients show an autosomal recessive inheritance pattern. Biallelic genetic mutations of the *CRBI* gene (called *CRBI* variants) can cause retinal pigmentosa (RP), Leber congenital amaurosis (LCA) and occasionally macular dystrophies [2]. *CRBI*-related RDs are one of the more frequently occurring IRDs with 7-17% of all LCA cases and 3-9% of all RP cases [3–7]. Patients with the LCA-form are generally legally blind around birth (*congenital*) and RP-*CRBI* in late adolescence. Currently, no effective therapy exists for RD- or LCA-*CRBI* patients. A large diagnosis overlap exists between LCA-*CRBI* and early RP-*CRBI* [8]. Initial LCA- and RP-*CRBI* symptoms range from night blindness, tunnel vision, and a progressive loss of the peripheral vision in patients, to LCA-only symptoms, such as non-recordable electroretinogram (ERG), nystagmus, and no oculodigital reflexes [8]. Vision loss in *CRBI*-patients is seen by full-field ERG recordings having lower scotopic a-waves (measuring the photosensitivity of rod photoreceptors), and lower scotopic b-waves (representing a loss of synaptic transmission through the neuroretina). Multifocal ERG recordings demonstrated a loss of ERG signal stemming by large of the rod-rich retinal periphery in early diagnoses and in later life also from a loss of central vision related to the loss of cone photoreceptor function [9].

So far, the *CRBI*-patient retinal morphology has only been studied by non-invasive imaging methods, such as fluorescein angiography, confocal Scanning Laser Ophthalmoscopy (FA cSLO, vascular leakage seen on *en-face* scans) and spectral-domain optical coherence tomography (SD-OCT, overall retinal morphology on *en-face* and OCT b-scans [retinal layer-by-layer visualization]), and similar to many other orphan diseases with limited patient numbers has not been studied on the morphology of cadaveric donor eyes. SD-OCT, cSLO and FA scans on LCA-*CRBI* patients may show a thickened neuroretina with no clearly visible synaptic layers, atrophy of retinal pigment epithelium (RPE), retinal oedema, and microvascular changes and osteoclast depositions (also called *bone-spicules* or *pigments*) close to venules [10,11]. The most common RP-*CRBI* morphological phenotypes are thinned photoreceptor nuclei layers (also called *outer nuclear layer* [ONL]), osteoclast depositions, Coats-like exudative vasculopathies, preserved para-arteriolar retinal pigment epithelia (PPRPE; definition: RPE cells are only preserved in proximity to arterioles), and preserved central fovea's; however, more severe phenotypes such as cystoid macular edema (CME) and macular atrophy can also be seen in late-stage and sporadically in early-stage RP-*CRBI* patients [2,12,13]. An absent ERG response and a thickened retina seen on SD-OCT in the first years of the life of some LCA-*CRBI* patients illustrates that LCA-*CRBI* is a developmental disease potentially affecting the embryonic retina [10,14].

A mix of morphology and retinal function test is the Fundus-controlled perimetry (FCP, also called *microperimetry*), a type of a visual field test. The FCP measures the light sensitivity of a defined retinal area(s) under scotopic (rods), mesopic (rods & cones), and photopic (cones) conditions. FCPs on RP-*CRB1* natural history studies are very promising for the preparation of *CRB1* gene therapy clinical studies because the photosensitivity of retinal areas can be related back on the SD-OCT/cSLO-based spatial markers (e.g. fundus) permitting tracking of specific scotomas (visual field *lesions*) and treated areas over time with a high retest-reliability in patients with no stable fixation [2,15,16]. The main treatment route of gene therapy products for ophthalmic diseases (**Chapter 1**) is delivered by local subretinal injection(s) preserving a limited retina area (called *islands*) that can be tracked by FCPs [17]. Other tests such as the classical Best-corrected visual acuity (BCVA) also showed promise in clinical trial preparations [2]. An rodent-adapted version of the BCVA is the optokinetic head-tracking response (OKT) [18]. It was further developed for measuring under low light and low contrast conditions [19,20]. The previous *proof-of-concept* (POC) *CRB* gene therapy in rodents showed a rescue on ERG and retinal morphology [21,22] (and **Chapter 1**). We also show that OKT contrast sensitivity is a very promising technique for screening *CRB* gene therapy vectors in mice *in vivo* (**Chapter 2**). We also generated retinal explants *ex vivo* (**Chapter 3**) and retinal organoids *in vitro* (**Chapter 4, 5**) which can be both modified for variant *CRB1* (RP-*CRB1* patient) expression. It will be interesting to correlate more patient findings to *CRB1* retinal organoids and other CRB models to generate better predictors (i.e., biomarkers) for monitoring the disease progression in patients and gene therapy trials. For example, the first preliminary experiments have measured retinal function and SD-OCTs on retinal organoids and organ-on-a-chip retina models [23–25].

CRB1 and CRB2 protein location and function in the neuroretina

Epidemiologic studies show a high genotype and phenotype heterogeneity in RD-*CRB1* patient pools [2,6,26]. Nowadays, RD-*CRB1* patients can be efficiently diagnosed by Next Generation Sequencing (NGS). Generally, RD-*CRB1* patients are found by linking a retinal phenotype to genes by whole-exome sequencing of retinal disease genes *only*. However, many (non-retinal disease) modifier genes may be missed by this method [2,12]. Efforts have been undertaken to screen also non-retinal diseases, such as *CRB2* along NGS of retinal patients [27] but the price for NGS and the limited information on retinal modifier genes have been obstacles in the field. RD-*CRB1*-based cell & molecular biology research studies what biological changes drive a RP-*CRB1* phenotype to an LCA-*CRB1* or *vice versa* (by therapies) by studying the *CRB1* gene function and (gene) therapies in different models. Research in the field may find (a) novel biomarkers (**Chapter 2, 5**), (b) develop therapies (**Chapter 1, 2, 3, 4**), (c) find modifier genes (e.g., other LCA/RP genes, apicobasal genes, unknown transcription factors, and other unidentified genes. See also **Chapter 2, 5**), (d) identify complex transcription and proteomic changes in cells affected by the loss of the CRB1 protein

or variant CRB1 protein expression (**Chapter 5**), and (e) predict the stability, folding, and trafficking of variant *CRB1* proteins by experimental methods (**Chapter 5**).

The mouse neuroretina like the human neuroretina contains rods and cones but the mouse retina lacks a cone-rich fovea. Human CRB1 (but not human CRB2) was found in both human PRCs and human MGCs at the subapical region in two-day-old human cadaveric retinas. Human CRB2 was found in the PRC inner segments but not at the subapical region. But in dissected non-human primate retinas and cultured human-derived retinal organoids (**Chapter 4**), CRB2 was found at the subapical region and in the PRC inner segments [28–30]. We propose that CRB2 location was lost at the subapical region in two-day-old cadaver human eyes due to post-mortem degradation processes because fresh non-human primate and cultured human organoids showed CRB2 expression at the subapical region adjacent to the adherens junctions at the outer limiting membrane (**Chapter 4**). In mouse, CRB1 is found exclusively in MGCs-villi at the subapical region and CRB2 in both PRCs and MGCs at the subapical region [31]. We also studied the onset of human CRB1 and CRB2 protein expression in retinal organoids and foetal retina showing that CRB2 precedes CRB1 during retinal development (**Chapter 4**).

The CRB1 protein, belonging to the CRB protein family member (CRB1, CRB2, or CRB3A), is a relative large protein of 160 kDa (1405 aa in mice and 1406 aa in humans; 200–220 kDa when glycosylated) [32]. CRB1 and CRB2 also share a large extracellular domain of three laminin A/globular(LamG)-like and 19 and 14 epidermal growth factor(EGF)-like-domain repeats [33]. Both CRB1, CRB2, and CRB3A proteins share a similar intracellular 37-aa C-terminal tail containing two protein-protein interaction motifs: the FERM domain (4.1 protein/*ezrin/radixin/moesin*) and the glutamic acid-arginine-leucine-isoleucine (ERLI)/PDZ (**P**ostsynaptic density/**D**iscs large/**Z**O-1) domain [34–38]. FERM domains are used by many transmembrane proteins as adaptors to the actin cytoskeleton [39]. CRB protein family members (CRB1, CRB2, or CRB3A) can participate in two apical polarity complexes: The core Crumbs (CRUMBS/PALS1/PATJ) and PAR complex (PAR3/ PAR6/aPKC). They are initiated by binding of Protein associated with Lin Seven 1 (PALS1; also called MAGUK p55 [MPP5]) or Partitioning defective-6 homolog (PAR6) to the ERLI/PDZ motif of the Crb protein [38,40,41]. The CRB apical polarity complex containing a CRB protein family member (CRB1, CRB2, or CRB3A) can be in complex with PALS1-MUPP1/MPP3/MPP4, PALS1-PATJ, EPB41L5(Yurt or Moe orthologue; cytoskeletal regulator)/PALS1/PAR6, PALS1/PAR6-LIN7c/PATJ, PAR6-CDC42/aPKC, or PAR6-PAR3(aPKC inhibitor & substrate)-FRMD4A/B-CYTH1 [3,32,42–45]. Yet, it is not clear whether MUPP1 and PATJ are in the same cell types and in the same complex with CRB1-PALS1(MPP5). Also, ablation of PALS1(MPP5) specifically in the neural retina in a Pals1 conditional short hairpin RNA (shRNA) knockdown mouse model using the Chx10Cre transgene did not significantly affect the retinal morphology or the Crumbs complex in photoreceptors/Müller glial cells, whereas

a severe RPE degradation phenotype was observed upon ablation of PALS1(MPP5) in both the RPE and neural retina in a Pals1 shRNA knockdown mouse model using the CrxCre transgene. These experiments indicated that PALS1 is essential at the tight junctions in RPE but not for the CRB apical complex in mouse photoreceptors/Müller glial cells albeit being overabundantly present [46]. Other protein complexes have been associated with the Crumbs complex and CRB binding, such as YMO1 (yurt/mosaic eyes like 1), EHM2, and moesin (FERM domain) proteins on the Crumbs complex; and, 14.3.3, CDC42, HOMER1-3, STXBP4 (Hippo pathway regulator) for the related PAR protein complex (Baz/PAR3-PAR6-aPKC) [36,44,47–50]. Interestingly, CRB's C-terminal phosphorylation by PKCa permits PALS1 binding but inhibits moesin binding indicating that the initiation of the Crumbs complex is less regulated by phosphorylation and more by CRB apical trafficking or ERL1/PDZ motif binding partners [50]. The CRB apical polarity complex in the neuroretina supports the maintenance and recruitment of tight-junction adhesion molecules (cadherins, catenins, zonula occludens proteins) at the adherens junction constituting the outer limiting membrane (OLM), acts as an intermediary for regulating development pathways (e.g. Notch & Hippo pathway), and regulates the recruitment of actomyosin cytoskeletal proteins [38,42,51–53].

The intracellular domain of CRB2 can also interact with the retromer sorting protein VPS35 [54]. The zebrafish CRB2A (a human *CRB2* orthologue) can interact with the recycling endosome protein RAB11A [55]. RAB11A and VPS35 are both essential proteins for efficient turn-over of membrane proteins on early endosomes, such as the cell surface proteins NOTCH1 and CRB1 (**Chapter 5**). We found a reduction in VPS35 and RAB11A in patient retinal organoids compared to their isogenic controls (**Chapter 5**). The long extracellular domain of CRB1 or CRB2 was proposed to form homophilic interaction *in trans* for stabilization at the apical membrane based on *Crb* fruit fly and zebrafish studies [56–58]. For example, the extracellular domain of the zebrafish CRB2A form homophilic interaction *in trans* contributing to the CRB2A apical membrane stabilization (apical protein turn-over) and overall cell adhesion [58]. Recently, also an *in cis* fruit fly Crumbs-Notch interaction on the extracellular domain was demonstrated that suppresses Notch receptor endocytosis and repress the Notch pathway activity [59]. We show that human CRB1-NOTCH1 can also interact on the extracellular domain in retinal organoids with little apical interaction and little apical NOTCH1 found in RP-*CRB1* retinal organoids (**Chapter 5**), potentially *in trans* or *cis* because we found NOTCH1 solely in MGCs and CRB1 in PRCs & MGCs. The results point to CRB1 stabilizing NOTCH1 at the OLM on apical early endosomes determining the apical protein turn-over (see section 3).

In previous studies, genetically modified mice were generated to knockout the *Crb1* gene and conditional knockout the *Crb2* gene in specific retinal cells (PRCs, rod PRC only, Müller glial cells [MGCs], or retinal progenitor cells [RPCs]) to study the function of the *Crb1* and

Crb2 gene [29,47,60–64]. The mouse studies (see also **Chapter 2**) and the RP-*CRB1* retinal organoid studies (**Chapter 4, 5**) show that the loss of CRB1 or CRB2 proteins coincide with the focal loss (*gaps*) of tight-junction adhesion molecules (cadherins, catenins, ZO-1) and subapical proteins (e.g., PALS1, MUPP1, PAR3, PATJ) at the OLM (called *OLM breaks*). The loss of the Crumbs complex in mice [29,47,60–64] (see also **Chapter 2**) and RP-*CRB1* retinal organoids (**Chapter 4, 5**) facilitates loss of cell adhesion between PRCs-PRCs, PRCs-MGCs, and MGCs-MGCs; and dysregulates the apical polarity signalling in the neuroretina (**Chapter 4, 5**).

The endolysosomal system and the apical CRB1 protein trafficking

The endosomal-lysosomal (endolysosomal) system is a complex dynamic intracellular vesicular trafficking and positioning system on the endocytic and secretory pathway. For example, the system regulates the sorting of proteins in correct vesicles, transporting the protein-loaded vesicles to correct microdomains at the cell periphery (along the cell-spanning endoplasmic reticulum [ER]), designation of proteins and vesicles to be sorted for degradation, recycling of proteins, and assisting the autophagic pathway [65,66]. The secretory pathway vesicles are termed secretory vesicles (includes lysosomes), transport vesicles (made on the *trans*-golgi network [TGN]), and exosomes. The endocytic pathway contains endocytic vesicles (clathrin-dependent/independent endocytosis), early endosomes (EE), recycling endosomes, late endosomes (LE), multivesicular bodies (MVB), and lysosomes. The secretory pathway, the endocytic pathway, and the autophagic pathway can converge on almost all vesicles. The endolysosomal system research field is rapidly expanding, even though complicated by the dynamic nature of the system. For example, many classical markers of endosome subpopulation of early/late endosomes and lysosomes are frequently found on all of them making identification of subpopulations difficult, different cells employ different endosome protein(s) (markers) for the regulation of the endolysosomal system, and many studies have been performed on single cells to track individual vesicles *in vitro* but vesicle-trafficking on cell-dense tissues may be quite different because of different apical protein expression profiles. Nonetheless, it is certain that a functional endolysosomal system is central to the health of all cells.

Some of the most studied diseases on (dys-)regulations of the endolysosomal systems are diseases with protein aggregation phenotypes (Parkinson's, Alzheimer's, Huntington's Disease), immune cells fighting pathogens, and monogenetic diseases on receptor-mediated endocytosis. Here, we focus on receptor-mediated endocytosis of intact or variant CRB proteins localized at the apical plasma membrane immediately adjacent to adherens junctions at the outer limiting membrane. At this apical membrane, cell surface CRB transmembrane proteins are internalized by clathrin-mediated endocytosis and packaged in endocytic vesicles maturing to early endosomes from where the vesicles can either be reintegrated back into the apical membrane or become designated for degradation in the lysosome. Recently, it

was indicated that NOTCH and CRB are endocytosed in the same apical vesicles [55]. The membranes of early endosomes (containing CRB/NOTCH) expand forming tubular vesicles containing retromer protein sorting complexes (SNX1/2, SNX5/6, VPS26, VPS29, and VPS35). The early endosomes then briefly peak in levels of PtdIns(3)P to bind to FYVE protein early-endosome-antigen-1 (EEA1), which is required for RAB11A-mediated removal of recycling cargo from endosomes [67,68]. The recycling endosomes then transport back the cargo to the membrane for membrane (re-)integration. It is thought that in an undisturbed endolysosomal system, most CRB/NOTCH is efficiently recycled and only a small fraction (e.g., variant CRB proteins) stays in early endosomes which then mature to late endosomes / lysosomes for protein degradation. New CRB protein is continuously produced in the ER, modified in the Golgi, and loaded on vesicles transported on the TGN moving on plus to minus-strand microtubules by dynein motors to the periphery (anterograde transport). Close to the apical membrane, the vesicles acquire RAB11A and Myosin V (attached on F-actin) guiding the cargo-release and CRB apical membrane integration [69]. The anterograde transport is mediated by a CDC42-dependent positive feedback loop and repressed (preventing overexpression) by Stardust (Sdt)/PALS1 [70,71].

Little is known about the specific regulation of variant CRB1 protein trafficking. Interestingly, the intracellular domain of CRB2 can bind to RAB11A and VPS35 potentially regulating the sorting and cargo-release on early endosomes [54,55]. Also, the loss of retromer induces an increase of lysosome degradation and a reduction of the apical Crumbs complex membrane-occupied area [54]. The intracellular domain of fruit fly Crumbs shows high sequence similarity to the intracellular domain of (human) CRB1 and CRB2 potentially also permitting mediation of sorting and cargo-release on early endosomes by CRB1/CRB2. We found a decrease of variant CRB1, NOTCH1, VPS35, and RAB11A protein expression at the apical membrane as well as an increase of degradative vesicles in *CRB1* patient retinal organoids (**Chapter 5**) providing evidence that variant CRB1 proteins are less efficiently sorted to the apical membrane and potentially dysregulating the CRB1/CRB2-VPS35 and CRB1/CRB2-RAB11A interactions. Interestingly, we also found an increase of two FYVE domain containing proteins EEA1 and WDFY1 on early endosomes in CRB1 patient organoids. The FYVE domains of EEA1 and WDFY1 can bind PtdIns(3)P. Overexpression of *Wdfy1* transcripts was also found in a RNAseq screen of *Crb1Crb2* cKO vs wildtype mice at E15.5 (**Chapter 5**). This suggest that variant CRB1 represses early endosome maturation causing an increase in degradative vesicle accumulation.

It will be interesting to find out (1) how cells upregulate *WDFY1* expression as a cellular response to inefficient sorting of variant CRB1 proteins, and (2) if the integration of more WDFY1 on early endosomes has a biological function such as initiating a less-well studied cell apoptosis pathway. WDFY3 (a WDFY1 family member which is 10x larger) mediates ATG5-guided selective autophagy by binding to the ubiquitin-binding protein p62 [72]. P62,

an autophagosome cargo protein, was also upregulated in *CRB1* patient retinal organoids (**Chapter 5**). Yet, the BEACH binding motif for p62 is not present on WDFY1. It is tempting to think that all WDFY proteins evolved around selective autophagy thus regulating variant CRB1 degradation. Moreover, an increase of WDFY1 protein can induce NF- κ B activation and pro-apoptotic pathways in immune cells [73], but conversely, NF- κ B activation was not found in neuronal cells expressing increased levels of WDFY1 [74]. These results further underline how the endolysosomal system is inherently differently regulated in immune and neuronal cells, and that more research is needed to delineate the effect of WDFY1 on RP-*CRB1* pathology.

Very little is known on how specific variant CRB1 proteins are regulated by the endolysosomal system in retinal cells. For example, when a human *CRB1* mutation was knocked in on a *Crb1*-null mouse (*Crb1*^{C249W/-}), normal amounts of CRB1 protein levels were found at the OLM suggesting that the CRB1 variant trafficking is intact. However, the OLM was more sensitive to light-stress demonstrating a loss of adhesion mediated by variant CRB1 [75]. Also, the natural occurring *Crb1*^{rd8} mouse – having a single nucleotide deletion on exon-9 corresponding to ~1150th aa of the 1406 aa in humans (the CRB1 variant contains only the extracellular domain) – express variant CRB1 proteins apically but at reduced levels in Müller glial cells [76]. However, the exact variant protein expression may be much lower because the antibody used in these studies to detect the variant CRB1 may also detect CRB2. Finally, fruit fly studies on a *Crb*-null background compared the effect of reintroducing different CRB variants including a variant similar as the *Crb1*^{C249W} (*Crb*^{C749W} in fruit fly). Very little variant CRB protein was detected in the rhabdomere (eight photoreceptor cells arranged in a stalk as seen in insects) [77]. Other *Crb* mutants in the LamG3 & EGF-like domain 21/22 on the extracellular domain (*Crb*^{T1386M}; *Crb*^{N1486S}; *Crb*^{C1540Y}) showed a much higher CRB protein expression at the rhabdomere compared to the wildtype control. What is more, these variant CRB1 proteins formed aggregates and mislocalized showing a typical gain-of-function phenotype. We found a reduction of potentially four different variant CRB1 proteins (*CRB1*^{M1041T}, *CRB1*^{Y631C}, *CRB1*^{E995*}, *CRB1*^{C948Y}; expressed in three RP-*CRB1* patients: *CRB1*^{M1041T/M1041T}; *CRB1*^{Y631C/E995*}; *CRB1*^{M1041T/C948Y}) in patient retinal organoids (**Chapter 5**). It will be exciting to study why certain variants become overabundantly expressed at the OLM and others are efficiently removed from the system. For example, *Crb1*^{C249W} showed protein expression in mice but a very similar *Crb*^{C749W} did not in fruit fly. Can the difference be explained by differences in the endolysosomal system in species? A study of the *CRB1*^{C250W} in human retinal organoids may solve the outstanding question. Furthermore, knowing what regulates CRB levels at the OLM will not only broaden our understanding of CRB function but may also contribute developing second generation *CRB* gene supplementation therapies where CRB overexpression can be prevented by including CRB regulators on the vector cassette. Fortunately, overexpression is most likely a lesser problem for gene therapy treated RP-*CRB1* patients because a low dose of CRB may already

be sufficient as indicated by the phenotypic rescue found in the isogenic *CRB* organoids expressing a variant *CRB1* on one allele and a wildtype *CRB1* on the other (**Chapter 5**), the mild phenotype seen in *Crb1*^{KO}*Crb2*^{LowMGC} mice (**Chapter 2**), and the overall tolerability of rAAV high vector doses injected to the mouse eye [21,22] (see also **Chapter 2**).

The total CRB levels at the OLM in photoreceptors and Müller glial cells determines the phenotype

The similar protein location and the mouse (conditional) knockout studies showed that *CRB1* and *CRB2* proteins have compensatory and overlapping functions in the neuroretina [29,47,60–64]. However, we did not know the contribution of *CRB2* protein to photoreceptors and Müller glial cells. A neuroretina consists of roughly ten photoreceptors per Müller glial cell. And one Müller glial cell wraps around ~10 photoreceptor nuclei column in the ONL. Thus, raising the question if a *CRB* gene supplementation therapy needs to target many photoreceptors, many Müller glial cells or a mix of PRCs-MGCs?

First, we generated a new *CRB1*-RP-like mouse model where we knocked out *Crb1* and conditionally knocked out one allele on the *Crb2* gene reducing the levels of *Crb2* in MGCs at the OLM (Mouse model: *Crb1*^{-/-}*Crb2*^{Floxed/wildtype}*Pdgfra-Cre*^{Transgene/+}. Shorted name: *Crb1*^{KO}*Crb2*^{LowMGC}). Early retinal disease phenotypes were seen on morphology, such as misplaced nuclei in the subretinal space (between the OLM and the RPE layer) and the outer plexiform layer (OPL; a synaptic layer between the photoreceptor nuclei and the inner retinal cells) in the inferior quadrants at 1 and 3 months-old animals. This was accompanied by an increase in gliosis (Glial fibrillary acidic protein [GFAP] expression), a reduction in MGC-microvilli length, and a reduction of PRC inner/outer segment length in 3-month-old *Crb1*^{KO}*Crb2*^{LowMGC} retinas. Then we found a correlation between the *CRB1*, *CRB2* and p120-catenin protein expression at the OLM and the number of OLM disruptions within four different *CRB1*-RP-like mouse models (*Crb1*^{KO}; *Crb2*^{ΔRods}; *Crb1*^{KO}*Crb2*^{LowMGC}; *Crb1*^{KO}*Crb2*^{ΔRods}) at 3-months-of-age. The study showed that PRCs and MGCs provide around half of the total *CRB2* protein to the OLM and that the *Crb1*^{KO}*Crb2*^{LowMGC} neuroretina had a 67% reduction of *CRB2* protein at the OLM (**Chapter 2**). Also, the more photoreceptor-based model (*Crb1*^{KO}*Crb2*^{ΔRods}) mouse had the highest number of OLM breaks compared to the other studied *CRB1*-RP-like models but a surprisingly well-preserved retinal function measured by ERG and retinal thickness for the first 3 months-of-age [61]. When *Crb2* was ablated in Müller glial cells lacking *Crb1* (*Crb1*^{KO}*Crb2*^{ΔMGC}) then no retinal function was detected with a severe retinal phenotype on morphology at 1-month-of-age [29]. These studies demonstrate that *CRB1/CRB2* expression in Müller glial cells is of high importance for gene supplementation therapies and should not be neglected by choosing only a photoreceptor-specific promoter. The current *CRB* gene supplementation therapy contains a ubiquitous promoter (CMV or CMVmin) that expresses the transgene in Müller glial cells as well as photoreceptor cells [21,78,79] (see also **Chapter 2+3+4**).

Viral vector-based gene supplementation therapy for RP-CRB1 patients

Finally, we show that the regenerative capacity of the neuroretina/OLM in a *CRB1*-RP-like mouse model can be reversed by supplementing human *CRB1* (h*CRB1*) or *CRB2* (h*CRB2*) cDNA to MGCs by recombinant adeno-associated viral (rAAV) vectors (**Chapter 2**). Gene supplementation therapies by rAAVs are promising techniques because the viral vectors are relatively safe (relative nonintegrative in the genome, replication deficient), many capsids with different cell & tissue-specific infection properties (managed tropism) are available, and the transgene expression can last for many years. Previously, we and others demonstrated that the rAAV6 capsid variant ShH10^{Y445F} can efficiently infect PRCs, MGCs and the epithelium of the ciliary body, and likely stem cells, and immune cells (e.g. dendritic cells, microglial cells). We injected the rAAVs by intravitreal injection targeting at least around 60% of all MGCs [79]. Our vector expresses upon cell infection and integration in the nuclei concatemerized cDNA of h*CRB1* or h*CRB2* under the control of a ubiquitous promoter (a minimal or full length CMV, respectively). We show that rAAV-based gene supplementation of h*CRB1* or h*CRB2* to *Crb1*^{KO}*Crb2*^{LowMGC} MGCs protected the neuroretina on morphology from degenerating under stress measured by retinal thickness, ectopic cells, photoreceptor inner/outer segments, MGC-microvilli length, and on SD-OCT imaging. Interestingly, only h*CRB2* protected the vision measured by ERG and OKT contrast sensitivity. Surprisingly, the h*CRB1* even reduced the ERG dark-adapted a-wave response and the OKT contrast sensitivity measured at 0.031, 0.064, and 0.092 cycles per degree. Further analysis indicated ectopic h*CRB1* expression in the ciliary body, an increase in vascular markers at the ciliary body and some infiltrating cells at the inner limiting membrane. We cannot exclude the possibility that the *Crb1* naïve mice upregulated an immune response upon being exposed to the (*de novo*) h*CRB1* protein in the eye, indicative that it is rather a species-specific response. More studies are needed to delineate the vision deficit with the therapeutic vector. Nevertheless, the study demonstrates that (a) h*CRB1* as well as the h*CRB2* protein, which are very similar in their protein domains, can support the regenerative morphological capacity of the neuroretina/OLM in a *CRB1*-RP like mouse model, and that (b) intravitreal injection is a powerful tool because one can supplement much more MGCs with the rescue vector. The vision deficits found in mice exposed to h*CRB1* also show that the rAAV-h*CRB1* therapy injections done intravitreally compared to subretinal injections have a higher risk of evoking side-effects and may require additional safety measures limiting (*de novo*) protein exposure to immune cells, preventing ectopic protein expression, and limiting the exposure of potential cis-regulatory toxicity found in some ubiquitous promoters to potentially sensitive cell populations. Several methods can be employed to reduce the risk (reviewed in **Chapter 1**): (a) more infective capsids such as AAV2-GL and AAV2-NN vectors may lower the dose requirement but these capsids tend to be overall less cell-specific, (b) more cell-specific capsids such as the AAV6 variant ShH10^{Y445F} infects more efficiently glial cells than the parent vector but AAV6 also infects immune cells (see also **Chapter 2+3+4**), (c) capsids that

pass more readily the rodent inner limiting membrane after intravitreal injection such as AAV2.7m8, (d) delineate the species-specific tropism in especially human retina models (**Chapter 2+3+4**), and (e) generate retina cell-specific promoters. We have shown that rAAV5 can more efficiently infect human photoreceptors and Müller glial cells in human retinal organoids and human retinal explants compared to rAAV9 (**Chapter 4**) without having the (theoretical) potential drawback of the rAAV6 variant ShH10Y infecting immune cells.

Conclusion

In conclusion, the thesis provides much needed information on rAAV-hCRB gene supplementation such as (a) rAAV vector optimization in the ophthalmic field (**Chapter 1**), (b) vector safety related to ectopic transgene expression (**Chapter 2**), (c) the overlapping and compensatory roles of both hCRB1 and hCRB2 protecting the OLM from stress in a challenged RP-CRBI mouse model (**Chapter 2**), (d) the development of rAAV-vector screens on the same donor neuroretina in parallel (**Chapter 3**), (e) rAAV5 infecting both human MGCs and PRCs on donor retinas and retinal organoids (**Chapter 4 part 1**), (f) the Crumbs complex changes during retinal development in retinal organoids and foetal retinas alike (**Chapter 4 part 2**), (g) the generation of a human RP-CRBI disease model on retinal organoids (**Chapter 4 part 3**), (h) that the human RP-CRBI retinal organoids have little variant CRB1 at the OLM which suppresses NOTCH1 expression at the OLM causing a dysregulation in the endolysosomal system (**Chapter 5**). With the previous studies, the new evidence in this thesis, and the ongoing natural history studies, the rAAV-CRB gene supplementation project paves the way for clinical studies in near future.

REFERENCES

1. Daiger, S.P.; Sullivan, L.S.; Bowne, S.J. RetNet. Retinal Information Network Available online: <https://sph.uth.edu/retnet/home.htm> (accessed on Aug 31, 2021).
2. Nguyen, X.-T.-A.; Talib, M.; van Schooneveld, M.J.; Wijnholds, J.; van Genderen, M.M.; Schalij-Delfos, N.E.; Klaver, C.C.W.; Talsma, H.E.; Fiocco, M.; Florijn, R.J.; et al. CRB1-associated retinal dystrophies: a prospective natural history study in anticipation of future clinical trials. *Am. J. Ophthalmol.* **2021**.
3. Gosens, I.; den Hollander, A.I.; Cremers, F.P.M.; Roepman, R. Composition and function of the Crumbs protein complex in the mammalian retina. *Exp. Eye Res.* **2008**, *86*, 713–26.
4. den Hollander, a I.; ten Brink, J.B.; de Kok, Y.J.; van Soest, S.; van den Born, L.I.; van Driel, M. a; van de Pol, D.J.; Payne, a M.; Bhattacharya, S.S.; Kellner, U.; et al. Mutations in a human homologue of *Drosophila* crumbs cause retinitis pigmentosa (RP12). *Nat. Genet.* **1999**, *23*, 217–21.
5. den Hollander, A.I.; Davis, J.; van der Velde-Visser, S.D.; Zonneveld, M.N.; Pierrottet, C.O.; Koenekoop, R.K.; Kellner, U.; van den Born, L.I.; Heckenlively, J.R.; Hoyng, C.B.; et al. CRB1 mutation spectrum in inherited retinal dystrophies. *Hum. Mutat.* **2004**, *24*, 355–69.
6. Talib, M.; van Schooneveld, M.J.; van Genderen, M.M.; Wijnholds, J.; Florijn, R.J.; ten Brink, J.B.; Schalij-Delfos, N.E.; Dagnelie, G.; Cremers, F.P.M.; Wolterbeek, R.; et al. Genotypic and Phenotypic Characteristics of CRB1-Associated Retinal Dystrophies: A Long-Term Follow-up Study. *Ophthalmology* **2017**, *124*, 884–895.

7. Corton, M.; Tatu, S.; Avila-Fernandez, A.; Vallespín, E.; Tapias, I.; Cantalapiedra, D.; Blanco-Kelly, F.; Riveiro-Alvarez, R.; Bernal, S.; García-Sandoval, B.; et al. High frequency of CRB1 mutations as cause of Early-Onset Retinal Dystrophies in the Spanish population. *Orphanet J. Rare Dis.* **2013**, *8*.
8. Bujakowska, K.; Audo, I.; Mohand-Saïd, S.; Lancelot, M.-E.; Antonio, A.; Germain, A.; Lèveillard, T.; Letexier, M.; Saraiva, J.-P.; Lonjou, C.; et al. CRB1 mutations in inherited retinal dystrophies. *Hum. Mutat.* **2012**, *33*, 306–315.
9. Yzer, S.; Fishman, G.A.; Racine, J.; Al-Zuhaibi, S.; Chakor, H.; Dorfman, A.; Szlyk, J.; Lachapelle, P.; Van Den Born, L.L.; Allikmets, R.; et al. CRB1 heterozygotes with regional retinal dysfunction: Implications for genetic testing of leber congenital amaurosis. *Investig. Ophthalmol. Vis. Sci.* **2006**, *47*, 3736–3744.
10. Jacobson, S.G. Crumbs homolog 1 (CRB1) mutations result in a thick human retina with abnormal lamination. *Hum. Mol. Genet.* **2003**, *12*, 1073–1078.
11. Beryozkin, A.; Zelinger, L.; Bandah-Rozenfeld, D.; Harel, A.; Strom, T.A.; Merin, S.; Chowers, I.; Banin, E.; Sharon, D. Mutations in CRB1 are a Relatively Common Cause of Autosomal Recessive Early-Onset Retinal Degeneration in the Israeli and Palestinian Populations. *Invest. Ophthalmol. Vis. Sci.* **2013**, *54*, 2068–2075.
12. Wang, Y.; Sun, W.; Xiao, X.; Li, S.; Jia, X.; Wang, P.; Zhang, Q. Clinical and Genetic Analysis of 63 Families Demonstrating Early and Advanced Characteristic Fundus as the Signature of CRB1 Mutations. *Am. J. Ophthalmol.* **2021**, *223*, 160–168.
13. Motta, F.L.; Salles, M.V.; Costa, K.A.; Filippelli-Silva, R.; Martin, R.P.; Sallum, J.M.F. The correlation between CRB1 variants and the clinical severity of Brazilian patients with different inherited retinal dystrophy phenotypes. *Sci. Reports 2017 71* **2017**, *7*, 1–9.
14. Tsang, S.H.; Burke, T.; Oll, M.; Yzer, S.; Lee, W.; Xie, Y.A. (Angela); Allikmets, R. Whole Exome Sequencing Identifies CRB1 Defect in an Unusual Maculopathy Phenotype. *Ophthalmology* **2014**, *121*, 1–10.
15. Pfau, M.; Jolly, J.K.; Wu, Z.; Denniss, J.; Lad, E.M.; Guymer, R.H.; Fleckenstein, M.; Holz, F.G.; Schmitz-Valckenberg, S. Fundus-controlled perimetry (microperimetry): Application as outcome measure in clinical trials. *Prog. Retin. Eye Res.* **2021**, *82*, 100907.
16. Roshandel, D.; Thompson, J.A.; Jeffery, R.C.H.; Sampson, D.M.; Chelva, E.; McLaren, T.L.; Lamey, T.M.; Roach, J.N. De; Durkin, S.R.; Chen, F.K. Multimodal Retinal Imaging and Microperimetry Reveal a Novel Phenotype and Potential Trial End Points in CRB1-Associated Retinopathies. *Transl. Vis. Sci. Technol.* **2021**, *10*, 38–38.
17. Ochakovski, G.A.; Ulrich Bartz-Schmidt, K.; Fischer, M.D. Retinal gene therapy: Surgical vector delivery in the translation to clinical trials. *Front. Neurosci.* **2017**, *11*, 174.
18. Thaug, C.; Arnold, K.; Jackson, I.J.; Coffey, P.J. Presence of visual head tracking differentiates normal sighted from retinal degenerate mice. *Neurosci. Lett.* **2002**, *325*, 21–24.
19. Prusky, G.T.; Alam, N.M.; Beekman, S.; Douglas, R.M. Rapid Quantification of Adult and Developing Mouse Spatial Vision Using a Virtual Optomotor System. *Invest. Ophthalmol. Vis. Sci.* **2004**, *45*, 4611–4616.
20. Alam, N.M.; Altimus, C.M.; Douglas, R.M.; Hattar, S.; Prusky, G.T. Photoreceptor Regulation of Spatial Visual Behavior. *Invest. Ophthalmol. Vis. Sci.* **2015**, *56*, 1842–1849.
21. Pellissier, L.P.; Quinn, P.M.; Henrique Alves, C.; Vos, R.M.; Klooster, J.; Flannery, J.G.; Alexander Heimel, J.; Wijnholds, J. Gene therapy into photoreceptors and Müller glial cells restores retinal structure and function in CRB1 retinitis pigmentosa mouse models. *Hum. Mol. Genet.* **2015**, *24*, 3104–3118.
22. Buck, T.M.; Vos, R.M.; Alves, C.H.; Wijnholds, J. AAV-CRB2 protects against vision loss in an inducible CRB1 retinitis pigmentosa mouse model. *Mol. Ther. - Methods Clin. Dev.* **2021**, *20*.
23. Cowan, C.S.; Renner, M.; De Gennaro, M.; Gross-Scherf, B.; Goldblum, D.; Hou, Y.; Munz, M.; Rodrigues, T.M.; Krol, J.; Szikra, T.; et al. Cell Types of the Human Retina and Its Organoids at Single-Cell Resolution. *Cell* **2020**, *182*, 1623–1640.e34.
24. Dorgau, B.; Felemban, M.; Hilgen, G.; Kiening, M.; Zerti, D.; Hunt, N.C.; Doherty, M.; Whitfield, P.; Hallam, D.; White, K.; et al. Decellularised extracellular matrix-derived peptides from neural retina and retinal pigment epithelium enhance the expression of synaptic markers and light responsiveness of human pluripotent stem cell derived retinal organoids. *Biomaterials* **2019**, *199*, 63–75.

25. Scholler, J.; Groux, K.; Goureau, O.; Sahel, J.-A.; Fink, M.; Reichman, S.; Boccarda, C.; Grieve, K. Dynamic full-field optical coherence tomography: 3D live-imaging of retinal organoids. *Light Sci. Appl.* **2020**, *9*, 1–9.
26. Ehrenberg, M.; Pierce, E.A.; Cox, G.F.; Fulton, A.B. CRB1: One gene, many phenotypes. *Semin. Ophthalmol.* **2013**, *28*, 397–405.
27. Hurk, J.J. van den; Rashbass, P.; Roepman, R.; Davis, J.; Voeselek, K.; Arends, M.; Zonneveld, M.N.; Roekel, M.V. van; Cameron, K.; Rohrschneider, K.; et al. Characterization of the Crumbs homolog 2 (CRB2) gene and analysis of its role in retinitis pigmentosa and Leber congenital amaurosis. *Mol. Vis.* **2005**, *11*, 263–273.
28. Quinn, P.M.; Buck, T.M.; Mulder, A.A.; Ohonin, C.; Alves, C.H.; Vos, R.M.; Bialecka, M.; van Herwaarden, T.; van Dijk, E.H.C.C.; Talib, M.; et al. Human iPSC-Derived Retinas Recapitulate the Fetal CRB1 CRB2 Complex Formation and Demonstrate that Photoreceptors and Müller Glia Are Targets of AAV5. *Stem Cell Reports* **2019**, *12*, 906–919.
29. Quinn, P.M.; Mulder, A.A.; Henrique Alves, C.; Desrosiers, M.; de Vries, S.I.; Klooster, J.; Dalkara, D.; Koster, A.J.; Jost, C.R.; Wijnholds, J. Loss of CRB2 in Müller glial cells modifies a CRB1-associated retinitis pigmentosa phenotype into a Leber congenital amaurosis phenotype. *Hum. Mol. Genet.* **2019**, *28*, 105–123.
30. Pellissier, L.P.; Lundvig, D.M.S.; Tanimoto, N.; Klooster, J.; Vos, R.M.; Richard, F.; Sothilingam, V.; Garcia Garrido, M.; Le Bivic, A.; Seeliger, M.W.; et al. CRB2 acts as a modifying factor of CRB1-related retinal dystrophies in mice. *Hum. Mol. Genet.* **2014**, *23*, 3759–3771.
31. van Rossum, A.G.S.H.; Aartsen, W.M.; Meuleman, J.; Klooster, J.; Malysheva, A.; Versteeg, I.; Arsanto, J.-P.P.; Le Bivic, A.A.; Wijnholds, J. Pals1/Mpp5 is required for correct localization of Crb1 at the subapical region in polarized Müller glia cells. *Hum. Mol. Genet.* **2006**, *15*, 2659–2672.
32. Kantardzhieva, A.; Gosens, I.; Alexeeva, S.; Punte, I.M.; Versteeg, I.; Krieger, E.; Neeffjes-Mol, C.A.; Den Hollander, A.I.; Letteboer, S.J.F.F.; Klooster, J.; et al. MPP5 recruits MPP4 to the CRB1 complex in photoreceptors. *Investig. Ophthalmol. Vis. Sci.* **2005**, *46*, 2192–2201.
33. Quinn, P.M.; Pellissier, L.P.; Wijnholds, J. The CRB1 complex: Following the trail of Crumbs to a feasible gene therapy strategy. *Front. Neurosci.* **2017**, *11*, 175.
34. Klebes, A.; Knust, E. A conserved motif in Crumbs is required for E-cadherin localisation and zonula adherens formation in Drosophila. *Curr. Biol.* **2000**, *10*, 76–85.
35. Bachmann, A.; Schneider, M.; Theilenberg, E.; Grawe, F.; Knust, E. Drosophila Stardust is a partner of Crumbs in the control of epithelial cell polarity. *Nature* **2001**, *414*, 638–643.
36. Laprise, P.; Beronja, S.; Silva-Gagliardi, N.F.; Pellikka, M.; Jensen, A.M.; McGlade, C.J.; Tepass, U. The FERM Protein Yurt Is a Negative Regulatory Component of the Crumbs Complex that Controls Epithelial Polarity and Apical Membrane Size. *Dev. Cell* **2006**, *11*, 363–374.
37. Médina, E.; Williams, J.; Klipfell, E.; Zarnescu, D.; Thomas, G.; Bivic, A. Le Crumbs interacts with moesin and β Heavy-spectrin in the apical membrane skeleton of Drosophila. *J. Cell Biol.* **2002**, *158*, 941–951.
38. Tepass, U.; Theres, C.; Knust, E. crumbs encodes an EGF-like protein expressed on apical membranes of Drosophila epithelial cells and required for organization of epithelia. *Cell* **1990**, *61*, 787–799.
39. Chishti, A.H.; Kim, A.C.; Marfatia, S.M.; Lutchman, M.; Hanspal, M.; Jindal, H.; Liu, S.C.; Low, P.S.; Rouleau, G.A.; Mohandas, N.; et al. The FERM domain: A unique module involved in the linkage of cytoplasmic proteins to the membrane. *Trends Biochem. Sci.* **1998**, *23*, 281–282.
40. Roh, M.H.; Fan, S.; Liu, C.-J.; Margolis, B. The Crumbs3-Pals1 complex participates in the establishment of polarity in mammalian epithelial cells. *J. Cell Sci.* **2003**, *116*, 2895–2906.
41. Lemmers, C.; Michel, D.; Lane-Guermonprez, L.; Delgrossi, M.-H.; Médina, E.; Arsanto, J.-P.; Bivic, A. Le CRB3 Binds Directly to Par6 and Regulates the Morphogenesis of the Tight Junctions in Mammalian Epithelial Cells. *Mol. Biol. Cell* **2004**, *15*, 1324.
42. Hurd, T.W.; Gao, L.; Roh, M.H.; Macara, I.G.; Margolis, B. Direct interaction of two polarity complexes implicated in epithelial tight junction assembly. *Nat. Cell Biol.* **2003**, *5*, 137–142.
43. Kantardzhieva, A.; Alexeeva, S.; Versteeg, I.; Wijnholds, J. MPP3 is recruited to the MPP5 protein scaffold at the retinal outer limiting membrane. *FEBS J.* **2006**, *273*, 1152–1165.

44. Tan, B.; Yatim, S.M.J.M.; Peng, S.; Gunaratne, J.; Hunziker, W.; Ludwig, A. The Mammalian Crumbs Complex Defines a Distinct Polarity Domain Apical of Epithelial Tight Junctions. *Curr. Biol.* **2020**, *30*, 2791–2804.e6.
45. Assémat, E.; Crost, E.; Ponserrer, M.; Wijnholds, J.; Le Bivic, A.; Massey-Harroche, D. The multi-PDZ domain protein-1 (MUPP-1) expression regulates cellular levels of the PALS-1/PATJ polarity complex. *Exp. Cell Res.* **2013**, *319*, 2514–2525.
46. Park, B.; Alves, C.H.; Lundvig, D.M.; Tanimoto, N.; Beck, S.C.; Huber, G.; Richard, F.; Klooster, J.; Andlauer, T.F.M.; Swindell, E.C.; et al. PALS1 Is Essential for Retinal Pigment Epithelium Structure and Neural Retina Stratification. *J. Neurosci.* **2011**, *31*, 17230–17241.
47. van de Pavert, S.A.; Kantardzhieva, A.; Malysheva, A.; Meuleman, J.; Versteeg, I.; Levelt, C.; Klooster, J.; Geiger, S.; Seeliger, M.W.; Rashbass, P.; et al. Crumbs homologue 1 is required for maintenance of photoreceptor cell polarization and adhesion during light exposure. *J. Cell Sci.* **2004**, *117*, 4169–4177.
48. Hurd, T.W.; Fan, S.; Liu, C.J.; Kweon, H.K.; Hakansson, K.; Margolis, B. Phosphorylation-dependent binding of 14-3-3 to the polarity protein Par3 regulates cell polarity in mammalian epithelia. *Curr. Biol.* **2003**, *13*, 2082–2090.
49. Laprise, P.; Lau, K.M.; Harris, K.P.; Silva-Gagliardi, N.F.; Paul, S.M.; Beronja, S.; Beitel, G.J.; McGlade, C.J.; Tepass, U. Yurt, Coracle, Neurexin IV and the Na(+),K(+)-ATPase form a novel group of epithelial polarity proteins. *Nature* **2009**, *459*, 1141–1145.
50. Wei, Z.; Li, Y.; Ye, F.; Zhang, M. Structural basis for the phosphorylation-regulated interaction between the cytoplasmic tail of cell polarity protein crumbs and the actin-binding protein moesin. *J. Biol. Chem.* **2015**, *290*, 11384–11392.
51. Varelas, X.; Samavarchi-Tehrani, P.; Narimatsu, M.; Weiss, A.; Cockburn, K.; Larsen, B.G.; Rossant, J.; Wrana, J.L. The Crumbs complex couples cell density sensing to Hippo-dependent control of the TGF- β -SMAD pathway. *Dev. Cell* **2010**, *19*, 831–844.
52. Richardson, E.C.N.; Pichaud, F. Crumbs is required to achieve proper organ size control during Drosophila head development. *Development* **2010**, *137*, 641–650.
53. Quinn, P.M.J.; Wijnholds, J. Retinogenesis of the human fetal retina: An apical polarity perspective. *Genes (Basel)* **2019**, *10*, 987.
54. Pocha, S.M.; Wassmer, T.; Niehage, C.; Hoflack, B.; Knust, E. Retromer Controls Epithelial Cell Polarity by Trafficking the Apical Determinant Crumbs. *Curr. Biol.* **2011**, *21*, 1111–1117.
55. Clark, B.S.; Miesfeld, J.B.; Flinn, M.A.; Collery, R.F.; Link, B.A. Dynamic Polarization of Rab11a Modulates Crb2a Localization and Impacts Signaling to Regulate Retinal Neurogenesis. *Front. Cell Dev. Biol.* **2021**, *8*, 608112.
56. Thompson, B.J.; Pichaud, F.; Röper, K. Sticking together the Crumbs - an unexpected function for an old friend. *Nat. Rev. Mol. Cell Biol.* **2013**, *14*, 307–14.
57. Letizia, A.; Ricardo, S.; Moussian, B.; Martín, N.; Llimargas, M. A functional role of the extracellular domain of Crumbs in cell architecture and apicobasal polarity. *J. Cell Sci.* **2013**, *126*, 2157–2163.
58. Zou, J.; Wang, X.; Wei, X. Crb apical polarity proteins maintain zebrafish retinal cone mosaics via intercellular binding of their extracellular domains. *Dev. Cell* **2012**, *22*, 1261–74.
59. Nemetschke, L.; Knust, E. Drosophila Crumbs prevents ectopic Notch activation in developing wings by inhibiting ligand-independent endocytosis. *Development* **2016**, *143*, 4543–4553.
60. Alves, C.H.; Bossers, K.; Vos, R.M.; Essing, A.H.W.; Swagemakers, S.; van der Spek, P.J.; Verhaagen, J.; Wijnholds, J. Microarray and morphological analysis of early postnatal CRB2 mutant retinas on a pure C57BL/6J genetic background. *PLoS One* **2013**, *8*, e82532.
61. Alves, C.H.; Boon, N.; Mulder, A.A.; Koster, A.J.; Jost, C.R.; Wijnholds, J. CRB2 Loss in Rod Photoreceptors Is Associated with Progressive Loss of Retinal Contrast Sensitivity. *Int. J. Mol. Sci.* **2019**, *20*, 4069.
62. Alves, C.H.; Sanz, A.S.; Park, B.; Pellissier, L.P.; Tanimoto, N.; Beck, S.C.; Huber, G.; Murtaza, M.; Richard, F.; Sridevi Gurubaran, I.; et al. Loss of CRB2 in the mouse retina mimics human retinitis pigmentosa due to mutations in the CRB1 gene. *Hum. Mol. Genet.* **2013**, *22*, 35–50.

63. Pellissier, L.P.; Alves, C.H.; Quinn, P.M.; Vos, R.M.; Tanimoto, N.; Lundvig, D.M.S.; Dudok, J.J.; Hooibrink, B.; Richard, F.; Beck, S.C.; et al. Targeted ablation of CRB1 and CRB2 in retinal progenitor cells mimics Leber congenital amaurosis. *PLoS Genet* **2013**, *9*, e1003976.
64. Quinn, P.M.; Alves, C.H.; Klooster, J.; Wijnholds, J. CRB2 in immature photoreceptors determines the superior-inferior symmetry of the developing retina to maintain retinal structure and function. *Hum. Mol. Genet.* **2018**, *27*, 3137–3153.
65. Repnik, U.; Česen, M.H.; Turk, B. The Endolysosomal System in Cell Death and Survival. *Cold Spring Harb. Perspect. Biol.* **2013**, *5*, a008755.
66. Neefjes, J.; Jongsma, M.M.L.; Berlin, I. Stop or Go? Endosome Positioning in the Establishment of Compartment Architecture, Dynamics, and Function. *Trends Cell Biol.* **2017**, *27*, 580–594.
67. Campa, C.C.; Margaria, J.P.; Derle, A.; Del Giudice, M.; De Santis, M.C.; Gozzelino, L.; Copperi, F.; Bosia, C.; Hirsch, E. Rab11 activity and PtdIns(3)P turnover removes recycling cargo from endosomes. *Nat. Chem. Biol.* **2018**, *14*, 801–810.
68. Gaullier, J.-M.; Simonsen, A.; D'Arrigo, A.; Bremnes, B.; Stenmark, H.; Aasland, R. FYVE fingers bind PtdIns(3)P. *Nat.* **1998**, *394*, 432–433.
69. Aguilar-Aragon, M.; Fletcher, G.; Thompson, B.J. The cytoskeletal motor proteins Dynein and MyoV direct apical transport of Crumbs. *Dev. Biol.* **2020**, *459*, 126–137.
70. Fletcher, G.C.; Lucas, E.P.; Brain, R.; Tournier, A.; Thompson, B.J. Positive feedback and mutual antagonism combine to polarize crumbs in the drosophila follicle cell epithelium. *Curr. Biol.* **2012**, *22*, 1116–1122.
71. Li, Y.; Wei, Z.; Yan, Y.; Wan, Q.; Du, Q.; Zhang, M. Structure of Crumbs tail in complex with the PALS1 PDZ-SH3-GK tandem reveals a highly specific assembly mechanism for the apical Crumbs complex. *Proc. Natl. Acad. Sci. U. S. A.* **2014**, *111*, 17444–17449.
72. Clausen, T.H.; Lamark, T.; Isakson, P.; Finley, K.; Larsen, K.B.; Brech, A.; Øvervatn, A.; Stenmark, H.; Bjørkøy, G.; Simonsen, A.; et al. p62/SQSTM1 and ALFY interact to facilitate the formation of p62 bodies/ALIS and their degradation by autophagy. *Autophagy* **2010**, *6*, 330–344.
73. Hu, Y.; Zhang, Y.; Jiang, L.; Wang, S.; Lei, C.; Sun, M.; Shu, H.; Liu, Y. WDFY1 mediates TLR 3/4 signaling by recruiting TRIF. *EMBO Rep.* **2015**, *16*, 447–455.
74. Sancho-Balsells, A.; Brito, V.; Fernández, B.; Pardo, M.; Straccia, M.; Ginés, S.; Alberch, J.; Hernández, I.; Arranz, B.; Canals, J.M.; et al. Lack of Helios During Neural Development Induces Adult Schizophrenia-Like Behaviors Associated With Aberrant Levels of the TRIF-Recruiter Protein WDFY1. *Front. Cell. Neurosci.* **2020**, *0*, 93.
75. van de Pavert, S.A.; Meuleman, J.; Malysheva, A.; Aartsen, W.M.; Versteeg, I.; Tonagel, F.; Kamphuis, W.; McCabe, C.J.; Seeliger, M.W.; Wijnholds, J. A single amino acid substitution (Cys249Trp) in Crb1 causes retinal degeneration and deregulates expression of pituitary tumor transforming gene Pttg1. *J. Neurosci.* **2007**, *27*, 564–573.
76. Mehalow, A.K.; Kameya, S.; Smith, R.S.; Hawes, N.L.; Denegre, J.M.; Young, J. a; Bechtold, L.; Haider, N.B.; Tepass, U.; Heckenlively, J.R.; et al. CRB1 is essential for external limiting membrane integrity and photoreceptor morphogenesis in the mammalian retina. *Hum. Mol. Genet.* **2003**, *12*, 2179–89.
77. Pellikka, M.; Tepass, U. Unique cell biological profiles of retinal disease-causing missense mutations in the polarity protein Crumbs. *J. Cell Sci.* **2017**, *130*, 2147–2158.
78. Buck, T.M.; Pellissier, L.P.; Vos, R.M.; van Dijk, E.H.C.C.; Boon, C.J.F.; Wijnholds, J. AAV serotype testing on cultured human donor retinal explants. In *Methods in Molecular Biology*; Boon, C.J.F., Wijnholds, J., Eds.; New York, NY: Humana Press: New York, NY, 2018; Vol. 1715, p. pp 275-288 ISBN 978-1-4939-7522-8.
79. Pellissier, L.P.; Hoek, R.M.; Vos, R.M.; Aartsen, W.M.; Klimczak, R.R.; Hoyng, S.A.; Flannery, J.G.; Wijnholds, J. Specific tools for targeting and expression in Müller glial cells. *Mol. Ther. — Methods Clin. Dev.* **2014**, *1*, 14009.

Chapter 7

Summary

Nederlandse Samenvatting

Acknowledgements

Curriculum Vitae

List of Publications

Summary

Around one out of 4000 people worldwide suffer from monogenetic hereditary retinal dystrophies (RDs; around 4000-6000 Dutch patients). Hereditary retinal diseases result from variations (*mutations*) on the genetic code (DNA) on genes causing changes on the gene expression and protein function. Biallelic *CRB1* gene variations can cause retinitis pigmentosa (RP), Leber congenital amaurosis (LCA), or in some cases macular degeneration. *CRB1*-related RDs account for around 7-17% of all Leber congenital amaurosis cases (1 / 250.000 people or 60-90 Dutch patients) and 3-9% of all retinitis pigmentosa cases (1/90.000 people or 130-390 Dutch patients). On *CRB1* animal models or eye scans of *CRB1* patients, it was shown that *CRB1*-related RDs (a) degenerate the light sensitive photoreceptors (PRs; especially in the retinal periphery), (b) reduce cell adhesion between Müller glial cells (MGCs)-PRs, PRs-PRs, and MGCs-MGCs, and (c) sometimes disrupts the cell cycle during retinal development. The consequence is vision loss and blindness. It is believed that the significance of *CRB1* in the neuroretina rests on the participation of *CRB1* in apical polarity complexes in Müller glial cells and photoreceptors – such as the Crumbs and PAR protein complex – at the outer limiting membrane (OLM). *CRB1* protein at the OLM can support adhesion/junction molecules, recruit actomyosin cytoskeletal proteins, and regulate the spatiotemporal retinogenesis via Notch, mTORC1 & Hippo pathways.

No treatments are available for monogenetic neuroretinal diseases. However, gene therapy is becoming a promising treatment option for many hereditary diseases. The development of gene supplementation therapies begins at (a) establishing relevant disease models, (b) generating & optimizing transgene sequences and vector cassettes, (c) screening of carefully selected viral capsids, and (d) testing gene therapy vectors in proof-of-concept studies in animals. Promising gene therapy candidates need to be screened on how efficient they can express the vector in the target cells while minimizing off-target effects. This can be illustrated on Luxturna® (voretigene neparvovec-rzyl), a gene therapy for biallelic gene variation on the *RPE65* gene causing LCA2 and RP. The *RPE65* protein is expressed in the retinal pigment epithelium (RPE). Luxturna® was the first retinal gene therapy approved both in the USA and Europe. The gene supplementation therapy is based on packaging the cDNA of the *RPE65* gene under the control of a ubiquitous promoter (CBA) into recombinant adeno-associated virus serotype 2 (rAAV2) particles. The rAAV-particles are then injected in the subretinal space where they can infect RPE cells. The single-stranded *RPE65* cDNA is then unpacked and transported to the nucleus where it forms episomal stable circular DNA structures from which the *RPE65* transgene is stably expressed rescuing the RPE phenotype. Similar strategies have been developed – but not approved yet – for many hereditary retinal dystrophies including *CRB1*-related RD (see for example **chapter 1, 2 and 4**). A summary of the clinical trials for ocular gene supplementation therapies, the different rAAV vector

cassettes (promoters, genes, polyadenylations sequences), the different rAAV capsid (tropism) studies, and the transgene & bioactivity assays are described in **chapter 1**.

We describe relevant human and mouse disease models for *CRB1*-related RP in **chapter 2+4+5**. In **chapter 2**, we describe a new RP-*Crb1* mouse model (*Crb1*^{KO}*Crb2*^{LowMGCs}) where we ablated *Crb1* expression and reduced the levels of the *Crb1* homologue *Crb2* in Müller glial cells. We also compared the OLM cell protrusion phenotype between four different RP-*Crb1* mice and wildtype mice. We find a negative correlation of the number of OLM breaks and the CRB1/CRB2 proteins (CRB's) at the OLM. It demonstrates that the amount of CRB proteins is important and not specifically the CRB1 or CRB2 proteins. Also, it was not known how important CRB1 or CRB2 is in MGCs at the OLM. It was interesting to see that reduction of CRB's in MGCs compared to rod photoreceptors caused a more severe OLM-phenotype. It means that a gene therapy should preferably also infect MGCs and not only photoreceptors. We also find that the reduced CRB2-protein expression at OLM in the *Crb1*^{KO}*Crb2*^{LowMGCs} mice still relatively preserved the OLM over 12 months. This was in stark contrast to a previous publication where we completely ablated *Crb2* (*Crb1*^{KO}*Crb2*^{ΔMGCs}), having a severe retinal (LCA-like) phenotype. Thus, the adhesion of neuroretinal cells is quite dependent on the level of CRB proteins in glial (meaning “glue” in Greek language) cells.

Although *Crb1*^{KO}*Crb2*^{ΔMGCs} mice compared to *Crb1*^{KO}*Crb2*^{LowMGCs} mice had a mild phenotype, they still need natural *Crb2* protein levels for proper retinal function and normal morphology. The mice lost their vision function earlier compared to *Crb1*^{KO} littermates measured by optokinetic head-tracking response (OKT) and electroretinograms (ERGs). Also, early effects on morphology were seen such as outer/inner segments of photoreceptor loss and more retinal cell protrusions. Also, when the *Crb1*^{KO}*Crb2*^{LowMGCs} retina was stressed by a low dose of a Müller glial toxin (DL-AAA), causing a breakdown of the OLM, then the vision function (measured by ERGs and OKT) was reduced one month after the DL-AAA injection. It shows that the recovery capacity of the *Crb1*^{KO}*Crb2*^{LowMGCs} neuroretina after aggravation is much lower compared to wildtype and *Crb1*-knockout neuroretinas.

Also, when codon-optimized human *CRB1* or *CRB2* cDNA is provided to *Crb1*^{KO}*Crb2*^{LowMGCs} Müller glial cells by rAAV-vector therapy, then the morphological phenotype caused by the toxin can be prevented. Thus, rAAV-*CRB1* or rAAV-*CRB2* gene therapy can increase the OLM stability in *Crb1*^{KO}*Crb2*^{LowMGCs} mice. Interestingly, only the rAAV-*CRB2* treatment protected the retina from vision loss measured by OKT and ERG, whereas rAAV-*CRB1* treated eyes had an unwanted increase of activated microglial cells and neovascularization events in the ganglion cell layer(GCL)/nerve fiber layer(NFL) and ciliary body. This and other studies show that CRB1 and CRB2 proteins have compensatory and overlapping functions in the neuroretina and that rAAV-*CRB2* is a promising candidate for clinical trials.

The protein shell (capsid) of the rAAV particle determines what cells are infected (tropism), to what degree (potency), and how easily it breaks down by enzymes or escapes immune recognition (capsid stability and potency). The rAAV infection of a cell is mediated by surface receptors on the host cell (see **chapter 1**). What is more, the surface receptors can be quite different depending on the species requiring screening of the rAAV capsids on human cells or non-human primates. In **chapter 3**, we set up a new rAAV transgene expression assay on (a) how to screen the tropism of rAAV capsids in parallel on human donor neuroretina's *ex vivo* and (b) how to keep the overall morphology intact for 21 days. In **chapter 4**, we tested three different rAAVs (rAAV9, rAAV5 and rAAV6-derived ShH10^{Y445F}) on their potency to infect the target cells of a gene therapy for *CRB1*-related RP patients: Müller glial cells and photoreceptor cells. We show on human donor retinal explants and human induced pluripotent stem cell (hiPSC)-derived retinal organoids that rAAV5 and rAAV6-derived ShH10^{Y445F} can efficiently infect Müller glial cells. Also, both rAAVs infected photoreceptors on human donor retinal explants. Surprisingly, they also outperformed on potency the rAAV9 on three different titers measured. Previously, rAAV9 showed excellent infection profiles in mice *in vivo* for *CRB1* rAAV therapies. These results demonstrate that (a) species-differences can influence potency and tropism, and (b) rAAV5 is a strong AAV-capsid candidate for *CRB1* rAAV-based treatments.

Finally, in **chapter 4** and **chapter 5**, we explore how *CRB1*-related retinitis pigmentosa can be modelled in a human cell system. First, we show that we can generate retinal organoids from hiPSCs of three different healthy donors (control retinas). We find back a laminated retina with all major types of retinal cells present (PRs, MGCs, amacrine cells, horizontal cells, ganglion cells, RPE cells). We then show that CRB2 protein precedes CRB1 protein expression at the OLM during retinogenesis in organoids and fetal retinal material. In the mature retinal organoid, CRB1 is found in the subapical region of photoreceptors & MGCs and CRB2 in photoreceptors and apical MGC-villi. In the mouse retina, CRB2 is found in PRs and MGCs. The protein location studies on immune-electronmicroscopy shows that CRB1 has a more prominent role in the human neuroretina when compared to the mouse retina where CRB2 is believed to compensate for the loss of *Crb1* in *Crb1*-null mouse models.

Second, we generated RP-*CRB1* organoids of three RP-*CRB1* patient donor hiPSC lines. They all developed a retinal volcanic-like cell protrusion phenotype as similar seen in *Crb1* and *Crb2*-RP mouse models. Interestingly, the OLM protrusions in RP-*CRB1* organoids do not only show a loss of the subapical & adherens junction proteins including variant CRB1 protein but also a strong decrease of apical NOTCH1. In control organoids, we find an extracellular domain (ECD) interaction of CRB1 and NOTCH1, which is largely lost in RP-*CRB1* organoids. This indicates that CRB1 is important for the recruitment of NOTCH1 or the stabilization of NOTCH1 at the OLM. Previously, it was shown that the neuroretina of

CRB1 LCA-like mice have an increase in the Notch pathway activation. The ECD interaction of CRB1/NOTCH1 could play an important role here.

Lastly, CRB1 and NOTCH1 need to be transported and continuously recycled (turned over) by the endolysosomal system at the OLM. We find much more early endosomes and an increase of the degradative cellular vesicles which is linked to decrease of RAB11A-positive recycling endosomes in RP-*CRB1* organoids. We hypothesize that the loss of CRB1 at the OLM, inhibits the maturation of early endosomes to recycling endosomes increasing the number of degradative vesicles. We also found an increase of WDFY1 proteins (especially in endosomes) in RP-*CRB1* organoids and an increase in *Wdfy1* mRNA expression in a *CRB1* LCA-like mouse model (*Crb1*^{KO}*Crb2*^{ARPC}). The WDFY1 and NOTCH1 proteins could be interesting biomarkers for *CRB1* gene therapies. Yet, little is known on the function of WDFY1 and the endolysosomal system in the neuronal retina. Especially, controlling the endolysosomal system to inhibit intracellular disease processes is an exciting treatment approach. But first more research into the endolysosomal system is needed to delineate (sub-)populations of endosomes in the neuroretina (and characterize RP- and control retinal organoids) to make such treatments more predictable.

In conclusion, we describe the generation and analysis of RP-*CRB1* mouse and human retinas: *Crb1*^{KO}*Crb2*^{LowMGCs} (**chapter 2**), human RP-*CRB1* organoids (*CRB1*^{M1041T/ M1041T}; *CRB1*^{Y631C/E995*}; *CRB1*^{M1041T/C948Y}; **chapter 4 and 5**). The data indicates that the human RP-*CRB1* disease can be studied in mice and human organoids. Then, we show that rAAV-*CRB* gene supplementation therapy to Müller glial cells of the *Crb1*^{KO}*Crb2*^{LowMGCs} mouse retina can protect it from stress-induced vision loss, and that human *CRB2* cDNA was superior to human *CRB1* cDNA (**chapter 2**). We then developed an improved rAAV tropism assay on human donor eyes (**chapter 3**). This assay shows that rAAV5 can efficiently infect Müller glial cells and photoreceptors, the target cells of a RP-*CRB1* gene therapy. Also, rAAV5 infection studies outperformed rAAV9 on human retinal organoids and human donor retinas (**chapter 4**). Thus, this thesis on both human and mouse models provides new insight into retinal degeneration and rAAV gene supplementation therapies.

Nederlandse Samenvatting

Wereldwijd lijdt 1 op de 4000 mensen aan een erfelijke netvliesziekte (ongeveer 4000-6000 Nederlandse patiënten). Erfelijke netvliesziekten ontstaan door afwijkingen in de genetische code (DNA) van genen, met gevolgen voor de functie en expressie van het eiwit. Genetische veranderingen op de twee *CRB1*-gen allelen kunnen retinitis pigmentosa (RP), Leber congenitale amaurose (LCA) of in sommige gevallen macula-degeneratie veroorzaken. *CRB1*-genvarianten op beide allelen komen voor in ongeveer 7-17% van alle gevallen van LCA (1 op de 250.000 mensen; 60-90 Nederlandse patiënten) en in 3-9% van alle gevallen van retinitis pigmentosa (1 op de 90.000 mensen; 130-390 Nederlandse patiënten). In *CRB1*-diermodellen of op oogscans van *CRB1*-patiënten is aangetoond dat (a) de lichtgevoelige fotoreceptoren degenereren (vooral in de retinale periferie), (b) de celadhesie kan verminderen tussen Müller gliacellen (MGCs) en fotoreceptoren (FR), FR-FR, en MGCs-MGCs, en (c) soms de celcyclus tijdens de ontwikkeling van het netvlies verstoord raakt. Het gevolg is vermindering van het zicht en uiteindelijk blindheid in deze patiëntengroep. Onderzoek heeft aangetoond dat het CRB1 eiwit in het neuronale netvlies een significante rol speelt bij apicale polariteitscomplexen – zoals de Crumbs en PAR eiwitcomplexen – in Müller gliacellen en fotoreceptoren bij het external limiting membrane (ELM). CRB1 kan door de polariteitscomplexen eiwit-adhesie-moleculen aansturen, actomyosine-cytoskeleteiwitten rekruteren en de ruimtelijk-temporele netvliesgenese reguleren via Notch/mTORC1/Hippo pathways.

Op dit moment zijn er geen behandelingen beschikbaar voor monogenetische neuronale netvliesziekten. Een veelbelovende therapievorm in ontwikkeling voor monogenetische ziekten is de gentherapie. De ontwikkeling van gentherapieën voor patiënten bestaat uit (a) het opstellen van relevante ziektemodellen, (b) het genereren en optimaliseren van transgenen en de vectorcassette, (c) het screenen van zorgvuldig geselecteerde virale capsiden, en (d) het testen van de gentherapie in proof-of-concept studies (POCs). De veelbelovende kandidaten (gentherapieën) moeten gescreend worden op hoe efficiënt ze de vector tot expressie kunnen brengen in de doelwitcellen, terwijl bijeffecten geminimaliseerd worden. Een voorbeeld van de werking van gentherapie is hier beschreven voor Luxturna® (voretigene neparvovec-rzyl), een gentherapie voor de biallelische *RPE65*-afgeleide erfelijke retinale pigmentepitheel (RPE) ziekte. Laatstgenoemde werd onlangs goedgekeurd door de EMA en FDA. Deze gentherapie is gebaseerd op het verpakken van het cDNA van het *RPE65*-gen onder controle van een ubiquitaire promotor (CBA) in recombinant adeno-geassocieerd virus serotype 2 (rAAV2)-deeltjes. De rAAV-deeltjes worden in de subretinale ruimte geïnjecteerd waardoor RPE-cellen geïnfecteerd worden. De *RPE65*-cDNA in de rAAV-deeltjes worden in de geïnfecteerde cellen uitgepakt en getransporteerd naar de celkern waar het episomaal stabiele cirkelvormige DNA-structuren vormt. Uiteindelijk komt het *RPE65*-transgen tot expressie in de RPE-cellen waar het het gevonden RPE-fenotype

herstelt. Soortgelijke strategieën zijn in ontwikkeling (maar nog niet goedgekeurd) voor vele erfelijke retinale dystrofieën, waaronder *CRB1*-gerelateerde netvliesziektes (zie bijvoorbeeld **hoofdstuk 2** en **4**). Een samenvatting van de klinische studies in oculaire genterapieën, de rAAV vectoren (promotors, genen, polyadenylatie sequenties), de rAAV tropisme studies, en het transgen en de bio-activiteit assay's zijn beschreven in **hoofdstuk 1**.

Het ontwikkelen en karakteriseren van een relevant ziektemodel voor RP-*CRB1* in muizen- en menselijke cellen is beschreven in **hoofdstuk 2+4+5**. In **hoofdstuk 2** beschrijven we een nieuw RP-*CRB1* muismodel (*Crb1*^{KO}*Crb2*^{LowMGCs}) waarin we de *Crb1* expressie hebben verwijderd en de niveaus van het *Crb1* homolog *Crb2* in Müller gliacellen hebben verlaagd. Bovendien vergeleken we in muizen het *Crb1*^{KO}*Crb2*^{LowMGCs} ELM-breuk fenotype met drie al eerder gepubliceerde RP-*CRB1* muizen. We vonden een negatieve correlatie tussen het aantal ELM-breuken en de totale hoeveelheid van CRB (CRB1/CRB2) eiwitten. Dat laat zien dat de hoeveelheid CRB belangrijk is en niet specifiek de CRB1 of CRB2 eiwitten. De vraag is hoe belangrijk de CRB1 of CRB2 eiwitten bij het ELM in fotoreceptoren en Müller gliacellen zijn. Interessant was dat het verwijderen van CRB-eiwitten in staafjes een minder erge ELM-fenotype veroorzaakte dan het verwijderen van CRB-eiwitten in Müller gliacellen. Dat betekent dat een rAAV-gebaseerde therapie bij voorkeur ook Müller cellen en niet alleen fotoreceptoren moeten infecteren. Verder hebben we gezien dat een lage CRB-eiwit-expressie in Müller gliacellen al beschermend is, toen we het fenotype van de *Crb1*^{KO}*Crb2*^{LowMGCs} muizen vergeleken met een eerder gepubliceerd fenotype waar *Crb2* geheel verwijderd was (*Crb1*^{KO}*Crb2*^{ΔMGC}). De *Crb1*^{KO}*Crb2*^{LowMGCs} muizen hadden een beter behoud van netvliesmorfologie, al te zien in 1 maanden oude dieren. Dus de adhesie van neuronale netvliescellen is bijzonder afhankelijk van de *CRB*-expressie in glia (Grieks voor "lijm") cellen.

Om een functionerend netvlies in muizen over langere tijd te behouden is het echter belangrijk dat *Crb2* in Müller gliacellen tot een natuurlijk niveau wordt gebracht. De *Crb1*^{KO}*Crb2*^{LowMGCs} muizen verloren eerder hun gezichtsvermogen in vergelijking met *Crb1*^{KO} control dieren, gemeten met behulp van opto-kinetische hoofd-tracking respons (OKT) en electroretinogrammen (ERGs). Ook werden vroege morfologische fenotypen gezien, zoals verlies van buitenste/binnenste segmenten van fotoreceptoren en een toename van verschoven fotoreceptorkernen in de subretinale ruimte (boven de ELM) van over de ELM in de subretinale ruimte. Ook wanneer de *Crb1*^{KO}*Crb2*^{LowMGCs} netvliezen werden blootgesteld aan stress door een lage dosis van een Müller gliaceltoxine (DL-AAA) dat een afbraak van de ELM veroorzaakt, was een maand later het zicht verminderd zoals gemeten met ERG's en OKT's. Hieruit blijkt dat het herstellvermogen van het *Crb1*^{KO}*Crb2*^{LowMGCs} netvlies lager is ten opzichte van de netvliezen van wildtype en *Crb1*-knockout muizen.

Wanneer codon-geoptimaliseerde humane *CRB1* of *CRB2* cDNA met behulp van rAAV genterapie vectoren wordt toegediend aan *Crb1*^{KO}*Crb2*^{LowMGCs} Müller gliacellen dan kan

het morfologische fenotype, veroorzaakt door de toxine, worden voorkomen. Het humane CRB1 of CRB2 eiwit is dus in staat om de ELM-stabiliteit of ELM-herstel in *Crb1*^{KO}*Crb2*^{LowMGCs} muizen te verhogen. Interessant is dat alleen de rAAV-*CRB2* behandeling het netvlies beschermd tegen verlies aan gezichtsvermogen, zoals gemeten met OKT en ERG. De met rAAV-*CRB1* behandelde ogen vertoonden een ongewenste toename van geactiveerde microgiale cellen en neovascularisatie in de ganglioncellaag (GCL) en het corpus ciliare. Deze en eerdere studies tonen aan dat de CRB1 en CRB2 eiwitten compenserende en overlappende functies hebben in het neuronale netvlies en dat rAAV-*CRB2* een veelbelovende kandidaat is voor de eerste RP-*CRB1* klinische studies.

Het eiwitomhulsel (capside) van het rAAV-deeltje bepaalt welke cellen worden geïnfecteerd (tropisme), in welke mate (potentie), en hoe gemakkelijk het door enzymen wordt afgebroken of aan de herkenningstaak van het immuunsysteem ontsnapt (capside stabiliteit en potentie). De infectie van een cel met het rAAV wordt gefaciliteerd door oppervlaktereceptoren op de gastheercel (zie ook **hoofdstuk 1**). Bovendien kunnen de oppervlaktereceptoren verschillend zijn naargelang de diersoort, waardoor het rAAV tropisme op menselijke cellen of niet-menselijke primaten moet worden onderzocht. In **hoofdstuk 3** hebben we een nieuwe rAAV transgeen expressie assay opgezet om (a) het tropisme van rAAV capsiden in parallel te screenen op humane donor neuroretina (*ex vivo*) en (b) de algehele morfologie intact te houden gedurende 21 dagen. In **hoofdstuk 4** hebben we drie verschillende rAAVs (rAAV9, rAAV5 en rAAV6-afgeleide ShH10^{Y445F}) getest op hun potentie om de doelwitcellen van het RP-*CRB1* netvlies te infecteren: Müller gliacellen en fotoreceptorcellen. We tonen aan dat rAAV5 en rAAV6-afgeleide ShH10^{Y445F} op efficiënte wijze de Müller gliacellen kunnen infecteren van retinale explantaten van menselijke donoren en menselijke geïnduceerde pluripotente stamcel (hiPSC)-afgeleide retinale organoïden. Beide rAAV's infecteerden ook fotoreceptoren op retinale explantaten van menselijke donoren. Verrassend genoeg overtroffen zij ook de infectiepotentie van rAAV9 op drie verschillende virusconcentraties (titers). Eerder toonde rAAV9 een uitstekend infectieprofiel in *in vivo* muisstudies. De resultaten op menselijk materiaal tonen aan dat (a) verschillen in diersoort de potentie en tropisme kunnen beïnvloeden en dat (b) rAAV5 een kandidaat is voor de *CRB1* rAAV-getherapie voor RP-*CRB1* patiënten.

Tenslotte, in **hoofdstuk 4** en **hoofdstuk 5**, onderzochten we hoe RP-*CRB1* gemodelleerd kan worden in een menselijk netvlies. Wij laten zien dat we retinale organoïden kunnen genereren uit hiPSCs van drie verschillende gezonde donoren (controles zonder bekende mutaties). In de controle-organoïden vinden we belangrijke celtypen (fotoreceptoren, Müller gliacellen, amacrine cellen, horizontale cellen, ganglioncellen, RPE-cellen) in de verschillende lagen van het netvlies terug. Wij tonen aan in organoïden en foetale retina's dat tijdens de ontwikkeling van het netvlies, het CRB2 eiwit veel eerder tot expressie op de ELM komt dan het CRB1 eiwit. In de oudere retinale organoïden wordt CRB1 aangetroffen in de sub-apicale

regio van fotoreceptoren en Müller gliacellen, terwijl CRB2 wordt aangetroffen de sub-apicale regio van fotoreceptoren en apicale Müller glia-villi. De locatiestudie van het eiwit op immuno-elektronenmicroscopie toont aan dat CRB1 een prominentere rol heeft in de menselijke neuroretina vergeleken met muizennetvlies. In het muizennetvlies wordt namelijk CRB2 gevonden in zowel fotoreceptoren als ook in Müller gliacellen, terwijl CRB1 alleen aanwezig is in Müller gliacellen.

Ten tweede, de RP-*CRB1* organoïden, die werden gegenereerd uit hiPSC donorlijnen van drie patiënten met RP-*CRB1*, vertoonden een netvliesfenotype bestaande uit protrusie van fotoreceptorkernen over de ELM in de subretinale ruimte. Dit fenotype hadden we eerder waargenomen in *Crb1* en *Crb2* RP muismodellen. Interessant is dat de ELM in RP-*CRB1* organoïden niet alleen een verlies laten zien van de sub-apicale en adherens junction-eiwitten inclusief variant CRB1 eiwit, maar ook een sterke afname van het apicale NOTCH1. In controle-organoïden vinden we een nog niet eerder beschreven interactie van CRB1 en NOTCH1 op hun extracellulaire domeinen (ECD). Deze interactie is grotendeels verloren gegaan in RP-*CRB1* organoïden. Dit wijst erop dat CRB1 belangrijk is voor de rekrutering van NOTCH1 of de stabilisatie van NOTCH1 op de ELM. Eerder is aangetoond dat LCA-*CRB1* muizen een overactieve Notch-pathway hebben. De CRB1-NOTCH1 ECD-interactie zou hier een belangrijke rol in kunnen spelen.

Tenslotte moeten CRB1 en NOTCH1 getransporteerd en continu gerecycled (turn-over) worden door het endolysosomaal systeem nabij de ELM. We vinden een toename in de hoeveelheid aan vroege endosomen en een toename van late endosomale afbraakvesikels. Dat lijkt gekoppeld te zijn aan een afname van RAB11A-positieve recycling-endosomen in RP-*CRB1* organoïden. Onze hypothese is dat het verlies van CRB1 op de ELM de rijping van vroege endosomen tot recycling-endosomen remt, waardoor het aantal afbraakvesikels toeneemt. Ook vonden we een toename van WDFY1 eiwitten (in het bijzonder in endosomen) in RP-*CRB1* organoïden, evenals een mRNA overexpressie van *Wdfy1* in RP-*CRB1* muizen. De WDFY1 en NOTCH1 eiwitten zouden interessante biomarkers voor *CRB1* gentherapie kunnen worden. Helaas is er nog weinig bekend over de functie van *WDFY1* en het endolysosomaal systeem in het neuronale netvlies. Vooral het specifieke aansturen van het endolysosomale systeem om intracellulaire ziekteprocessen te remmen, zou in de toekomst een significantere rol kunnen spelen. Maar eerst is er meer onderzoek nodig om de (sub-)populaties van endosomen in netvlies te karakteriseren in RP en controle-organoïden, om het effect van het aansturen van het endolysosomaal systeem beter te kunnen voorspellen.

Samengevat beschrijven wij de generatie en analyse van RP-*CRB1* muizen in **hoofdstuk 2** en menselijke RP-*CRB1* organoïden (*CRB1*^{M1041T/M1041T}, *CRB1*^{Y631C/E995*} en *CRB1*^{M1041T/C948Y}) in **hoofdstuk 4 en 5**. De gegevens tonen aan dat de menselijke RP-*CRB1* ziekte gereproduceerd kan worden in muizen en in menselijke organoïden. Vervolgens laten we zien dat rAAV-*CRB* gentherapie op Müller gliacellen van de *Crb1*^{KO}*Crb2*^{LowMGCS} muizen

het netvlies kan beschermen tegen stress-geïnduceerd zichtverlies en dat humaan *CRB2* cDNA superieur is aan humaan *CRB1* cDNA (**hoofdstuk 2**). We ontwikkelden een verbeterde rAAV tropisme assay op menselijke donorretina's (**hoofdstuk 3**). Vervolgens laten we zien dat rAAV5 efficiënt humane Müller gliacellen en fotoreceptoren kan infecteren, de twee voornaamste doelcellen van een RP-*CRB1* gentherapie. Ook presteerde rAAV5 beter dan rAAV9 in infectiestudies op menselijke retinale organoïden en menselijke donorretina's (**hoofdstuk 4**). Zowel menselijke modellen als muismodellen verschaffen dus nieuwe inzichten in retinale degeneratie en rAAV-gentherapieën.

ACKNOWLEDGEMENTS

Time flies at the LUMC! It has been a wonderful, sometimes frustrating but exciting PhD time, working side-by-side with all of you over the last six years. I very much enjoyed the comradeship, guidance and all the helping hands! I would not have lasted so long without you (and you made the ride much more enjoyable).

Thank you, Jan Wijnholds (supervisor) and Prof. Gré Luyten (promoter), for the patience and mentoring over the years. You always placed importance on having students around to sharpen our minds & giving back to the next generation, a tradition I will take with me.

To the current and former members of the Jan Wijnholds lab: Rogier, Peter, Jeroen, Lucie, Henrique, Albena, Michaela, Nanda, Andy, Carmen, Charlotte, and Xuefei. Special thanks to Lucie (my MSc student supervisor), Rogier (AAV production / cell culture / subcloning) and Henrique (retina research / co-supervisor) who all helped me transitioning from a MSc student to a PhD student and stoke the fire for the field of gene therapy. It was my privilege to supervise so many students. Thank you for your efforts: Martijn, Sarina, Ayse, Charlotte, Mees, Hind, Ilse, Yacintha, Ariadna, Mariska, and Daniëlle.

Thanks to all people in different departments. OOG: Camiel, Martine, Mieke, Elon, Danial, Annemijn, Mays, Annelies, and Judith. Transgenic animal unit: Jan-Bas, Ben, Fred, Martine, Ewoud, Jos, Nelleke, Marloë; and, the fruitful discussion during the experimental animal coordinator meetings. We could not have done all the mouse behaviour studies (ERG, OKT, cSLO, OCT) and viral injection rescue studies without you. The microscopy team & microscope user meetings: Joop, Annelies, Karien, Aat, Bram, Carolina, Lennard, and Willem. You made my images pop! The Virus / Stem Cell Biology / Human iPSC Hotel groups: Rob, Martijn, Harald, Christian, Christiaan, Marga, Arnaud, Maaïke, Manuel, Diana, Amiet, Anna, Francesca, Hidde, Igno, Iris, Jin, Kim, Marjolein, Sanne, Timo, Tobias, Vera, Xiaoyu, Marcella, Silvana, Qian, Zhen, Merve, Sanne, Selas, Willemijn, Sofia, and Lonneke. Thanks Sanne for organizing game nights! Also, the generation of viral vectors and iPSCs has been essential for my thesis. Special thanks to Steve for his guidance on all molecular techniques & whisky. The CCB: Sjaak, Ilana, Marlieke, Peter, Catalina, Chuannan, Dieuwke, Joke, Tom, Mayke, Felix, Marten, David, Zary, Pauline, Julia, and Marianne. Thank you, Ilana, for bringing the endolysosomal system a bit closer to me.

To my paranympths Nanda and Francesca, thanks for all your support and advice. Additionally, I would like to thank my Alb friends, the CV Parterretrap VC group, and my NOLA friends.

Thanks to my extended family (Böckeler, vd Brand, Broeders/Adams, Buck, Calmbach). A special thanks to my grandpa Theo who inspired me to become a scientist. Finally, I would like to dedicate the Thesis to my wife Claartje and my child Luna. Thanks for staying patient with me during the many stressful hours as a PhD student.

Curriculum Vitae

Thilo Matthias Buck was born on June 22nd, 1988 in Esslingen am Neckar, Germany. After finishing his business & economics high school at the Theodor-Heuss-Gymnasium (Abitur), Reutlingen, Germany, he went on to study psychology and economics in his bachelor studies at the University of Innsbruck, Austria. He transferred to the University of New Orleans, USA, in 2009, finishing his Bachelor's Degree (*magna cum laude*) in psychology with minors in chemistry and biology in 2012. During his bachelor studies he broadened his skills in internships in stress research (SPIT lab; supervisor: Dr. Elizabeth Shirtcliff), brain development (supervisor: Dr. Ben Hall), and Huntington's disease (supervisor: Dr. Gerald J. LaHoste).

He was awarded to the Erasmus Mundus NEURASMUS master's scholarship program in neuroscience in 2012. During 2012-2014, he interned at the labs of Dr. Marc Landry (chronic pain mouse models, INSERM/CNRS, France), Dr. Olaf Strauss (RPE and bestrophin-1, Berlin Charité, Germany), and Dr. Jan Wijnholds (rAAV tropism in mouse models, NIN, Amsterdam). He received his Master's Degree in Neuroscience from the VU Amsterdam (The Netherlands), the Bordeaux University (France), and the Humboldt University (Germany).

After a short stay as an English teacher in Siem Reap, Cambodia, in 2014/2015, he continued his work first as a research analyst (2015/2016) in Dr. Jan Wijnholds laboratory, and then later as a PhD candidate at the Department of Ophthalmology, at the Leiden University Medical Center (LUMC), in Leiden under the supervision of Dr. Jan Wijnholds on rAAV vectors and CRB1/CRB2 protein functions in the retina.

In 2021, he works as a viral vector specialist at the Netherlands Center for the Clinical Advancement of Cell & Gene Therapies (NecstGen), Leiden. NecstGen helps early-stage research organizations and start-ups to enter the clinical stage by bringing together the required expertise from R&D, development, production, QA and regulatory affairs in a non-profit GMP production.

List of Publications

Buck, T.M., Wijnholds, J (2020). *Recombinant Adeno-Associated Viral Vectors(rAAV)-Vector Elements in Ocular Gene Therapy Clinical Trials and Transgene Expression and Bioactivity Assays*. Int. J. Mol. Sci., 21, 4197.

Buck, T.M., Vos, R.M., Alves, C.H. Wijnholds, J. (2021). *AAV-CRB2 protects against vision loss in an inducible CRB1 retinitis pigmentosa mouse model*. Molecular Therapy: Methods & Clinical Development, 20, 423-441.

Buck, T.M., Pellissier, L.P., Vos, R.M., van Dijk, E.H.C., Boon, C.J.F., Wijnholds, J. (2018). *AAV serotype testing on cultured human donor retinal explants*. Methods in Molecular Biology, 1715, 275-288.

*Quinn, P. M., ***Buck, T.M.**, Mulder, A.A., Ohonin, C., Alves, C. H., Vos, R. M., Bialecka, M., Herwaarden, T. v., van Dijk, E. H.C., Talib, M., Freund, C., Mikkers, H. M. M., Hoeben, R. C., Goumans, M.-J., Boon, C. J. F., Koster, A. J., Chuva de Sousa Lopes, S. M., Jost, C. R. and Wijnholds, J. (2019). *Human iPSC-derived retinas recapitulate the fetal CRB1 CRB2 complex formation and demonstrate that photoreceptors and Müller glia are targets of AAV5*. Stem Cell Reports, 12, 906–919. ***Authors contributed equally to this work.**

Buck, T.M., Quinn, P. M., Pellissier, L.P., Mulder, A.A., et al. (2022). *CRB1 is required for the recruitment of NOTCH1 and proper recycling by RAB11A+ vesicles in human retinal organoids*. Manuscript submitted.

Quinn, P. M., **Buck, T.M.**, Ohonin, C., Mikkers, H. M. M., Wijnholds, J. (2018). *Production of iPS-Derived Human Retinal Organoids for Use in Transgene Expression Assays*. Methods Mol. Biol., 1715, 261–273.

Boon, N, Alves, C.H., Mulder, A.A., Andriessen, C.A., **Buck, T.M.**, Quinn, P.M.J., Vos, R.M., Koster, A.J., Jost, C.R., Wijnholds, J. (2021). *Defining Phenotype, Tropism, and Retinal Gene Therapy Using Adeno-Associated Viral Vectors (AAVs) in New-Born Brown Norway Rats with a Spontaneous Mutation in Crb1*. Int. J. Mol. Sci., 22, 3563.

Schoonderwoerd, R.A., **Buck, T.M.**, Andriessen, C.A., Wijnholds, J., Hattar, S., Meijer, J.H., DeBoer, T. (2021). *Sleep deprivation does not change the flash electroretinogram in wildtype and Opn4^{-/-}Gnat1^{-/-} mice*. J. Biol. Rhythms 37, 216-221.